In-situ surface wear processes of Gold coated carbon nanotube MEMS electrical contacts

PhD Thesis

Author

Thomas Gregory Bull

University of Southampton

Faculty of Engineering and the Environment

Submitted for consideration

1st November 2019

Primary Supervisor

Prof JW McBride

Secondary Supervisor

Prof L Jiang

Declaration of Authorship

I confirm that:

I declare that this thesis and the work presented in it is my own and has been generated by me as the result of my own original research.

1. This work was done wholly or mainly while in candidature for a research degree at this University;
2. Where any part of this thesis has previously been submitted for a degree or any other qualification at this University or any other institution, this has been clearly stated;
3. Where I have consulted the published work of others, this is always clearly attributed;
4. Where I have quoted from the work of others, the source is always given. With the exception of such quotations, this thesis is entirely my own work;
5. I have acknowledged all main sources of help;
6. Where the thesis is based on work done by myself jointly with others, I have made clear exactly what was done by others and what I have contributed myself;
7. Either none of this work has been published before submission, or parts of this work have been published as: [please list references below]:

Bull, Thomas G., and McBride, John W. "Transient Contact Opening Forces in a MEMS Switch Using Au/MWCNT Composite." *Technologies* 7.4 (2019): 69.

Bull, Thomas, and McBride, John. "In-situ contact surface characterization in a MEMS ohmic switch under low current switching." *Technologies* 6.2 (2018): 47.

McBride, John W. and Bull, Thomas G. "The in-situ wear of a hot and cold switched Au on Au coasted MWCNT electrical contact for a MEMS switch application." *2019 IEEE Holm Conference on Electrical Contacts, Milwaukee, USA*. IEEE, 2019.

Bull, Thomas G., John W. McBride, and Liudi Jiang. "The influence of Circuit Parameters on Molten Bridge Surface Degradation in a Au/MWCNT MEMS Switch Contact." *2018 IEEE Holm Conference on Electrical Contacts, Albuquerque, USA*. IEEE, 2018.

Mcbride, John and Bull, Thomas (2016) The influence of circuit parameters on molten metal bridge energy in a mems relay testing platform. *28th International Conference on Electric Contacts (ICEC2016), United Kingdom. 06 - 09 Jun 2016.* 6 pp .

Bull TG, Jiang L and McBride JW. “Investigating micro-scale surface change of an Ohmic MEMS switch between switching cycles”, *13th International Conference on Advances in Experimental Mechanics, Southampton, UK*

Bull TG, McBride JW, Jiang L (2017) An Investigation of the application of gold coated multiwalled carbon nanotubes surfaces for use in low current switching. *2017 University of Southampton Faculty of Engineering and the Environment Post Graduate Conference*.

Thomas Gregory Bull

Acknowledgements

This research was completed at the Mechatronics Research Group in the Faculty of Engineering and the Environment at the University of Southampton between 2016 and 2019. It was funded in part by EPSRC Grant EP/M508141/1.

I would like to thank my supervisory team, Professor John McBride and Professor Liudi Jiang, for the opportunity to undertake the project.

My thanks to:

John, I would not have completed this project without your time and support – often from across multiple time zones or while jetlagged. I have lost count of the number of times you have told me to keep it simple, so I will – you have my eternal and heartfelt thanks.

Liudi, your welcoming me, positivity and enthusiasm for the work settled me in a profoundly alien environment and gave me the confidence to make my way through it.

Professor John Atkinson for his advice and feedback from my 9-month review and transfer viva and the advice that a mature student could and would make it.

Mr David Oakley who provided the instrumentation that made this investigation possible.

Dr Kevin Cross for modifications the system control software and assistance with automating waveform analysis.

Mr Tim Hartley who always found a way to get things made for me and has been a good friend since.

Dr Dongkyu Shin, now half a world away, for being a sounding board, your help, friendship and ‘coffee time’.

To Em. For taking 8 years out of our lives so I could be a student again and prove to myself I could do this, for your support, for keeping me sane and for your love.

Thank you.

Commonly used Abbreviations and Symbols

CNT	Carbon Nanotubes
MWCNT	Multi-walled CNT
SWCNT	Single Walled CNT
Au/MWCNT	Gold coated MWCNT
505 Au/MWCNT	Au/MWCNT 50 µm high MWCNT coated with 500 nm of Au
MMB	Molten Metal Bridge
MEMS	Micro-electromechanical System
DE	Delamination Event
PZT	Piezoelectric Transducer
RF MEMS	Radio Frequency MEMS
tCVD	Thermal Chemical Vapour Deposition
peCVD	Plasma Enhanced Chemical Vapour Deposition (Sputter Coating)
CL	Confocal Laser sensor
WL	White Light sensor
ICE	In-situ Contact Evolution apparatus
a	Radius of an individual asperity contact area
α	Radius of cluster of asperities (Holm radius)
L	Characteristic length of a device
L^2	Characteristic area of a device
L^3	Characteristic volume of a device
R_c	Contact Resistance
V_c	Contact voltage drop

Abstract

This thesis describes the development, and use, of an apparatus to investigate lifetime switching wear of micro electromechanical system (MEMS) switch contacts. The investigation is focused on a composite contact material that is composed of vertically aligned multiwalled carbon nanotubes (MWCNT) with a conductive gold film coating to form an Au/MWCNT composite. A testing system, termed the In-Situ Contact Evolution (ICE) apparatus, is developed to provide the first system capable of in-situ, nanometre scale measurement of the MEMS contact surface, during sustained high-speed, low force MEMS contact cycling required for lifetime MEMS switch contact testing. The apparatus includes instrumentation that detects the formation of the transient molten metal bridge (MMB) phenomenon known to cause contact wear when hot switching. The apparatus is tested during an investigation of thin-film Au contacts under both cold and hot switching conditions. Microscopic wear from individual switching cycles is detected and a new wear mechanism is observed where a microscale delamination of the Au film interrupts the formation of a MMB.

The Au/MWCNT MEMS contact material is investigated switching below the arcing voltage (~12 V). The upper limit for switching is found and the failure mechanism characterised. Above circuit currents of 302 mA the Au surface film is thermally ruptured and as the contacts open the exposed carbon nanotubes become involved in circuit conduction. The circuit current causes thermal decomposition of the nanotubes observed as a series of discrete steps in contact resistance linked to the consecutive thermal failure of the outer walls of the conducting nanotube.

The influence of circuit parameters (current and voltage) and contact texture on the energy of the MMB is characterised. In an important observation the energy of the MMB is found to have a linear relationship to circuit current, rather than the i^2 relationship previously reported. The delamination event (DE) is also detected switching the Au/MWCNT contact. The DE and MMB are found to be mechanically distinct, with the DE characterised by ~20% increased separation force. Circuit conditions are shown to influence the MMB energy and number of DE. The lowest voltage and current show the highest occurrence of the DE and the lowest surface wear.

Lifetime testing is carried out at low force (150 µN) under hot and cold switching conditions. Under cold switching conditions the contact is switched to 4 $x10^9$ (4 billion) cycles while the microscale wear caused by DEs is detected and quantified. Under hot switching conditions of 200 mW DC power the contact fails after 140 $x10^6$ cycles switching, by an excessive increase in contact resistance. The

composites Au upper surface is found to have transferred to the opposing contact by a mixture of MMB and DEs.

The results are used to develop an enhanced model for the prediction of Au/MWCNT contact lifetime which considers the influence of contact force, DE wear and the switching current. The model shows good correlation with both the results of this work and previous investigation.

1 Introduction

1.1 Structure

This thesis is structured into the following chapters.

Chapter 1 – An introduction to outline the problem the project intends to address.

Chapter 2 – A review of the literature deemed significant in the context of the project.

Chapter 3 – Experimental methodology and the development of testing apparatus.

Chapter 5 – Experimental results.

Chapter 6 – Summary of the significant findings and conclusions

Appendix

1.2 Introduction

Electrical contact wear is a key problem in developing reliable microelectromechanical system (MEMS) switches. The size and contact closure force available in the MEMS switch limits the size of contact such that even microscopic levels of surface wear can disable the device. Gold coated multi-walled carbon nanotubes (Au/MWCNT) are a novel composite contact material developed as a wear tolerant electrical contact for MEMS switches. The material is manufactured by depositing a thin Au film onto thermally grown, vertically aligned nanotubes. This creates a composite with an electrically conductive upper Au surface, embedded into a mechanically compliant sublayer of nanotubes. When used as one side of a contact pair the enhanced compliance increases the contact area and wear tolerance. While the mechanical compliance and electrical resistivity of the composite have previously been investigated, the evolution of wear with switching and the ultimate switching lifetimes it can tolerate has not been characterised. This is due to the microscopic nature of the wear and the high number of switching cycles required.

Contact wear in the MEMS switch is a complex electromechanical process influenced by multiple processes. As well as the mechanical wear from switching the contacts without an electrical signal (cold switching) switching contacts while they carry a signal of more than ~1 V (hot switching) introduces additional wear processes. As contacts open Joule heating from current constriction drives the formation of a microscopic molten metal bridge (MMB) between the contacts. The current is interrupted when the MMB ruptures and is scattered, resulting in a surface wear process characterised by the fine transfer of contact material. Investigation of wear processes has previously been limited by the complexity, micro-scale and number of switching cycles involved.

1.3 MEMS Switching

Micro-Electro-Mechanical-System (MEMS) switches are sub-millimetre scale devices that integrate a mechanical mechanism to open and close the pathway for an electrical signal. The size of these devices allows their manufacture with materials and techniques commonly used in the semiconductor industry that have manufacturing advantages of high throughput and low-per-unit-cost.

MEMS switches are an attractive technology for the electronics industry as they offer several major advantages over semiconductor switching technologies [1]; however despite their demonstration in

the late 1970s [2] they have only relatively recently begun to encounter adoption in commercial applications [3] in a large part due to poor reliability of the switch contact surfaces [4], practical difficulties encountered when scaling up manufacture from prototype to production, and more recently due to lack of sensitivity in identifying market applications [5].

When MEMS switches are compared to semiconductor switch alternatives, such as P-I-N diodes and field effect transistors (FETs) they present outstanding performance in the following areas:

Isolation – the physical separation between the contacts provides a switch with a large off state resistance and low capacitance. This results in substantial attenuation of the input signal measured at the output port when the contacts are open. Isolation is expressed as a ratio of the output power to the input power when the contacts are open [6].

$$Isolation\ (dB) = 10\log_{10}\left(\frac{P_{out}}{P_{in}}\right)\ Switch\ Open \qquad (1\text{-}1)$$

Insertion loss – the low 'on' state DC contact resistance (typically 1-5 Ω) of the Ohmic (metal-metal) contact strategy minimises signal power loss across the switching element. Insertion loss is expressed as the ratio of output power to input power when the contacts are closed [6]

$$Insertion\ Loss\ (dB) = 10\log_{10}\left(\frac{P_{out}}{P_{in}}\right)\ Switch\ Closed \qquad (1\text{-}2)$$

Power consumption – the most common method of closing the contacts is by electrostatic bias. Once charged the bias electrodes consume no current. The electrostatically actuated MEMS switch therefore consumes no power while it is kept switched on [4].

A summary comparison of typical properties of the MEMS switch and semiconductor competitors (the P-I-N diode and the field effect transistor) is presented in Table 1-1.

Parameter	MEMS Switch	PIN Diode	FET
Isolation (1-10 GHz)	Very high	High	Medium
Isolation (10-40 GHz)	Very high	Medium	Low
Isolation (60-100 GHz)	High	Medium	None
Inline (Series) Resistance (mΩ)	200 - 2000	2000 - 4000	4000 - 6000
Insertion Loss (1-100 GHz) dB	0.05 – 0.20	0.30 - 1.20	0.40 – 2.50
Power Use (mW)	0.05 – 0.10	5 – 100	0.05 – 0.1

Table 1-1 – Comparison of the properties of MEMS switches to semiconductor alternatives

It can be seen that the MEMS switch performance can be characterised with higher isolation, lower insertion loss and lower power consumption that the P-I-N diode and the FET [7].

1.4 Description of a Typical MEMS Switch

At its most basic a MEMS switch consists of a mobile contact, a static contact and an actuation method. The switches can be classified according to the strategy used for the contact – Ohmic (resistive) or capacitive types.

The resistive switch strategy is a conventional switch but scaled down. Ideal switch states correspond to open and short circuit conditions. This is achieved by creating a metal-metal conductive path between the mobile and fixed contacts. The structure and scale of a typical metal-metal MEMS switch is shown in Figure 1-1 with an electron micrograph of the internal switch structure, alongside a fully packaged device mounted on a production circuit board.

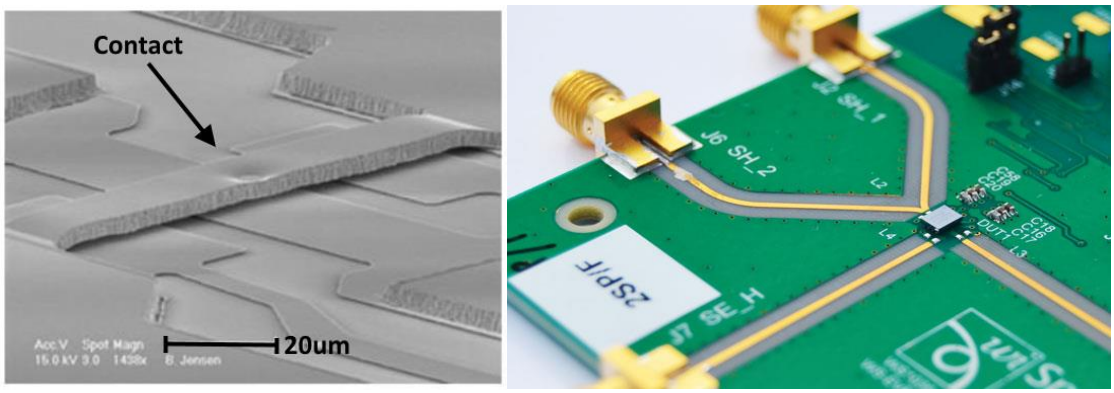

Figure 1-1 SEM image of RADANT MEMS switch (left) and packaged Wispry MEMS switch on PCB (right) [8]

In contrast, a capacitive switch uses a layer of dielectric between the contacts so that bringing the contacts together increases their capacitance and presents a low impedance circuit path for RF (radio frequency) signals.

Either contact strategy can be used to switch RF signals. The capacitive switch offers advantages such as greater resilience to contact damage from mechanical and electrical mechanisms, due to the presence of the dielectric; however direct current (DC) switching applications may only be realised with the resistive switch. While the capacitive switches' generally greater contact area allows superior power handling, it typically exhibits a capacitance of 2-5 pF in the down state limiting its

range of switchable frequencies to above 6 GHz. Thus the resistive switch is the only effective option for devices required to switch signals in the DC to 6 GHz range [4].

The topology of the switch can be configured with the transmission line in series or parallel (shunt) depending on the required application or circuit characteristics. The moving contact may be designed as either a cantilever (fixed-free) or bridge/membrane (fixed-fixed) strategy. Figure 1-2 shows diagrams for (a) fixed-free resistive cantilever in the up state (switch open) before it is pulled down to close the contact with the transmission line by electrostatic force. The force is applied by applying a signal to the pull-down (bias) electrode. Figure 1-2 b shows a fixed-fixed bridge arrangement in the open state.

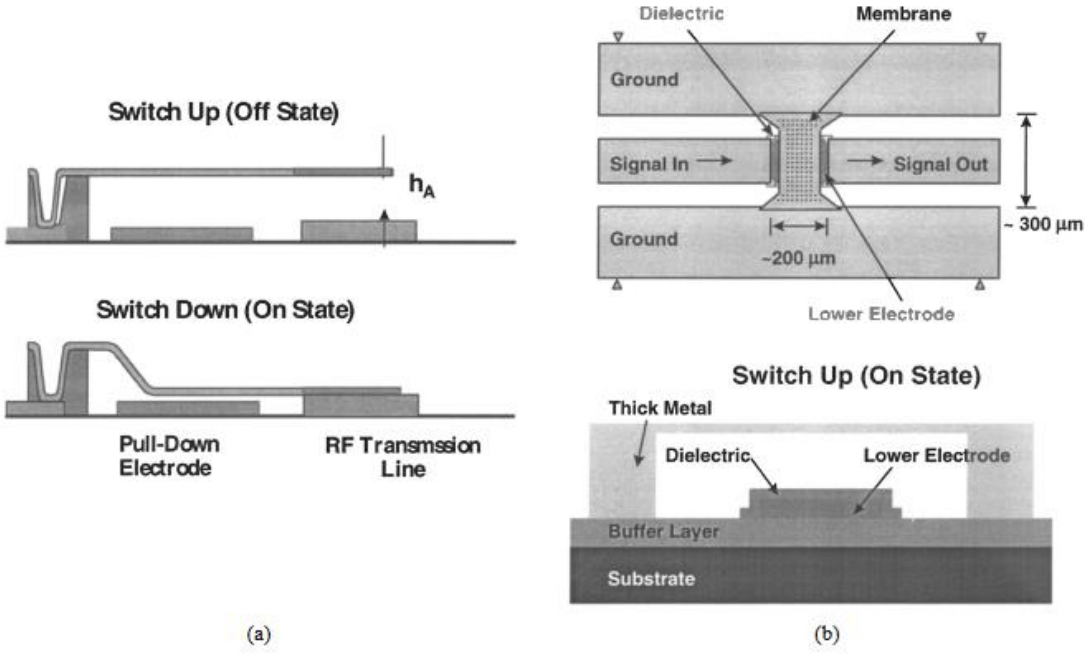

Figure 1-2 - Diagram of an resistive cantilever (a) and a capacitive bridge (b) MEMS switch strategy [4]

The moving contact may be actuated electrostatically, magnetostatically, thermally, or piezoelectrically. Most practical MEMS switches developed to date have been actuated electrostatically through biasing an electrode beneath the moving contact. When a DC bias voltage is applied to the electrode, the electrostatic force causes the mobile contact to deflect towards the static contact. When the bias voltage is removed the restorative spring force of the cantilever returns it to its original position as shown in Figure 1-2.

Electrostatic actuation is advantageous as the required electrode and cantilever structures are relatively simple to manufacture and package together using microfabrication techniques. The electrostatic force relationship is dependent on area, rather than volume as in the case of magnetic or thermal actuators, and therefore proportional to the characteristic scale of the device L^2 rather than L^3 [9]. As the scale of a device decreases this makes electrostatic actuation more attractive, particularly if we consider the typical flat, thin film structures employed in microfabrication. Of most benefit is that electrostatic actuation utilises no DC power once the electrode has been charged and can be designed for rapid charge dissemination when switched off achieving a rapid transition between the on and off state (switching time).

There are several disadvantages with the electrostatically actuated resistive MEMS switch. A significant disadvantage of electrostatic actuation is the bias voltage is generally large (20-80 V) when compared to traditional electronics voltage levels (1-5 V) [4] [10]. The introduction of a mechanical cycled mechanism introduces material problems of stress, creep flow, deformation and work hardening of the contact surface to a field of electronics and microfabrication where experience of such mechanisms may be limited [4]. The low contact opening force of the MEMS cantilever requires a careful consideration of bonding forces that may occur between contacts, such as cold welding and adhesion caused by contamination [4].

1.5 Problems with Resistive MEMS Switching and a potential solution

The impedance between the contacts is the single most critical specification for the resistive switch. It presents the primary source of insertion loss [6] and drives localised Joule heating in the surface when switching carrying a signal (hot switching).

In the context of this investigation hot switching is defined as the switching operation occurring while the switch carries a signal with enough electrical power to cause some migration or alteration of the contact material. It will be seen later in this chapter that for a gold conductor the potential drop for this to occur can be as little as 80 mV across the contact. Conversely, cold switching is defined as the switching operation being performed while the carried signal has a negligible effect on the contact material.

The most common failures of the resistive MEMS switch directly involve the contact surface. These failures can be generally be classified as an excessive increase in the contact resistance (R_c) or as the contacts sticking to one another so the opening force is unable to separate them [4] [11] [12] [13].

A novel metal-matrix carbon-nanotube composite material has been engineered at the University of Southampton for use as a high performance contact surface for the resistive MEMS switch [14]. The material consists of a thin film of gold (Au) film coated onto a vertically aligned 'forest' of multi-walled carbon nanotubes (MWCNTs), herein referred to as Au/MWCNT or 'the composite'. The Au does not simply sit on top of the MWCNT but partially penetrates the nanotube forest creating a composite upper layer (Au/MWCNT) with an under layer of pure MWCNT. Figure 1-3 shows a side view of a cross section of the composite under scanning electron microscopy (SEM). The vertically aligned nanotubes are visible as the lower darker region of the image, while the brighter region at the top is where the Au has penetrated the top of the nanotube forest. Variation in the depth of penetration (~ 0.7 and 1.3 µm) is illustrated shown at two locations only a few microns apart.

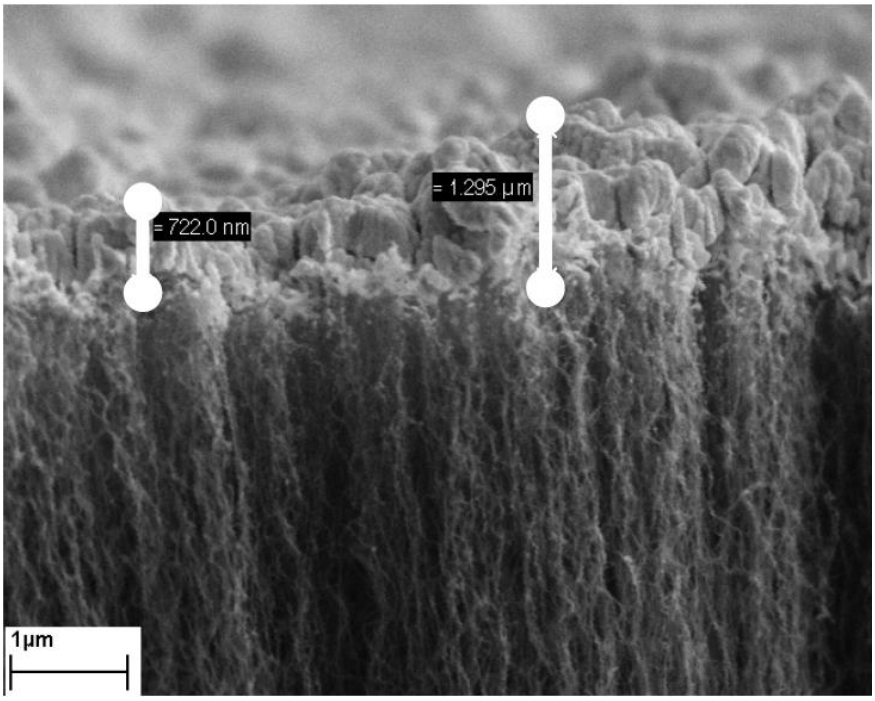

Figure 1-3 - SEM image of Au/MWCNT composite surface with scale showing Au penetration into MWCNT [15]

The composite provides electrical conductivity close to that of pure Au while the MWCNTs provide enhanced mechanical compliance, reducing impact damage from the mechanical closure and improving the contact interface area. This has been shown to increase the contact switching lifetime by several orders of magnitude over an equivalent gold film without a sub layer of nanotubes [16].

The composite has been demonstrated to provide extended contact lifetime, by both dissipating the impact energy from contact closure, and enhancing the area of contact. Both properties provided by the increased elasticity introduced by the MWCNT layer.

It has previously only been investigated at low currents switching, <200 mA with the focus on the 1-50 mA range [14, 17, 18]. In this current range the dominant method of contact failure appears to be the fine transfer of Au linked to the occurrence of microscopic transient molten-metal-bridges (MMBs) formed between the contacts as they open under hot switching conditions.

Many electrical devices require greater current levels. The advent of high energy density battery technology and mobile computing power has recently led to a wide range of smart devices with current requirements in the range of several amps. Switching contact technology for this current range could benefit from a resistive contact with enhanced lifetimes, as offered by the Au/MWCNT composite. The composite surface has not been investigated at currents >200 mA and it is likely that other failure modes will dominate the fine transfer mechanism proposed for the very low current regime. It is apparent that characterisation of the composite performance under higher current switching will be required to determine suitability for this type of application.

Before this investigation the evolution of the contact resistance and thermal energy associated with the MMB phenomena was observed over hundreds of millions of hot switched cycles, but could not be linked to changes of the contact surface [19]. The failure to link the contact surface change to the evolution of electrical characteristics of the contact was primarily due to two factors - the difficulty in locating and quantifying the extremely small levels of surface wear - and investigation of the contact surface being limited to the completion of switching.

1.6 Current State of MEMS Switching

An in depth study of the current 'State of the Art' for MEMS switching is also included in Appendix 1 - Market Predictions for MEMS Growth and Current State of the Art. However, this section provides a broad overview of the current state of MEMS switching.

While this work is predominantly interested in the evolution of the resistive MEMS switch, it is recognised that the capacitive MEMS switch can fulfil many of the same functions and it is useful to have a broad overview of the relative strengths of both technologies so key benefits and disadvantages can be recognised.

In 2004 - 2005 there were predictions that the RF-MEMS market would reach 0.7 - 1.0 B$ (billions of dollars) by 2009 [20]. Initial predictions for market uptake of RF-MEMS devices have generally not been met. This is in a large part due to failure to achieve the performance advantages that make

their adoption attractive. Rather than general adoption as high-performance alternatives to traditional devices such as P-I-N diodes and GaAs devices, they have found only niche market adoption. The practical difficulties in realising their performance can be attributed to three main areas; device reliability, complexity of packaging, and integration.

1.6.1 Reliability

There are currently several resistive MEMS switches commercially available that claim cold switching lifetimes of > 10^{12} of cycles. The lack of published data on device materials together with large activation voltages and low contact forces suggest these devices have not solved the fundamental reliability issues associated with surface failure and stiction, rather engineered solutions that avoid the root cause. This includes approaches such as utilising refractory metals to improve wear characteristics or using multiple cantilevers in parallel to reduce on state resistance to acceptable levels [4]. Refractory metals exhibit high hardness and melting points but generally rely on hermetic packaging to avoid oxide formation. While this approach provides a reliable switch, the superlative properties offered by the MEMS switch have been compromised – particularly in terms of on-state resistance, packaging size and activation voltage required to provide a contact force that keeps contact resistance to an acceptable level.

In capacitive devices, while the dielectric apparently provides an inherent protection mechanism to contact failure it introduces reliability issues at least as complex as those in resistive switches. The significant obstacle to reliability has been avoiding unintentional charging of the dielectric material in the on-state. This results in a permanent shift of the capacitance-voltage characteristic curve for the device and failure of the device by stiction of the contacts [20]. Early devices utilised silicon nitrides (SiN) as the dielectric and significant effort has gone to developing high performance dielectrics, including multiwall carbon nanotube and silicon nitride composites [21, 22].

Reliable devices have compromised by using low strength dielectrics (such as SiO_2) that have provided a reliable switch at the expense of a lower than desired on-to-off state capacitance ratio [23].

1.6.2 Packaging

The ultra-low forces involved in the MEMS switch operation mean that trace quantities of contaminants can significantly alter performance of the contact surface or cause the device to fail

altogether. This can be through physical and chemical processes such as cold welding, stiction, oxidation and corrosion fatigue. Practical management of this problem requires the hermetic packaging of active switch components to ensure particulate, hydrocarbon and water vapour contaminants cannot get in. Often the hermetic packaging encapsulates an inert gas, to minimise oxidation of the contact surface.

This packaging requirement presents several important considerations: firstly it leads to a component that can be considered discrete, limiting further processing of the substrate. This is important if trying to include the MEMS switch in very large scale integration (VLSI) processes or manufacturing a complex array of switches on a single wafer. Secondly packaging adds significant bulk and height to the component increasing its footprint and mass. The encapsulation process can also introduce material or pathways that have a negative influence in terms of RF performance and so additional constraints are imposed on the switch designer. Finally, it adds a complex stage at the end of processing where reduction in manufacturing yield would be the most costly [9].

The packaging choice depends on the switch construction – for instance the Radant MEMS RMS102 device uses a sintered glass capping process that provides a reliable and low cost seal, but this requires processing at >400 ^{o}C to glaze, a level where thermal degradation of MWCNTs can be expected in an environment containing oxygen [24] [25].

Additional complexity arises due to the incorporation of the actuation circuitry. The low power consumption offered by electrostatic actuation requires a relatively high bias voltage (5-80 V) that is generally not available directly from the batteries employed in modern mobile devices. The integration of charge pump circuitry to the device packaging has been adopted [4] [26] [27] to allow operation from low voltage supply. An impetus for driving the performance of the charge pump further is being provided by the proliferation of non-volatile memory storage solutions, which require a relatively high voltage for programming, with the trend for required voltage decreasing as shown in Table 1-2 [28].

Year	2001	2005	2010	2015
Supply voltage (Vdd)	1.2	1.1	0.97	0.81
Write/Erase voltage (NOR logic)	*8-10*	*7-9*	*7-9*	*6-8*
Write/Erase voltage (NAND logic)	19-21	17-19	17-19	15-17

Table 1-2 - The trend in supply and programming voltages for flash memory (29)

In considering both reliability and packaging of the MEMS switch there exists opportunities for novel materials to provide the MEMS switch designer with additional capabilities and design freedom. The current trend in small scale switching is a demand for higher signal frequencies where the performance of traditional semiconductor switch solutions fall off and an alternative solution is no longer just desirable but a requirement [29].

1.7 Aims

The following work is an investigation of the wear mechanisms of a composite Au/MWCNT electrical contact for MEMS switching. As well as wear from the mechanical effects of switching contacts with no electrical signal (cold switching) there is also wear caused when there is an electrical signal across the contacts (hot switching). Hot switching damage to the MEMS contact is a complex process that is not explained by a single mechanism. The mode and direction of contact wear is influenced by circuit conditions and operational parameters as well as the formulation of the composite and the geometry of the contact interface. Lifetime evaluation of the in-situ surface evolution has not previously been investigated.

Through the application of advanced optical surface profiling and electrical measurement instrumentation the evolution and behaviour of the Au/MWCNT composite is investigated at electrical switching conditions below the arcing threshold (< ~12 V) and at low forces (>1 mN) equivalent to a practical MEMS switch. The parameters that influence the energy of the molten metal bridge phenomenon, which has been linked to hot switching wear are also investigated

The aim is to characterise the Au/MWCNT composites' mechanisms of wear during switching conditions and determine the influence of circuit conditions and switching parameters on these mechanisms, through the in-situ measurement of the contact surface and concurrent measurement of transient electrical phenomena associated with electromechanical wear effects arising from the switching process.

This is done with a view to demonstrate the validity of the Au/MWCNT material as an enhanced-life contact surface for use in a practical MEMS switch and provide practical performance characterisation for the MEMS switch designer.

1.8 General Scientific Objectives of the Project

To evaluate the evolution of Au/MWCNT contact wear and its influence on the electrical performance of the contact.

To classify and evaluate the mechanisms of switching wear in the Au/MWCNT contact and the circuit parameters that influence the wear regime below the arcing threshold.

To empirically determine the ultimate switching lifespan of the MEMS scale Au/MWCNT contact.

2 Literature Review

This literature review is formed of three main sections based around 1) the Au/MWCNT contact material, 2) electrical contact theory, and 3) strategies for MEMS contact testing. First, the properties of Au, the manufacture, growth and properties of carbon nanotubes, and their use together as a composite (Au/MWCNT) for MEMS electrical contacts is reviewed. Secondly, theory on the relationship between contact force and contact area, how contact resistance arises from current constriction, and how this drives a mechanism for electromechanical wear is introduced. The third section reviews the strategies and apparatus previously used to investigate the behaviour of the Au/MWCNT contact and MEMS switches. The chapter is ended with a summary of the deficiencies in the literature around Au/MWCNT behaviour, and the primary considerations for a MEMS testing apparatus that would allow its investigation.

This is the motivation for this is the research question asked by this work – *What effect does switching below the arcing threshold have on the Au/MWCNT surface?* – and the methodology that will be used to attempt its answer.

2.1 Gold as an electrical contact

The material properties of the conductive surfaces have a profound influence on switch performance. In this study gold (Au) is used as the conductive material and its benefits, and weaknesses are here reviewed.

Gold is widely used as a contact surface due to its ability to form reliable, low resistance interfaces. This ability is derived from golds properties of softness, ductility, chemical stability and high self-adhesion, so it readily forms a low resistance contact interface. The same properties present key difficulties in using it as a thin film in a MEMS contact surface. The softness and ductility make it susceptible to mechanical wear processes, while the adhesion can lead to cold welding of the contacts at low forces and delamination of the contacts [30]. The malleability of Au is well known, and it can be plastically deformed to films thinner than the crystal grain from bulk material. This property extends from two properties, a face-centred-cubic (FCC) lattice and chemical stability. The FCC structure provides the largest number of slip systems while the chemical stability resists the formation of oxides that would otherwise trap dislocations and limit slippage [31, 32]. The relatively low melting point of gold also increases susceptibility to thermo-electrical wear processes [33-35].

To reduce wear in macro scale contacts, gold is often hardened by alloying with elements such as nickel, palladium, platinum and silver [36]. But this reduces a key benefit for MEMS contacts where Au forms a good contact interface at low force.

In practice, while chemically stable and resistant to oxidation, clean Au readily absorbs a thin contaminant film. In the study of single asperity Au-Au contact Tringe and Uhlman detected the presence of such films were found even when electroplated Au film samples were kept in a clean dry nitrogen environment. The films were found to be composed primarily of hydrocarbon whose electrical resistance was broken down by the effects of hot switching (5.6 V , 1 mA peak) and treatment with O_3 (ozone). It was noted that contamination reduced the Au-Au adhesion and if such a layer were not present contacts may have failed through cold welding together [37].

Dickrell and Dugger found contaminant film on a Au-Pt contact resulted in the increase of contact resistance (from ~ 2 to 200 Ω) in < 15 contact hot switched cycles (3.3 V 3 mA). When the experiment was repeated with a quenching RC circuit, which suppressed the formation of a transient electrical arc, the contact resistance remained low and stable (~2 Ω) until the quench circuit was removed. No surface damage was apparent and the increase in resistance was attributed to break down of the contaminant film into insulating compounds by micro-arcing [38].

Hyman and Megrahany found increasing contact closure force resulted in increased opening time and decreased contact resistance in sputter coated Au micro-contacts. Decreased resistance and increased adhesion indicated greater metal-metal bonding had occurred. In ambient atmosphere opening time was increased, while the contact resistance remained stable, compared with vacuum conditions. The effect suggested metallic bonding was comparable in both cases but the reduction in water vapour under vacuum had reduced the number of Van der Waals and hydrogen bonds. The study concluded that for the most rapid opening of a Au-Au MEMS switch the apparent contact area should be minimised [39]. It is observed that minimising contact area conflicts with the requirement for low contact resistance.

While Au is a well understood contact material with a balance of properties that are attractive in a MEMS contact, it's low melting point, ductility and self-adhesion make it susceptible to wear. Alloying systems can decrease the wear by increasing hardness, but this is at the expense of increasing the contact force required. This is already critical in the electrostatically actuated MEMS switch. Reducing contact area, to decrease contact opening time, also has the effect of increasing

the low contact resistance of the MEMS switch, the key property in achieving a low insertion loss. Even when protected by dry nitrogen atmosphere, contaminant films are detected, and their influence is different dependant on the switching conditions. Water vapour as a mechanism to increase surface adhesion is also noted. The Au contact interface is influenced chemically, mechanically and electrically, and evolves dynamically with the switching process. Understanding the contact wear process can be partially inferred from instrumentation (e.g. measurement of contact resistance and force) and post switching inspection, but the contact surface evolves every switching cycle and cannot be assumed to be constant.

2.2 Carbon Nanotubes

The manufacture and use of a carbon nanotube composite material as a functional electrical contact material is integral to the purpose of this study and this section introduces the background to the carbon nanotubes, their manufacture and typical properties.

The nature of the electronic arrangement in atomic carbon makes it usually effective in making relatively short and stable bonds to other carbon atoms [40]. As well as being the basis for its ability to form polymers and the ability to exist in multiple, atomically pure structural (allotropes). The structural differences between allotropes result in wide differences in behaviour. For instance a 4-way covalent, diamond-cubic bonding structure results in diamond with hard and insulating properties, whereas in the 3-way covalent, layered, hexagonal-planar structure in graphite with strong intra-layer bonding and the final valent electron available to migrate along the layer plane, such that the layers experience weak interbonding and electrical conduction can occur. Graphite can be regarded as stacked layers of graphene.

Graphene is currently of exceptional interest in many fields of research due to it possessing several superlatives, including tensile strength hundreds of times greater than steels, and thermal and electrical conduction properties better than silver. It is the remarkable properties of graphene that give rise to similar properties in fullerenes, where the graphene sheet structure is wrapped into balls and tubes [41].

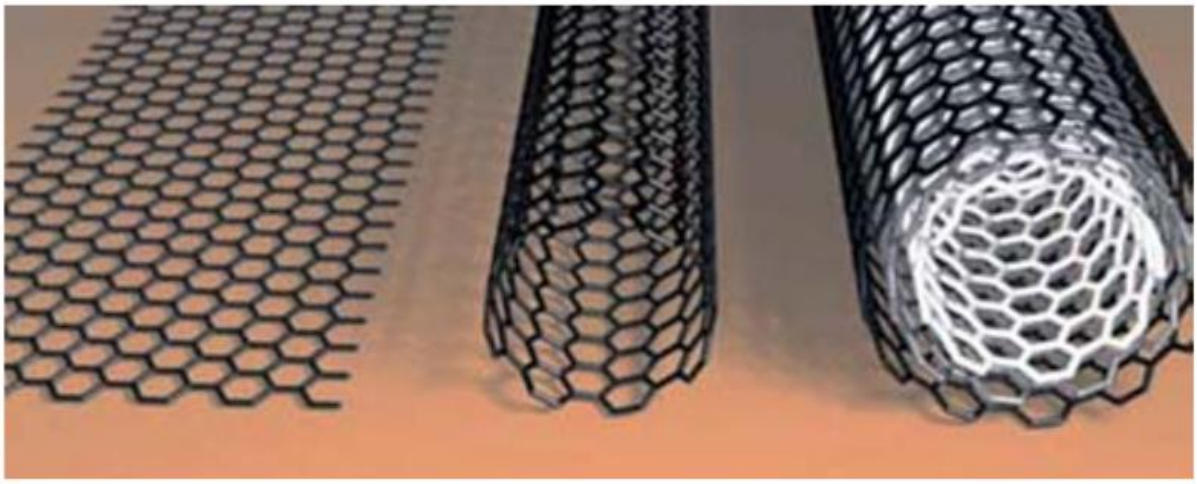

Figure 2-1 – Structural representations of graphene (left), SWCNT (middle) and MWCNT (right) [42]

In 1985 carbon structures, dubbed Buckminsterfullerenes, were identified by Kroto et al [43]. These share hexagonal and pentagonal layer bonding structures such that a layer can be wrapped around to meet itself resulting in a hollow spherical body. Iijima et el reported the identification of new form of fullerene in 1991 [44]. The sharp, hollow, "needle-like tubes" with a structure composed of multiple concentric graphitic sheets with an extremely high aspect ratio: the first reported identification of the carbon nanotube (CNT). Two main forms of CNT are identified (illustrated in Figure 2-1): the single-walled CNT (SWCNT) (center) and multi-walled CNT (MWCNT) (right), that may be visualised as an arrangement of multiple, concentric SWCNTs. In both cases the end of the structure tends to be capped by a hemispherical structure similar to Buckministerfullerenes [42].

CNT growth has to date been achieved by three main methods: arc discharge, laser ablation or catalytic growth. The first two methods are not considered further here as they are not practical where anchorage of the CNT to a substrate is required [45].

Yacaman first demonstrated catalytic growth of CNT in 1992 utilising thermal chemical vapour deposition (tCVD) of ethlene precursor decomposed via an iron particle catalyst [46]. The process involved exposing iron nano particles in a tube furnace raised to 700 ^{o}C to a carbon stock precursor in the form of a flow of ethylene gas where the temperature was sufficient for the catalyst to decompose the carbonaceous precursor. The decomposed carbon is absorbed by the iron catalyst. As the carbon solubility limit is reached the carbon is desorbed and precipitates into a stable graphitic structure defined by the shape of the catalyst particle [47]. This method has been used to

manufacture MWCNT with various precursor stock gases, including methane, carbon monoxide, benzene, xylene, but most commonly ethylene and acetylene [42, 45, 47].

The iron is an effective catalyst because of its solubility for carbon at raised temperatures, and diffusion rate for carbon; however several other transition metals with similar properties have also been successfully used as CNT catalysts including cobalt (Co), nickel (Ni) and gold (Au). It is of note that Fe, Ni and Co demonstrate a stronger adhesion to the nanotube as it grows and this property may be exploited to create tighter curvatures, thus narrower CNT diameters [47, 48]

The direction of growth is not well established, with contradictory observations from different groups reported, suggesting that the mechanism is highly sensitive to the growth parameters and may vary dependant on the shape of the catalyst particle and it's adhesion to the substrate, as well as the growing conditions; however two widely accepted mechanisms exist for a) tip or b) base growth and these are described below with reference to Figure 2-2 [42, 47]. The tip growth process in Figure 2-2 (a) is the mechanism observed during the growth process used in this work and described in the next chapter.

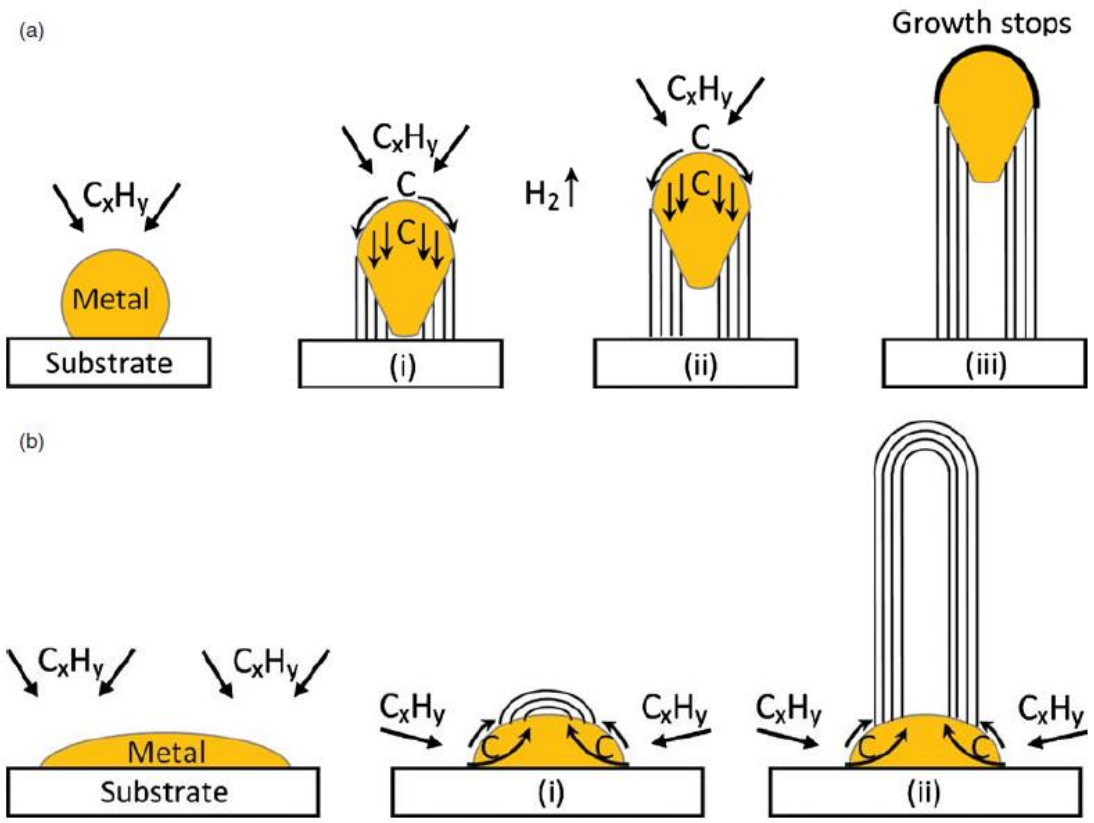

Figure 2-2 – Tip and base growth mechanisms described by [49] figure reproduced from [47]

In the tip growth model (a), the wetting angle between the substrate and catalyst is high, leading to a small contact patch and low adhesion between the catalyst and the substrate. Precursor hydrocarbon is broken down on the upper side of the catalyst with carbon diffusing to the underside, where the nanotube precipitation begins (i), first adhering itself to the substrate and eventually lifting the catalyst particle away from the substrate. The process continues to grow the nanotube from the underside of the rising catalyst particle (ii) until the source of carbon is cut off or the catalyst is poisoned by excess carbon [49, 50].

In contrast, the base growth model (b) begins with a catalyst that is strongly adherent to the substrate and the desorbed carbon can only exit the catalyst particle at the exposed upper surface where nanotube formation commences. Nanotube growth continues from the base, raising the tube above the catalyst with growth again ceasing when the carbon source is cut off or the catalyst is poisoned. Additionally, considering the case of many tubes growing together, they may limit the diffusion of the stock gas to the catalyst. It can be seen for both mechanism that the size and adherence of the catalysts as well as its distribution on the substrate effect the size, rate of growth and density of the nanotubes produced and the location of any residual catalyst. Both mechanisms can result in single or multi walled tubes but lower temperature growth conditions favour MWCNT growth as the proximity of bonds shared between adjacent layers suggests a lower activation energy; however, this distinction is beyond the scope of this review. Individual nanotubes may also continue to increase in diameter, by the growth of additional outer concentric shells, even after the new tube formation and vertical growth has stopped [47, 49].

While it seems contradictory, the conduction properties of CNT are not the main interest of this work. It is instead the mechanical properties that are the key to an enhanced contact material with perhaps the ability for nanotubes to recover from large strain and tight radius bending without experiencing fracture that is of most interest. Falvo et al demonstrated bending a single CNT tube back upon itself and subsequent recovery of form to a radii of curvature (20 nm) approaching the diameter of the tube [51]. However, as an electrical contact material we must consider the properties of nanotube arrays rather than individual nanotubes. Arrays of nanotubes have the potential to absorb mechanical energy and conform to the shape of an incoming MEMS contact. The CVD method described above can produce large fields of vertically aligned nanotubes – described as forests – with the areal density of the individual nanotubes determined by the initial distribution of the catalyst particles. The property of vertical alignment arises from simultaneous growth where individual nanotubes are supported from collapse by mechanical forces supplied by the surrounding

nanotubes. Additionally, they are observed to adhere to one another in bundles via weak Van der Waals force resulting from the very smooth and regular surfaces of the tubes. The process allows for the creation of vertically aligned and self-supporting regions of high aspect nanotube growth on the substrate as shown in the patterned array of MWCNT in Figure 2-3 [52].

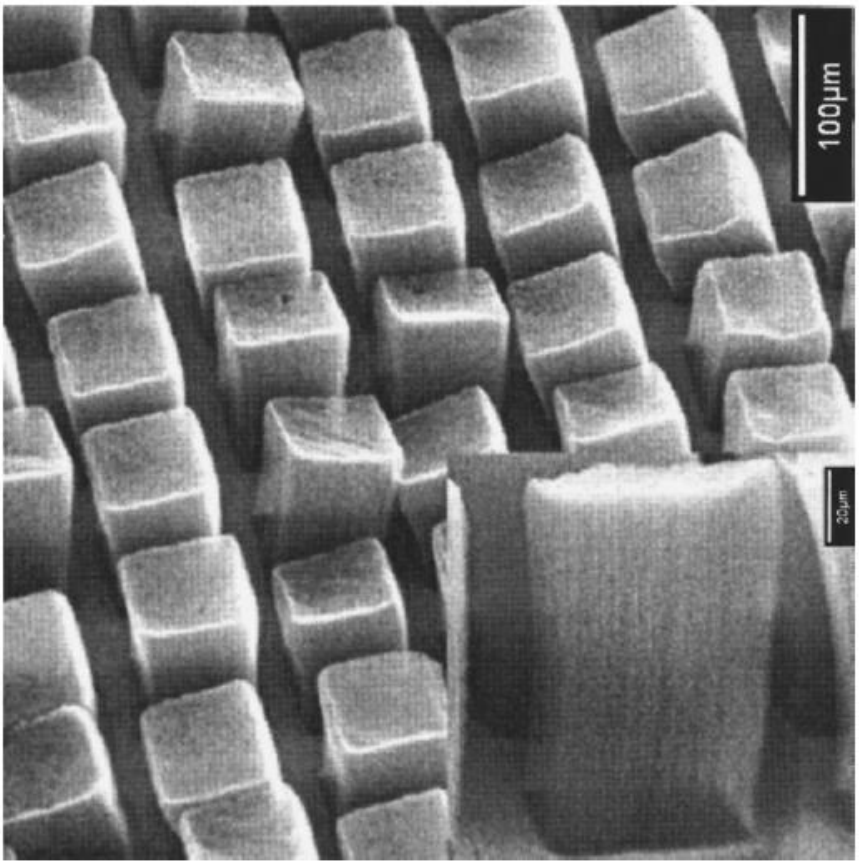

Figure 2-3 – Arrays of vertically aligned MWCNT on 1.5 nm Fe catalyst at 650C (Inset image scale bar = 20 um [52]

The low density and highly stiff forests of vertically aligned MWCNT (VA-MWCNT) have been demonstrated to exhibit properties of high mechanical energy absorption when loaded along the long axis of the tube; however the resultant deformation is typically permanent and a function of their height, not just due to the overloading and plastic failure of individual tubes, but through the trapping and tangling of elastically deformed tubes in the loaded position by adhesive van der Waals forces with the surrounding tubes [18]. Bradford et all demonstrated enhanced strain recovery in MWCNT forests by modifying the tCVD growth process [53]. The post growth process was to deliberately poison the catalyst using a brief overdose of stock gas before returning to the growing conditions. Nanotubes were grown that had an increased number of concentric shells with a rougher outer surface. The mechanism for enhanced strain recovery observed was attributed to the increase

in the tube surface roughness resulting in decreased bundling despite the contradictory observation that overall tube diameter increasing from 7-9 nm to 14nm, decreasing overall tube separation. Figure 2-4 shows the difference in the forest alignment with and without the post growth treatment while Figure 2-5 demonstrates the strain recovery behaviour observed [53].

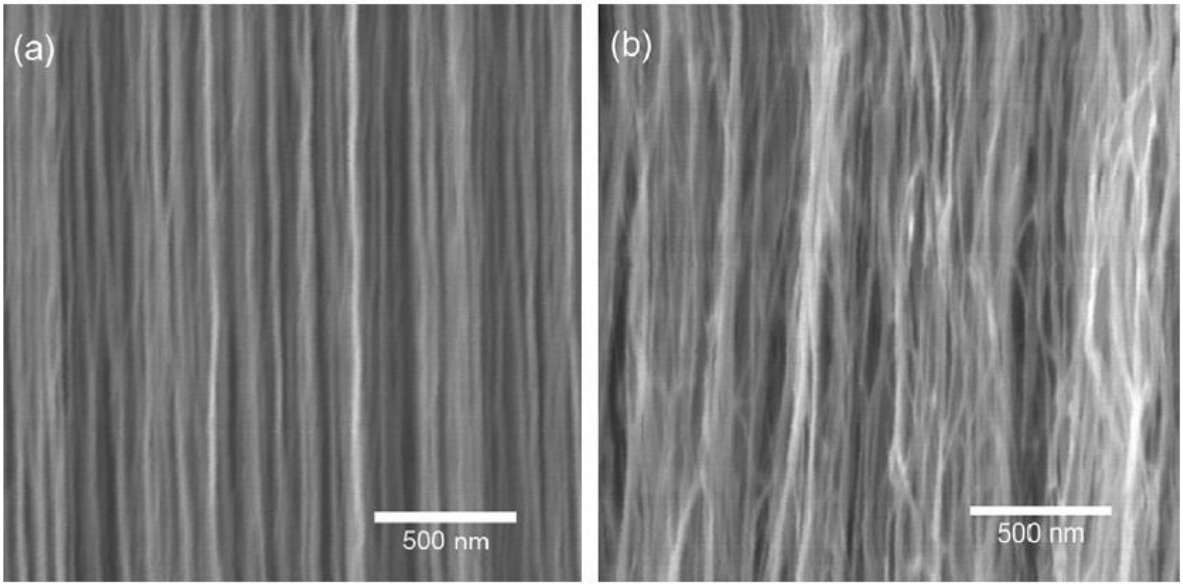

Figure 2-4 – Electron micrograph of MWCNT forest grown by tCVD a) conventionally and b) with a post growth exposure process to roughen the CNT surface [53]

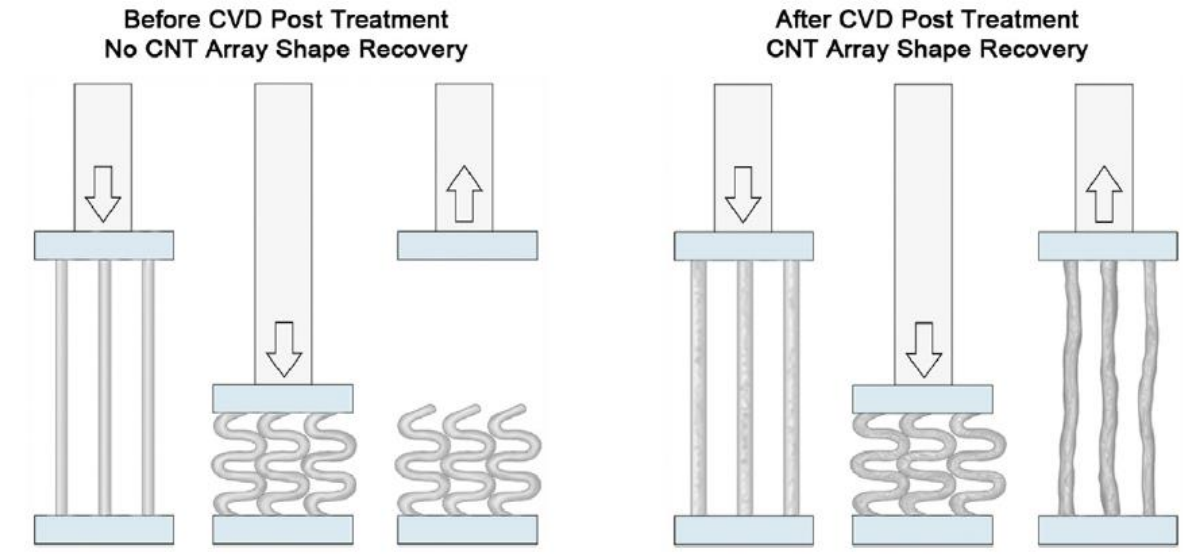

Figure 2-5 – Recovery behaviour of cyclically loaded tCVD grown MWCNT a) conventionally grown and b) with post growth exposure process [53]

Individual SWCNT can vary between 0.4 to 4 nm in diameter while MWCNT ranging from 1 to around 100 nm and can develop structures with hundreds of concentric tubes [45]. Separation between concentric tubes is observed to be 0.34 nm; the same as adjacent sheets of graphene in graphite [42]. The aspect ratio of the tubes may be of the order of hundreds of thousands with Zhang et al reporting the growth of a 550 mm specimen in 2013 [54].

Mechanical properties vary widely with the structure and aspect ratio of the tubes but empirical measurement and modelling has reported some of the highest elastic modulus and strength of any materials as well as the low density tube structure offering superlative specific properties. Single tubes have demonstrated stiffness's from 300 to 1450 GPa, similar to graphene (~1000 GPa) and diamond (1220 GPa) with tensile strength as high as 10 GPa – ten times greater than steel [42]. Bending and buckling strengths are a complex subject and depend strongly on the structure, aspect ratio and presence of adjacent tubes; however, the tailorability of CNT arrays that make it clear they present potential as a powerful engineering material.

In the context of developing a long lifetime switching contact MWCNTs presents a material with superlative damage tolerance and ability to absorb energy, while manufacture allows control of the geometry, strength, stiffness, distribution and adhesion between tubes to alter the compliance and recovery required from the material.

2.3 Au/MWCNT Composite as an Enhanced MEMS Switching Surface

The unmatched strength and conduction of heat and electricity offered by single layers of carbon atoms such as of graphene and fullerene based materials have relatively recently been proposed for many applications. The potential benefits have not been generally been realised because of practical issues related to the manipulation or purity of the material. In terms of their application to a MEMS electrical contact, while the tensile strength and electrical conduction are excellent, their contact resistance is poor and they do not form a good contact material in isolation. An alternative strategy is to engineer a composite material, where a graphene based fibre, selected for strength and damage tolerance, is embedded in a metal-matrix chosen for low resistance [55].

Such a material was demonstrated by Yunas et al, consisting a sublayer of partially tangled forest of carbon nanotubes with a thin layer of gold deposited into the top of the forest [14]. It was demonstrated that the top layer of Au bonded to the MWCNT forest and drastically improved the electrical contact resistance characteristics. Further it was demonstrated that the thin Au layer, and

the sublayer of compliant MWCNT, allowed the contact to deform to the incoming contact at MEMS scale forces. This both enhanced the contact area available for conduction and dissipated kinetic energy from the incoming contact to reduce mechanical contact damage [56] [30]. The important point is that the MWCNT is employed for its mechanical, and not electrical, properties to enhance the wear characteristics of a thin film Au contact.

Yunas demonstrated that the composite material has an enhanced switching lifespan for stable contact resistance achieving an extended switching lifetime over a thin film Au electrode as shown in Figure 2-6. Contact resistance was demonstrated between three contact pair types: MWCNT-MWCNT, Au-Au and Au-Au/MWCNT with contact resistances of ~160, 0.2, and 0.5 Ω at 1 mN respectively [56] [55].

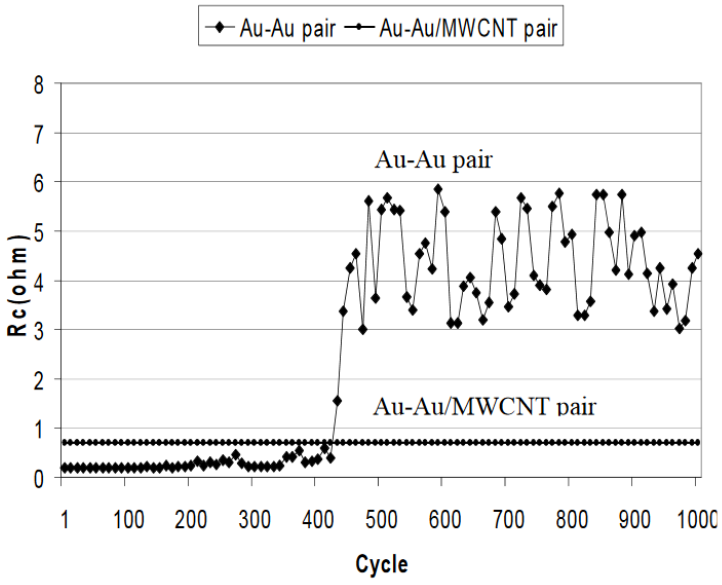

Figure 2-6 – The evolution of contact resistance cold switching cycles for an Au-Au and Au-Au/MWCNT contact pair [56]

It is of note that this study employed thin film Au coatings on silicon substrate without an adhesion promoter. Au is well known to be difficult to adequately bond to Si and the failures observed in the thin film Au coatings may be due to this mechanism. The switches forces used were high relative to the typical maximum force applied by an electrostatically actuated cantilever (~100 - 200 µN) [57].

Chinrabutra demonstrated wear processes on the composite surfaces, under hot switching conditions at low currents and mN scale forces, described by the ψ – θ theorem. An empirically derived model of the transfer of Au from the Au/MWCNT contact was developed that included opening and closing events due to contact bounce and predicted a potential lifespan of 28 billion hot

switched cycles at 4 mW signal power. However switching rates were not high enough to empirically test lifetimes at this level, and the predicted number of switching cycles included the multiple contact bounces which results in a longer predicted lifespan. [58].

The composite was further characterised by Down who demonstrated stable contact resistance over 12 million cycles of hot switching a 400 mW DC signal. Contact resistance was compared between control samples of thin film Au with an adhesion promoter of Cr, and the composite at 1 mN of applied contact force and found to be 0.15 and 0.24 Ω respectively. Contact lifetimes were shown to be an order of magnitude higher for the Au/MWCNT composite for given test conditions. For a contact geometry of a 2mm diameter hemisphere to planar contact the best switching lifetimes were achieved between forces > 4 mN. Above this force the composite was observed to plastically collapse [59].

Down considered the mechanical and electrical performance and characterisation of several compositions of the composite. It was found that the load to contact resistance curves match the shape of the Holm prediction according to *Equation (2-7)* indicating the composite behaves as a single bulk material [60]. The contact resistance was found to decrease with the increasing thickness of the Au coating, between 300 and 800 nm. The thickness of the Au was defined by the coating depth on a sacrificial Si chip and this is not necessarily a linear relationship with Au penetration depth into the nanotubes and homogeneity of the resultant Au in the composite [16]. It is also noted that increasing the Au thickness also increased the hardness of the composite. This demonstrates that the composition of the material can be optimised for a given application in terms of the applied force and required electrical performance.

Perhaps the most significant finding was that an increasing the CNT height, expected to increase surface compliance and so reduce contact resistance, was found to increase it [16]. A possible mechanism for the increase in resistance with CNT height is the forest becoming less dense [61] resulting in deeper penetration of the Au to the forest and a more porous, less conductive composite layer. The author has observed anecdotally that increased height in CNT shows increased tangling at the upper region of the forest. This can be explained by the Fe carbon saturation mechanism hypothesised for CNT growth, where enhanced nanotube height restricts diffusion of stock carbon to the metallic catalyst at the base [42, 47]. It is apparent that the CNT layer has a significant influence on the electrical performance of the composite and the apparent Au thickness is not necessarily linearly related to the penetration depth [16].

Critically the contact forces and geometry employed in these studies were larger than those associated with electrostatically actuated MEMS devices with the force regime an order of magnitude higher than a practical device will realise.

Lewis extended the performance characterisation of the composite scaling down the contact size and closure forces equivalent to the MEMS regime and increasing the switching rate for accelerated lifetime testing. A contact pair was constructed consisting of an Au/MWCNT planar contact formulated for long lifetime (30 μm MWCNT with 500 nm Au) with an electrostatically actuated Au coated MEMS cantilever upper contact. This was used to apply a closed contact force of 35 μN under hot switched conditions of 40 mW (4V 10 mA) and 200 mW (4V 50 mA). The evolution of the contact resistance and thermal energy associated with the MMB transient were then recorded. The evolution of the contact resistance for the 40 mW and 200 mW cases are presented in Figure 2-7 and Figure 2-8 .

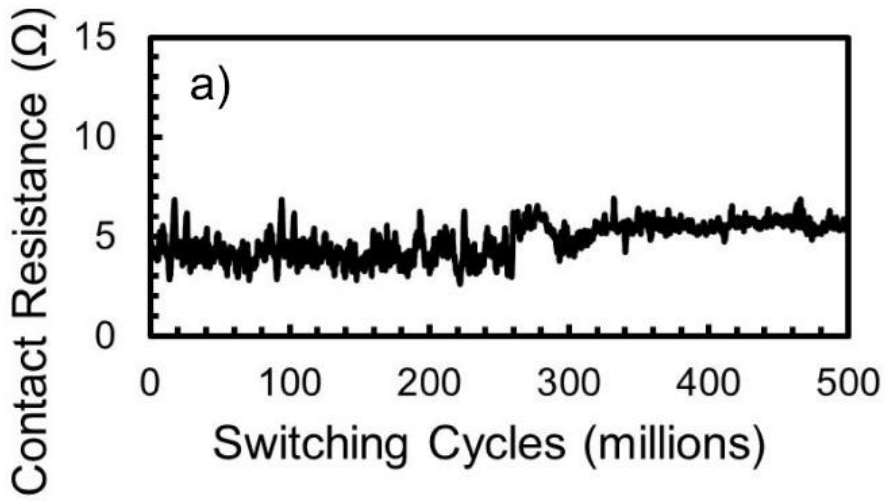

Figure 2-7 – The evolution of contact resistance with hot switching cycles in a MEMS scale Au/MWCNT contact at 35 μN contact force, 4V DC and 10 mA (40 mW) [19]

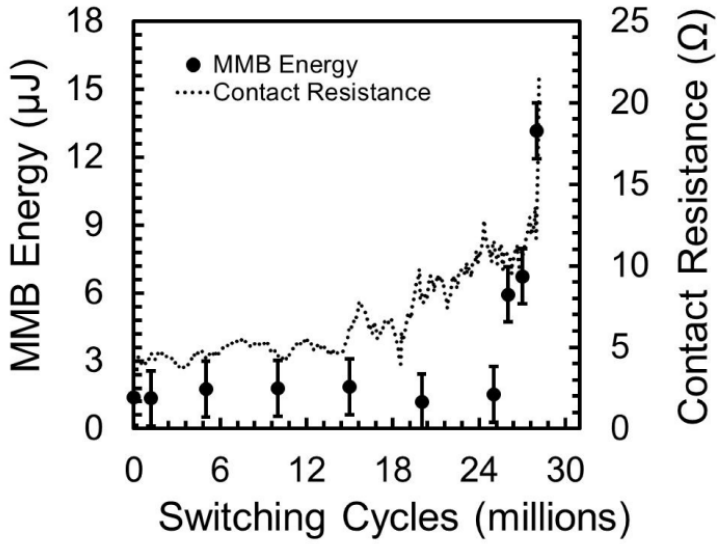

Figure 2-8 – The evolution of contact resistance and MMB energy with lifetime hot switching in a MEMS Au/MWCNT contact at 35 µN contact force at for 4 V DC, 50 mA (200 mW) load [19]

The 40mW case shows a stable contact resistance throughout the experiment (Figure 2-7) and the contact has not failed after 500M cycles. In contrast the 200 mW case (Figure 2-8) demonstrates a steady increase in contact resistance from approximately 15 M cycles before it is deemed to have failed at 28 M cycles.

The transient voltage waveform just prior to the contact opening and characteristic of the MMB was shown to evolve in the 200 mW case, increasing slightly in both length and energy until a sudden and rapid increase immediately prior to ultimate failure [19].

As the fine transfer mechanism is thermal and the thermal power (P_t) related to i^2 according to *Equation (2-1*),

$$P_t = V_c i \qquad (2\text{-}1)$$

The point of expected failure for the 40 mW case was extrapolated from the failure time of the 200 mW case. The fine transfer model in [57] proposed an i^2 relationship with wear. As the current is 5 times smaller the life of the contact was expected to be (28 M x 5^2) or 700 M cycles, if the wear mechanism follows the same trend. In this case, at 500M cycles we would expect the contact to be well into the increasing resistance stage exhibited by the 200 mW case, but this is not clearly

observed. This suggests the directional fine transfer mechanism may not be occurring as rapidly as expected or is being offset by another mechanism. An empirical test to ultimate failure under these conditions has not yet been carried out with the Au/MWCNT material.

An attempt was made to improve the conductive properties of a precious metal/CNT composite by increasing the metallic film thickness by Yukiyoshi et al [62]. While noting a key reliability issue for a MEMS contact is the limited contact area at low force and a susceptibility to wear the study concluded that the problem with a composite contact material is the slightly increased contact resistance. A process of electroplating was found to increase the metallic penetration of the nanotubes upto 5 μm but only moderate improvements in contact resistance were observed. It is noted that these were in line with the results of increasing the Au film thickness observed by Down et al. Following exposure to a hydrogen annealing process, the contact resistance was reduced significantly and Yukiyoshi concluded the improvement was due to increased flexibility of the metallic film. The motivation of the Yukiyoshi research was to reduce contact resistance by increasing the metallic layer thickness and the results show this approach is detrimental to the performance of the composite. While increased metal film thickness marginally improves the contact resistance it reduces longevity provided by enhanced conformity and enhanced damage tolerance demonstrated by Down et al [59, 60]. This is evidenced by the manufactured materials failing to demonstrate life spans that were greater than conventional metallic films [16, 62]. While the poor wetting of CNT makes direct electroplated coatings impractical for CNT, it is observed that a CVD layer of Au could act as a seed layer for control over the subsequent electroplating and tuning the composite properties, particularly when combined with the hydrogen annealing.

This work concerns the investigation of a Au/MWCNT composite where the MWCNT are vertically aligned to provide increased compliance. The benefits of compliance provided by the MWCNT alignment are emphasised by the study of Au/MWCNT composite where there is no alignment between nanotubes. Izuo et al [63] and Kageyama et al [64] investigated such composites. In the Izuo investigation the MWCNT were co-deposited with Au during electroplating; however, this resulted in aggregation of the MWCNT and poor dispersion. The hardness of the composite was found to be equivalent to an Au/Pt film. The Kageyama investigation addressed the dispersion issue by spray coating MWCNT in suspension before electroplating with Au. Attempts to sputter coat Au onto the surface of the MWCNT Au layer resulted in failure of the composite to attach to the substrate. The spray coated/electroplated Au/MWCNT composite demonstrated a lifetime of ~9,100 switching cycles before failure compared with ~3600 cycles for an equivalent Au-Au contact. The

increased adhesion of the electroplated Au film to the substrate suggest the electroplated Au had fully penetrated the MWCNT and attached to the substrate. This is supported by the reported hardness of the film cf. the vertically aligned Au/MWCNT characterised by Down [16] and it is apparent that the switching lifetime demonstrated by the compliant vertically aligned Au/MWCNT composite is much greater [19].

2.4 Au/MWCNT Force and Load Relationship

Mcbride et al investigated the load to contact resistance relationship at the <35 μN contact force range [65]. They found that the relatively low Youngs modulus and hardness of the composite, compared to conventional metal films, provided a material whose contact resistance was highly sensitive to the contact force at the μN scale. This property combined with the corrosion and wear resistance of the composite make it a candidate for a durable micro force measurement sensor. Two mechanisms of operation were investigated using a 10 mm long electrostatically actuated MEMS scale cantilever beam, suspended over a fixed Au/MWCNT contact surface. The intended mode of closure and contact is illustrated in Figure 2-9. Firstly, the deflection of the central portion of the cantilever continues to deflect nearly linearly with voltage, even after contact with the surface is made.

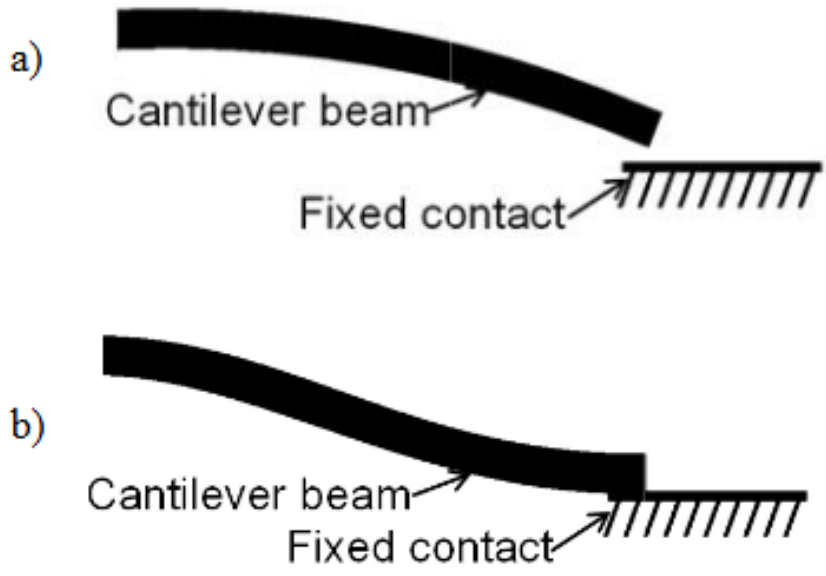

Figure 2-9 – The mode of deflection of an electrostatically actuated MEMS cantilever a) before surface contact and b) after surface contact [65]

By applying a known contact force and measuring the resultant deflection the tip force to central beam deflection the relationship can be calibrated and subsequently the deflection of the beam used to deduce the applied contact force at the tip. The mode of the beam deflection before and after contact is shown in Figure 2-9 and the linearity of the central deflection is plotted in Figure 2-9. The smooth displacement of the central region of the cantilever is observed (x = 4 and 6 mm from cantilever anchor) even after the tip has made contact (dotted line) with the Au/MWCNT fixed contact. The deflection of the cantilever with electrostatic potential is shown in Figure 2-10 where the tip of the cantilever (x = 9.5mm) shows non-linear displacement as it reaches the contact indicating contact force is increasing.

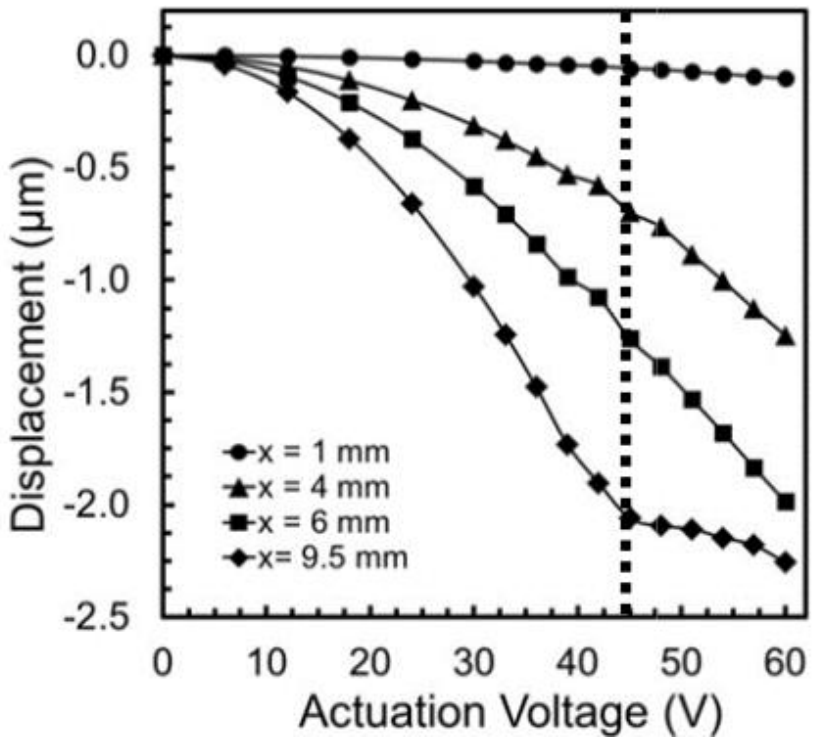

Figure 2-10 – Measured deflection of an electrostatically actuated cantilever vs bias voltage, at various distances from the anchor [65]

The sensitivity of the contact resistance to changes in contact force was directly used to calculate the contact force at the tip. The measured contact resistance are shown in Figure 2-11 alongside contact resistance predicted by a finite element (FE) model of the Au/MWCNT using material parameters for modulus and hardness obtained from nanoindentation and show good correlation at the low force levels used. The empirically measured contact resistance is both highly sensitive to the contact force at micro Newton levels and correlates well with the FE model.

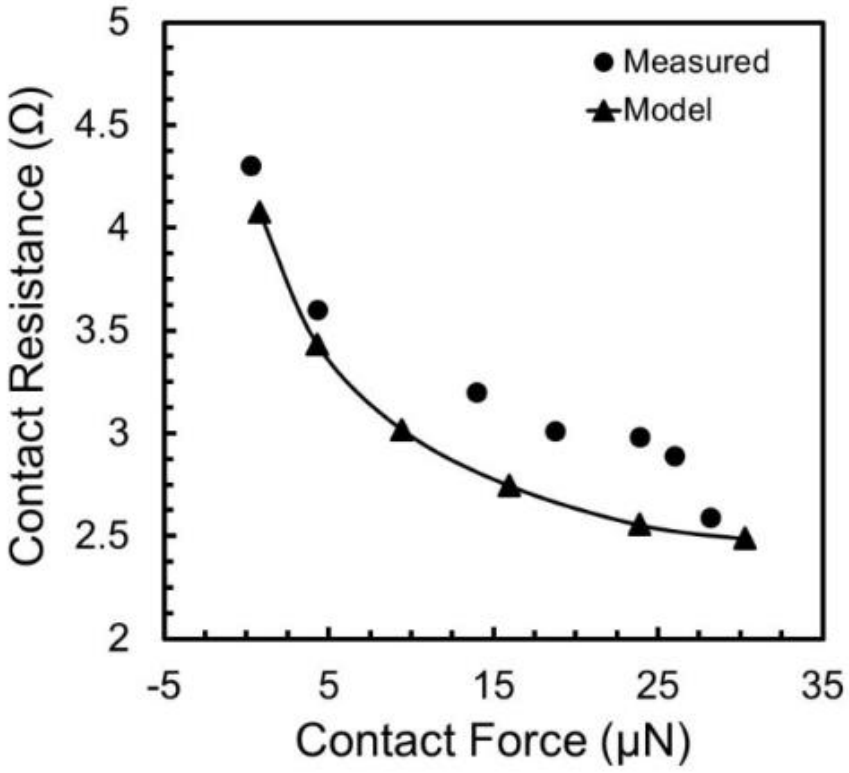

Figure 2-11 – Contact resistance vs measured and modelled contact force for an electrostatically actuator MEMS cantilever to Au/MWCNT fixed contact pair [65]

While the relationship between contact resistance and contact force, outlined in the next section of this chapter, is well understood at the macro scale, the composite presents two significant enhancements to employing this relationship as a micro scale force sensing technique. The greater sensitivity of the force/resistance relationship, and a resistance to both wear and corrosion that would otherwise cause sensor behaviour to change significantly over time. This property is of interest in the context of this study as it offers compact and highly sensitive force measurement at the MEMS contact scale.

2.5 Classic Contact Theory – Contact Force and the Real Area of Contact

A key advantage of a MEMS switch over semi-conductor alternatives is the property of low insertion loss. This property is a result of the metal-metal contact interface that provides a low resistance pathway for the electrical signal. In the simplest case the resistance is introduced by the body of the conductors (bulk resistance) and current constriction in the contact area (contact resistance).

If we consider a simple cylindrical homogenous conductor with equipotential end surfaces of diameter 2r, the impediment to current flow along the conductor is from the bulk resistance of the

cylinder [66]. Where ρ is the resistivity of the bulk cylinder material and *L* is the long axis of the cylinder parallel to current flow the bulk resistance of the cylinder can be expressed as *Equation 2-2.*

$$R = \rho L/A = \rho L/(\pi r^2) \qquad (2\text{-}2)$$

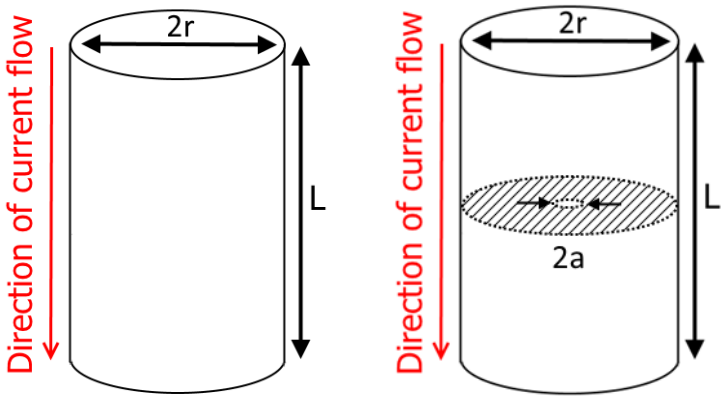

Figure 2-12 - Bulk conduction (a) and bulk conduction with a circular constriction imposed (b)

If we introduce a thin perfectly insulating disk as a restriction to current flow with only a small circular conducting region of diameter *2a* at the centre (Figure 2-1 b) we have created a simple geometric constriction in the conductor. This models a contact interface where there is only a single circular point at which the contacts meet.

Current flow lines must constrict together leading up to the contact interface and then spread out again after passing through it. The constriction and spreading of the current flow lines leads to an additional resistance component caused by the crowding of charge at the constriction. The magnitude of the resistance is determined by the geometry of the restriction and the resistivity of the conductor. Figure 2-13 shows a visual representation of the current flow lines (in red) through the constriction caused by the contact. An overview of current flow lines (red) in the conductor is shown in the right image while the shape of equipotential surfaces (blue lines) in the immediate vicinity of the constriction is shown in the right image.

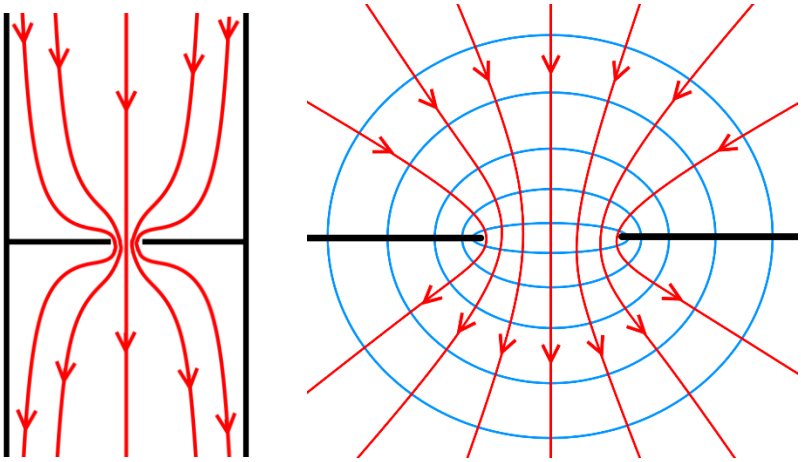

Figure 2-13 – A visual representation of current flow in the conductor (left) and in the immediate location of the constriction created by the contact area (right). Current flow lines are shown (red). At the constriction equipotential lines (blue) are described by flattened (oblate) spheres

Assuming peak current density occurs at the constriction and current flow lines are parallel far away from the constriction the shape of the equipotential surfaces can be determined as flattened (oblate) spheroids. An analytical solution of the problem was presented by Maxwell where the contact resistance can be expressed as *Equation 2-3* for a monometallic contact. [67].

$$Monometallic\ Contact \qquad R_{constriction} = {}^{\rho}/_{2a} \tag{2-3}$$

Experimentally it is observed that influence of the texture on real surfaces means the contact area does not consist of a single continuous circular spot but many smaller contact regions. The number, size and distribution of the contacts vary with the force applied to the contacts [66] [68] [69]. The micrographs shown in Figure 2-14 show the indentations left by a flat but rough surface pressed into a flat smooth surface under an increasing load. They demonstrate the irregular distribution of points that form the real area of contact and that these points increase in both number and area with increasing load. The real area of contact occurs inside a cluster of surface asperities on opposing contacts and these contact points are termed ‘a-spots’.

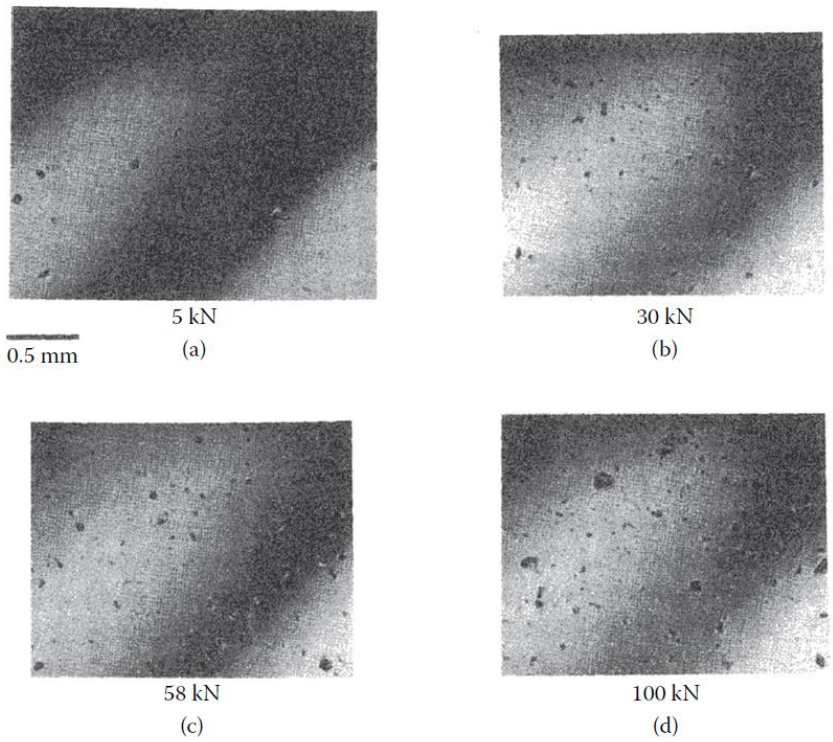

Figure 2-14 - Optical micrographs of smooth steel that has experienced contact with a rough surface at various loads showing the locations of the real area of contact (21)

Several cases of the multiple contact resistance problem were considered by Holm. In the simplest case, where *n* a-spots of an equal radius *a* are well distributed within a circular cluster of radius *α* the resistance that arises is given by *Equation 2-4* [70].

$$Rc = \rho\left(\frac{1}{2na} + \frac{1}{2\alpha}\right) \qquad \textit{(2-4)}$$

Where the number of the individual a-spots becomes large, then the 1/2α term dominates and the expression simplifies to *Equation (2-5)* closely resembling *Equation 2-3* [69].

$$Rc \approx \rho\left(\frac{1}{2\alpha}\right) \qquad \textit{(2-5)}$$

Greenwood showed that where many a-spots of an equal radius with a dense and uniform distribution the contact resistance expressed as *Equation 2-5* held as a good approximation for a variety of a-spot sizes and distributions. Figure 2-15 shows several different cases of a-spot distributions and a dashed circle representing the single contact area that would give rise to the same resistance as the a-spot distribution. It is noted the effective contact radius varies little and is close to the perimeter of the a-spot clusters. The cluster radius can therefore be used to determine

the practical constriction resistance in a wide variety of contact problems and was termed the 'Holm radius' by Greenwood.

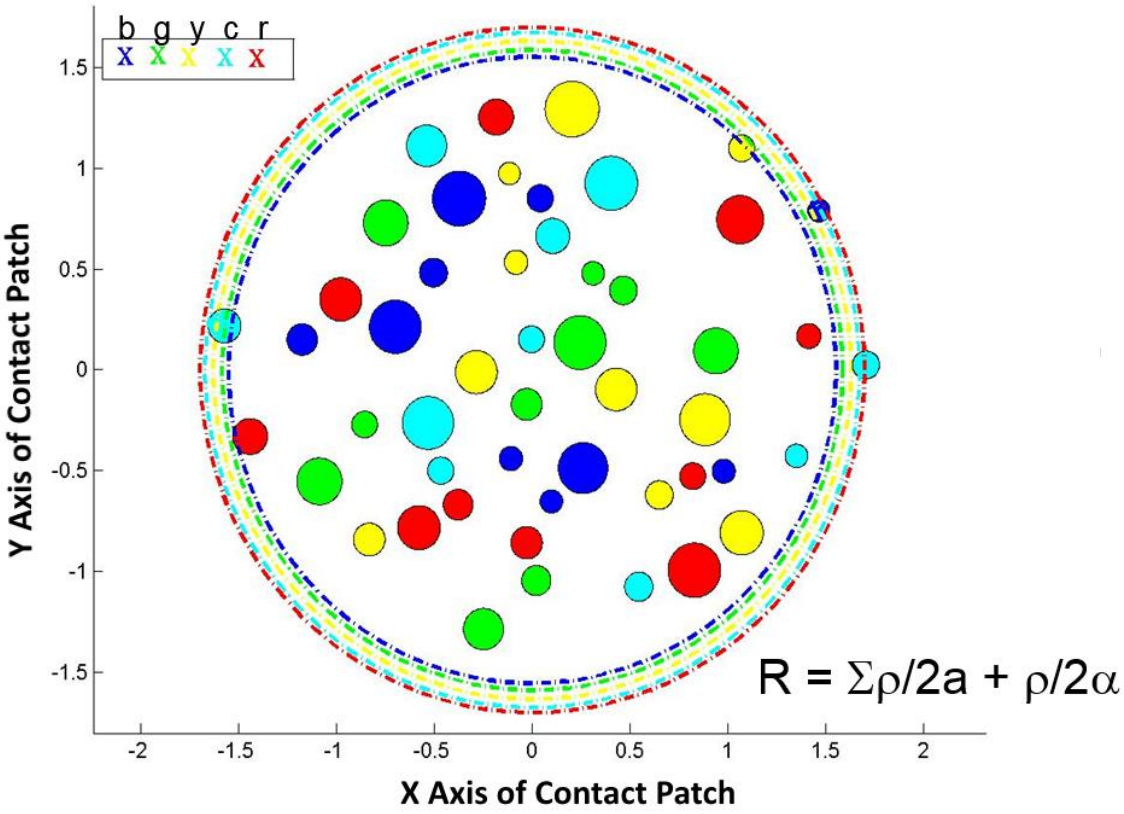

Figure 2-15 – The equivalent cluster radius of groups of a-spots [71]

This is a useful observation, as while it is difficult to measure the cluster radius, it is easier than measuring the average a-spot radius. Equation (2-5) shows good agreement with empirical observation of many practical contact problems. The key requirement for this agreement is that the contact load must be sufficient to result in a large number of well distributed contact points [66].

Practically, the Holm radius remains a useful approximation even when the number of a-spots is reduced to very few and the predictions only deviate significantly where the distribution of a-spots is no longer homogenous.

Research carried out by Myers et al of current pulsing in thin film conductors indicates that the peak contact temperature, therefore the location of the conductive a-spots, occurs in an annular (donut shaped) ring at the periphery of the apparent area of contact [72]. This is in keeping with analytical

observations by Malluci who, using models by Greenwood, showed that the current density between a-spots is influenced by both the distribution and size of the a-spots within the distribution [73]. The general trend Malluci observed was for the highest current densities to occur in small spots furthest from the centre of the contact region.

2.5.1 Deformation of Asperities and Variation of Area with Force

As the force applied to the contacts is increased the regions in contact must deform according to the stress they are individually experiencing; however, when surface roughness is considered it is obvious that the real contact area is much smaller and independent of the apparent area of contact.

Surface roughness is typically multiscale such that the real area of contact may be considered fractal over several orders of scale. The apparent area of contact and the true area of contact vary with force for multiple and single asperities and the possibility this extends to the atomic roughness scale [74].

Hertz developed a solution for the surface area between two perfectly smooth elastic bodies in the late 19th century; however, a practical surface has roughness. In the practical surface the real contact and load sharing area is formed at the a-spots. As the total contact area between a-spots is much smaller than the apparent contact area between surfaces then they must experience greater stress than calculated by the apparent area supporting the load [70] [75] [74].

In 1933 Abbott and Firestone measured surface roughness and considered the problem of the load to contact relationship and developed the bearing area curve to describe the cumulative distribution of the surface height. Bowden and Tabor extended this work in 1939 [76] and proposed that the real area of contact was due to plastic deformation in the surface of contacts. The real contact area could then be derived from the bulk plastic flow modulus or yield stress (Hardness, H) of the softest contact material and the force orthogonal to the contact surfaces, F [77] according to

$$A_{cp} = F/H \qquad (2\text{-}6)$$

By relating the real contact area, A_{cp} to the effective contact area derived from the Holm radius, α and assuming the number of a-spots to be large and well distributed then *Equation (2-6)* can be substituted in *Equation (2-3)* such that contact resistance becomes a function of the contact load

and bulk material properties, where η is an empirically determined coefficient equal to 1 for a clean contact interface [66]

$$R_c = \left(\frac{\eta\rho^2\pi H}{4F}\right)^{1/2} \quad (2\text{-}7)$$

Greenwood and Williamson observed that, in practice, there must exist a balance between the elastic and plastic regimes. They developed the concept of a plasticity index in a model with non-interfering (mechanically independent), elastically deforming asperities, the height of which are described by a Gaussian distribution [74]. A key advantage of this approach is that the model only requires two measurable qualities – the standard deviation of the surface distribution and the curvature of the surface peaks. This allows the rapid interchange of parameters within the model to evaluate different surfaces.

While the Greenwood elastic model was updated [74] it was later shown by Yamada et el in 1977, using a glass pin-disk system that experimentally obtained values of contact radius were larger than predicted by the elastic Greenwood model, particularly at low loads, and that the observed load on individual asperities radius remained relatively independent of the total applied load [78]. The latter aspect suggests that it is the number of asperities that grow with increasing load rather than the contact area of an individual asperity.

The model also assumes that elastic theory alone is enough to describe the asperity deformation. The assumption is that as only a small proportion of the contact area experienced plastic deformation and those that collapse will have their load taken up elastically by the remaining asperities. This fails to consider the volume conservation of the plastically deformed regions and leads to an underestimation in the predicted contact area thus an overestimation in the local stress [79]. Only under very low force regimes (<10 μN) can the deformation of asperities can be considered to be elastic [66]. This is of interest as typical MEMS switches provides a contact closure forces in this range, and as the deformation regime is therefore expected to be a mixture of both elastic and plastic. Models that address a mixed deformation regime are discussed in the next section.

It is noted than the Greenwood model assumes a Gaussian distribution of asperities which is generally not valid for any worn surface. For instance a switch contact that has undergone multiple

cycles, will not demonstrate a Gaussian distribution of asperities; however, the residual uppermost peaks, the most likely to be in contact, may still have a Gaussian distribution [71].

2.6 The Micro-contact Regime

A typical MEMS contact is constructed using microfabrication techniques where the conductors are thin metallic films and the actuation mechanism provides a very low contact force. This reduction in the characteristic scale of the switching device introduces additional considerations. Material properties are scale dependant and for the MEMS device we approach dimensions where bulk properties do not accurately describe material behaviour. Additionally, the ratio of effects may scale disproportionately according to surface area to volume relationships. For instance, inertial forces may depend on mass, thus will depend on volume assuming homogenous density, whereas electrostatic force will scale according to area [9]. This section describes where the influence of the conductor dimensions and contact area introduce additional considerations for calculating contact resistance.

2.6.1 Thin Films

In a MEMS switching device the conductive surface would typically be created by a process such as chemical vapour deposition (CVD), plasma vapour deposition (PVD), photolithographic masking, etching and spin coating. These techniques are widely used in microfabrication to create homogenous layers a fraction of a nanometre in thickness, over silicon wafers up to 450 mm in diameter, termed ‘thin film’ technology. When thin films are used as an electrically conductive contact surface for MEMS switching the sharp deviation of flow lines and restriction to spreading in the immediate locality of the constriction imposes an additional resistance [80]. This effect is illustrated in Figure 2-16 where the conducting film thickness approaches the scale of the restriction and the flow lines are forced to ‘hairpin’ near the constriction [81].

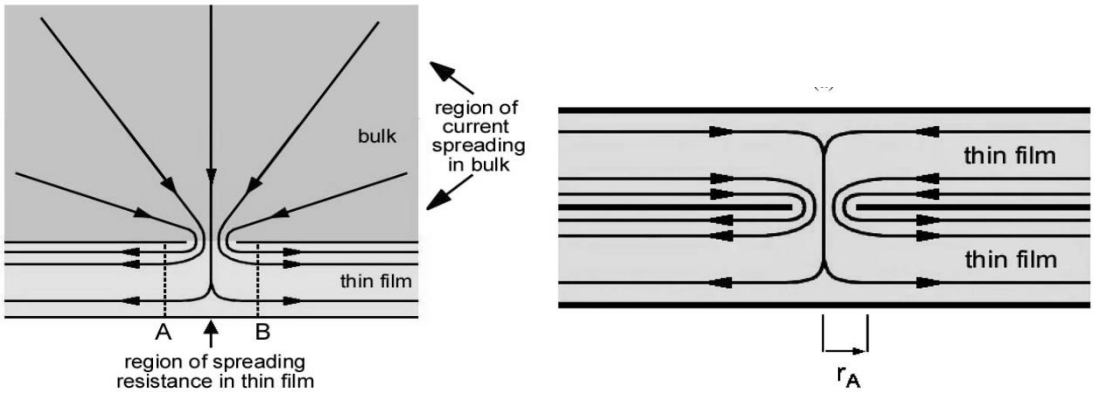

Figure 2-16 - Current flow lines due to a constriction in a bulk material to thin film (left) and a thin film to thin film (right) [81]

The additional resistance that arises to current flow between a bulk conductor and a thin film conductor (illustrated Figure 2-16 (left)) occurs mostly due to radial expansion of current flow lines away from the constriction in the thin film. Because lines of current flow can expand only minimally in a film of depth *L* it will have parallel flow lines in the film a short distance away from the constriction r_a. The thin-film restriction resistance R_{tf} for current spreading between r_a and some radius further from the constriction, b is given by

$$R_{tf} = \frac{\rho}{2\pi L}\ln\frac{b}{r_a} \qquad (2\text{-}8)$$

Using Bessel functions to provide approximate solutions Timsit showed analytically that the additional resistance caused by the thin film restriction becomes significant when the a-spot radius, *a* (shown as r_a in Figure 2-16) to the thickness of the conducting film, *L* ratio (a/L) ≥ 0.02 [81]. This guideline serves as a useful tool to quickly estimate the contribution towards contact resistance where the a-spot/Holm radius and film thickness are known.

This analytical approach, like the single contact spot Maxwell model and multiple a-spot Holm model, also relies on previous assumptions of Ohmic conduction and circular geometry. An additional point is that the approach requires the use of average current density as a parameter, as the boundary conditions result in current density tending to infinity at the limits of the constriction. It is an acceptable approximation in the context of providing an estimate of the overall contribution from thin film constriction, but it is noted that the approach assumes a single average current density while in a real contact the current density varies [73, 82].

Additional complication arises if the transmitted signal approaches frequencies typical of the radio band, that of skin effect whereby the alternative current (AC) reduces the effective area of conduction. As signal frequency reaches the 10^9 Hz (GHz) range the effective skin depth approaches that of the metallic conduction films in use in MEMS devices and will become a consideration in the device design parameters; however this work is restricted to direct current and the skin resistance will not be considered further [66].

2.6.2 Diffusive to Ballistic Electron Transfer

Classic theory uses the simplification that electrons behave diffusively, and the many individual charged particles that are really moving rapidly and colliding and scattering randomly in the conductor behave as if they are a slower and steady continuous flow.

As the scale of the current restriction is reduced and approaches the distance an electron usually moves before encountering a collision this clearly no longer holds.

It becomes increasingly likely that the boundary of the restriction will itself scatter the particle rather than the material in the conductor itself and a scale dependent behaviour is observed. The influence can be characterised by the dimensionless Knudsen number, K, which is a ratio of the lengths characterising the system. In the case of the restriction to conduction, the ratio of the mean free path of the electron, l_p to the a-spot radius, a.

$$K = \frac{l_p}{a} \qquad (2\text{-}9)$$

As the Knudsen number approaches 1 the additional consideration becomes appreciable. The mean free path of the electron in pure gold is given as 38.3 nm [66] and it can be seen that the scale of the MEMS contact approaches a limit where failure to consider this effect will result in an incorrect prediction of constriction resistance.

Figure 2-17 illustrates the path of an electron (a) diffusively and (b) ballistically traversing a restriction. The concept this illustrates is that an electron traversing the restriction ballistically is not being scattered by the medium. As the restriction dimension approaches the mean free path of the electron, the Holm model underestimates the constriction resistance.

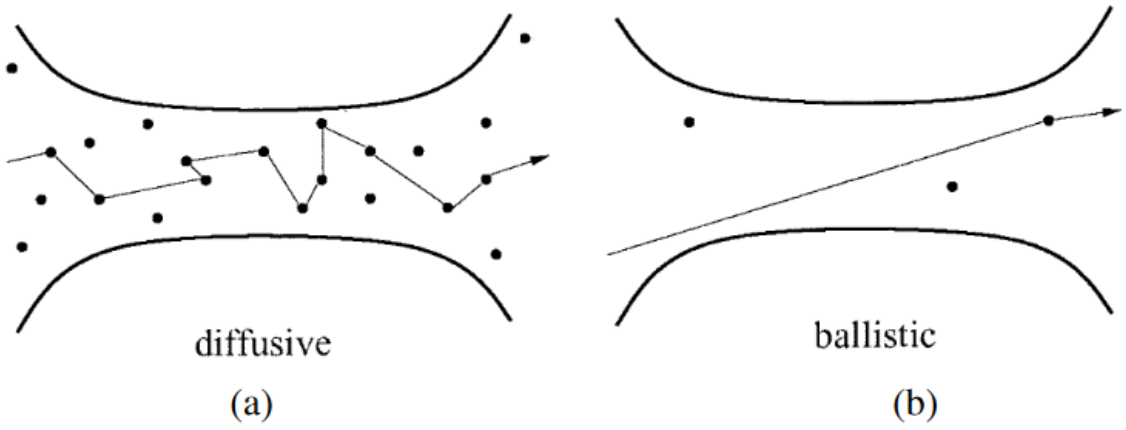

Figure 2-17 – Schematic of diffusive and ballistic motion in a constriction [12]

2.6.3 Models that consider the incorporation of thin film and electron transfer mechanisms

Chang et al considered a plastic-elastic model (later revised and enhanced by Chang) that linked the predictions of both elastic and plastic deformation models and included the effects of conserving the volume of the plastically deformed asperities [79]. Mikrajuddin et al examined contact resistance from both quantized effects and classically described effects and derived a function to account for the contribution of the mechanisms depending on the scale [83]. Coutu et al noted the lack of inclusion of ballistic transfer and developed a model that considered the transition between ballistic and diffusive electron transfer in the elastic-plastic regime [12]. Considered in the range of contact forces from 10 μN to 1 mN, the diffusive and ballistic contact resistances were respectively defined as

$$R_{diffusive} = \frac{\rho}{2}\sqrt{\frac{H\pi\left(1.062 + 0.354\left(\frac{2}{3}K_y - 3\left(\frac{\alpha}{\alpha_c}\right)\right)\right)}{F}} \qquad (2\text{-}10)$$

$$R_{ballistic} = \frac{4\rho K}{3\pi}\sqrt{\frac{H\pi\left(1.062 + 0.354\left(\frac{2}{3}K_y - 3\left(\frac{\alpha}{\alpha_c}\right)\right)\right)}{F}} \qquad (2\text{-}11)$$

Where ρ is contact resistivity, H is the plastic flow modulus, F the nominal load, K the Knudsen number, α and α_c are the asperity vertical elastic deformation and critical plastic yield deformation respectively. Where the Poisson ratio is *v*, the yield coefficient K_y is defined by

$$K_y = 1.128 + 1.158v \qquad \textit{(2-12)}$$

The total contact resistance is defined by a function of the Knudsen number, Γ(K) that smoothly varies between 0 and 1 and defines the dominant transfer regime and overall contribution.

$$R_c = R_{ballistic} + \Gamma(K) R_{diffusive} \qquad \textit{(2-13)}$$

Coutu et al utilised the continuously variable Gamma function (Equation 2-14) proposed by Mikrajuddin. The function is plotted against Knudsen number and the region where mixed diffusive and ballistic behaviour is expected in highlighted in Figure 2-18.

$$\Gamma(K) \approx \frac{2}{\pi}\int_0^{\infty} e^{-Kx}\ \mathrm{sinc}(x)\ dx \qquad \textit{(2-14)}$$

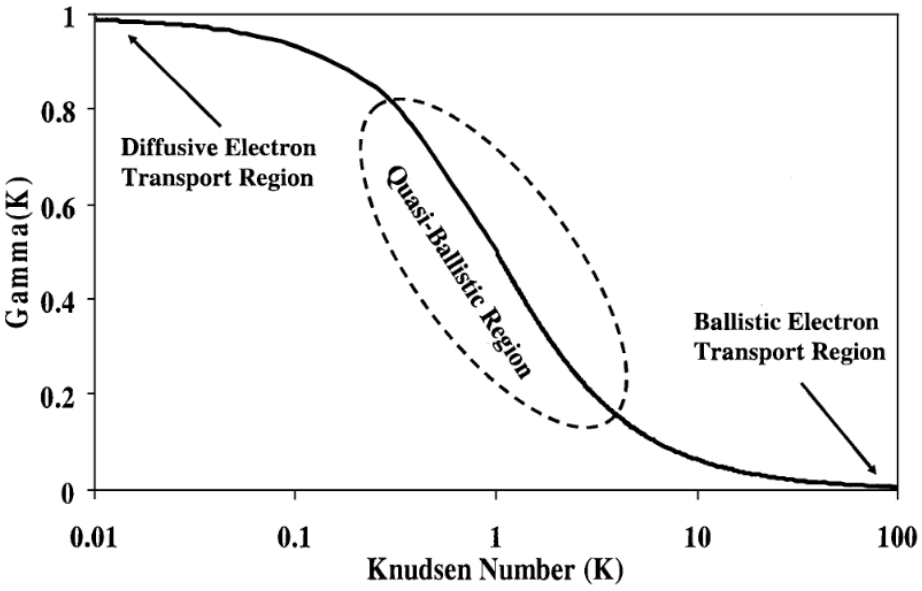

Figure 2-18 – A plot of the Mikrajuddin et al Gamma function reproduced from Coutu et al

Critically the Coutu model *(Equation 2-13)* assumes the individual a-spots are close together and therefore a single effective a-spot region may be considered. In practice this depends on the micro-roughness characteristics of the surface.

Yunus et al noted the lack of consideration of the effects of thin films and in the Coutu model was updated by to include the sharp deviation of current lines in thin films according to *Equation 2-8* and spreading resistance. Their contribution to the diffusive resistance component is weighted by coefficients derived from FEA models of the contact interface [13, 55]. It is noted that there is a relatively large discrepancy between the modelled and experimental values attributed to measurement bias; a conclusion the experimenters support through observing the analytical models converge as force increases; however, the discrepancy is substantial and merits further investigation. The model does not consider a material, such as a composite, whose hardness may vary significantly with the depth in the material or the effect of contaminant films. Further the effects of micro-roughness are not considered that have been shown computationally by Pennec et al to be potentially considerable though not yet experimentally validated [84].

The updated Coutu et al model is currently the most comprehensive for a MEMS application as it considers the force scale and likely deformation between elastic/plastic. Consideration of conduction between diffusive/ballistic and makes contribution for the sharp deviation of flow lines in thin film conductors. It is noted that it does not consider the influence of multiple a-spots and the model still shows discrepancy between modelled and empirically measured contact resistance. However, despite its simplicity the Holm model for contact resistance shows excellent agreement with a wide variety of contact problems and is considered to be appropriate for this study.

2.7 Voltage-Temperature Relationship

Due to the current flowing through a-spots the diffusive conduction will result in Ohmic heating (Joule heating). Assuming the conductor is thermally insulated from the surroundings and the constriction is symmetrical and the resistivity and thermal conductions vary minimally with temperature, then the heat will flow from the hotter constriction to the cooler bulk material, with the thermal conduction lines following the current flow lines i.e. isotherms and equipotential lines are superimposed.

The relationship between thermal and electrical conduction in metallics is described by the Wiedemann-Franz Law where T is the metal temperature, κ the thermal conductivity and σ the electrical conductivity.

$$LT = \frac{\kappa}{\sigma} \qquad \textit{(2-15)}$$

The potential and thermal gradients are therefore related. This gives rise to an expression for the local temperature of the a-spot as

$$T_m - T_0 = \sqrt{V^2/4L_0} \qquad \textit{(2-16)}$$

In conditions known as the ψ – θ theorem [70]. Where T_m is the maximum spot temperature (contact super temperature), T_0 is the ambient temperature of the bulk material, V is the potential across the contact and L_0 is the Wiedemann-Franz-Lorentz number (Lorentz number) [66]. This predicts theoretical values for the melting voltages of pure gold as V_m = 0.42 V which shows close agreement with the experimentally obtained value of V_m = 0.43 V [85].

The voltage drop across the contact is assumed to be related to the contact resistance via Ohms law

$$R_c = V_c/I \qquad \textit{(2-17)}$$

The ballistic resistance component does not give direct rise to Joule heating at the constriction as shown in Figure 2-19 because electrons tend to collide elastically with the constriction boundary and so do not transfer energy to the lattice and hence Knudsen resistance does not result in the expected additional heating at the immediate location of the constriction [66]. Under low force conditions (30 μN) under the quasi-ballistic Knudsen regime below (K = 0.1 > 10) the empirically measured softening voltage was significantly higher than predicted by classical theory [35]. Figure 2-19 shows the deviation of the empirically measured softening voltage to the classical prediction from the Holm contact resistance model for an Au-Au contact. This illustrates the mechanism is of greater importance for MEMS scale contact where the a-spots are expected to be small due to the low force applied to the contacts. In the context of the Au molten metal bridge, discussed in the next

section, this is a useful observation as it implies that for melting to occur in the ballistic regime the voltage drop must be greater than 0.43 V.

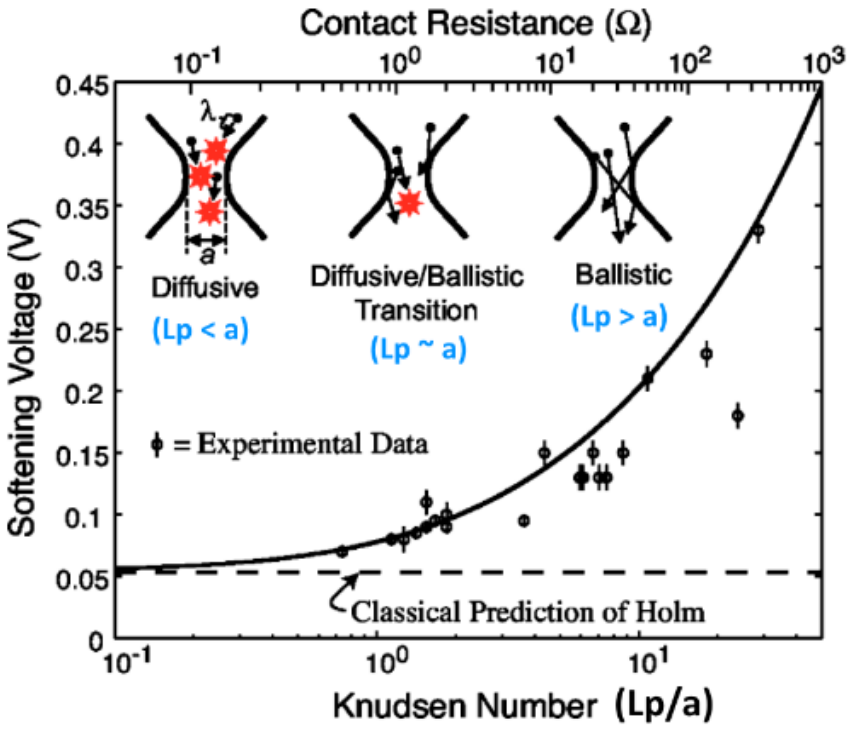

Figure 2-19 – Measured Softening voltage for a Fixed Contact Area compared with the Holm predicted values and the expected electron transport regime in an Au contact [35]

It is noted that the Lorentz number is not in fact a constant of proportionality but varies slightly between materials and temperatures; however the Lorenz number of Au has been experimentally determined to increase only slightly at cryogenic temperatures, 2 – 30 K (2.47 to 2.51 x10^{-8} WΩK^{-2}) and is given as 2.42 x10^{-8} WΩK^{-2} between 300 and 1200K [86] [70] [87].

The switching carried out in this study is of surfaces that have been exposed to ambient atmospheric conditions, thus will have been contaminated by substances such as hydrocarbon and moisture. Further the material is a composite. This means for the ψ – θ theorem the contact surface can not necessarily be assumed to be pure clean Au.

2.8 Molten Metal Bridge

The obvious aspect of the ψ – θ theorem, is that assuming a constant Lorenz number and diffusive electron transfer, the only variable effecting the contact super temperature is the voltage drop

across the contact. The softening, melting and boiling voltages for pure gold (Au) are given as 0.08, 0.43 and 0.88 V respectively [66].

If we apply simple elastic behaviour to a contact that is opened while carrying an electrical signal then as the contact opens, the contact force reduces, and the contact area smoothly decreases. The constriction resistance and the potential drop across the contact must also increase. If the potential drop exceeds the melting voltage, a liquid bridge must form between the contacts. If the boiling voltage is exceeded the bridge must then rupture by boiling.

When the size of the asperity, contact opening velocity, contact potential and current density are considered it is apparent that the phenomenon must be extremely brief. The occurrence of the phenomenon can be detected by measuring the potential across the contact where the MMB is associated with a characteristic transient waveform.

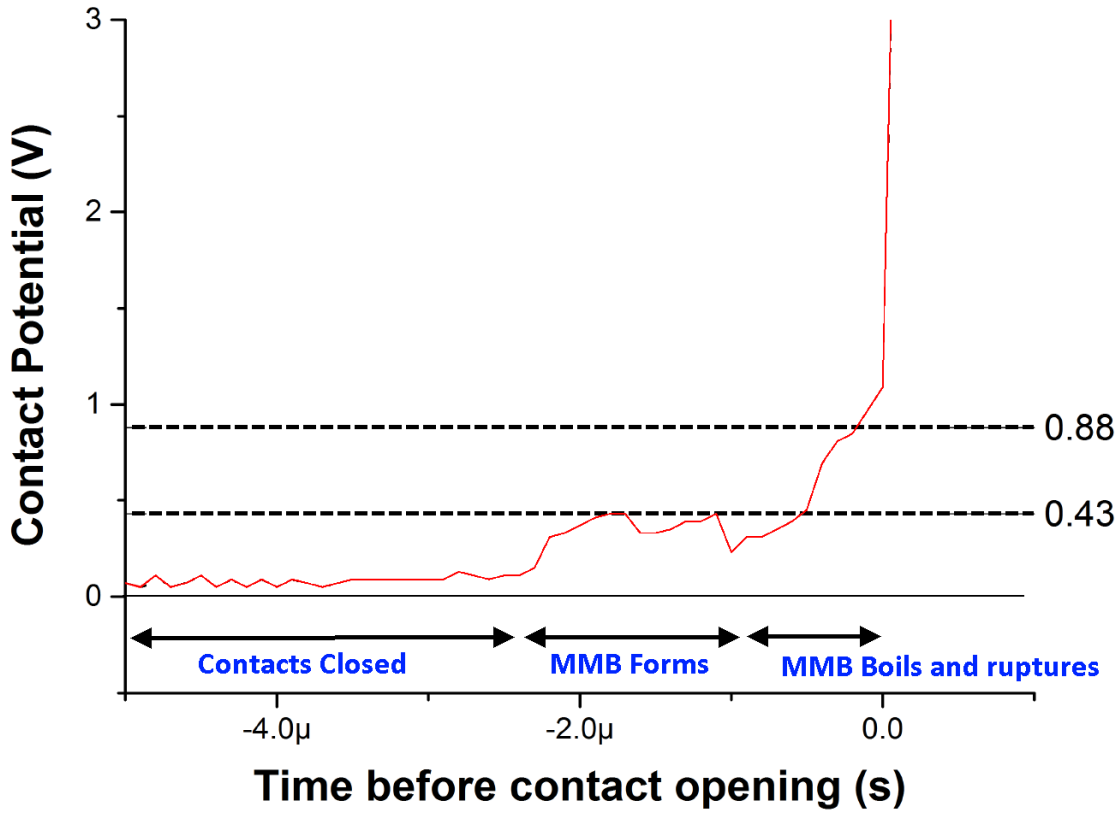

Figure 2-20 – An illustration of the transient voltage across a Au contact showing stages of closed contact, formation of the MMB and drawing out (Potential drop = 0.43 V), and the constriction increase and boiling before the bridge ruptures (Potential drop rises from 0.43 to 0.88 V)

Koren et al characterised three stages of the MMB for boiling rupture as shown in Figure 2-20; the initial creation where the contact voltage rises from the closed contact potential to the melting voltage, a stable region where the bridge is drawn out and lengthened and the contact voltage smoothly increases, followed by an region where the bridge becomes unstable and ruptures by boiling [88]. It is noted that the Koren investigation was in the context of the MMB as a prelude to arcing, where the boiled metal provides a medium for gaseous conduction before a plasma arc is formed. The currents and voltages investigated were therefore much greater than considered in this work.

Price and Llewellyn-Jones studied the behaviour of several metals during the MMB in the current range between 10 and 100 A and observed the bridge fluctuated [89]. Their results showed contaminated electrodes exhibited a greater repeatability of the measured rupture voltage and hypothesised the mechanism was the presence of impurities reducing fluctuations in surface tension caused by temperature variation in the MMB surface. Ultimately, they concluded greater temporal resolution was required for appropriate analysis. They also observed that Au tended to create relatively narrow and unstable bridges. This is in keeping with their observation regarding impurities stabilising the bridge and the propensity of Au to behave as a Nobel metal.

Slade et al [90] considered three modes of bridge formation and observed they could occur in conjunction with one another; 1) the classic Greenwood elastic-contact reduction in area resulting in MMB, 2) the plastic drawing of a cold-welded cylindrical metal filament between the electrodes which then softens, and melts forming the MMB and 3) the brittle fracture of the filament prior to boiling rupture. This would in turn give rise to three distinct forms of transient contact opening voltage waveform. It was proposed that the bridge instabilities are caused predominantly by; onset of boiling, magnetic pinch effect and hydrodynamic considerations; however, it was concluded that rupture processes are dominated by the hydrodynamic considerations where circuit conditions are <1 kA. In the cases cited above the circuit conditions were above the threshold for arcing to occur.

Wakatsuki and Honnma investigated silver (Ag) contact opening time under 12 - 50 V and 0.1 - 20 A and varying contact opening force [91]. By examining the transient voltage and current waveforms they found contact opening force did not appear to be linked to the time between the onset of melting and interruption of current. The opening time was also found to be “almost independent” of circuit voltage but proportionally linked to current. Results below 400 mA were not published reportedly as they could not clearly define the opening time at these currents.

The duration of the MMB can be linked to the length the bridge reaches before rupture (if contact velocity was measured) but does not necessarily link to the energy input to the bridge or the volume of contact material involved. As the MMB process is driven by Joule heating it is a reasonable assumption the energy input is proportional to i^2r as proposed in the fine transfer model [57] but the observation in [91] shows MMB duration is proportional with current suggests otherwise. However, as the melted region on the surface was not reported the MMB size cannot readily be verified and it is noted that MMB duration and energy are not necessarily linearly related. MMB duration below 400 mA were not published but they reported they could not clearly define the opening time at these currents, which illustrates the temporal resolution required for MMB detection is high. This result suggests there may be additional complexity in the current range > 400 mA and provides scope for further investigation.

Lewis et al investigated a gold coated MEMS cantilever along with the Au/MWCNT composite at circuit conditions of 4 VDC and 50 mA [19]. By measuring the transient voltage waveform and integrating it with respect to time, the energy of the MMB was calculated. It was found that the duration of the molten bridge, while highly variable from one event to the next, remained in a stable range with a steady average value, while in contrast the closed contact resistance rose gradually over 28 million switching cycles. In the final ~10% of the contact life the MMB energy increased suddenly along with contact resistance. The increase observed in the MMB energy in the 50 mA case suggests the surface interface had changed and Lewis hypothesised the surface had become smoothed leading to an increase in the contact area that could take part in a MMB. While no surface damage could be detected on the composite surface there was evidence of molten transfer of Au from the Au/MWCNT on the opposing gold coated cantilever. The same experiment carried out at a lower current of 10 mA demonstrated 500M cycles with stable contact resistance. Average MMB energy showed correlation with an i^2 relationship, while MMB duration was linked to current by a linear relationship, but no surface wear could be detected on the Au/MWCNT contact.

In real contacts it has been shown that contact area consists of multiple a-spots (Figure 2-14). The geometry, area and distribution of these regions is not uniform and so the current flow will also be influenced. As the surface experiences softening, the contact interface changes and the current distribution must also change [73, 82]. It is noted that Au, is observed to form smaller bridges, and consequently a greater circumference to cross sectional area ratio, would have a greater proportion of the current carrying region at the perimeter [89]. Malucci further observes that in practical contacts multiple adjacent bridge structures are thought to exist [92].

MMB formation, duration and stability depends upon multiple factors including circuit and opening conditions, electrode properties, surface tension and convection within the bridge [66]. The $\psi - \theta$ theorem is dependent on the system reaching equilibrium which does not occur in a MMB which is evolving dynamically. That is if the reduction of contact area and consequent increase in constriction resistance occurs slowly enough for the temperature in the a-spot to stabilise. Clearly if contact opening velocity is sufficiently high then there will not be time for a thermal equilibrium to be reached [88, 90]. Slade et al showed with nickel electrodes and varied contact opening velocity that this effect showed a practical limit to the theorem after which the melting voltages are higher than predicted values for circuit currents ~500 A [90]. For the opening velocities typical in MEMS switching this effect is not expected to be of significance. A final note is that Koren observed events where the contact ruptured before reaching the melting voltage, suggesting additional mechanisms may be at work.

The MMB is thus an exceptionally complex and rapidly fluctuating phenomena involving a dynamic interplay of competing forces. This results in variability in form from one switching event to the next, even for effectively identical switching conditions. The evaluation of the MMB therefore requires the high-resolution capture of the transient voltage waveform during the contact opening over many consecutive switching operations.

2.9 The Molten Metal Bridge (MMB) as a Wear Mechanism in the MEMS (Low Current Low Voltage) Regime

Rebiez states the primary cause of failure in the resistive MEMS contact is damage, pitting and work hardening of the surface caused by the impact between contacts [4]. This generally applies to the 'cold switching' regime where the contact is cycled without carrying a signal and the damage occurs mechanically. The MMB presents an additional wear mechanism for the electrical contact during hot switching.

Provided the steady state voltage is below the arcing threshold and circuit current and reactance is minimal an arc will not be drawn between contacts thus the contact surfaces will not experience the damage associated with micro-arcing. Contact failure in these sub-arcing conditions has been linked to the transfer of material during the MMB phenomenon – termed the fine transfer model. [66] [15]. Fine transfer occurs because of the softening, melting and boiling of the metallic surface and the transfer of this material between electrodes. At high currents the transfer is often observed from the

anode to the cathode though the direction of transfer is a complex interaction and not fully described by literature [66] [93] [94].

Figure 2-21 is an electron micrograph of a Au/MWCNT contact surface that has experienced 4V DC hot switching conditions for 12 M cycles at 1 mN closure force and shows signs of fine transfer wear [57]. The number of cycles includes ~14 separate contact bounces for each closure and the demanded number of switching operations is therefore ~850k cycles. The opposing contact was a Au coated hemisphere and a nominally circular wear pattern, that corresponds to this shape is apparent (indicated by a red dashed circle). The darker patches within the circular region (two of which are arrowed) are where the upper Au film has been thinned and transferred to the opposing contact. There is a relatively homogenous distribution of wear sites indicating a good distribution of a-spots within the contact region and fine transfer wear has occurred at multiple discrete spots within the contact area. It is observed that the region of greatest wear appears to be the perimeter of the contact site, particularly at the left side. This is in keeping with the predictions for peak current density occurring at the perimeter of the contact area [73]. During the contact cycling the contact resistance rose from 0.43 to 0.79 Ω indicating the switching performance was degrading but the contact had not failed.

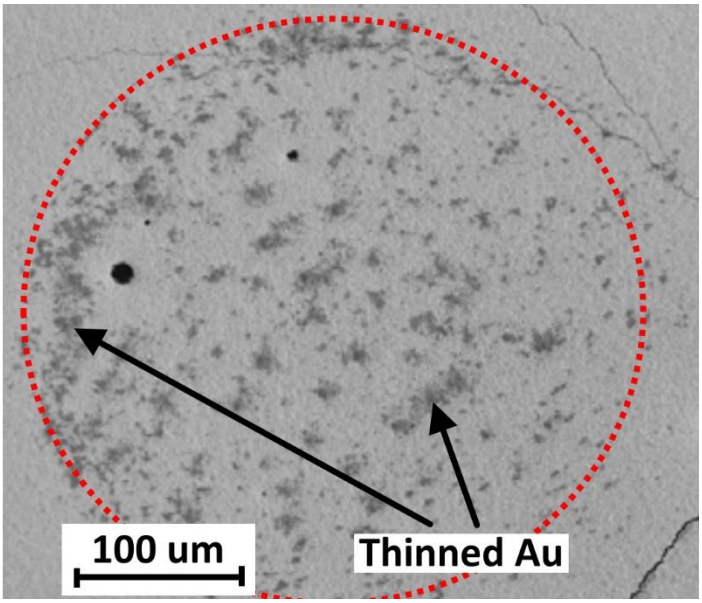

Figure 2-21 – Contact sites showing evidence of Fine transfer on Au/MWCNT composite surface after hot switching for 12M cycles at 1 mN force and at 4 VDC 10mA circuit conditions. Examples of the darker, thinned Au surface are arrowed. The area where the opposing contact mated is indicated by a red dashed circle [57]

Down et al postulated that the plastic mode of bridge creation, where contacts are initially cold welded and begin to separate before melting occurs and the electrode is a metal thin film, could give rise to unpredictable and catastrophic contact failure in MEMS devices through contact separation force causing film delamination [17]. The fine transfer mechanism observed by Down et al gave a more gradual, and predictable, mode of failure when compared to the catastrophic and unpredictable failure seen in in an equivalent Au/Cr/Si film without a MWCNT sublayer. McBride et al also observed a delamination/adhesion failure mechanism in the Au/MWCNT for currents above 20 mA. In the lower current cases, after the fine transfer had eroded through the Au material, it led to an additional wear mechanism whereby delamination of larger pieces of surface material would occur at the edges of the puncture site [15].

Down also proposed the mechanism of the direction of the fine transfer could be explained by the asymmetric rupture of the MMB arising due to differences in thermal properties of electrode material [60].

The evolution of the MMB energy is again identified as a key metric for evaluating the contact wear process during hot switching. As the switching current is strongly linked to the material volume transferred and the bridge thermal energy, evaluation of the MMB is key to investigating the fine transfer mechanism [95]. However, this strategy cannot be used to evaluate wear during cold switching or investigate the evolution of the contact surface. Surface wear is practically difficult to measure, even with the most sensitive of measurement techniques. Direct measurement of the Au/MWCNT contact surface during the switching process has not previously been investigated. It would allow the evolution of contact wear to be evaluated directly. That the MMB demonstrates directional wear in where an Au coated to Au/MWCNT contact pair is used demonstrates that both the influence of circuit parameters on the MMB and the influence of MMB energy on wear must be known to link circuit conditions to the wear.

The in-situ measurement of surface wear, and the characterisation of circuit parameters on the MMB energy are identified as a key objectives for this work.

2.10 MEMS Testing Strategy and Previous Test Apparatus Employed

The development of a state-of-the-art MEMS testing apparatus will be required to investigate the surface evolution and electromechanical phenomena related to contact wear over lifetime cycling of a MEMS contact. The following section describes strategies and apparatus previously used to

investigate MEMS switching devices with a view to develop the operational parameters of such a system.

The operation of the electrostatically actuated MEMS cantilever is of importance as it is the most likely to be employed as the mobile contact in a realised device. The operation of such a cantilever provides guidance in the contact separation and force parameters a testing apparatus should be capable of providing. The likely number of testing cycles, which motivates the required switching rate is then discussed with reference to published data from a commercial MEMS switch alongside the parameters previously used to evaluate contact performance. Isolation from vibration at the level of the intended operational forces is then considered. Finally, apparatus previously developed to characterise the switching performance of the Au/MWCNT surface by Yunas, Chianrabutra and Lewis, as well as those used recently to investigate MMB phenomenon and MEMS switching by Ren and Toler are discussed.

2.10.1 Actuation of the practical MEMS contact

The MEMS switch is discussed in Chapter 1 and the prevalent strategy in current designs is the use of an electrostatically closed and restoring-spring-opened cantilever as the mobile contact. This highlights that the closing and opening of the MEMS switch can be expected to occur under different motive forces and determined by different parameters.

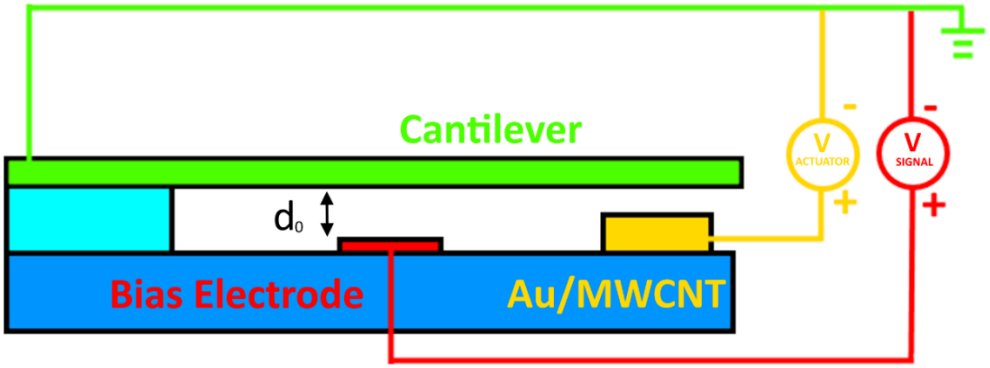

Figure 2-22 – Configuration of an Electrostatically Actuated Cantilever Beam as a MEMS switch showing the unbiased electrode separation distance d_0

A diagram of a typical MEMS anchored cantilever (green), with the positions of the actuating bias electrode (red) and functional contact electrode (yellow) is shown in Figure 2-22. If these electrodes

are considered as simple parallel plates separated by an air gap distance, d with an overlap area, A in a uniform electrical field then the capacitance of the pull-down electrode system is

$$C = \frac{\varepsilon_0 A}{d} \qquad \textit{(2-18)}$$

In practice this simplification underestimates the capacitance by 20-40% [4] due to the field edge effects being ignored but the simplification is still useful in highlighting the balance of forces and their dependant parameters. Applying a voltage, V across the electrodes will result in each receiving a charge, Q with a surface charge density on the electrodes, σ described by

$$\sigma = Q/A \qquad \textit{(2-19)}$$

If the overlapping area of the electrodes were considered as infinite in extent then the resultant electric field, E at each electrode would be of magnitude

$$E = \frac{\sigma}{2\varepsilon_0} \qquad \textit{(2-20)}$$

And the voltage required to create the field between electrodes separated by an air gap, d can be described by

$$V = E_{total} d = \frac{Qd}{A\varepsilon_0} \qquad \textit{(2-21)}$$

Thus, the electrostatic attraction between the plates can be derived as

$$F_{attr} = \frac{QE}{2} = \frac{\varepsilon_0 A V^2}{2d^2} \qquad \textit{(2-22)}$$

This force is countered by the restorative spring force created by the deflection of the beam according to the spring constant, *k* at the point of load application (i.e. the electrode position) and

the distance it is deflected, *x* (i.e. Hookes Law). The displacement x can also be more practically described in terms of the separation between electrodes with no applied bias voltage, d_0 and the separation between the electrodes for a given position, d as follows

$$F_{beam} = kx = k(d_0 - d) \quad \textit{(2-23)}$$

Equating forces gives rise to an expression that can be solved for the situation to be in equilibrium

$$\frac{\varepsilon_0 A V^2}{2d^2} = k(d_0 - d) \quad \textit{(2-24)}$$

Rearranging for the pull-down voltage, V gives the expression

$$V = \sqrt{\frac{2k\ d^2(d_0 - d)}{\varepsilon_0 A}} \quad \textit{(2-25)}$$

If we consider the effect of increasing the bias voltage on the beam the effect is to increase the electrostatic force, increasing the beam deflection, reducing the electrode separation which increases the capacitance, in turn increasing the electrode charge and the strength of the electric field. This positive feedback relationship will reach a critical separation point to be reached at which the applied voltage will be enough to cause the beam to become unstable and accelerate towards the opposing contact. The reverse is also true if the beam begins in the pulled down position and the bias voltage is reduced, eventually it will reach the same critical voltage and the restoring spring force will overcome the electrostatic force and the beam will snap open.

For a given contact type k, A and ε_0 are all constants and we can simplify *Equation 2-25* to

$$V = C_1\sqrt{d^2(d_0 - d)} \quad \textit{(2-26)}$$

Where C_1 is a constant of k, ε_0 and A. Solving for the derivative determines that the critical voltage will be reached when the separation between the electrodes reaches 2/3 d_0. Figure 2-23 shows a plot of cantilever displacement with bias voltage from fully open (d/d0 = 1) to fully pulled down

(d/d0 = 0) - the black portion of the graph represents the stable region during pull in and the red portion during the release.

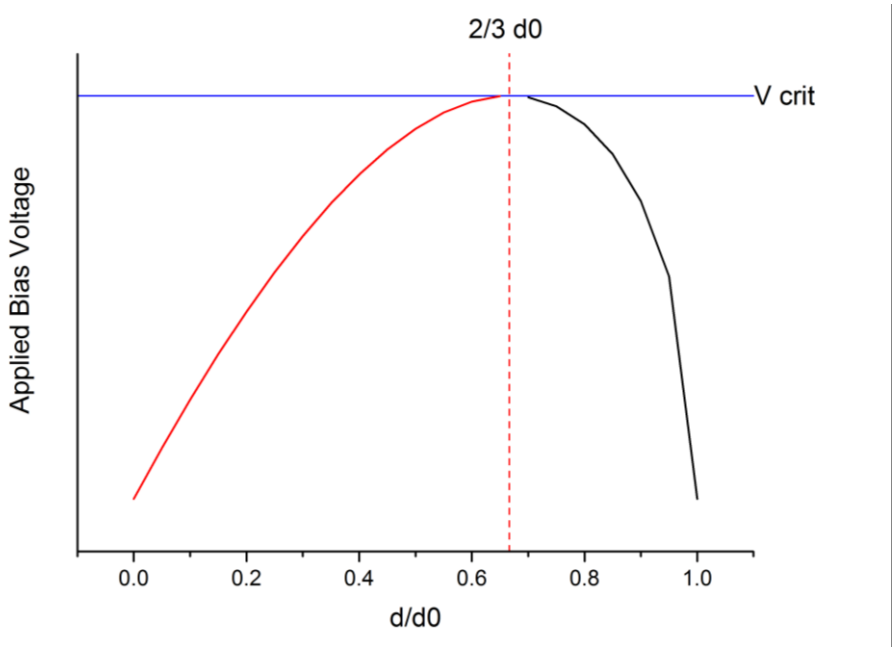

Figure 2-23 – Graph of Electrode Bias Voltage as a Function of Beam Displacement

When *Equation 2-26* is applied to typical beam geometry and for Au and Al beams it becomes apparent that the practical contact separations are very small (<4 um) before required actuation voltages exceed 100 V [4]. It is also apparent by applying *Equation 2-23* to a theoretical device with unbiased contact separation of 3 µm, applied voltage of 50 V and an electrode area of 100 x 100 µm, that the electrostatic pull down force is <28 µN at the critical separation distance. While direct measurement of the contact force is desirable its accurate measurement becomes difficult at these scales due to considerations of both the instrumentation and influence of environmental vibrations [96].

Optimising the actuation voltage profile has been proposed as a control strategy for dynamically controlling the contact closure to minimise contact bounce and mechanical damage to the contact surfaces whilst also achieving adequate static closure force [4]. Portable electronic devices are a key potential application for the MEMS resistive switch where the available actuation voltage will be determined by the power source [97]. Typical lithium battery technologies offer cell voltages around 3-4V and while strategies exist to upscale these voltages [98] the MEMS switch designer will generally minimise the required actuation voltage where possible favouring minimising contact separation [4, 10]. In competition with the requirement to minimise the pull in force is the

requirement for the restoring spring force to overcome any stiction or cold-welding effects. Considering the typical separation distance of the contacts in the off-state configuration the requirements for actuation voltage and switching time must be balanced with the requirements for an adequate restoring spring force and isolation. With the practical MEMS switch often hermetically encapsulated in a nitrogen or Nobel gas environment and the current and voltage of the switched signal below the arcing threshold the separation required between the contacts for good isolation characteristics in the off-state this optimisation of contact separation is generally at the scale of several to tens of microns.

With these considerations it is appropriate to consider a testing apparatus actuation method that can vary the displacement-velocity profile of the moving contact, as well as the static closure force applied, to investigate different actuation strategies or configurations. The testing apparatus should be capable of manipulation of the mobile contact over a motion range of several to 10's of μm at forces commensurate with electrostatic actuation (10's to 100's of μN).

2.10.2 Required Switching Rate

Perhaps the most important single specification for a testing apparatus is the switching rate. Radant claim switching lifetimes for the RMSW101 device as $>10^{11}$ and $>10^{9}$ cycles for cold-switched and hot-switched at 100 μW respectively [99]. These values effectively describe a non-perishable device at cold switching and very low power switching conditions. Demonstrating the Au/MWCNT technology can achieve lifetimes of the same magnitude is important in establishing its validity thus these figures serve as a practical benchmark. At the time of writing the highest number of cycles the Au/MWCNT surface has been tested to is 0.5×10^{9} under hot-switched condition at 40 mW [19]. The testing process was interrupted without contact failure but required two months cycling at a switching rate of 100 Hz. In order to demonstrate the potential of the Au/MWCNT technology in a practical timeframe a greater switching rate for testing is highly desirable.

Instrumentation is required for the measurement and logging of multiple experimental parameters. Contact resistance, contact force, voltage and current waveforms as well as changes in the structure of the surface. The time and voltage resolution required should be considered in terms of the events under investigation. In the case of the Au/MWCNT MMB transient the duration is of the order of 10-200 μS [19, 95] with the onset of softening ~80 mV and open circuit voltages in the nominal non-arcing regime < 12V. This leads to a requirement for measurement and recording resolution at the

nanosecond and millivolt scale. Illustratively, if a MMB has a duration of 200 µs a switching rate of 5 kHz would begin to interrupt the process and influence the results of the wear process, and this is without considering the time required to achieve a stable contact interface when closing the switch.

Static contact resistance is a key electromechanical metric in evaluating the contact pair inline insertion loss. Previous research has defined the point of contact failure as the contact resistance reaching a multiple of three times its nominal initial value [15, 19, 58]. As a parameter for evaluating the contact over its lifetime it requires that the applied circuit conditions (current, voltage) and contact force are precisely controlled and isolated from external influence. Contact resistance for the MEMS scale contact is typically in the range of 0.5 to 10 Ω [19, 58].

2.10.3 Environmental Vibration Isolation

Local air pressure fluctuation because of noise, doors opening and closing, air conditioning and audible noise may directly influence the contact force. As an example, the author has noted that even the vibrations from nearby human speech are enough to causes fluctuations in the contact force at the µN level and corresponding variation in the contact resistance measurement at the mΩ scale. External ambient vibrations transmitted through the ground arise as a result of road traffic, operation of nearby heavy machinery, with ground transmitted vibrations typically in the region of 4-20 Hz [100]. Additionally wind and weather conditions can induce sway in the building and are typically of relatively low frequency ~1-5 Hz for low rise blocks typical of the University laboratory facilities [101]. Internal vibration source such as foot traffic, lift equipment, mechanical instrumentation such as pumps and motors also create vibrations that are transmitted through the structure of the building typically in the 5-100 Hz range. It is therefore apparent that to stabilise the measurement of contact parameters and the switching regime care must be taken to isolate any apparatus from the influence of building and air transmitted vibration [96].

2.10.4 The Yunas Apparatus

Early investigation of the Au/MWCNT contact surface by Yunas employed a modified nano-indenter apparatus [55] that is not described in detail here, primarily as the cyclic rate is too low for practical lifetime testing; however it is worth mentioning the nano-indenter approach offers precise control of the contact force in an environment that is both temperature controlled and well isolated from vibration and drafts. This is relevant as they are key considerations in the lifetime testing of a MEMS scale contact.

Yunas also developed an apparatus for an enhanced rate of switching [56]. This uses a rigid frame with a system of cantilevers and hand operated adjustment screws to set the static separation between the contact pair. The apparatus is shown in Figure 2-24 and a schematic diagram in Figure 2-25.

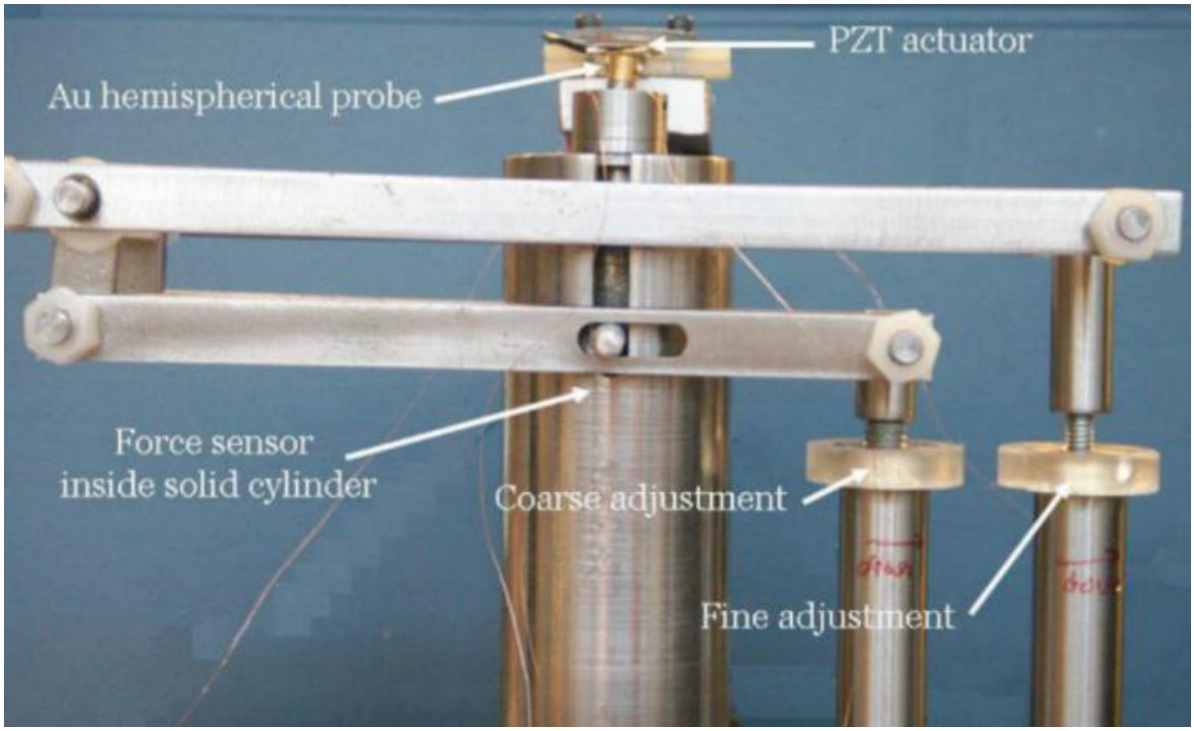

Figure 2-24 – Yunas Apparatus for Testing a MEMS contact

The lower contact is a hemispherical ball held parallel to the Z axis, this is itself connected to a force transducer that is held inside a steel cylinder such that it may translate in the Z axis but not the X and Y axes. The contact force may be controlled in three modes: via adjustment of the contact separation in the Z axis, by changing the length of the beam free to bend or by changing the actuation voltage of the beam. The cantilever system allows for coarse and fine adjustment of the contact separation distance using two different ratio 2nd class levers; however, precise adjustment was hindered by poor tolerance of the threads of the adjustment mechanism.

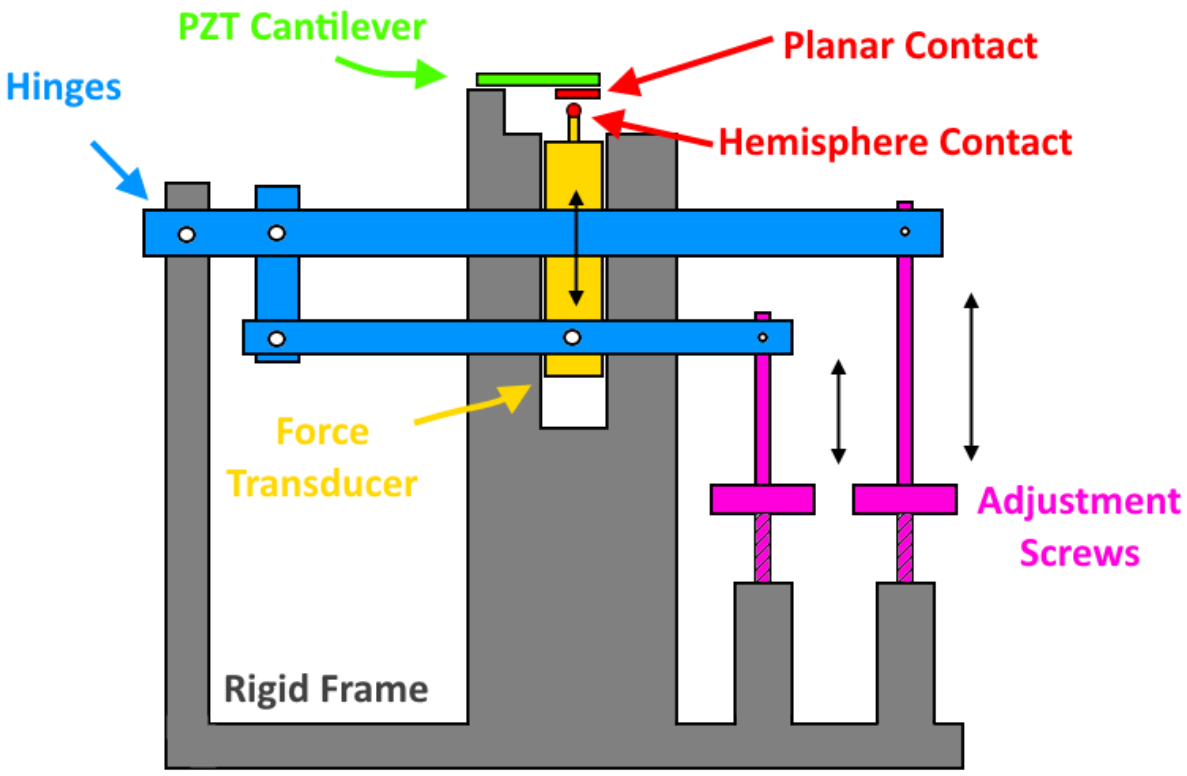

Figure 2-25 – Schematic of Yunas Apparatus

Dynamic contact motion is controlled using a piezo-electric transducer (PZT) actuated, fixed-free cantilever of a four-layer laminar construction of nickel, lead zirconate titanate, nickel and Kovar™ (a proprietary nickel-cobalt-ferrous alloy). The application of a voltage across the PZT portion induces a piezoelectric response and a longitudinal expansion resulting in the cantilever tip deflecting orthogonally – much as a bimetallic strip deflects under variation of temperature. Under typical operating conditions of a 0 - 20 V square wave actuating signal and a static contact separation of ~40 µm this system results in a static contact closure force of approximately 1 mN. The long-thin cross section of the cantilever beam magnifies a small change in the length of the PZT layer to create a large displacement of the tip; however the geometry of the long-thin beam has an inherently low second moment of area with little damping, making it prone to vibration. Practical switching rates are limited to approximately 30 Hz by bouncing effects investigated by Chianrabutra and described in 2.10.5. The fixed end of the PZT is held rigidly to the steel cylinder with the upper contact mounted, inverted, on the cantilever tip. The inverted planar contact obscures effective visualisation of the contacts meeting point and cannot be adjusted in the XY direction without disassembly of the mount. A schematic of the cantilever operation is included in Figure 2-25to show particularly show the contact orientation and difficulty in visualising the contact interface. The system is mounted on a

vibration control platform in a temperature controlled environment with the 4-wire resistance measurement (described in the Methodology chapter) used to measure contact resistance.

Weaknesses in the ability to manipulate the contact position were addressed by Chianrabutra; however three key points are recurrent in the review of following apparatus and they are specified here.

1) The apparatus requires the destructive or invasive disassembly of the contact pair in order to image or measure the morphology of the surface. As the surface will be melted, reformed and transferred during hot switching and surface texture is key in determining the contact a-spot distribution, understanding surface evolution during electromechanical wear is of great importance.
2) The 30 Hz cycling rate limitation of the PZT cantilever would require more than a year to achieve a billion switching cycles – a level at which the Au/MWCNT technology must practically demonstrate to establish itself as a viable technology. Lifetime test cycling has been reported at switching rates of 10 kHz achieving 1 billion cycles in 28 hours [99].
3) A protective environment, such as dry nitrogen, that would be expected in the practical hermetically sealed MEMS switch is not provided, thus the influence of atmospheric contamination is unknown. While the Au surface is Nobel and resistant to corrosion there is an unknown influence on surface adhesion and electromechanical effects due to the presence of moisture and hydrocarbon contamination.

2.10.5 Chianrabutra Testing Apparatus

The Chianrabutra apparatus incorporates the ability to cycle a contact at forces close to MEMS contact operation while resolving the transient forces associated with the contact operation through a vertically aligned micro force transducer [102]. It is an evolution of the apparatus developed by Yunas and as it has been used in the preparation of results during this study. An outline of its operation is given in Section 3.2.

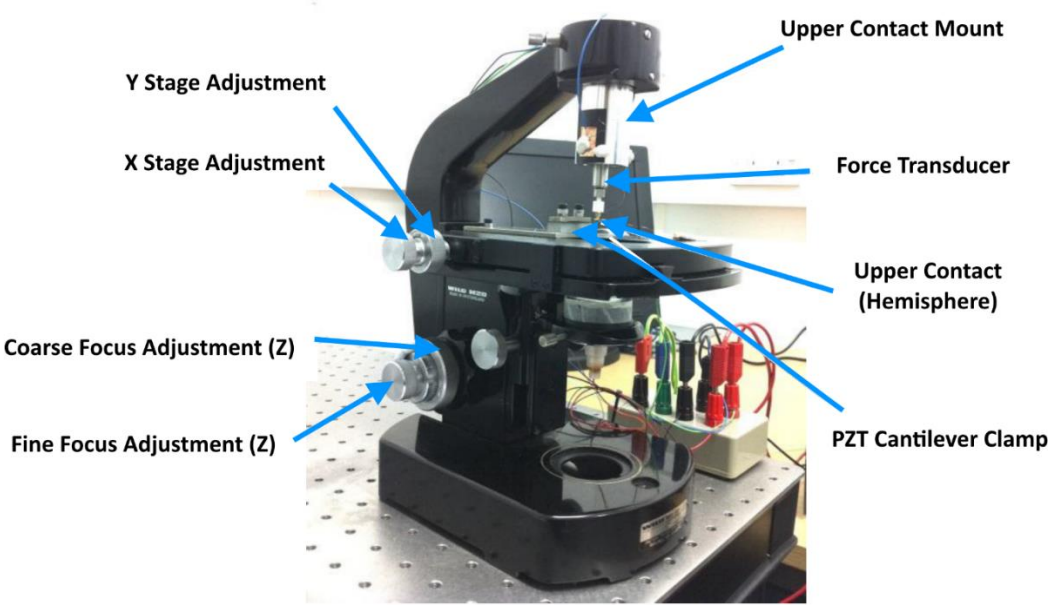

Figure 2-26 – Chianrabutra MEMS Testing Apparatus

The frame of reference between the upper and lower contact is derived from a Wild Heerbrugg M20 microscope modified by the removal of the optics, turret and condenser and is shown in Figure 2-26 with captions to illustrate the main controls. The microscope provides a stiff box-section steel-cantilever frame with a force transducer and the hemispherical contact mounted in place of the optics on the upper limb. The PZT cantilever and lower contact are mounted on the stage. The fine focus mechanism allows relative positing of the contact pair in the Z axis to a resolution of ~1 µm while the XY stage Vernier have increments of 10 µm.

When compared to the Yunas apparatus, it offers a much finer control of contact meeting point in the Z axis with the author finding it possible to adjust the static contact force with a resolution of +/- 100 µN. The precise control of the contact meeting point in the XY axes is now possible using the microscope stage Vernier controls that feature a 10 µm graduated scale. In practice the author found that the lack of a magnified visual feedback limited the positional resolution to no better than 100 µm but it does allow for quick and reliable repositioning of the upper contact over a new location on the planar contact; however it is noted that the precision is not sufficient to allow repeatable placement of a MEMS scale contact pair at the XY coordinates and the lack of visual feedback makes in-situ alignment of a specific location on the contact problematic.

Dynamic actuation of the contact is achieved using the same PZT cantilever as the Yunas apparatus with the planar contact on the PZT cantilever tip. In the Chianrabutra design the contact is oriented

with the planar contact lowermost such that it can be more easily visualised. At the point of contact closure with a non-zero arrival velocity the kinetic energy from the moving contact must be dissipated. Some of the energy will be dissipated via a mode of free vibration being induced in the beam causing the contacts to "bounce", with the energy dissipated by internal friction in the beam and the contacts. In the PZT beam design described, the first harmonic frequency is ~900 Hz. When the mass of the planar contact is added to the end of the beam this frequency will be reduced. If the beam is not clamped at the base, such that the freely vibrating length is reduced the frequency of the first free mode of vibration will increase. It is noted that the cantilever clamping mechanism does not allow the precision alignment of the PZT and in practice it is difficult to locate a cantilever in the same place once it has been disturbed. This lack of precision is placement will influence the frequency of the cantilever resonance.

Chianrabutra observed contact bounce using the described PZT arrangement with a planar contact affixed to the tip of the beam. The contact "bouncing" is shown in Figure 2-27 and of the order of ~500 Hz with ~15 bounces, (B_c) over ~0.03 s (T_c) before the contacts remain in continuous contact.

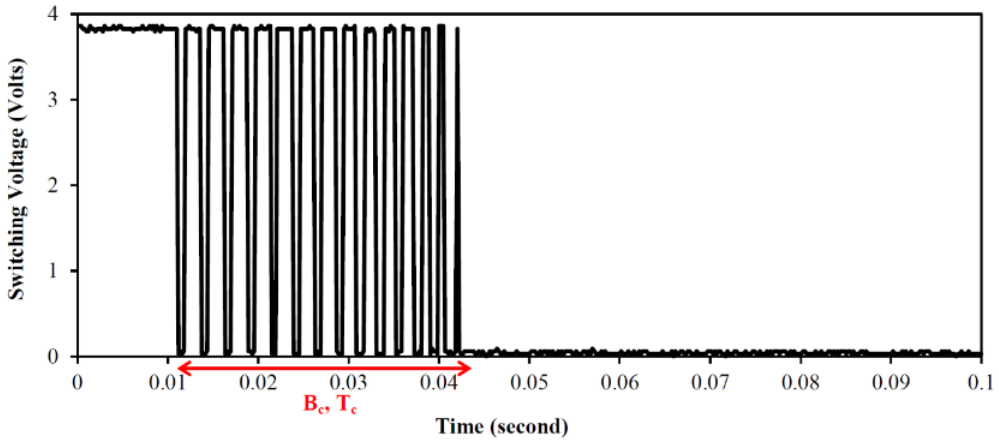

Figure 2-27 – Graph showing the unstable bouncing time after contact closure for an Au/MWCNT contact

This is significant as the time required for the contact to settle places a practical limit on the maximum switching rate for this PZT beam design (~ 30 Hz).

Both the Chianrabutra and Yunus apparatus cycle the contact by moving the planar contact. In the practical MEMS switch this is unrealistic as the mobile contact would be the cantilever side of the contact. This becomes relevant for the Au/MWCNT surface as, unlike thin film coatings, at this stage in the research it cannot practically be applied to a MEMS scale cantilever. It follows that the

movement of the planar contact introduces additional vibration in the Au/MWCNT structure that may have an undesirable electromechanical effect.

While the system is limited to forces that are above or borderline with those practically realisable for the MEMS switching regime, the apparatus is preserved as it offers the ability to carry out contact testing with a calibrated force transducer, and this will be important in calibrating the contact resistance/contact force relationship described in 2.4. The same limitations of environmental protection, non-invasive surface measurement and switching rate are noted.

2.10.6 Lewis Testing Apparatus

The Lewis apparatus was developed in order to test the Au/MWCNT contact at a force regime more likely to be experienced in a practical MEMS switch and an electrostatically actuated cantilever beam was produced [19]. Reduction of the contact force is desirable for practical testing as at the MEMS force scale the transition from diffusive to ballistic transfer is expected. This will result in an increase in the softening voltage thus a mechanism that may increase contact lifetime above the macro force regime [35].

The cantilever beams' first mode of resonance was designed to be ~275 Hz resulting in dimensions of 2 mm wide by 10 mm long and approximately 20 μm thick. These dimensions are significantly larger than devices found in commercially available MEMS switches but offer the ability to achieve a large air gap, useful for the easy manipulation of the contact separation, with a relatively low pull-in voltage achieving a realistic MEMS contact closure force. Manufacturing variation caused a greater than anticipated etch and a reduction of the beam thickness thus a reduction in the designed stiffness. The first mode of resonance was measured experimentally at 235Hz thus switching rates of ~150 Hz could be achieved but considerations of the logging instrumentation limited the switching rate to 100 Hz. The mobile contact cantilever is micro fabricated via the lithographic mask patterning and inductively-coupled plasma (ICP) etching of a silicon wafer before being coated with a 10 nm adhesion promoting layer of Cr and a final electrode layer of 500 nm of Au. The contact actuation is achieved electrostatically via a bias electrode under the cantilever with the cantilever acting as a common ground for the electrostatic actuation and signal circuits [103].

Commercial relay testing equipment (ART Reflex 51) was employed to automate contact cycling and the measurement of contact resistance to known British and military standards (BSEN116000-3, MIL-PRF-83536), while a high-speed digital storage oscilloscope was used to capture transient voltage

waveforms associated with the electromechanical wear phenomenon. A force transducer is not incorporated to the apparatus design; however the contact force was modelled computationally and derived from the in-situ cantilever deflection measured via a chromatic aberration displacement probe thus calculated indirectly and is described in 2.4.

Overall arrangement of the system is shown in Figure 2-28 and a close-up view of the contact arrangement in Figure 2-29.

Alignment of the contacts achieved using a lever operated XY translation stage and a machine screw to adjust the cantilevers static height. Static separation between the actuation electrode and the cantilever was controlled via a 25 μm Mylar film. This leads to a dense and complicated arrangement of electrodes with no active control over the contact motion during the opening phase.

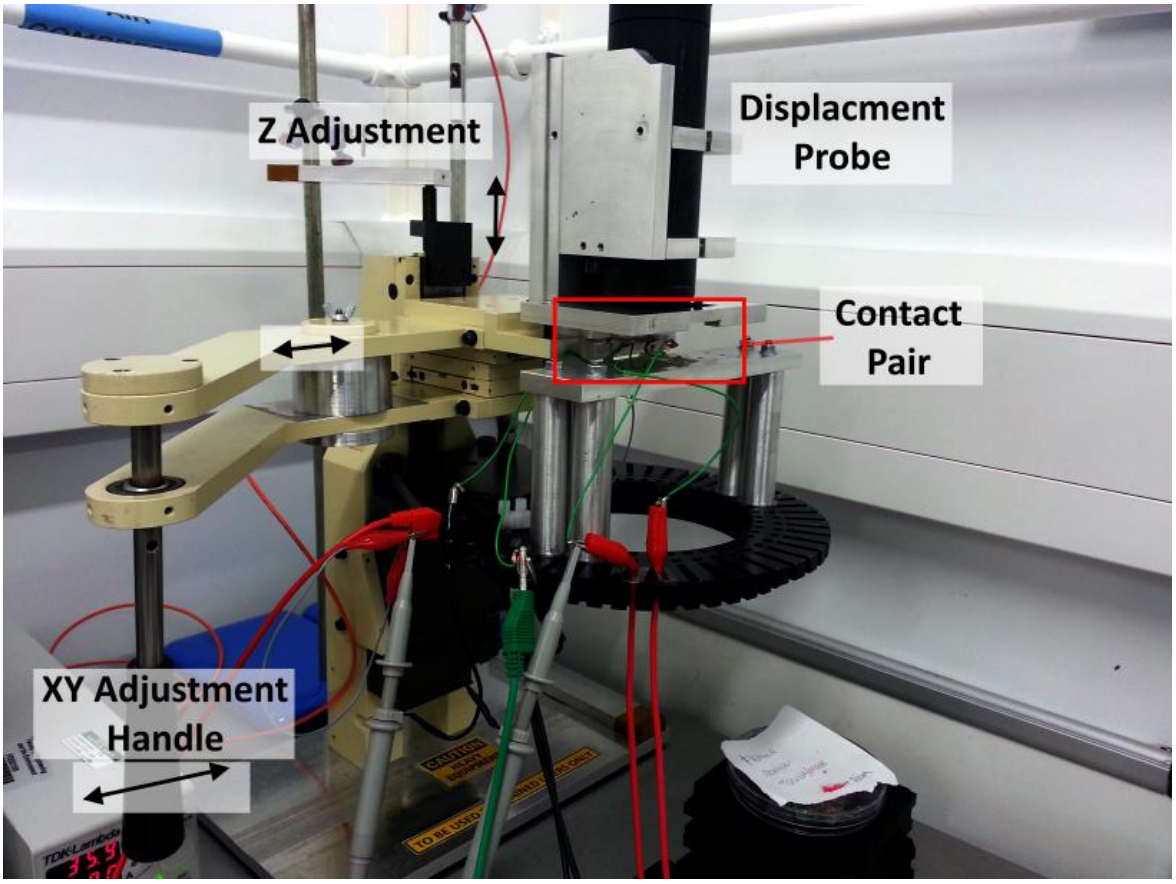

Figure 2-28 – Lewis Apparatus for MEMS contact testing

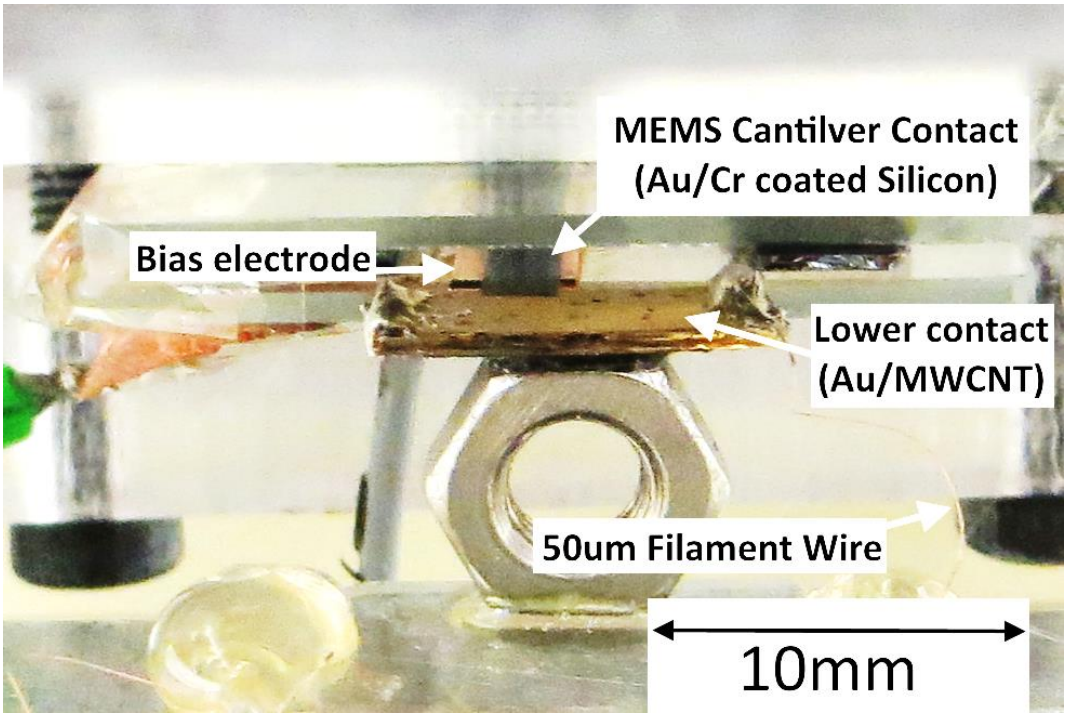

Figure 2-29 – Electrostatic Actuated Cantilever and Au/MWCNT Contact Pair in Lewis Apparatus

An issue with this design is that if contact stiction overcomes the restorative spring force of the cantilever the contact will fail in the down position and testing cannot continue. This may be acceptable where a practical cantilever is in use as it is representative of real performance; however, where the contact lifespan is under investigation and the cantilever is not representative of a practical device this introduces a weakness in the apparatus. While switching rate is now possible at 100 Hz and the apparatus has been demonstrated to cycle to 500M operations this required two months of continuous operation and a greater cyclic rate is required to achieve practical testing of the Au/MWCNT composite. The lack of protective environment and ability to measure in-situ surface evolution is observed again. The acquisition rate of the instrumentation and harmonics of the cantilever limit the switching rate. It is noted that to achieve the number of switching cycles required in a practical time frame will require an actuator with higher stiffness.

2.10.7 Ren Apparatus

The Ren study of the MMB phenomenon in Au contacts utilised a testing apparatus developed in the investigation of Au plated contacts under conditions of low force (50 mN) and ultra-low speed contact opening (25 to 150 nms^{-1}) [104]. The objective of the low speed opening was to ensure thermal equilibrium in the bridge; however it is unclear if the phenomena observed during this study were in fact MMBs as the circuit conditions are above those normally associated with the reported

arcing threshold for Au of 12 ~ 15 V and the contact potential drop remains below the accepted melting voltage for Au of 0.43 V [66, 85]. It is noted that the instant of bridge rupture needs to be resolved in greater temporal detail and slower opening of the contact will not affect the extremely rapid transient nature of ultimate bridge rupture.

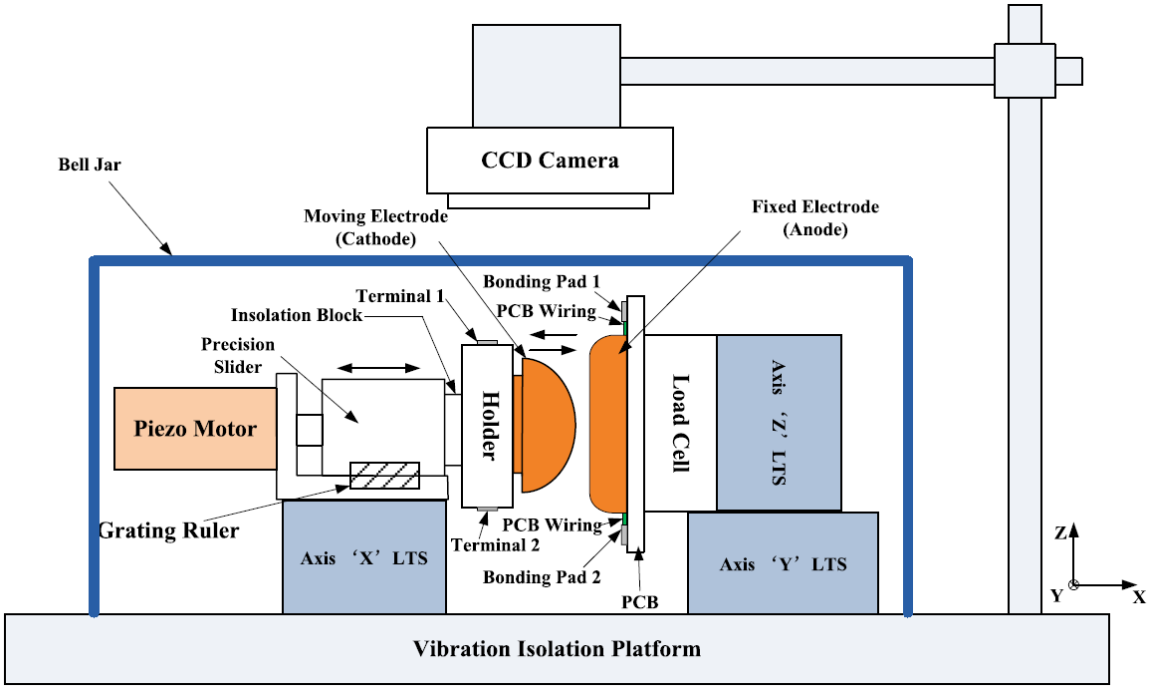

Figure 2-30 - Apparatus developed by Ren et al for low force contact opening [105]

The system is housed on a vibration isolating table and beneath a dust tight bell jar to reduce contamination and air transmitted vibration that causes the contact force to vary at the levels required for testing (10 µN ~ 4 mN). A CCD camera is used to monitor the contact position and the control of position is achieved via manual Vernier stages. Contact closure is controlled with a piezo motor with a linear encoder providing 5 nm resolution. It is noted that the uni-directional velocity profile of the piezo motor is not continuous but a high acceleration, stop-start, micro-stepping profile that will introduce a vibration of 5 Hz due to the stepping interval. The sample rate of the voltage recording instrumentation (1 ms) is significantly below transient voltage changes in the MMB events that appear linked to changes in contact force prior to bridge rupture, observed by the author to be of the order of 20 ns.

This testing rig was modified and reused in a further study to examine what the author identified as contact bounce phenomena at low force under hot switching conditions of 10 V and 2 mA; however the phenomena is likely to of been instability due to the vibration in the mobile contact mount. The

modifications included placing the moveable contact on a bow type spring (Figure 2-31). Unstable contact behaviour was proposed to be a competitive balance between the spring force and electrostatic force; however both the adhesive force observed due to the MMB in their previous work [105] and vibration in the spring were ignored as possible influences. The MMB adhesion force is clearly not present until the contact first closes and re-opens but the spring vibration is a significant issue. The stepping of the piezo motor would produce vibration due to the acceleration and the author has observed that the vibration force caused by nearby human speech is detectable at these force levels with a rigidly mounted contact isolated by enclosure. The low spring constant of the bow type spring may exacerbate the sound transmitted vibration forces by acting as an amplifying membrane. This could influence oscillation between restorative spring force and electrostatic force as illustrated in Figure 2-31.

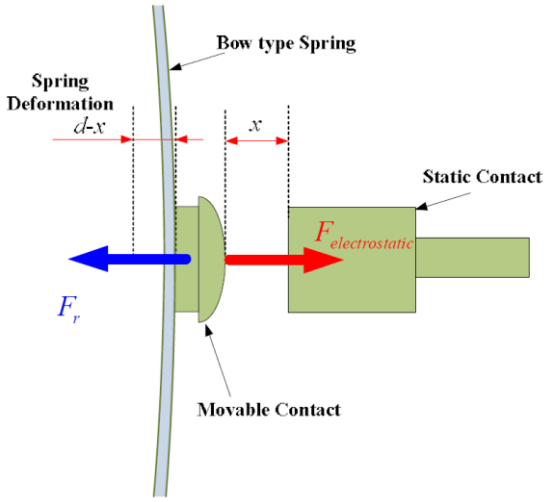

Figure 2-31 - Bow type spring arrangement used by Ren et al to examine contact oscillation [106]

2.10.8 Toler Apparatus

Toler et al developed a piezoelectric actuator driven MEMS testing apparatus (Figure 2-32) that is capable of high cyclic contact rates (~3 kHz) that allow 10^9 cycles to be reached in under 93 hours of continuous testing [107]. The MEMS switch under test was a complete pair of contacts consisting a mobile contact of a fixed-fixed bridge with a hemisphere contact to a fixed planar contact both with a sputtered Au coating. It is enclosed in a hermetically sealed polycarbonate test chamber kept under a nitrogen atmosphere test environment. This minimises the development of oxide and organic contaminant films associated with degradation of MEMS contact resistance and failure [4]

[81]. The contact force is applied via the piezo actuator driving a force measurement probe that pushes the fixed-fixed bridge down onto the contact. The contact force is derived by modelling the fixed-fixed beam deflection force and subtracting from the total applied force. The contact force was thus calculated indirectly as ~100 μN.

Contact resistance is measured using a dedicated MEMS contact pad arrangement according to the the 4-wire method described in section 3.3.

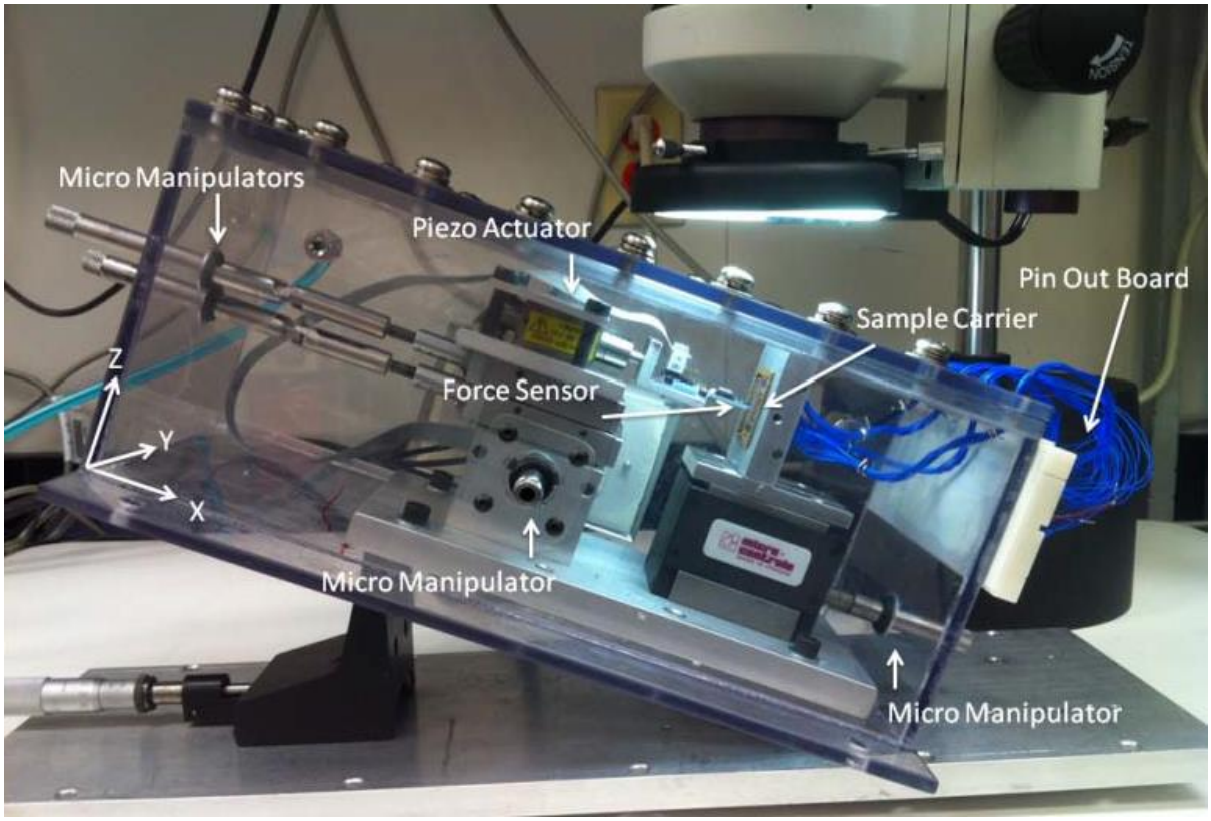

Figure 2-32 - MEMS lifetime testing apparatus developed by Toler et al [107]

As the fixed-fixed type moving electrode is brought into contact with the lower electrode by a piezo motor actuator with a force probe attached. This introduces an additional source of physical damage, that of the physical contact between the force probe and the top side of the moving electrode. Vernier micromanipulators are incorporated to adjust the actuation point with an overhead magnified viewer to assist in accurate positioning.

The system represents the most advanced test apparatus described and offers the ability for the application and measurement of force with micro Newton resolution in a protective atmosphere at a switching rate of 3 kHz. While the apparatus operates a realistic MEMS switch device it is noted that

the measurement of force is indirect and relies on the accurate modelling of the fixed-fixed bridge. The bridge was observed to plastically deform during lifetime testing to ~ 10 million cycles thus the contact force could not be accurately judged, only the total applied force. In order to evaluate the contact surface, the device required destructive disassembly thus measurement of surface evolution is not possible with this apparatus.

2.11 Summary and gaps identified

Au demonstrates low resistivity, is chemically stable and forms a good contact interface at low force. However, Au is relatively soft and has a low melting point making it susceptible to wear, adheres to itself and absorbs a layer of contaminants that break down under micro-arcing to highly insulating compounds. The use of Au and MWCNT together provides a tailorable composite system that provides a low modulus MEMS contact material that simultaneously increases contact area and provides a mechanism for energy dissipation. Both properties improve the tolerance of Au to switching wear while retaining conductive properties close to pure Au. Composites using the vertically aligned MWCNT forests have demonstrated superior switching lifetimes to non-aligned MWCNT. Thermal catalytic growth of MWCNT allows both vertically aligned growth in patterns defined by the catalyst deposition, and the anchor of the MWCNT to a substrate surface. Application of Au by sputter coating Au only partially penetrates the MWCNT and retains the compliance of the MWCNT.

The MMB in the Au/MWCNT composite is linked to a fine transfer wear mechanism. The stability of the MMB is influenced by its surface tension and magnetic pinch effects and it is noted that varying the contact opening acceleration or circuit voltage may in turn influence the MMB. The effect of circuit voltage and contact opening velocity have not been reported for the Au/MWCNT contact. The upper limit of the composites current carrying ability has not been characterised. Previous study of the vertical aligned Au/MWCNT composite has mostly been under closed contact forces greater that those identified as likely for electrostatically actuated MEMS switches (~ 1000 cf. 10s-100s µN) and increased force has been linked to increased damage to the Au/MWCNT and consequently reducing the contact force may also increase lifespan. The exception is the Lewis study where the contact force was ~ 35 µN. However, while MMB were detected, no surface wear could be detected after 28 M hot switching cycles at 4 V 50 mA. Just prior to the contact failure the average MMB energy rose from 1.5 to 13.2 µJ and a mechanism was proposed were changes in surface texture resulting in a larger MMB. In these studies, the surface wear has only been detected and quantified at the

completion of switching or not at all. After 2 months continuous hot cycling and completion of 500 M switching cycles the contact had neither failed nor could any wear be detected meaning the prediction of ultimate lifetime cannot be accurately inferred. The lifespan of the composite under cold switching conditions has not been determined.

2.12 **Aim and Objectives**

The motivation of this work is to establish the composite is an advanced engineering material that can be used as a long-life MEMS electrical contact and provide data to the MEMS switch designer. The aim of this work is to characterise the influence of switching processes on the lifetime surface wear of the Au/MWCNT composite, at the force regime expected for an electrostatically actuated MEMS switch, and so model and predict switching lifetime under a range of conditions. The objectives of this work are:

1) Develop apparatus that can detect and capture the MMB waveform, the microscale wear in the Au/MWCNT contact surface and cycle the contacts to the failure at low force switching equivalent to the electrostatic actuated MEMS switching regime.
2) Determine the current switching limit of the Au/MWCNT and the mechanism of the failure when the limit is exceeded by investigation of the contact surface and the MMB waveform. This will provide fundamental information towards characterising the composites performance.
3) Measure the influence of circuit voltage, current and contact roughness on the MMB phenomenon. This is to characterise the influence of the circuit conditions composite texture on the fine transfer wear mechanism and provide empirical data to aid the prediction of contact lifetime under a range of switching conditions.
4) Determine if the opening velocity of the contacts is linked to the MMB behaviour. This is to provide data linking switch design parameter to the rate of fine transfer wear and therefore the lifetime of the composite.
5) Measure the evolution of surface wear linked to the MMB in Au/MWCNT contact while circuit parameters are varied. This purpose is to link the MMB characteristics to the rate of surface wear.
6) Determine the evolution of surface wear under cold switching conditions. This is to characterise the influence of the mechanical effects on switching of the composite. Then

apply the empirically derived data to develop an enhanced model for surface wear to enable the lifespan of an Au/MWCNT contact to be predicted under a given switching regime.

3 Experimental Methodology and Development of Apparatus

This chapter describes the manufacture and testing of the Au/MWCNT material and the development of apparatus required to meet the research objectives of this work.

The two main manufacturing processes used, plasma enhanced chemical vapour deposition (peCVD) and thermal chemical vapour deposition (tCVD), are described. Catalytic nanotube growth is highly sensitive to the manufacturing conditions and small variations can result in significant variation in the structure, composition and homogeneity of the nanotubes produced [46]. To produce contact material equivalent to, and therefore comparable with previous study the manufacturing methodology is largely unchanged from previous investigation; however, improvements to the thermal control of the process have been made.

While improving production control improves manufacturing yield, the variance in the manufactured materials still requires they are physically characterised. The characteristics critical for performance as a contact material are the growth height and homogeneity of the nanotube forest, and the thickness of applied gold coating. The characterisation is described using advanced optical profilometry techniques. These techniques are also evaluated for their ability to characterise the microscale texture of the composite surface as the texture approaches the scale of the diffraction limit.

A previous developed MEMS testing apparatus is described which has been enhanced during this investigation with instrumentation to provide better resolution of contact force and MMB transients. The legacy system is used to establish equivalent results from previous investigation while validating the new instrumentation before it is incorporated in a new apparatus for in-situ MEMS surface testing.

A novel, state-of-the-art MEMS testing apparatus developed for this study is described. It provides the ability to investigate how the MEMS contact surface evolves over a lifetime but at accelerated rates.

Finally, a series of experiments are described, related to the numbered research objectives described at the end of the previous chapter.

3.1 Manufacturing Process Used for Au/MWCNT

The research objectives of this work require the availability of Au/MWCNT composite material for experimentation. The following outlines the production method and equipment involved. The growth process for the nanotubes is catalytic thermal chemical vapour deposition (tCVD) based on a hybridisation of methods well described by literature [108-113].

The manufacture of each composite contact begins with the preparation of a substrate material. The substrate is a 5 mm by 10 mm silicon wafer chip. Wafer chips are cut by dicing saw from a larger 100 mm diameter silicon wafer. The wafer provides a flat substrate that is easy to handle and can tolerate the manufacturing process. The type of silicon wafer is not critical for the growth process as there is no etching of the silicon, while chemical and adhesive properties are largely determined by the subsequent coating process. The wafer type used is single side polished (SSP), N<100> silicon wafer with a 1 μm thick silicon oxide coating.

The wafer chips are then cleaned. Organic contamination is removed using acetone under ultrasonic agitation for 10 minutes followed by rinsing with Class III distilled water from a reverse osmosis purifier to remove debris and waste acetone. Acetone residue is removed by rinsing in ethanol under ultrasonic agitation for a further 10 minutes. The chips are rinsed again in distilled water again before forced drying with ‘dry’ nitrogen to minimise water marks that are known to influence manufacture with even ultra-pure water through the presence of dissolved gases [114]. The chips are mounted on a microscopy slide (also cleaned) with carbon tape for the plasma enhanced chemical vapour deposition (peCVD) or ‘sputter’ coating.

The chips require coating with alumina (Al_2O_3) buffer layer then an iron (Fe) catalyst layer using a low-pressure sputter coating system (Kurt Lesker). The sputter coater and interior of its reaction vessel are shown in Figure 3-1 with four locations for different source materials visible as the circular features in the reaction chamber. The sputter coating process is also used to apply the gold (Au) upper layer to the Au/MWCNT after their manufacture [115]. The sputter coating process is advantageous as it repeatable and provides fine control of the applied coating thickness.

The deposition process is first to remove the atmosphere from the reaction chamber down to high vacuum which requires several hours and is typically carried out overnight. A small quantity of ‘process gas’ is then introduced. The process gas is the source for the carrier plasma. The quantity introduced is optimised to minimise the energy for igniting and maintaining the plasma arc, and to

maximise the material transfer rate. The process gas used is argon (Ar) at a pressure of approximately 2 $x10^{-2}$ Pa.

Electrical potential is then applied between the reaction chamber electrodes to ignite a plasma arc and cause it to strike on the source material. Thermally emitted electrons ionise the process gas atoms which are in turn accelerated towards the target electrode containing the coating material. As the highly energetic ions arrive, they impact and dislodge atoms of the coating material to form a vapour that is transferred to the target as a thin layer. This process is called plasma enhanced chemical vapour deposition (PECVD) or "sputter coating" and is attractive for processing as it offers a relatively rapid deposition of homogenous, well adhering layers while the low overall temperature of the process minimises oxidation of the catalyst [47].

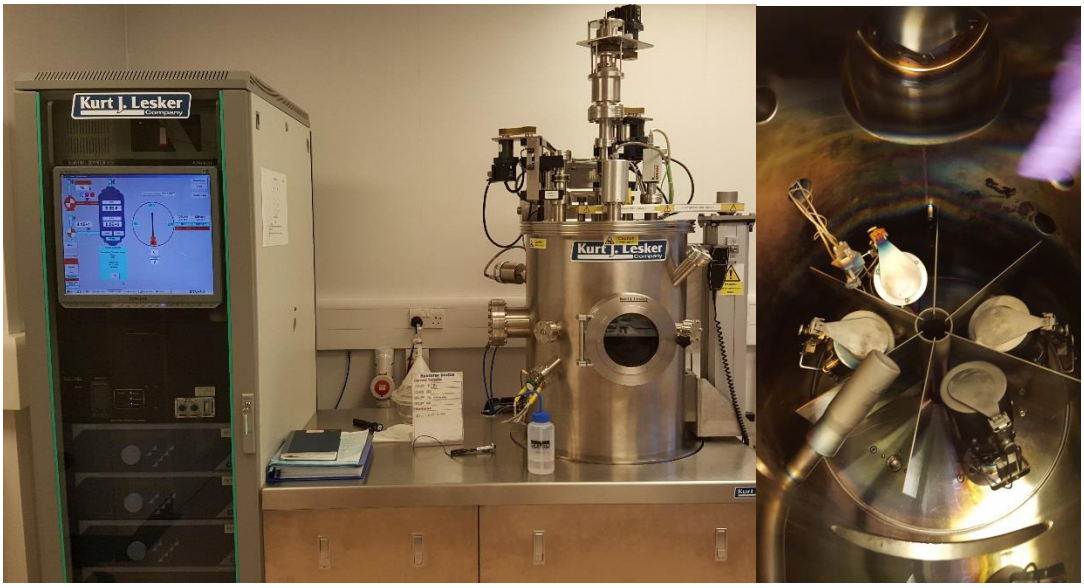

Figure 3-1 - Lesker PECVD Apparatus (left) and inside of coating chamber (right)

The PECVD process is used to coat the silicon substrate with a buffer layer of alumina (Al_2O_3) that provides a low energy coating and 'de-wets' the surface, such that the subsequent coating layer of iron (Fe) forms discrete and well distributed catalytic seed particles during the later thermal annealing process. The thickness of the iron layer is a key parameter in determining the properties of the nanotube forest as it determines the size and distribution of the catalysing nanoparticles. The de-wetting of the surface allows the catalyst Fe particles to form 'bulbs', and a tip growth mechanism in the MWCNT [42].

Following sputter coating, of alumina and iron layers, the substrate silicon is transferred to a thermal reactor vessel for thermal chemical vapour deposition (tCVD). The reactor consists of a quartz chamber approximately 300 mm long and 25 mm in diameter. It is enclosed in a three-zone furnace that can control the reactor temperature at up to 1425 ^{o}C. The apparatus is shown in Figure 3-2 with the furnace in the open position after a nanotube growth process. Signs of carbon deposits becoming increasingly heavy in the direction of gas flow on the inside walls of the reaction vessel are apparent.

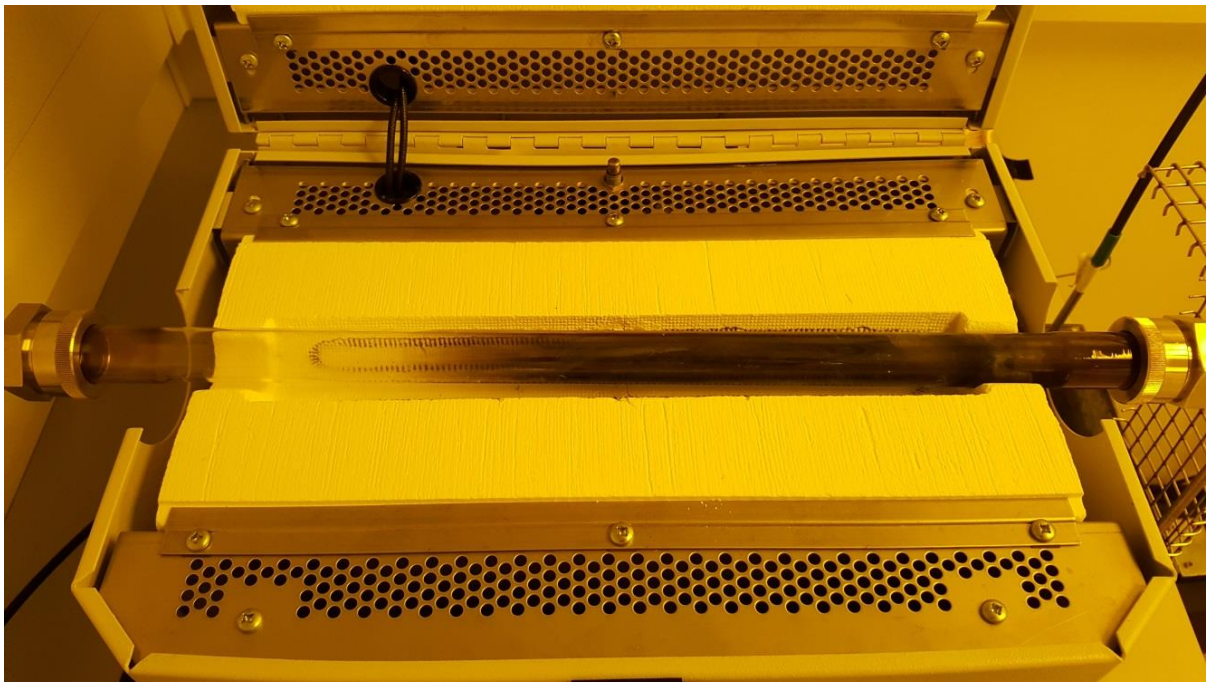

Figure 3-2 – tCVD Furnace (opened) showing quartz reactor vessel after CNT production

The substrates are loaded into the tube in a ceramic carrier (boat) before the tube is sealed and immediately purged with an argon and hydrogen (H_2) gas mixture to minimise oxidation of the catalyst [46]. Nanotube growth is achieved by exposing the coated wafers to a specific gaseous environment and thermal profile. A 'stock gas' of ethylene is used to provide the source carbon for nanotube growth. A typical profile for thermal and gas conditions required for growth are presented in Figure 3-3.

The furnace temperature control is achieved by microprocessor closed loop PID feedback between a thermocouple in the heating chamber and the furnace heaters. A programmable gas controller is used to control a mixture of argon, hydrogen and ethylene (C_2H_4) gases and follows three stages.

The furnace is gradually heating the reaction chamber from ambient laboratory temperature up to the catalyst annealing temperature of around 900°C over 30 minutes. The temperature is then held constant for several minutes during the annealing phase. During this phase the temperature is high enough for the thin iron film to form into discrete particles [47]. The gas mixture during the initial purge of the reactor and both heating and annealing phases is a mixture of argon and hydrogen. This gas composition provides strongly reducing conditions that assists the reformation of Fe from Fe_xO_y, that may have formed from exposure to ambient atmosphere during transfer of the silicon wafers from the PECVD apparatus [112]. The conditions also inhibit the formation of Fe_3C in the presence of any contaminant carbon. The temperature is then programmed to change to the growth temperature for carbon nanotubes. As the reactor temperature reaches the programmed growth temperature the composition of the gaseous environment is changed. Ethylene stock gas diluted with argon is introduced at the ratio required for the MWCNT growth. At the end of the growth phase the chamber is purged with argon while the chamber is gradually reduced to ambient laboratory temperature. It is possible to reopen the vessel and expose the nanotubes without damage from around 150 °C [116].

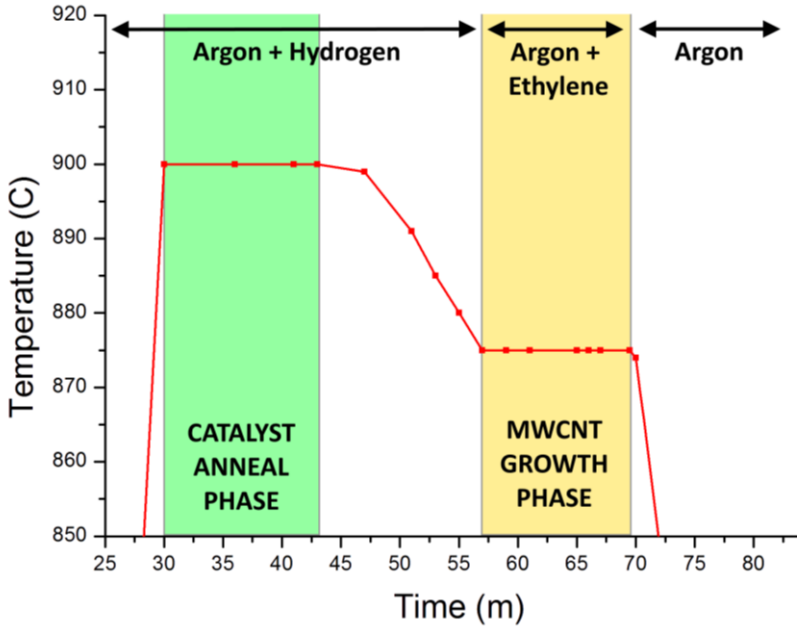

Figure 3-3 – The Gas Environment and Thermal Conditions for a MWCNT growth process

After cooling the samples are removed for characterisation of nanotube height, distribution, alignment and homogeneity with scanning electron microscopy (SEM) images (Figure 3-4) and optical surface profiling (Figure 3-5). The remaining samples are transferred back to the PECVD

apparatus where they are coated with an upper layer of gold (Au) particles that embed and entangle with the top of the carbon nanotube forest. A key point is that the attachment of Au nanoparticles to a substrate is difficult due to their low adhesion, but the micro texture of the MWCNT forest upper surface shown in Figure 3-4 provides a textured interface that improves attachment [115].

Modification of the iron deposition rate, annealing temperature, annealing time or reducing conditions all affect the size and distribution of the catalyst particles that in turn determine the size, distribution and type of the nanotubes grown. Similarly, the growth time, temperature and gas conditions also effect the dimensions, growth rate and alignment of the tubes, as well as the strain recovery they demonstrate. The duration of the final Au coating determines the thickness of the upper Au layer. The thickness of the Au layer has a significant effect on the mechanical properties of the composite [16]. In this work the desired composite material is 50 µm high MWCNT coated with a 500 nm layer of Au as this composition has previously been indicated as optimal for achieving the long switching life under a range of circuit conditions [103].

In practice the manufacturing process for nanotubes is exceptionally sensitive to changes in the manufacturing parameters and entirely different materials have been observed from seemingly identical production runs. The apparatus requires careful set up and tuning for each production run, with the samples inspected after manufacture to classify the material that has been produced.

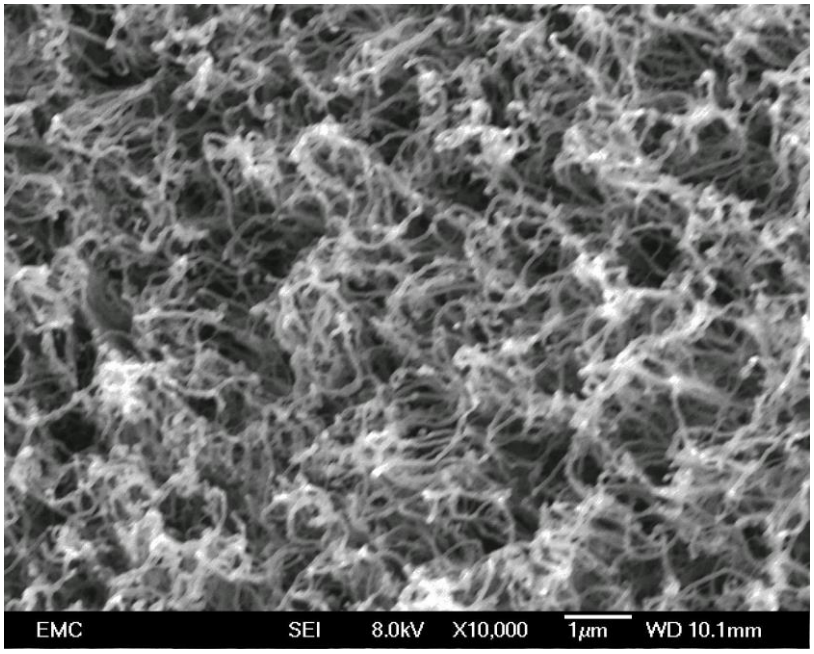

Figure 3-4 – Micrograph of Carbon Nanotube Forest upper surface at x10k magnification showing individual tangled nanotube structure creating microscopically roughened surface texture

An electron micrograph of the upper surface of a forest of MWCNT grown during this work is presented in Figure 3-4. The micrograph shows that the MWCNT tangle and clump together at the exposed upper surface. The brighter regions at the ends of the MWCNT indicate a higher atomic number than the darker regions. This observation supports the tip growth mechanism expected for this method of manufacture. The surface tangling of the MWCNT at provide a characteristic micro-texture to the material, that is preserved even when the final Au coating is applied.

Figure 3-5 shows the surface of a MWCNT forest grown over a 10 mm x 5 mm silicon wafer chip. The MWCNT growth process was classified as failure in this example as the manufacturing target was a 50 µm field. The colour scale represents the height of the field above the surface of the wafer. The nominal height of the MWCNT is approximately 30 µm and the presence of several contaminant spots on the surface can be detected. However, the micro-texture of the MWCNT surface can be detected as the speckled pattern, particularly in the homogenous regions on the left side of the figure

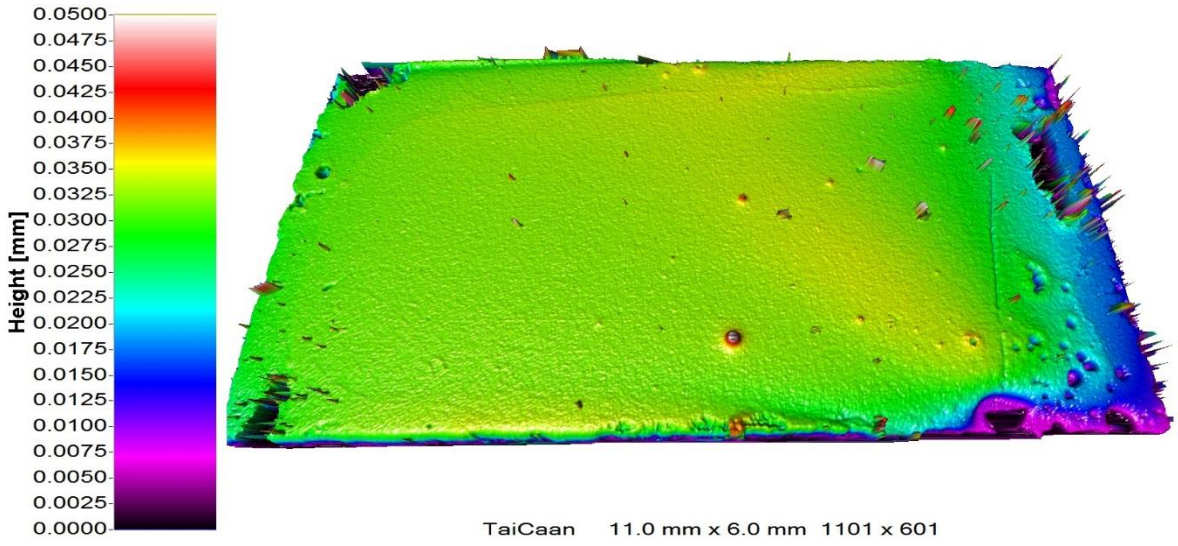

Figure 3-5 – Results from optical profilometry of a 30 µm high Carbon Nanotube forest on 10mm x 5mm Si wafer with height shown by the colour scale referenced to the substrate wafer surface

3.2 Height, Coating Thickness and Surface Characterisation

The characterisation of surface texture (roughness parameter), height of the carbon nanotubes and thickness of the gold coating is measured using two optical confocal optical surface measurement techniques. Either technique could also be incorporated in an apparatus developed to detect

microwear which is a key objective of this work. However, the level of wear expected in the Au/MWCNT MEMS contact is expected to be at a level that approaches the detection threshold of these techniques. In the next section the sensor operating principles are described, and two key effects are described that distinguish their performance in characterising surfaces. Both techniques are employed to characterise the Au/MWCNT surface and these mechanisms give rise to a discrepancy between measurements that is explained with reference to their operating principles and physical limits.

While both techniques are used to characterise the manufactured material, the confocal laser sensor provides the best sensitivity for detection of microscale wear in the contact surface. It is for this reason that the confocal laser measurement technique is chosen over the white light technique for incorporation in the novel MEMS testing apparatus developed during this study and described later in this chapter.

3.2.1 Confocal laser (CL) sensor

The principle of operation is a monochromatic collimated beam of light is passed through a focusing lens that is vibrating on the end of a tuning fork at a controlled frequency and is illustrated in Figure 3-6. Light reflected from the surface is passed back to a detector via a semi-silvered mirror arrangement. As the beam is focused on a surface a peak in intensity is recorded that correlates with the position of the end of the tuning fork and the relative height (Z position) of the surface recorded. Vertical (Z) resolution is 10 nm and spatial resolution (minimum XY feature size detectable) is a function of the spot diameter (2 µm).

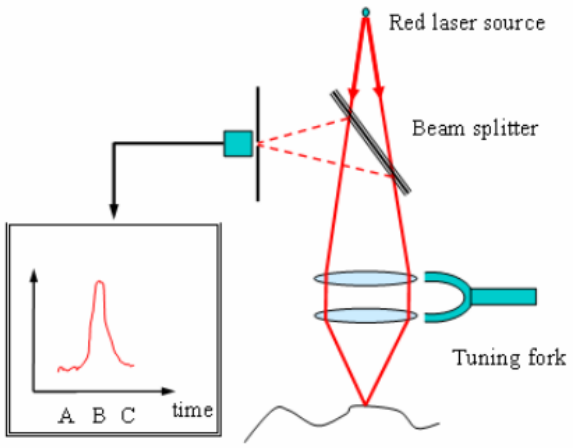

Figure 3-6 - Operating principle of confocal laser (CL) sensor

The advantage of the technique is that is utilises a smaller spot and thus resolves finer detail than compared with the white light sensor described in the next section. The disadvantage is that the reduced incident light makes refraction by sharp feature more likely or total loss of signal if the surface is heavily disrupted, particularly in the case of light absorbent deposits, such as carbon.

3.2.2 White light (WL) sensor

The white light (WL) sensor operates on the chromatic aberration principle illustrated in Figure 3-7 [117]. A polychromatic beam of light is passed from a halogen source through a barrel lens design to enhance chromatic aberration (separation of the wavelengths). Short wavelength blue light experiences a greater refraction and will have a focal point closer to the optic and red light further away. Light reflected from the surface is passed back to a spectrometer. A peak in light intensity correlates to a surface in focus and the surface displacement is determined by the wavelength of the detected peak. The technique is also capable of measuring multiple transparent layers.

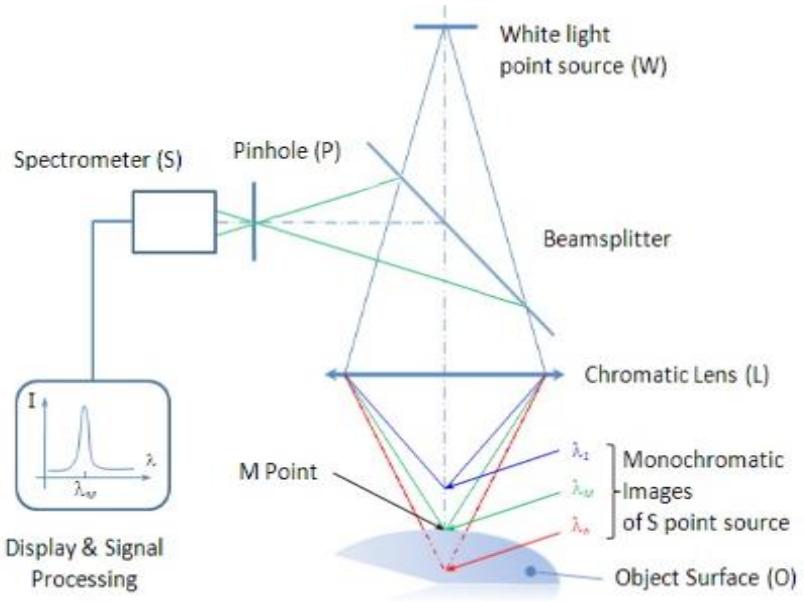

Figure 3-7 - Operating principle of the white light (WL) sensor

The advantage this technique offers over the CL sensor is has a greater spot diameter of 7 µm that allows significantly more light to be reflected from the surface allowing performance on light absorbent surfaces. The polychromatic technique is also less disturbed by large changes in surface reflectivity (i.e. from specular to diffuse surfaces). The larger spot also allows a greater angular tolerance and can measure surfaces with greater slope.

3.2.3 Summary of Optical Surface Measurement Techniques

While the CL and WL measurement techniques provide different advantages they represent practical limits to measuring surfaces using light. The performance of the instruments is dependent on decreasing the spot size of the optics to provide the best spatial resolution while a conflicting requirement to for enough light to detect the reflection requires increasing the spot size.

As a key goal in this work is to detect microscale wear it is decided that the optimal technique is the confocal laser displacement meter will be used for the novel apparatus described in the next chapter. However, the systematic errors inherent in the technique must be considered, and it for this reason that the switching surfaces will also be imaged using scanning electron microscopy (SEM). While it is impractical to use SEM to image the contact surfaces in-situ, SEM can be used to compare and validate the surface measurement at the end of the contact investigation.

3.3 4-Wire Resistance Measurement

The low contact resistance is a key property of the MEMS switch contact but presents a practical difficulty for measurement due to the presence of wiring between the measurement instrument and the contact. Increase of contact resistance is associated with contact wear and provides a clear definition of where the contact has considered to have failed. Further, it is planned to use the relationship between contact resistance and contact force to determine the closed contact force. For these reasons the 4-wire method to measure contact resistance is described.

A known current supply, I_{known} in series and a voltmeter in parallel with the resistance under investigation are configured as shown in Figure 3-8 such that the voltage drop V_{drop} be related to the resistance by Ohms law.

$$R = {V_{drop}}/{I_{known}} \qquad (3\text{-}1)$$

As negligible current is carried through the voltmeter the voltage drop measured is only across the subject resistance and the effect of the resistance in the wires to the voltmeter can be disregarded. This is known as the 4-wire or Kelvin resistance measurement and it is implemented in this study for the measurement of the contact pair resistance.

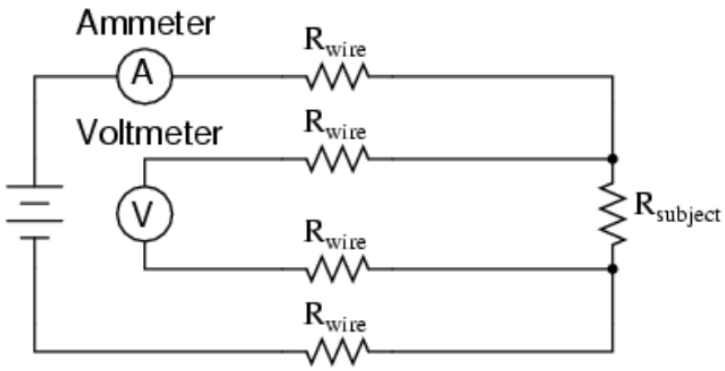

Figure 3-8 - 4-wire resistance diagram

The contact pairs are connected to the circuit via 50 μm diameter copper filament held to the contact by conductive epoxy in an arrangement analogous to the crossed rod method developed by Holm [70] to allow the mating of circular, equipotential surfaces, and implemented at the MEMS scale by Toler et al [7] using a hemispherical to planar contact pair. The contact arrangement is illustrated in Figure 3-8 showing the arrangement of wiring. Two wires are connected immediately above the Au coated hemisphere, and two wires are connected to the Au/MWCNT contact under investigation. A Keithley 580 Micro-Ohmmeter (Keithley Instruments) provides both the current source and high-resolution voltmeter. The instrument limits the potential applied during resistance measurement to < 20 mV which is below the softening voltage for Au.

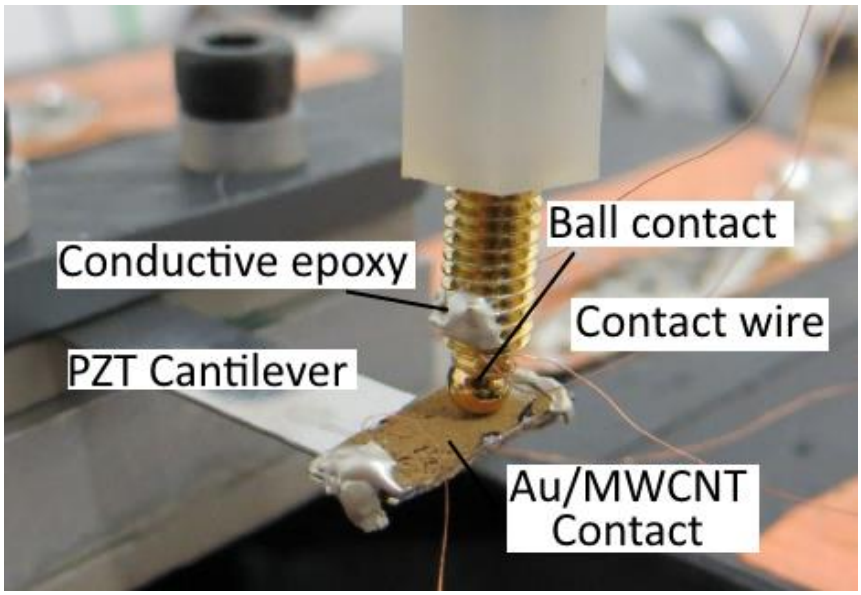

Figure 3-9 - 4-wire "Holm crossed rod" method implemented in a gold coated ball to Au/MWCNT planar contact

3.4 Molten Metal Bridge duration and energy

The molten metal bridge (MMB) can be described by the transient voltage waveform observed just prior to the contacts separating. To accurately measure the waveform the potential between the contact must be captured at the point of contact opening. The key difficulty is measuring this waveform with enough resolution and at a high enough sample rate to capture the a rapidly fluctuating, transient and non-periodic signal.

In this study the signal is captured by a Tektronix MDO4054B digital storage oscilloscope with a bandwidth of 500 MHz. The maximum real-time sample rate is 2.5 GS/s (samples/second) or every 0.4 nS at a record length of 20 M samples. In practice it was found the longest duration MMB events detected in this work are ~200 µs in duration and capturing at 250 MS/s (every 4 ns) provides excellent resolution while reducing download time.

Figure 3-10 shows a voltage transient across the contact typical of a molten bridge event with the defined beginning and end points (t1, t2) shown.

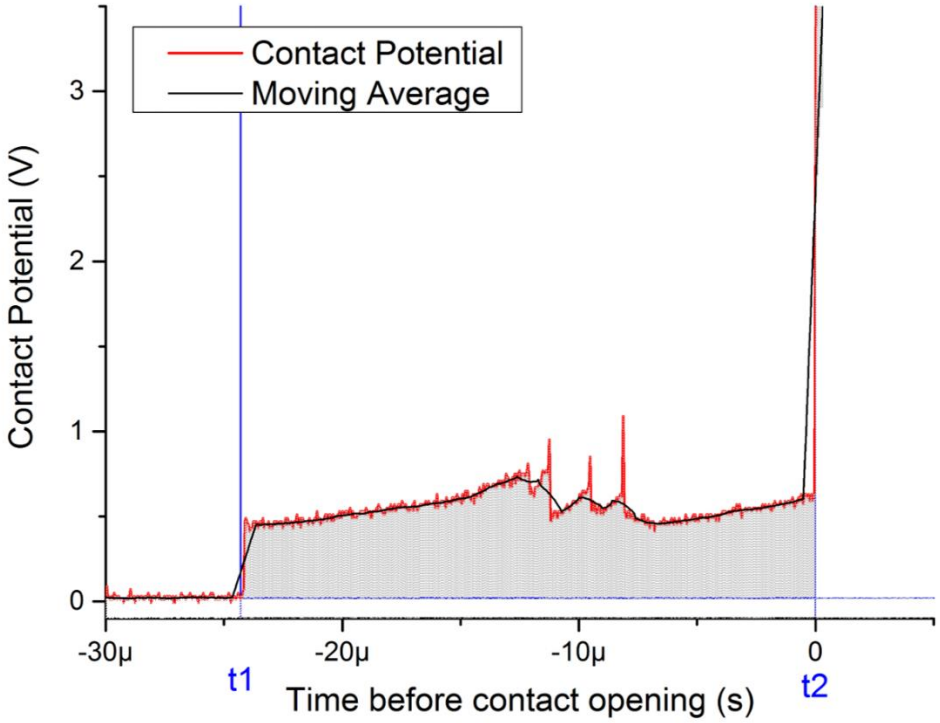

Figure 3-10 – Molten metal bridge transient voltage waveform with moving average, beginning (t1) and end (t2) times. The lower blue line represents the normal closed contact potential. The shaded region between the blue lines and the red contact potential line represents the thermal energy of the molten bridge

The contact potential can vary significantly between consecutive samples such that a subtle trend in voltage can be difficult to distinguish against the background of a rapidly fluctuating signal. To define the starting point of a molten bridge event, t_1 it is convenient to apply a low-pass filter the signal. The filter used is a 51-point moving average and an example is shown in Figure 3-10. A 51 point filter is chosen as optimises between accurate detection of the start of a gradually changing signal and minimises error where there is a step change in signal. The maximum error in determining the beginning of a MMB (t1) is 100 ns (half the filter length). Figure 3-10 illustrates the trace of the moving average filter (black line) against the real contact potential (red line) for a MMB of ~25 µs duration. In this case a 100 ns error represents a 0.4 % error in the duration of the MMB which is acceptable for this study. Note that the moving average filter is only used to determine the onset time of the MMB, t1 and once the onset time has been determined the real (unfiltered) signal is used to derive the energy of the MMB.;

The point a molten bridge event begins (t_1) is defined as where the moving average rises 40 mV above the potential drop across the contact when it is closed. The value of 40 mV is chosen as it is the noise floor of the oscilloscope and below the softening voltage for Au (~80 mV). The potential drop across the closed contact is defined as the arithmetic average value from the first 50 samples of the waveform. The point at which the contact opens (t2) is defined as where the contact potential first rises above 3 V and remains above 3 V for a minimum of 5 consecutive samples.

The duration of a molten bridge is defined as the time elapsed between t_1 and t_2.

With the start (t_1) and end (t_2) points of the MMB defined the thermal energy associated with the molten bridge waveform can now be calculated by integration of the real (unfiltered) waveform with respect to the times defined according to Equation (3-2) and represents the grey shaded region enclosed between the blue lines and the red contact potential graph in Figure 3-10

The energy associated with the MMB is defined by Equation (3-2).

$$E = I \int_{t1}^{t2} V \; dt \qquad \textit{(3-2)}$$

3.5 PZT MEMS Testing Apparatus

This section describes an apparatus developed by during previous research by Chianrabutra that simulates the mechanical action of a MEMS switch using a piezoelectric transducer (PZT) cantilever [119]. The apparatus has limitations, making it unsuitable for investigation of the objectives of this work related to micro-wear and lifetime switching (discussed in the previous chapter). However, it can be used to achieve and support the pursuit of several objectives identified for this work around the characterisation of the MMB and the calibration of the Au/MWCNT contact force to contact resistance relationship.

The system uses the frame and micro-manipulation system from a laboratory microscope to manually position the opposing halves of the contact. The contact is then opened and closed by a piezoelectric cantilever while a microforce transducer allows the applied contact force to be measured.

The instrument is shown in Figure 2-26 and a schematic of the system is shown in Figure 3-11. It is located on an anti-vibration work surface in a temperature & humidity-controlled environment (20 ^{o}C variance ± 1 ^{o}C, 60 %RH variance ±10 %RH).

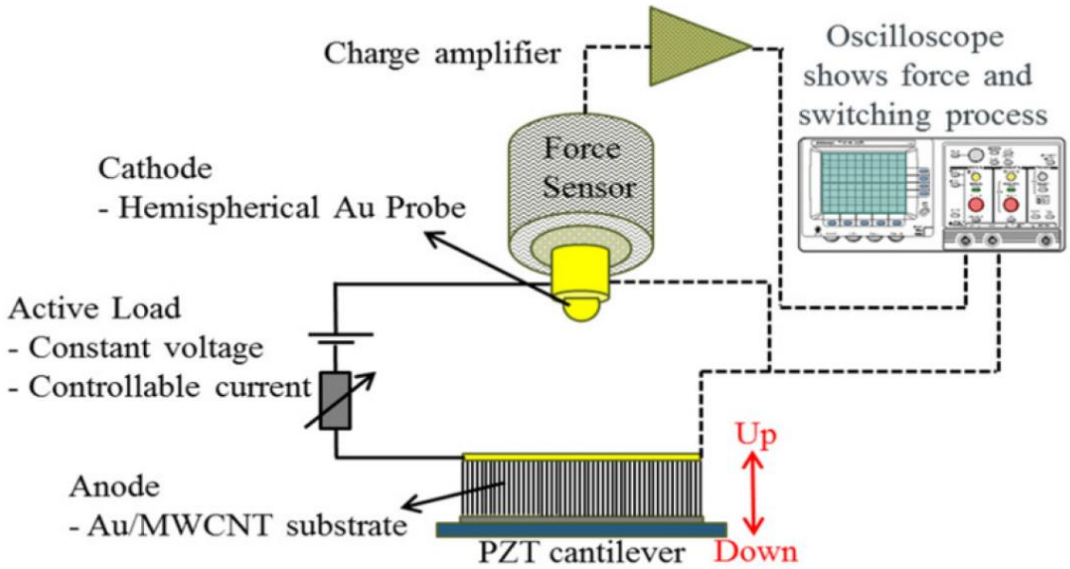

Figure 3-11 - Schematic of the PZT switching apparatus

The switching rig consists of a rigidly held upper contact (2 mm diameter stainless steel ball with a 500 nm Au coating) mounted on a quartz force transducer (Kistler Model 9207). The force

transducer is connected to a charge amplifier. As the load on the upper contact is varied, the electrostatic charge on the quartz crystal also varies which is detected and amplified by the charge amplifier. The technique can be used to detect rapidly changing and very low forces; however, the small charges involved mean that with even well-designed insulation the charge rapidly 'leaks' away when the force is static. As a result, it is difficult to measure static force, but with a measurement circuit with a time constant designed to slow the leak of charge it is possible to make "quasi-static" measurements.

The lower switching contact (Au/MWCNT composite) is attached to the end of a lead zirconate titanate piezoelectric cantilever (~50mm long and 8mm wide). When a voltage is applied to the cantilever, the beam bends and opens the contact. As the voltage is removed the beam returns to its neutral position. The cantilever motion is driven by a voltage signal from a function generator and provides a range of motion of around 100 μm. It is more accurate to measure the static closed contact force by measuring the rapid decrease in force that occurs as the contact is opened. This is because the contact force requires time to stabilise when it is closed due to the cantilever oscillating.

The contacts may be adjusted by hand in the XY plane using the microscope stage controls (this adjusts the lower contact position) and the vertical (Z) contact position by using the focus and fine focus controls. This allows the static contact force to be adjusted with an accuracy of +/- 100 μN of static contact force. The time required for the contact force to stabilise limits the system to cyclic rates of a maximum of ~ 30 Hz.

Circuit potential is supplied by lead acid batteries (Sonnenschein A500 Series) connected to a variable in-series load resistance that provides control of the steady state current. Battery temperature is maintained by the environmental control. The battery voltage is monitored to ensure it is stable while the maximum current drawn is limited to <1% of the rated peak current of 88 A.

The synchronised capture of voltage waveforms from the charge amplifier, function generator and contact potential are by the same digital storage oscilloscope described in the previous section on the capture and characterisation of the MMB.

In this work the PZT apparatus is used to carry out three experiments related to the research objectives of this work and outlined as follows and described in more detail at the end of the chapter. Experiment 1 – investigation of the hot switching current carrying capacity of the Au/MWCNT composite. Experiment 2 – to determine the influence of surface texture, circuit current

and voltage on the energy of the MMB. Experiment 3 – the influence of contact opening velocity on the energy of the MMB. The PZT system is also used force/resistance curves for the composite contact to be measured.

3.6 Development of a State-of-the-Art MEMS Lifetime Testing Apparatus with Surface Evolution Measurement Capability – the ICE Apparatus

A key objective of this study is the development of MEMS testing apparatus to repeatably cycles contacts at MEMS scale forces over billions of cycles and detect the wear in-situ. Existing studies have not measured the switching surface in-situ but have permanently interrupted the switching process through either invasive or destructive disassembly of the contact pair [15, 58, 102, 120].

A novel apparatus has been developed that allows accelerated lifetime testing of a MEMS contact and the measurement of in-situ evolution of contact wear. The system is termed the In-situ Contact Evolution (ICE) apparatus. An overview of the design is given in Figure 3-12 with close up images of the measurement head arrangement, that contact the displacement sensor, actuator and video microscope in Figure 3-13.

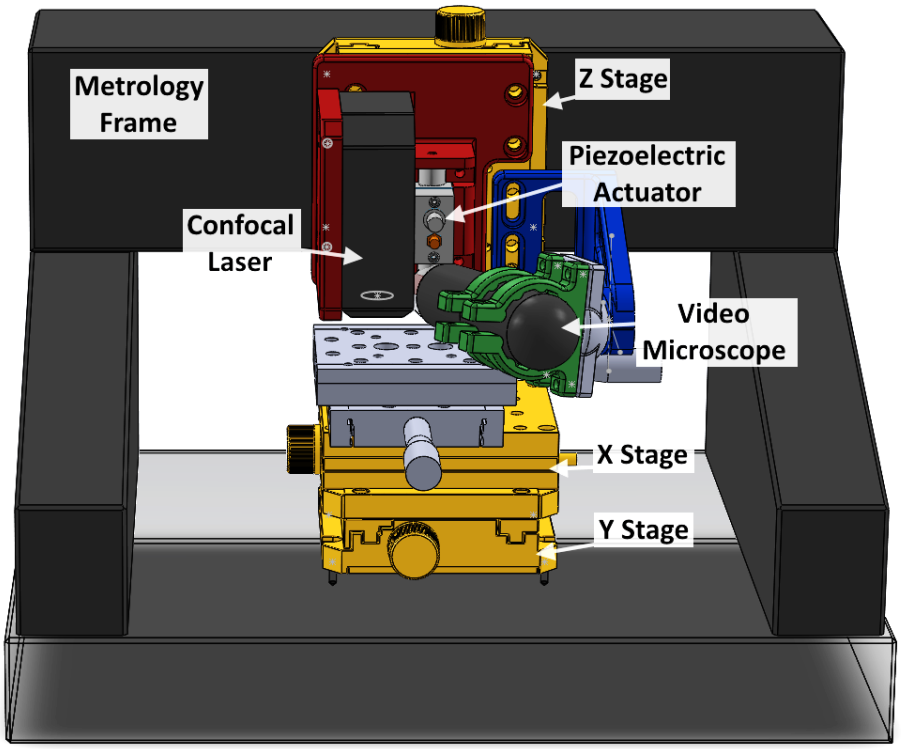

Figure 3-12 – Overview of novel MEMS testing apparatus

The system is based on an H-beam granite metrology frame as a rigid frame of reference for three automatic linear motion stages and a confocal laser displacement meter arranged as Cartesian XY and Z axes. Two additional Vernier linear stages allow the manipulation of one half of the contact with reference to the other while a video microscope provides live imaging of the contact positions. Control of the contact switching rate and motion profile is driven by a function generator whose signal is amplified and used to drive a piezoelectric actuator that provides the motive force of the MEMS contact. The frame, motion control and automatic motion system are adapted from a commercial surface profiler (TaiCaan XYris 4000 CLx).

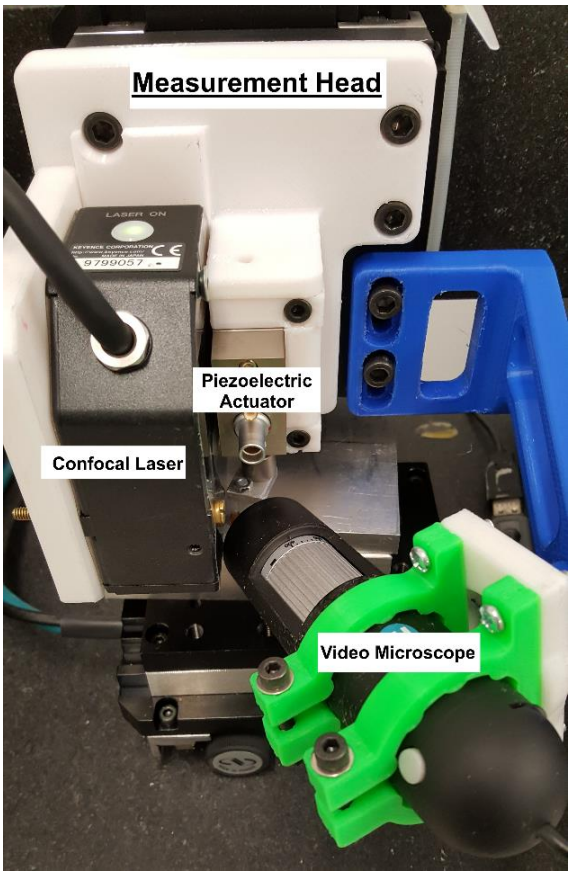

Figure 3-13 – The arrangement of the novel testing apparatus actuator, video microscope and displacement meter

The system allows the contact pair to be separated, for measurement of the contact surface, then return them to their original position with high precision for continued switching operation. The actuator can operate at cyclic rates of greater than 4 kHz, requiring less than 3 days to reach 1 billion cycles.

3.6.1 Overview of Operation

In the direct mode of operation, the upper contact is mounted directly on the tip of the piezoelectric actuator. This allows the contact geometry of the PZT apparatus to be replicated.

The operation follows four stages that are shown diagrammatically in Figure 3-14.

1) The upper contact is installed directly to the piezo actuator tip and the microscope is focused at the tip (dark grey triangle) for operator feedback of the alignment process. Concurrently the lower planar contact (light grey rectangle) is arranged on top of the XY stage assembly

2) The control software is then used to lower the automatic Z stage that brings the apparatus "head" down towards the planar contact. This is necessary to facilitate sample loading as the maximum extension of the piezo actuator is only 20 μm. Microscope feedback can be used for visual feedback of the alignment process as well as the contact resistance instrumentation that can be used to determine a precisely defined position.

3) A function generator provides a signal of the desired waveform of the actuator motion and rate. This is sent to an amplifier unit that upscales the signal to the 0 to 75V signal required by the piezo actuator. The contact is then opened at closed at the set parameters while a high speed DSO captures the transient electrical waveforms.

4) The driving signal is stopped and the XY stages translate the contact surface to beneath the confocal displacement meter for surface measurement. Upon completion the contact is returned to position where cycling can continue.

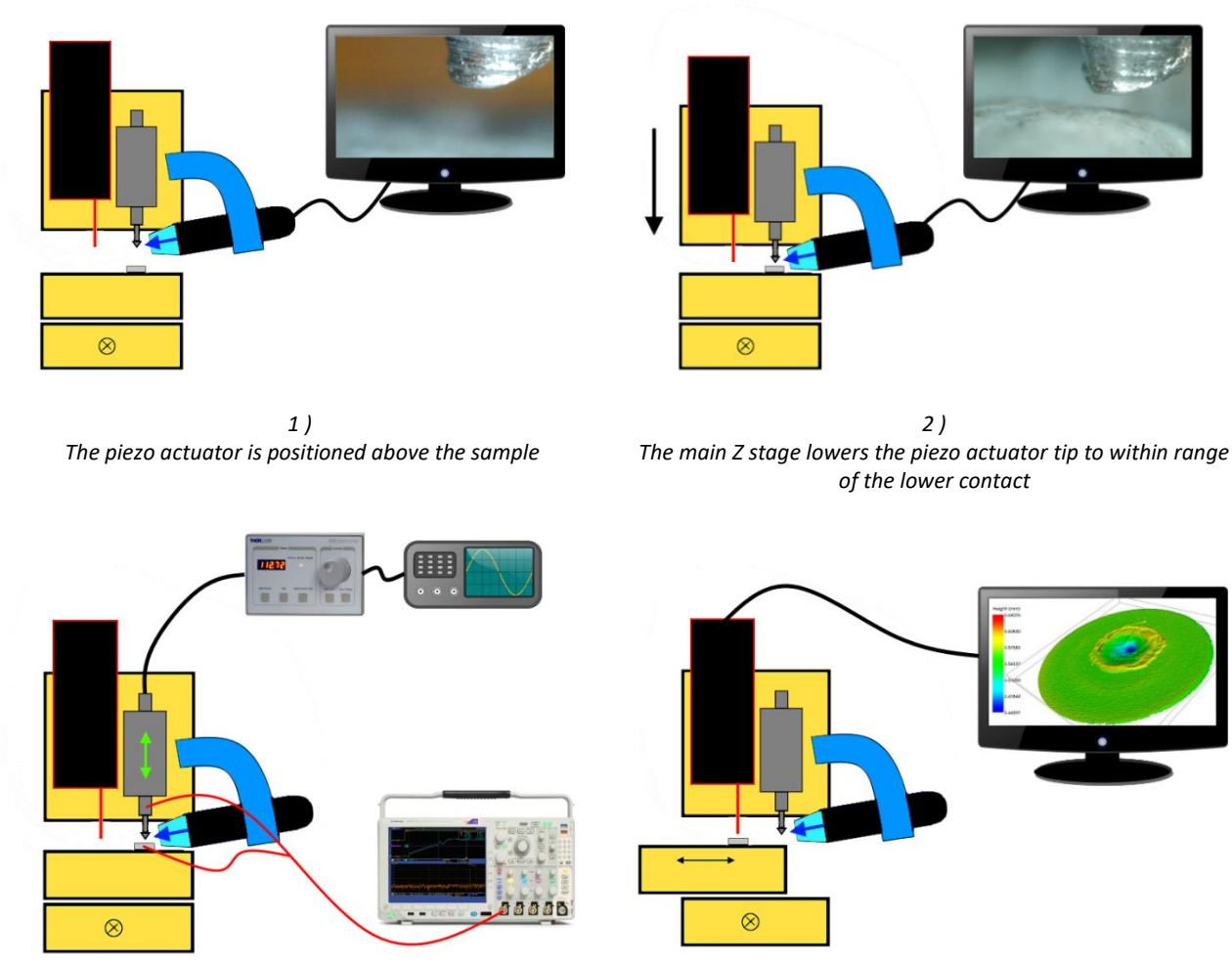

1)
The piezo actuator is positioned above the sample

2)
The main Z stage lowers the piezo actuator tip to within range of the lower contact

3)
The piezo actuator is cycled to open and close the contact while instrumentation gathers data

4)
The main XY stages move the lower contact beneath a displacement meter to record a map of the surface

Figure 3-14 – Schematic showing operation of the novel testing system in a Direct Contact Mode

3.6.2 Measurement of Contact Surface

The height of the lower contact surface is measured by the confocal laser sensor. By moving the XY stages in a raster scanning pattern a series of height measurements is built up into a rectilinear grid of XYZ coordinates creating a point cloud map of the surface. The XY area and the spacing of the height measurements is programmed through the software interface (TaiCaan Stages v1.98). Extraction of surface parameters (e.g. feature height, volume and roughness) and imaging of the

surface are prepared by commercial surface analysis software (TaiCaan Boddies 2.18 and TaiCaan BEX 1.1.7).

3.6.3 Controlling the Contact Force

As the contact resistance is linked to the contact force it is desirable that a MEMS testing apparatus can maintain contact force at least as stable as can be expected in a practical device. In direct mode of operation, the upper contact is mounted into a threaded nylon mount. The nylon mount both insulates the contact from the actuator and provides an elastic component between the actuator and the contact. Contact force is controlled by the precise position of the actuator and the compression of the contacts.

The initial contact force is set by the position of the actuator. The relationship between actuator position and contact force is calibrated using the PZT MEMS testing apparatus to calibrate the relationship between force and contact resistance. An example of this relationship is shown for a thin film gold coated silicon contact mated to a gold coated hemisphere contact in Figure 3-15. The relationship between actuator extension and contact force is linear (as shown by the inset graph) for even a relatively hard contacts due to the use of the elastic nylon mount.

The Au-Au contact requires the actuator to extend by 3 µm to increase the contact force from 0 to 2 mN. This contrasts with the highly elastic Au/MWCNT composite which requires approximately 10 µm to increase the contact force by the same amount.

The composites high elasticity can be exploited such that the composite can itself be used as a force sensor by calibrating the relationship between the contact resistance and the force applied to a contact pair.

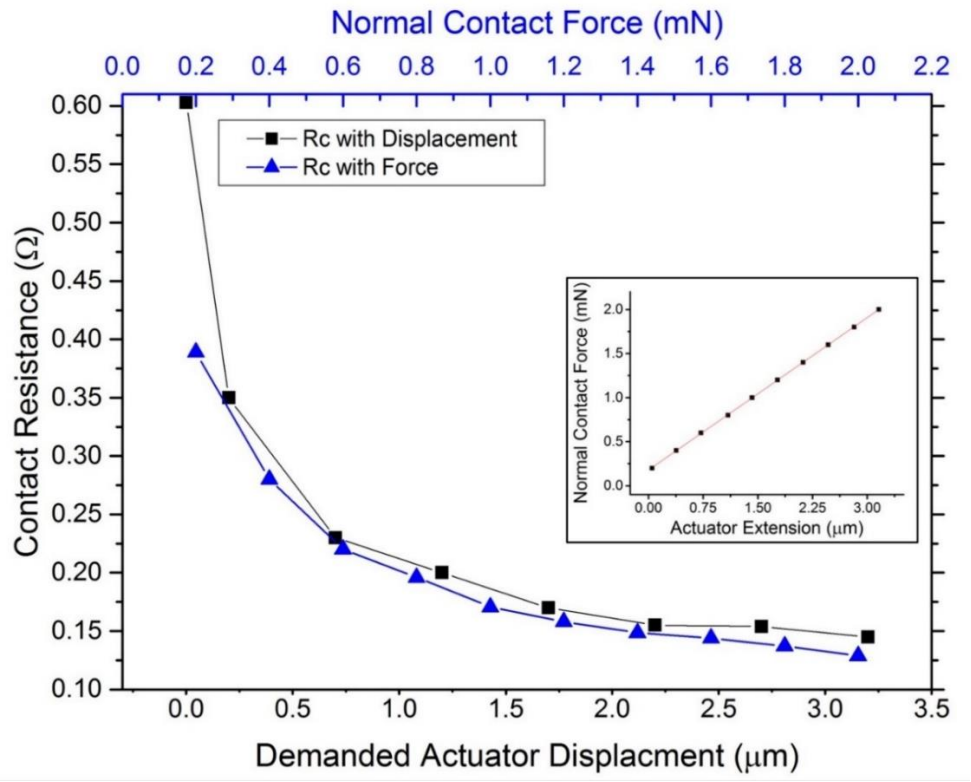

Figure 3-15 – The relationship between contact force and contact resistance with force to actuator extension (inset) for an Au coated ball to thin film Au contact pair [121]

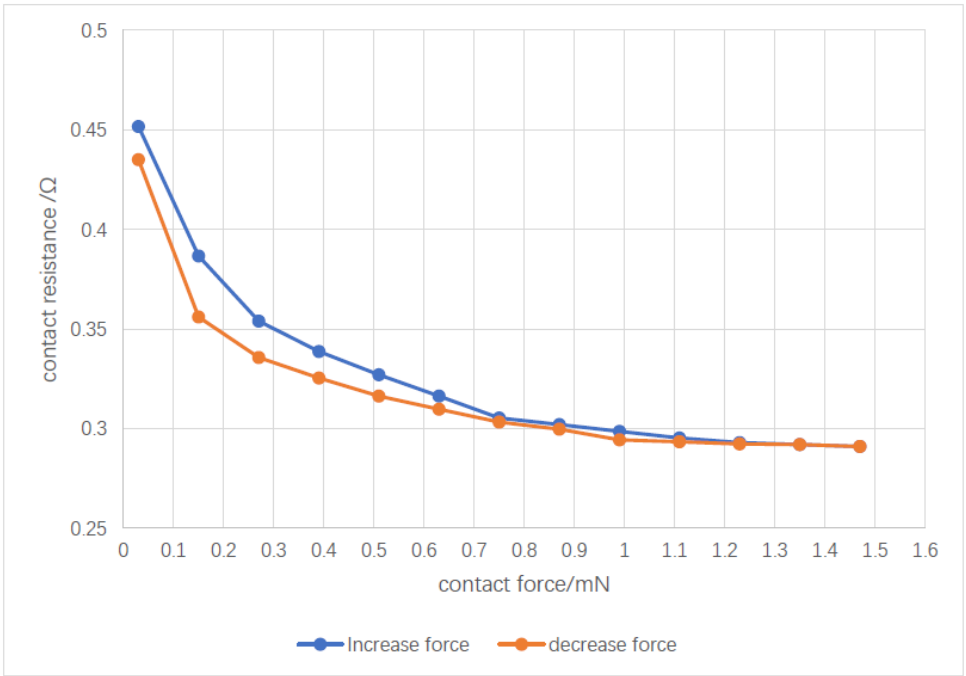

Figure 3-16 – The relationship between contact resistance and the loading and unloading force for a Au coated ball to 505 Au/MWCNT Contact Pair [Mr Wu Sample 6 Site 5]

At low forces the sensitivity to change is as great as 0.5 mΩ/μN. While the loading and unloading curves are distinct, they are unidirectional repeatable i.e. loading curves are highly repeatable. The main difference between using a rigid thin film Au contact and the more compliance Au/MWCNT contact is the latter allows force control at a lower level. Figure 3-15 shows this is limited to around 100 μN in a thin film Au surface. But similarity between loading and loading curves in Figure 3-16 shows the contact force is repeatable as low as 20 μN with an Au/MWCNT surface. This force level is equivalent to levels reported by studies using an electrostatically operated MEMS scale cantilever [122].

3.6.4 Actuation of Contact and Enhancing the Switching Rate

To achieve the required high switch actuation along with control of the motion profile of the moving contact a monolithic stack piezoelectric actuator has been selected. The stack approach offers several advantages over a cantilever.

Firstly, the monolithic stack design is very stiff, compared to a cantilever device. The first harmonic of the device used is at 22 kHz. This is much greater than a cantilever and allows an increased switching rate without the actuator resonated and bouncing during operation.

Secondly stack designs can provide a much greater blocking force. Blocking force is defined as the maximum force generated by the piezo against an infinitely stiff load. As this is not physically possible it is practically measured by extending the piezo and measuring the force required to return the piezo to the pre-extended position. Thus, the displacement with a light but varied load remains very linear. This is particularly true when the scale of the typical MEMS contact force is considered along with the blocking force generated by the device selected (>1000 N at 60 V). This is an important parameter when operating the device at frequencies >300 Hz where closed loop feedback from the inbuilt strain gauges cannot be employed to control the piezo position and the applied force must be considered.

The piezo actuators unloaded range of motion is controllable from 0 to 20 μm by the application of a voltage of between 0 to 75 V. The rate at which the piezo can change position is limited by the slew rate. In this case the slew rate, SR is limited by the maximum amplifier current, and the capacitance of the piezo, C_{piezo} where V_{out} is the amplifier output.

$$slew\ rate, SR = \frac{dV}{dt} = \frac{I_{max}}{C_{piezo}} \quad (3\text{-}3)$$

This will limit the switching frequency of the device over the full range of motion for a slew rate limited triangular waveform drive, f_{max} described by

$$f_{max} = \frac{I_{max}}{2V_{max}C_{piezo}} \quad (3\text{-}4)$$

To minimise contact impact velocity and switching time, a sinusoidal drive voltage profile is desirable. If we describe such a voltage profile

$$V(t) = A\sin(2\pi ft) + A \quad (3\text{-}5)$$

And its rate of change as

$$\frac{d}{dt}\big(V(t)\big) = 2\pi Af\cos(2\pi ft) \quad (3\text{-}6)$$

The maximum rate of voltage change is reached at zero and every n^{th} π. Solving for t=0 linking to Equation (4-2) for slew rate and substituting V_{max} = 2A the maximum sinusoidal displacement frequency, $f_{max\ sin}$ is

$$f_{\max sine} = \frac{I_{max}}{\pi V_{max}C_{piezo}} \quad (3\text{-}7)$$

For the instrumentation and piezo stack selected the maximum current, I_{max} is 500 mA and C_{piezo} is 3.6 µF this gives a slew rate of 0.139 V/µS. The highest frequency of sinusoidal cycling over the full 20 µm motion range $f_{max\ sine}$ is 589 Hz. For a reduced 5 µm motion range this is increased to 2.4 kHz.

The highest frequency achievable over the full motion range is using a square drive f_{max} of 926 Hz. For a reduced 5 µm range this is increased to 3.7 kHz.

3.6.5 System Specification

The performance of the MEMS testing apparatus performance is summarised in Table (3-1)

	Specification	Notes
Switch cycling frequency (kHz)	3.7*	5 µm range*
Measurement Resolution Surface Height (nm)	10	
Measurement Resolution Volume (μm^3)	2.5 $x10^{-3}$ **	* at 250 nm XY grid spacing
Contact Potential sampling (GHz)	2.5	
Contact Potential noise floor (µV)	130	

Table 3-1 – A summary of the performance specification of the ICE Apparatus

3.6.6 Positional Feedback using Video Microscopy

Previous systems featured limited or no operator visual feedback in the set up and operation of the system. To address this limitation a 400x optical video microscope with adjustable focus and light source has been integrated to provide a magnified view of the contact pair. The microscope is nominally held just off horizontal, to allow the contact separation to be easily viewed. Cylindrical clamps and a ball joint mechanism hold the body of the microscope such that its orientation can be adjusted. The mount is held fixed to the automatic Z stage such that the field of view is fixed with reference to the piezoelectric actuator. The video feed is sent to the command and control computer system and the status of the apparatus can be remotely monitored (e.g. for contacts sticking).

The magnification is enough for the operator to visually detect micron scale adjustments in the contact position within a field of view ~ 0.50 mm by 0.35 mm and hence assists with both the coarse and fine positioning of the contacts. The shallow depth of field is set such the contact point is in sharp focus. This provides the operator with a degree of depth perception in the imaging. The two images below (Figure 3-17) show a 5 µm vertical adjustment in the Z position between a test target

(white modelling clay) and a test tip (M4 screw turned down to ~200 µm point). It is noted that is easier to visually detect motion using a video feed rather than static imaging.

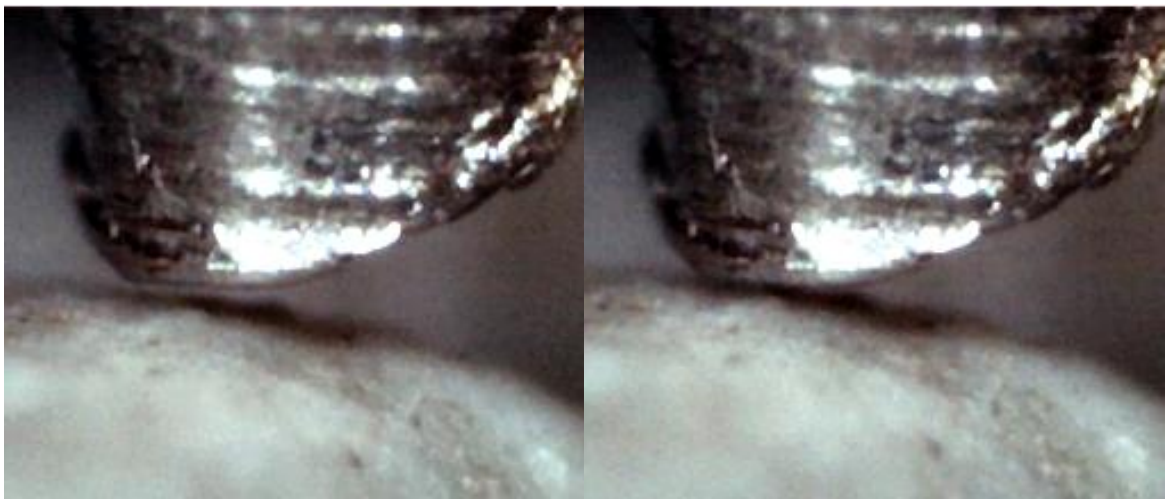

Figure 3-17 – Visual Feedback of a 5 µm Height Change of the Upper Contact (silver) to the Lower Contact (white) – (left higher with perceptible gap – right lower with no gap perceptible) lowering

3.6.7 Thermal Considerations

While changing to an electrostatic from a displacement-based actuation provides simplification in terms of the packaging and arrangement of the mobile contact with an electrostatic contact, it is important to consider the applied force is now dependant on a motion rather than an electrostatic force. As such any variation in the absolute position of the actuator, rather than applied voltage, can introduce a variance in the contact force.

Thermal effects on the performance of the apparatus can be considered due to thermal expansion of materials, variation of resistance with temperature (and humidity) and the change in the refractive index of air with temperature (also humidity and pressure).

Many of the parameters to control thermal effects are considered in the design and selection of the XYris 4000CLx profiling instrument for incorporating in the MEMS testing apparatus. The use of a stone metrology frame provides a high thermal mass and a low coefficient of thermal expansion. The gabbro-norite mineral, known commercially as Belfast Black Granite, has a low thermal expansion coefficient, α of $< 8.4 \times 10^{-6}\ K^{-1}$ with a specific heat capacity of 790 $Jkg^{-1}K^{-1}$ and a low thermal conductivity [123]. The mass of the frame is 38.97 kg, providing a heat capacity of 30.8 kJ/K. The

high mass and specific heat capacity with low thermal conductivity help to stabilise the temperature of the frame with respect to small oscillatory fluctuations in the local air temperature.

The automatic linear stages are selected to control contact position. They incorporate absolute linear encoders manufactured from a proprietary aluminosilicate glass-ceramic (Zerodur by Schott AG) with an extremely low α value, 0.05 $x10^{-6}$ K^{-1}. The encoders serve to provide an absolute reference for the on axis position of the stage that is thus minimally effected by temperature fluctuation [124].

3.6.8 Vibration Isolation and Damping

The apparatus is isolated from floor transmitted vibration by a 750 mm x 750 mm x 110 mm vibration damping optical breadboard surface. It has stainless steel honeycomb cell internal structure coated in elastomeric polymer that provides a work surface with broadband damping properties. The work surface is supported by a 4-point, self-levelling pneumatically-damped spring system (Newport Corporation, USA). The damping system isolates the work surface by means of a chamber of compressed air with a flexible membrane sealing the top and a pneumatic release valve designed for a highly laminar flow during operation.

The work surface is connected to the chamber by a piston that rests on the flexible membrane. Motion of the lower section is isolated by the inertia of the work surface and the low viscosity of the air. The energy of the vibration is dissipated by the viscosity of the laminar flow of air into and out of the pneumatic valve. A schematic of this damping mechanism is shown in Figure 3-18.

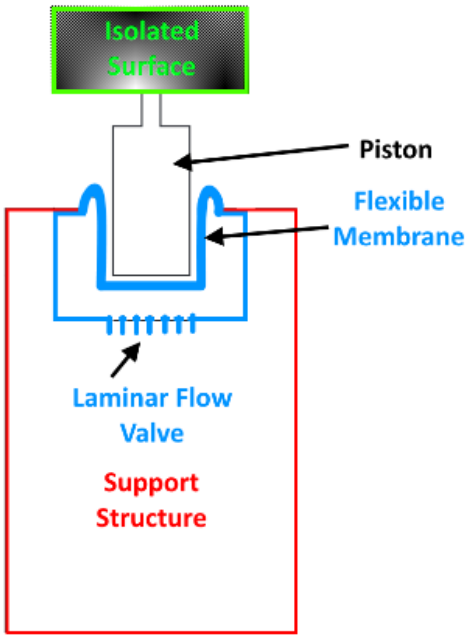

Figure 3-18 – Schematic of the air damping mechanism supporting the isolated surface

Damping characteristics of the air damping are optimised for attenuation of vibration to -40 dB in the 20 - 50 Hz band most prevalent in multi floor buildings [101]. The primary mode of resonance is at 1.5 Hz.

The optical breadboard surface provides a stiff support surface with broadband damping in the 100 to 250 Hz range. The first fundamental resonance occurs at ~350 Hz that is a significantly higher frequency than typical floor transmitted vibration.

The enclosure and isolation from drafts and other air transmitted vibration is achieved using a simple box structure, constructed from 10 mm transparent acrylic sheet with small cut outs for instrument and power cables. This is placed over the apparatus during operation. The thermal output of the system components results in a small temperature rise in the enclosure and the system must be left to reach thermal equilibrium before operation. This stabilises temperature to better than 0.2 ^{o}C over 24 hours.

A final note is that the use of a hermetically protected environment was desired for operation. The potential leak risk of an asphyxiant gas in a laboratory with no outside ventilation has serious safety implications. Demonstrating the performance of Au/MWCNT contact material in ambient atmosphere illustrates a significant practical advantage over technologies that require hermetic

packaging. However, control of the gaseous environment in the testing apparatus is identified as a target for future work.

The results from a validation and testing program are appended [Appendix 2 –Validation and Test of the ICE Apparatus Performance].

3.7 Experimental Plan

The sequence of planned experiments is related to the task based objectives of this project and are as follows:

Experiment 1. The capabilities of the newly developed ICE apparatus for MEMS testing will be tested by investigating in-situ contact wear during individual hot and cold switching cycles of a thin film Au contact. The objectives are to determine the lower limits of surface evolution as a result of individual low force contact cycles, and to demonstrate the development of a system that detects in-situ contact evolution. Before studying the Au/MWCNT contact material the novel ICE MEMS testing system is used to investigate the surface of a thin film Au contact. The thin film Au contact is used to demonstrate the actuator displacement to contact force relationship is accurate. The low compliance of the thin film Au results in the most sensitive actuator displacement to contact resistance relationship. Further, the surface of the thin film Au is very smooth and small changes in the surface can be visually detected more easily than against the background of a rough surface such as the Au/MWCNT composite.

Experiment 2. The investigation is moved to the study of the 505 Au/MWCNT contact material using the PZT apparatus to determine the current switching limit of the Au/MWCNT surface. A Au coated hemisphere contact is paired with a planar 505 Au/MWCNT contact. A switching current of 10, 20, 50, 100, 200, 345, 450 and 600 mA is applied to the contacts while they are cycled and the transient voltage waveform is captured. The point at which the characteristic transient voltage waveform of the Au MMB is used to determine where the contact surface has failed. The breakdown mechanism of the Au/MWCNT during current overload is analysed and characterised.

Experiment 3. The second experiment using the PZT apparatus is to investigate the influence of current, voltage and surface roughness on the molten metal bridge phenomenon during hot switching of the Au coated ball to Au/MWCNT contact pair. The energy of the molten metal bridge is

evaluated in the current range below the determined failure limit (10 – 200 mA) while the circuit conditions (current and voltage), surface texture and contact opening velocity are varied.

Experiment 4. The third experiment using the PZT apparatus is to investigate the influence of contact opening velocity on the molten bridge phenomenon and the forces that occur during contact separation. An Au coated ball to Au/MWCNT contact is hot switched at 4V 50 mA while the contact opening velocity is varied from 80 to 8000 μm/s while the MMB is evaluated. A limit to the MMB is detected and this leads to the investigation of the transient contact separation force associated with the MMB.

Experiment 5. Using the new MEMS testing apparatus, the influence of circuit current and voltage on surface wear in the Au/MWCNT contact will be investigated. The influence of circuit current (20 and 50 mA) and voltage (4 and 8 V) on the fine transfer process is investigated using the ICE MEMS testing system. Au coated hemisphere to Au/MWCNT contacts are cycled over 100,000 switching cycles while the surface wear is measured in-situ. The evolution of the surface texture and the influence of the circuit conditions are characterised.

Experiment 6. The enhanced switching rate of the new MEMS testing apparatus is used to carry out switching cycles of Au coated hemisphere to Au/MWCNT until contact failure or reaching more than 3 billion cycles while contact wear is characterised. Two circuit conditions are investigated: effectively cold switching conditions and hot switching conditions at 4 V 50 mA.

The empirically derived lifetimes are then used, along with the data developed in the previous experiments, to develop an enhanced model for predicting the switching lifetime of the Au/MWCNT contact under a range of force and current conditions.

4 Results

In this chapter the findings of the work are presented. The chapter covers six main sections related to the research objectives identified in the previous chapters and the experiments intended to achieve them.

4.1 Experiment 1 - In-situ Surface Wear Switching a Thin Film Gold Contact

Previous investigation of surface wear in MEMS switching surfaces has been limited to the completion of switching. In this section the surface change that occurs in the first few operations of a thin film Au contact are detected and characterised under both hot and cold switching conditions using the ICE apparatus. The objectives are to demonstrate the performance of the newly developed ICE apparatus in the detection of in-situ wear and to determine the lower limits of the evolution of surface wear.

The ICE apparatus is used to switch a contact pair, where the upper ball contact is mounted directly on the piezoelectric actuator. The contacts are brought into proximity and then pushed together by bringing the upper contact down until the contact closes. The contact closure process is shown by video microscope in Figure 4-1.

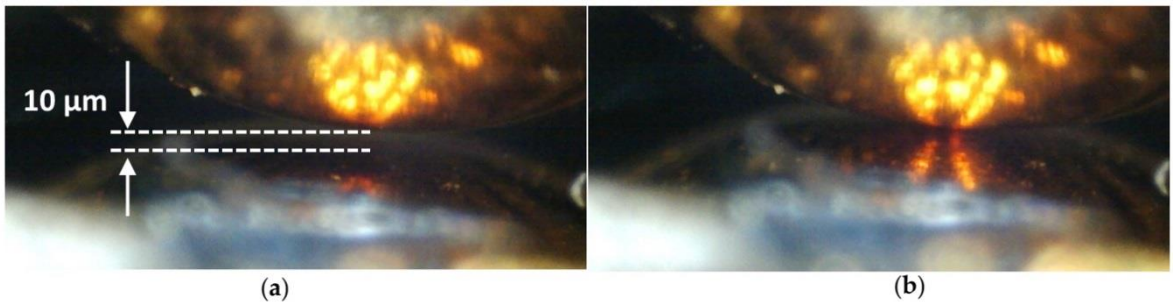

Figure 4-1 - The contact pair shown through the 400x integrated video microscope a) with a 10 µm separation between contacts and b) in contact

The relationship between contact force and contact resistance is calibrated using the PZT Cantilever apparatus described in section 3.5, by setting the contact force to the required level and recording the corresponding contact resistance. The relationship between contact force, the demanded contact displacement and contact resistance is shown in Figure 3-15.

The contacts are pressed together until the contact resistance is reached that corresponds to the normal contact force required for the test. This is either 100 µN (cold switched test) or 500 µN (hot switched test). A higher contact force is used for the hot switching case to minimise contact heating while the contact is closed. The contact is held stationary for 30 seconds to allow the contact interface to stabilize before the resistance is recorded.

The circuit load of 4V DC 20 mA is then connected, and current allowed to flow for 10 seconds before the contacts are demanded to open by 0.1 mm at a maximum acceleration of 100 mm/s^2. The load circuit is then disconnected, and the lower contact surface is measured using the laser profiling system. Once the surface is measured the contacts are brought together at the same position and the process is repeated. The surface measurements are evaluated for roughness and the volume of material that has been transferred using commercial metrology software (Boddies 3D v2.18, TaiCaan Technologies).

4.1.1 Contact Switching with no signal (Cold Switching) at 100 µN

The measurements of the Au contact surface after switching the contact with no load power over 10 cycles at 100 µN of closure force are shown in Figure 4-2.

The number at the bottom left of each image indicates the number of switching cycles the surface has experienced. The contact surface is measured before any switching has occurred (0 cycles) over a 0.7 mm by 0.7 mm region. After a single switching cycle the area is remeasured and the precise point of contact is located and remeasured in greater detail. The colour scale indicates the surface height and the full colour scale is set to +4 to -2 µm from a reference plane of best fit to the nominal surface. At the completion of switching the contact is removed from the ICE apparatus for imaging using colour video microscopy (bottom right image).

After a single switching operation, a roughened and raised pattern appears. The pattern is raised approximately 500nm above the nominal surface and is around 50 µm in diameter. The shape of the site corelates well with microscopy of the same region, which also shows the pattern to be gold coloured.

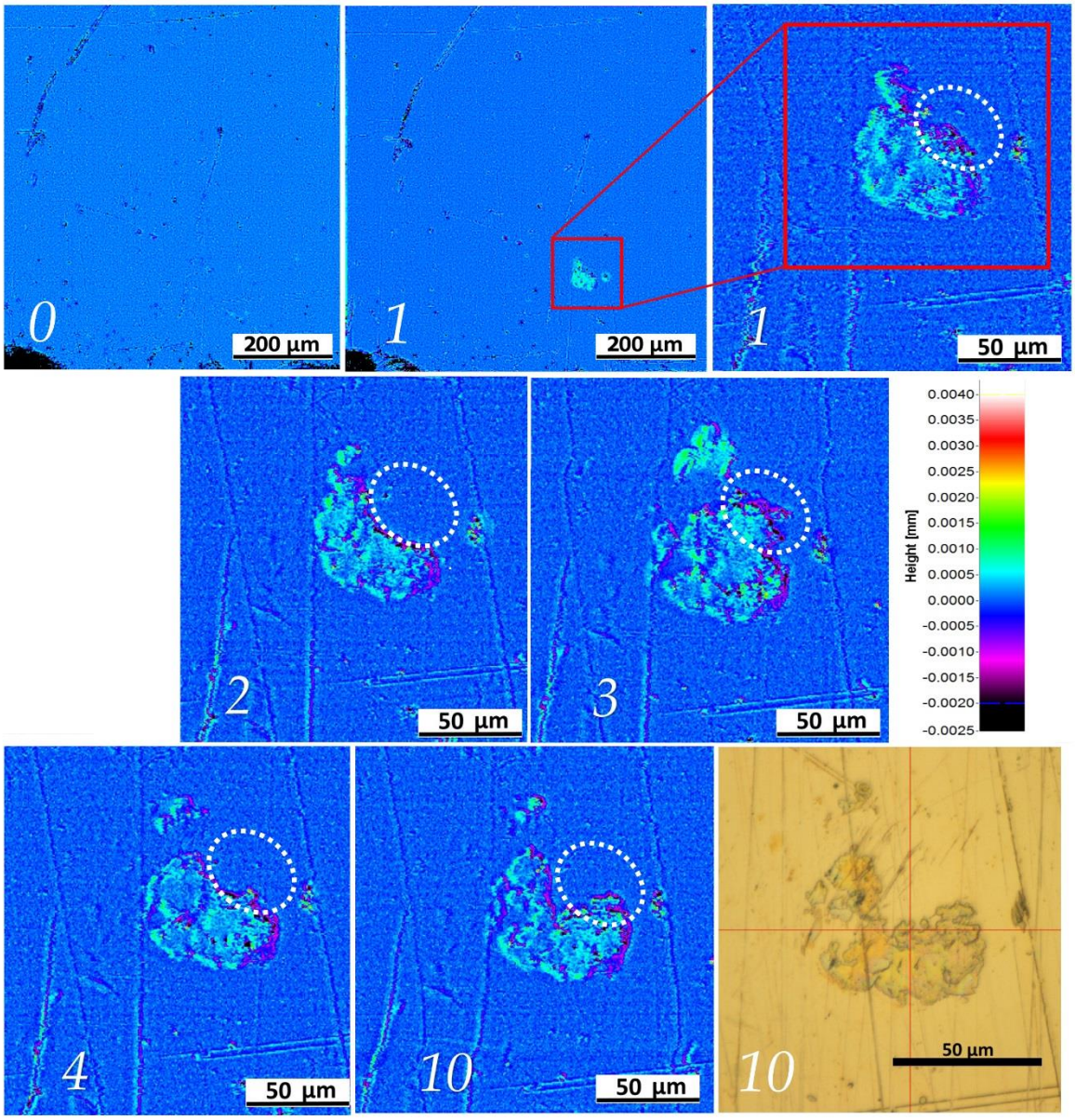

Figure 4-2 – Surface measurements of the lower contact during a cold switching sequence at 100 uN normal contact force. At 0 (before switching), 1, 2, 4, and 10 cycles. The white dotted region shows an area of material transfer

The progression of contact resistance and the surface roughness is presented in Figure 4-3. Contact resistance initially increases and is relatively unstable over the first 5 switching cycles varying ~250 mΩ, before it stabilises over the next 5 switching cycles and variance decreases to ~40 mΩ. The surface roughness increases over the first 5 cycles to 200 nm and fluctuates by upto 50 nm, while the second 5 cycles show the roughness stabilises around 175 nm varying no more than 10 nm. The overall trend between contact resistance and surface roughness (inset graph) shows a correlation between increasing surface roughness and increasing contact resistance.

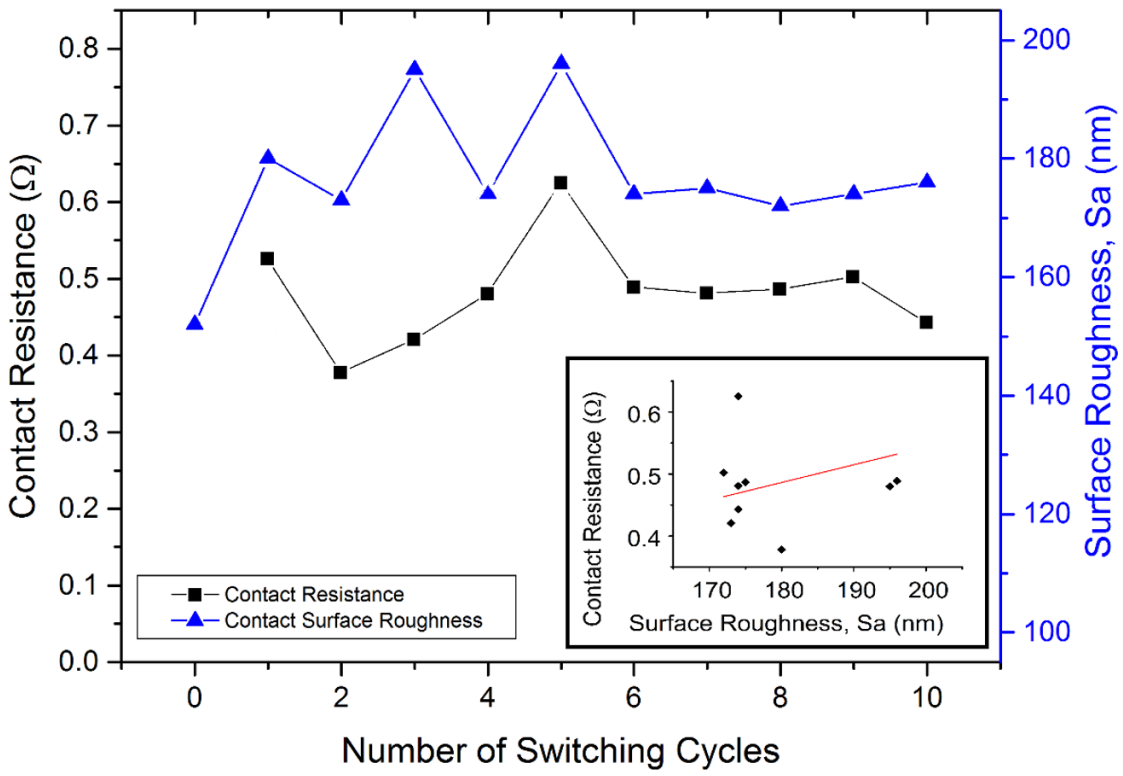

Figure 4-3 – The evolution of contact resistance and surface roughness over 10 cold switched cycles

The evolution of the volume of material transfer to the lower planar thin film Au contact surface is shown in Figure 4-4. The zero datum for volume transfer is defined by a plane fitted using a linear least squares method to the nominal surface (i.e. the unworn region). Net material above this plane is defined as positive transfer (deposition) onto the lower contact. The figure shows that after a single cold switching event there is a net deposition of 0.38 μm^3 of material. After the second cycle the deposited volume decreases to 0.22 μm^3, before increasing again to 0.43 μm^3 after the third cycle. This pattern of transfer continues but decreases in magnitude, until after the 8th cycle the material transfer stabilises at around 0.22 μm^3 of material deposited on the lower contact surface. This transfer pattern correlates with the appearance and disappearance of material highlighted by the white dotted region shown in Figure 4-2.

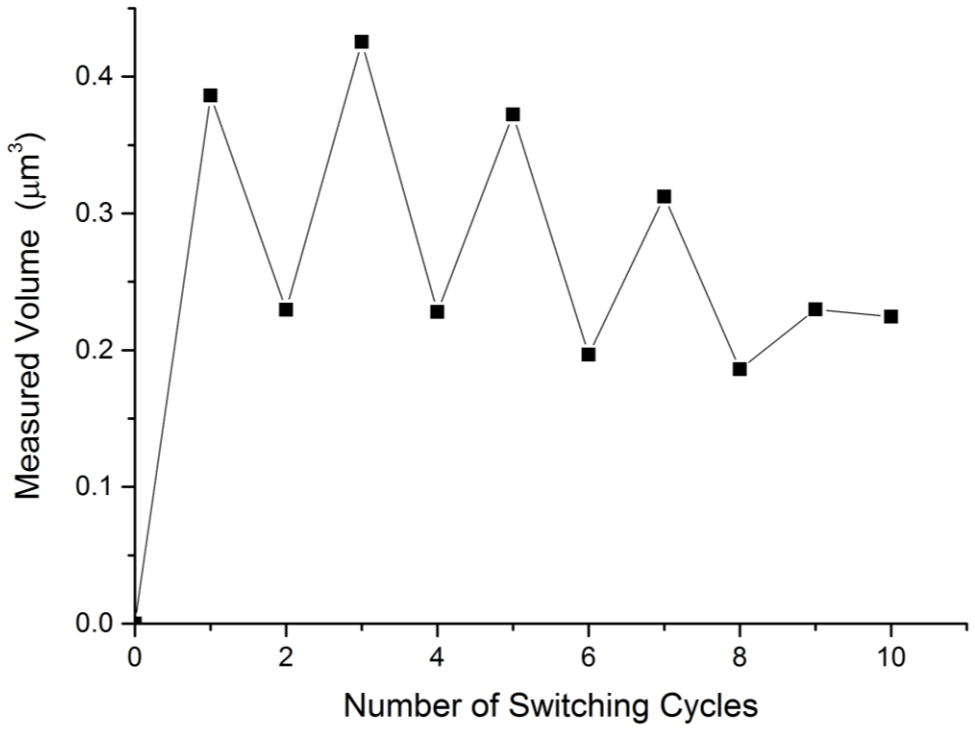

Figure 4-4 – The evolution of volume of material deposited on the lower contact surface over 10 cold switching cycles

4.1.2 Contact switching with a 4V DC 20mA Signal (Hot Switching)

A hot switched contact surface is investigated using the same method, but with a normal contact force 500 µN. The evolution of the measured surface is shown in Figure 4-5. The vertical scale is again indicated by colour scale, but in this case the scale is +1.0 µm to – 0.5 µm. This is 25% of the range scale used in the cold switched surface shown in Figure 4-2.

A circle with a white dashed outline is used to indicate the region of wear. Height cross sections of surface features labelled AB and CD are presented after 1 and 20 switching cycles. A wear pattern can be seen in a ring-shaped region approximately 50 µm in diameter. After a single switching cycle features AB and CD can be observed as a step approximately 500nm below (purple/black) to 500 nm above (green) the nominal surface of the gold film. After 4 cycles the width of these features, as well as the height/depth decreases. After 20 hot switching cycles the CD feature is nearly imperceptible, while the AB feature has reduced in magnitude. The height and depth suggest delamination of the 500 nm Au film.

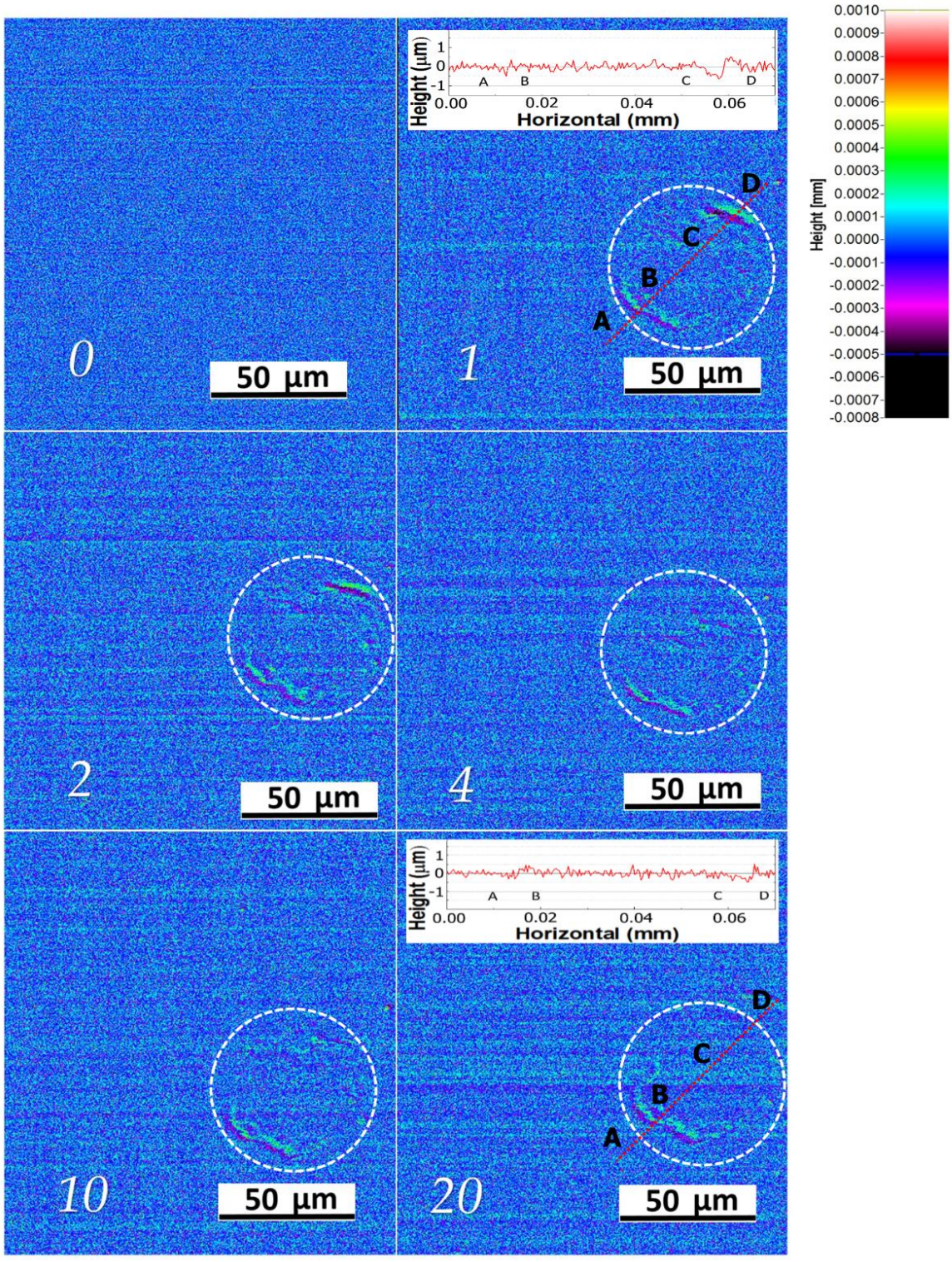

Figure 4-5 – A sequence of measurements of the lower contact during a hot 20mA 4 VDC switching sequence at 500 uN normal contact force. 0.15 mm x 0.15 mm region after 0, 1, 2, 10 and 20 cycles

The progression of the contact resistance (black squares) and surface roughness (blue triangles) is presented in Figure 4-6, together with the trend between surface roughness and contact resistance

(inset graph). Both roughness and contact resistance show an increase over the first two contact cycles, before they both settle and relatively stable between cycles 5 and 20. The observed trend is again for an increase is surface roughness to correlate with an increase in contact resistance.

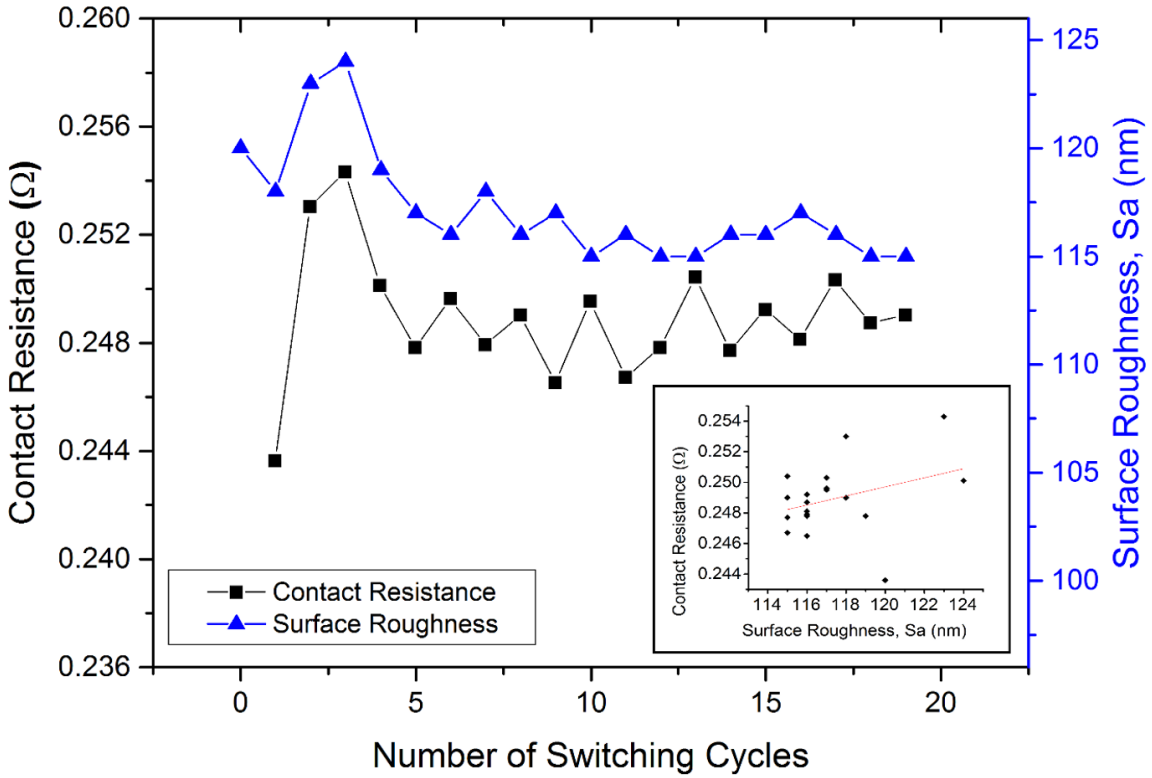

Figure 4-6 – The evolution of contact resistance and surface roughness over 20 hot switched 4V 20mA switching cycles

4.1.3 Delamination Event Voltage Waveforms between thin film Au contacts

The transient voltage waveform between contacts is recorded immediately prior to the contact opening for each hot switching cycle. Two distinct types of waveform are observed, and examples are presented in Figure 4-7.

The first type (cycles 16 and 20 – red and blue traces) is characterised by a rise from the small voltage drop associated with the normal closed contact resistance, to an irregular fluctuation between 0.38 V and 0.88 V before the contact potential rises abruptly to the open circuit voltage (nominally 4 V). These voltages are the melting and boiling voltages for Au. The observed waveform is characteristic of a molten metal bridge (MMB) forming between the contacts as the reduced

contact area results in increased current constriction and the surface interface changes through softening melting and boiling before the final asperity in contact becomes liquid, boils and the contact is broken. The 3rd, 5th to 13th and 15th to 20th opening events are of this molten metal bridge (MMB) type.

The second waveform (cycle 1 – black trace) is an abrupt increase from the normal closed contact voltage drop, to open circuit potential with no intermediate process apparent. This waveform is observed to occur immediately before the appearance of the AB and CD features suggesting the gold film has torn and delaminated from the surface. We term this new waveform a "delamination event" or DE. The 1st, 2nd, 4th and 14th cycle are DE type waveforms.

When the change in surface roughness is evaluated for each waveform type it is found the MMB event is associated with an average change of 1.06 nm, while the DE waveform is associated with a much greater change of 3.25 nm.

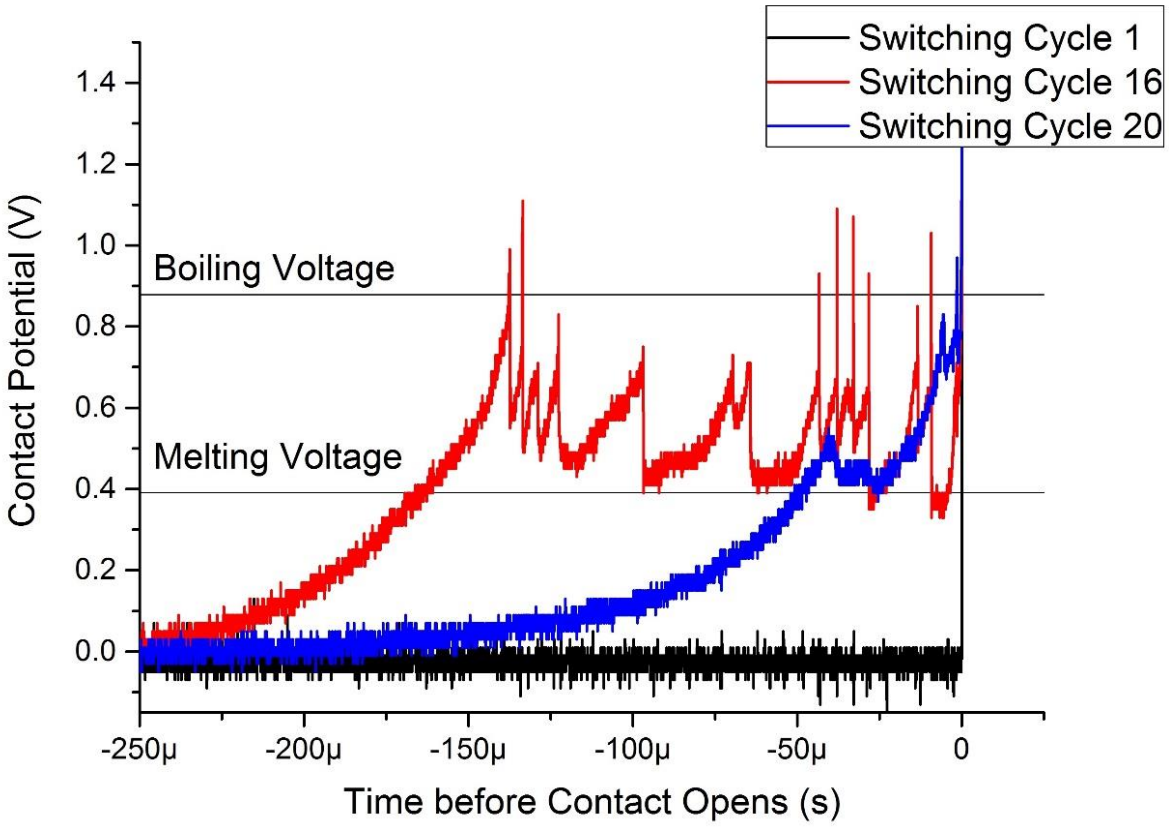

Figure 4-7 – Contact potential immediately before contact opening showing MMB and DE type opening waveforms

4.1.4 Discussion

Cold Switched Contact Sequence

The contact resistance, surface roughness (Figure 4-3), volume transfer (Figure 4-4) and surface imagery (Figure 4-2) all suggest that the contact pair experienced a delamination of the Au film from the upper hemispherical contact during the first switching cycle. Some of this material was then transferred back and forth between the contacts with the volume of transfer decreasing with continued cycles, shown in Figure 4-4. The initial phase of switching is well known to demonstrate a gradual decrease in contact resistance as the surfaces begin to conform to one another and 'bed in'. Laurvick et al observed the initial phase of switching with Au-Au MEMS contacts coincides with the greatest variation in contact resistance during the switching lifetime; however they noted that where the decrease in contact resistance was not smooth and gradual, it correlated with the premature failure of the device [125]. It is seen that over the first 5 cycles both the contact resistance and surface roughness do not show a smooth and gradually decrease but fluctuate. In this study the appearance of a deposit on the lower Au contact, that is gold coloured indicates a delamination of the Au film from the upper contact. The relatively large variance of contact resistance of ~250 mΩ indicates the contact interface is unstable during this period. That a delamination of the Au film on the upper contact does not result in total failure is expected. This is because the substrate of the upper contact is a stainless-steel ball and continues to prove a conductive pathway. The observation in this study of an initial delamination effect linked to unstable contact resistance suggests a mechanism where initial variability of the contact resistance indicates a defect in the contact interface which can be initially tolerated but will result in premature failure [125].

The trend observed for increasing roughness to correlate with increasing contact resistance (inset graph Figure 4-3). As the surface volume change stabilizes the contact resistance is also stabilized, but at a higher level than the 0.45 Ω measured at the initial closure on the undamaged interface, suggesting the change in surface texture is at least partially responsible. As the material transfer is reduced, the contact interface will evidently be more stable, and therefore the contact resistance also stabilizes. This suggests the Au film has at least partially re-adhered to the ball. Jensen et al observed the adhesive forces between Au-Au MEMS switches were dependent on both adhesive forces between surfaces in the apparent contact area but of also by the metal-metal adhesion in the real contact area [39]. With the contact resistance primarily dependent on the real contact area any

change in adhesion between contacts cannot be inferred from the contact resistance alone. It is noted that the observed detachment of the Au film from the substrate will allow significantly increased rates of strain in the film and thus an increased rate of strain-hardening. This may be a contributory factory to the increased contact resistance as a harder contact material evidently provides a smaller contact area for a given force.

Adhesion in Au contacts is a recognized problem and this presents a significant failure mechanism for the MEMS switch, particularly when the poor adhesion of Au to Si/SiO substrates is considered. In this study an adhesion promotor (Cr) was used, previously demonstrated by Lewis et al to enhance switching lifetimes in Au contacts [126]. However, while this study was carried out under controlled temperature and humidity, the test environment was not under hermetic seal or inert gas, and the presence of water vapor and hydrocarbon contamination is expected. These are both recognized as factors in influencing self-adhesion of Au, an effect would be reduced in a practical Au thin-film device by sealing under an inert atmosphere [39, 127].

Hot Switched Contact Sequence 20mA

A wear scar appears after a single switching event that is described by a toroid where the thin-film surface shows partial tearing and wrinkling at opposing sides (Figure 4-5, cycles 1 and 2). The height of the features AB and CD shown in Figure 4-9 are ~500 nm. This is the deposited Au film thickness and it suggests that the film has torn, delaminated from the substrate and shifted laterally to expose the Si wafer. The toroidal wear shape is significant as it has been previously been shown analytically and empirically that the maximum current density occurs preferentially at the edges of the contact region [6,34]. The visual representation of the surface height in Figure 4-5 show the greatest change occurring at the 1st, 2nd and 4th cycles at the AB and CD features. The voltage waveform observed at these cycles was not representative of a MMB event and suggests the contact area has not decreased gradually, but suddenly. The change in surface roughness associated with this “delamination” type waveform is over three times greater than observed for the MMB type.

Cross sections comparing the AB and CD features in Figure 4-5 after the 1st and 20th cycle show they have reduced in magnitude after 20 cycles. The trend of decreasing surface roughness is also seen in Figure 10 from the 5rd to 20th switching cycle onwards. The 14th cycle shows also corelates to an increase in roughness and this is the final “delamination” type voltage waveform. It appears that the feature at CD is a tear in the Au film that is gradually closed as switching continues. During the initial

phase of switching it is apparent that the local contact pressure in the real area of contact will be higher as the most prominent surface asperities in contact undergo plastic deformation and additional surrounding asperities begin to distribute the contact load more elastically as the contacts "bed in" [70, 125]. It is during this initial phase where the higher local pressures and plastic deformation are most likely to result in cold welding. The observation of the delamination waveforms occurring in early switch operations (1st, 2nd and 4th) suggests a correlation with the period of highest plastic deformation. Recent study has shown that hot switched MEMS contact welding is observed regularly at conditions of 10 VDC and 80 mA, and sporadically at 10 VDC and 60mA; however the study did not specify the contact closure force, and the reported contact resistance suggests it was higher than this study [128].

As the switching sequence continues, it is apparent from Figure 9 that the tear in the thin-film Au observed at the CD feature of the contact region is visible reduced and appears to be smoothed out. The smoothing effect is confirmed by the progression of roughness from the 5th switching cycle (Figure 10). The surface roughness and contact resistance decrease, with all but one of the last 15 opening waveforms characterized by MMB type events. The observations of Laurvick et al, that over long term switching the irregular progression of contact resistance corelated to premature device failure [125] is noted, as in this study the largest changes in contact resistance correlated with the largest changes in surface texture and the appearance of apparent tears in the Au film.

These observations suggest the delamination events are associated with a higher level of damage to the Au film, while the MMB type events correlate to decreased damage, film smoothing and perhaps even repair of the film.

Summary

In summary, the results demonstrate that the ICE apparatus achieves a key objective of this work, and can detect microscale surface change resulting from individual switching cycles at the low force MEMS switching regime. The surface changes are linked to the contact performance by the correlation between increasing surface roughness and increased contact resistance in both cold and hot switched cases. This is as expected for first few cycles of a very smooth thin film Au contact, where any increase in surface roughness indicates wear / material transfer has occurred and the pristine hemisphere on planar contact geometry is altered which would increase the current constriction at the interface and increase contact resistance.

In an unexpected finding, the hot switching condition, expected to provide a more demanding conditions for the contact where both mechanical and electrical wear mechanisms are present, corresponds to lower overall surface wear than the cold switching. A previously unreported case where a MMB is not formed during hot switching is observed and linked to an increased level of surface wear cf. where the MMB is observed. The event is characterised by a three times greater change in surface roughness caused by apparent delamination of the Au film. The abrupt increase in contact potential where no MMB is termed a delamination event (DE). The observation is significant as it indicates that hot switching conditions at 4V 20mA are less strenuous for the contact than cold switching conditions for a thin film Au contact.

The DE is investigated further in the Au/MWCNT composite contact in Experiment 4 where the force at the contact and mechanism is investigated further.

4.2 Experiment 2 - The hot switching current tolerance of the Au/MWCNT material

In this experiment the practical upper limit to the hot switched current carrying capacity of Au/MWCNT is investigated using the PZT apparatus. This data is required to determine the mode of failure when the surface experiences too great a DC current, and to establish a suitable current range for investigating the behaviour of the molten metal bridge in the following section. A Au/MWCNT lower contact is paired with a Au coated hemisphere upper contact and switched at 4 V while the load current is varied. A Au/MWCNT composite with greater than usual surface roughness is used. This is because it provides relatively large MMB that are convenient in this experiment as deviation from the MMB waveform is easier to detect. The rough sample and the influence of Au/MWCNT surface roughness on the MMB are described in more detail in the next section.

The contact is operated using the PZT cantilever apparatus (Figure 2-26) as we are only interested in a small number of switching events. The contact mechanism is driven open and closed by a 0.5 Hz square wave signal at a closure force of 150 µN. For each condition the contact is cycled 100 times with no current to allow the contact interface to mechanically stabilise or “bed in”. Contact potential is captured as the contact opens for fifty consecutive hot opening events at currents of 10, 20, 50, 100, 200, 350, 450 and 600 mA. The upper current limit of 600 mA is imposed by the fusing limit of the filament used to wire up the contacts. The test circuit is arranged as per Figure 3-11. Contact resistance is recorded before and after hot switching.

The contact resistance before and after 50 hot switched cycles against the switching current is presented in Figure 4-8. The figure shows that after 50 hot switching cycles there is a slight decrease in the contact resistance for switching currents between 10 and 200 mA. As the current is raised to 345, 450 and 600 mA the contact resistance after switching rises by 48, 122 and 430 mΩ respectively.

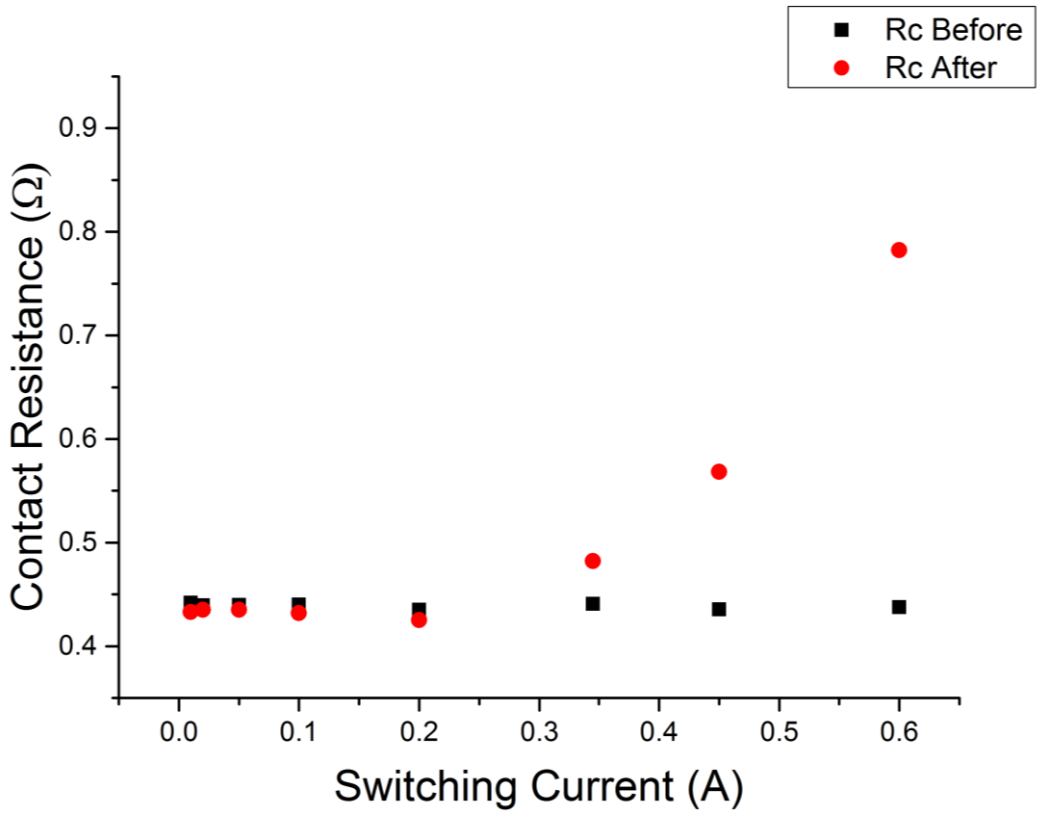

Figure 4-8 – The change in contact resistance (Rc) after 50 hot switching cycles as current is varied.

The captured contact opening voltage waveforms are synchronised in time by defining t=0 (the oscilloscope trigger point) as where contact potential reaches 3 V and the contacts are defined to be fully open. The mean potential at each point in time is calculated for all 50 waveforms to create an average waveform at each current condition. The average waveforms are presented in Figure 4-9.

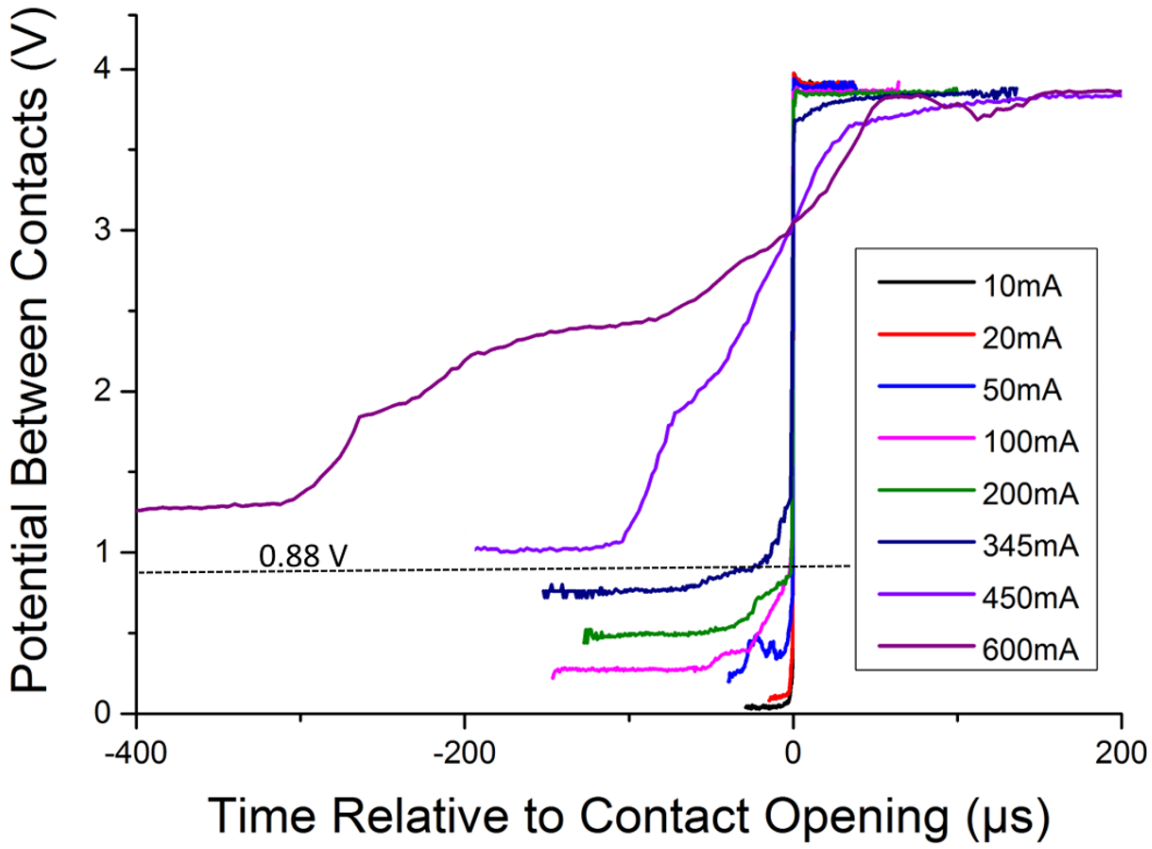

Figure 4-9 - Variation of Contact Potential during Opening with Steady State DC Current between 10 and 600mA with the boiling voltage for Au indicated by horizontal dashed line

Each waveform is initially level and stable, indicating the contact is closed. The potential drop associate with the closed contact resistance increases with current. This is expected as the load and closed contact resistances act as a potential divider for the circuit voltage. As the load resistance is decreased, circuit current is increased, but the potential drop across the closed contact resistance becomes a proportionally larger potential drop. At circuit currents of 10, 20, 50, 100 and 200 mA there is a gradual rise to 0.88 V (the boiling voltage for Au) before there is an abrupt increase to 4 V open circuit potential. This indicates that a MMB has been formed in the Au and when it boils it ruptures interrupting the circuit. The time between the onset of the voltage increasing and the contact opening (MMB duration) appears to increase with current.

As the current is increased to 345 mA the average duration of the molten event increases to more than 70 µS but circuit potential reaches 1.2 V before the circuit is interrupted. This is significantly above the boiling voltage for Au [85]. Illustratively, the ψ – θ theorem equates a contact voltage drop of 1.2 V to a contact super temperature of approximately 3,600 ^{o}C.

For circuit currents of 450 and 600 mA the contact potential rises nearly continuously and there is not an obvious point where the contact opens. As such the waveforms are not necessarily synchronised. Figure 4-10 and Figure 4-11 show individual consecutive waveforms captured at 450 and 600 mA conditions respectively. They show that, while there is significant similarity between waveforms at each condition and the average waveforms are representative, they do obscure some detail.

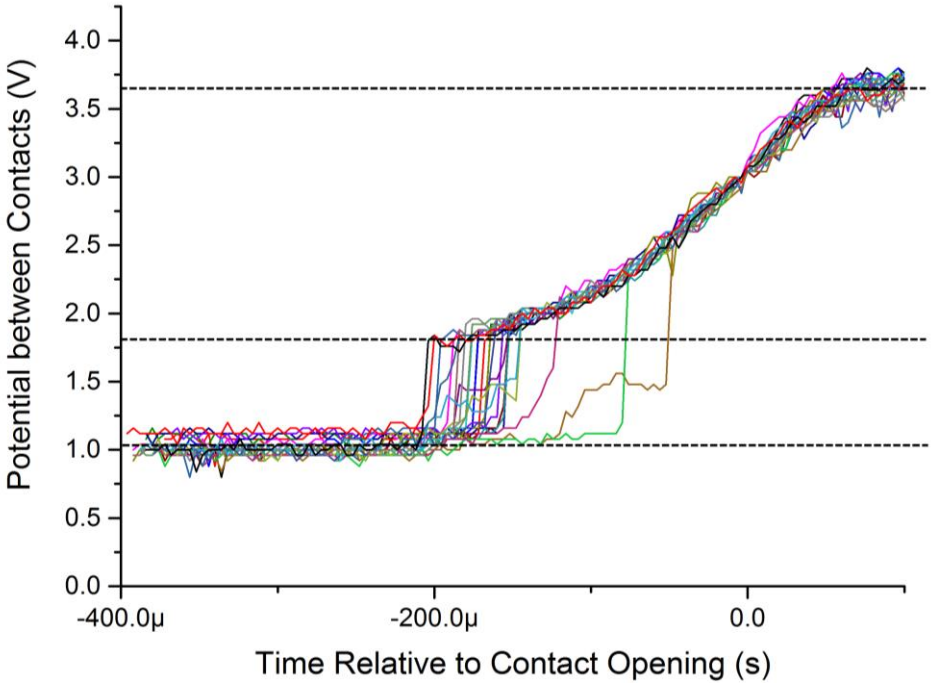

Figure 4-10 – The Contact Potential during 25 Consecutive Opening Events with at 450 mA Circuit Current

At 450 mA there is a rapid onset to opening events characterised by an abrupt increase from the closed contact potential (first dashed line) to 1.8 V (second dashed line) or higher. The potential then rises more steadily for approximately 220 µs to 3.3 V (third dash lined) of full open circuit potential 200 µs later. The reduction in open circuit voltage is due to the much larger current demand on the battery causing a recovery effect in the lead acid cell from chemical diffusion last several milliseconds after the contacts have opened.

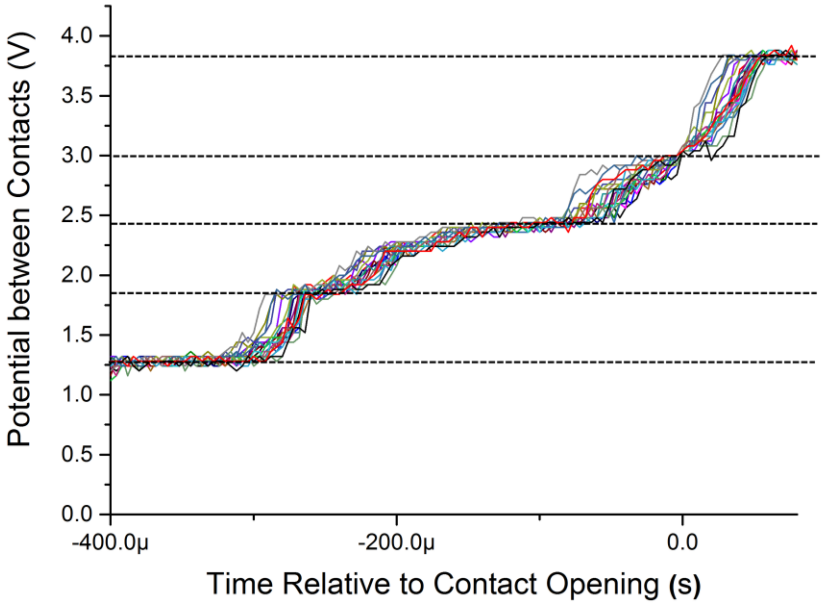

Figure 4-11 – The Contact Potential during 25 Consecutive Opening Events with at 600 mA Circuit Current

Figure 4-11 shows 25 consecutive openings at the 600 mA conditions. Similar to the 450 mA case there is a distinct beginning to the opening event characterised by sudden increase in contact potential to 1.8 V (between first and second dashed lines). The voltage then rises continuously to the full open circuit potential over 350 µs with two steps or plateaus apparent at 2.4 and 3.1 V.

Following testing the Au/MWCNT contact is removed for microscopic examination of the contact sites. Contact sites for currents between 10 and 200 mA show brightening and evidence of fine wear on the surface. Where currents above 200 mA have been switched there are multiple dark sites. Micrographs of the 200 and 600 mA switching sites are presented in Figure 4-12 and Figure 4-13.

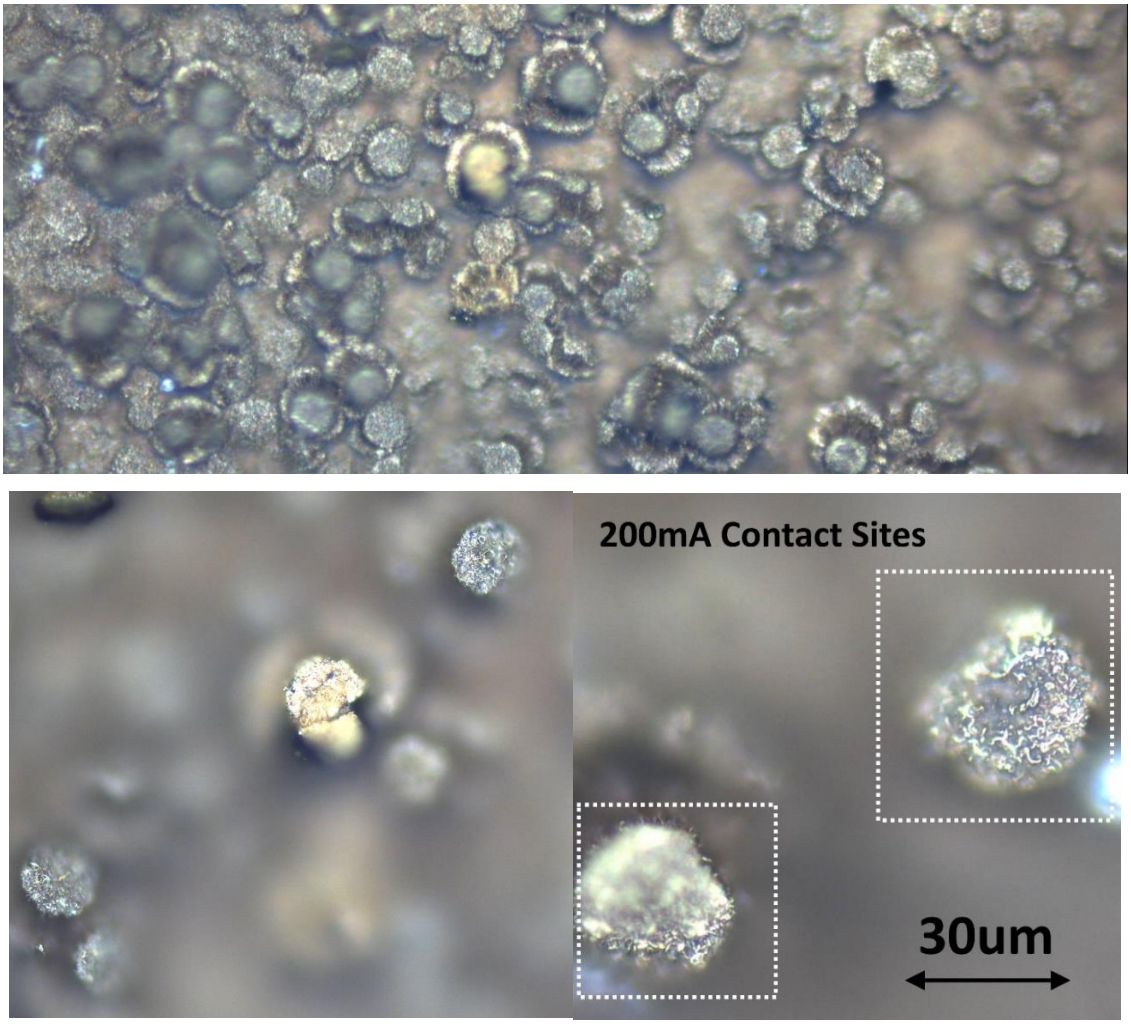

Figure 4-12 – (Top) The 100 mA switching site shown at 200x optical magnification. (Left) Location of the 200mA Contact Site at 1000x optical magnification showing a rasied microscale texture of the brighter material (Right) Location of the 100 mA Contact Site at 500x magnification showing some peaks inside the contact region are brighter than other peaks after switching.

The left image in Figure 4-12 shows a view of three raised regions that were in mechanical contact during hot switching of the 100 mA signal. The feature in the center of the contact region appears much brighter. At the 200 mA switching site (Figure 4-12 right) a similar pattern is observed. Two 30 µm wide raised regions on the Au/MWCNT contact are highlighted by a dotted white box. Each of these regions shows a raised and deformed microscale texture of gold coloured material. The microscale asperities appear to be partially flattened and brighter than the lower material. Both observations suggest that the contact is experiencing mechanical and thermal wear at the higher points but it is limited to microscale changes. The contact surface appears to be Au. These observations were made in all contact sites between 10 and 200 mA switching with the amount of contact brightening increasing with current.

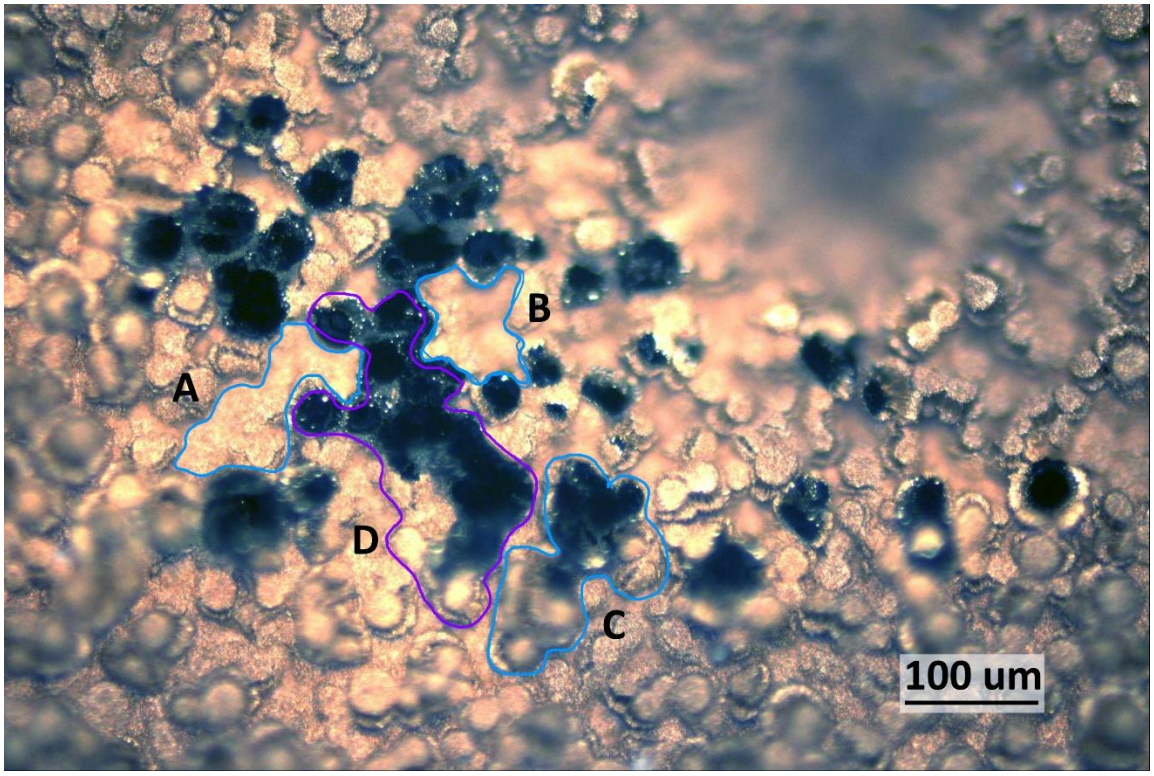

Figure 4-13 - Location of the 600mA Test on the Rough Sample at 200x optical magnification showing flat regions (A and B) and asperities with damage (C and D)

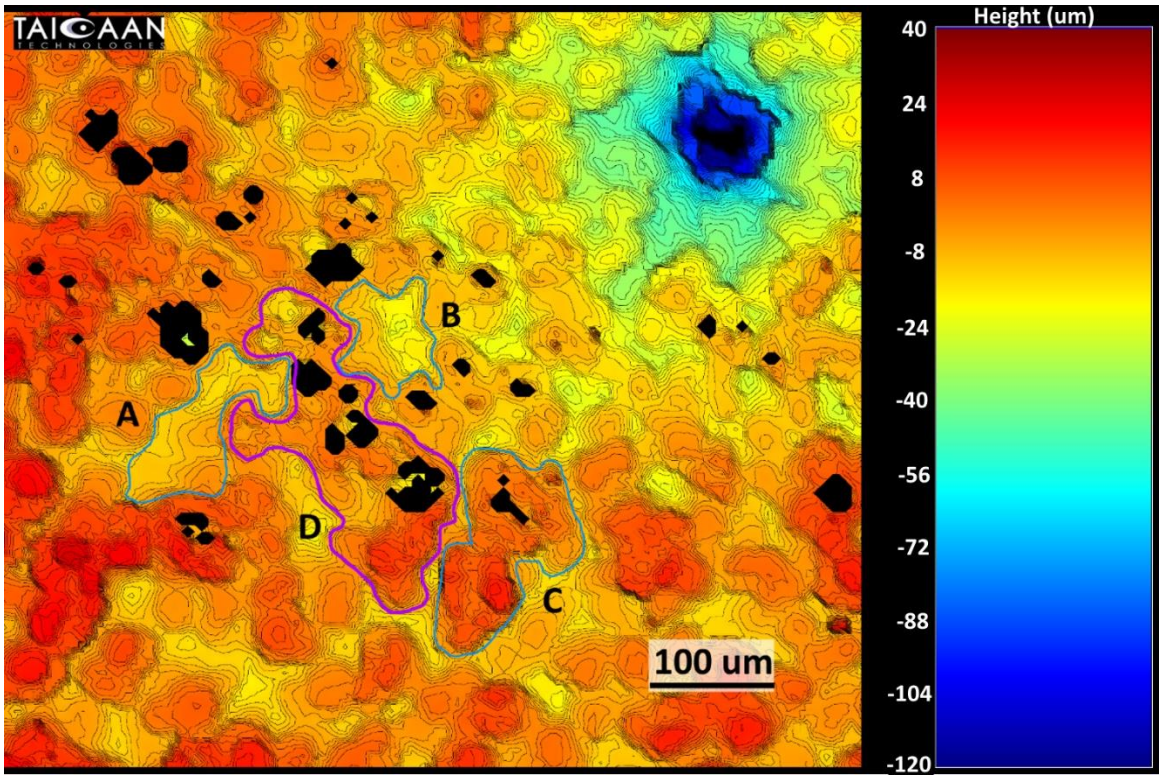

Figure 4-14 – Surface Height Map of the Au/MWCNT contact with contouring at the same location as Figure 4-13. Regions A and B are lower plateaus. Regions C and D are rasised asperities. Black regions denote no height measurement has been recorded (due to poor signal return)

The location of the 600 mA switching site is shown by micrograph in Figure 4-13 with a surface height map of the same region taken post switching shown in Figure 4-14. The black regions in the surface height map show where no surface height measurement has been possible. This is typically due to the surface being poorly reflective. The regions where no signal has been returned in the height map correspond to within the darkened regions of the micrograph. In the upper right-hand corner of both Figures is the location of a nanoindentation site. The site is blurred in the micrograph due to the narrow focal plane but is clearly shown as a pit 100 µm wide and 50 µm deep in the surface height map. Four more regions are highlighted in both Figures for orientation. Sites A and B show two lower and flatter regions, while sites C and D indicate the location of two raised regions. An important feature of the micrographs at switching currents of 350, 450 and 600 mA is the appearance large dark regions. The dark regions in the micrograph correspond to the peaks in the surface on the height map, such as regions C and D. This appears to be the removal of Au film from the surface, exposing the MWCNT beneath. This shows the exposed MWCNT are still the highest points on the surface. Around the edges of the dark regions small bright spots are visible suggesting Au has become molten and been finely scattered. There is a general pattern of the gold coloured regions being bright at the switching site and dull around the edges. In comparison to the lower current sites (Figure 4-12) this suggests the thermal effect from current is more widespread as the mechanical conditions were the same.

To verify the MWCNT has been exposed an energy dispersive x-day (EDX) analysis is carried out at the edge of the region labelled D in the previous Figures. An electronmicrograph of the investigated region is presented in Figure 4-15 with the EDX spectra presented in Figure 4-16. The electron micrograph shows the presence of spherical features around 100 nm in diameter (red arrow) that are widely distributed over the surface and show up as brighter spots. On the left side of the image the upper Au film is mostly intact and features a spherical feature (region i) around 5 µm in diameter embedded into a surface of ireggularly shaped flat features. This appears to be part of the Au film that became molten and has reformed. The iregular flat features are sections of the Au film that have become flattened and broken up at the edge of the dark regions seen in the previous figures. To the right of Figure 4-15 there are darker and more regularly textured features that appear to be the underlying MWCNT with a very fine scattering of Au particles.

EDX analysis of regions i and ii are shown in Figure 4-16. Peaks appear for C, O and Au in both regions however region (ii) has greater intensity in the C peak (45.4 vs 28.9) and lower intensity in

the Au peak (48.4 vs 78.9). This shows that region (ii) has a significantly lower presence of Au and increased C compared with region (i).

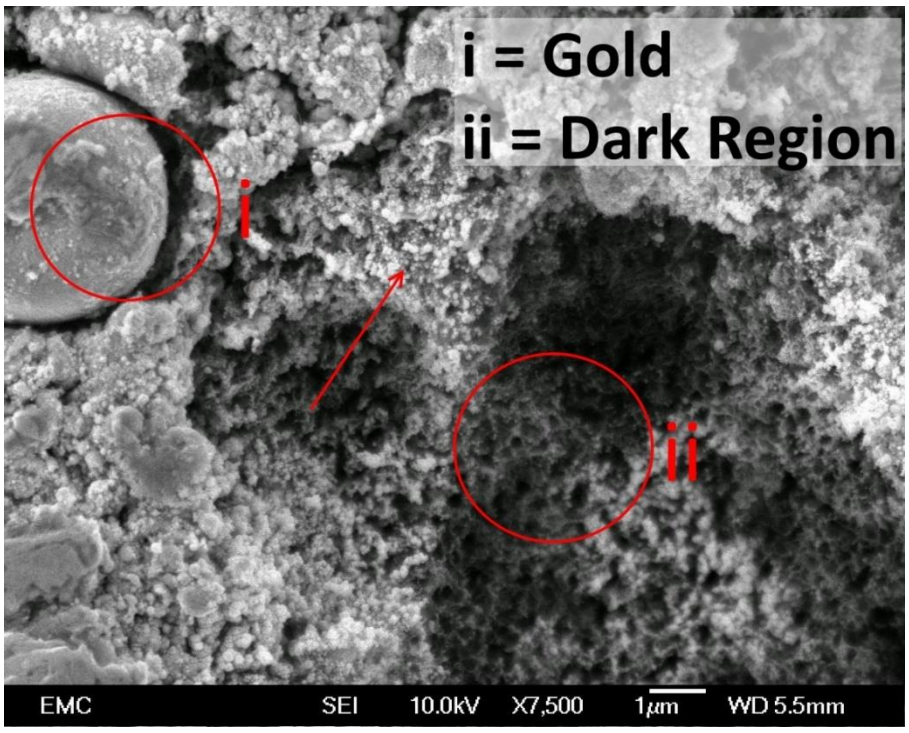

Figure 4-15 – SEM image of the edge of the 600 mA contact site. The location is at the edge of one of the dark regions. Energy dispersion X-ray analysis (EDX) is carried out at the sites labelled I (an Au region & ii an Au depleted region).

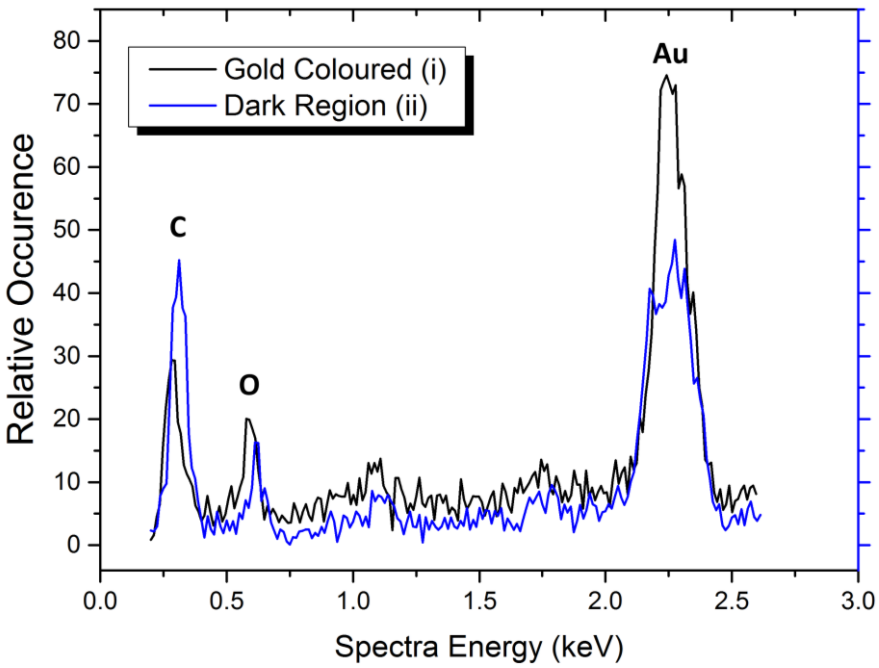

Figure 4-16 – Energy dispersive X-ray (EDX) analsysis of the surface composition at (i) a gold coloured region and (ii) a darker region as indicated by Figure 4-15

4.2.1 The Opening Behaviour of a Hot Switched MWCNT contact

The results from the previous section showed when the switching current was raised to 345 mA and above the Au surface was instantly damaged, exposing the underlying MWCNT. The contact opening voltage waveform no longer corresponds with a Au molten metal bridge. These observations suggest the carbon nanotubes had become involved in conduction during the final stage of contact separation.

In this section the behaviour of current carrying carbon nanotubes during hot switched contact opening are investigated and compared during hot switched contact opening. The lower contact now consists only of vertically aligned MWCNTs with no upper layer of Au. The experimental arrangement is shown in Figure 4-17 is replicated from the previous section. The opposite contact is again a Au coated ball. The same closed contact force (150 µN) and switching circuit arrangement is used. The circuit current is again provided by a 4 V battery but an important difference is peak circuit current is limited to 100 mA as the combination of the MWCNT bulk resistance and contact resistance (~ 28 Ω) is much greater than the Au-MWCNT composite contact resistance of < 1 Ω.

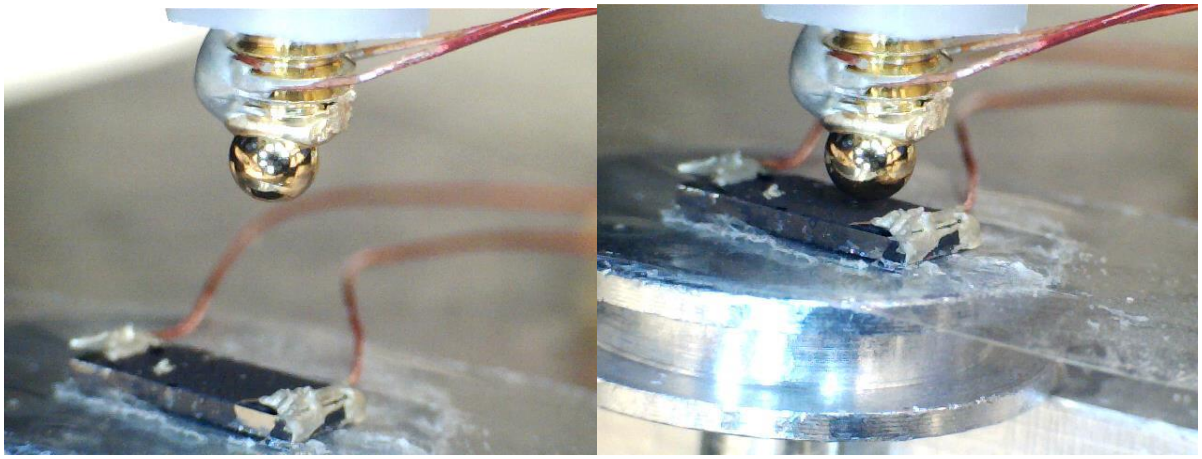

Figure 4-17 – The arrangement of upper Au coated sphere contact and lower vertically aligned MWCNT lower contact (left) with contact open and (right) contact closed

Ten consecutive opening waveforms observed at 4V and 20 mA switching conditions are presented in Figure 4-18.

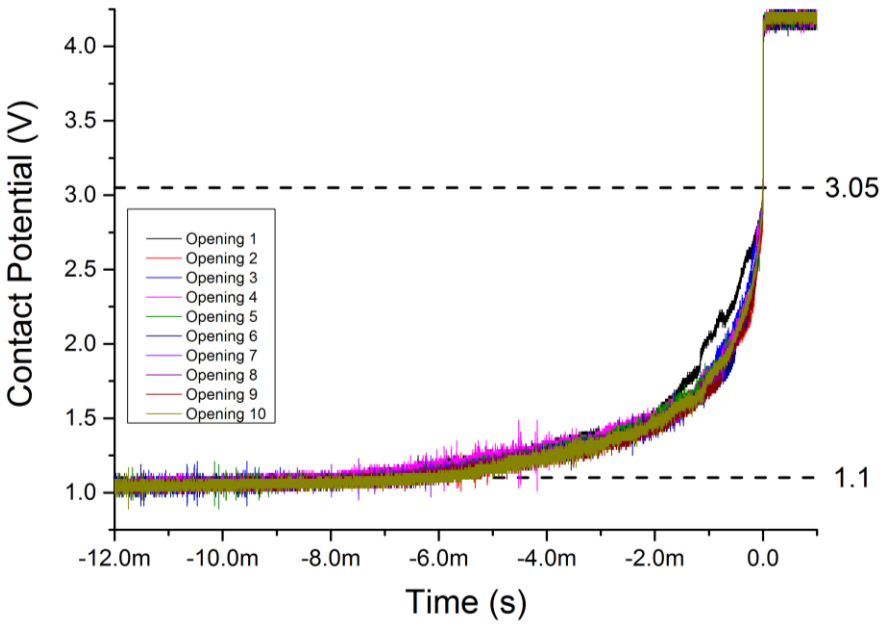

Figure 4-18 – Ten Contact Potential Waveforms during Hot Opening a MWCNT contact at 4V 20 mA

The difference in contact resistance between the MWCNT and Au-MWCNT contacts is seen when the waveforms are compared (Figure 4-9 cf. Figure 4-18) by the potential drop when the contact is closed being much greater (1 V cf. 0.02 V) as expected. The duration between the closed contact resistance beginning to increase and reaching full open circuit potential is also much greater than the Au/MWCNT contact 6 ms cf. 5 µs under the same switching conditions. This is anticipated as without the upper Au coating of the MWCNT only contact is more elastic with a lower stiffness [16]. The contact area at the same force is therefore larger for the MWCNT only contact, with the upper contact penetrating farther into the MWCNT. As the contacts are opened with the same velocity profile it takes longer for the contacts to open, the contact area takes longer to decrease and the current constriction increases more gradually.

The contact potential rises to a much higher potential (3.05 V cf. 0.88 V) before it instantaneously rises to the full open circuit potential and the contact is deemed to be open. While the contact supertemperature cannot be accurately deduced according to the $\psi - \theta$ theorem relationship (because the potential drop across the contact arises not solely from constriction resistance but also the bulk material resistance of the MWCNT) an estimate can be made from the difference between the closed contact potential (lower dashed black line in Figure 4-18) and the point where the potential begins to increase abruptly to the open circuit potential (upper dashed black line). The difference in potential is 1.95 V. Even excluding the effect of contact resistance, this predicts a

contact super temperature of approximately 6000 K, and above the generally reported melting temperature of carbon nanotubes of 3200 to 4800 K [129, 130].

Several steps in the contact potential can just be seen in Figure 4-18 however at the timescale shown they are difficult to detect. Figure 4-19 shows the 4th opening from Figure 4-18 in detail from 1.2 ms before the contact opens

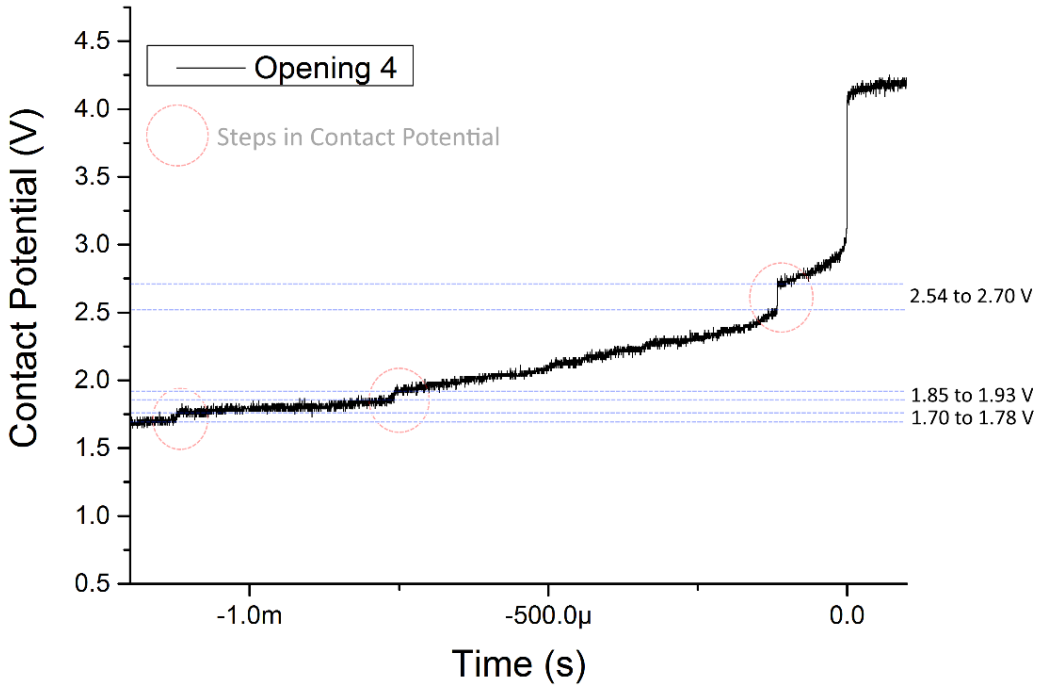

Figure 4-19 – Detail of a Single Contact Potential Waveforms during Hot Opening a MWCNT contact at 4V 20 mA with steps in the contact potential indicated by a red dashed circle

Three steps in the contact potential are apparent. Their location is indicated by a red dashed ring while the voltage levels are shown by blue dashed lines. At 1100 µs before the contact opens the first step in contact potential occurs from 1.70 to 1.78 V (0.08 V) before continuously and gradually increasing for another 350 µs. At this point (750 µs before contact opening) there is a second step from 1.85 V to 1.93 V (0.08 V) in the contact potential. The potential continues to rise quite steadily until 100 µs before the contact opens where there is a third step from 2.54 to 2.70 V (0.16 V). Over the next 100 µs the potential rises more rapidly, sharply increases to 3.05 V, then instantaneously rises to over 4 V (the open circuit potential) indicating the contact has fully opened. The steps appear in all opening waveforms with the MWCNT only contact.

4.2.2 Discussion

Failure Current Experiments with Au/MWCNT and MWCNT Only

The Au/MWCNT surface has been hot switched at 4 V while the current is varied from 10 to 600 mA. At currents between 10 and 200 mA the contact resistance shows a small drop after 50 switching cycles. This is expected as the microscale molten metal bridges (indicated by the transient voltage waveforms) will allow the contact microstructure to reflow. This allows the contacts to conform to one another and exposes clean metallic surface (indicated by the brightening of metallic Au observed at the contact sites), both factors that increase the area for conduction and decrease the contact resistance. This behaviour is expected and routinely observed as a bedding in process for electrical contacts [66, 125].

At currents of 345 mA and above there is a progressive increase in the post switching contact resistance with switching current. Micrographs of the contact surface show that the metallic Au has become molten and removed from the surface, piercing the Au film and exposing the MWCNT beneath. The increase in contact resistance can be linked to destruction of the conductive surface in the contact area by Equation (2-3) and the thermal input power P_t linked to the square of the circuit current according to

$$P_t = i^2 r \qquad (4\text{-}1)$$

Figure 4-20 shows the change in contact resistance after 50 hot switching cycles against the switching current squared. A linear best fit shows a good fit to the contact resistance and is used to extrapolate the point where 50 hot switching cycles are expected to result in reduction in the conductive Au contact area and increasing contact resistance to the Au/MWCNT contact. This is found at i^2 is 0.0912 A^2 and therefore i is 302 mA. It is important to note that at high current levels the molten Au material is observed to be entirely removed from the MWCNT so an Au-Au contact interface cannot be reformed. This contrasts with currents below 200 mA where the Au is transferred within the contact area and can again become part of the contact interface. The failure current limit is therefore related to the power dissipated in the Au film and therefore the film thickness. The contact wear process below the overload current is linked to the MMB energy, and not to film thickness, and the relationship between circuit current and MMB energy is investigated in the next experiment.

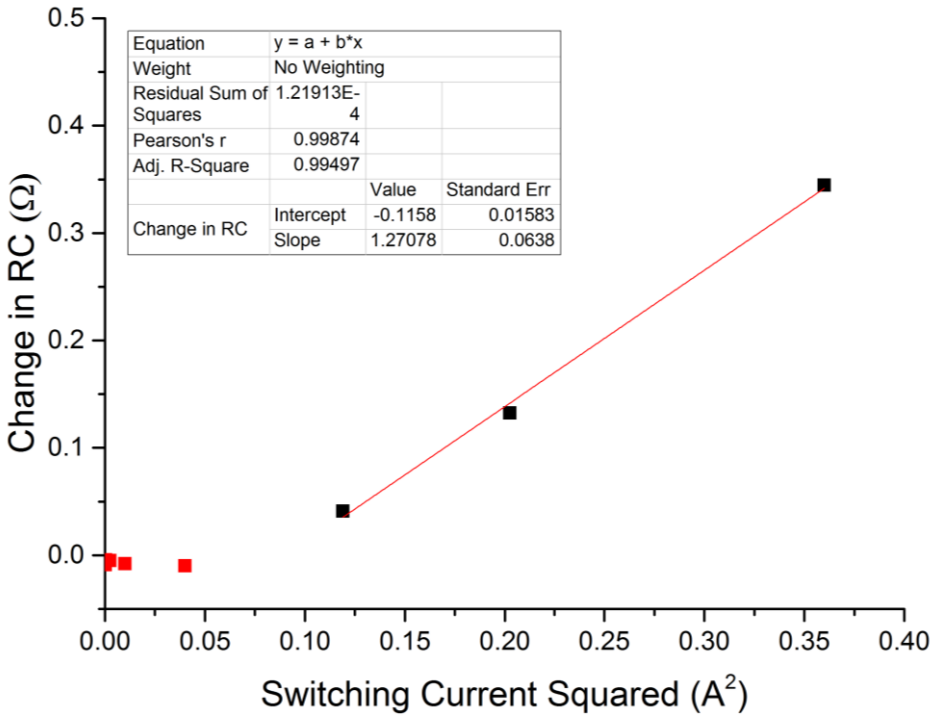

Figure 4-20 – Change in Contact Resistance after 50 hot switched cycles against the switching current squared

Between 10 and 200 mA the voltage waveform across the contacts indicate a Au MMB is formed and the contact separate when the boiling voltage for Au (0.88 V) is reached (Figure 4-9). In each case the contact potential rises to 0.88 V before abruptly increasing to 4 V (the open circuit potential). The duration and energy of the events increases with current. Imaging of the switched surface between 10 and 200 mA (Figure 4-12) shows evidence of microscale softening and melting of the Au layer at the peaks of the asperities in the contact region, without the Au film being punctured.

At currents of 350 mA and greater the contact potential exceeds the boiling voltage for Au before the contact opens (Figure 4-9). Steps in the contact potential are observed at 1.2 V (350 mA) and 1.7 V (450 and 600 mA) (Figure 4-10 and Figure 4-11). Using the ψ – θ theorem these potentials are used to calculate contact super-temperatures of ~3600 and 5200 ^{o}C respectively. It is noted that this is close to the reported value for the melting point of graphite (3550 ^{o}C) and single walled carbon nanotubes without defects (4500 ^{o}C) and approaches that for bulk single walled carbon nanotubes [130]. At 350 mA the contacts open immediately after reaching 1.2 V but at 450 and 600 mA the voltage continues to rise, without exhibiting the ringing response caused by stray capacitance and typically observed as the contacts open abruptly (this ringing behaviour is described and modelled the discussion of Experiment 4). This suggests that there is still a very high resistance circuit pathway

present. As the contact separation is only ~20 µm and the nanotubes are ~50 µm in length the mechanism proposed is individual nanotubes still bridging between the contacts.

Imaging of the Au/MWCNT surface after switching currents of 350, 450 and 600 mA showed the appearance of darkened regions with bright spots. Surface profilometry showed the darker regions were the highest locations on the surface and are therefore the most likely point of final contact and greatest current constriction as the contact opens (Figure 4-14 and Figure 4-15). SEM and EDX compositional analysis (Figure 4-16) showed the darker regions had a greater proportion of carbon and lower proportion of Au than the brighter gold coloured region. This indicates that the Au film had broken down by melting, boiling and scattering to expose the carbon nanotubes. The nanotubes become the final point of physical contact as the switch opens and the contacts separate when the current constriction raises the temperature of the final nanotube in contact until it sublimes/pyrolyzes [116].

At currents of 450 and 600 mA the contact potential does not show a discontinuity but either an exponential rise or a stepped rise to the open circuit potential. The voltage levels are significantly greater than associated with the melting or boiling of the contact material and suggest a different mechanism. The increase is explained by the presence of multiple parallel and serial current paths through exposed MWCNTs [82]. Illustratively, the contact resistance of MWCNT to MWCNT bundles has been reported above 100 kΩ [131]. However, a nanotube embedded in Au at either end could provide a better contact interface and a lower resistance path for most of the current that rapidly causes the nanotube to pyrolyze by Joule heat from current constriction and the stepped failure of the outer walls previous described. Because the resistance that arises is no longer contact resistance but the bulk resistance of a carbon nanotube, and as such the $\psi - \theta$ theorem cannot be used to infer the contact super temperature. Once the lower current path enabled by the MWCNT embedded in Au is destroyed there are still multiple highly resistive paths between the contacts through nanotubes just touching the opposing contact (not embedded in the Au) with much higher contact resistance. This mechanism would be observed as a step-in potential to the melting voltage for the nanotube followed by an exponential rise in potential as the current is restricted by the much higher resistance path.

When switching the MWCNT with no Au coating the final current constriction is intended to occur in a carbon nanotube as the bonding between individual nanotubes in the “forest” is weak compared to that in the Au layer on the upper contact. As the contacts separate individual nanotubes are

expected to adhere to the upper contact and be drawn out, creating a circuit pathway through an individual nanotube. The voltage steps are therefore linked to the conduction mechanism in the nanotube. It is proposed the steps in contact potential are the consecutive thermal failure of the walls in the final MWCNT as the contacts separate [129].

For cases of contacts of vastly dissimilar resistivity, the supertemperature will occur embedded in the material with higher resistivity [66]. Determining the temperature at which the thermal failure is expected to occur is difficult as the precise chemical properties of the manufactured MWCNT have not been identified. Predicting contact supertemperature by the $\psi - \theta$ theorem is also complicated by the circuit pathway of the 4-wire measurement of contact resistance. Practically it is not possible to eliminate the more resistive nanotube-nanotube junctions from the measurement of the contact resistance. As a result, the voltage drop cannot be entirely attributed to the constriction resistance and the contact supertemperature will be overestimated. Real-time TEM observation of wall-by-wall thermal failure of MWCNT under vacuum was indirectly measured at 3200 K reported by Begtrup et al [116]. Ambient temperature was determined by the melting of adjacent nanoparticles with the local sublimation temperature of the nanotube derived by FEA from a diffusive model of conduction. This approach is likely to underestimate the temperature due to the lack of inclusion of ballistic conduction effects [132].

As it is the mechanical attributes of the MWCNTs that are important for the contact performance the precise chemical properties of the nanotubes used in the Au/MWCNT material have not yet been isolated and this is identified for future work. Because the MWCNT is a bulk material manufactured by thermal vapour deposition, a mixture of compounds with contaminants is expected. The apparent supertemperature in the 345 mA case and the observation of step pyrolysis at 450 and 600 mA suggest the thermal failure temperature is between 3200 and 3600 ^{o}C**.**

Summary

The current switching limit and the mechanism of failure have been identified for the 505 Au/MWCNT. The Au/MWCNT contact tolerates a switching current of 200 mA for 50 switching cycles without puncture of the Au film. Switching currents of 345 mA and above result in almost immediate thermal deterioration of the Au surface, characterised by the puncturing of the Au film and exposure of the underlying carbon nanotubes. The overload current where the current interruption is no longer characterised by rupture of a Au MMB is calculated to be 302 mA based on an i^2r relationship

with the thermal input power and is related to the thickness of the Au film coating. The damage to the Au film exposes the underlying MWCNT which become involved in the conduction at the final stages of the contact opening.

In each of the higher current cases (350, 450 and 600 mA) the opening waveform changes. Surface imaging, compositional analysis and profilometry show the underlying carbon-rich material has been exposed and suggests carbon nanotubes become involved in the current path as the contact opens. While nanotubes are highly conductive, they demonstrate high contact resistance and are not considered to be viable as a MEMS switching surface when used alone [30].

Surface imaging and profilometry indicate surface asperities are the location of the MMB as expected. The MMB is shown to increase in duration and energy with current. The Au/MWCNT contact well tolerates switching currents upto 200 mA where the Au MMB is detected and this defines the range of current that will be investigated in the next section.

4.3 Experiment 3 - Molten Metal Bridge Energy relationship with Contact Surface Roughness, Current and Voltage

In this section the energy and duration of the molten metal bridge is evaluated while current, voltage, Au/MWCNT surface texture and the contact opening velocity are varied. The lifetime of the Au/MWCNT contact has previously been linked to a process of fine transfer driven by the molten metal bridge formed during hot switched contact opening. Fine transfer is a cumulative process that can only be effectively quantified from the surface wear after many switching cycles. However, the molten metal bridge is the driving mechanism for fine transfer and the influence of the circuit parameters and surface texture can be characterised without lifetime switching. The PZT apparatus is used as the number of switching cycles investigated is low. The objective is to provide empirical data that can be used to aid the prediction of the Au/MWCNT contact lifetime. The range of circuit current that will be investigated has been determined by the previous experiment (10 – 200 mA) and the range of circuit voltage by the arcing threshold (4 – 12 V). The surface roughness is varied using two Au/MWCNT samples with different surface texture.

4.3.1 Molten Bridge Energy with Surface Roughness and Circuit Current

Two Au/MWCNT samples have been investigated. Both nominally consist of a 505 Au/MWCNT (500nm layer of sputtered gold supported on a vertically aligned forest of MWCNT 50 µm high).

The key difference provided by changing the surface micro texture is changing the distributions of a-spots within the contact area.

Rough Sample 1) Minor manufacturing process variation led to a sample with an increased variation in the heights of CNT growth giving rise to rougher composite surface. There is also some evidence of film irregularity in the rougher surface. The mechanism is not fully understood but believed to be the result of residual surface tension in the Au coating as well as increased variability in the heights of the MWCNT forest. This is referred to as the *Rough sample*.

Smooth Sample 2) A sample previously used for a 50 mA lifetime measurement at one edge of the surface served as a reference for a normal surface. This is referred to as the *smooth sample*.

Optical micrographs of the sample surfaces are shown in Figure 4-21 to indicate the difference in surfaces. The rough sample has been extensively switched at this location when the image was captured. The region labelled A) is the location of high current switching damage from the previous experiment.

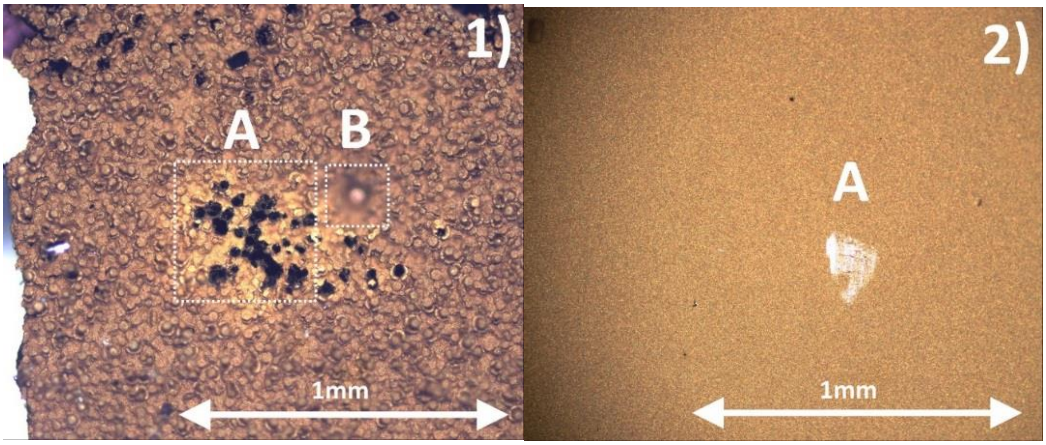

Figure 4-21 – Optical micrographs of the rough (1) and smooth (2) Au [500nm]/MWCNT [50um] shown at 100x magnification. The rough sample has experienced extensive hot switching in the imaged region with surface damage at a high current switching site shown by the white dotted box (A).

The surface roughness is characterised before switching. A 1mm x 1mm area is measured every 5 µm. The roughness is characterised using the 3D Arithmetic Absolute Average (S_a) parameter with a

0.25mm Gaussian form filter. The rough and smooth surfaces are characterised as having S_a of 7.822um and 0.231um respectively.

Figure 4-22 shows the surface height map of the rough surface (left) and the smooth surface (right) over a 200 µm x 200 µm with a +/- 20 µm colour scale with a cross of the surface profile along the black dotted line below. The rough surface features flattened peaks approximately 30 µm in diameter and 25 µm in height.

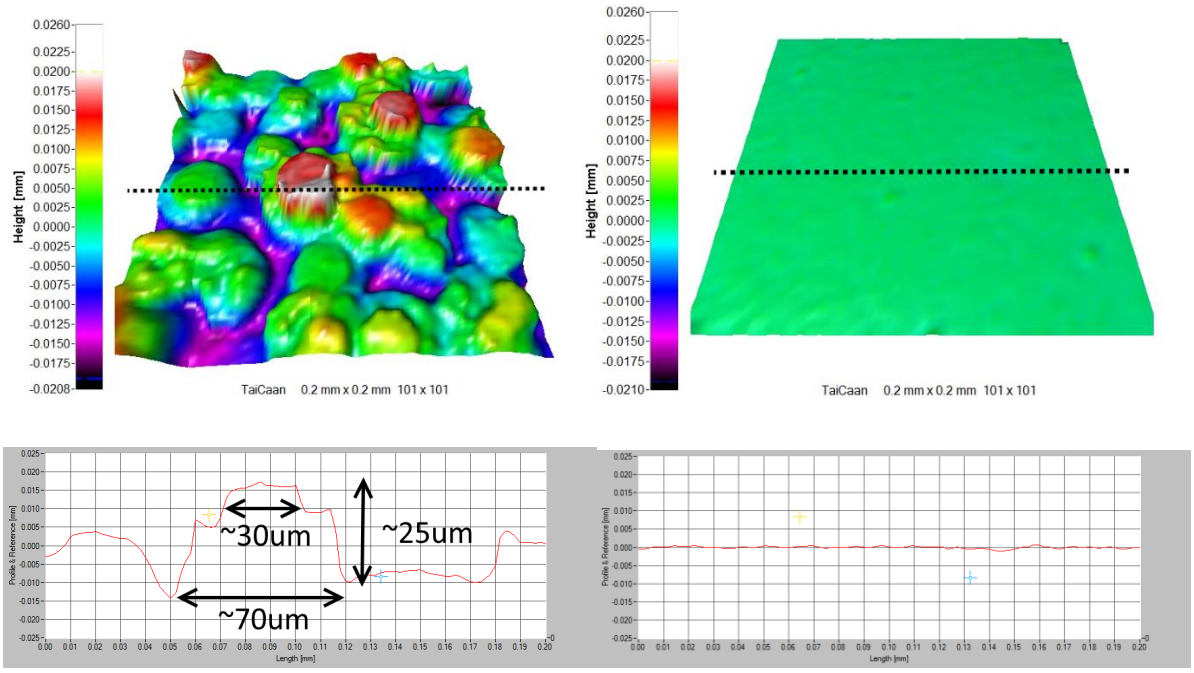

Figure 4-22 - Surface profile of the rough (left) and smooth (right) samples

Texture Parameter	Rough surface	Smooth surface
3D Roughness, Sa (um)	*7.822*	*0.231*
2D Peak to Valley (µm)	*31.225*	*1.651*

The contacts are closed to 1 mN static contact force and the contact resistance recorded. The contacts are cold switched for 100 cycles to allow the contact area to mechanically conform. The contacts are then hot switched for a further 200 cycles with the opening transient waveform captured for the final 50 events. Contact resistance for the smooth and rough samples is 5.7 and 1.1 Ω while the bulk resistance across the Au/MWCNT contact is 55 and 57 mΩ respectively.

4.3.2 Molten Bridge Energy with Circuit Current and Surface Roughness

The average MMB energy against circuit current is presented in Figure 4-23.

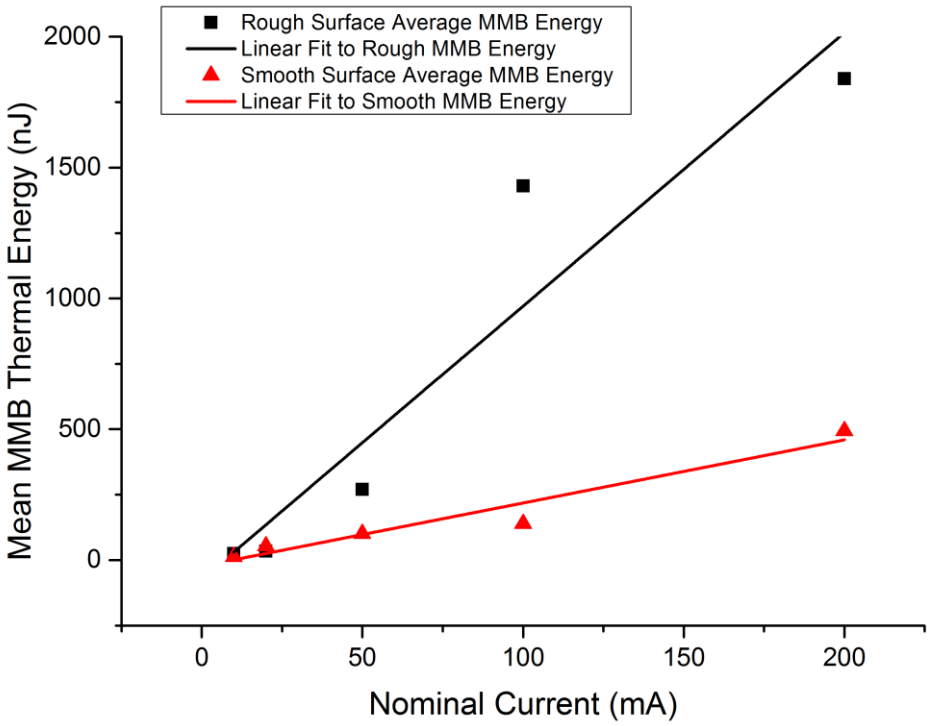

Figure 4-23 - Graph of MMB Trend with Current for a Smooth and Rough Au/MWCNT Contact at 4V DC with Original (right) and Enhanced (left) Instrumentation. Note the enhanced instrumentation shows the same trends but a much lower overall energy level due to the improved resolution

A linear best fit is plotted for the MMB energy on the rough and smooth surfaces. The results show there is linear correlation between increasing circuit current and the average MMB energy in both the smooth and rough surface cases; however, the rough surface shows a greater average MMB energy to the smooth case.

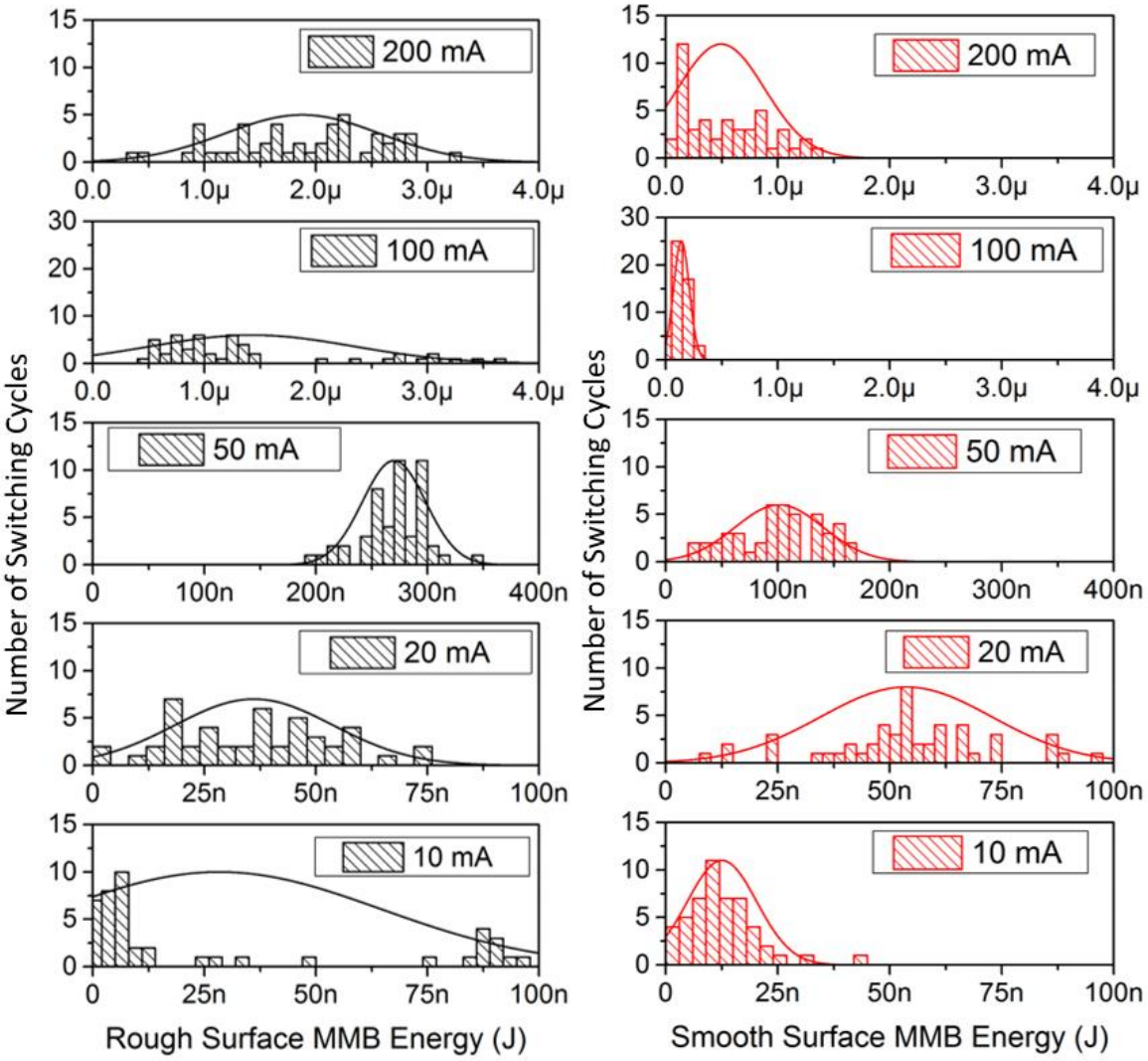

Figure 4-24 shows histograms distributions of the individual MMB energy for contact openings of the rough surface (left in red) and the smooth surface (right in black). A normal distribution curve is fitted to the data. To clearly show the distribution the scale increases with current but at a given current the scale is the same to allow comparison between smooth and rough surfaces.

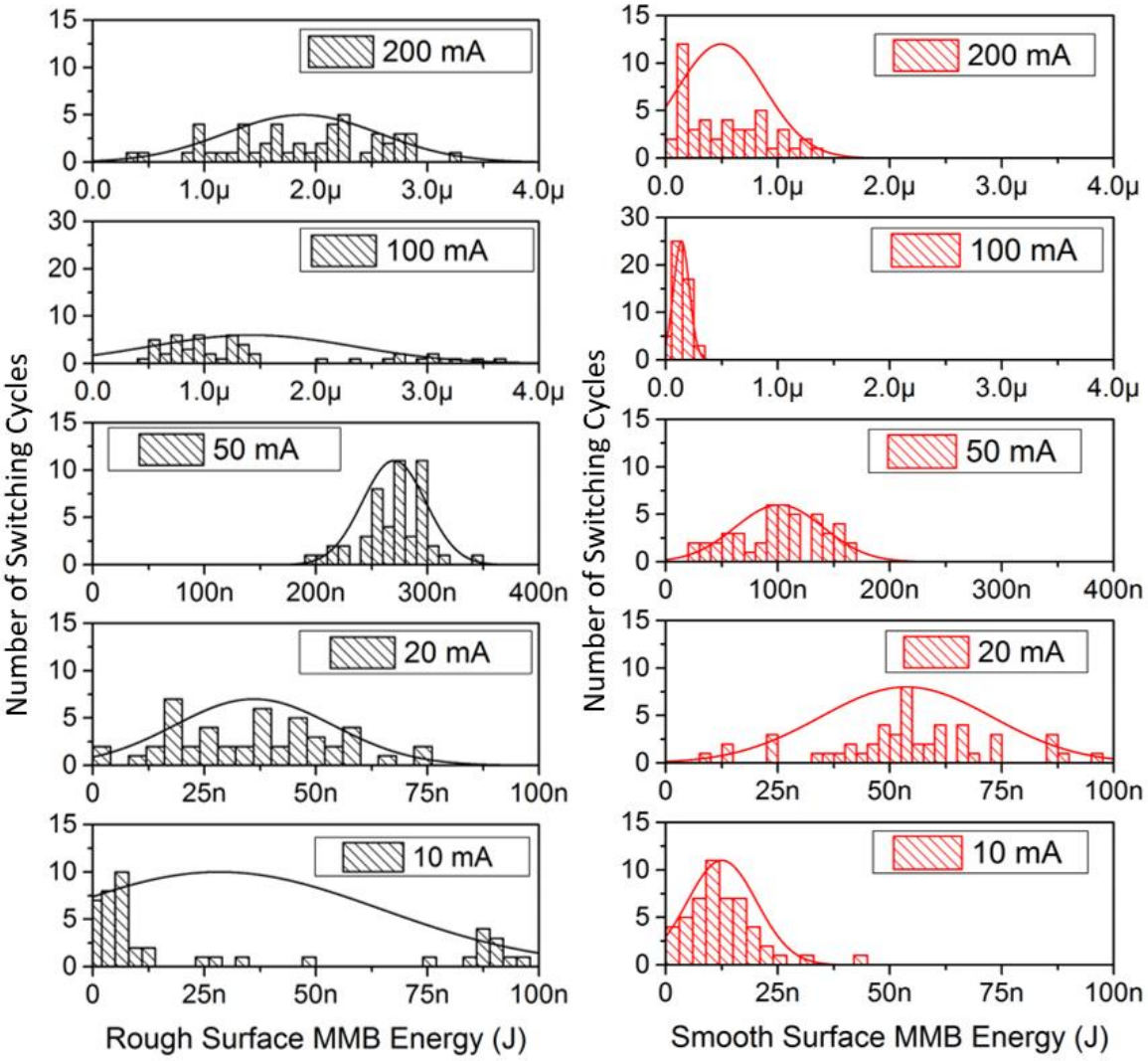

Figure 4-24 - MMB Energy Distribution for Consecutive Opening on Rough and Smooth Samples at 10 to 200 mA 4V DC

Two general trends are observed. The distribution of molten bridge energy at a given current is greater for the rough surface that the smooth surface, that is the MMB energy is more variable. Secondly, the overall energy is higher for the rough surface than the smooth. The only exception is at the 20 mA switching condition where the energy distribution for rough and smooth surfaces overlap. The average MMB energy and the variance (characterised by standard deviation) are summarised below in Table 4-1 for each switching condition.

MMB Energy (nJ)	10mA		20mA		50mA		100mA		200mA	
	Rough	Smooth	Rough	Smooth	Rough	Smooth	Rough	Smooth	Rough	Smooth
Mean	28.3	12.5	36.1	53.7	270	*101*	1430	140	1880	494
Standard Deviation σ	36.4	*7.7*	17.7	*19.2*	28.3	*39.4*	909	*70.2*	695	*391*

Table 4-1 - Summary of MMB Distribution Parameters for Currents from 10 to 200mA

4.3.3 Molten Bridge Energy with Circuit Voltage

The distribution of MMB as circuit potential is varied is presented in Figure 4-25 with lines fitted for a normal distribution. There is no clear trend in the average MMB energy as the voltage is varied between 4 and 12V DC at 50mA circuit current. The overall average MMB energy across all voltage cases is 209 nJ. It is noted that the lowest average MMB occurs at 10 V (89 nJ) while the highest occurs at 6 V (357 nJ).

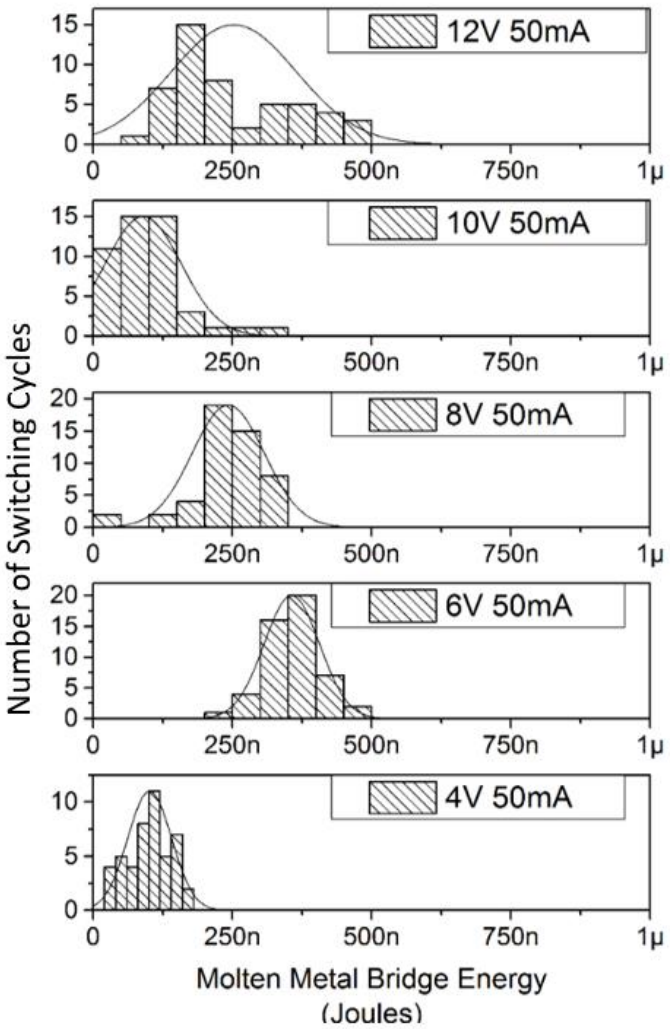

Figure 4-25 - Variation of MMB Thermal Energy Distribution with Circuit Potential

There is a small correlation between the distributions of MMB energy increasing with voltage which is more apparent if the variance of the MMB energy at each condition is plotted against circuit potential. The average MMB energy and variance (standard deviation) are shown in Figure 4-26.

When a linear best fit is applied to the variance it indicates the trend is for the variance in MMB energy (standard deviation) to increase by 8 nJ/V between 4 and 12 V.

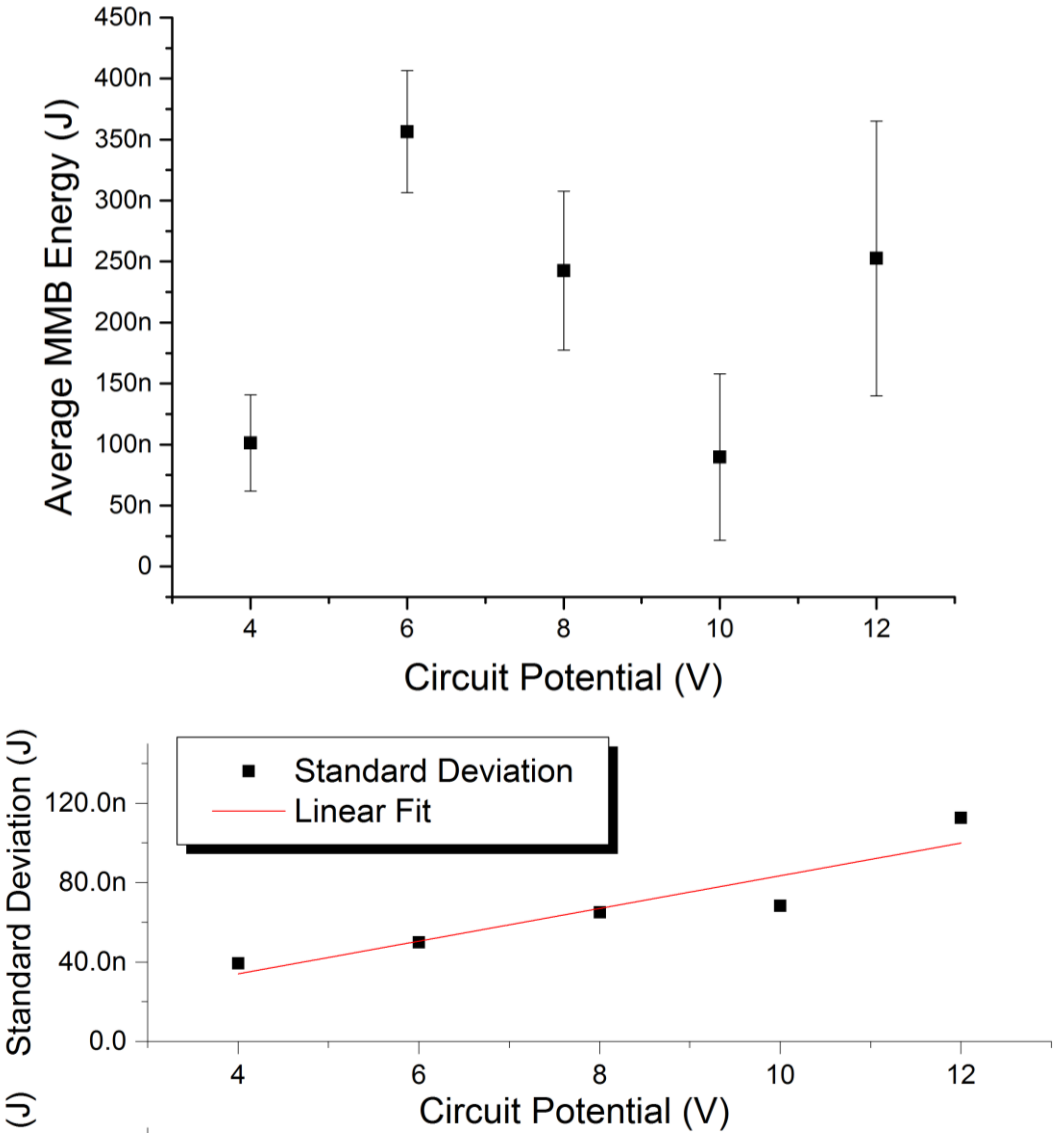

Figure 4-26 – Average MMB Energy against Circuit Potential – Standard Deviation shown as vertical error bars (Top) and the Standard Deviation in MMB Energy against Circuit Potential with a Linear Fit (Bottom)

MMB Energy (nJ)	4 V 50 mA	6 V 50 mA	8 V 50 mA	10 V 50 mA	12 V 50 mA
Mean	**101**	**357**	**242**	**89.7**	**253**
Standard Deviation σ	39	50	65	68	110

Table 4-2 - Summary of MMB Average Energy and Distribution between 4V 50mA and 12 V 50mA

4.3.4 Discussion

Repeatability of the Molten Metal Bridge

The results show that the MMB energy is highly variable, even for 50 consecutive switching cycles at the same conditions. It is also shown that changing the surface micro texture has a significant influence on the MMB energy. The variability of MMB energy over 50 consecutive hot switching cycles demonstrates a distribution close to a normal distribution curve, as shown in Figure 4-24 and Figure 4-25. Evaluating a larger number of switching operations would provide a histogram with more detail and so a more detailed representation of the probability distribution of MMB energy. The problem this presents is that each MMB alters the surface micro texture which is shown to influence the MMB energy. Therefore, evaluating a larger number of switching cycles would increase the influence of surface change due to the MMB, particularly at higher currents where the duration and energy of the MMB is greater. That the MMB distributions appear to be approximately normal and the trend between switching current and the mean MMB energy is close to linear indicates that an average of 50 cycles provides adequate repeatability for this study.

MMB Energy Relationship with Current

The linear relationship shown between MMB energy and circuit current is unexpected. The molten metal bridge is a thermal process driven by Joule heating from DC power. The relationship between switching current and MMB energy has been proposed to be an i^2r relationship. In the previously proposed process of fine transfer wear in the Au/MWCNT contact [133], the relationship is based on this assumption. The discrepancy can be explained with reference to the constriction resistance which is not a constant but evolves dynamically. As material is melted the size of the MMB must increase and as the contacts continue to separate the MMB will be elongated. It is the geometry of the MMB that determines the constriction resistance, which in turn drives the Joule heating, which in turn influences the geometry of the MMB.

That the average MMB energy has a linear relationship with current is therefore an important empirical observation in developing an enhanced model for predicting contact lifetime, which is a key objective of this work.

A fine transfer model proposed by Chianrabutra et al was later proposed [57]. Where the load current is I, the maximum volume of material for transfer is V_{max} and k is an experimentally determined transfer constant, then the number of cycles to contact failure N_f is given by

$$\frac{V_{max}}{kI^2} \qquad (4\text{-}2)$$

In a the study by Lewis et al [103] where a MEMS scale cantilever was used with a lower contact force of 35 µN the trend of MMB duration also appears to be linearly dependant on current. The plot from the previous study is shown in Figure 4-27

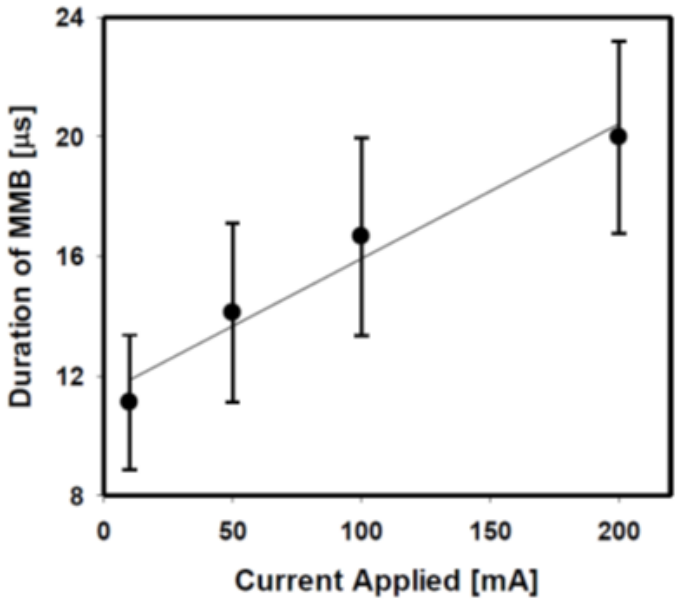

Figure 4-27 – MMB Duration with Switching Current for a MEMS Cantilever to Au/MWCNT Surface [103]

In practice, the end point of the molten bridge is it's rupture, and this may be caused by a variety of factors such as collapse of surface tension, convection turbulence in the bridge, rupture by boiling or being pulled apart [89]. As such the energy and duration of the bridge are not determined solely by the thermal input power.

The overall MMB energy observed in this experiment is lower than reported by Lewis et al [19]. This is attributed to significant differences between this experiment and the Lewis study where the test apparatus, contact opening velocity and contact geometry are different. The Lewis study employed the tip of a low stiffness MEMS cantilever (resulting in a line contact) closed to 35 µN and opened at

relatively low velocity. This study uses a high stiffness PZT cantilever with a ball contact closed with a 1000 µN closure force. The contact opening velocity is shown to influence MMB duration in the next section.

The results demonstrate that re-evaluating the fine transfer model with a linear dependence on switching current should provide more accurate model for determining contact lifetimes at the range of currents investigated.

Increase in MMB Average Energy and Variance with Rough Surface

The increase in the variability of the MMB energy of the rough surface can be attributed to the nature of the surface. At the scale of the contact interface the rough surface has relatively few irregularly shaped peaks while the smooth surface has a more homogenous distribution of regular peaks. Any molten bridge event will microscopically alter the shape of the contacting asperities as the molten material re-solidifies. If an asperity is melted its height may have decreased such that for the next switching cycle it is no longer the final point of contact. Because the smooth surface has more regular and numerous asperities the molten bridge of each subsequent switching cycle is likely to be formed at a point with similar geometry. The energy of each molten bridge is therefore expected to be similar.

The increase in molten bridge energy observed with the rough surface can also be attributed to the distribution and geometry of asperities [71]. As the overall closed contact force is the same for both smooth and rough contact switching the reduced number of asperities means the local peak loads are expected to be higher.

Higher peak loads will cause more plastic deformation of the asperities causing flattening and a larger final area of contact. This is supported by the difference in closed contact resistance between the rough and smooth contacts (5.7 vs 1.1 Ω) while the bulk resistance is very similar (55 vs 57 mΩ) which indicates the effective contact radius (Holm radius) is expected to be smaller for the rough contact interface. It is noted that the rough surface represents an exception to the contact resistance to force relationship described by Equation (2-7) as the ratio of elastic deformation of the nanotubes to plastic deformation of the asperities is not the same i.e. the differences in deformation regime between the smooth and rough material cannot be described by bulk modulus.

With a larger, more conformal final contact area the molten bridge can be expected to be larger. Lewis noted that worn Au/MWCNT surfaces demonstrated increased MMB energy as the contacts entered the end of life stage [103]. The effect was attributed to smoothing of the contact surface by the flattening of many asperity peaks resulting in a single larger final area of contact. While both results are attributed to similar changes in the contact interface geometry it is noted that they are described in this study by an increase in roughness, and by Lewis as a decrease in roughness. This highlights that the roughness parameter is not enough to well describe the behaviour of the Au/MWCNT surfaces.

The decrease in molten bridge energy with the smooth surface illustrates that the hot switching longevity of the Au/MWCNT is enhanced by its texture which provides numerous and well distributed asperities. This is an important observation as it is the first time the texture of the Au/MWCNT composite has been shown to have an influence on the MMB energy a key objective of this work.

Influence of Contact Potential on MMB Average Energy and Variance

There is no clear correlation between the circuit voltage and the average MMB energy which is as expected. However, there is a small correlation between an increase in circuit potential and an increased variance of the MMB. This suggests the maximum MMB energy may increase with contact potential. A possible mechanism is the increase in energy of individual charge carriers with increased circuit potential. While it is concluded that circuit potential does not have a substantial influence on the MMB energy, it may still be related to surface wear by other mechanisms and increased circuit potential is identified as a condition for Experiment 5, where in-situ wear of the Au/MWCNT contact will be investigated.

4.4 Experiment 4 - Molten Bridge Energy and Duration with Contact Opening Velocity and the Delamination Event

The literature review indicates that surface tension of the MMB is a factor that influences its rupture. The rate of contact opening is identified as a parameter that can both be controlled by MEMS switch designer and influence surface tension. As this has potential to influence switching wear, and therefore contact lifetime, the influence of contact opening velocity on the MMB energy has been identified as a key objective of this work.

The investigation of the contact opening velocity suggests the occurrence of delamination events (DE) as seen during the investigation of the thin film Au are also occurring in the Au/MWCNT contact. This leads to two follow up experiments where DE behaviour is analysed. Firstly, the same switching conditions are applied to a bulk AgNi contact where no evidence of the DE are observed. Secondly the force as the contacts separate are analysed and found to be different between MMB and DE.

In the contact opening velocity experiment the PZT apparatus is used to hot switch an Au/MWCNT lower contact and Au coated hemisphere upper contact while the opening velocity of the contact is varied between 80 and 12,000 µm/s. Contact velocity is controlled by altering the frequency of the triangular waveform signal driving the PZT cantilever. The contact velocity is checked by laser displacement meter. Circuit conditions are 4V DC 20 mA with the closed contact force of 150 µN and a switch cycling rate of 0.5 Hz.

The contacts are bedded in for 100 cold switched cycles before being switched at 4V 20 mA for 200 cycles with the final 75 opening waveforms captured. A new location of the Au/MWCNT contact is used for each case. Histogram distributions of molten bridge energy are presented for each opening velocity in Figure 4-28.

Between 80 and 1,600 µm/s contact opening velocity the average MMB energy is consistently around 1.5 µJ but variability of the bridge energy increases with opening velocity.

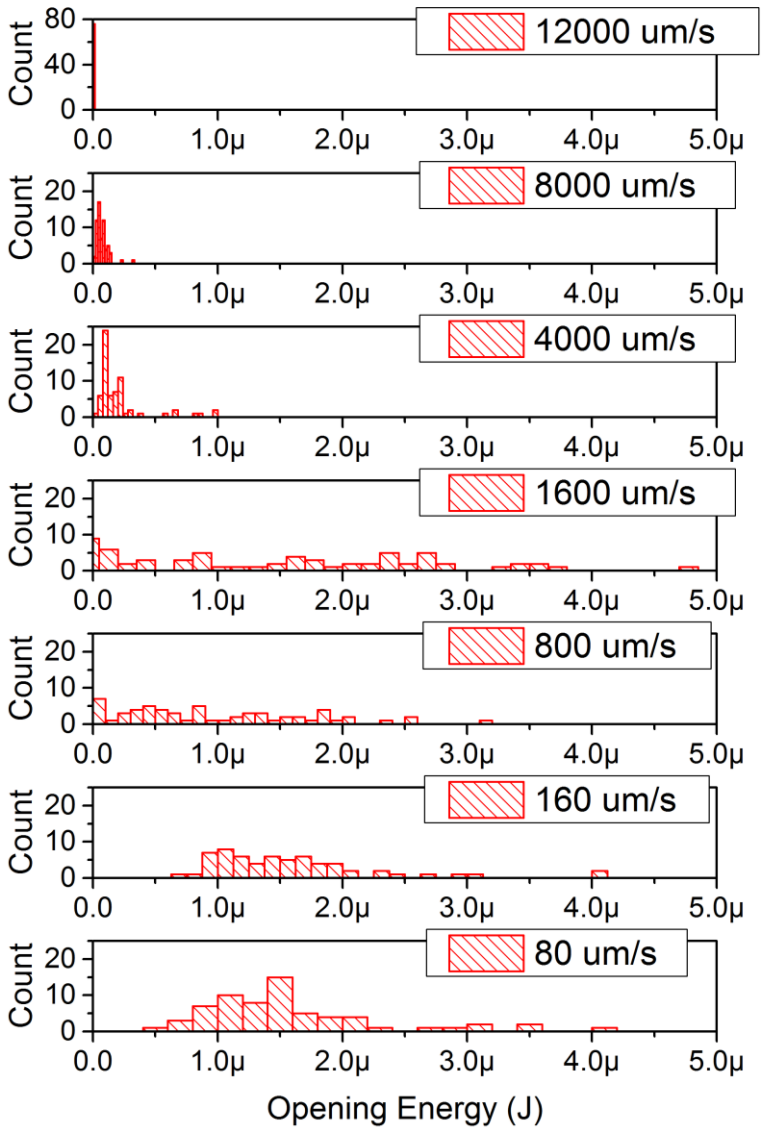

Figure 4-28 – Histograms of MMB energy as Contact Opening Velocity is varied

As the opening velocity is increased to 4,000 µm/s there is a decrease in the average MMB energy from 1500 to 500 nJ. Doubling the contact velocity to 8,000 µm/s corresponds to a decrease in molten bridge energy to around 100 nJ.

As the contact opening velocity is increased to 8,000 µm/s a new opening waveform is observed where there is instantaneous transition to the open circuit voltage without transition to the melting or boiling voltages for Au. The occurrence of the waveform is detected as a MMB of energy below 10 nJ indicating the contact voltage has risen from the closed circuit voltage to above the 3 V trigger threshold in single time step of voltage measurement.

The calculated MMB energy is presented in Figure 4-29 for each cycle with a vertical log scale. The smaller red ring indicates these events occurring at 8,000 µm/s while the larger red ring indicates the 12,000 µm/s events.

These waveforms were also detected during the study of the thin film Au contact (Experiment 1) where they were linked to the delamination of sections of the surface and interruption of molten bridge formation.

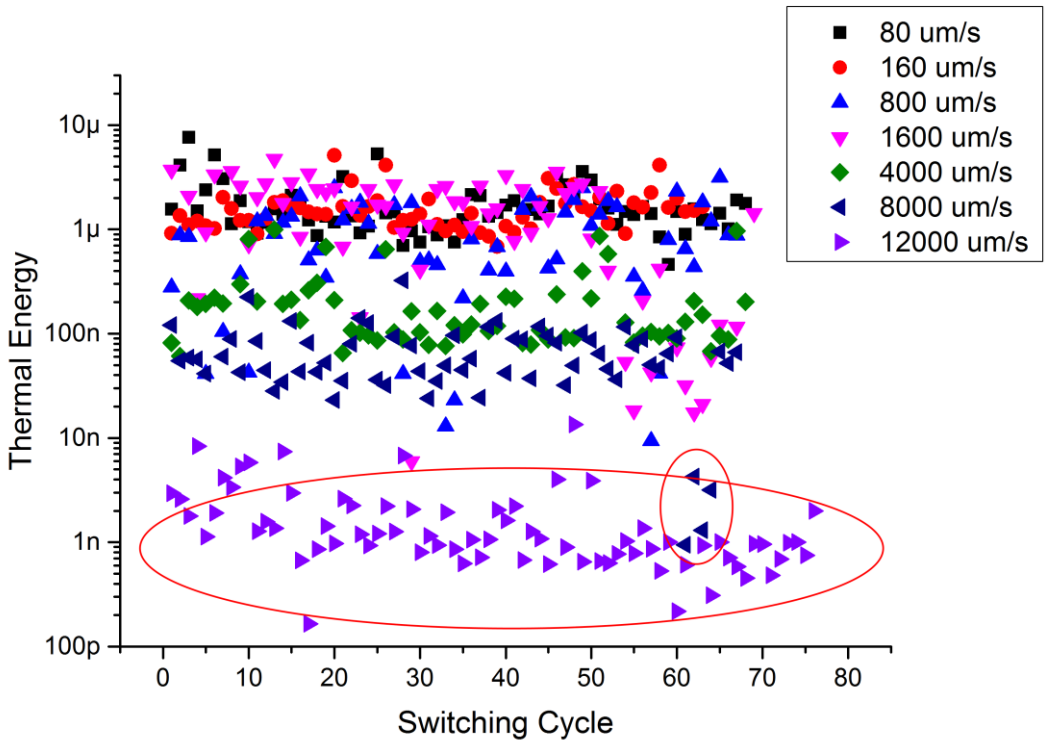

Figure 4-29 – The calculated MMB Energy for 75 consecutive switching cycles as contact opening velocity is varied

The average energy of the bridge and the variance (standard deviation) as contact opening velocity is varied is presented against contact velocity as a log scale in Figure 4-30. The figure illustrates that the molten bridge energy remains consistent between contact opening velocities of 80 to 1,600 µm/s but after exceeding around 1,600 µm/s the MMB is still present but with a significant decrease in energy.

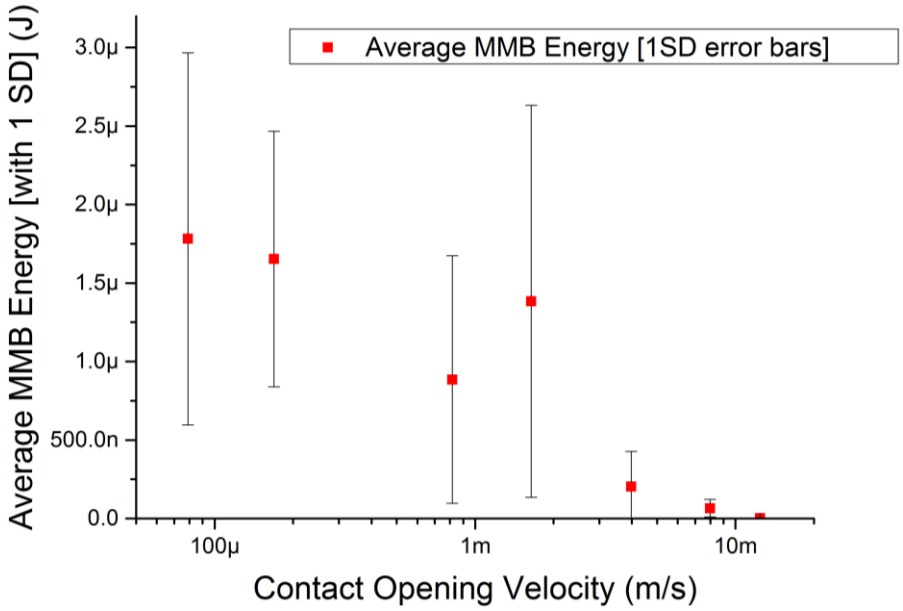

Figure 4-30 Average Molten Bridge Energy against Contact Opening Velocity with 1 Standard Deviation Error Bars

Because the effect is thought to be attributed to delamination of part of the thin film Au surface, a comparison experiment is carried out on a bulk silver nickel (AgNi) contact at the same circuit conditions and opening velocity.

4.4.1 Delamination Events in Au/MWCNT contacts cf. AgNi Bulk Contacts

In this experiment a contact pair made of bulk contact material (silver nickel – AgNi) is investigated at the same conditions as the Au thin film coated ball to Au/MWCNT composite contact pair. The same instrumentation is used to capture the transient voltage waveform. The objective is to show no DE occur in the bulk contact which should not be associated with delamination.

The 4V 20 mA circuit condition is used as it is linked to the highest occurrence of the delamination events (DE) in the next section – Experiment 5. A simple electromagnetically operated microswitch testing apparatus is used to operate a AgNi contact pair at 4 V DC 20 mA circuit conditions for 1,000 switching cycles at closure force estimate as ~ 2 mN from the contact resistance. The results are then compared to the results from switching the Au/MWCNT composite at similar conditions. Waveforms typical of the MMB and DE waveforms are presented in Figure 4-31 where the MMB waveform (red) fluctuates between the melting and boiling voltages for Au, the DE waveform transitions from the closed contact condition to the open circuit voltage immediately.

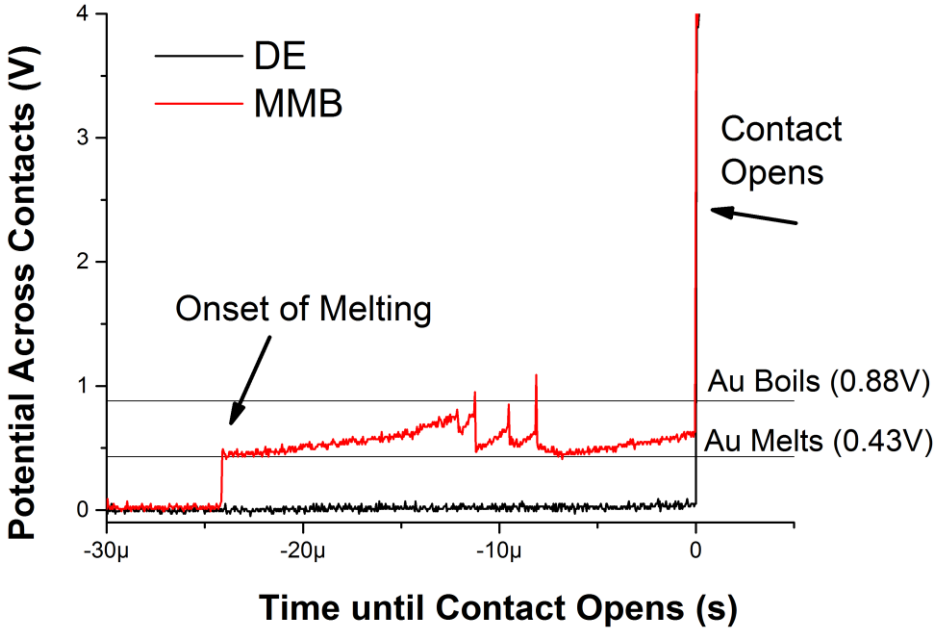

Figure 4-31 –Contact opening voltage waveforms typical of the molten metal bridge (MMB) in red and a delamination event (DE) black.

Figure 4-32 shows the distribution of calculated opening event duration as defined by the time taken to rise from 0.04 V to above 3 V for 5 consecutive samples. The figure shows that the Au/MWCNT and AgNi contacts have overlapping distributions for the MMB events. The Au/MWCNT contact has a shorter average duration of ~25 µs cf. ~50 µs for the AgNi contact. The AgNi distribution is normal with peak frequency in the middle of the distribution range. The Au/MWCNT contact demonstrates many events (more than 50 of 120) that are classified as having the shortest duration with the remainder distributed between 10 and 200 µS in duration.

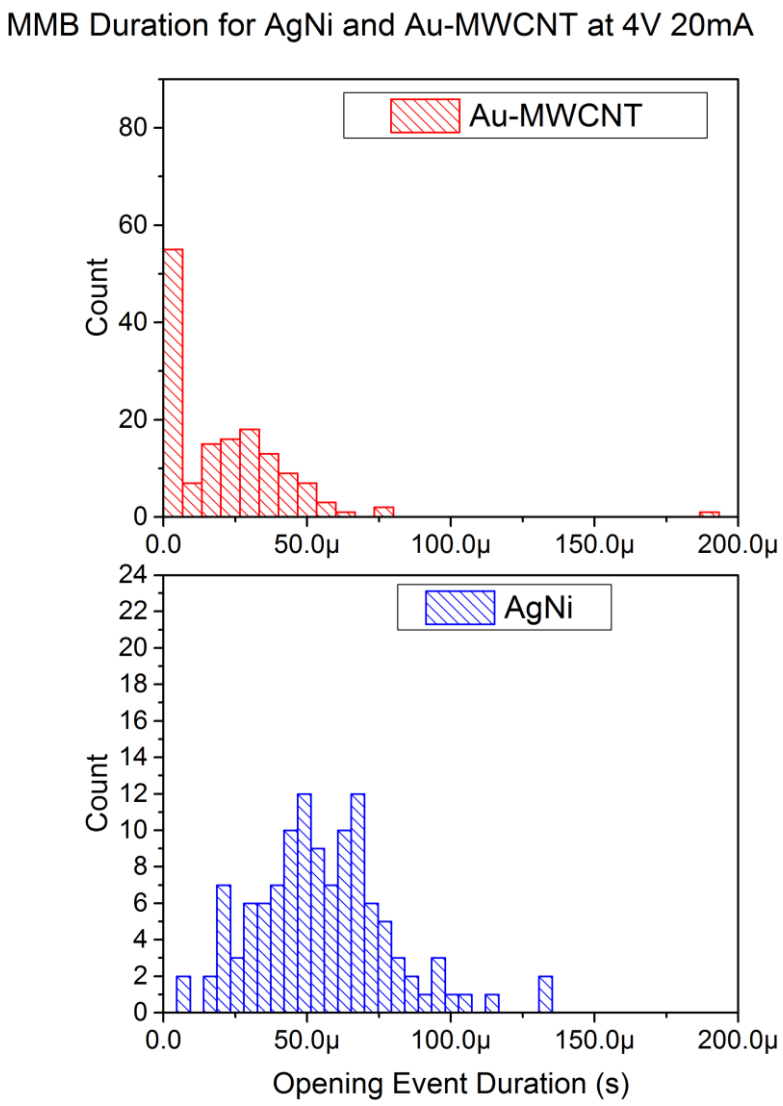

Figure 4-32 – Comparison of Au/MWCNT and AgNi Contact Molten Metal Bridges at 4V 20 mA Hot Switched Conditions – Molten Bridge Duration (left) and Molten Bridge Energy (right)

The duration of the opening events is then plotted against their occurrence in the switching sequence and the result is presented in Figure 4-33. The figure shows a trend in the duration of the Au/MWCNT opening event. Around switching cycles 20, 50 and 100 there are clusters of the contacts opening immediately one after another. Between cycles 55 and 80 there are no instant opening events detected and the event duration increases then decreases between these cycles. The suggested trend has been indicated with black arrows to highlight them. In contrast the AgNi opening durations appear to be far more randomised.

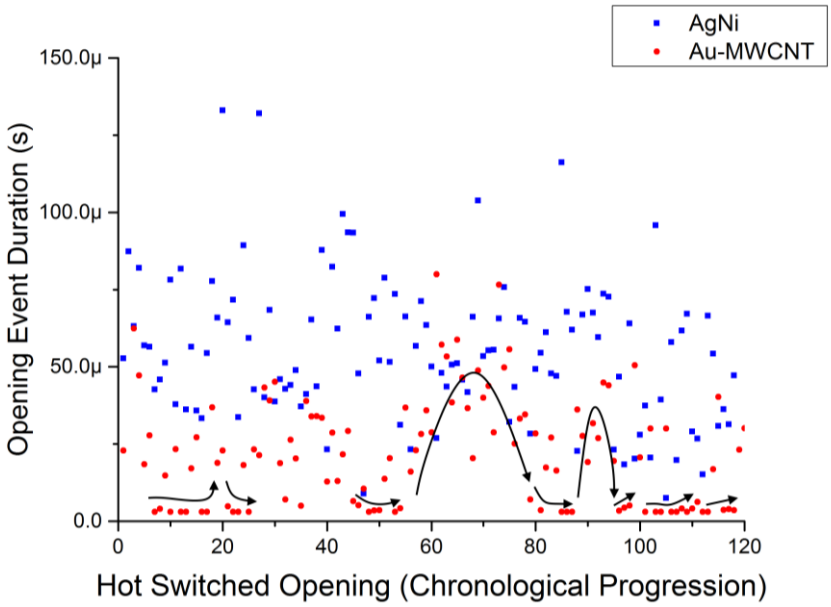

Figure 4-33 – Evolution of Au/MWCNT and AgNi Contact Molten Metal Bridges at 4V 20 mA Hot Switched Conditions with ongoing switching cycles – The black arrows indicate trends as the duration of the MMB changes gradually with ongoing cycles

4.4.2 Transient Forces Associated with Delamination Events and Molten Metal Bridges

In this section the PZT apparatus is used to capture the contact opening waveform of the hot switched Au/MWCNT contact but at the same time the transient force experienced at the contact is also captured. The objective is to characterise any difference in the forces observed between the MMB and DE contact openings.

The contacts are positioned to achieve a 150 µN static closed force. The static closed force is determined using the same charge amplifier with a 20 s time constant. The contacts are opened to a clearance of ~ 25 µm by applying a 20 V signal to the piezoelectric cantilever. The contact closes when the signal to the piezoelectric cantilever is 0 V. The drive signal to the cantilever is an offset 0 – 20 V square wave 0.5 Hz signal. The contacts are 'bedded in' for 1,000 cycles with no circuit load to allow the contact interface to mechanically stabilize. After 1,000 cycles with no electrical signal the load circuit is switched on. A further 100 cycles are carried out hot switching a 4 V DC, 20 mA signal. The contact potential and transient forces associated with these 100 contact openings are captured. The voltage and force signals are sampled at 0.4 ns over 80 µs (200,000 points). A schematic of the contact interface and a free body diagram of the force sensor showing the convention used in the graphs for positive and negative force is shown in Figure 4-34

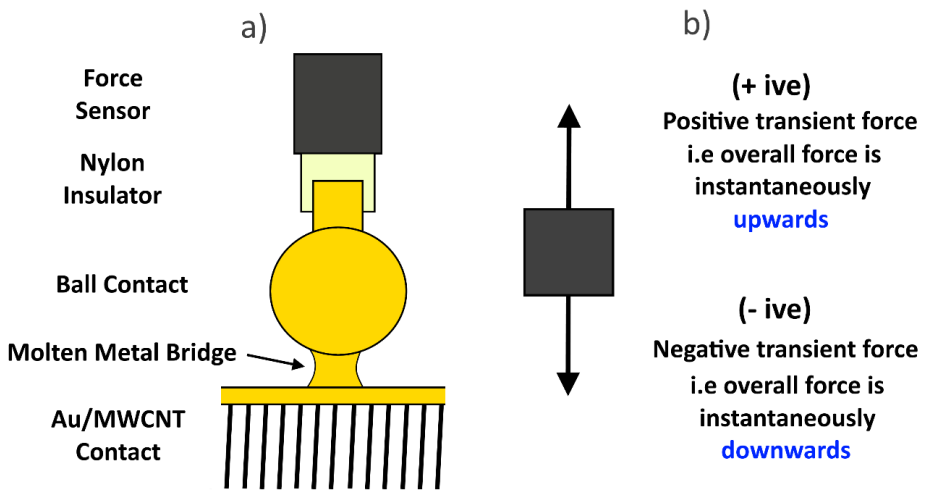

Figure 4-34 – The contact force measurement arrangement a) and a free body diagram of the force sensor showing the convention used in graphs for positive and negative force (b)

Examples of the contact opening voltage and transient force detected during a molten bridge opening and a delamination event opening are presented in Figure 4-35. The figure shows the contacts from 500 ns before the contacts open to 100 ns after.

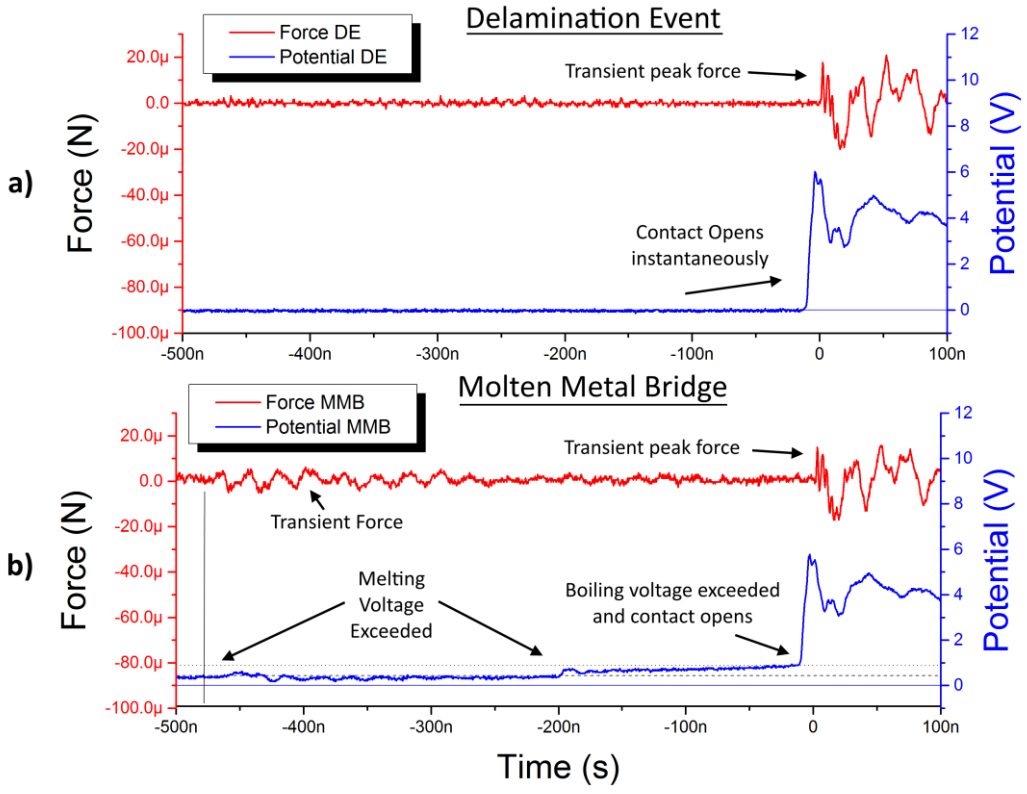

Figure 4-35 – Examples of the force and contact voltage during a Delamination Event (top) and Molten Metal Bridge (bottom) from 500 ns before the contact opens with the transient peak force as the contact opens indicated.

The DE force graph Figure 4-35a (red trace) shows the force sensor at the noise floor (~ 1 µN) while the contact potential graph Figure 4-35 a) (blue trace) remains at the closed contact potential. At time = 0 the contact potential instantly rises above the open circuit voltage and a positive force event around 20 µN is detected. Both force and the voltage potential oscillate after this event.

The MMB force graph Figure 4-35b (red trace) shows force events above the noise floor of the force sensor. The contact potential varies above the normal closed contact potential, with steps shown to correspond with the melting voltage (horizontal dashed line) and boiling voltage (dotted black line) for Au. The contact potential rises to the boiling voltage for Au where it then rapidly rises above the open circuit voltage and a positive force event of ~ 20 µN is detected. The force and voltage oscillations observed are like the DE example.

The Molten Metal Bridge and the Transient Contact Force

While each MMB event is unique, a representative example is presented in Figure 4-36 over a longer time duration that Figure 4-35.

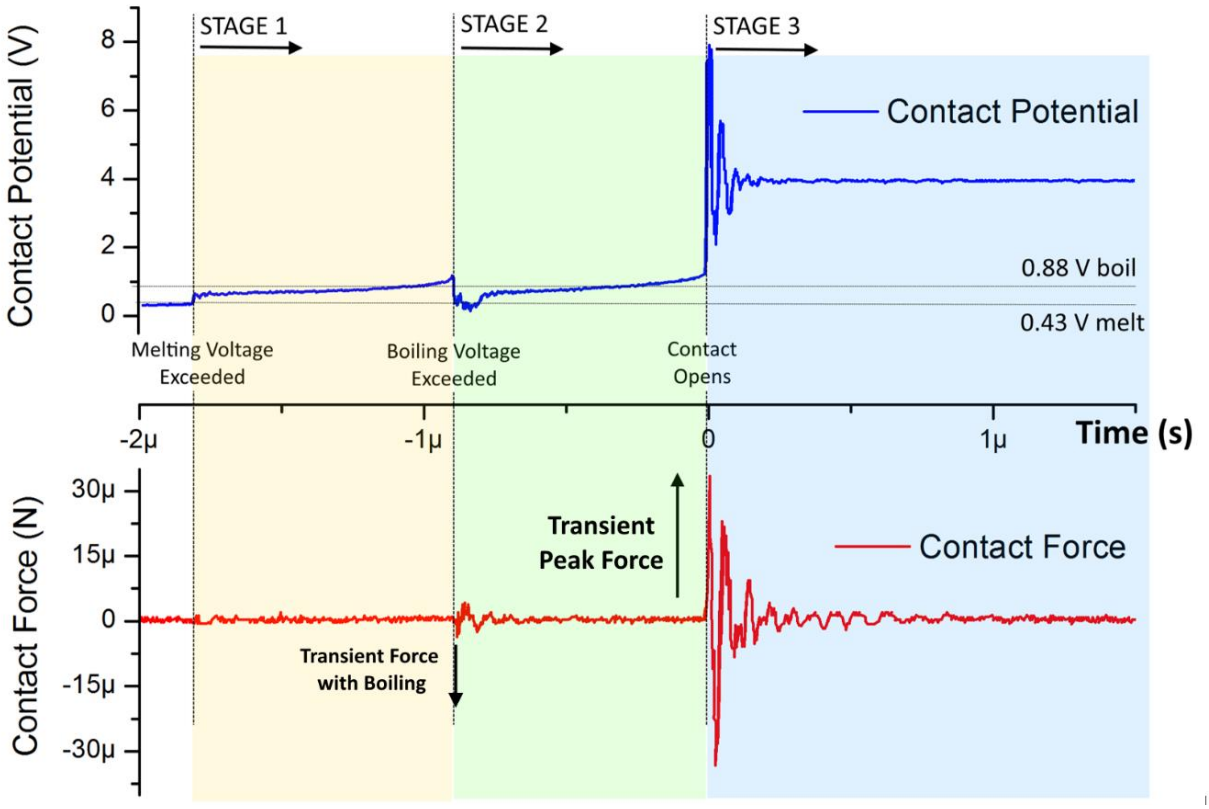

Figure 4-36 – Molten metal bridge contact potential and the corresponding Transient Peak Force.

Stage 1 Melting Voltage Exceeded (from ~1.8 µs before contact opening)

Contact potential (blue) and the transient force experienced by the upper contact (red) are shown from 2 µS before to 1.5 µS after contact opening. The time scale shows t = 0 s as the contact opening. The event labelled as Transient Peak Force in both Figure 4-35 and Figure 4-36 is a positive event showing the net force acting upwards on the upper contact has increased. The opening event is described in three stages. As the contact potential steps from just below 0.4 V to above 0.6 V (this is above the melting voltage for Au), there is a very low-level force that is within the noise level of the sensor. At end of stage 1, the contact potential rises to 0.9 V before rapidly increasing to 1.1 V exceeding the boiling voltage for Au at time = -0.9 µS. The rapid increase from 0.9 V to 1.1 V occurs over 30 nS.

Stage 2 – Boiling Voltage Exceeded (from ~ 0.9 µs before contact opening)

At the start of stage 2, the contact potential drops sharply from 1.1 V to 0.2 V. After a further 150 ns the contact potential rises back to 0.6 V. When the contact potential drops from 1.1 V to 0.2 V a force transient is detected peaking at 5 µN and lasting 150 ns. The force is initially in the opposite direction to the transient peak opening force in Fig 6. is damped after 150 ns. From t = -0.75 µs the contact potential slowly rises from 0.6 V to 0.9 V and above the boiling voltage. The contact potential increases more rapidly from 0.9 to 1.1 V over 100 ns before a step change to nearly 7.8 V occurs.

Stage 3 – Contact Opens

This is the point at which the contacts are deemed to be open and the circuit has been interrupted. After the circuit is open the contact potential oscillates 5 times over 260 ns around the open circuit voltage of 4.1 V varying between a maximum of 7.8 V and a minimum of 2.2 V. The time period of each oscillation in contact potential is 52 ns. The force is initially positive and then oscillates 8 times over the next 700 ns with a time period of 87 ns. The peak force when the contact opens is defined as the Transient Peak Force.

The Classification of Delamination Events (DE) and Molten Metal Bridge (MMB) Events

The type of opening event is classified by the transient voltage waveform. DE show a single abrupt voltage step to the open circuit voltage while MMB show multiple stages of rising and falling contact potential as the bridge is formed. Figure 4-37 shows 100 consecutive hot opening events as both

contact potential vs time (left) and the number of events of a given duration (right). The MMB events waveform are highly variable from one event to the next. It has previously been shown that groups of consecutive cycles at the same switching conditions are well described by a Gaussian distribution [95]. It is possible to distinguish a clear difference between the DE and MMB events in Figure 4-37 (left) as there are no MMB apparent with a duration of less than ~10 µs. However, it is difficult to see the number of DE as each trace is effectively overlaid. By evaluating the duration of each event and plotting the number of events at a given duration (Figure 4-37 right) it is very clear that there are two distinct type of event. Approximately half the events are classified with a duration under 7.5 µs while the remainder have a duration above 10 µs. Using this methodology, the short duration events are classified as DE and the longer duration events as MMB. No events are classified with a duration between 7.5 and 10 µs.

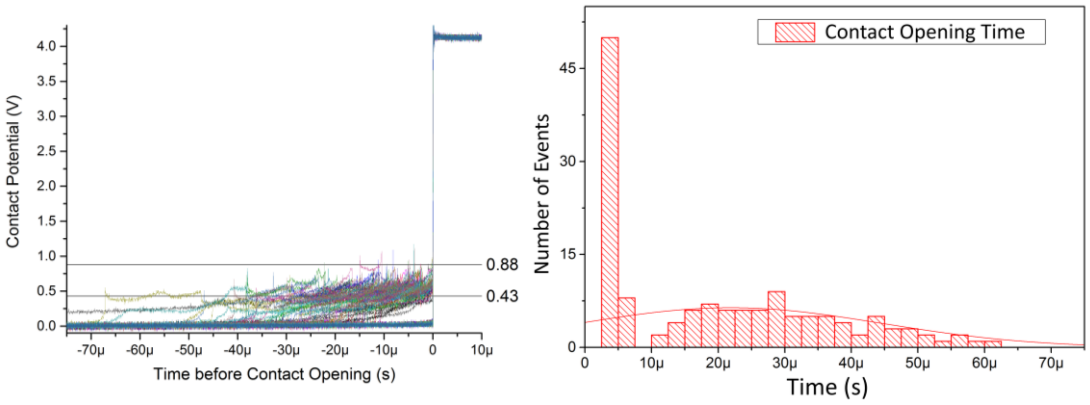

Figure 4-37 – The transient voltage waveforms of 100 consecutive switching cycles (left) and a histogram showing the calculated duration of the opening event. The individual molten metal bridge (MMB) waveforms are highly variable but rise to 0.43 and 0.88 V prior to opening. The delamination events (DE) show no increase in the contact potential until the contact abruptly opens.

With the contact opening now classified as either MMB or DE events, the contact force can be evaluated and according to the type of opening event.

The Contact Opening Force for Delamination and Molten Metal Bridge Events

Figure 4-38 shows a histogram distribution of the Peak Transient Opening Force of the 100 hot switched (4 V DC, 20 mA) opening events. The colour scale shows the contact opening type by colour with MMB (blue) and DE (red) with a normal distribution curve fitted to each type. The figure demonstrates a nearly equal number of DE and MMB events.

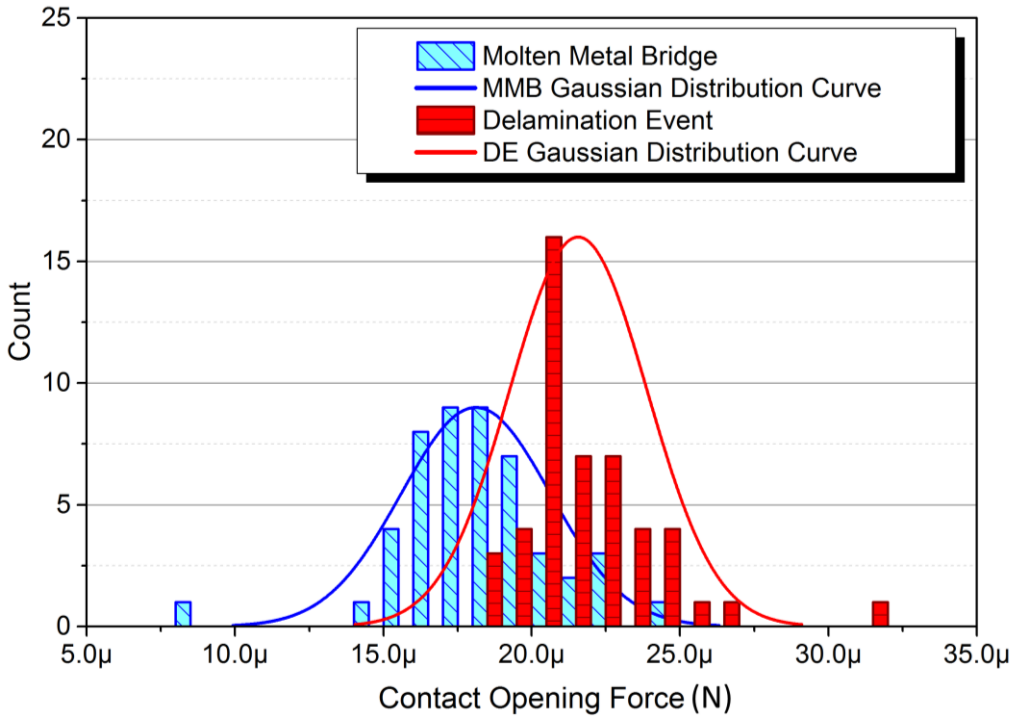

Figure 4-38 – A histogram of the Transient Peak Force of 100 consecutive hot switched contact openings at 4V 20mA. Delamination events (DE) are shown in red while the molten metal bridge (MMB) events are shown in blue. The average Transient Peak Force is 18.1 µN for MMB and 21.6 µN for DE.

The distribution of Transient Peak Force for MMB is close to Gaussian distribution with a mean opening force and standard deviation of 18.1 ± 2.5 µN. The distribution of DE type demonstrates a slightly more leptokurtic (peakier) distribution with a higher mean opening force of 21.6 ± 2.3 µN. This represents the DE contact openings having a ~ 20% higher average Transient Peak Force than the MMB type.

4.4.3 Discussion

Variation of Contact Opening Velocity

In this section the contact opening velocity was varied between 80 and 12,000 µm/s. Average MMB energy was around 1.5 µJ per cycle between 80 and 1,600 µm/s with a but the distribution of MMB energies increasing with opening velocity (Figure 4-28). Average bridge duration is illustratively 200 – 400 µs. An estimate for bridge length is between 32 and 640 nm by approximating the real contact separation speed using the peak contact opening velocity and assuming the MMB begins to extend as soon as it is formed. It is noted that the contact opening velocity is not the actual speed of contact separation as the point the MMB forms for two reasons. Firstly, the contact will be accelerating from

rest, and secondly the highly elastic and compliant nature of the Au/MWCNT surface means the surface will be restoring to its unloaded condition. However these lengths are in keeping with previous observations that Au tends to form short bridges at micron scale in length at currents of 10 – 1000 A when the reduced current is considered [89].

The relatively stable average energy MMB across a wide range of opening velocity (80 – 1,600 µm) suggests that the surfaces are separating in a similar way each time. This can be explained by the surfaces being microscopically cold welded together at the conduction interface. There would therefore be a small force required to pull the surfaces apart which means there is slight tension through the contacts at the final point of contact. As the molten bridge develops, the tension between contacts would be a function of the closed contact force and would not be expected to be influenced until the opening velocity exceeds the speed that the deformed Au/MWCNT surface can restore. The bridge then fails by boiling rupture, and the boiling voltage (0.88 V) is seen to be reached in the opening waveforms.

As contact opening velocity is increased to 4,000 µm/s there is decrease in the average MMB energy from 1.5 to 0.5 µJ. The opening waveforms still reach the boiling voltage which indicates that the current constriction has occurred more rapidly . This is explained by the opening velocity being large enough to mechanically extend draw out the bridge so its cross section is decreased and its constriction resistance increases, increasing the heating in the bridge and resulting in a faster rupture of the bridge by boiling.

At 8,000 µm/s the average MMB energy decreases further and there are contact openings observed where there is no MMB waveform. The waveforms suggest the delamination events detected in the thin film Au contact (Experiment 1 - 4.1.3) also occur in the Au/MWCNT composite. It is proposed the contacts are now opening with enough velocity and force that the adhesive energy between contacts is overcome by the tension force without the surfaces melting. A mechanism proposed is insufficient time for the Joule heating from the current constriction to raise the temperature of the constriction to the melting point. If the tension force causes a small area of the contact surface to breakaway rapidly such that the current constriction does not reach the critical point where Joule heating results in melting a molten bridge will not be formed.

An estimate for the time required is now made using the ϑ-ψ theorem. Assuming the constriction is modelled by an electric current passing through a semi-infinite body with a circular constriction of

radius a, and that resistivity (ρ) and thermal conductivity (λ) are independent of temperature, and current density is j, heat capacity per unit volume is c, the increase in temperature (T) with time (t) can be described in spherical coordinates in differential form [66]

$$\lambda\left\{\frac{\partial^2 T}{\partial r^2}+\frac{1}{r}\frac{\partial T}{\partial r}+\frac{1}{r^2\sin^2\vartheta^2}\frac{\partial^2 T}{\partial \vartheta^2}\right\}-\frac{c\,\partial^2 T}{\partial t^2}-\rho j^2=0 \qquad (4\text{-}3)$$

The solution can only be arrived at numerically, but it is shown in [134] that the solutions are of the form

$$\frac{A}{c}\frac{e^{-\frac{cr^2}{4\lambda t}}}{\left(\frac{4\pi\lambda t}{c}\right)^{3/2}} \qquad (4\text{-}4)$$

And at the location of the constriction r ~ a, the time constant for temperature rise to steady state is

$$\frac{ca}{4\lambda} \qquad (4\text{-}5)$$

Taking values for Au of c = (specific heat capacity / density) = 2.43 x106 Jm^3K, λ = 297 $Wm^{-1}K^{-1}$ and ρ = 2.19 μΩcm and assuming a likely constriction diameter of between 100 nm and 10 μm (based on SEM surface imaging of the Au/MWCNT Figure 4-39) the time constant is calculated as between 0.20 μs and 0.02 ns respectively. An estimate for the time required for the contact region to rise in temperature to reach peak temperature can be made using 5-time constants which gives a time of between 1 μs (for a 10 μm constriction) and 0.1 ns (for a 100 nm constriction). It is noted that the duration of the shortest MMB at 8,000 μm/s is around 2 μs. If the final area of contact can separate either as an instantaneous step change (delamination) or more rapidly the Joule heating can melt the constriction, then a limit is reached where no molten bridge will form as the contacts separate. It is noted that the molten bridge is a dynamic and highly unstable phenomenon and by its nature will never reach thermal equilibrium. However, the estimate gives a useful guide to speed and scale of a delamination event.

Sequences of DE

The sequence of opening energy can be explained with reference to the mechanism for delamination. Once a delamination of the surface material has occurred the material is still a prominent part of the contact interface – only transferred to the opposing contact. As the contacts come together again it can again form part of the conductive path again, and as an already weakened part of the surface detach again. Back and forth transfers were observed in the thin film Au contact (Experiment 1 - 4.1.3). and this provides the mechanism for delamination events to occur in sequences. The mechanism also suggests why the Au/MWCNT has demonstrated tolerance to the effect, particularly when the microroughness characteristics of the Au/MWCNT are considered. This suggests the area of the delaminated section is smaller than observed in thin film Au.

At similar switching conditions in a bulk Ag/Ni contact there was no evidence of the DE in 1000 consecutive switching operations. The consistent occurrence of the molten bridge during hot switching openings in the AgNi contact in similar switching conditions to the Au/MWCNT contact supports the observation that the delamination event is specific to the thin film nature of the surface of the Au/MWCNT composite.

The Molten Metal Bridge and the Transient Contact Force

The results show that the MMB event can be detected by the force sensing method. The force events are synchronized with step changes in the contact potential linked to phase changes in the contact material predicted by the ϑ-ψ theorem [70].

Stage 1 – Melting Voltage

The first force event is a small shock or vibration caused by liquid surface tension as the MMB is formed. The observed force indicates that as the liquid bridge initially forms there is a small increase in adhesion force. Over the following 900 ns the contact potential rises smoothly as the constriction resistance increases, with no force transients detected at the contact. This indicates the contacts are separating while the molten bridge is elongating and reducing in cross section while its temperature rises.

Stage 2 – Boiling Voltage

As the contact potential reaches 0.9 V it begins to rise more quickly reaching 1.1 V before suddenly dropping to 0.2 V in Figure 4-36. The observed drop in potential across the contact shows the current path has rapidly decreased in resistance. This suggests that on this occasion the circuit path is not interrupted by the onset of boiling but rather it has been deformed or distorted to include a part of the contact that is much cooler and in still in solid phase. This event is not typical and attributed to the unique properties of the Au/MWCNT surface. The MWCNT under the Au coating is acting like a spring with the deformation of the surface returning its non-loaded condition. The introduction of cooler material to the MMB momentarily reduces the average temperature of the bridge to below the melting (freezing) point for around 80 ns before the potential again exceeds the melting voltage. This period is explained by the new solid material becoming heated to a molten state.

As the contacts are separating, the refreezing of MMB causes an instantaneous force. This is experienced as a force by the force transducer, followed by a mechanical ringing that is damped as the bridge re-liquifies. It is noted that this is in the opposite direction to the defined Transient Peak Force and indicates that the Au/MWCNT surface is applying a force to the upper contact, as would be expected with the spring like nature of the surface.

Stage 3 – Contact Opening

Prior to stage 3 in Figure 4-36 the potential rises steadily from 0.6 to 0.9 V, and before again increasing more rapidly after reaching 0.9 V; however, this time the contact potential rises instantaneously (in less than 4 ns) to over 3 V. Simultaneously a sudden increase in force of 32 µN is detected at the upper contact. This event describes the rupture of the molten bridge by boiling, and the contacts separating. For the contacts to separate they must be under enough opening force to overcome the adhesive forces between the contacts. As the MMB boils it is broken and the surface tension that was acting as an adhesive force between contacts is instantaneously removed. The measured Transient Peak Force is therefore equal and opposite to the adhesive tension force in the MMB the instant before the bridge ruptures.

After the contacts have separated there is a transient ringing in both the electrical circuit and the response of the force transducer. The oscillation in force can be explained as mechanical vibration of the upper contact as MMB ruptures and its tension force is lost. The vibration characteristics are therefore related to the stiffness and the mass of the upper contact mount. It is interesting to note

that the time period of force and contact potential oscillations are of the same order at 52 and 87 ns respectively. Similar phenomenon were reported during opening of MEMS scale contacts, however the study used extremely low opening velocities that were unrepresentative of a practical device and subject to influence from environmental vibration [105].

Modelling Voltage Oscillation after Contact Separation

The observation of oscillation in contact potential following contact separation appears highly repeatable suggesting a ringing response in the electrical circuit. The response is modelled to check the empirically observed response matches the predicted response. The over voltage at the point of circuit rupture is critical to maintain below ~ 12 V as above this level micro arcing can be induced. The magnitude and time period consistent the circuit's inductance and capacitance are estimated from a series LCR model of the switching circuit behaviour (Matlab Simulink 2015) according to the second order transient response Equation (4-6).

$$V_s = LC\frac{d^2v_c(t)}{dt^2} + RC\frac{dv_c(t)}{dt} + v_c(t) \qquad (4\text{-}6)$$

Capacitance is estimated using a parallel plate model, while inductance is estimated as the self-inductance of a single loop of wire. The modelled and empirically observed values for overvoltage, time period and damping are summarised in

	Peak Over Voltage (V)	Time Period (ns)	Damping Time /6db (ns)
Experimental	**3.7**	**52.5**	**260**
Modelled	**3.8**	**69.4**	**427**

Table 4-3 - Summary of MMB Average Energy and Distribution between 4V 50mA and 12 V 50mA

The modelled values for peak overvoltage and the frequency of the response closely correlate with the experimentally observed voltage transient at contact opening. The damping observed is higher than predicted by the model. This is expected as the model does not consider the influence of circuit capacitance changing (as would occur between real separating contacts), nor the dynamic impedance of the lead acid voltage source to a high frequency signal, both factors that would damp the response. The good agreement observed between the modelled and empirically observed values for overvoltage and frequency support the observation that the oscillation in the contact potential is

the circuit electrically ringing after opening due to its micro-inductance and pico-capacitance. Both empirical and modelled responses indicate the MMB test circuit does not exceed the threshold voltage for arcing [85].

It is noted continuous increase in separation of contacts means the capacitance will change dynamically. Both more advanced modelling of capacitance and load circuit inductance are identified for future investigation.

4.2. Classification of MMB and DE

The classification of opening events by duration demonstrates a distribution with a clear region of separation. This shows the classification method is effective at separating the MMB and DE events. It is noted that the use of the moving average filter will result in overestimated DE duration, which are effectively instantaneous but, the primary purpose is to classify the opening event type and this method provides a clear distinction between MMB and DE. The switching conditions were chosen as they have previously been linked with a frequent occurrence of the DE. The occurrence of DE marks a limiting condition for the formation of the MMB. Increasing either the current of voltage from circuit conditions of 4V 20mA demonstrated the number of DE decreased, while as the number of switching cycles increased the frequency of the DE increased [135]. The limiting case to the formation for the MMB can be explained by step changes in the conduction area. A requirement for the Holm ϑ-ψ theorem is that Joule heating raises the conductor temperature nearly instantaneously to a point of thermal equilibrium [66]. This is reasonable assumption provided the contact area and therefore constriction resistance change gradually. If there is a step change in the contact area occurring (such as a delamination), this may occur too rapidly for thermal equilibrium so no MMB is formed. The time constant for thermal equilibrium is dependent only on the thermal conductivity and heat capacity per unit volume of the conducting material and proportional to the contact area. Illustratively, for a circular constriction of diameter 10 µm in a Au conductor the thermal equilibrium time constant is calculated as 0.198 µs. It is noted than the observed MMB duration and contact areas reported in low force studies of the Au/MWCNT material are of similar magnitude [95, 121].

4.3. Distribution of Contact Opening Force

The distribution of Contact Opening Forces shows that DE are associated with a greater adhesion force between contacts than the MMB events. Figure 4-39 shows scanning electron micrographs of

the Au/MWCNT contact surface before and after hot switching at 4 V DC and 20 mA. There is evidence of both softening and melting as well as mechanical flattened and cracking of the surface. It is proposed that because of the speed of the DE there is insufficient time for a MMB to form. The Contact Opening Forces observed are evidence the adhesive force released during a DE are ~ 20% greater than during the MMB formed at 4 V 20 mA circuit conditions.

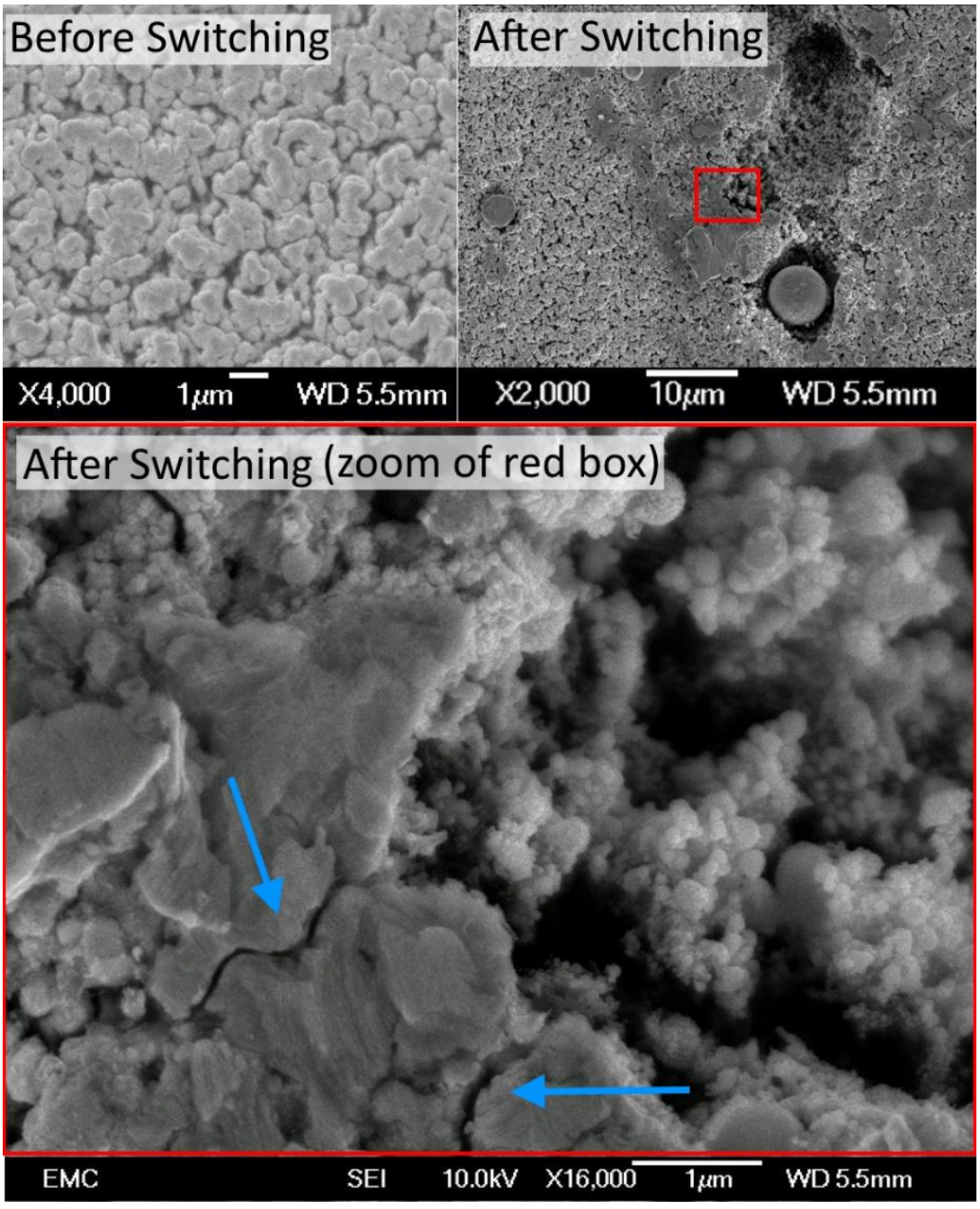

Figure 4-39 –Evidence of surface cracking and delamination of the Au surface after 1M Hot Switching Cycles at 4V 20 mA imaged by scanning electron microscopy following disassembly

In the MEMS switching regime contact opening force is limited. Small increases in adhesion are therefore linked to increase risk of the contacts failure by sticking [39]. It has previously been shown that varying the circuit conditions will influence the duration, thermal energy and size of the MMB.

Conclusion

The Contact Opening Forces in molten metal bridge (MMB) and delamination events (DE) have been investigated during hot switching of a Au/MWCNT composite contact at forces and switching conditions representative of the MEMS switch regime.

The magnitude and direction of micro force transients are observed under contact closure force and opening velocities realistic for a practical device. The force transients are linked to the melting and boiling processes that are also linked to a fine transfer wear process. A limiting case for the formation of the MMB is proposed where step changes in contact area occur too rapidly for thermal equilibrium.

Finally, the Transient Peak Force required is found to be ~ 20 % greater when DE are observed cf. MMB events. The observation suggests that the delamination events may result in greater force transferred to the contact surface. This is significant as it suggests that switching the contacts with a small signal present may be less damaging than where no signal is present.

4.5 Experiment 5 – In-situ Measurement of Fine Transfer in Au/MWCNT

In the previous sections the experiments were carried out using the PZT apparatus. The results from relatively low numbers of switching cycles have illustrated the linear dependence of molten bridge energy on current, increase in MMB energy variability with circuit voltage, and the presence of a waveform associated with surface delamination in thin film Au contacts and the interruption of the molten bridge.

In this section the newly developed ICE MEMS testing apparatus is used to study the evolution of wear on the Au/MWCNT switching surface. Empirically defining the evolution of wear in the Au/MWCNT contact is a key objective of this study as it provides data to more accurately model the contact lifetime.

The influence of current and voltage on fine transfer is investigated under three switching conditions. Contact pairs consisting an Au coated ball upper contact paired with a planar Au/MWCNT contact are hot switched at MEMS scale force (500 µN) for 100,000 cycles. The influence of circuit voltage and current are investigated using three switching conditions. A baseline case of 4 V 20 mA, an increased voltage case of 8 V 20 mA and an increased current case of 4 V 50 mA. These are referred to as the 4-20, 8-20 and 4-50 cases. The evolution of contact resistance, surface wear and contact opening waveform are evaluated. The switching process is interrupted to measure the surface of the contact over a 150 µm x 150 µm area around the contact site and the contact resistance. The first 10 cycles are measured. Measurements are then repeated at 100, 1k, 10k and 100k cycles. The MMB energy and contact opening waveform are captured for 150 cycles with 200 ns resolution immediately after a surface measurement. The effects of changing the voltage from 4 to 8 V and the current from 20 to 50 mA are reported.

4.5.1 In-situ Evolution of Contact Surface over 100,000 Hot Switching Cycles

The contact resistance was recorded before switching, after each of the first ten, 100, 1k, 10k and 100k switching cycles. The results are presented in Figure 4-40. In each switching case there is a settling process over the first 10 cycles where the contact resistance drops from the initial value to a lower stable value. Contact resistance then remains low and stable between and is between 0.34 and 0.39 Ω after 100k cycles.

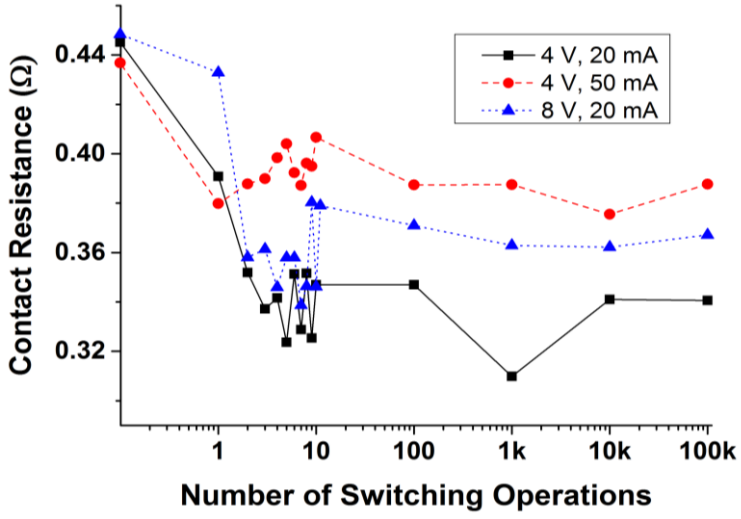

Figure 4-40 – Evolution of Contact Resistance over 100,000 Hot Switching Cycles

The captured contact opening waveforms are classified as either a molten metal bridge (MMB) or a delamination event (DE). A DE is considered to have occurred if contact opens with no transition to the melting or boiling voltage and rises to above 3 V in one step of the capture resolution (200 ns). The ratio of MMB to DE opening events expressed as a percentage is shown in Figure 4-41. For example, where all opening events are classified as MMB the percentage is 100; however, if all events are classified as DE then the percentage is of MMB is 0.

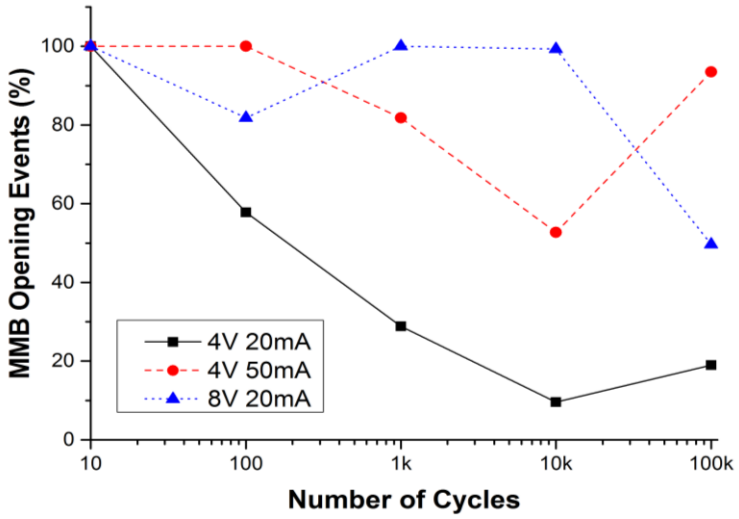

Figure 4-41 – Frequency of Delamination Event Occurrence during 100,000 Hot Switching Cycles

There is a 100% occurrence of the MMB in all three cases during the first ten switching cycles (no DE occur). As switching cycles increases all three cases show the presence of the DE. Over 100k cycles the control case demonstrates the highest occurrence of DE. Increased voltage (8-20 case) or current (4-50 case) show a decreased occurrence of the DE cf. the baseline (4-20 case). The increased voltage case demonstrates the lowest overall number of DE. In the 4-20 case there appears to be a trend of increasing numbers of DE with switching cycles, while the 4-50 and 8-20 cases do not show an obvious trend.

With the opening events classified the average molten bridge energy can be calculated. The average MMB energy with increasing switching cycles is presented in Figure 4-42. The error bars indicate the max-min energy of the sample. Over the first 100 cycles the lowest average energy is the 4-20 baseline (400 nJ), the increased voltage case is 1,000 nJ and the highest average energy occurs for the increased current 10,000 nJ. However as switching progresses there is significant variance in the average energy. The baseline (4-20 case) shows the most stable average energy over 100k cycles

(around 200 to 1000 nJ) while the increase current case shows the largest variance (around 50 to 10,000 nJ).

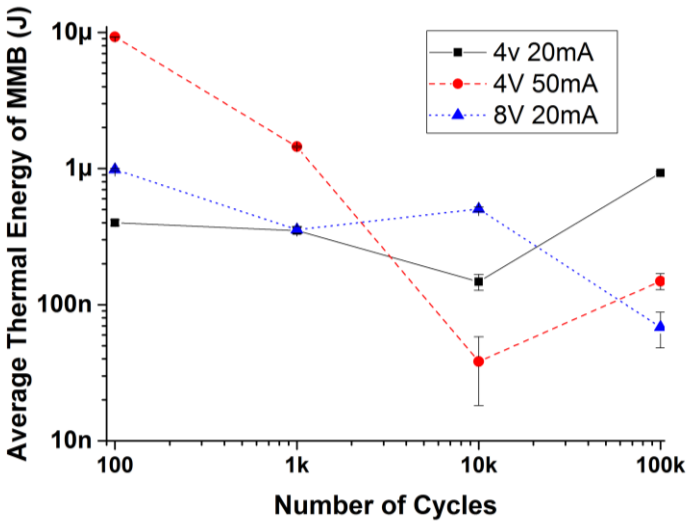

Figure 4-42 – Average Thermal Energy of the MMB during 100,000 Hot Switching Cycles

The areal (3-D) surface roughness parameter is calculated from the ICE system surface measurements quantitatively assess surface change. The contact site is evaluated over a 150 µm (x) by 150 µm (y) for height (z) at equally spaced 250 nm intervals (361,201 data points). The surface is then levelled to a linear least squares plane-of-best-fit to the surface data. The change in S_a from the original unswitched surface is then plotted against switching cycles and presented in Figure 4-43.

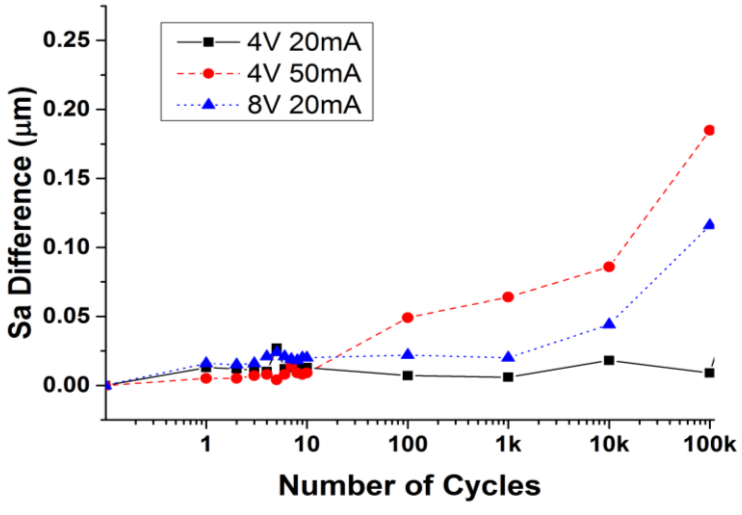

Figure 4-43 – 3D Surface Roughness against Hot Switching Cycles for 4V 20 mA, 4V 50 mA and 8V 20 mA conditions. Zero roughness is defined as the surface roughness before any switching has occurred.

Sa is used as it provides a highly stable parameter to quantify surface texture; however, it only evaluates surface amplitude change (height) and does not evaluate the scale (spatial frequency) of the texture. Over the first 10 cycles there is a trend for the surface roughness to vary slightly before stabilising. This trend is similar but inverted to the contact resistance trend. The greatest roughness increase in the first 10 cycles is 27 nm in the 4-20 case. The average change is 12 nm. The 4-20 case demonstrates a stable roughness over 100k cycles with a small overall increase of 9 nm. Both the increased voltage and current cases show progressive increase in surface roughness with switching cycles. The 4-50 case increases the most (185 nm after 100k cycles). The 8-20 case follows the same trend (116 nm after 100k cycles).

A visual evolution of the Au/MWCNT surface height is presented in Figure 4-44. Each panel represents a plan view of the contact surface over a 150 µm (x) by 150 µm (y) area. To clearly indicate the location of the highest surface peaks (contact asperities) and lowest troughs (wear regions), the scale for height is restricted to three colours – white regions are above +5 µm (peaks) and black regions are low than -5 µm (troughs). All other regions are coloured grey. Each column shows the circuit switching condition. Each row compares the same number of switching cycles. Both the 4-50 and 8-20 cases show measurable surface features after only a single switching operation. The features are labelled as B and C. Features B and C shows circular regions 3-6 µm in diameter. The edges are raised ~5 µm above the nominal surface on one side and depressed ~ 5 µm below the surface on the opposite side. In the 4-50 case there are two raised features separated by ~ 60 µm (feature B), while the 8-20 case shows three features separated by approximately 30 µm (feature C). After 10k cycles features are apparent at the same locations; however, the features show greater evidence of wear. In the 4-50 case the wear is described by features that are around 5 µm in height spread over a region approximately 100 µm in diameter. After 100k cycles a similar wear region and distribution of high points is seen to 10k cycles; however, there are significant areas where the surface has been penetrated by 5 to 6 µm. The wear region is irregular, made up of 4 or 5 sub-regions. The 8-20 case shows a smaller region of wear when compared to the 4-50 case after 10k cycles. The features of 8-20 are however broadly similar with a single significant difference, labelled feature D in Figure 4-44. Feature D presents as a donut shaped region ~ 10 µm in diameter but the edges show a significant increase in height. After 100k cycles the 8-20 case shows multiple areas raised ~20 µm above the nominal surface, labelled feature E with arrows. A donut feature is still apparent at the previous location of feature D. In the 8-20 case the most apparent change after

100k cycles is a region of continuous wear of 5 to 6 µm in depth. The 4-20 case demonstrates negligible wear after 100k cycles.

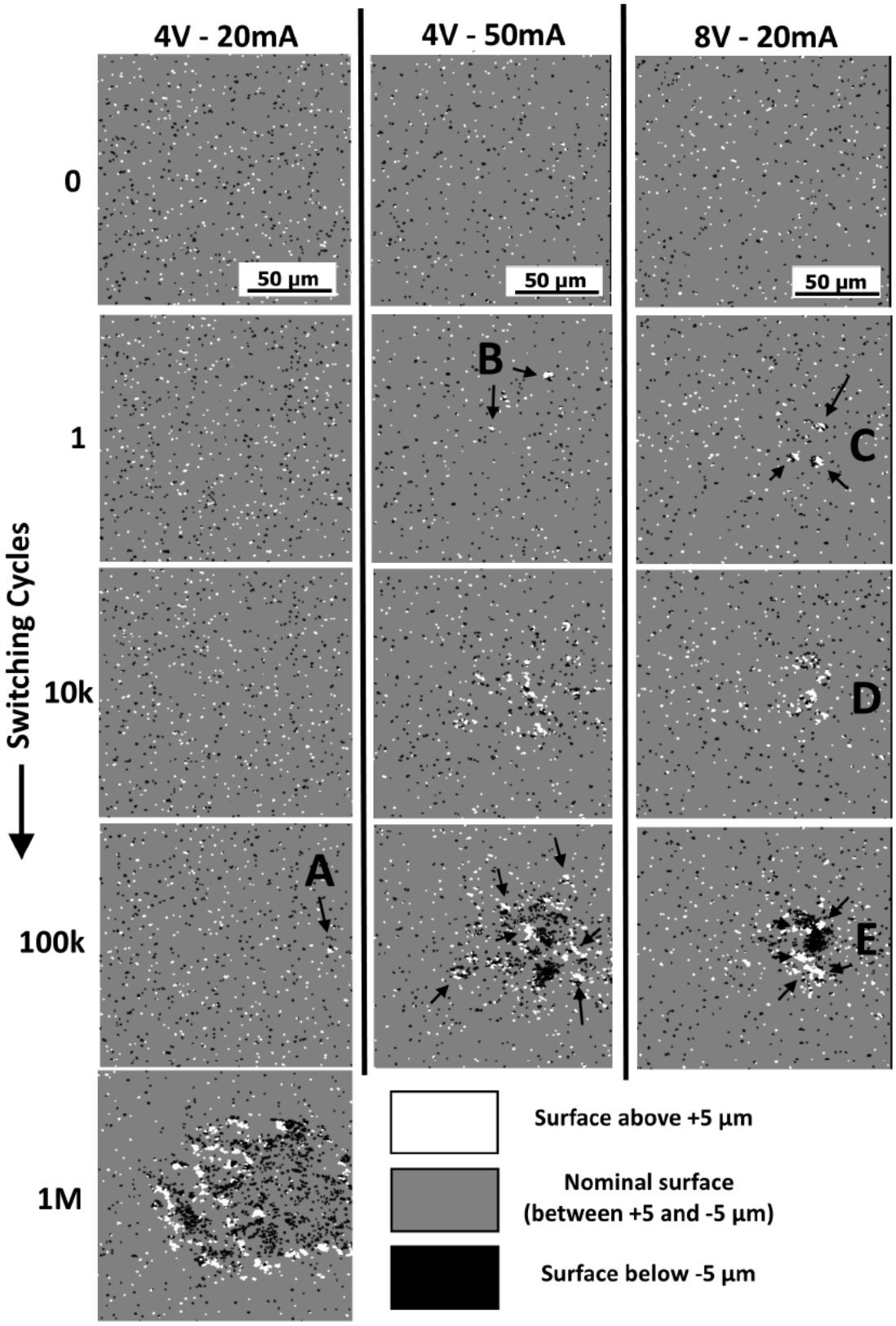

Figure 4-44 – Mapping the Development of Wear Pits (black) and Asperities (white) with increasing hot switched contact cycles using the ICE Apparatus

Figure 4-45 shows the volume of the asperity tips with switching cycles. The calculation is performed using commercial surface analysis software (Boddies 2.18, TaiCaan Technologies, UK). The volume is defined by a plane 5 µm above the nominal surface and any surface above this height. It therefore describes the total volume of the features shown in Figure 4-44 as white. The unswitched surface (i.e. 0 cycles) is plotted as 0.1 cycles on the logarithmic axis for convenience. After a single switching cycle all three cases show a measurable increase in the asperity volume, before a small decrease after 100 cycles. From 100 to 100k cycles the 4-20 case shows a consistent volume but the 4-50 and 8-20 cases show increase in volume, with the 8-20 case showing the greatest increase.

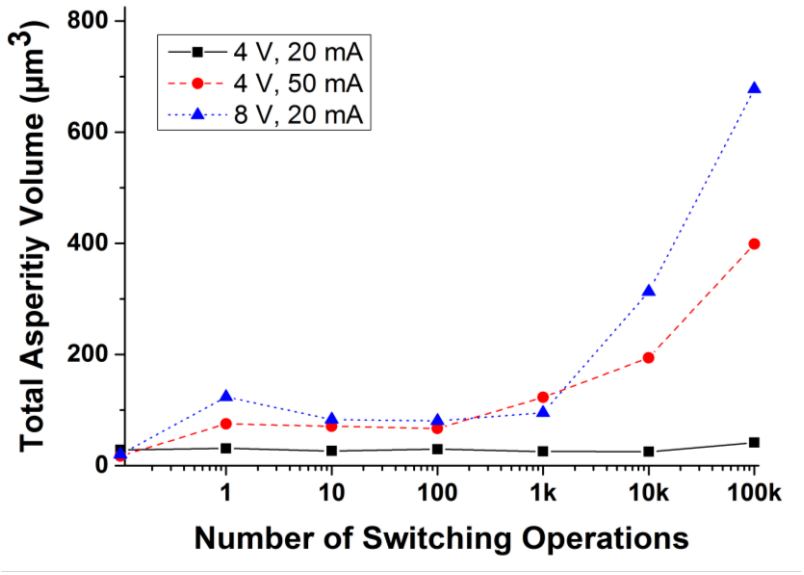

Figure 4-45 – Volume of the Surface Asperities against Hot Switching Cycles for 4V 20 mA, 4V 50 mA and 8V 20 mA conditions

Figure 4-46 shows the surface height map of the Au/MWCNT contact after 100k cycles. In each image a 150 µm x 150 µm area of the contact surface is shown. The surface height in each image is linked to the same ± 6 µm colour scale and relates to the 100k cycles 'row' in Figure 4-44. The dotted line indicates the location of the inset 2-D cross section. The scale of the cross section a 150 µm length and 40 µm in height in each image. After 100k cycles the 4-20 case shows minimal surface change while both the 4-50 and 8-20 case show significant evidence of wear. The 8-20 case shows the surface wear is confined to a smaller area than the 4-50 case, with the 2-D cross section showing the peaks higher (~20 µm v. 10 µm) and less numerous. In the 8-20 case the highest peaks are located immediately at the perimeter of the material loss region, while in the 4-50 case they are spread out and occur mostly in regions with no obvious material loss.

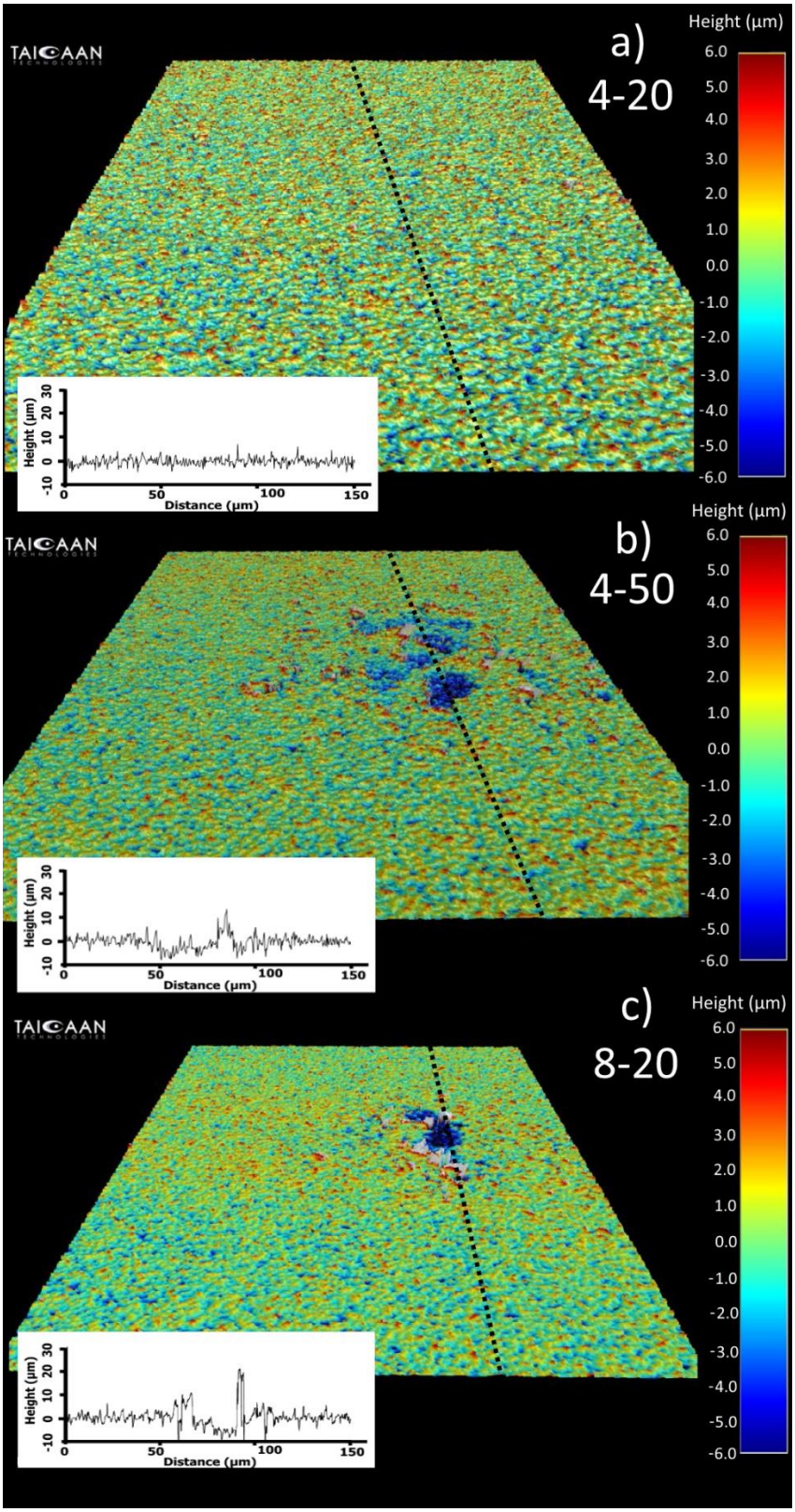

Figure 4-46 – The colour enhanced 3-D profile of the contact surface after 100,000 hot switched cycles for the (a) 4-20, (b) 4-50 and (c) 8-20 cases. The contact region is 150 µm by 150 µm. The colour scale represents regions of height difference. A 2-D cross section along the black dotted line is inset to each image at the same scale.

4.5.2 Post Switching Imaging of the Au/MWCNT Surfaces

At the completion of switching the contact surfaces are imaged with scanning electron microscopy (SEM) and compared to the ICE apparatus surface measurements. Figure 4-47 shows the surface measurement of the 4-20 case after 100k cycles (top), with a 2D cross section along a 125 µm segment, and a SEM image of the surface at the contact interface.

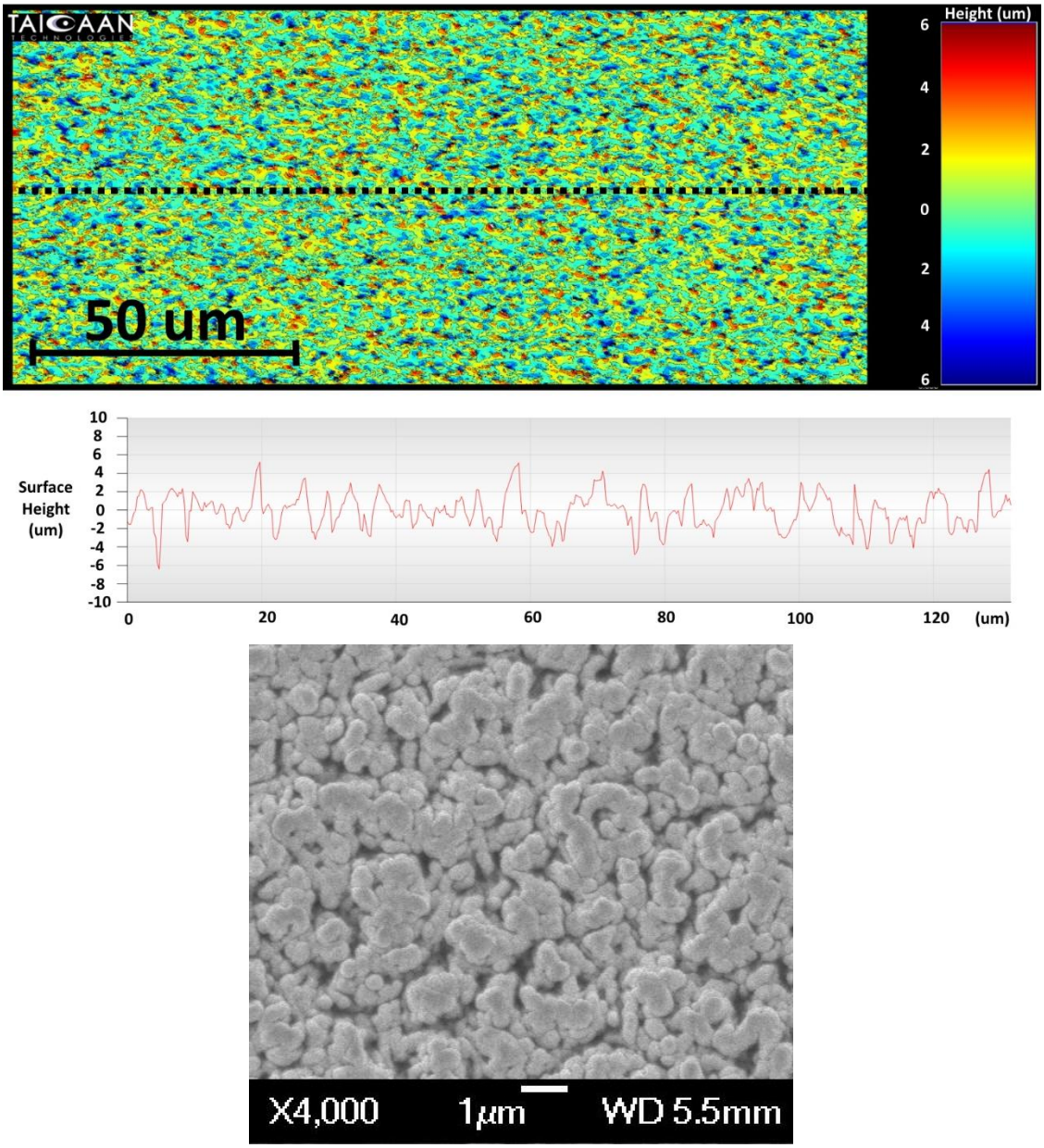

Figure 4-47 – The Au/MWCNT surface after 100k Cycles of 4V 20 mA Hot Switching measured in-situ by the ICE Apparatus (top) and imaged by scanning electron microscopy before switching begins (bottom)

The surface consists of numerous and well distributed Au particles. This provides an excellent conduction interface when mated with the smooth Au coated ball as it allows the formation of multiple a-spots and increases the apparent contact area, decreasing contact resistance. It is noted that there are no obvious signs of wear from switching, which is expected from the quantitative evaluation of surface roughness.

The surface of the 4-50 case is presented in Figure 4-48 with the ICE apparatus surface height (top) and the same region imaged with SEM (bottom).

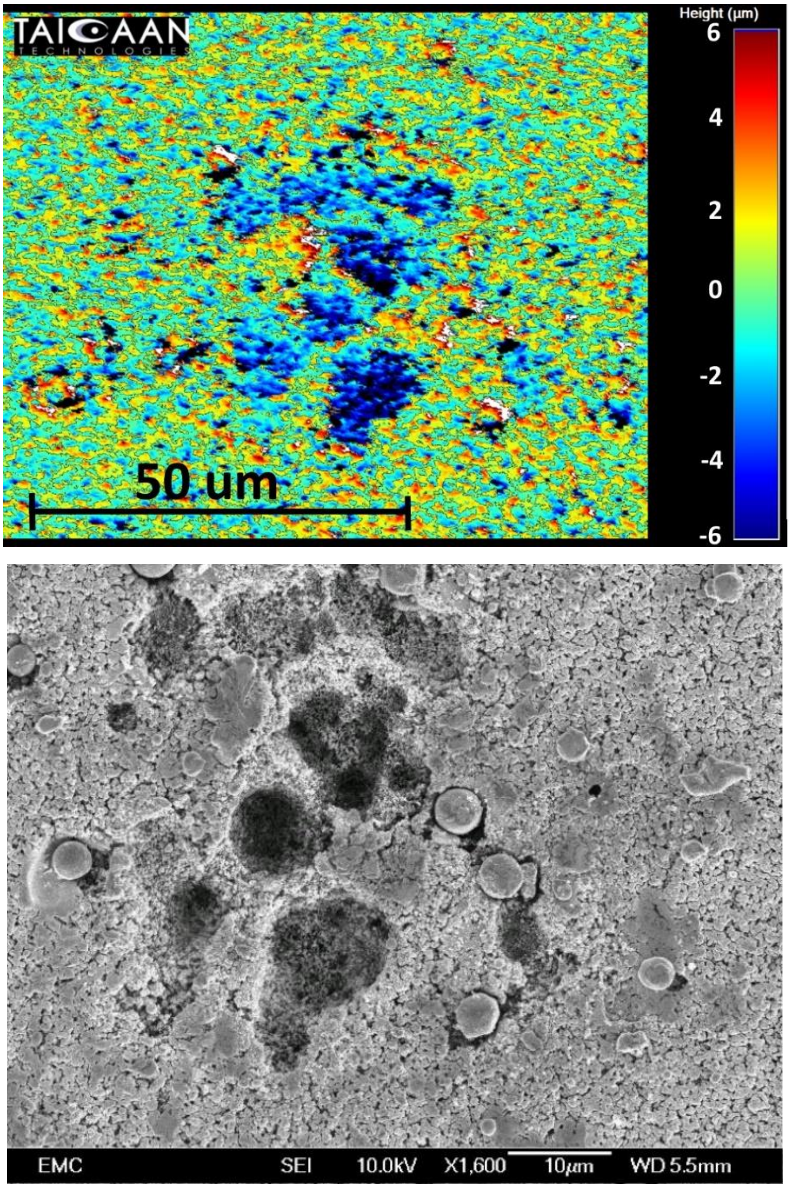

Figure 4-48 – The Au/MWCNT surface after 100k Cycles of 4V 50 mA Hot Switching measured in-situ by the ICE Apparatus (top) and imaged by scanning electron microscopy following disassembly (bottom)

The surface shows significant signs of wear characterised by a wide distribution of pits 2 – 6 µm in depth and around 10 µm in width, that have pierced the upper Au film to expose the underlying MWCNT. These regions appear as dark blue/black regions in the surface height map and dark grey/black region in the SEM image. The second features of note are Au features that appear to be nominally spherical and embedded so their crowns are nearly flush with the top surface. They are clearly visible in the SEM image as light grey circles between 2 and 5 µm in diameter. They are harder to detect in the surface height map (as they are embedded in the surface) but can be detected as rings of higher area (red/white) with a central depressed region (green or blue). The third features of note are flattened, smoothed regions 5 – 10 µm wide with irregularly shaped edges. These appear as dark grey regions immediately next to the pits in the SEM image. They are, again, less obvious in the surface height map, where they appear as slightly raised sections (red/yellow) with fewer peaks than the surrounding surface, indicating flattening.

The surface of the 8-20 Au/MWCNT contact after 100k switching cycles is presented in Figure 4-49 with the ICE apparatus surface height map (top) and the same region imaged by SEM (bottom). The surface height map shows a similar level of wear to the 4-50 case but in a more confined region. A single elongated pit is apparent with a large, apparently spherical particle at the lower edge ~7 µm in diameter. Smoothed and flattened regions with irregularly shaped edges are again apparent in the SEM image, at the edges of the pit.

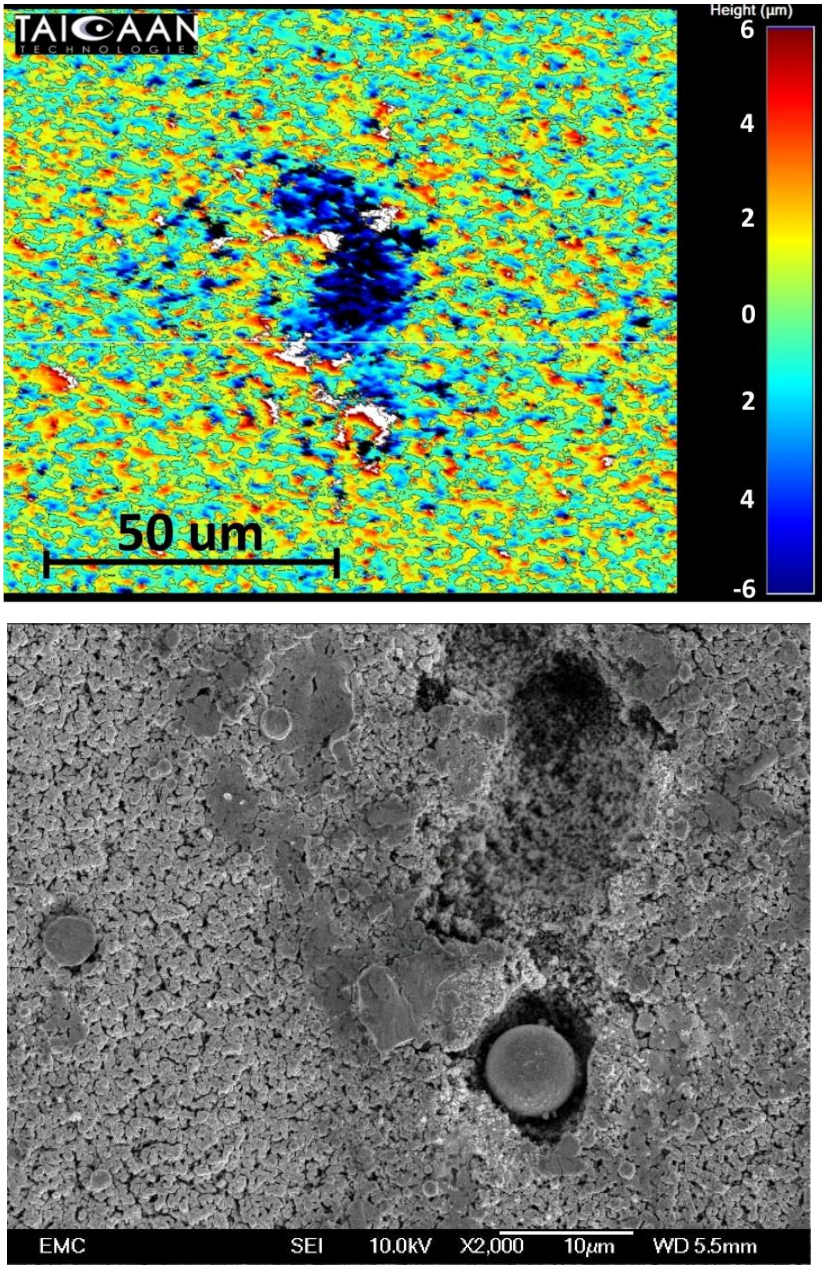

Figure 4-49 – The Au/MWCNT surface after 100k Cycles of 8V 20 mA Hot Switching measured in-situ by the ICE Apparatus (top) and imaged by scanning electron microscopy following disassembly (bottom)

4.5.3 Discussion

Investigation of Fine Transfer over 100k Hot Switching Cycles

Both MMB and DE type openings are observed under all three circuit conditions. The frequency of the MMB and DE events show variability, but as previously noted the 4-20 case shows the highest occurrence of the DE events (Figure 4-41), the least variability and lowest overall average MMB energy (Figure 4-42). The frequent occurrence of the DE waveform is with negligible surface change

is unexpected, as in a previous study of Au/Si contacts it was associated with the delamination and tearing of the conductive film and greater increase in surface roughness, when compared with MMB events [120, 121]. In the case of Au/MWCNT contact materials it was previously observed that delamination occurred after the contact surface was worn to a thinner Au layer by the MMB process [120]. The increased current (4-50) and voltage (8-20) cases both show much greater evidence of surface change, and an increased number of MMB events with a higher average opening energy than the 4-20 case. In the 4-50 case this is the anticipated result, with the MMB energy linked to Joule heating and the MMB previously shown to be proportional to current. The 2.5-fold increase in circuit current between the 4-20 and 4-50 cases is expected to result in a 2.5-fold increase in the thermal energy. This trend is broadly observed as the ratio of the MMB energy between the 4-20 and 4-50 cases (Figure 4-42). The increased voltage case (8-20 cf. 4-20 case) was not expected to show an increase in the opening energy or surface wear. It was previously shown during investigation of a rough and smooth Au/MWCNT surface that for the same circuit conditions the rougher surface demonstrated a higher energy associated with the MMB [95]; however, there is no clear explanation for the increase in surface wear with an increase in circuit voltage below the arcing threshold. Previous investigation showed no consistent correlation between the circuit voltage and the energy associated with the MMB over a range of 4 to 12 V; however, of a much lower number of switching cycles was investigated and a slight increase in the MMB energy was observed between 4V, 50 mA and 8V, 50 mA [95]. It is noted that increase in voltage was also linked to an increase in the energy distribution of the MMB. The increased wear is explained if the most energetic bridges cause disproportional amounts of surface damage (by melting much larger areas) and changing the scale of surface change.

Surface changes are detected in each case with new surface features detectable after only a single switching cycle in both the 4-50 and 8-20 cases. The 8-20 case demonstrates a more concentrated region of wear to the 4-50 case, with the surface material depleted and drawn into peaks that are observed after a single switching operation The surface roughness alone does not clearly describe the differences in the surfaces; however, it is quantified by surface asperity volume. Previous investigation has shown the transfer of Au contact material is always observed from the Au/MWCNT to the Au contact, and independent of polarity or gravity [19]. A proposed mechanism was differential cooling in the MMB caused by the material properties of the contacts resulting in asymmetrical MMB rupture [60]. The wear observed in this study suggests that if mechanism occurs the rupture is closest to the Au contact. An alternative explanation is the the Au-Au adhesion is

greater than the Au-MWCNT. The dimensions of the peak features shown are suggestive of the dimensions of the MMB formed. These are in agreement with previous observation, with the significant difference that a much lower current has been used in this investigation (20 to 50 mA vs 10 to 100 A) [89].

The apperance of spherical particles suggests an additional mechnism for the longevity of the Au/MWCNT material over a conventional thin Au film. The uniform spherical nature of the particles suggest they were formed while molten. The obvious mechnism being the collapse of the molten metal bridge to its root following rupture. The size of the particle therefore also indicates of the dimension of the MMB. Assuming such particles may also be formed in a conventional Au film their diameter is greater than the film thickness and they would act as an impediment to the contacts closure. This mechanisms would decrease contact area and increase the contact resistance. In the Au/MWCNT composite the particles appear to be pushed into the MWCNT below as their crowns are flush with the surface. This provides a mechnism that mitigates the spheres stopping contact closure and becoming an impediment, particularly when the low force available for contact closure is considered.

4.6 Experiment 6 - Lifetime Switching Ability of the Au/MWCNT Composite and an Enhanced Fine Transfer Model to Predict Au/MWCNT Contact Lifetime

In the final experiment the ultimate lifetimes of the contact under hot and cold switching conditions are determined. The objective is to switch the contacts to failure condition, where the contact resistance has increased excessively, and to detect and quantify the wear that has caused failure. This data is required to determine coefficients for an improved model of fine transfer to predict contact lifetime of the Au/MWCNT.

Two conditions are investigated. The first is a hot switched case at 4 V DC 50 mA (200 mW switching power) circuit conditions. This represents conditions that resulted in wear detectable after a single cycle in the previous experiment. A second case of near cold switched conditions, 4 V DC 4 µA (4 µW switching power) is also investigated. The Au coated hemisphere to Au/MWCNT planar contact arrangement is used with a contact closure force of 150 µN. Contact opening velocity is the same in both cases as a square wave drive with the same slew rate is used to drive the contact motion

profile. During cold switching the contact is cycled at 1157 Hz - one complete cycle in ~900 µS and 100 M cycles per day. In the hot switched case, to allow time for the MMB to occur without interruption the switching rate is decreased to 500 Hz. During cold switching the contact potential is monitored during opening at 100 MHz and no MMB waveforms are detected.

4.6.1 Hot Switching Lifetime at 4 V 50 mA (200 mW)

The progression of contact resistance with switching cycles is presented in Figure 4-50. The contact resistance begins below 0.5 Ω and remains below 3x this value until suddenly increasing to more than 2 Ω after 140 M cycles have been completed indicating the failure of the contact surface. At this point the contact is considered to have failed by excessive increase in contact resistance. The progression of contact resistance with switching cycles is presented in Figure 4-50.

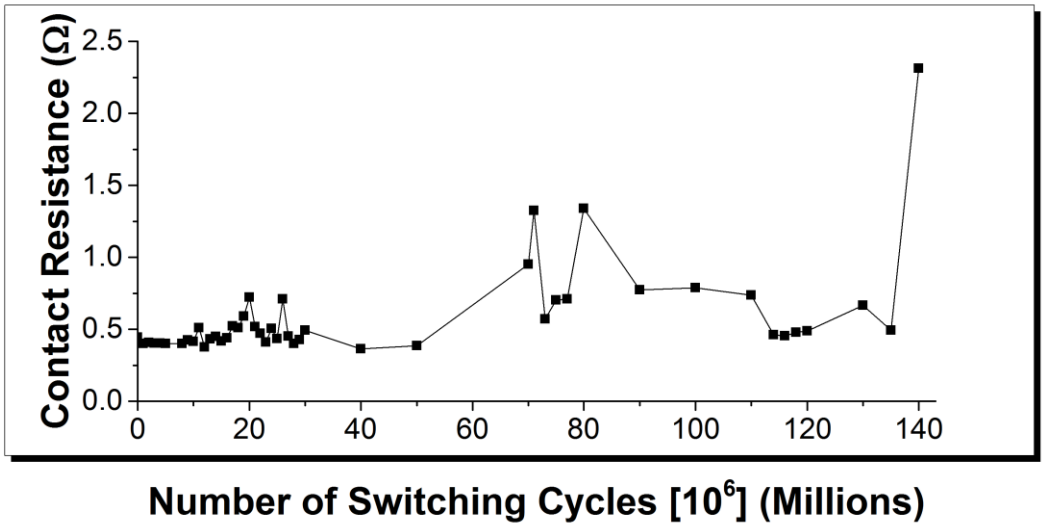

Figure 4-50 –The Contact Resistance evolution of an Au coated ball with Au/MWCNT contact over 140M hot switching cycles at 4 V DC 50 mA. The contact is considered to have failed at 140M cycles due to an excessive increase in contact resistance (>3x nominal Rc)

The progression of surface wear is shown in Figure 4-51 where the surface of the Au/MWCNT contact has been mapped after 10, 20, 50 and 100 M switching cycles. The figure illustrates a wear process characterised by an initial puncturing of the Au film (10M cycles yellow regions). The wear grows from these regions (green regions at 20M cycles and blue regions at 50M cycles) before they coalesce into much larger regions of Au film depletion. There is a deformation to the form of the Au/MWCNT contact that is not apparent in the cold switched experiment. This effect was due to the actuator displacement being fixed during the cold switched experiment and being slightly adjusted

after each measurement of the contact surface (every 10 M cycles) during the hot switched experiment. This implies that the contact displacement and therefore the contact force increased slightly with the number of switching cycles.

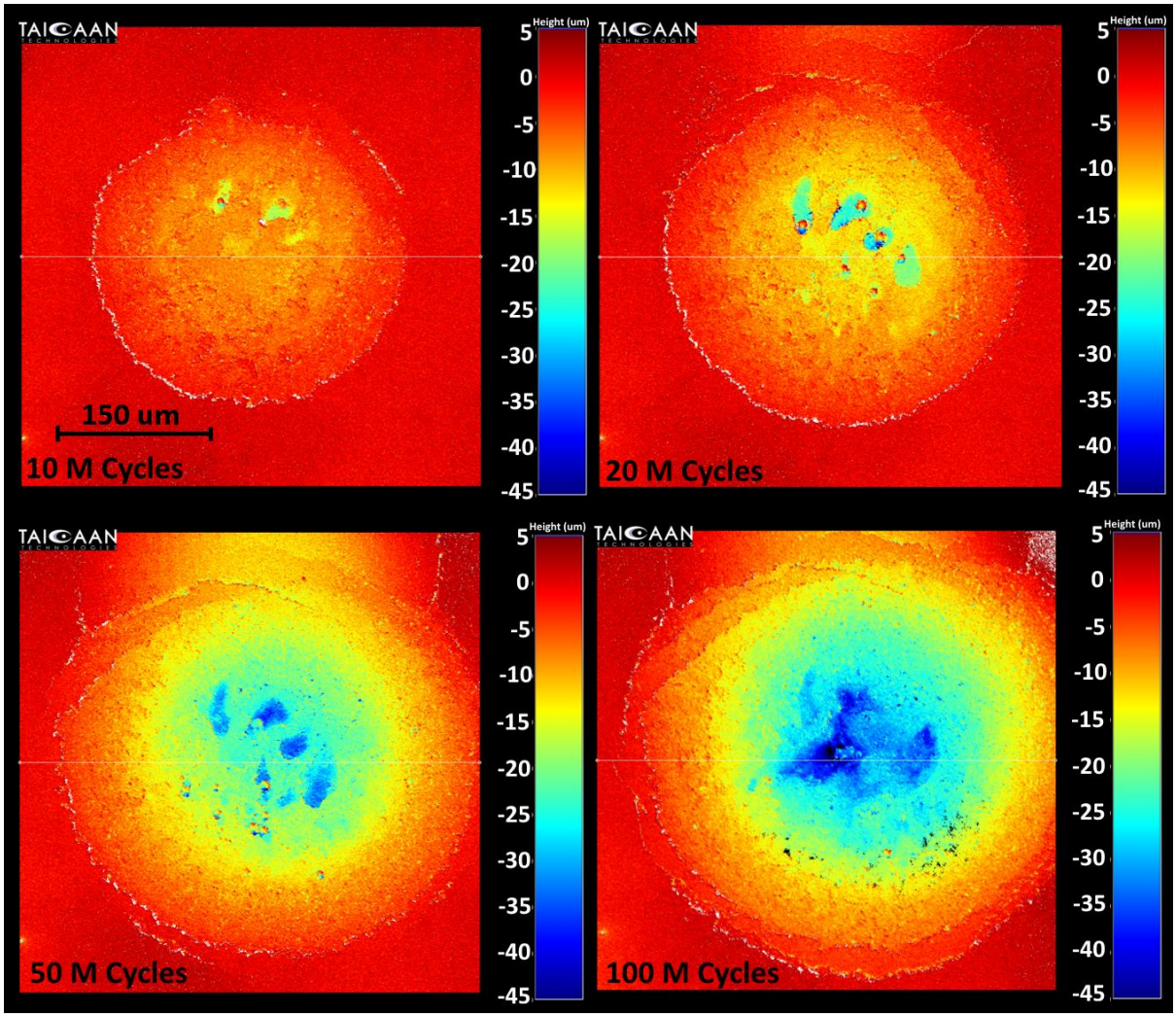

Figure 4-51 –The progression of surface wear in the Au/MWCNT contact after 10, 20, 50 and 100 Million switching cycles at 4V 50 mA. 500 µm (X) x 500 µm (Y) Colour scale +5 to -45 µm. 1001 x 1001 data points

Figure 4-53 and Figure 4-52 presents the surface height map of the Au/MWCNT and Au coated ball after contact failure (140M hot switching cycles) with micrographs of the same region of the Au/MWCNT contact and the corresponding surface area of the upper Au coated ball contact. The Au/MWCNT contact has taken the form of the hemispherical upper contact It can be seen that there nearly all the Au film has been removed from the contact area; however several regions of thinned Au film are still apparent in the micrograph of the Au/MWCNT as dark shiny irregularly shaped regions in bottom left image in Figure 4-52.

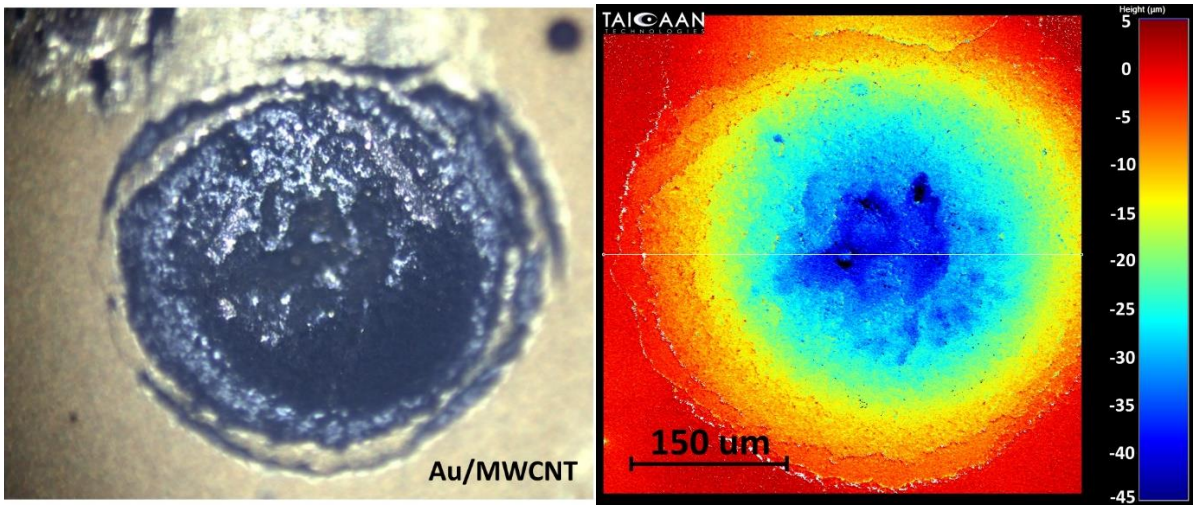

Figure 4-52 – Au/MWCNT Contact at Failure after 140M cycles – Micrograph of Au/MWCNT (left) and Surface height map of same region over 500 µm (X) x 500 µm (Y), 1001 x 1001 data MWCNT (right). The micrograph is showing fully exposed MWCNT (dark black), thinned and damage Au film (dark shiny regions) and cracking and separation of the Au film.

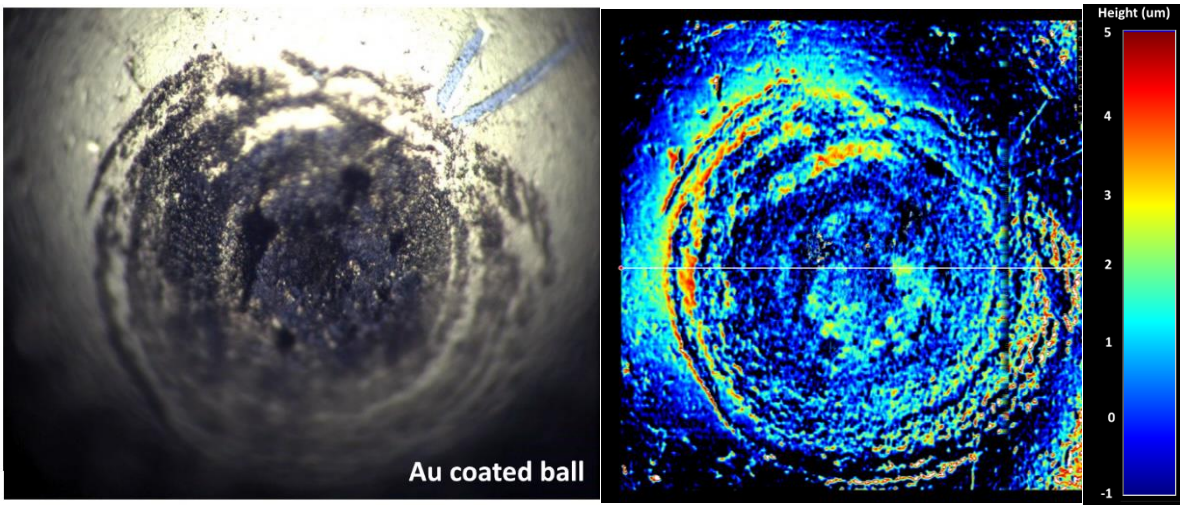

Figure 4-53 – Au Coated Ball Contact at Failure after 140M cycles – Micrograph of Au Coated Ball (left) and Surface height map of same region 500 µm (X) x 500 µm (Y), 1001 x 1001 data (right). The spherical form of the ball has been removed from the height map to better show the high regions (red) that indicate black MWCNT material has transferred onto the surface of the ball

Around the perimeter of the contact site the Au film is partially intact but is breaking away from the main body of the film. The micrograph of the Au coated ball (Figure 4-53) shows a corresponding wear pattern to the Au/MWCNT (Figure 4-52) with a significant amount of MWCNT (black regions) that have transferred to the surface. The direction of wear is from the Au/MWCNT to the Au coated ball. It is interesting to note that it is not just the Au that has transferred but the subsurface MWCNT has also been transferred. The patterns of surface cracks and deep pits, where the surface has been

entirely removed are apparent in both the surface height map and the micrograph of the Au/MWCNT.

The surface volume change is evaluated after fitting the form of the upper ball contact (2 mm diameter) to the surface and the volume loss calculated as 0.154 $x10^{-3}$ mm^3.

4.6.2 Cold Switching Lifetime

After 40 days of continuous switching the cold switching test is halted without surface failure. The progression of the contact resistance is presented in Figure 4-54. The initial contact resistance is 0.4 Ω and shows a gradual increase with cycles but does not reach the failure condition of > 3 Ω. The contact resistance has a trend of gradual increase with switching cycles and has risen from ~0.5 to ~ 1 Ω after 4 B cycles which shows the contact continues to perform well but contact wear is occurring.

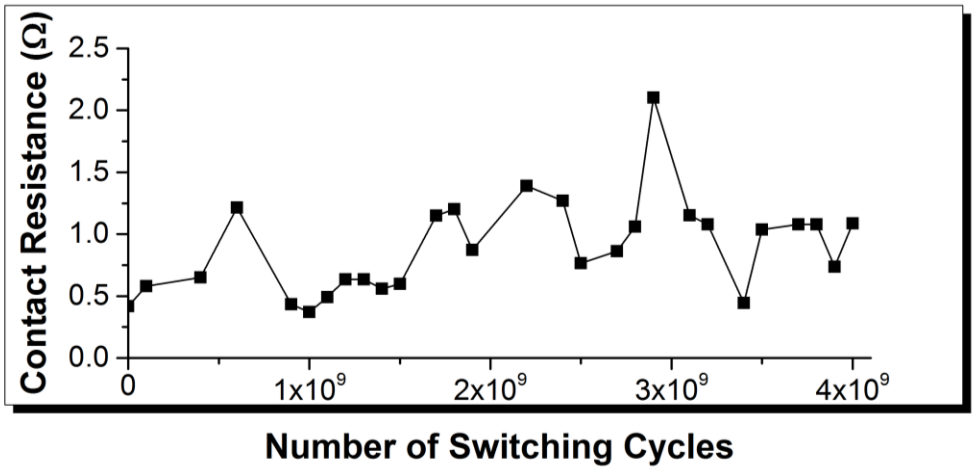

Figure 4-54 – The Contact Resistance evolution of an Au coated ball with Au/MWCNT contact over 4B cold switching cycles. The contact is still operating well after 4 B cycles as shown by the continued low contact resistance

The evolution of the Au/MWCNT contact surface is shown after 1, 2, 3 and 4 billion cycles over the 500 µm (X) by 500 µm (Y) region in Figure 4-55. This is same area as the previous figures for the hot switched wear but the colour scale has been enhanced to better show the more limited wear. The areas of wear are apparent in the central region approximately 300 µm in diameter. These regions become progressively greater, and by 4 billion cycles the outer edge of the contact area is clear.

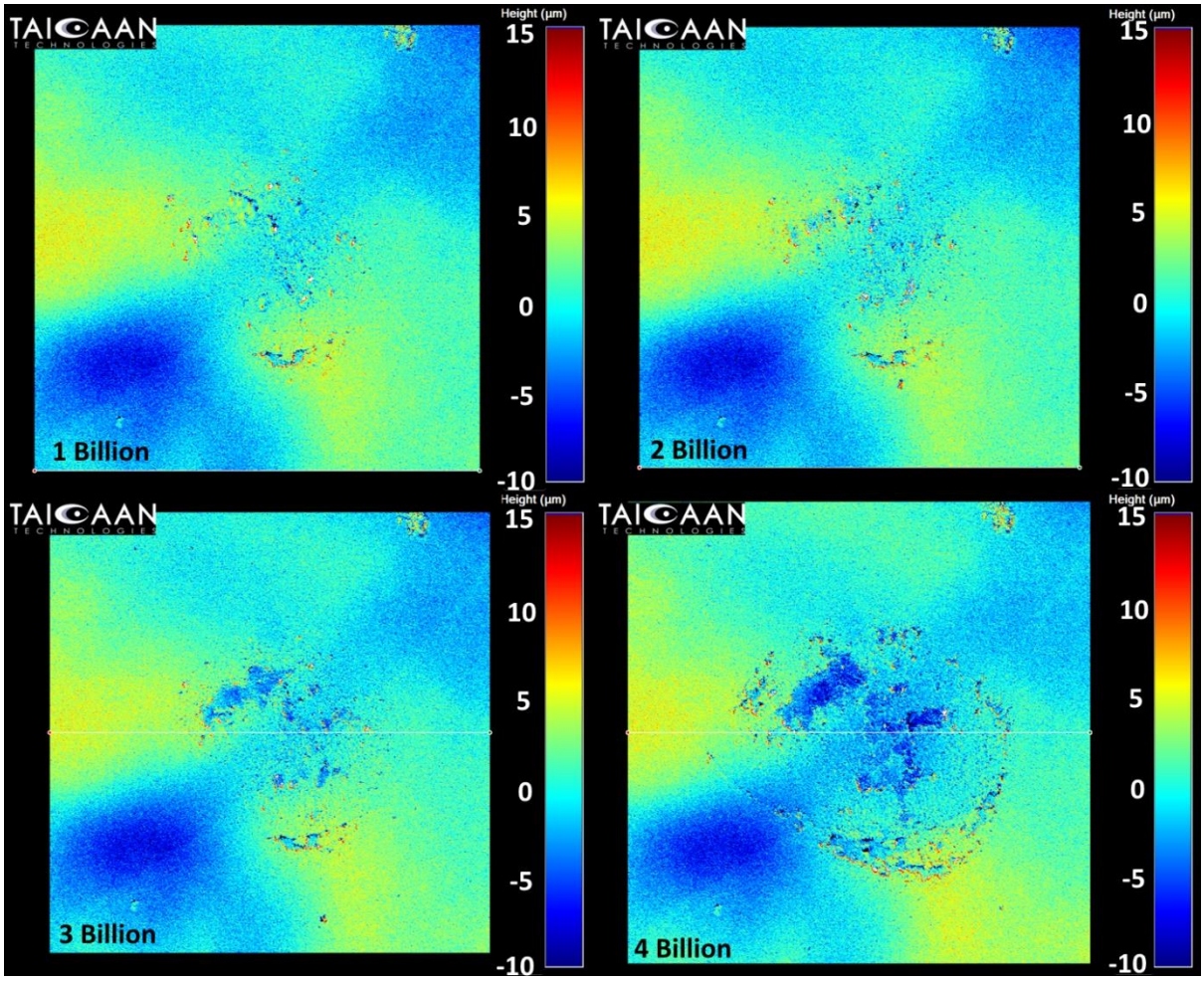

Figure 4-55 – ICE Apparatus Surface Measurement of the Cold Switched Au/MWCNT Contact Site after 1, 2 3 and 4 Billion Switching Cycles over a 500 µm (X) by 500 µm (Y). The height scale (Z) is 25 µm

As the Au film is transferred from the surface the area for metallic condition (Au-to-Au contact) is reduced and the contact resistance increases. The depth of the wear regions is around 5 µm, which is consistent with the previous measurements of in-situ wear in section 4.5.

The volume of material removed from the surface is presented in Figure 4-56. The volume of material removed after 4 billion cycles is 0.201 x 10^{-3} mm^3

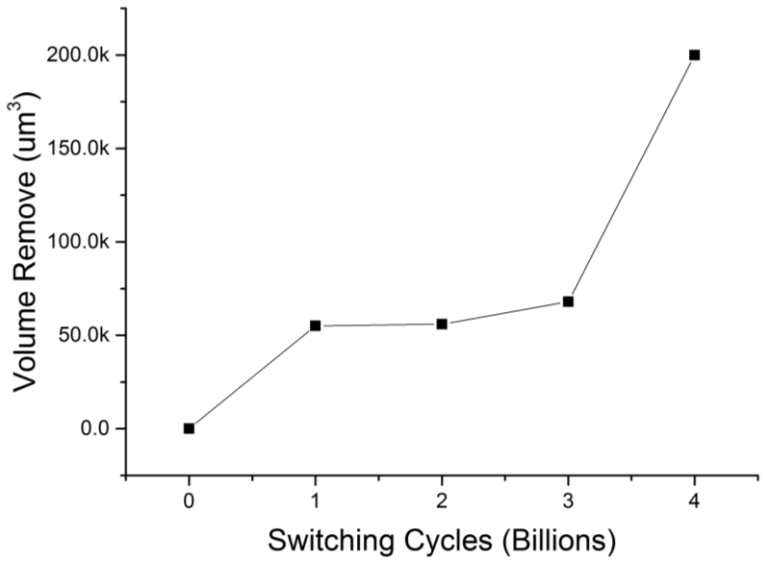

Figure 4-56 – Evolution of contact wear at 150 µN closure force and 4 µA circuit conditions on a Au/MWCNT composite contact

4.7 Predicting the Number of Cycles to Contact Failure – An Enhanced Model of Fine Transfer

The summary of results from switching in this experiment and previous investigation of the Au/MWCNT contact are presented in Table 4-4

Experiment	Contact Force (µN)	Switching Current (A)	Cycles to Failure	Volume of Wear ($x10^{-3}$ mm^3)
Bull - Hot Switched [a]	**150**	**50m**	**140 $x10^6$**	**0.154**
Bull - Cold Switched [b]	**150**	**4µ**	**4 $x10^9$ (6.92 $x10^9$)***	**0.201**
Lewis [c]	**35**	**50m**	**28 $x10^6$**	**Not detected**
Chianrabutra [d]	**1000**	**20m**	**910 $x10^6$**	**0.444**

Table 4-4 - Summary of MMB Average Energy and Distribution between 4V 50mA and 12 V 50mA

Explanatory note **a)** the contact force started at 150 µN but increased slightly during the switching process, **b)** the contact had not failed at 4 Billion cycles but predicted to be 6.92 Billion, **c)** no wear could be detected on the Au/MWCNT surface, **d)** the number of cycles was originally reported as 70 M but later revised to 910 M through the inclusion of an average of 13 contact bounces per switching cycle

The existing model for fine transfer Equation (4-2) [57], predicts a switching lifetime of 22.8 $x10^6$ Billion switching cycles at 4 µA. Figure 4-55 shows significant wear after 4 Billion cycles and it is clear

the prediction of the model is not correct at this low current level. While the contact surface had not failed after 4 Billion cycles at 4 µA switching the average wear per cycle can be predicted based on the total volume available for transfer V_{max} and the average volume transferred per switching cycle. Based on a contact force of 150 µN and a total volume for transfer of $V_{max} = 0.27 \times 10^{-3}$ mm^3 the predicted switching lifetime is 6.92 Billion cycles.

Two significant changes are proposed to the fine transfer model. Firstly, the relationship between switching cycles and current is assumed to an i^2 relationship; however, this work has shown the influence of current on the MMB and surface wear to follow a linear relationship. Secondly, the micro delamination of the contact material has been observed and is not considered in the existing fine transfer model.

The energy of the MMB, calculated by Equation (3-2), is a linear function of current and this has been shown during investigation of current in the 10 to 200 mA range in this work. If we assume that the fine transfer wear driven by the MMB is proportional to the MMB energy, then it will also be proportional to current according to Equation (4-7)

$$n_f = \frac{V_{max}}{k\, i} \qquad (4\text{-}7)$$

This observation is supported by the wear detected in the previous results section. The new coefficient for wear, *k* is calculated by applying the relationship to the Chianrabutra data ($V_{max} = 0.444 \times 10^{-3}$ mm^3, i = 50 mA) and gives a new value of $k = 2.44 \times 10^{-11}$ mm^3/A per switching cycle. At 4 µA this predicts 4550 Billion cycles compared to the 6.92 Billion cycles based on extrapolation from the empirically observed wear. This demonstrates the model requires the consideration of the influence of the delamination wear on contact lifetime at low currents.

The existing model for fine transfer does not explicitly include the influence of force, as the maximum volume available for transfer is itself determined by force. From Figure 4-55 it is apparent that wear occurs even when no MMB is detected. It is proposed that the delamination wear observed in this work is the result of adhesion at the level of the asperities which is linearly linked to the contact force according to Equation (2-6). The contact wear is therefore a combination of MMB driven wear proportional to the switching current, and delamination wear proportional to the contact force. The coefficient for transfer linked to the circuit is k_1 previous defined to be 2.44×10^{-11}

mm^3/A per switching cycle. The maximum volume available for transfer, V_{max} is also a function of the contact force. The maximum number of switching cycles as a first approximation then becomes Equation (4-8)

$$n_f = \frac{V_{max}}{k_1\, i + k_2 F} \qquad (4\text{-}8)$$

By assuming the wear observed at 4 µA is dominated by delamination wear a value for the coefficient k_2 as is function of the contact force is derived as $k_2 = 3.33 \times 10^{-10}$ mm^3/N per cycle.

The new model is applied to the three contact forces (35, 150 and 1000 µN) and presented along with indicators of empirical results of this and previous studies in Figure 4-57.

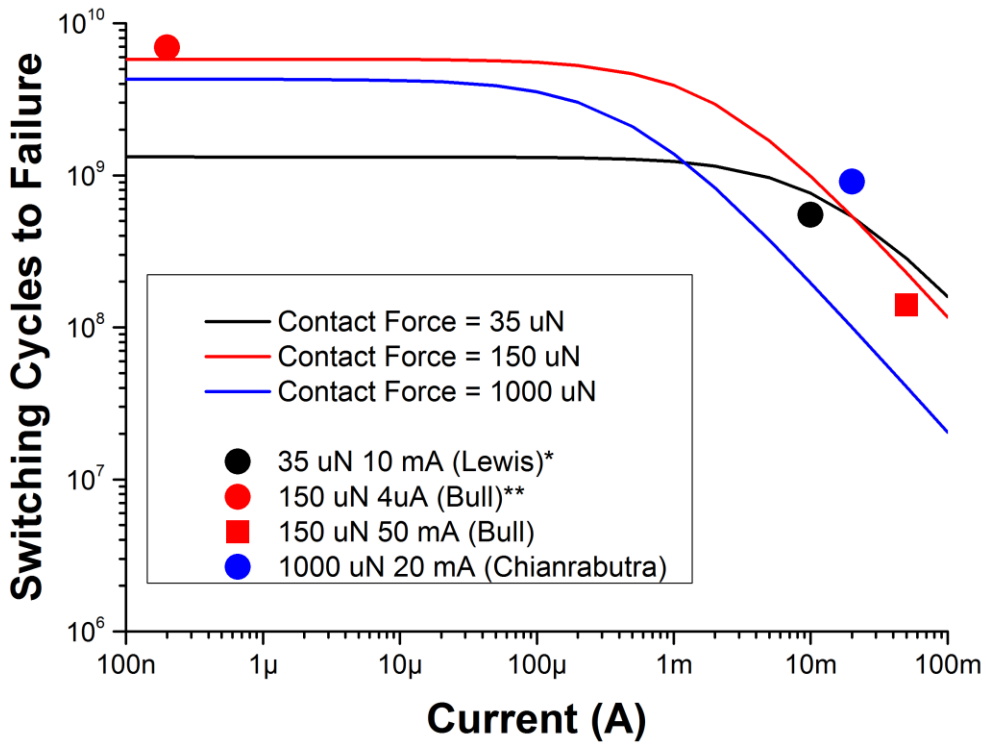

Figure 4-57 – The new Fine Transfer Model for Au/MWCNT contact lifetime applied to 35, 150 and 1000 µN contact force. Empirical results from switching lifetimes are indicated by symbols.

Where the coloured shape (empirical result) lies near to the line of the same colour (modelled result) this indicates the empirically observed data matches the prediction of the model. The only exception is the Chianrabutra investigation (blue circle) which the model predicts around 100M

cycles while the reported number of switching cycles was 910M. It is noted that he reported number of switching cycles was originally 70 M which is much closer to the 100M cycles predicted by the model [19, 119]. It has already been noted that each subsequent bounce would be at a reduced force reducing surface wear. With this discrepancy accounted for Figure 4-57 shows the new model demonstrates good agreement with empirically observed data over range of contact forces likely for a practical MEMS contact 30 to 1000 µN and switching currents from effectively 0 to 100 mA. The model provides the MEMS switch designer with a practical and easy to use predictor for contact lifetime of the Au/MWCNT contact.

4.7.1 Discussion

The 4 billion cold switched cycles are the highest number of switching cycles ever demonstrated by the Au/MWCNT composite under any condition. The contacts had not failed but cycling was halted at a number of cycles equivalent to an effectively imperishable switch contact [136]. The strict definition of cold switching requires there is no electrical signal across the contacts and a 4V 4µA signal was applied. The signal was applied to allow instrumentation to count the switching cycles and ensure that the contact was operating correctly during the experiment.

The hot switched experiment contacts failed after 140M cycles by an excessive increase in contact resistance (exceeding 3x nominal). At 4 V 50 mA (200 mW) this represents the greatest number of switching cycles achieved. Lewis et al demonstrated 28 M cycles to failure at the same circuit conditions but there were two significant differences between these experiments [19]. The first is the contact force used (150 vs 35 µN) and the second is the contact geometry (Au coated ball vs Au cantilever). The increased force provides an increased contact area, and therefore more contact material is available for transfer. The contact geometry created by a cantilever on a planar Au/MWCNT contact also presents a potential reduction in contact area, as any misalignment would result in a point or line of contact rather than an area.

The ability of the composite to conform at low forces is in competition with increasing the thickness of Au applied that increases the volume of material available for wear. Only a single composition of the Au/MWCNT contact (500 µm MWCNT with a 500 nm Au coating) has been characterised in this study and the investigation of wear rates in other compositions is also identified for future work.

The prediction for the hot switching case investigated in this study 4 V 50 mA at 150 µN is a lifetime of 214M cycles to failure which is greater than the 140M cycles observed. It is noted that the contact

force was increased slightly during the experiment and this may have resulted in greater than anticipated wear. The new model shows that above switching currents of ~500 µA the wear mechanism is driven by current, while below 500 µA the switching lifetime is determined by micro delamination wear. Contact life at a given switching condition can be optimised by controlling the contact force. This is an important observation as it provides practical guidance for the MEMS switch designer in application of the Au/MWCNT contact material.

The model shows good correlation with the empirically obtained results for lifetime switching the Au/MWCNT. There is a significant deviation from the modelled result to that reported by Chianrabutra at 20 mA [19, 119]. The reported number of switching cycles was 910M but this was based on multiple contact bounces per switching cycle. It is noted that actual number of demanded switching cycles was 70 M and of the same magnitude predicted by the new model (100M cycles). It has already been noted that each subsequent bounce would be at a reduced force and expected to result in a reduced level of surface wear.

The new Fine Transfer Model does not yet account for the influence of circuit voltage, the variation of MMB energy with contact opening velocity and contact texture which have been shown to influence the MMB or surface wear directly. These are identified for future study and inclusion in the model.

5 Conclusions and Summary

5.1 Conclusions

The aims of the study were to demonstrate the Au/MWCNT composite could achieve lifetimes that would enable its use as a practical contact surface in a MEMS switch, and provide the MEMS switch designer with data to predict its performance under a range of switching conditions.

This characterised the ultimate switching lifetime of the Au/MWCNT composite at low force MEMS switching conditions. The lifetime of the Au/MWCNT composite electrical contact has been shown to be a combination of wear from the mechanical and electrical influences of switching. This has been achieved by the development and application of an advanced MEMS wear testing apparatus and the study of the influence of circuit parameters on the molten metal bridge phenomenon. The study provided the empirical data to extend and revise a model that predicts the composite lifetime under a range of switching current and contact force conditions and shows good correlation with the results of this and previous study of the Au/MWCNT composite.

Development and Test of the ICE MEMS Testing Apparatus

The development of a new testing apparatus designed to detect the microscopic wear in the Au/MWCNT contact was tested on thin film coated Au/Cr hemisphere to planar contacts. The contacts were cycled at conditions where surface wear has not previous been detected in-situ - 100 µN with no signal (cold switched) and 500 µN with a 4 V 20 mA signal (hot switched). The resolution of the apparatus allowed the wear caused by a single switching cycle at these conditions to be detected and demonstrated that switching wear is significant and can be characterised from the first cycle. The cold switching conditions caused a 30 µm section of the Au film to delaminate from the hemisphere and part of it to transfer back and forth between contacts over the following cycles. The contact wear was linked to the evolution of contact resistance with increases in the surface roughness found to correlate with an increased contact resistance. In the hot switched case surface damage was also detected from individual cycles; however, the level of damage was much lower than the cold switched condition which was unexpected. The damaged was characterised by a tearing and delamination of the planar Au film with increases in surface roughness again linked to increases in contact resistance. The presence of two distinct opening voltage waveforms were detected as the contacts opened. The first indicated a MMB had been formed, while the second was linked to the occurrence of the film delamination. The new waveform was termed a delamination

event (DE) and linked to a three times greater level of change in the surface roughness than the MMB event.

Failure Mechanism with Current Overload

A thin film coated Au hemisphere to planar 505 Au/MWCNT contact pair was investigated under low force (150 µN) switching conditions at 4 V DC while the switching current was varied between 10 and 600 mA. As the current exceeded 300 mA the contact was found to fail. This failure was characterised by the rapid piercing and removal of the Au film. The removal of the Au film exposed the underlayer of MWCNT. Analysis of the transient voltage waveform during contact opening revealed the characteristic MMB waveform gave way to a more complex and stepped waveform as the Au surface failed. The process was linked to the involvement of MWCNT in the conduction process where the interruption to current was no longer by the rupture of the MMB but by the thermal failure of a conducting MWCNT and the consecutive breakdown of the outer walls of the nanotube by thermal processes caused by current overload. Analysis of the rupture indicated this thermal failure occurred at the melting point of graphite.

The Relationship between MMB Energy and Switching Current, Voltage, Contact Roughness and Opening Velocity

The influence of switching conditions on the MMB energy was investigated using Au coated ball to Au/MWCNT contacts during switching at 1000 µN. The switching current was varied between 10 and 200 mA on two Au/MWCNT samples, each with a different surface texture. In both cases the energy of the MMB was found to correlate linearly with the switching current and is explained by the relationship between the size of the MMB and the geometry of the current constriction. The linear relationship with current is an important observation as wear modelling of requires that circuit current is a modelled parameter.

Increasing the surface roughness of the Au/MWCNT contact resulted in a significant increase in the MMB energy, and the influence of surface texture on electrically driven wear below the arcing threshold was demonstrated. Analysis of the surface microstructure suggest that the cause of the increased MMB energy is the distribution and shape of the contact asperities, and increased peak loading resulted in larger final areas of contact and consequently larger MMB. It is concluded that surface roughness as a parameter does not adequately describe the surface texture in terms of the geometry that influences the MMB.

The circuit voltage was not expected to have an influence on the MMB energy and there was no clear correlation detected. However, there was a small positive correlation between voltage and the variance of the MMB energy.

At 4 V 20 mA the MMB energy was found to be influenced by contact opening velocity above 1,600 µm/s, Below this velocity the MMB energy was found to have a consistent average energy. Between 1,600 and 8,000 µm/s the average MMB energy was observed to decrease with a mechanism proposed whereby the geometry of the MMB is influenced and results in more rapid constriction and early rupture. The presence of the DE waveform where no MMB was apparent was also detected as the opening velocity was 8,000 µm/s. From 12,000 µm/s the number of DE increased significantly. During study of a bulk AgNi contact at low force and the same circuit conditions no evidence of the DE was identified.

The force transients at the contact interface were investigated during MMB and DE events in the Au/MWCNT contact. It was found the DE correlated with a 20% greater force required to open the contact than a MMB. The result indicated similar behaviour to that observed during hot switching a AuSi contact where a MMB was associated with a lower level of surface change than a DE. The mechanism by which the DE interrupts the formation of a MMB is proposed to be step change in contact area where there is insufficient time for the current constriction to result in melting of the contact material.

Micro delamination in the Au/MWCNT contact

Surface wear of the Au/MWCNT contact was investigated in-situ during hot switching circuit conditions at 150 µN contact force. Three circuit conditions were investigated – a baseline case, and increased current case, and an increased voltage case. The surface wear from a single switching cycle was detected in all three conditions. The presence of both MMB and DE were detected under all three conditions but the highest occurrence of the DE was under the baseline case with the lowest voltage and current conditions (4 V 20 mA). After 100,000 switching cycles the Au/MWCNT surface demonstrated negligible wear. In both the increased current case (4 V 50 mA) and an increased voltage case (8 V 20 mA) the number of MMB events, surface roughness and surface volume wear increased. Between the 4-20 and 4-50 cases the increase in wear was proportional to the increase in circuit current as expected but the increase in wear with circuit voltage was not expected and this is identified as a subject for future work.

Lifetime Wear of the Au/MWCNT contact and New Model of Fine Transfer

The in-situ wear of the Au/MWCNT contact was investigated at 150 µN contact force for lifetime switching wear under two conditions. First, an effectively cold switched condition where the dominant wear mechanism was expected to be the micro delamination caused by asperity level adhesion. Secondly, a 4 V 50 mA hot switched case, where the dominant wear mechanism has been shown to be the fine transfer of contact material driven by the MMB.

In the 4 V 50 mA case the contact demonstrated a low and stable contact resistance for 140M cycles before it suddenly increases to ~2.5 Ω indicating the contact has failed. Post switching analysis of the surface reveals the Au film has been worn away and transferred to the Au coated ball contact along with MWCNT. In-situ analysis reveals the wear process occurs simultaneously in multiple sites, which increase in size and coalesce until the surface is depleted of Au.

The cold switched case demonstrated a low and stable contact resistance for 4 Billion cycles, at which point switching was interrupted as this number of switching cycles represent an effectively imperishable contact. The in-situ detection of wear reveals a pattern of Au wear with more numerous but much smaller wear sites to the hot switched case. The wear rate and total volume available for transfer extrapolate an ultimate switching lifetime of 6.92 Billion cycles at these conditions.

A new model for predicting switching lifetime of the Au/MWCNT contact is developed based on a linear, rather than squared, relationship with the switching current. Contact force is now included in the model to account for the influence on asperity level adhesion which drives the observed micro delamination wear. The empirically observed wear is used to determine coefficients of material transfer. The influence of switching current and contact force is then modelled and compared to the results of this work and previous study where it shows good correlation.

5.1.1 Summary

This work has characterised the wear of the Au/MWCNT contact over billions of cycles, demonstrating its effectiveness as a practical MEMS switching contact, and provides a model that allows the contact lifetime performance to be predicted over a range of switching currents and contact forces.

-

6 Future work

Micro texture of the contact surface was shown to influence the energy of the MMB but the characterisation of the surface using roughness was not adequate to define the relationship. Further study of the influence of the micro texture would provide enhanced understanding of the MMB wear process. The characterisation of the contact surface texture using hybrid amplitude and spatial parameters defined by ISO standard BSEN25178-2 would provide a more complete description of the contact surface and may reveal correlation with the energy of the MMB. Parameters are suggested to characterise the surface texture slope (the Root Mean Square Surface Slope, S_{dq}), the ratio of the 3D to projected surface area (Developed Interfacial Area S_{dr}), the number of peaks per unit area (Summit Density S_{ds}) and the curvature of the peaks (Mean Summit Curvature S_{sc}). It is noted that the data from this study could be used for this characterisation.

The influence of DC circuit voltage was not shown to significantly influence the average energy of the molten metal bridge; however, the wear of a Au/MWCNT contact demonstrated greater and more concentrated wear with increased circuit voltage. A possible explanation is the increased contact potential causing increased electrostatic transfer of any charged particles formed as the MMB ruptures. An expansion of the study to measure the contact opening force as circuit voltage is varied and circuit current is kept constant would provide evidence of this effect if it were present.

In this study the switched signals were limited to DC current as this was expected to cause the greatest levels of wear; however, a significant advantage of the MEMS switch over semiconductor devices is its ability to switch RF signals. A report appended to this thesis has outlines a range of practical applications for the Au/MWCNT contact. These applications (communications, radar, smart devices and sensors) can be used to define RF frequency bands where wear tolerance of the Au/MWCNT would be crucial and has not yet been demonstrated e.g. 5G applications operate around 600 MHz to 6 GHz.

The hemisphere incoming contact to planar Au/MWCNT geometry was chosen for the contacts in this study to provide a localised contact interface and ease of manufacture, but a practical MEMS switch will be actuated by a MEMS cantilever. A reduced contact radius would reduce the device scale but reduce the contact interface area, and therefore wear tolerance. The geometry of the

incoming contact and the pattern of MWCNT growth should be investigated with a view to optimising the switching life.

The contact opening velocity demonstrated a significant effect on the MMB energy, and it is suggested that the contacts may reach a separation velocity where the MMB does not thermally rupture but is pulled apart by the force from the separating contacts. This phenomenon is expected to be detected by a change in the final separation force as the MMB would be under tension (from the contacts pulling apart) rather than compression (from the force caused by the boiling rupture). The ICE apparatus could be modified to include a force transducer to further investigate this process. It is noted that the contact opening velocity is a parameter that can be controlled by the MEMS switch designer and information on this process would provide a valuable design insight to mitigating contact wear.

The observed transfer of Au from the Au/MWCNT to the Au coated contact suggests an adhesion wear mechanism. Changing the coating on the opposing contact may reduce the transfer of Au and extend the switching life of the Au/MWCNT contact. A coating of ruthenium is suggested as it has been previously demonstrated a MEMS switching coating, possing wear resistant properties and does not readily oxidise.

The ICE testing apparatus has scope to be improved to allow a greater range of investigation including those area identified above. The addition of a piezo force transducer in the ICE apparatus would allow the investigation of the contact force associated with individual switching cycles and the wear that results. The acquisition of data for surface height and contact resistance, as well as the stopping and starting of contact cycling are currently carried out manually. Using a programmable data acquisition device (DAQ) and modifications to the surface profiling control software would provide significant automation to the testing process and allow greater MEMS switching testing throughput.

The Au/MWCNT has not been tested under variable humidity or dry atmosphere conditions that are typically used for encapsulated MEMS switches. The addition of atmospheric control can be safely achieved with minimal cost by hermetically sealing the test chamber and applying an inert switching atmosphere, such as dry nitrogen from a low volume bottle, or a water vapour using a humidifier. This will provide appropriate conditions for testing a range of MEMS switching materials. It was noted anecdotally during this investigation that the presence of water vapour appeared to increase

the duration of the MMB, and this would be expected to influence the fine transfer contact wear. The addition of such a capability would allow the influence of humidity on the MMB to be investigated.

7 Appendix 1 - Market Predictions for MEMS Growth and Current State of the Art

In 2011 the MEMS market was valued at $10B with a prediction to increase to $21B by 2017. Real growth exceeded predictions and by 2016 the market was valued at $38B with a predicted increase to $66B by 2021. The market has been driven by new applications such as 3D sensing, 5G communications and increasingly autonomous vehicles, and the increased adoption of MEMS sensors in smart devices.

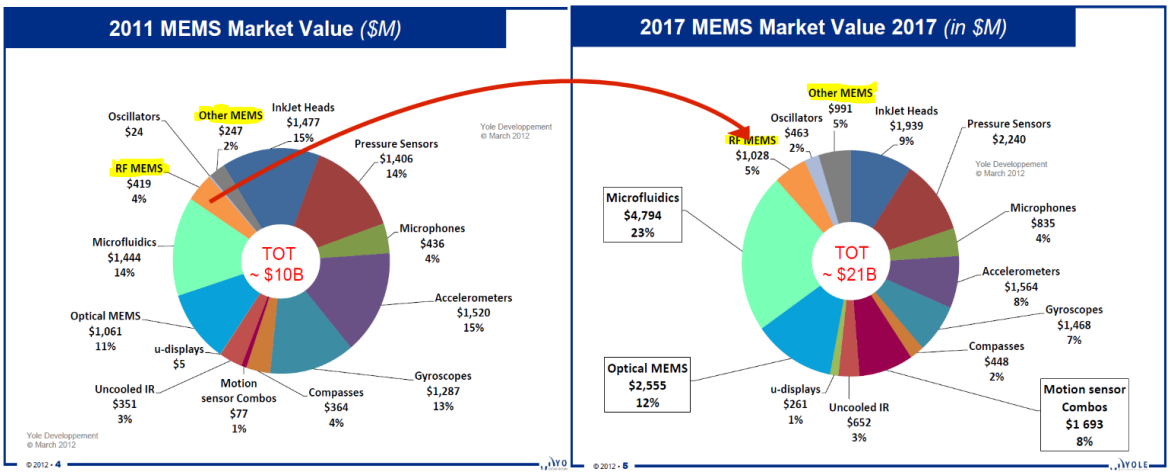

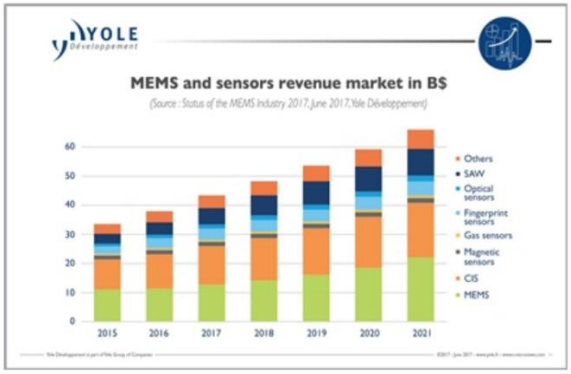

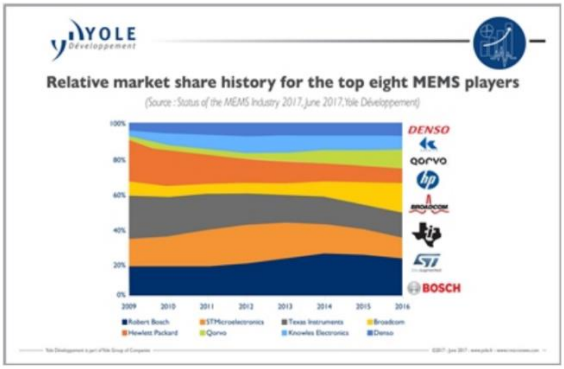

Figure 7-1 - MEMS market value in 2011 (top left) with 2011 prediction for 2017 (top right). Actual market value is shown from 2015 with predictions to 2021 (bottom left), along with the market share of the main foundries (bottom right). Source Yole Developpment Group

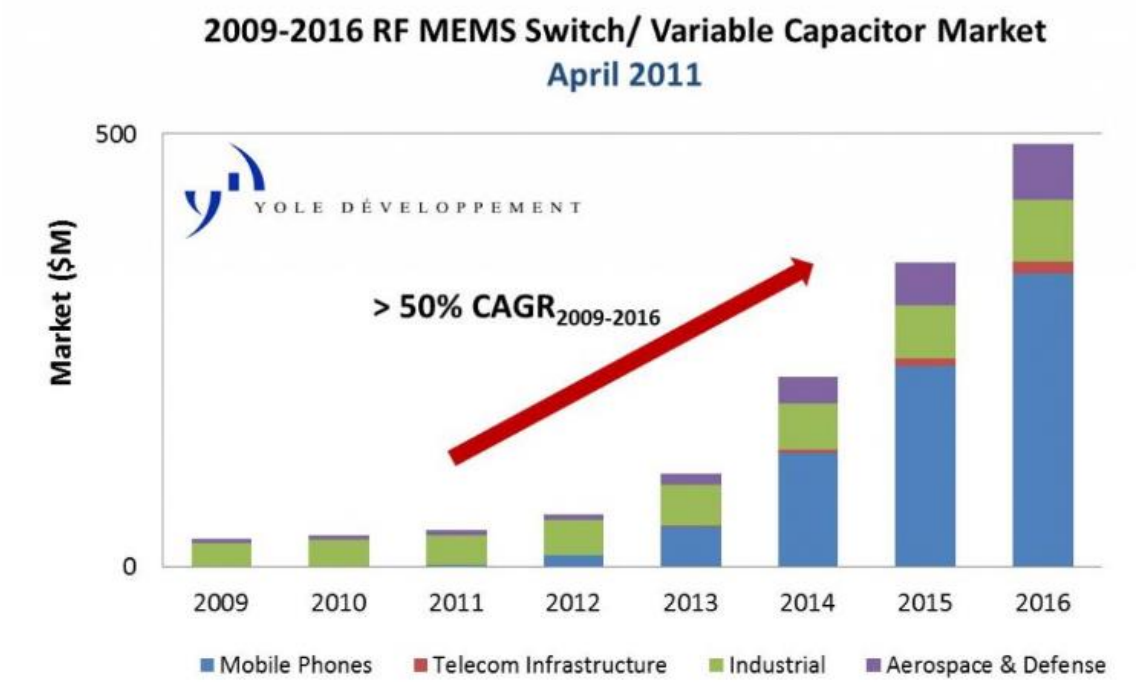

Figure 7-2 - Historic growth prediction for MEMS switches from 2009 to 2016. Note the relative scale of mobile phone and defence market applications. Source IC Insights [31]

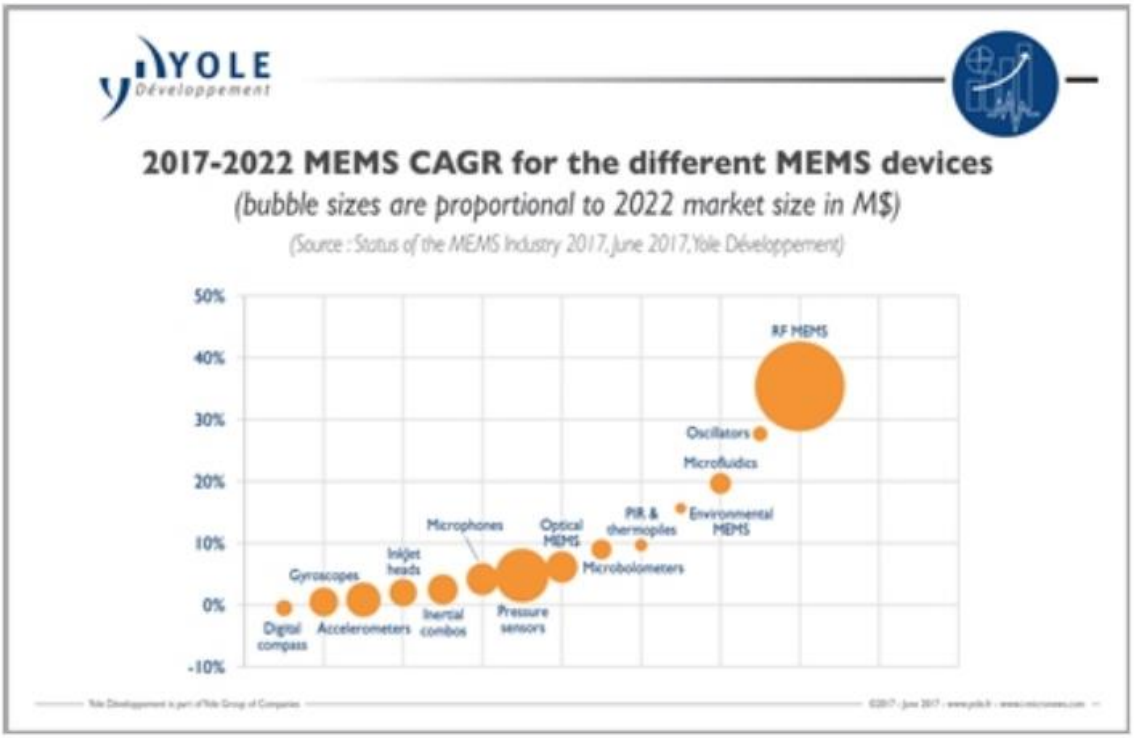

Figure 7-3 - The compound annual growth rate (CAGR) prediction (from June 2017) for 2022 with RF MEMS demonstrating the largest proportion of MEMS device market and a 35% CAGR. Source Yole Developpment Group [32]

7.1.1 Overview of Technologies Enabled or Enhanced by MEMS Switches

The key advantages of using a MEMS switch is their ability to outperform semiconductor, or solid-state device when switching high frequency signals. As the frequency of the transmitted signal increases the capacitive reactance falls and the solid-state device cannot effectively turn off, or "isolate", the transmitted signal. The mechanical opening MEMS switch puts an air gap between the contacts and achieves a much high impedance in the off-state and is capable of effectively switching much higher frequency signals.

Where the contacts are metal-metal the switch offers a very low impedance in the on-state and the power loss in the signal caused by inserting the switch in the signal path (insertion loss) is low. It also provides the capability of transmitting DC signals.

Finally, the MEMS switch device is typically electrostatically actuated, with no actuation power flowing once the actuation electrodes have been charged – therefore the device has a low power consumption to actuate.

- excellent isolation of RF signals
- low insertion loss (power losses to transmitted signal)
- low power consumption

7.1.2 Enhancement Provided by Au/MWCNT Technology

The compliant Au/MWCNT contact technology extends the MEMS switch contact lifetime. The Au/MWCNT provides low contact resistance equivalent to gold film contacts but with enhanced damage tolerance. The high compliance provides a much larger contact area that reduces the mechanical impact damage when switching the contact and limiting the thermal degradation effects by reducing current constriction when transmitting electrical power, particularly as the switch opens [16].

The currently available MEMS switches are unable to tolerate hot switching conditions and their hot switched specifications are limited to low power (~10 mW) while the Au/MWCNT technology has demonstrated switching lifetimes in excess of 150M cycles at 200 mW DC power.

The hot switching capability removes the need to shut off the signal power before changing the switch state and the additional componentry required. This saves cost and space/volume in the device. Cold switched power handling is also enhanced over conventional thin film approaches due to the enhanced contact area and reduced contact resistance [16].

Manufacturers typically quote AC power switching lifetimes, as AC hot switching significantly limits the damage to the contact [136]. DC hot switching is typically more demanding, and the Au/CNT technology shows much greater performance in this area [16]. The advantages are made possible by the enhanced contact area of the conducting surfaces and a greater tolerance for the damage inherently caused by hot switching. AC arcing in the RF range has been observed to surprisingly little damage to thin film metallic contact surfaces. This is due to the arc duration decreasing with frequency, with less damage expected a result [137]. Conversely AC switching in the low frequency range (100 to 100kHz) has been shown to be related to more rapid device failure, thought to be due to the frequency response characteristics of the switch causing an extended arcing period [125].

While the Au/CNT technology has been investigated in the sub arcing DC range, it has not been characterised hot switching low frequency (100-100kHz) frequency AC signals and the literature suggests these switching conditions may accelerate wear. High frequency (RF) AC signals are expected to be better tolerated than DC conditions but have not yet been investigated.

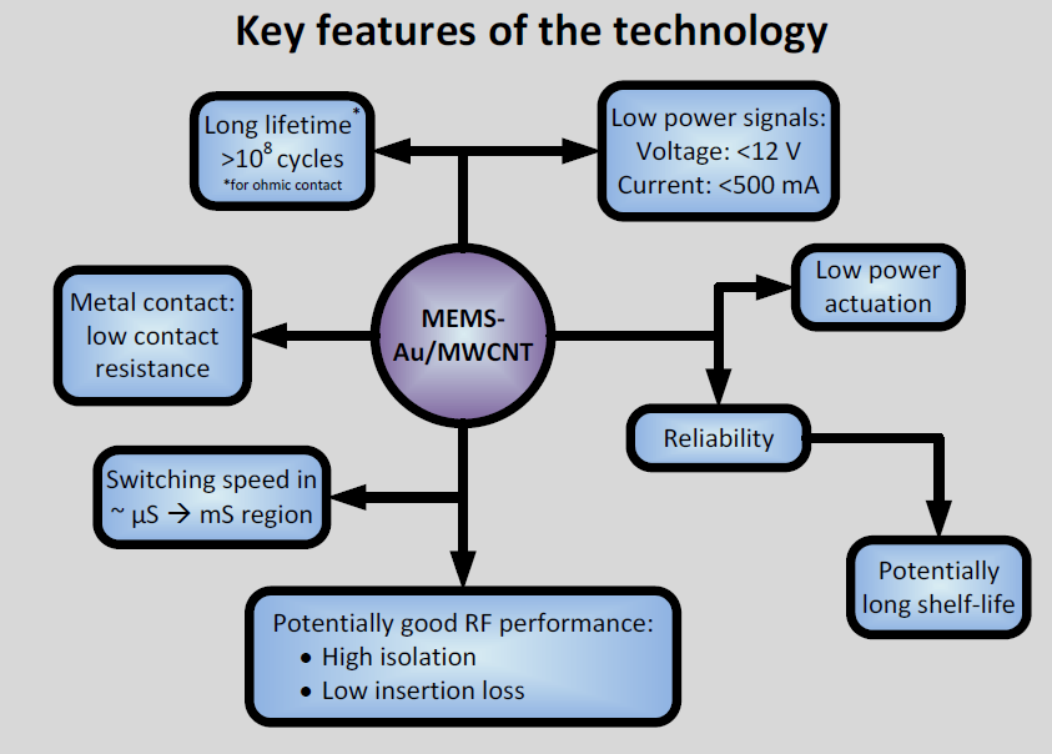

Figure 7-4 - Key features of the Au/CNT technology. Source Lewis Report 2013

7.1.3 Hot Power Switching Limitations of Au/CNT Surface

During DC hot switching circuit loads of up to ~ 200 mW (4V 50mA) the contact lifetime is defined by a gradual fine transfer wear process [Ongoing Testing – Not Published – Bull/McBride]. Increasing the circuit load beyond this causes a more rapid thermal degradation of the contact surface. As the circuit load is increased to ~2 W (4V, 500mA) the Au/CNT contact surface is permanently thermally degraded in only a few cycles of hot switching. By comparison an Au thin film contact would fail catastrophically (destroying the device) at ~30% of this load current.

7.1.4 Reliability and Packaging Requirements

The reliability required for switching devices means that a practical Au/CNT switch will require encapsulating the active element to prevent moisture and HC contamination (these lead to contact stiction) with the control circuitry and voltage upscale (for electrostatic actuation) also incorporated. In practice this leads to a much larger discrete component. The incorporation of the switching device with the application circuitry may be required before encapsulation.

This would mean the manufacture of a discrete device, or to improve packing efficiency integration with the “customer” device fabrication. In practice the Au/CNT switch manufacture would be subsumed as one of the assembly processes.

This case is illustrated by the successful Radant MEMS switch designs that were integrated into steerable radar and satellite communications systems. Radant MEMS were bought out by CPI in April 2017 and integrated to their radome manufacture division.

7.1.5 Manufacturing Process or Discrete Device

Few companies (Omron, GE, Analogue Devices, ST, Texas Instruments, Menlo Micro) offer a discrete packaged ohmic MEMS switch component. Most organisations that possess metal-metal MEMS switch technology appear to use it to enhance their production capabilities as a foundry for VLSI.

The list of metal-metal MEMS switch devices listed below with reference to who has demonstrated such technology and how few offer a discrete device is a useful illustration of how the technology is monetised. The list is expanded from Rebeiz 2003 [4].

Manufacturer	Actuation	V, I, Power (V, mA, W)	Switching Time (µs)	Contact Force (µN)	Lifetime (10^9)	Status
Motorola	Electrostatic	40-50, 0, 0	4-6	100	60+	Foundry services
Radant MEMS	Electrostatic	70-80, 0, 0	3-6	100	60+	Bought out by CPI for their own Radar manufacture
Omron	Electrostatic	17-20, 0, 0	300	1000	1+	Discrete device
Cronos	Thermal	5, 40, 200	10000	2000-3000	1+	Liquidation - technology bought by MEMSCAP foundry services
Rockwell Scientific	Electrostatic	60, 0, 0	8-10	50-100	1+	Unknown
Samsung	Electrostatic	5-8, 0, 0	100	50-100	0.5+	Foundry services
Hughes Research Labs	Electrostatic	20-30, 0, 0	30-40	50-100	0.1+	Foundry services
Lincoln Labs	Electrostatic	70, 0, 0	<1	50-100	0.1+	US Department of Defence
ST-Microelectronics	Thermal	5, 4, 0	300	50-100	0.5+	Discrete device, USB switching etc
Microlab	Magnetostatic	5, 100, 0	500	50-100	0.1+	Then MagFusion - manufacture in Grenoble, France (PHS MEMS) – gone?
NEC	Electrostatic	30-50, 0, 0	30-40	50-100		
DelfMEMS	Electrostatic	ILO -0.18dB, ISO -52dB @ 2GHz				Liquidation
Teledyne Dalsa	Electrostatic					Foundry Services
TDK-Tronics						Foundry services
MenloMicro (GE)	Electrostatic	150, 1000, 25	10		3+	Discrete Device - no charge pump - needs 70V driver
Coto Technology (RedRock)	Magnetostatic	100, 50, 0.3	500			Discrete Device (micro reedswitch)
Analogue Devices	Electrostatic	10, 6, 1.8	75		1+	Discrete Device, $40/1000

Table 7-1 - Comparison of Metal-Metal MEMS Switches Source: [4, 27, 136, 138]

Since 2003 several companies that have demonstrated proven technology have gone into liquidation (DelfMEMS, Microlab). Others have been absorbed by organisations that provide foundry services (Chronos) or bought out as they provided key components (RadantMEMS).

7.2 Applications for MEMS Switches

The high performance of MEMS switches in the transmission and attenuation of DC to RF signals by a device offering low volume, low weight, high reliability and low power consumption devices tend to lend themselves to high efficiency and mobile applications where device size and minimised power loss are critical to performance.

Existing MEMS switch technology requires the signal power is interrupted before switching requiring an additional component to switch the power. The Au/CNT technology offers the opportunity to remove the requirement for additional component required for power switching and simplify the circuitry and its footprint. This would benefit applications that require large numbers of switches and are sensitive to mass/volume. An extreme case would be the RF tuning circuitry in a satellite.

The tolerance for hot switching also provides an advantage were an application may have an in-rush current from an inductive load. Figure 5 illustrates the numerous applications of a MEMS switch in an RF Front End (RFFE) application

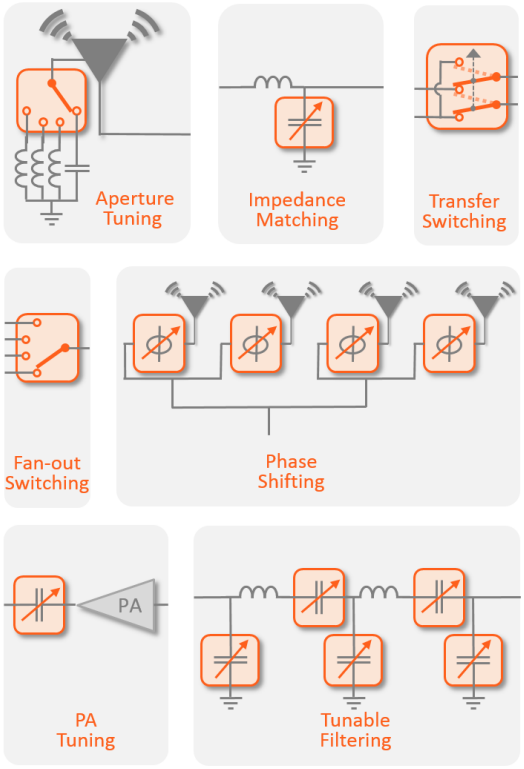

Figure 7-5 - Example applications for a MEMS switch with illustrative circuits in an RF Front End (RFFE) for wireless communications, smart phones, mobile communications infrastructure, radar, frequency agile communications, etc. Source Cavendish Kinetics

7.2.1 Phased Array Antenna (Communications and Radar)

Networks featuring multiple transmitting or receiving elements require precise control of the phase of the signals in each antenna to function. For instance, in a linear antenna the transmission elements must all be precisely in phase to maximise signal power and avoid destructive interference, while in a steerable antenna array the elements must be precisely out of phase to control the pattern of interference between individual antenna signals and "steer" the resultant signal.

A larger number of antennae and switches provides greater performance, with each device in-line with the signal presenting a source of signal loss e.g. Lockheed Martin RRP-117 Air Radar has 1584 radiating elements.

7.2.2 RADAR Basics

The two types of radar are pulse Doppler – 1) where a chirp and echo strategy is used, or 2) frequency modulated continuous waveform (FMCW) where the system transmits and receives simultaneously. Beam steering is by physically rotating the transmit and receive (T/R) arrays and/or by phase shifting the signal to electronically steer the resultant beam from constructive/destructive interference. Passive scanned arrays use a common transmitter, while active scanned arrays have their own T/R for each element of the array.

7.2.3 Application 1 – Microwave Circuitry Protection

Where a ferrite circulator is used as a duplexer to switch between transmit and receive elements the low noise amplifiers requires protection. This application is one where hot switching capability is useful. Currently the pull in time required for an Ohmic MEMS switch device would be at the microsecond to 10s of nano second range.

The hot switching tolerance of the Au/CNT surface provides an opportunity to use a highly linear, high bandwidth metal-metal circuit interruption device with inherently low insertion loss as circuit protection for arrays using a circulating duplexer.

7.2.4 Application 2 – The T/R Switch (Duplexer) in pulse Doppler arrays.

Broadly speaking pulse Doppler systems provide the best long-range performance but have a "blind spot" caused by the time required to switch between transmitter and receiver arrays. This blind spot

is directly related to the switching time between the T/R elements. While the RF performance of a single pole double throw (SPDT) MEMS switch (high bandwidth, low insertion loss) – the longer switching time of the MEMS switch drastically increases this blind spot. Solid state devices achieve switching times of the order of 10's of nanoseconds but suffer from poor linearity and insertion loss– requiring amplification.

The low contact force required for the Au/MWCNT surface presents an opportunity to optimise a MEMS switch for low contact force, and therefore reduce switching time. The application would be the T/R duplex switch element in a pulse Doppler system. This would provide the benefits of high linearity, low insertion loss, and remove the need for amplification thanks to lower inline losses.

7.2.5 Application 3 – Switchable Tuning/Matching Networks

In order to maintain maximum transmission power when the carrier frequency is varied, the load impedance must be matched to the antennae impedance. While this can be achieved by capacitive MEMS switches, an Ohmic switch used with a capacitor can provide a much larger capacitance ratio.

7.2.6 Application 4 – Phase Shifters

Phase Shifters are used to give a delay to a group of active elements, allowing the beam to be steered. MEMS switches can provide a highly linear response with frequency with low insertion loss. Combined with lower noise and power consumption they provide an excellent alternative to solid state alternatives.

Previous problems with MEMS switches used in phase shifters have been phase errors arising from manufacturing variance (for instance variability in base Rc). This problem could be reduced by using an Au/CNT surface whose elastic performance provides repeatable contact resistance reducing variability the phase error. The Au/CNT surface also has the possible benefit of cold switched power handling over alternative MEMS devices due to it's larger contact patch for a given switch force. This also provides the capability to reduce the package volume for a given transmission power.

As examples the Radant MEMS ohmic switch can switch 16W cold and 0.1W (20 dBm) hot with a 10 uS switching time.

[139-141]

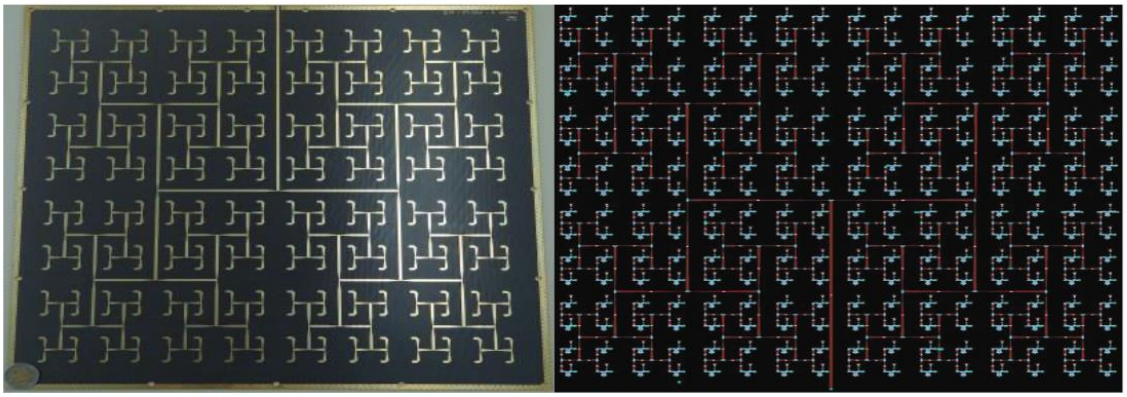

Figure 7-6 - Example array of 16 x 16 ~10mm x 10mm MEMS Antennae with MEMS switch phase shifters for beam steering (right) and without (left)

7.2.7 Mobile Phones Transmission Equipment and Smart Devices

The current trend in smart phone use is for a greater number of operating bands that are also tending to increase in frequency (900/1800 MHz 2G, 900/2100 MHz 3G, 800/1800/2600 4G, 3400/3800 MHz 5G Europe, 4400/4990 GHz Japan).

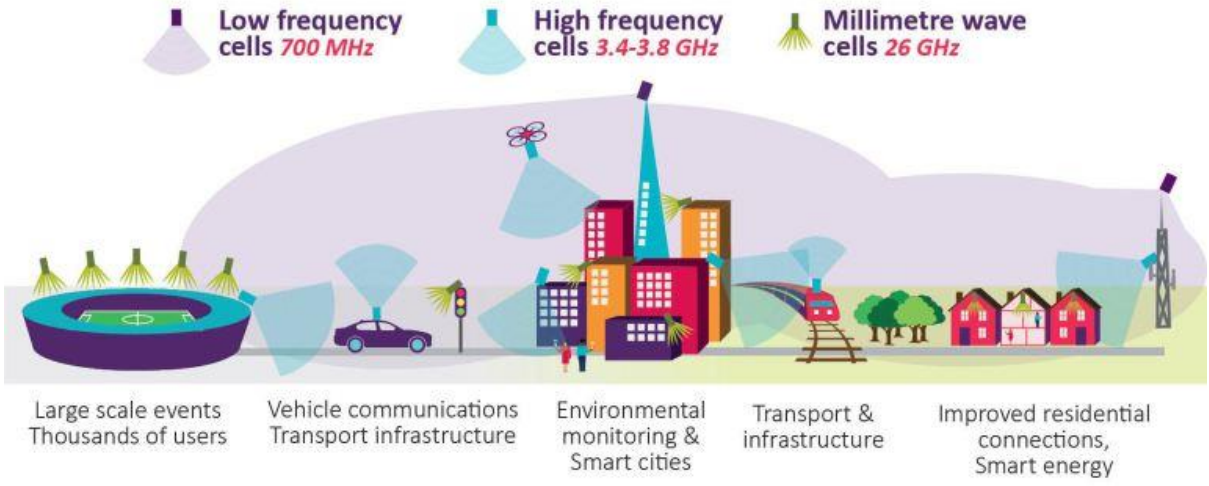

Figure 7-7 - Example of the typical switching frequencies used in mobile communications network. Note the emphasis on higher and agile frequencies ranges where semi-conductor switch performance falls off

7.2.8 Military Communications

Frequency agile software driven RF hardware applications such as encrypted communications, signal jamming and anti-jamming require the ability to rapidly tune and retune antennae elements while continuously receiving or transmitting the signal.

7.2.9 High Frequency RF Sensors

There are multiple applications for high resolution sensors for distance and shape sensing. These can be as simple as accurately monitoring the level of a fluid in a tank and proximity sensing in pre-programmed environments such as a robotic vacuum, to those as demanding as self-driving vehicles and drones, where there is a requirement to differentiate between other vehicles, pedestrians, road furniture and so on. The motivates a requirement for high frequency and frequency agile sensing that can be enhanced by the MEMS switch.

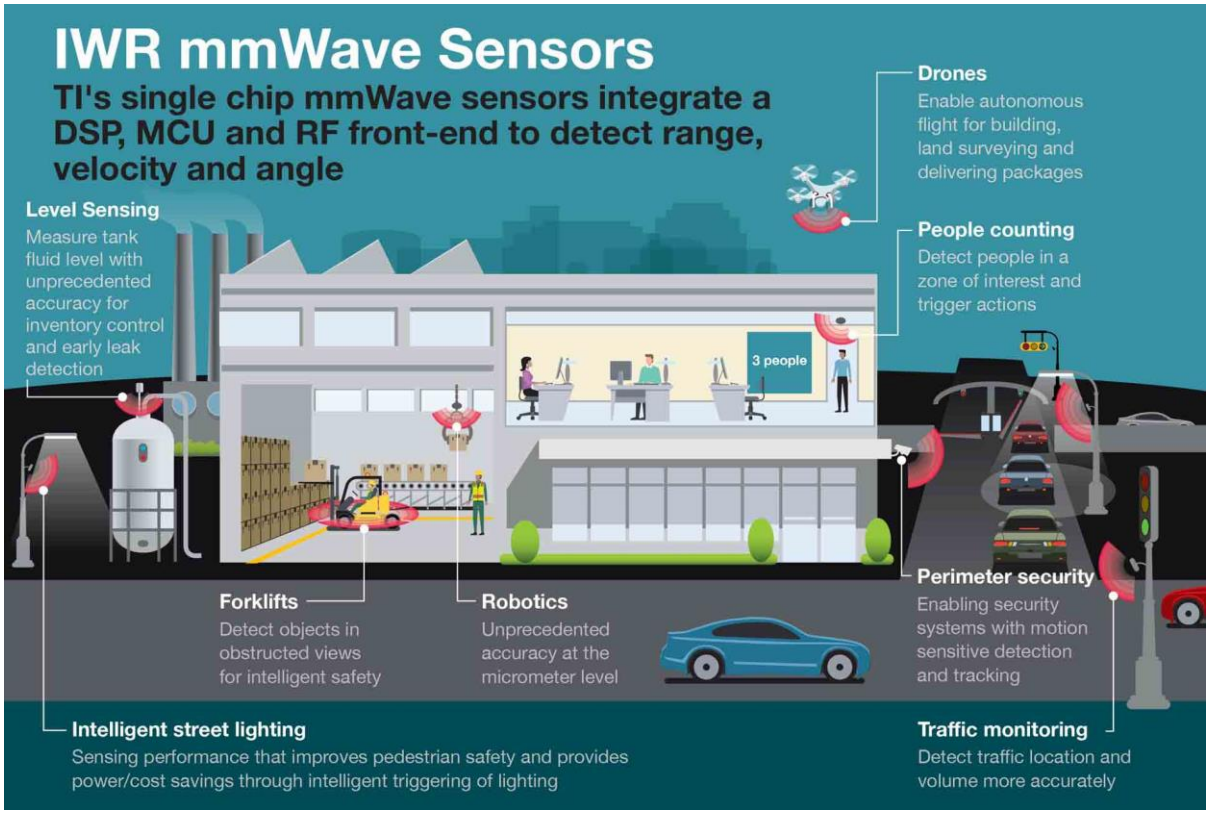

Figure 7-8 - Example applications for high frequency proximity sensors. Source Texas Instruments

7.2.10 Wireless Power Transmission

While wireless (RF) power transmission is particularly inefficient it is being used as a method to improve packaging efficiency in consumer electronics by removing the requirement for alkali batteries or battery access. It is also increasingly being desired as a method to provide “top up” power for devices such as smart phones and tablets to extend their usage time, without resorting to charging stations or plug-in chargers. This application has a wide range of applications including wearable medical devices (such as hearing aids, cardiac monitors, blood glucose monitors). A few

new patents, companies and registrations for frequency bands are being reported that covers this technology (2017-2018). Tuning the transmission and reception devices is critical to maximising power transfer efficiency and this is a target application for the ohmic MEMS switch.

7.3 Market Leading Performance in Ohmic MEMS

There are two relatively new discrete Ohmic MEMS switches brought to market that offer significantly increased performance – particularly the specification for cold switched power handling. The devices are from Analogue Devices and MenloMicro (General Electric). Both devices use multiple cantilevers and contact pads to increase the cold switched power handling and reduce the on-state resistance (R_{on}). It is notable that the mechanism for contact degradation at sub arcing voltages (molten bridge transfer) only occurs at the final point of contact, therefore adding multiple contact pads does not solve hot switched opening wear problem as the Au/CNT does.

7.3.1 MenloMicro MM3100 Ohmic MEMS Switch

Maximum continuous RF power handling of 25 W and DC voltage and current maximums of 150 V and 1 A. On state resistance is quoted as typically better than 0.5 Ohm with a switched lifetime of better than 3 billion cycles either cold or hot switching at 30 mW (15 dBm) at 900 MHz. The target applications for the device include tuneable filters, filter bank selectors, antennae tuners, programmable phase delays and tuneable oscillators [142].

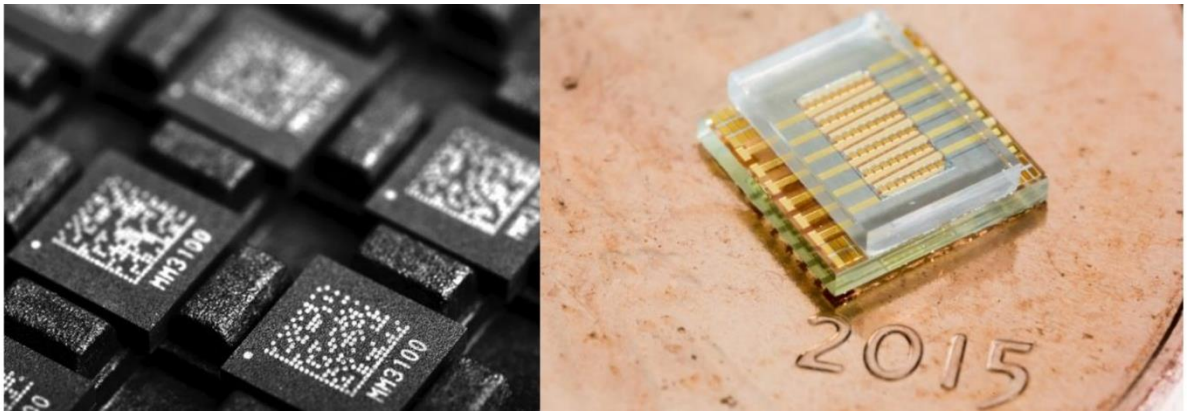

Figure 7-9 - The MenloMicro MM3100 switch packaged (left) and capped wafer showing switch cantilevers (right).

7.3.2 Analogue Devices

The Analogue Devices ADGM1004 switch is optimised for a greater RF bandwidth (DC to 13 GHz) than the MenloMicro MM3100 (DC to 3 GHz). A charge pump is incorporated in the package so TTL voltage (3.3 V) is used to operate the switch. Target applications are again tuneable filters and attenuators [138].

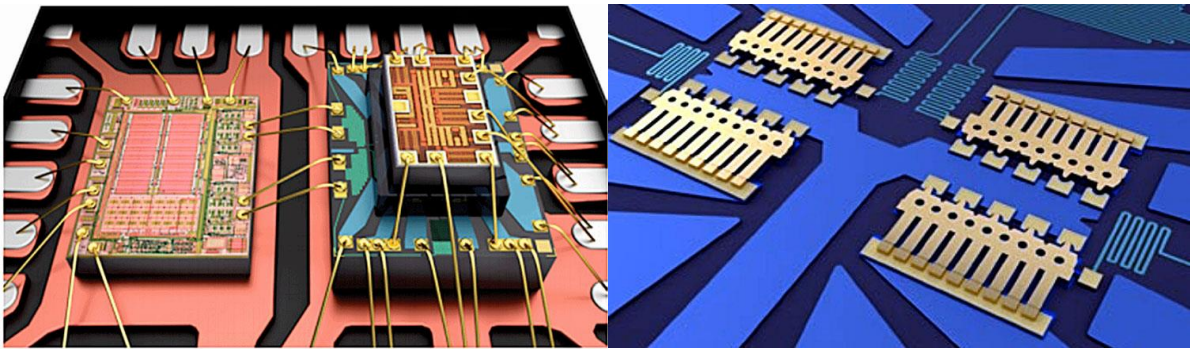

Figure 7-10 - Gold cantilever Analogue Devices ADGM1004 Single pole 4 throw 4 Switch package with voltage pump and control system (left). Switches encapsulated, and wire bonded with drive circuitry (only 3.3 V required to operate). The internal metal-metal contacts are shown (right) Note use of 5 contact pads per switch - configuration provides a maximum RF power handling of 4 W (Released August 2018)

	MenloMicro MM3100	**Analogue Devices ADGM1004**
Max Isolation Signal (V)	+/- 150 (AC or DC)	+/- 20 (DC)
Max Transmit Signal (V)	+/- 45 (AC above 10MHz)	+/- 6 [10 Max] (DC)
Max Current DC (mA)	1000	250
Closed Resistance (Ron Ohm)	0.75	1.8 Rises to 3.5 after 10^9 220 mA cold cycles
Maximum Continuous RF Power (W)	25 (above 2 MHz) 1 (below 2 MHz)	1.6 (32 dBm) 2.0 (33 dBm Max)
Maximum Hot Switched Current	10 mA (1 V)	
Lifetime (cold cycles)	>3 x10^9	>1 x10^9
Lifetime ('hot' RF cycles)	>3 x10^9 (15 dBm @ 900 MHz)	3 x10^9 (10 dBm @ 2 GHz) 3.3V 2.5 x10^6 (15 dBm @ 2 GHz) 400 x10^3 (20 dBm @ 2 Ghz)
Switch Format	6 channel SPST	SP4T – 4 groups of 5 cantilevers
Bandwidth	DC to 3 GHz	DC to 13 GHz (<3 dB)
Closed Resistance Ron (Ohm)	0.75	1.8 Rises to 3.5 after 10^9 220 mA cold cycles
Guaranteed Switching Time (uS) **[Typical]**	<10 [6]	<75 [30]
Insertion Loss (Test Frequency)	0.30 dB (3 GHz)	0.45 dB (2.5 GHz)
Isolation	25 dB (3 GHz)	24 dB
Brought to Market	August 2018	2017
Package Size (mm)	6 x 6 x 1.3	5 x 4 x 1.45

Table 7-2 – Comparison of the key specifications of the market leading metal-metal MEMS switches

7.4 Recommended MEMS Switch Specification

The Menlo Micro device currently demonstrates the cutting edge of metal-metal MEMS switch performance. The key metrics that must be achieved or surpassed by a device incorporating the Au/CNT technology are the switching lifetime (>3 billion), bandwidth (0-3GHz), closed state resistance (0.75 Ω) and isolation (25 dB @ 3GHz).

Cold switched power handling is also important, but this specification is most commonly met by adding switch cantilevers parallel.

Hot switched power handling of greater than 10 mW and approaching 3 billion cycles would demonstrate a real advantage for radar, communications and wireless power applications.

8 Appendix 2 –Validation and Test of the ICE Apparatus Performance

8.1 Validation and Testing the Operation of the New MEMS Lifetime Testing Apparatus

The development of a testing apparatus is, in itself, novel and state-of-the-art and pushes the limits of what is possible with the available technology; however the development of the system is not itself a primary goal of this project and is engineering application to support the scientific objectives of this project. This does not remove the requirement for the performance of the system to be characterised and the work to do this is described in this section.

8.1.1 Characterising the Accuracy, Repeatability and Switching Rate of the Piezoelectric Actuator

The piezoelectric actuator is required to accurately and repeatable achieve the position demanded of it at cyclic rates that are at the limit of performance such that the MEMS switching contacts and reliably and repeatable operated, as well as held statically so the contact resistance and switching surface of the device can be measured reliably. It is therefore necessary to characterise performance in these areas.

Short Term Static Positional Performance of the Piezoelectric Actuator

The worst case on-axis accuracy and linearity errors of the actuator are characterised by manually driving the actuator forward and back to fixed set points over the full 20 μm range in open loop control mode (no strain gauge feedback) while recording the position of the tip using a calibrated optical probe. It is carried out over a short timeframe and as such the thermal effects are not considered significant. It is important to note that the actuator is not incorporated to the system for this test, but rather tested in isolation.

The position of the piezoelectric actuator tip is recorded via a confocal white light displacement meter (nominally a 1 kHz sample rate and 0.01 μm resolution) arranged on axis with the actuator and targeted at the centre of the actuator tip, arranged such that the beam of the displacement meter is central and parallel with the actuator travel. The piezo controller is used to reset the piezo to zero by fully discharging the actuator and referencing this to the controllers 0V output with the corresponding displacement recorded by the confocal sensor defined as zero displacement. Voltage steps of 7.50000 V +/- 18.75 mV (equivalent to 2 μm steps +/- 0.005 um) are demanded from the controller and the corresponding displacement of the piezo tip recorded.

The demanded and reported position is recorded. Figure 8-1 shows the error in the recorded position for the actual position demanded. The expansion (black) and then contraction (red) of the piezo actuator over the 20 μm range are shown as two traces.

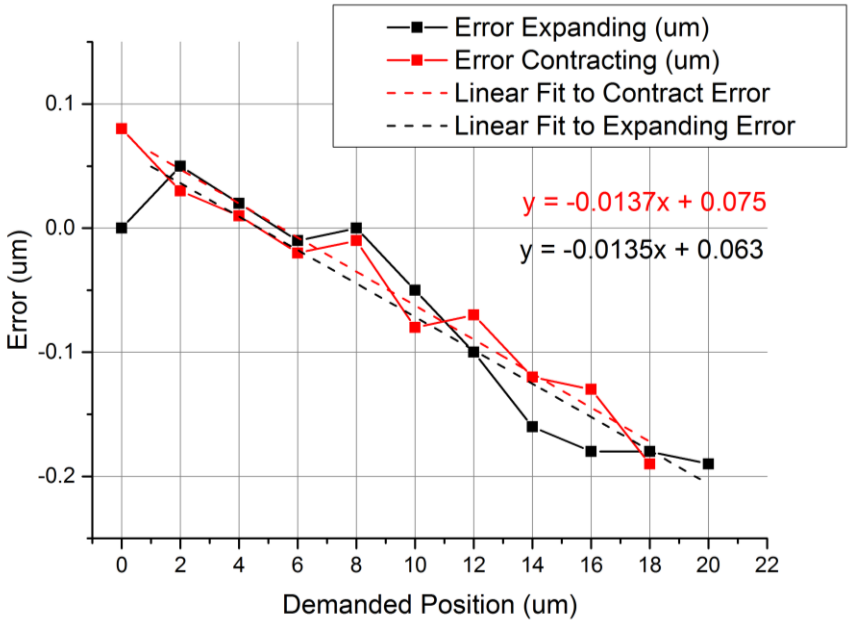

Figure 8-1 – Graph of Recorded Positional Error vs Demanded Displacement for the Piezoelectric Actuator

On axis accuracy was quantified by the trend line to the expansion and contraction error. The trend indicates that the demanded position is on average under achieved by during expansion (1.35 %) and during contraction (1.37%) an average of 1.36% underachievement. The maximum absolute error was at the demanded extension for full range (20 μm) and was underachieved by 190 nm (-0.95%) at the endpoint. The precision was quantified by positional repeatability with maximum variation of 80 nm and a standard deviation of 36 nm.

These measurements characterise the linearity as -1.36%, the worst case on-axis accuracy as 190 nm and the worst case repeatability as 80 nm. It is concluded that the driving signal must be increased by 1.36% to compensate for linearity error and the operating range should avoid the endpoints to avoid the limits of actuator range to minimise positional error.

Dynamic Measurement of Switching Motion Amplitude Variance with Drive Frequency

In order to characterise the accuracy of the piezoelectric actuator when it is in motion (dynamic accuracy) investigation of the actuator position measured directly using a displacement meter is described.

For switching rates >300 Hz the bandwidth of the piezoelectric amplifier/controller is not high enough to support closed loop feedback control from the inbuilt strain gauge arrangement. To evaluate the precision of the piezo amplitude in the open loop mode the amplitude of a square wave motion profile has been measured with a nominal but uniform amplitude (2.33 μm) of drive signal over a range of frequencies. The driving voltage has been increased by 1.36% based on the previous test results to compensate for the under extension observed in the previous test. The position of the piezoelectric actuator tip is recorded via a confocal white light displacement meter (nominally a 1 kHz sample rate) targeted at the actuator tip such that the beam of the displacement meter is parallel to the actuator travel.

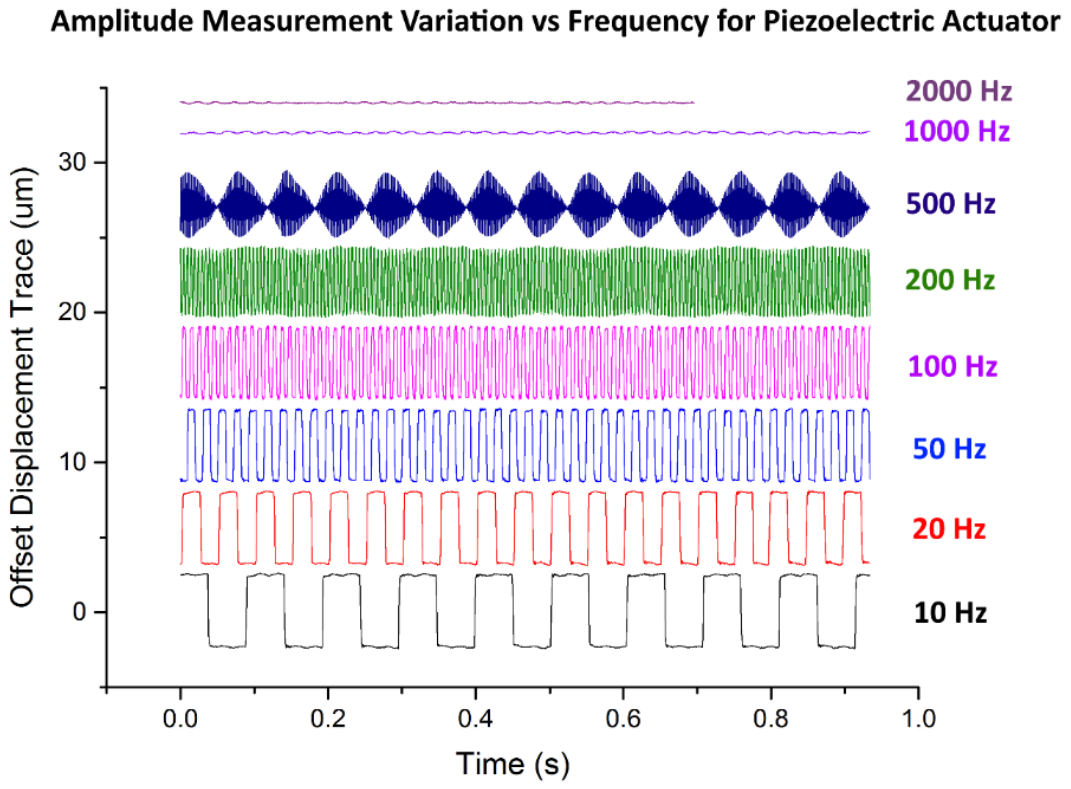

Figure 8-2 – Displacement vs Time for a Piezoelectric Actuator Driven by a Variable Frequency Square Wave

The influence of the sensors sampling frequency will, according to the Nyquist theorem, introduce an aliasing effect. In Figure 8-2 the recorded position of the piezo actuator tip is reported against time for a range of operating frequencies. It can be seen that the measurement of amplitude does not appear stable from 200Hz with aliasing effects becoming increasingly apparent, caused by the switching frequency approaching the sensor sampling frequency.

To evaluate the influence of the aliasing effect on the misrepresentation of the real switching amplitude the absolute arithmetic average of the measured signal is derived and the trend with actuator frequency extrapolated as follows.

Where the amplitude of actuator motion, A in the z axis is calculated using the absolute arithmetic average $A_{\bar{z}}$ of the measured displacement signal according to

$$A_{\bar{z}} = \frac{1}{n}\sum_{i=1}^{n}|z - \bar{z}| \qquad \textit{(8-1)}$$

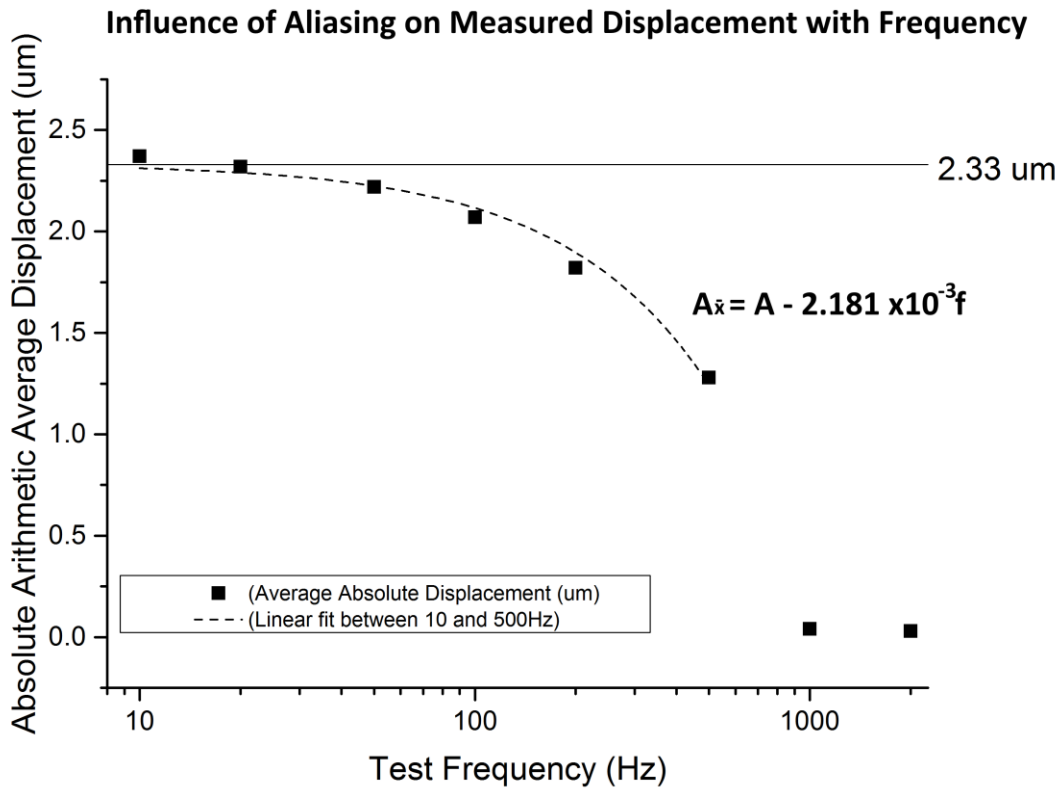

Figure 8-3 – Plot of Arithmetic Absolute Average of Measured Displacement vs Switching Frequency for a Piezoelectric Actuator

In Figure 8-3 the $A_{\bar{z}}$ parameter is plotted against the actuation frequency with a linear line of best fit (note frequency scale is logarithmic). The variation of the $A_{\bar{z}}$ parameter showed a linear response with cycling frequency, f where A is the demanded amplitude of motion in microns and is best described by

$$A_{\bar{z}} = A - 2.181 * 10^{-3} f$$

Rearranging and solving for the 2.33 μm switching amplitude investigated predicts the $A_{\bar{z}}$ parameter would be zero as f reaches 1068 Hz. This cut off is close to the nominal 1000 Hz sampling frequency of the white light displacement sensor. At 10 Hz switching the $A_{\bar{z}}$ parameter was 2.33 μm

The lower amplitude observed with higher switching frequencies is attributed to the limitation of measurement sampling frequency and the trend agrees with the ultimate limit of the displacement sensor sample rate. The measured and demanded switching amplitude were in agreement to the resolution of the measurement instrumentation (0.01 μm) at the 10 Hz rate where the trend observed would have resulted in an underestimation of 22 nm. It is therefore concluded that the dynamic switching amplitude at 2.33 um is 2.33 um +/- 0.02 um upto a switching frequency of 500 Hz. A final note is that a sensor with a 4 kHz sampling rate and enhanced on-axis accuracy is being sourced and will be able to improve upon this characterisation.

8.1.2 Characterising the Influence of Thermal Effects on System Stability

In the context of the system performance the effects of long term positional stability (drift) is predominantly dependant on thermal effects and the range of thermal variation the operational environment will experience over a lifetime testing experiment. In this section the thermal variation is monitored in the laboratory the apparatus is to be used. In the following section the correlation between thermal variation and positional change is investigated.

Long Term Variation of Temperature in Operating Environment

The location of the apparatus is a nanometrology laboratory where the temperature is set to be controlled at 20 C +/- 1 C and humidity to 40 % +/- 10 %. Temperature and humidity in the laboratory are recorded at the location of the apparatus at 1 second intervals with 0.1 ^{o}C and 0.5 %RH resolution (Lascar EasyLog EL-USB-RT Temperature and Humidity Logger). Figure 8-4 shows the temperature and humidity monitored over a continuous 7 day period. Mean recorded temperature was 20.64 ^{o}C fluctuating between maximal and minimal values of 21.7 and 18.8 ^{o}C respectively.

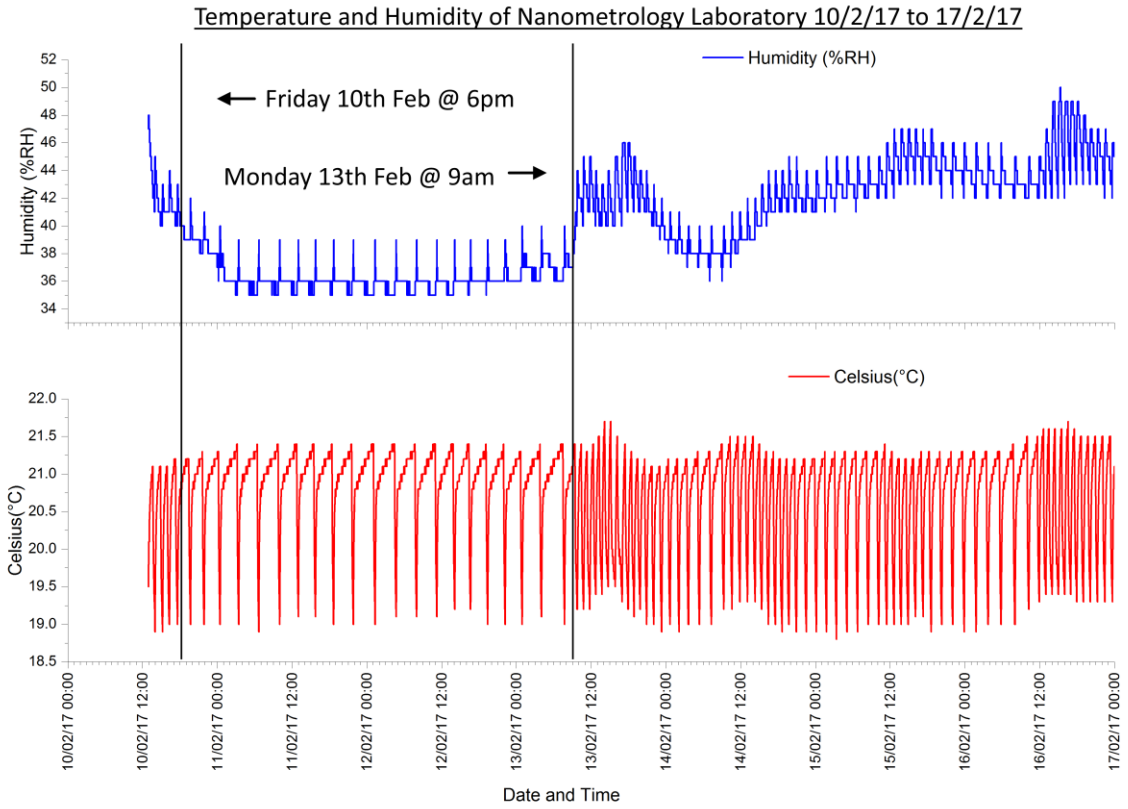

Figure 8-4 – Graph of a 7 day temperature and humidity log in the University of Southampton, Lanchester Building, Nanometrology Laboratory

These values are slightly outside the limits specified for the laboratory; however they are within 0.3 ºC of the plant control set points, suggesting that a better tolerance for temperature control may reasonably be achieved by adjusting the HVAC plant control. Mean recorded humidity was 40.3 %RH fluctuating between maximal and minimal values of 35 and 50 %RH. Where the laboratory was unoccupied the control of humidity was improved and stayed between 35 and 39 %RH.

The air conditioning plant introduces a thermal cycle that begins to cool the laboratory air supply when a control sensor measures the air temperature has reached 21.0 ^{o}C. The cooling is stopped when the sensor indicates the ambient laboratory air has reached 19.0 ^{o}C. Most equipment and instrumentation is left switched on continuously to achieve good thermal stability; however the presence of the human operators and increased equipment activity introduces additional heat sources of the order of 130W per person [143]. Thus the cycle time varies from approximately 360 minutes to as little as 75 minutes long depending on the thermal load in the laboratory. This is clearly observable by the most stable humidity and longest temperature cycle times occur over the weekend where laboratory occupancy and equipment use in minimal.

The most rapid temperature change occurs during the cooling phase where the laboratory air temperature can typically drop from 21.0 to 20.0 ^{o}C in less than 10 minutes. It was observed that the position of the temperature logger was directly in the flow path of the air being returned from the HVAC plant. Future measurements were taken in ambient air but shielded from the direct flow path and show slower decreases in temperature as the HVAC plant begins to cool the laboratory air.

General good practice for metrology laboratories [96] recommends the control of dimensional and optical laboratories (Type 2) to 20.0 ^{o}C +/- 0.3 ^{o}C. This may be contrasted to the UK NAMAS accredited NPL Metrology Laboratories that are controlled to 20.0 ^{o}C +/- 0.1 ^{o}C and humidity to 40 %RH +/- 5 %RH. Humidity control kept the laboratory between 35 and 50 %RH. It is noted that 65 %RH is a key threshold in metrology laboratories as it is above this level where tribo-corrosive attack on ferrous materials is observed to accelerate significantly. Where this is not a consideration in this case as the major components are non-ferrous based, general good practice suggests control between 35 and 55 %RH. It is also noted that the laboratory climate control system appears to be effective in keeping the temperature and humidity controlled close to the set point values but these are considerably greater than those specified in UKAS.

The conclusion there is scope for improvement to the thermal stability in the laboratory but the long term control of temperature is performing as expected and short term fluctuation is of the order of 2C over a period of ~ 2 hours. University of Southampton Estates and Buildings Services are currently being queried regarding possible improvements to the temperature control set point values for a tighter control of the laboratory temperature to minimise uncertainty in dimensional and instrumentation measurements due to thermal variation.

Effect of Thermal Fluctuations on Long Term Positional Stability of the Measurement Head (Upper contact holder) to XY stages (Lower contact holder)

To investigate the effect of laboratory temperature fluctuation on the stability of the system that holds the halves of the contact relative to one another a study is carried out a study of the measured displacement between the upper and lower contact mounting locations. A confocal laser displacement meter (Keyence LT9010M), also used as the measurement sensor in the new testing apparatus described earlier, is attached to the upper contact mount and aligned vertically. The target for measured displacement is an optically flat surface placed horizontally on the lower contact mount. The total static displacement is set to be nominally 6 mm. The variation of the sensor displacement from the nominal static set point and the laboratory temperature is then logged over a 2 hour period identified in the previous section as encompassing the significant period of thermal variation.

Two conditions are investigated. Firstly the apparatus is left exposed to ambient laboratory air, and secondly, the apparatus cover is used to enclose the system such that the metrology frame, motion system and sensor are protected from drafts. Both experiments were carried out in the evening to ensure minimal disturbance from mechanical vibrations in the laboratory.

The results are presented in Figure 8-5 and show that despite the enclosure being only partially sealed, it provides a significant improvement in the stabilisation of the temperature and positional stability of the contact separation in the apparatus. The use of the enclosure to stabilise temperate resulted in a decrease in the standard deviation of ambient apparatus temperature and static displacement from 0.473 ^{o}C to 0.069 ^{o}C and 1.049 μm to 0.164 μm respectively.

The results conclude the apparatus will achieve significantly stabilised from drift effects using an enclosure and this should be employed during lifetime switching investigation; however it is not completely clear if the variation is due to drift of the motion control or the sensor itself. These

effects are difficult to investigate in isolation and to some extent this is unimportant as it is the overall error that is of significance and the purpose of this study was to characterise this error.

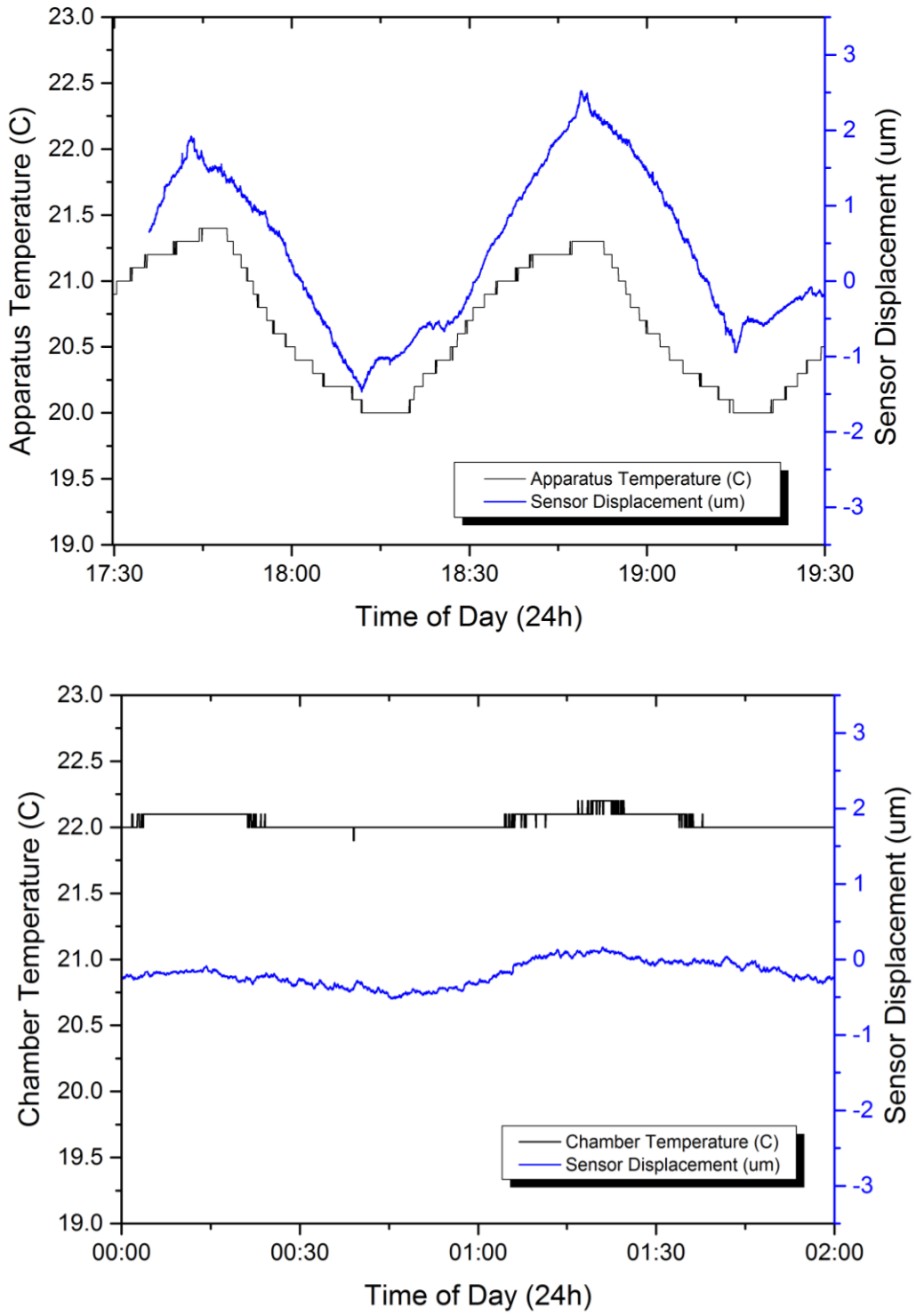

Figure 8-5 – Graphs of Apparatus Ambient Temperature and the Separation between Upper and Lower Contact Mounts (above) without apparatus enclosure and (below) with apparatus enclosure

8.1.3 Determining Reliable Switching Rates for System Operation

During accelerated lifetime testing it is a requirement to drive the switching contact at cyclic rates that are generally far above those that are experienced in operation service. This section reviews the new testing system operating a test contact at enhanced switching rates using the Direct Mode of operation (page 101) where the upper contact is directly driven by the piezoelectric actuator. As the cycle rate is increased the time required for the contact force to stabilise due to effects such as becomes appreciable in terms of the overall cycle period. The objective of these tests is to demonstrate that the system can reliably operate (open and close) the contact at enhanced switching rates.

Dynamic Measurement of Switching Rate by Measuring Closed Contact Condition – Set up

Initial testing of the switching rate that may be achieved with the apparatus has been carried out utilising a contact pair consisted an Au/Cr coated 2mm diameter ball as the mobile contact and a simple planar bulk Cu plate at the lower electrode. The contacts are brought into initial proximity manually by 100 nm steps until a closed circuit condition was measured by the 4-wire resistance method. The first point at which a static position maintained a constant closed circuit was set as the centre of the switching action. The contact was then cycled over nominally +/- 2.5 µm driven by a triangular waveform provided to the piezo actuator controller from a function generator. The triangular waveform is chosen such that the contact is open and closed at a constant velocity for a given switching rate and acceleration of the contact pair is minimised. The contact potential and driving waveform are monitored using a high speed digital storage oscilloscope (DSO). A load circuit provides a constant current of 10 mA at 4 VDC to the electrode pair. The DSO instrumentation is set to record the closed contact potential with the highest resolution such that potentials above 0.145V are out of range of the measurement; however when the waveform is inspected including this range the normal open circuit voltage is observed (~4.1 V). The purpose of this arrangement is to evaluate that the circuit is opening and closing at the intended rate and to investigate the stability of the dynamically changing contact resistance. The contact is then operated at driving frequencies of nominally 120, 200 and 1250 Hz for 60 seconds.

Dynamic Measurement of Switching Rate by Measuring Closed Contact Condition – 120 Hz Switching

A section of the recorded waveform at 120 Hz is presented in Figure 8-6.

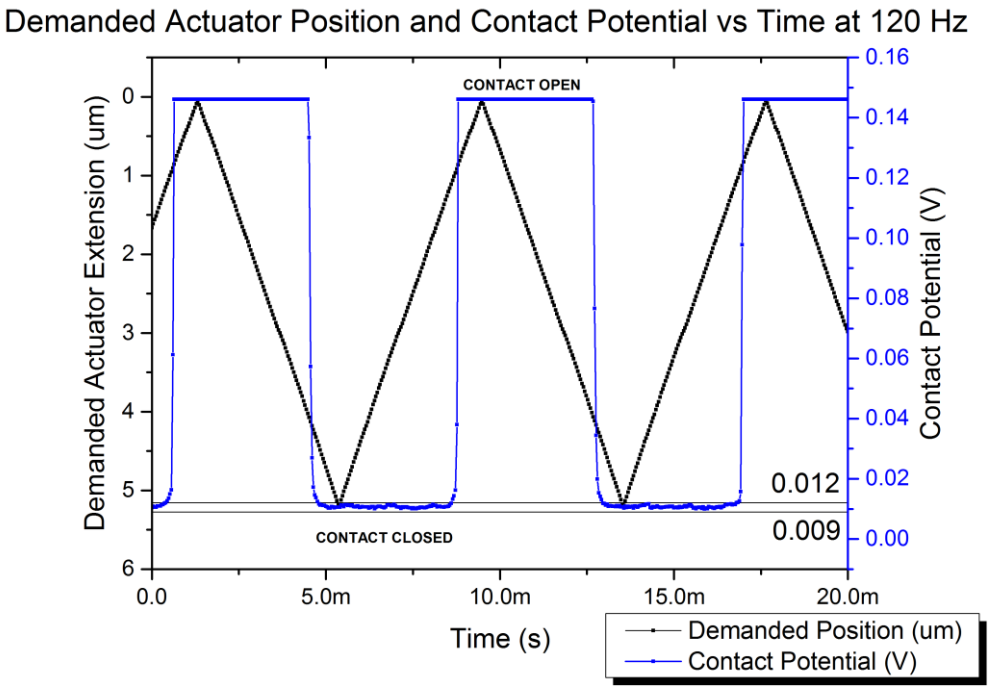

Figure 8-6 – Graph of the Piezoelectric Actuator Drive Waveform and the Contact Potential for 120 Hz Switching

We observe the time period of a cycle, T is 8.12 ms (123 Hz) and the ratio of switch closed circuit time to overall cycle time (duty cycle) appears correct and is measured at 0.54T (54%). The contact potential during contact closure is stable between 9 and 12 mV equating to contact resistance of between 1.08 and 0.81 Ω for the 40 mW test conditions

As the duty cycle is close to 50% we expect the maximum demanded extension of the actuator to be coincident with the midpoint of the contact closure; however it is observed there is an offset in these positions with the midpoint of contact closure occurring 16% of a time period (0.16T) after the time of maximum demanded actuator displacement.

Dynamic Measurement of Switching Rate by Measuring Closed Contact Condition – 200Hz Switching

A section of the recorded waveform at 200 Hz is presented in Figure 8-7.

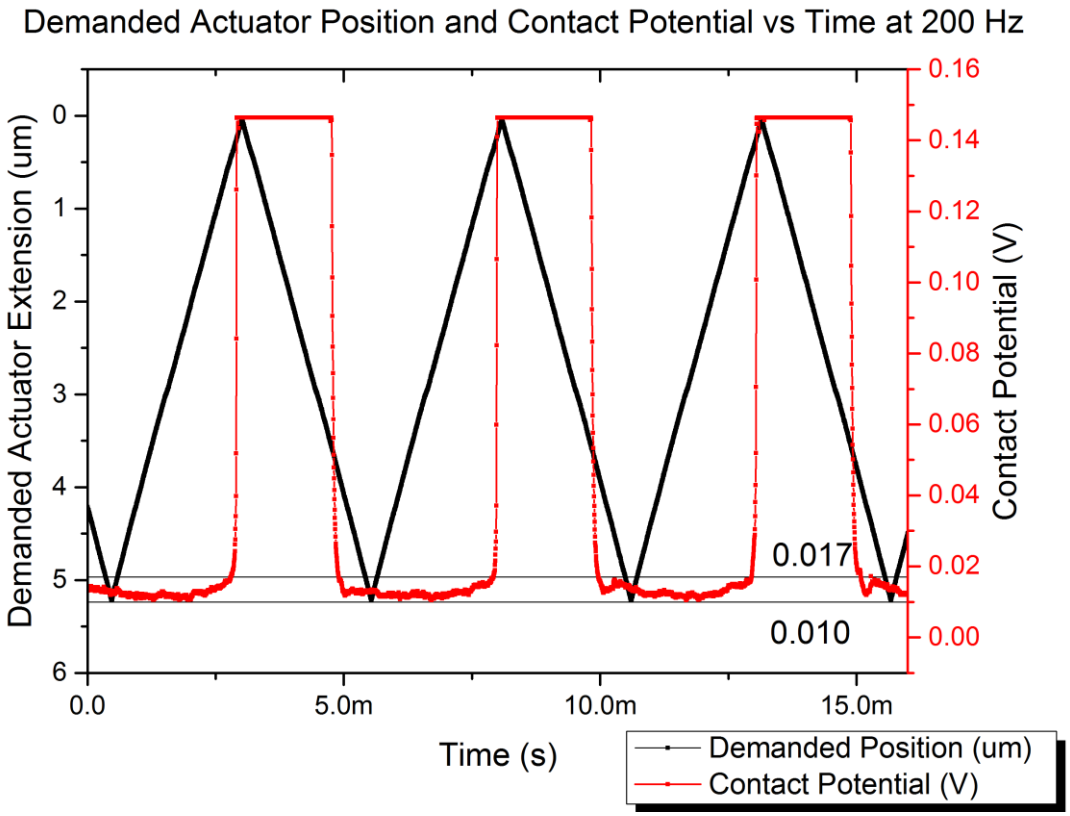

Figure 8-7 – Graph of the Piezoelectric Actuator Drive Waveform and the Contact Potential for 200 Hz Switching

Time period of 5.09 ms (196 Hz) are noted with an increase in the duty cycle observed to 0.64T (64%). The closed circuit voltage shows increased fluctuation, measured between 10 and 17 mV, equivalent to contact resistance of 0.90 to 1.53 Ω. The contact resistance is repeatedly observed to show a slight increase immediately approximately 0.5 ms after contact closure before beginning to unsteadily decrease again to a minima approximately halfway through the closed circuit condition. Just prior to opening a small plateau is observed in the contact potential indicating the contact resistance is briefly stabilised for approximately 0.5 ms.

Dynamic Measurement of Switching Rate by Measuring Closed Contact Condition – 1250 Hz Switching

A section of the recorded waveform at 200 Hz is presented in Figure 8-8. This shows significantly greater resolution of time that Figure 8-6 and Figure 8-7 to represent an equivalent waveform sample. This makes the gradual decrease in contact resistance at closure more obvious.

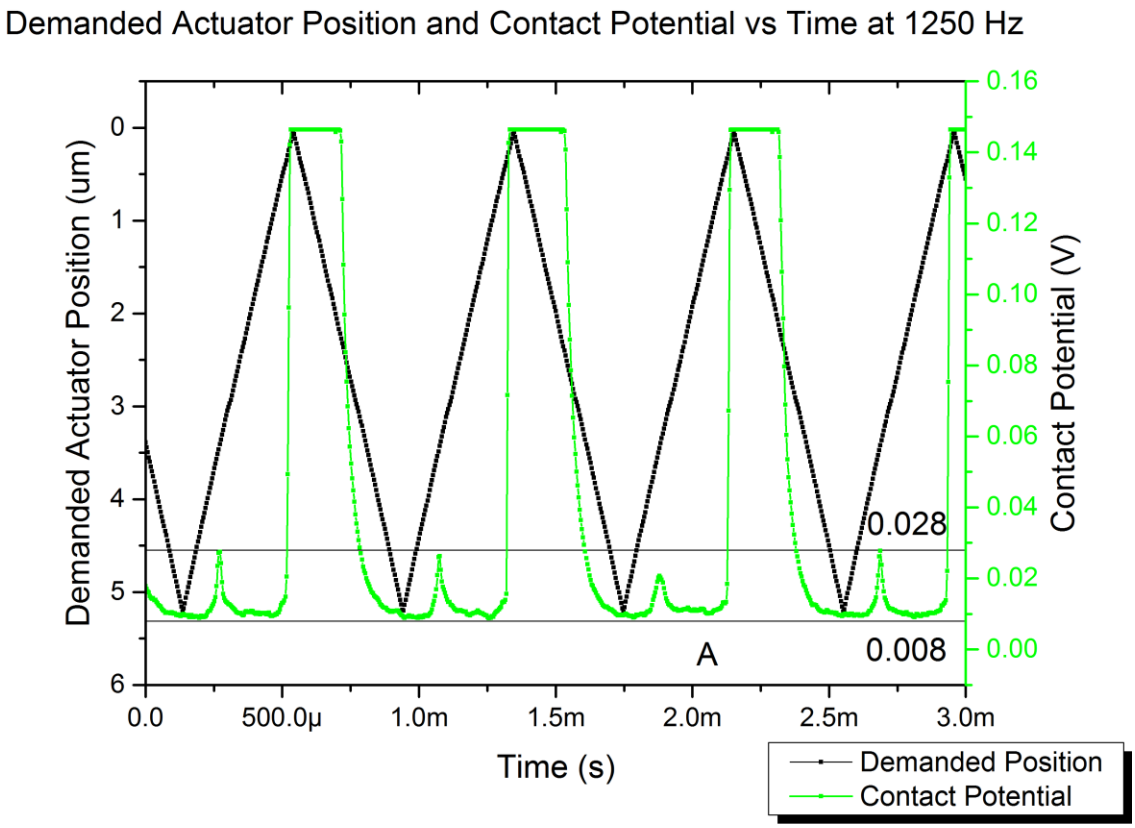

Figure 8-8 – Graph of the Piezoelectric Actuator Drive Waveform and the Contact Potential for 1250 Hz Switching

A time period of 0.81 ms (1238 Hz) is measured along with a duty cycle of 0.78T (78%). The lag between the contact maximum demanded position and centre of the closed circuit contact is measured at 10% of the time period.

The most significant difference that is observed is the presence of a spike in contact resistance approximately hallway through the closed circuit period where the contact potential increases from approximately 8 to 28 mV indicating an increase in the contact resistance from 0.72 to 2.53 Ω. The contact potential does drop again after this event but in many waveforms (as per the waveform labelled “A” in Figure 8-8) it does not reach the previously observed level.

Comparison of the Contact Potential at Closure at 200 and 1250 Hz

It was observed the rate of decrease of contact potential during onset of the closed circuit condition was very similar in all three test frequencies. A graph of the contact potential at contact closure in the 1250 and 200 Hz tests is presented in The 120 Hz test was carried out at a lower sampling frequency and is presented in Figure 8-9.

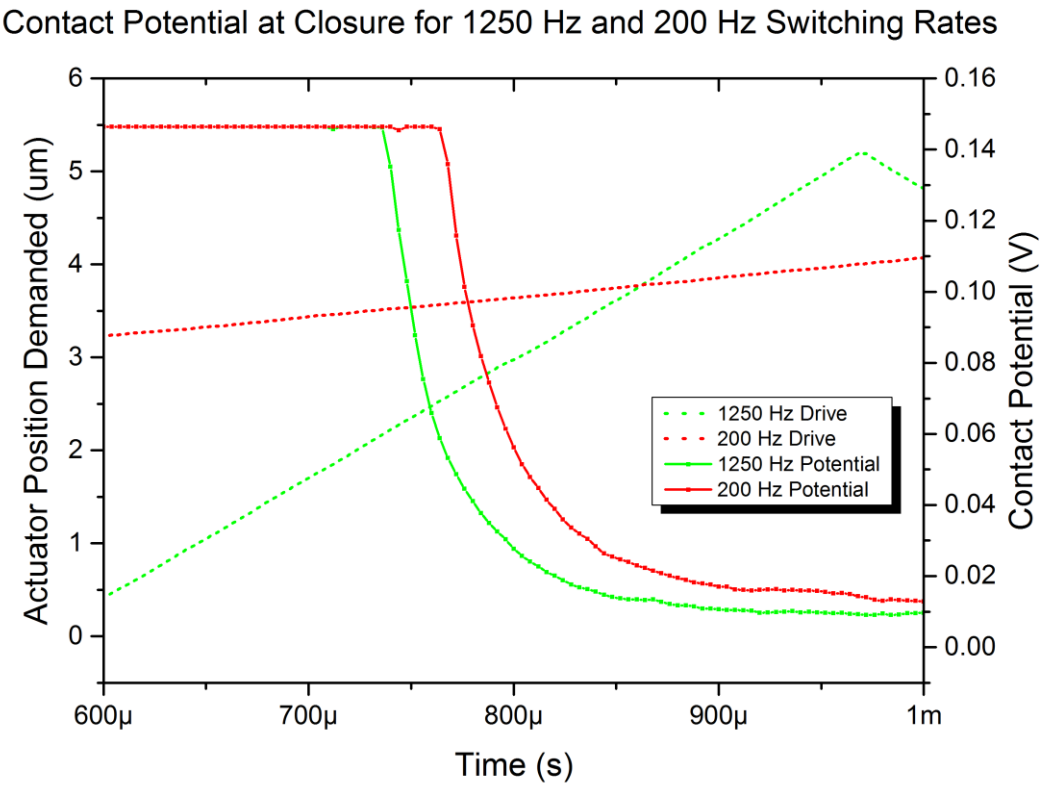

Figure 8-9 – Graph of the Contact Closure at 200 Hz and 1250 Hz vs Time

It is observed that despite an increase in the contact closure velocity of greater than six fold, the rate of decrease in contact potential is very similar. Close observation of the switching operation at very low frequency using the magnified visual feedback revealed that as the contact closes the planar contact surface does not deform significantly but is in fact pushed down.

8.1.4 Summary of ICE System Switching Performance

Measurement Performance

Measurement Principle	Vertical (Z) Resolution	Vertical Range	XY Range	XY On-Axis Repeatability	Sensor Light Source	Sensor Spatial (XY) Resolution
Point Autofocus	10 nm	0.6 mm	25 mm x 25 mm	±50 nm	655 nm (Red Laser)	<1 µm

Noise Floor (Optically flat standard) S_a	Step Height Accuracy (2.660 μm standard) Mean	Step Height Repeatability (2.660 μm standard) Standard deviation
24.2 nm	2.660 μm	32 nm

Switching Performance

Sustained Contact Cycling Rate	Minimum Contact Force	Resolution of Contact Force
20 μm Cycle - 10 μm Cycle - 1250 Hz 5 μm Cycle – 3700 Hz	~ 20 μN (Indirect Mode) ~100 μN (Direct Mode)*	

*Minimum Contact Force in Direct Mode is dependant on the spring constant of the contact interface

8.1.5 Conclusions from Switching Performance Testing of ICE Apparatus

The higher switching rate performance of the apparatus shows that the contact is being opened and closed reliably at the frequency demanded up to 1250 Hz, the highest frequency tested; however a skew between the driving signal and the displacement profile, and a fluctuation in the contact resistance at the higher switching rates was observed. The source of skew may be that the A to D conversion of the drive signal by the amplifier has a frequency dependence on the drive signal. This is in keeping with the observation that the skew had a consistent offset as a fraction of the time period and can be readily tested by measuring the output waveform from the amplifier to test this hypothesis. Assuming the drive waveform and motion of the actuator are offset then appearance of the increase in contact resistance at the mid-point of contact closure during 1250 Hz switching may be related to the change in direction of the actuator. The change in jerk would cause the force between contacts to decrease if the returning spring force of the lower contact was rate limited by internal viscosity.

It is also noted that the contact is being overdriven and this was intended as the 2.5 um over drive was representative of the deflection seen in an Au/MWCNT contact surface at closure. In the case of the planar Cu contact, with much greater modulus and hardness, this may have resulted in one or both of the contacts being crushed. As the hardness of the Au is lower than Cu it is logical that the Au would have been crushed first potentially exposing the steel substrate ball. The drop in contact resistance at higher frequency may be due to the thin film Au coating becoming punctured by asperities in the Cu.

The measurement of duty cycle indicated the contact remained closed for an increasing proportion of the switching cycle as the switching frequency was increased. When the contact motion was visually inspected at lower velocity it was observed that the entire lower contact was being microscopically deflected down rather than the lower contact being deformed. This indicates that the entire lower contact assembly was behaving as a spring with a very low spring constant. This would present itself as a small contact load being achieved quickly but additional displacement of the actuator resulting in very little additional contact force. This is supported by the observation that the rate of change of contact resistance is not dependent on the contact velocity for the switching frequencies observed. This mechanism suggests that the contact form does not entirely marry to the surface of the glass substrate and the cyanoacrylate adhesive was unable to fix the air voids such that the copper plate is bowing macroscopically rather than locally at the contact interface.

Additionally this may be due to the lower stage requiring an additional static preload to remove any lash as the load on the XY stage is changed. A further test is planned with an epoxy based adhesive to support the lower contact and a static load plate.

It is concluded that system is effectively opening and closing the contact at rates of up to 1250 Hz. The direct mode of operation appears to have a reliable relationship with contact closure and applied force at 200 Hz but will not be suitable for operating at the cyclic frequencies intended for lifetime testing (> 1 kHz) as the contact force is too variable. This may be due to unintended compliance in the lower contact support mount though it was always the intention to use a MEMS scale cantilever in the Indirect Mode of operation for testing at these rates. Further attention to the design and implementation of the mount that holds the lower contact will be required to stabilise the fixture during high frequency testing and this will be incorporated to the next phase of testing which is the implementation of the MEMS contact Indirect mode of operation.

8.2 Surface Measurement Performance Testing of ICE Apparatus

In this section the results from the performance characterisation of the XYRIS instrument that forms the basis of the newly developed lifetime testing apparatus, and two optical measurement techniques, intended to be a primary tool for surface investigation during this study are presented.

An initial investigation of the influence of surface texture on the fine transfer wear mechanism during hot switching is then carried out with Au/MWCNT contacts. This employs the Chianrabutra PZT MEMS testing apparatus to evaluate the energy associated with the MMB when current and voltage are varied.

Finally, the preliminary results from an in-situ measurement of a contact surface during a switching sequence are presented. This is achieved with the newly developed lifetime testing apparatus.

8.2.1 Characterisation of Surface Measurement System Performance

It is recognised that no measurement system provides infinite resolution and the limitations and systematic errors that result from the practical limits of the technology must be understood and where possible quantified to allow meaningful evaluation of the data or comparison with measurements by other methods where discrepancy may arise. The XYRIS measurement system has been characterised with reference to calibrated standards as well as an Au/MWCNT surface.

Performance has been quantified using calibrated standards for the system flatness, the noise floor of the sensor and the accuracy to which step height and roughness is measured. The influence of systemic error as a result of the spatial resolution (a function of the spot size of the displacement sensor) and the speed and mode of data acquisition is also evaluated quantitatively. Finally the measurement is compared qualitatively to scanning electron micrographs of an Au/MWCNT sample.

Two displacement sensors are evaluated, the confocal laser (CL) and the white light (WL). The CL sensor is evaluated in two modes, a standard mode and a “high gain” mode where the sensitivity of the detector is increased at the expense of an increased noise floor.

8.2.2 Quantitative Characterisation of Measurement System against Calibrated Standards

The inaccuracy arising from a lack of perfect vertical stability of the motion system was characterised by the measurement of an optically flat surfaces deviation from an ideal plane. The optical flat is measured over the full measurement region of the instrument (25mm x 25mm). As the form of the motion system motion is very repeatable but the micro up-and-down "jitter" (caused by microscopic movements of the recirculating ball bearings) is not repeatable, the measurement has a 0.8mm moving Gaussian filter applied to remove the repeatable form from the quantification of the error. The 3D arithmetic absolute average roughness parameter, S_a, is then used to quantify the average error over the XY measurement area.

The stability of the system and the influence of any environmental vibration (noise floor) was quantified by gathering continuous data from the displacement sensor such that any movement, system noise or drift would show as variance in the measurement. A 5,000 point sample was gathered over approximately 5 seconds. The deviation of the signal is characterised by twice the standard deviation (2σ) of these values such that 64.2% of measurements would fall between within this range.

Z axis accuracy was quantified by measurement across a calibrated step feature – an etched trench. The step was arranged orthogonal to the measurement direction and an average of 11 measurements taken, equally spaced over a 1 mm section of the step feature. This repeats the methodology of the original calibration method that accounts for slight variation of the step geometry over its length. The data was then imported to TaiCaan Boddies analysis software where the surface of the trench sides were then levelled and set to be the zero datum and the depth of the trench at the centre recorded.

Performance over a discontinuous rough surface was quantified by the measurement of a calibrated roughness standard sampled over 1 mm x 1mm region with 201 x 201 data points.

All parameters were in keeping with the system resolution and environment. The results of the system performance evaluation are summarised in Table 8-1.

Characteristic Evaluated	Evaluation Method	Confocal laser (CL) Normal Mode	Confocal Laser (CL) High Gain Mode	White light (WL)
System flatness	Sa with 0.8mm Gaussian Filter over 625mm^2	24nm	26nm	25nm
Sensor Noise Floor	*5000 point capture on static target, 2σ [nm]*	*12.88nm*	*12.92nm*	*32.44nm*
Step Height Accuracy	Calibrated trench (2.66um)	2.660um (+0nm)	2.657um (-3nm)	2.676um (+16nm)
Discontinuous Surface	*Ra Standard (0.79um) over 1mm^2*	*0.835um (+45nm)*	*0.815um (+25nm)*	*0.750um (-40nm)*

Table 8-1 – Summary of XYris 4000 System Performance

The system flatness measurement includes the effects of all operational errors – sensor noise, environmental vibration, thermal drift, electronic noise, motion system errors and so on. This makes it an excellent overall measure of the system performance and the limit of the resolution to which it measures height. All three sensor strategies showed a very similar result at 24 to 26 nm which represent 2-3 resolution steps. The noise floor for all three also falls within approximately 3 steps of resolution but it appears the WL sensor is significantly noisier than the CL sensor; however this does not appear to have a significant influence on the overall noise floor of the system. The agreement between the step height measurement and the calibrated value is within the margin of uncertainty of the calibration certification (+/- 10nm) for the CL measurement but slightly overestimated by the WL sensor. The measurement of the roughness standard has, as expected, proven the most challenging measurement with the largest variation between methods and from the calibrated value. The variation can be explained with reference to the size of the sensor spots and the acquisition method of the sensors. The WL sensor has the largest spot (~7 μm) and it is expected this will have a smoothing effect on edges where there is a sharp discontinuity. It is therefore expected to result is a systematic underestimation in the amplitude of the square wave form of the roughness standard. By contrast the smaller spot size of the CL results in a brief loss of signal at the edge of the discontinuities. The influence of the CL discontinuity and WL smoothing effects are investigated further in the next two sections.

It is concluded that the system provides the vertical resolution and control of Z height required for the accurate investigation of the Au/MWCNT wear evolution process; however the two sensors show a discrepancy of up to 85 nm when measuring a discontinuous surface but the discrepancy is reduced when the CL sensor uses the High Gain mode.

8.2.3 Quantitative Evaluation of CL Sensor Mode on the Error over Continuous and Discontinuous Surfaces

To better understand the influence of the discrepancy observed between roughness measurements in the previous section the CL sensor is now evaluated on continuous, discontinuous and an Au/MWCNT surface in the high and low gain modes.

Performance on a Continuous Surface

The optical flat continuous surface was measured over 201 x 201 points over a 25 mm x 25 mm range in both low and high gain modes. And the measured data is shown with a +/- 5µm colour scale and 2D cross section in Figure 8-10 with (left) standard gain and (right) high gain mode. The measurements returned values of 0.162 µm and 0.161 µm for the unfiltered S_a roughness parameter. This shows effectively no difference in sensor performance for the different gain modes on continuous surfaces and no evidence of sensor acquisition loss or the Gibbs phenomena.

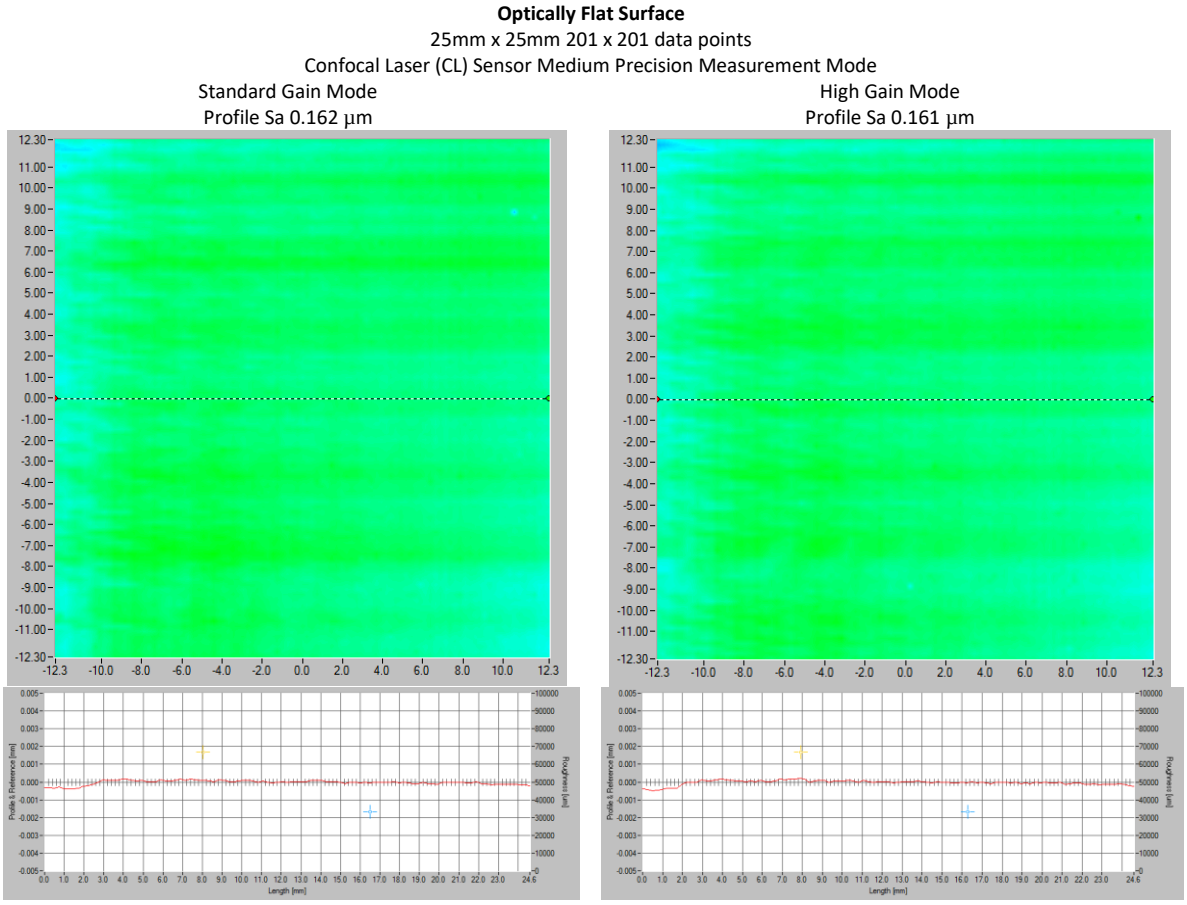

Figure 8-10 - Sensor shows negligible Gibbs Error on continuous surface in either normal or high gain modes

Performance on a Discontinuous Surface

Calibrated region of square wave trenches (Ra 0.79 um) with sharp edges tend to cause overshoot on rising edges and undershoot on falling edges due to signal processing of discontinuous data. By tilting the sample away from horizontal the trapezoid trench edges become effectively step discontinuities where the reflected light may not be returned and any Gibbs error on the processing of a discontinuous sensor signal is exaggerated. It can be seen that the CL sensor high gain mode significantly reduces the effect as the sensor is more likely to maintain a continuous signal from the surface light reflected.

Calibrated region of square wave trenches Sa = 0.80µm
1mm x 1mm
201 x 201 data points
Confocal Laser (CL) Sensor Medium Precision Measurement Mode

Standard Gain Mode
Profile Sa 1.331 µm
+531nm over calibrated value

High Gain Mode
Profile Sa 0.855 µm
+55nm over calibrated value

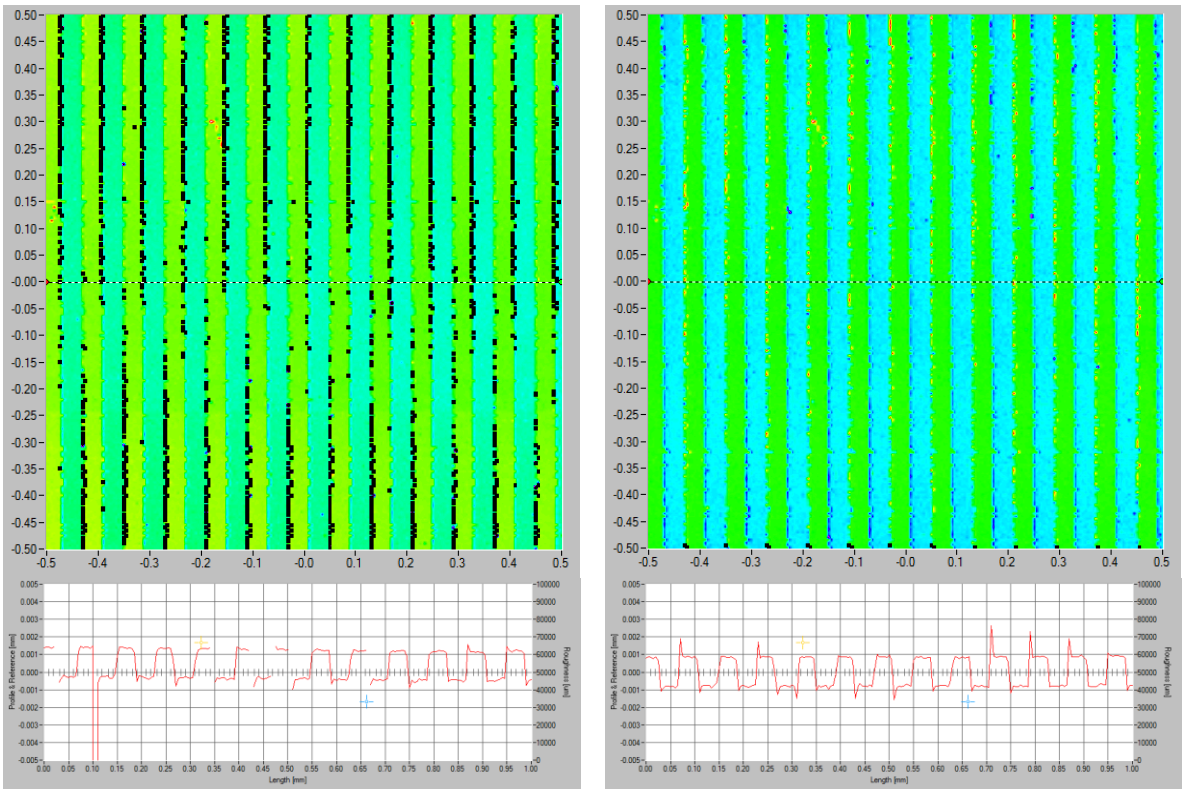

Colour image shows 2D plan view of measurement area in X and Y
Colour represents Z height

Graph shows profile along dotted line

Figure 8-11 - Sensor shows significant Gibbs Error on discontinuous surface in standard gain but not high gain mode

Figure 8-11 shows that the standard gain mode (left) exhibits greater variation of the reflected signal at the step discontinuities and this leads to large artefact spikes at discontinuities seen in the red 2D trace and an over estimation of the calibrated sample roughness by 531 nm. The high gain mode improves the signal available for processing and reduces the overestimation of roughness to 51nm in this case, but does not completely eliminate the phenomena as can be seen from the smaller spikes at discontinuities.

It is concluded that while the high gain mode reduces the artefacts are apparent on visual inspect and the rest of the surface appears to be measured well. Care should be taken when employing the high gain mode as it may make these artefacts less obvious and prone to inclusion as valid data. Finally it is noted that a simple back to back measurement in both gain modes will show up any difference that is being caused by this error and this is attempted in the next measurement on a typical Au/MWCNT composite surface.

Performance on a Typical Au/MWCNT Surface

Review of SEM and optical microscopy imaging suggest the typical Au/MWCNT composite surface is mostly continuous (shown later Figure 8-17 and Figure 8-18). Some surface fissures are observed during microscopy but these do not represent a large proportion of the surface. From the previous result we only expect to see a large difference between gain mode performances if the surface under investigation is strongly discontinuous. The surface is measured over a range where the influence of the micro topography of the surface geometry is expected to be observed based on SEM imaging. The Au/MWCNT surface is measured over a 0.2 mm x 0.2mm region sampled at 1 µm intervals and is presented inFigure 8-12 - Data suggests minor Gibbs Error on continuous surface in normal gain mode Figure 8-12 with a +/- 5 µm colour scale and 2D cross section.

Au/CNT Sample Number 112
201 x 201
0.2mm x 0.2mm
Confocal Laser (CL) Sensor Medium Precision Measurement Mode

Standard Gain Mode
Profile Sa **1.068um**

High Gain Mode
Profile Sa **1.018um**

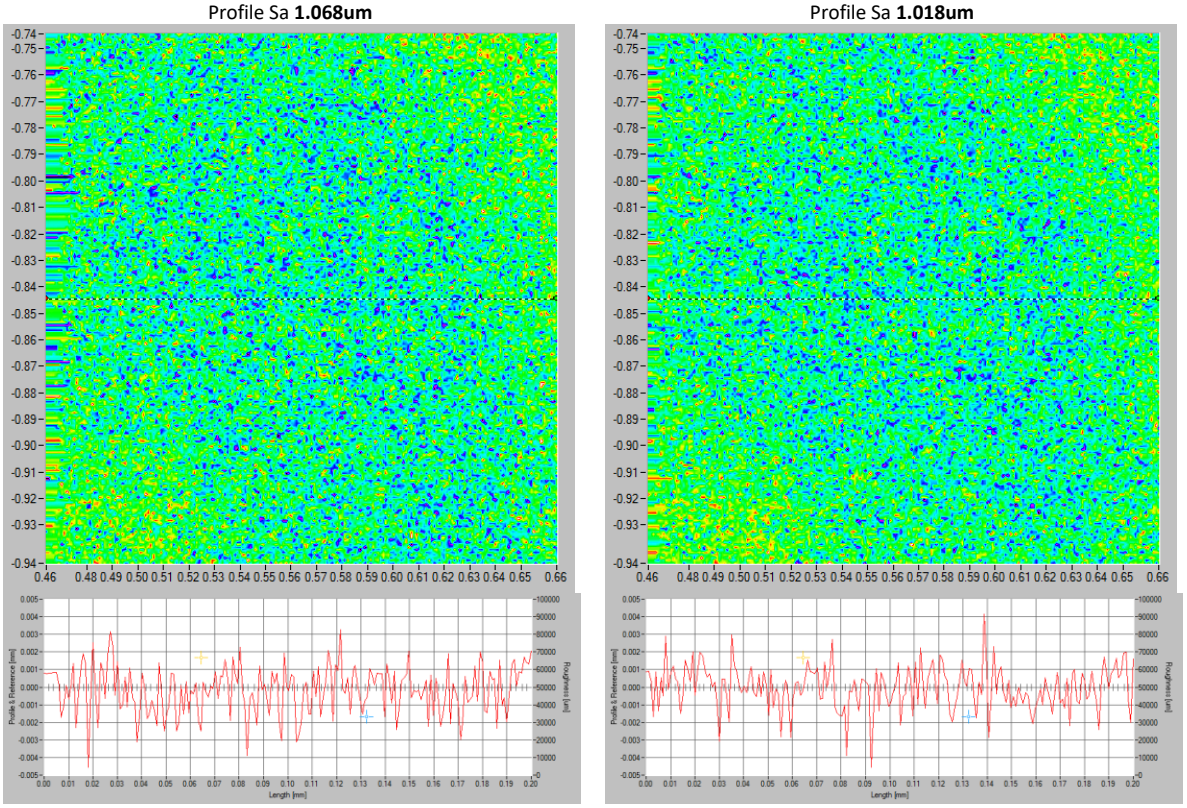

Colour image shows 2D plan view of measurement area in X and Y
Colour represents Z height

Graph shows profile along dotted line

Figure 8-12 - Data suggests minor Gibbs Error on continuous surface in normal gain mode

The measurement data shows a small difference (50nm) in the S_a value between measurement gain modes which supports the Gibbs error is not introducing a significant effect. This supports the microscopy observations of the Au/MWCNT surface being strongly continuous and it is concluded that the use of the high gain mode is practical for unworn Au/MWCNT contacts though care should be taken as a heavily worn surface will show greater discontinuity and the evolution of the surface itself may lead to an exaggeration in wear.

8.2.4 Quantitative Evaluation of WL Smoothing Error

The influence of the underestimation of the roughness of the calibrated standard by the WL sensor smoothing effect, introduced by the spot size, is further investigation in this section. First the spectral return of the sensor is investigated to estimate the range of vertical displacement on the measured surface within the spot area. A filtering effect is then applied to surface data measured with the CL to simulate the effect of a larger spot size, and this is compared to data measured directly with the WL sensor.

Smoothing Error Evaluated by the WL Reflection Spectrum

The WL sensor uses a chromatic aberration technique to derive the measurement of displacement. Light is passed through a lens designed to enhance the chromatic expansion of the incident light such that different wavelengths are focused at different displacements from the sensor. By detecting the wavelength of peak intensity in the reflection the distance to the surface can be deduced. Because the spot size of light is finite, there is practically a range of wavelengths returned. A rough surface will reflect a broad peak, while a smooth surface will return a sharper peak. Examining this range can give an estimation of the range of surface heights that area within the incident spot.

The reflection spectra from the optical flat target, arranged approximately orthogonally to the incident beam returns a very narrow range of wavelengths varying by ~0.22 nm. This corresponds to a variation in Z height within the sensor spot of 105 nm or a deviation from the optical flat being orthogonal to the beam of 0.85 °.

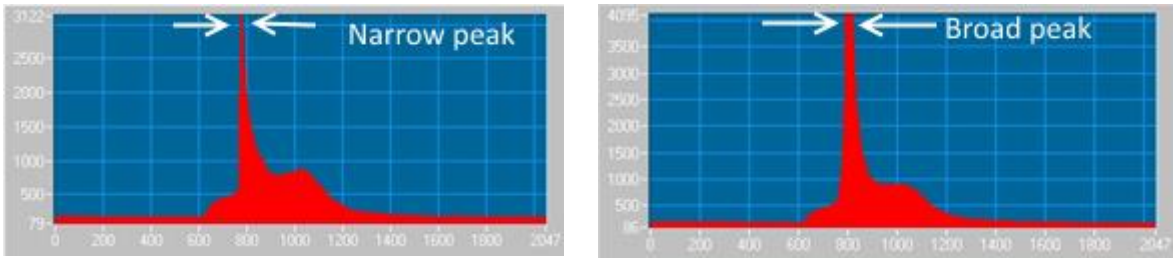

Orthogonal optical Flat reflection spectra **Au/CNT reflection spectra**

Figure 8-13 – Narrower reflection spectra observed from a flat, smooth surface orthogonal to the incident beam when compared to a microscopically rough surface from a WL sensor

The peak width of reflection spectra found to be returned from a nominally smooth and levelled Au/MWCNT surface was found to be of 1.575 nm. The same peak width was obtained from the

optical flat surface tilted to an angle of 15^{o}. Trigonometrically this predicts a 1.8 µm variation in height of the surface under the spot for the tilted optically flat surface.

By assuming the sensor optics gauge range to wavelength relationship is approximately linear then the range of frequencies returned from the composite surface when compared to the gauge range of 350 µm gauge and the 400nm wavelength detection range of the sensor equate a 1.575 nm peak width to a 1.8 µm change in Z position.

Both the inclination of a flat smooth surface and assuming the WL sensor wavelength detection to gauge range is nominally linear give rise to the same estimation of surface heights under the WL spot area of 1.8µm. This is in keeping with observations made via SEM imaging in section 8.2.7.

The conclusion is that the WL spot size is spatially larger than the features on the Au-MWCNT surface that result in a-spots, hence while it may still be possible to quantify wear the spatial resolution is probably insufficient to quantitatively evaluate the surface change due to a-spots forming and reforming.

Filtering CL Data to Approximate Effect of WL Spot Size on CL Measurement

Measurement of the Au/MWCNT composite by CL and WL sensors shows a significant discrepancy. Observation of the Au/MWCNT surface suggests the CL sensors enhanced spatial resolution is accurately reporting the surface and the discrepancy is due to the smoothing effect of the WLs larger spot size. By applying a Gaussian filter to data measured with the CL data it is possible to approximate a loss of spatial resolution and the smoothing effect of a larger spot size.

A 0.2mm x 0.2mm area of the Au/MWCNT composite sample number 112 was measured using WL and CL sensors. The raw CL sensor data then has a long pass 8µm Gaussian filter applied such that waveforms shorter than 8 µm are smoothed. This approximates the data the CL would have measured if its spot size was increased to that of the WL sensor. The measurements are presented in Figure 8-14 showing (left) WL data, (middle) CL data and (right) smoothed CL data.

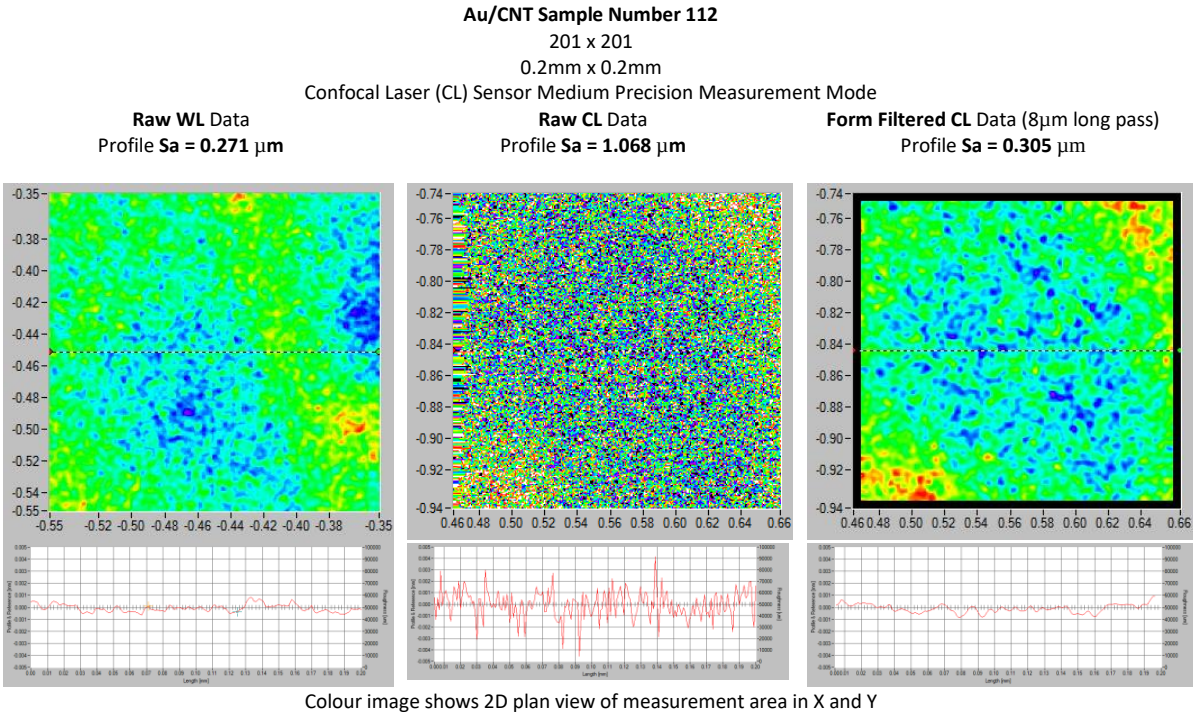

Figure 8-14 – The effect of simulating a larger spot size on CL data

Measurements of the 3D roughness (S_a) were then taken to see the effect of smoothing the CL data. The results showed that the CL filtered roughness (0.305 µm) was brought into close agreement with the value obtained with the WL sensor (0.271 µm). It would be preferably to have better parity

between measurements through duplication of the exact same area, though the surface regions measured in this test were observed to be in close proximity and with homogenous texture.

It is concluded that the discrepancy between sensors can be largely attributed to the lower spatial resolution of the WL sensor.

Using narrow focal plane of microscope to measure Z range

A parity check on height range of the surface within the field of view was carried out by making use of the very narrow focal depth at high magnification. Using calibrated trenches the optical microscope was brought into focus on the trench wall (high) and then trench base (low) at 1000x magnification and the increments on the Z stage Vernier control recorded.

The process was repeated for the Au/MWCNT bringing the low range and highest range of features into focus e.g. 2.7 steps equated to a peak to valley range of approximately 2.6 μm for a 140 μm by 160 μm region

Microscopy gave an indicative spread of 2.6 μm that is in keeping with the CL measurement of the similar sized region

8.2.5 Systematic Errors

An ongoing study in this research group has anecdotally shown that micro roughness measurements taken with the white light sensor agree with measurements from an Alicona InfiniteFocus (Alicona Imaging GmbH) coordinate measuring machine that uses an automated focal variation technique. This disagrees with the measurement data from the CL technique which reports a higher surface roughness. There are two reasons for the discrepancy. The first is that the smaller spot size of the CL sensor provides higher spatial resolution and can therefore detect the height changes of smaller features on the surface, which increases the reported surface height variation. The second is that at surface step discontinuities the CL shows a small displacement error similar to the Gibbs phenomena at the points immediately before and after the step. The error arises as a result of discontinuous function being represented by only a finite series of continuous sine/cosine functions. An example is shown in **Error! Reference source not found.** where the red plot shows the surface under investigation and the green plot shows the reported height.

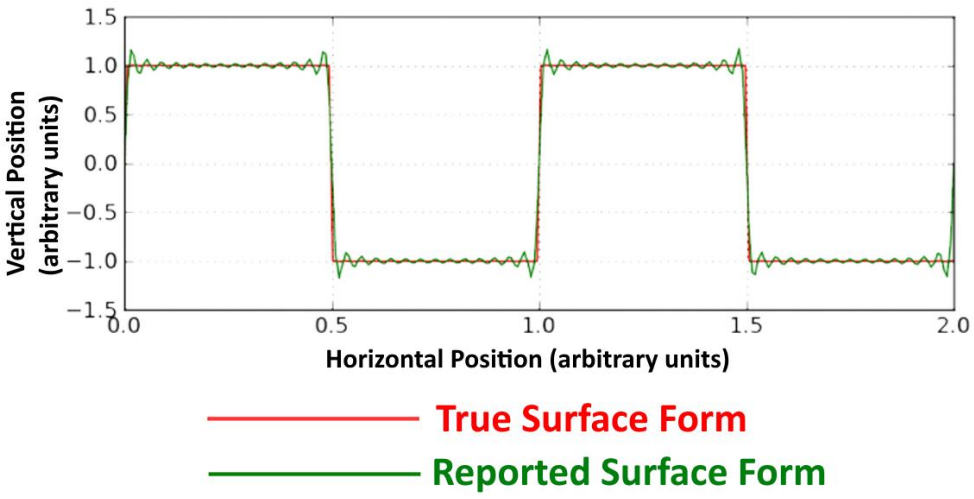

Figure 8-15 - Gibbs error in signal processing that arises when approximating with a finite Fourier series

While roughness is a measure of height variation the spatial characteristics of a surface influence the ability of the instrumentation that is measuring height. It is recognised that the spatial resolution will be practically limited by the diffraction of wavelength of the incident light according to the Rayleigh criterion [118] [117].

8.2.6 Increasing data point averaging and slowing measurement acquisition

A final test for the surface measurement system was to evaluate the influence of the measurement mode the system operates in. The TaiCaan XYRIS instrument control software (STAGES) provides low, medium and high precision modes that optimise the precision required against the time taken for the measurement.

In low precision mode the system optimises performance for the lowest acquisition time. The system acquires a single measurement at each point in the measurement grid and traverses the measurement area as rapidly as the sensors acquisition rate (1 kHz) will allow. In medium precision mode the system improves precision by taking the average of two measurements at each point in the grid, and slowing the motion system down such that unrepeatable error caused by the motion system is reduced and precision enhanced. High precision measurement mode was not investigated as the time required for these measurements would be prohibitive.

The same region was measured on a nominally smooth Au/MWCNT sample using low and medium precision measurement modes with the CL sensor and is presented in Figure 8-16. The black circles are peaks and valleys that have been removed from the graphical representation so the nominally flat regions are shown, the better to compare the samples.

Au/CNT Sample Number 112
251 x 251 data points
0.5 mm x 0.5 mm
Confocal Laser (CL) Sensor

Low Precision Mode
Profile **Sa 1.386um**

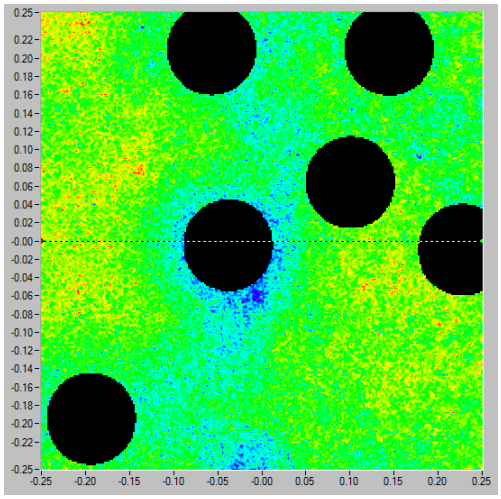

Medium Precision mode
Profile **Sa 1.417um**

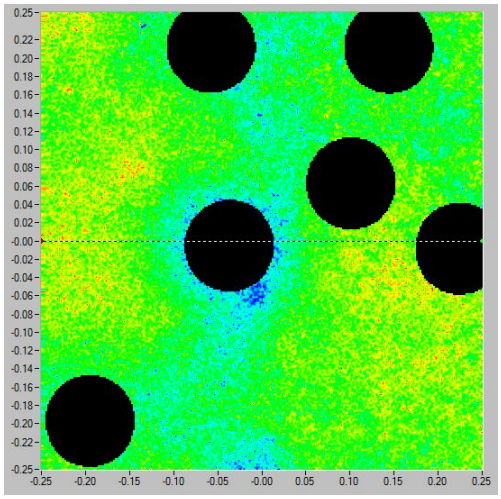

Colour image shows 2D plan view of measurement area in X and Y
Colour represents Z height

Figure 8-16 - Measurement variation with XYris precision mode

The results show that the enhanced precision strategy does not introduce significant variation in the measurement. There is a marginal increase (31nm) in the measured roughness. This indicates that the measurement precision mode has a minor effect at the relatively high roughness values seen for the nominally smooth composite samples.

It is concluded that as it is the variation in roughness during switching surface lifetime the medium precision strategy is preferable as the changes in profile roughness are likely to be very small and the enhanced precision will be required.

.

8.2.7 Conclusions from Surface Measurement Performance and Parity with Other Measurement Strategies

The surface amplitude parameter is an important variable in models for contact dynamics and understanding the profiler behaviour at the limits of its performance is important in interpreting the data it provides. There is significant difference in the spatial and height resolution of different methods as well as the filter length employed for the separation of roughness and form. The Au/MWCNT surfaces demonstrate multiscale roughness apparent which is apparent from the surface measurements and SEM imaging. While the images are not measurements, they can be used to identify and estimate the scale of features and compare to the measurement data.

SEM imaging at 1000x (Figure 8-17) clearly shows breaks in the composite surface of around 2 µm in width occurring with relatively wide spacing of 20-30 µm.

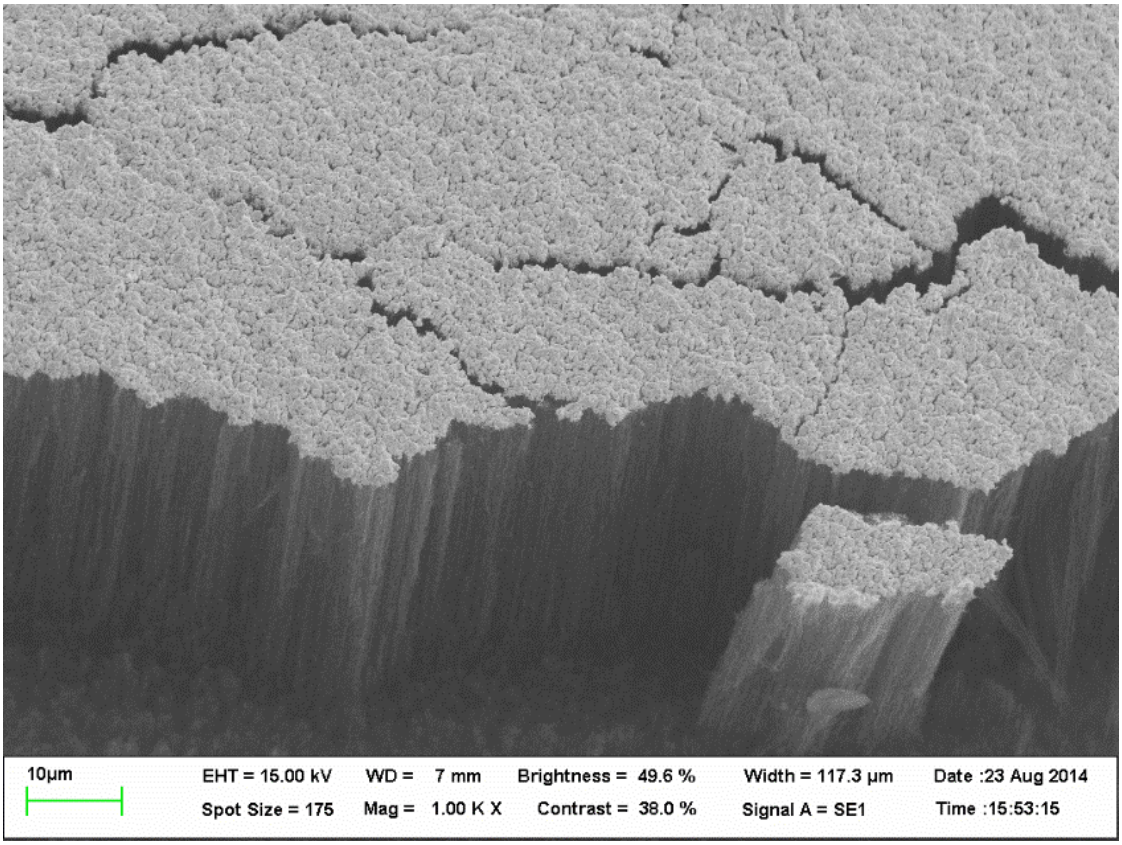

Figure 8-17 - SEM of nominally smooth Au/MWCNT Sample 112 at 1000x

Enhancing the magnification to 3000x shown in Figure 8-18 - SEM of nominally smooth Au/MWCNT Sample 112 at 3000xFigure 8-18 shows sub-micron scale features that would be smoothed by WL

measurement (7 µm spot) but on the threshold of detection for the CL sensor (2 µm spot). Visual examination of SEM image and scale suggests Z scale of small features appear to be vary from ~0.2 to 2.0 µm in diameter. The Z range is not clear due to the angle of imaging but visually estimated at ~2 - 4 µm of waviness with height of the individual Au particles around 0.2 to 0.5 µm.

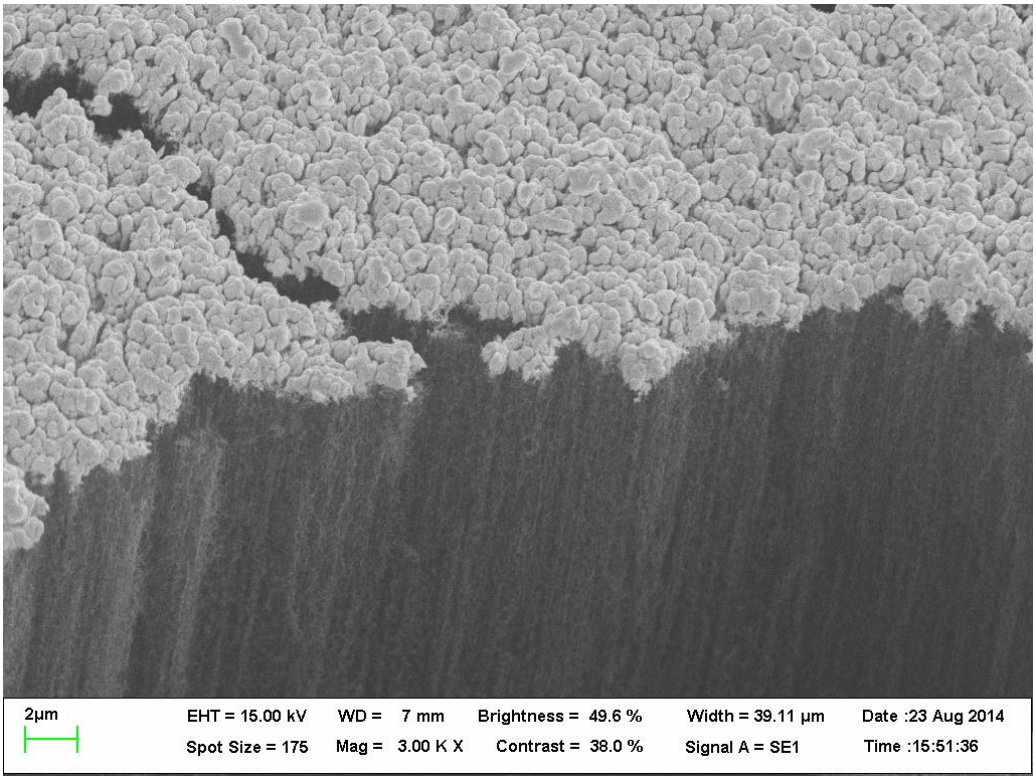

Figure 8-18 - SEM of nominally smooth Au/MWCNT Sample 112 at 3000x

AFM measurement of the Au/MWCNT by Liu et al has reported the surface with a peak to valley of 1.9 to 2.3 µm over a 40 µm evaluation length with the Ra roughness characterised as 0.18 to 0.19 µm using a 2.5 µm Gaussian filter. The characterisation of the surface was also reported as closely agreeing with a TaiCaan XYRIS with a WL sensor over a 40 µm x 40 µm region at 0.2 µm intervals with Ra roughness characterised as 0.22 um using a 2.5 µm Gaussian filter [144].

When the results from this investigation are considered it appears to strongly support that WL measurement represents a significant smoothing of the surface micro-roughness. When this smoothing effect is applied to the CL data the CL and WL agree closely. The composite surface appears to be generally continuous without sharp discontinuities. The key difference between the measurements by Liu and those reported here is the much greater spacing between measurements in this study. This makes the application of a similar roughness filter impractical as it would result in

a null value. The higher roughness values observed can be accounted for by the increased spatial resolution of the CL over the WL, and the relatively large sample spacing that results in a greater proportion of the surface waviness to be included in the roughness parameter.

A parity check on Z range within the field of view was carried out making use of the very narrow focal depth at high magnification. This provided a peak to valley microscopy estimate of 2.6 μm in a 0.14 mm x 0.16 mm field of view. It is noted that the spatial resolution of the microscopy will be limited to around 300 nm at best and the focal method employed attempted to keep a range of features in focus at both the upper and lower areas. This means the measurement is closer to taking the difference in distribution of asperity heights rather than a true peak to valley measurement. Thus it is approximates a value of double the S_a rather than S_z measurement.

In conclusion it has been shown the micro roughness of the nominally smooth Au/MWCNT surface is occurring due to features of spatial dimension of the order of 1um and less. This is practically beyond the resolution of the WL instrumentation and the sensor is smoothing data at this level significantly. The CL data does not demonstrate significant artefacts due to discontinuities on the unworn surfaces and the high gain mode appears to offer minimised error as the surface becomes more discontinuous

It is concluded that the measurement system, and both sensors report surface form accurately and provide highly repeatable (precise) data that correlate very closely with calibrated features. The variance between measurement methods due to the difference in spatial resolution of the techniques and the existence of multiple scales of roughness on the Au/MWCNT samples. The use of either sensor is justified but it is desirable to use one sensor where the data is to be compared and parity is required.

Ultimately the CL sensor has been chosen for integration with the novel testing system as its performance is greater at the scale where the a-spots are expected to change due to hot switching effects.

8.3 Preliminary Results from New MEMS Lifetime Testing Apparatus

To establish that the new apparatus is capable of detecting in-situ measurement of the surface wear occurring during switching two initial tests have been carried out. The first is carried out on a relatively rough bulk copper surface where the detection of small amounts of wear is difficult due to the relative scales of the roughness and wear features. This test place focus on the apparatus being able to precisely relocate and measure the switching location. The second test is carried out on a MEMS scale thin film contact to see if a minimal number of switching cycles in hot and cold conditions can be detected. The thin film surface is very smooth and simplifies the detection of small features

8.3.1 In-situ Surface Measurement of a Roughened Bulk Copper Contact

The capability of the test apparatus to precisely remeasure the same contact area has been investigated. This is an important performance criterion as the ability to quantitatively detect electromechanical wear at a submicron scale is often limited by the 'ambient' surface roughness obscuring small changes arising due to electromechanical effects.

The performance has been evaluated by analysing the change in the surface measurement of a bulk copper contact after hot switching at 200 mW (4 V DC, 50 mA). The Cu surface is chosen as it has similar surface roughness to the Au/MWCNT contact surfaces and provides a useful datum for the physical scale of geometric surface change that can be evaluated. The switching conditions are chosen as similar conditions proved difficult to detect any wear until a magnitude higher switching cycles had been completed [15].

An Au/Cr coated (500/10nm) 2mm stainless steel ball in used as the mobile upper contact in the direct drive mode of the new test apparatus. The lower contact is a simple bulk copper plate fixed to a glass microscope slide by cyanoacrylate adhesive. Wiring to allow 4-point resistance measurement is attached to the lower contact by lead based solder and the upper contact by silver based conductive epoxy.

The static contact closed position is achieved by lowering the upper contact in 100 nm steps until a short circuit is achieved continuously with this point defined as the centre of the cyclic motion.

The contact is then cycled over a range of +/- 2.5 μm driven by a square wave 100 Hz function. The square wave function is selected to approximate the switching action used by the PZT device in a previous study [15]. The square wave profile is used such that the contact force is stabilised for the longest period possible whereas in previous studies this switching action resulted in a bouncing phenomenon. The surface of the planar electrode is measured using the apparatus over a 0.5 mm x 0.5 mm region at 1 μm intervals in the X and Y axes.

The region was evaluated from three measurements. The first and second measurements were carried out with no switching between but the apparatus motion control system was moved from the measurement to the switching site and back again. This was to quantitatively characterise the error attributable to any lack of precision in the motion and sensor system. The third measurement was carried out after hot switching.

Analysis of the measurements was undertaken using TaiCaan Boddies surface analysis software and images representing the surface profile, before and after hot switching, are presented in Figure 8-19 where the colour scale represents a height range of 10 μm and a zoom is shown into the 100 μm x 100 μm region of contact that shows clear evidence of a wear effect.

The contact area was found to be approximately 25 μm across. The S_a roughness of the 100 μm x 100 μm region following increased from 1323 to 1385 nm (62 nm) before and after switching. The change in the surface is predominantly due to a deposition process as evidenced by the increase in height of the sample around the contact region. The deposition is believed to be the transfer of Au contact material from the opposing contact; however the contact has not had a material analysis (performed by EDX or similar) at the time of writing.

This is supported by the fitting of a linear least squares plane of best fit to both datasets and then evaluating the volume. This showed the volume above the datum had increasing from 7860 to 8500 μm^3. Assuming this additional material to be Au due to its lower hardness and fractionally lower melting point, and solid, then this equates to a transferred mass from the ball to the planar contact of 12.4 $x10^{-12}$ kg (0.0124 μg).

It is concluded that the system is accurately locating the switching region and has sufficient resolution to quantitatively detect the changes that arises due to hot switching conditions.

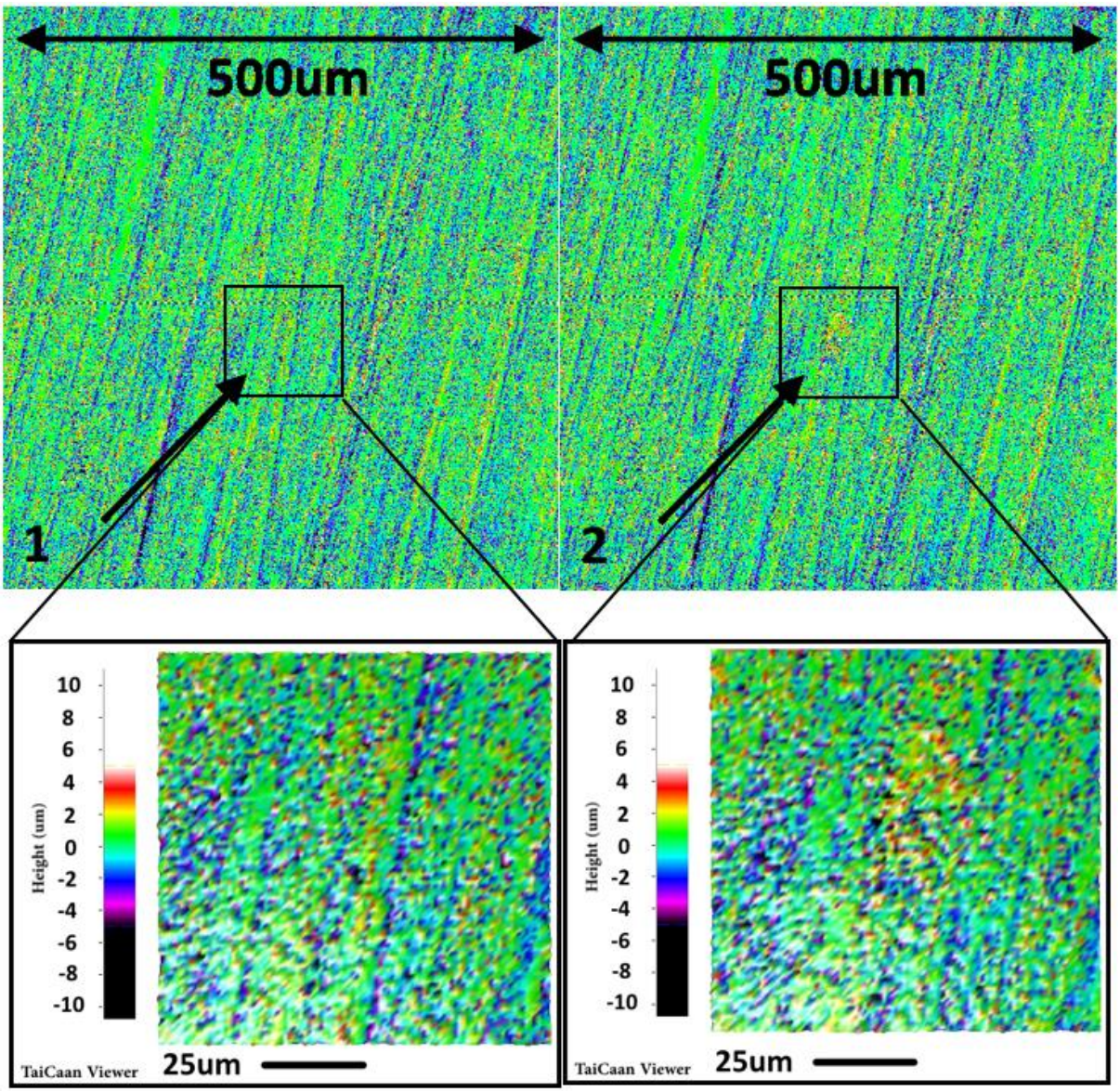

Figure 8-19 – Colour scale representations of the surface height of a planar Cu contact before and after hot switching (0.5 mm x 0.5 m, 501 x 501 data points) and (below) Zoom in to a 100 um x 100 um area of the contact region of the planar Cu contact before and after hot switching

8.3.2 In-situ Surface Measurement of a Smooth Thin Film Au Contact

The capability of the apparatus to detect changes due to a very low number of switching cycles has been investigated by carrying out cold, then hot switching on a planar thin film Au/Cr coated silicon contact.

An Au/Cr coated (500 nm / 10 nm) 2mm stainless steel ball is used as the mobile, upper contact in the direct drive mode of the new test apparatus. The lower contact consists a silicon wafer chip that has been sputter coated with a 10 nm adhesive layer of chromium with an upper 500 nm thick coating of Au. It is fixed to a glass microscope slide by cyanoacrylate adhesive. Wiring to allow 4-point resistance measurement is attached to the contacts by silver based conductive epoxy.

The contact is then brought into contact in the same method as the Cu contact (100 nm steps until closed contact). The switching motion range is set such that after initial contact the actuator pushes the upper contact down into the lower contact by 2 μm, then moves up by 20 μm such that there is an 18 μm clearance between contacts.

The contact surface is measured A) before switching, B) after 10 cycles of cold switching (no signal carried) and C) after a further 10 cycles of hot switching at 4 VDC 50 mA. All surface measurements are carried out at 0.2 mm x 0.2 mm with 401 x 401 data points (0.5 μm sampling)

The results of the surface measurements are presented as a plan view of the contact region Figure 8-20 (left) and as 3D representations of the contact region**Error! Reference source not found.** (right) where the white dotted line shows where a 2D cross section is evaluated and presented as a graph in Figure 8-21

The progression shows A) the presence of surface irregularities before switching is commenced. These serve as a useful reference that the switching site is being correctly located as the same features are clearly visible after cold and hot switching. Following cold switching B) there is a clear appearance of a pile up feature on the planar electrode surface. The deposition pattern is approximately circular with a diameter of approximately 25 μm, with a rough and jagged surface of approximately 7 μm in height at the peak. This is significant as the film thickness is only 500 nm and suggests the contact material has been torn away. Pitting damage that is ~ 2 μm deep can be observed on the right hand side of the site. This indicates not only has the surface film being punctured but the underlying substrate has also been damaged.

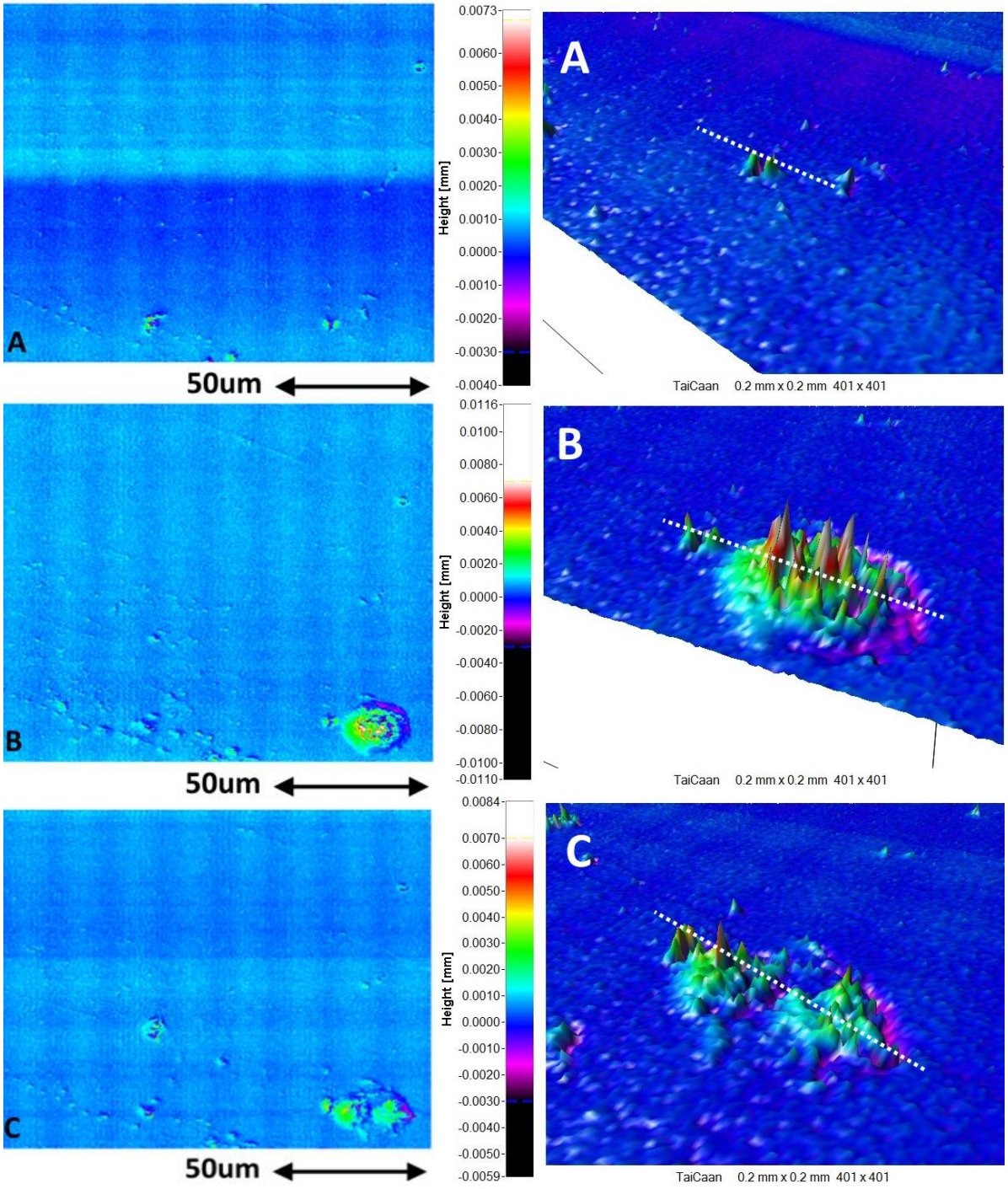

Figure 8-20 – 2D Representations Au/Cr coated Si sample A) before switching, B) after 10 cold switched and C) after 10 hot switched cycles

(left 2D – right 3D)

Dotted line indicates where 2D profile is measured

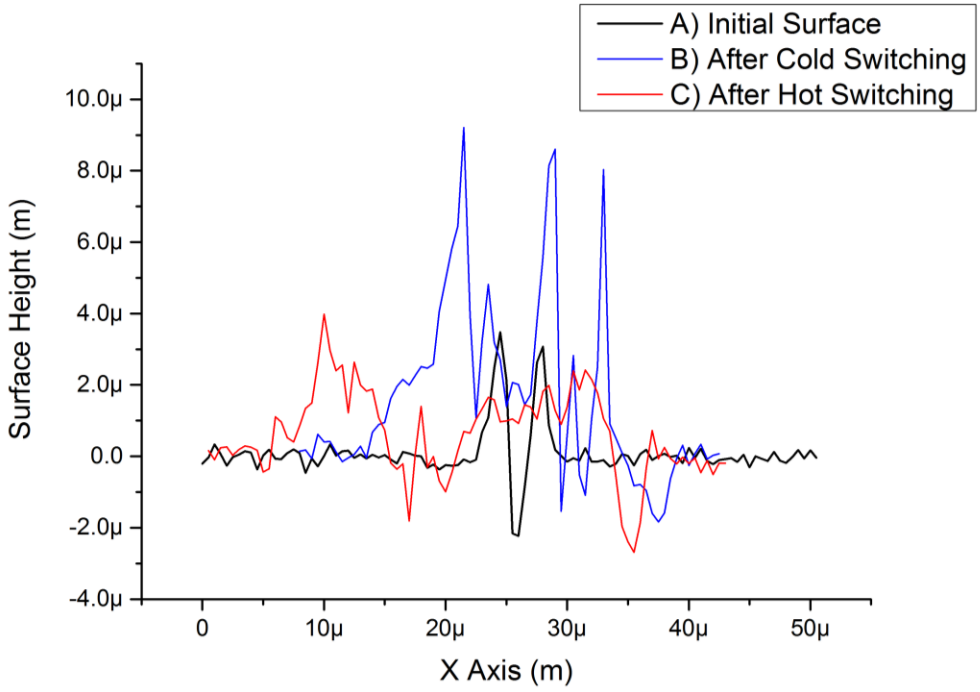

Figure 8-21 – Cross sections of the height through the same location A) before switching, B) after 10 cold switched and C) after a further 10 hot switched cycles – measured along dotted line shown in previous Figure

The wear pattern that can be seen in **Error! Reference source not found.** B is not uniform and shows, from left to right, a rise above the background on the left hand side, followed by a very rough central region and an exposed region on the right. This is reminiscent of a film that has been torn at one edge and shifted laterally. This effect was observed by Lewis et al during the MEMS scale testing of hot switching on thin film Au on Si and a micrograph of the switching sight is presented in Figure 8-22 [122]. The key difference between the measurements presented here is the use of a much greater contact force that will accelerate wear. The damage observed by Lewis resulted from hot switching, and a large region of the contact material is worn away at the contact site with the film tearing effect shown at the edges of the contact site when the main site had worn away. It is interesting to note the scale of the film shifting effect observed at the edge is in keeping with the in-situ measurement of this study (~25 µm).

Following C) the hot switching process the peaks of the transferred material are significantly reduced in height and the erosion site is observed to be partially filled in. The wear pattern observed suggests the most smoothing has occurred at the center of the switching location (i.e. the region associated with the first and highest contact force).

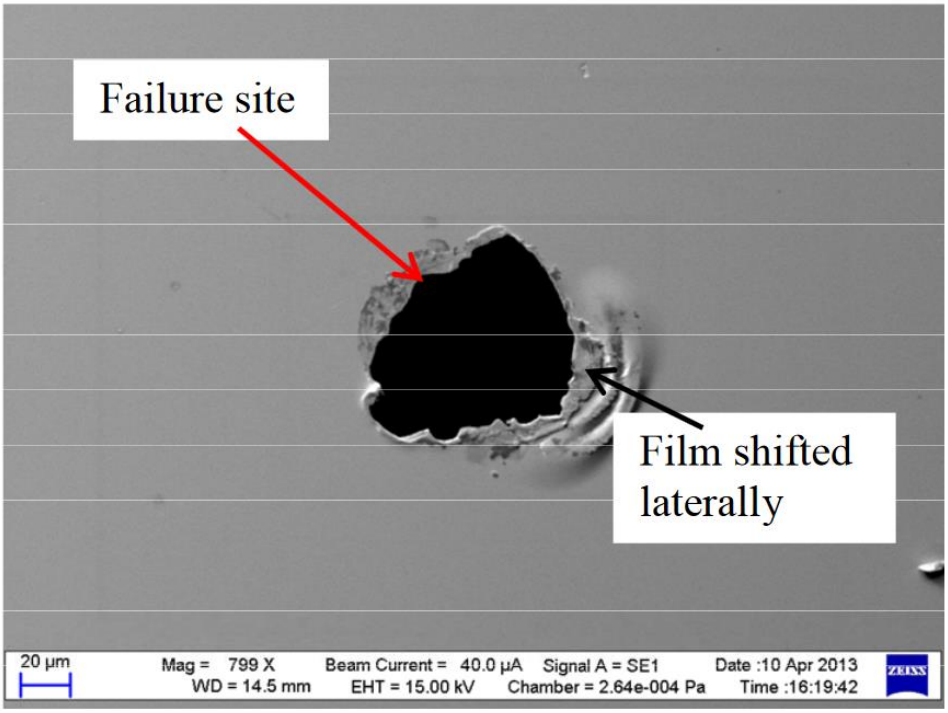

Figure 8-22 – SEM Micrograph of a thin film Au coating on silicon that has experienced 600k hot switched cycles at 50mA from Lewis et al [122]

More material appears to of been pushed from the center of the contact site to the edges, as evidenced by the difference between the surface profiles (blue and red lines in Figure 8-21). This suggests that the hot switching conditions have allowed the thin film to reflow and partially repair themselves. The act of hot switching could allow the thin film soften locally and re-adhere to the substrate. The subsequent hot switched contact opening will cause the formation of an MMB phenomena which may result in and less adhesion force between contacts immediately prior to contact separation thus reducing the tendency of the thin Au film to become detached.

8.3.3 Conclusion from preliminary testing of the ICE Apparatus

The purpose was to establish if the novel apparatus could evaluate the changes at a switching contact surface between small numbers of switching cycles. It is concluded that the apparatus clearly demonstrates this ability. To the authors knowledge the in-site measurement of a MEMS scale thin film being damaged then redistributed by cold then hot switching has not been reported and an expansion of this study presents the opportunity to present original findings.

9 Appendix 3 – Publications

9.1 Summary of Publications

Journal Papers

Bull, Thomas, and McBride, John. "In-situ contact surface characterization in a MEMS ohmic switch under low current switching." *Technologies* 6.2 (2018): 47.

Bull, Thomas, and McBride, John. "Transient Contact Opening Forces in a MEMS switch using Au/MWCNT composite." ***Technologies* 6.2 (2019): 47**.

Conference Papers

Mcbride, John and **Bull, Thomas** (2016) The influence of circuit parameters on molten metal bridge energy in a mems relay testing platform. *28th International Conference on Electric Contacts (ICEC2016), United Kingdom. 06 - 09 Jun 2016.* 6 pp .

Bull, Thomas G., John W. McBride, and Liudi Jiang. "The influence of Circuit Parameters on Molten Bridge Surface Degradation in a Au/MWCNT MEMS Switch Contact." *2018 IEEE Holm Conference on Electrical Contacts, Albuquerque, USA*. IEEE, 2018.

McBride, John W. and **Bull, Thomas G**. "The in-situ wear of a hot and cold switched Au on Au coasted MWCNT electrical contact for a MEMS switch application." *2019 IEEE Holm Conference on Electrical Contacts, Milwaukee, USA*. IEEE, 2019.

Bull TG, Jiang L and McBride JW. "Investigating micro-scale surface change of an Ohmic MEMS switch between switching cycles", *13th International Conference on Advances in Experimental Mechanics, Southampton, UK*

Bull TG, McBride JW, Jiang L (2017) An Investigation of the application of gold coated multiwalled carbon nanotubes surfaces for use in low current switching. *2017 University of Southampton Faculty of Engineering and the Environment Post Graduate Conference*.

9.2 Journal Papers

MPDI Technologies 2018

technologies

MDPI

Article

In-Situ Contact Surface Characterization in a MEMS Ohmic Switch under Low Current Switching

Thomas G Bull* and John W McBride

Mechanical Engineering, University of Southampton, UK; tb10g11@soton.ac.uk
* Correspondence: tb10g11@soton.ac.uk; Tel.: +44-23-8059-5568

Received: date; Accepted: date; Published: date

Abstract: To develop robust MEMS switching technology for low voltage DC applications (1 - 12 V) there is a requirement for the investigation of wear caused by hot switching (contact operated while carrying a current load). Previous investigation of contact wear in the ohmic MEMS switch has been limited to either the completion of the contact switching cycles, where the device is destructively opened, or by low switching rates, making lifetime testing impractical. A novel MEMS testing platform is described that is capable of both resolving microscale changes on the contact surface between switching events and sustained high frequency switch cycling, enabling practical lifetime testing. The platform is used to investigate early surface changes in a thin-film Au contact pair on a cycle-by-cycle basis. The contact is closed at forces representative of a practical MEMS contact (< 1 mN). The apparatus reveals the microscopic surface change between individual switching events. Hot switched contact wear is dominated by the molten metal bridge (MMB) phenomenon, linked to a characteristic voltage transient at contact opening and the gradual process of contact material transfer; however, during hot switching delamination phenomena are also observed, and associated with a step change in contact voltage and a greater level of surface damage.

Keywords: MEMS switching; contact wear; surface wear; DC switching; hot switching; low current switching

1. Introduction

Ohmic MEMS switching offers the advantage of smaller devices made by microfabrication manufacture to reduce cost-per-unit [1]. The metal-to-metal interface strategy offers several advantages over the capacitive switch alternative. It is capable of transmitting DC signals, while offering higher isolation (ratio of on-to-off state impedance) and lower insertion loss (power loss in the on-state) than the capacitive MEMS switch alternative [2]. However, it is the metal-to-metal interface of the ohmic MEMS switch that presents the single most common point of device failure. The contact surface generally fails through either contact adhesion (static friction, cold welding), where the surfaces cannot be separated under the available restorative force, or through wear processes, that cause excessive increase in contact resistance [3,4].

Under low contact closure force the experimentally measured contact resistance [5] is higher than predicted by the Holm model [6]. This effect is largely due to the contacts being formed from thin metallic films where the conduction mechanism is not accurately described by simple diffusion of electrons through a bulk material. The most common design of MEMS switch employs an electro-statically actuated, micro-machined cantilever with conductive surfaces formed from thin-films. Under these conditions the assumption of contact material behavior according to the bulk properties does not accurately describe the contact interface [7,8].

While improvements to analytical models have been made to account for factors such as, the scale dependence of the electron transfer mechanism [9], the additional constriction arising from

conduction path in thin-films [10], and the elastic-plastic deformation of the contact surfaces [11,12] their predictions still differ from study.

The influence of practical surface roughness ensures the true area of switch contact, and therefore conduction, is limited to points where surface asperities meet, referred to as a-spots. The a-spots have a significant influence on contact resistance and this has been shown by modelling changes in their geometry [13] and their distribution inside the apparent contact area [14], as well as the influence of multi-scale surface roughness [15]. If we consider that the surface is changed each switching cycle by the electromechanical effects of switching it is apparent that accurate modelling of the MEMS switch requires measurement of the real contact surface. The investigation of contact behavior is therefore vital in developing an understanding of switching phenomena at the MEMS contact scale.

The investigation of contact surface wear has been limited to the completion of switching. This is because access to the contact surface has required cutting open the device, or the due to the inability to precisely realign the contacts to their original positions. This is an important consideration as towards the end of switching life the contact resistance rises more rapidly, and thus increased effects of Joule heating at the final stage of switch lifetime may obscure evidence of early switching wear [16]. Reported strategies for MEMS switch investigation have included apparatus based on atomic force microscopy (AFM) , nano-indenters [17], scanning probe microscopes (SPM) and ultra-low velocity piezo-actuator closure for low cyclic rate testing [18], and high speed piezo actuated mechanisms for high speed accelerated-lifetime testing [19]. To date an apparatus capable of both in-situ measurement of the contact surface, and accelerated lifetime testing has not been reported.

When the contact is opened while carrying a signal (hot switching) the contacts experience wear caused by both the mechanical cycling of the mechanism and the influence of the electrical signal. Where circuit conditions are greater than ~1 V the melting voltage for many metals is exceeded [20] and the MMB phenomenon is observed [21], described with reference to the θ-ψ theorem [6]. Immediately prior to contact opening, the reduction in contact area results in a constriction of current flow lines, an increase in Joule heating at the a-spots and the formation of a microscale molten-metal bridge (the MMB). This phenomenon results in the transfer of molten contact material between contacts and contact wear [22]. The MMB event is described by the transient voltage waveform just before contact opening which has also linked to the contact surface roughness [23].

The contact surface conditions will vary significantly over the switching lifetime, from an initially smooth, reflective surface, to a worn surface. Techniques that are sensitive to variations in the optical and roughness properties are therefore unsuitable for contact surface measurement. Such techniques include phase shifting interferometry (PSI), coherence scanning interferometry (CSI) and digital holographic microscopy (DHM) [24].

Optical measurement of the contact surface requires a disruption to the switching process. For switching operation to continue after surface measure the contacts must be precisely realigned. 3D measurement systems that utilize point sensors such as confocal chromatic aberration or autofocus sensors already have precision motion systems to allow the measurement sample to be 'scanned'. Point based sensors are insensitive to variations in the optical properties of the surfaces under investigation and offer large inherent measurement range with an ability to measure strongly sloping surfaces (angular tolerance) and have been previously demonstrated to be highly effective in measurement of the electrical contact surface [22]. The lateral resolution of these techniques is limited by the spot size of light, but this is close to the diffraction limit imposed by the numerical aperture (NA) of the optics and wavelength of light imposed by other techniques [25].

The following describes a novel apparatus for investigating In-situ Contact Evolution (ICE) of microscale wear in the ohmic MEMS switch contact, which we define here as the ICE apparatus. The apparatus can achieve cyclic rates of up to 1250 Hz (100M cycles per day), with the capability to interrupt switching at any point to measure the contact surface with sub-micron resolution before continued switch cycling. The ICE apparatus is used here to measure and compare very early contact damage under cold and hot switched conditions in a thin-film Au contact pair at low contact force (<1 mN).

2. Materials and Methods

2.1. In-Situ Contact Evolution (ICE) Apparatus for MEMS Contact Testing

The testing apparatus allows the separation of switching contacts and the lower contact surface to be profiled using a laser displacement meter, before relocating the contacts to their original position. Figure 1 presents an overview of the main apparatus components. The apparatus consists of a granite frame that provides a fixed geometry between a lower XY motion stages and an upper Z motion stage that carries a piezoelectric actuator and displacement sensor system. The apparatus is developed from a commercial metrology system [26]. The system provides a stable metrology frame, combined with a 3D confocal laser scanning system (XYRIS 4000CL, TaiCaan Technologies Ltd, UK), which has been modified to incorporate a MEMS switching system. In the system described a piezo electric actuator is used to directly actuate the switching mechanism. The system has been designed to also allow the incorporation of a MEMS cantilever, such that the cantilever is actuated by the piezo electric actuator; however, in this study the contact is attached directly to the actuator. The switching pair (not visible in Figure 1) is arranged with the lower contact placed level and 'face-up' on the XY motion stages. The upper contact is held above the lower contact, on the tip of a piezo-electric actuator, such that raising or lowering the actuator will open or close the contact. Contact force is precisely controlled by positioning the actuator.

A 400x video microscope is used to provide visual feedback of the contact closure process.

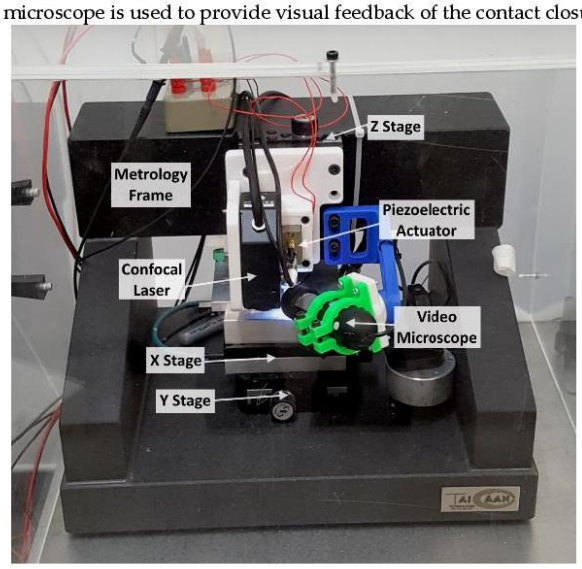

Figure 1. The In-situ Contact Evolution (ICE) apparatus, based on a TaiCaan Technologies Ltd, XYRIS 4000CL. The lower contact is carried on the XY motion system, while the upper contact is carried on the lower tip (obscured by video microscope) of the piezoelectric actuator.

During switching (Figure 2a), the actuator (ThorLabs, USA) moves the upper contact to open and close the contact. The actuator is capable of high speed cyclic operation (>1.25 kHz). In this study the switching cycling is interrupted after each switching operation to allow contact surface measurement.

The 3D profile of the contact surface may be measured at any point during the investigation (Figure 2b). This is performed by opening the contacts, then using the XY motion system to move the lower contact beneath a confocal laser displacement meter. The system allows placement the contacts in a reference XYZ coordinate system to +/- 50 nm repeatability (XYZ positional repeatability). The

laser displacement meter can resolve spatial (XY) detail at the sub-micron level on the lower contact surface with a height (Z) resolution of 10 nm. Key system specifications are summarized in Table 1.

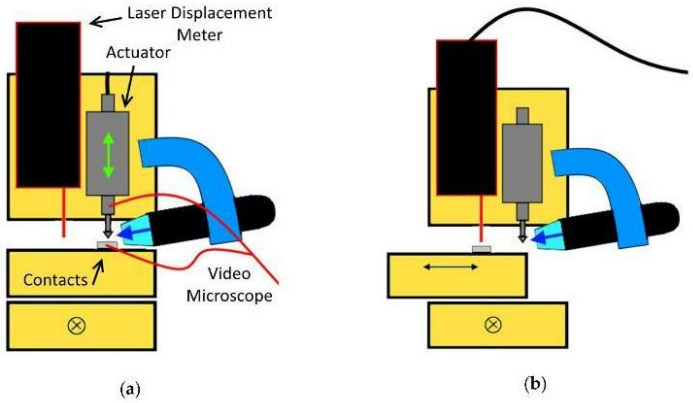

Figure 2. Schematic of In-site Surface Evolution (ICE) testing apparatus during a) Switching Mode, where the piezo-electric actuator opens and closes the switch and b) Surface measurement mode

Table 1. Summary of key specifications of the ICE apparatus

Measurement Principle	Vertical (Z) Resolution	Vertical Range	XY Range	XY On-Axis Repeatability	Sensor Light Source	Sensor Spatial (XY) Resolution
Point Autofocus	10 nm	0.6 mm	25 mm x 25 mm	±50 nm	655 nm (Red Laser)	<1 µm

The apparatus is mounted in an temperature controlled metrology laboratory within a chamber to further damp thermal effects and air transmitted vibration. Temperature and humidity is continuously monitored and maintained at better than 22.0 +/- 0.2 °C and 40 +/- 4 %RH over a 24-hour period. Ground vibration isolation is by a passively damped optical-grade work surface supported by four laminar-flow air dampers (Newport Corporation, USA).

Instrumentation for data capture includes a high-speed oscilloscope (Tektronix, USA) to characterize the transient voltage waveform across the contact at the point of contact opening (related to the formation of the MMB), and a four terminal micro-ohmmeter (Keithley, USA) for contact resistance measurement under dry test conditions (< 20 mV).

System measurement performance is characterized against two traceable standards. The combined noise floor of the sensor and motion system is characterized by the measurement of an optically flat target (Edmunds Industrial Optics, USA) over the full 25 mm x 25 mm measurement area at 125 µm intervals (40,401 evaluated points). The absolute arithmetic average (equivalent to the unfiltered S_a roughness) is then recorded. Step height accuracy is characterized by measurement of a 2.660 µm step height (AMETEK Taylor Hobson, UK) at 15 equally spaced intervals. The mean and standard deviation of these values is then recorded to respectively characterize the step height accuracy and the step height repeatability. The obtained values are presented in Table 2.

Table 2. Summary of key system performance on traceable standards

Noise Floor (Optically flat standard) S_a	Step Height Accuracy (2.660 µm standard) Mean	Step Height Repeatability (2.660 µm standard) Standard deviation
24.2 nm	2.660 µm	32 nm

2.2. *Contact Manufacture*

The test contacts are: 1) an hemispherical upper contact, manufactured from a 2 mm diameter precision ground stainless-steel ball, coated with a 20 nm Cr, then 500 nm Au and 2) a planar lower contact, of a SiO_2 on Si substrate (IDB Technologies, UK), coated with 20 nm Cr and 500 nm Au. The contact substrates are prepared by solvent cleaning (20 minutes ultrasound in acetone, followed by 20 minutes in isopropanol), and drying (blown dry with nitrogen then placed on a hot plate at 65 °C for 15 minutes). They are then coated by a plasma vapor deposited 20 nm Cr adhesion promotor layer, followed by 500 nm Au conductor layer (Kurt J Lesker, USA). The Au film thickness is verified by exposing a pre-masked section on a test piece which is then measured for the film step height using the XYRIS 4000CL.

2.3. *Test Circuit*

The circuit configurations for switching and contact resistance measurement are shown in Figure 3. The contact resistance is measured by the 4-terminal method using a micro-ohmmeter (Keithley, USA) Figure 3a. The switching circuit is a simple series loop incorporating a 4V battery with current controlled by a resistive load – Figure 3b.

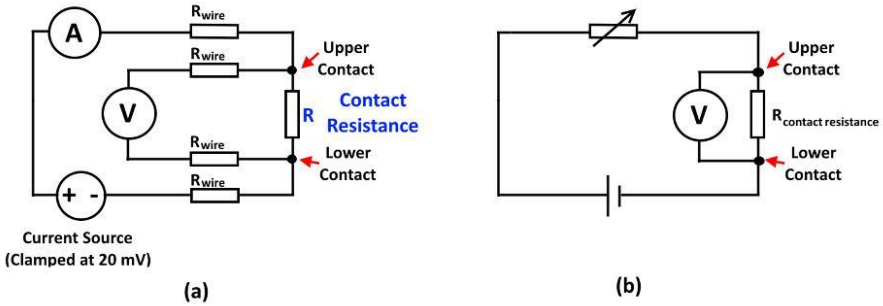

Figure 3. a) Contact Resistance Measurement Circuit and b) Contact Load Circuit

2.4. *Contact Force Determination*

The applied contact force is controlled by bringing the contacts to the point of just meeting, and then demanding further extension of the actuator. As the actuator continues to be extended the contact closure force increases. The ICE apparatus as presented does not include a transducer to directly measure force. To determine the contact force a second apparatus is used [27], to calibrate the relationship between the initial applied force and the contact resistance for the contact samples. In the ICE apparatus a new undamaged surface contact resistance is thus linked to the calibrated force. The actuator displacement to contact force relationship is derived from the contact pair resistance/force curve measured by 4 terminal micro-ohmmeter (Keithley, USA) and piezo force sensor (Kisler AG, Switzerland) in the Holm crossed bar configuration with apparatus previously described in [27].

2.5. Switching Test Procedure

The initial contact closure position for the test is obtained by slowly closing the contacts until they are in close proximity (shown in Figure 4). The contacts are then pushed together by the actuator until the contact resistance is reached that corresponds to the normal contact force required for the test. The actuator position is repeated for subsequent cycles. The contact is held stationary for 30 seconds to allow the contact interface to settle before contact resistance measurement is recorded. The load circuit is then connected, and current is allowed to flow for 10 seconds before contact opening to a separation of 0.1 mm is demanded at a maximum acceleration of 100 mm/s^2. The load circuit is then disconnected, and the lower contact measured by the laser displacement meter. After contact surface measurement the contacts are repositioned to the original coordinates and the process repeated.

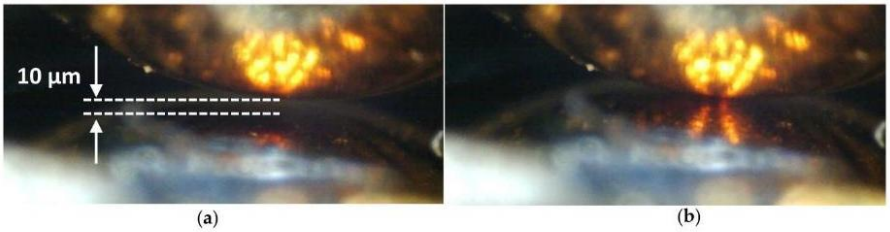

(a) (b)

Figure 4. The contact pair shown through the 400x integrated video microscope a) with a 10 µm separation between contacts and b) in contact

2.6. Surface Measurement Analysis

The lower contact surface measurements are evaluated for surface roughness and volume wear (Boddies 3D v2.18, TaiCaan Technologies, UK). The lower contact surface wear is measured under two conditions and these are summarized in Table 3.

Table 3. Circuit and Force Conditions for each switching sequence

Test Condition	Circuit Voltage (V)	Circuit Current (mA)	Contact Force (µN)	Number of Switching Cycles
Cold Switched	0[1]	0[1]	100	10
Hot Switched 20mA	4.1	20	500	20

[1]During the cold switched sequence the battery is removed from the circuit, but the contact resistance measurement applies a 20 mV potential during the contact closing process and for a further 30 seconds after the contact closure

3. Results

3.1. Contact Force and Demanded Actuator Displacement vs Contact Resistance

Figure 4 shows the contact resistance to contact force and demanded contact displacement and contact force. The new apparatus allowed the contacts to be positioned to achieve a stable contact resistance of 0.6012 Ω. The lowest stable contact force that could be measured with the force testing apparatus was at 200 µN at a contact resistance of 0.3808 Ω. The inset figure shows the relationship between the extension demanded from the actuator and the contact force.

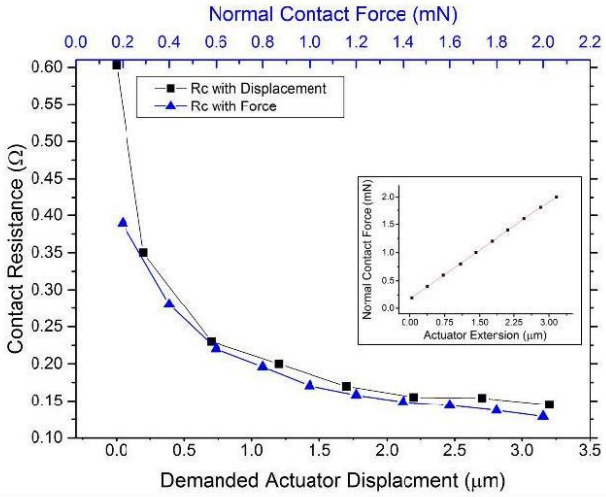

Figure 5. Contact Resistance to Contact Force (blue triangles), and Contact Resistance to Contact Demanded Displacement (black squares) with Contact Force to Actuator Displacement (inset)

Over the range of measured force to contact resistance (200 to 2000 μN) there is good agreement between the displacement and force curves. This provides a range of contact resistance between ~ 0.15 and 0.60 Ω where the relationship between actuator displacement and contact force is linear as shown in Figure 5. This means contact resistance can reasonably be used to determine the initial contact force.

3.2. Cold Switched Contact Sequence

The evolution of the cold switched contact surface over 10 cycles at ~ 100 μN is presented in Figure 6. The surface height is represented by a colour scale set to the same height range (+4.0 to -2.0 μm) for each panel in Figure 6 to provide a fixed reference for visual inspection. The contact surface is measured before switching (0 cycles) over an area of 0.7 mm by 0.7 mm, but a smaller and more detailed measurement of 0.15 mm by 0.15 mm is taken of the precise contact location following the first switch cycle. The number of switching cycles the surface has experienced in shown in the lower left corner i.e. 0 is before any switching.

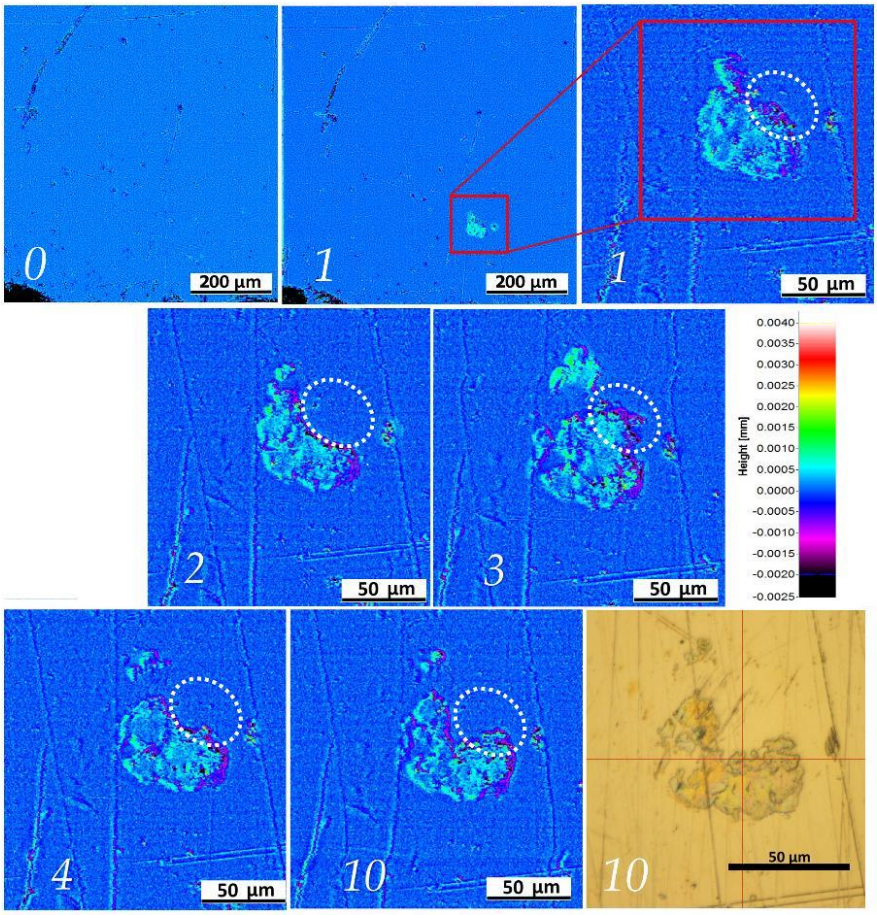

Figure 6. A sequence of measurements of the lower contact during a cold switching sequence at 100 µN normal contact force. At 0 (before switching), 1, 2, 3, 4 and 10 cycles. The white dotted region shows an unstable region of deposition.

Figure 6 shows a pattern raised above the nominal surface that is approximately 50 µm in diameter appears after a single switching operation (from 0 to 1 cycles). The pattern presents as a roughened, raised region approximately 500 nm above the nominal contact surface, with an irregular circular shape. Following the completion of the switching sequence the contact region is imaged with true colour optical video microscopy. The shape of the site is well correlated between the micrograph image and the final measurement of the wear site with the micrograph showing the wear region to be gold colored (cycle 10).

The progression of the contact resistance and lower surface roughness is shown against the number of switching cycles in Figure 7 with a subplot of contact resistance against surface roughness.

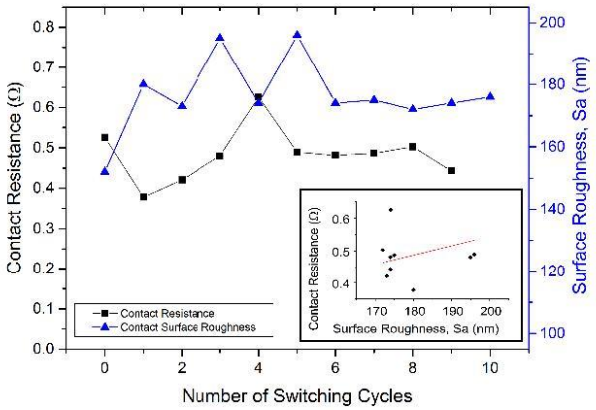

Figure 7. The evolution of contact resistance and surface roughness over 10 cold switching cycles

The contact resistance and surface roughness are shown to be initially unstable between cycles before stabilizing after five cycles. The inset figure shows a trend for the contact resistance to increase with the surface roughness.

The volume of material above the nominal surface of the lower contact before switching is evaluated from the surface measurements on a cycle-by-cycle basis and presented in Figure 8 [28]. The datum of zero volume transfer (0) is defined as the volume measured above the plane of best fit to the unswitched contact surface. A positive volume indicates there has been net surface deposition upon the contact surface. It is apparent from Figure 8 that after the first cycle 0.38 μm^3 of material have been deposited on the surface, after the second cycle the deposited volume has reduced to 0.22 μm^3 but following the third cycle increases to 0.43 μm^3. Figure 6 shows that the top right region of the deposit (enclosed by a dashed white oval) appears to be transferred back and forth between contacts. Figure 8 shows that the volume transferred back and forth each cycle is reducing over the following 10 cycles with the smallest volume of material transfer occurring between the final switching cycles. After 10 cycles there is a net positive volume deposited of ~ 0.22 μm^3.

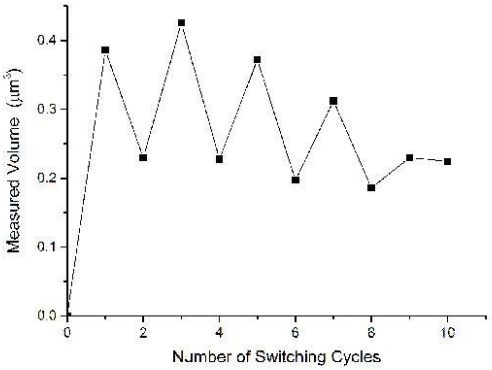

Figure 8. The evolution of material deposited on the lower contact surface over 10 cold switching cycles

3.3. 20 mA 4V Hot Switched Contact Sequence

The evolution of a hot switched contact surface over 20 cycles at ~500 μN is presented in Figure 9. The measurement area is 150 μm by 150 μm. The surface height is represented by a colour scale set

to the same height range for each panel in Figure 9 (+1.0 to -0.5 µm). It should be noted that the range of this scale is one quarter of that used in Figure 6 to better enhance the subtle surface features in this sequence. A white dashed ring is used to indicate the wear region, with the features of note labelled AB and CD. A cross section of the surface along the red dotted line is presented after 1 and 20 cycles.

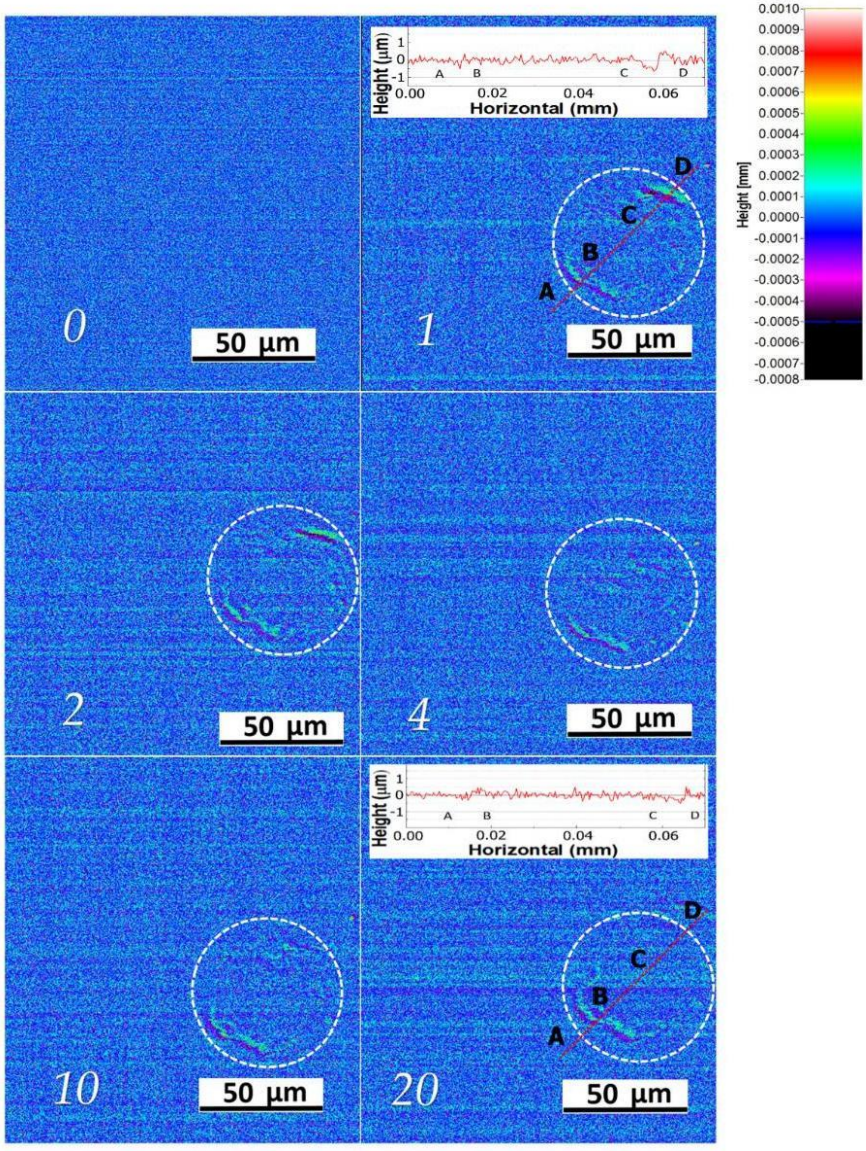

Figure 9. A sequence of measurements of the lower contact during a hot 20 mA 4 VDC switching sequence at 500 µN normal contact force. 0.15 mm x 0.15 mm region after 0, 1, 2, 4 ,10 and 20 cycles

Figure 9 shows the contact surface at 0 cycles (before switching) and after 1, 2, 4, 10 and 20 cycles. The wear pattern presents as a toroidal region approximately 45 µm in outer diameter, highlighted

by a dashed circular line, with the most significant change in surface height occurring after 1 and 2 cycles in the lower left (AB), and upper right (CD) of this region. The surface colour map shows the lowest area to be ~500 nm below the nominal surface (purple areas) with the highest area immediately alongside and ~500 nm above the nominal surface (green areas). Features AB and CD appear to be tears in the Au film, with the film lifting off the Si substrate at the edges of the tear.

After four switched cycles the height and width of the tears appear to both decrease in magnitude and begin to smooth, particularly in the CD region of the wear pattern where the surface height stabilizes. This smoothing trend continues until the completion of switching after 20 cycles.

The evolution of the lower contact surface roughness and the contact resistance is presented in Figure 10 along with a subplot showing the relationship between contact resistance and surface roughness. Both roughness and resistance show an initial rise over the first switching cycles before settling between cycles 5 to 20. After cycle 5 there is a trend of the surface roughness decreasing while contact resistance is broadly stable.

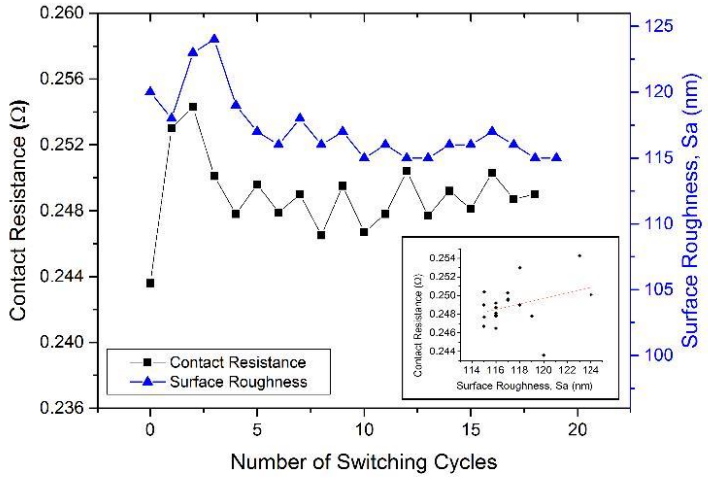

Figure 10. The evolution of contact resistance and surface roughness over 20 hot switched 4V 20 mA switching cycles

The voltage waveform at the point of contact opening is captured at each cycle of switching. Two types of waveform are observed with examples shown in Figure 11. The first is a less stable and unrepeatable event where the contact potential is observed to vary between ~0.4 and 0.9 V before finally rising abruptly to the full open circuit potential – termed "MMB" (molten metal bridge) type. The MMB type occurs as the gradual reduction in the contact area constricts current flow leading to increased Joule heating and the local softening, melting and boiling of the contact surface at the contacting asperities. The second type of waveform observed is an abrupt and instantaneous rise in contact potential to the full open circuit voltage. We term this waveform here a "delamination" type.

Figure 11 shows the 1st, 16th and 20th opening waveforms as examples of the types of waveform. The 1st cycle (black) shows the abrupt "delamination" waveform suggests that as a MMB event is not observed the contact area has not decreased gradually, but rather has separated suddenly.

The longer waveforms (16th – red and 20th - blue) are typical of the MMB phenomenon, where the gradual reduction in contact area causes the microscale melting and boiling of the contact surface and the contact opens as the molten bridge ruptures by boiling and cannot reform. The reported voltages for the melting and boiling of Au (~0.38 and ~0.88 V respectively) are plotted for comparison. [20,29].

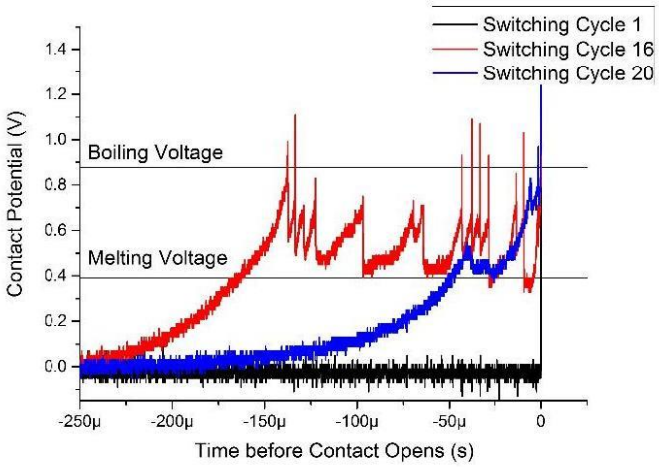

Figure 11. Contact Potential immediately before contact opening showing MMB and delamination type openings

Each switching waveform is classified for the type of opening as either a "delamination" or "MMB" type, with 4 events classified as "delamination" type and 16 as "MMB". The waveform type is then compared to the magnitude of surface roughness change before and after the opening event.

The 1st, 2nd, 4th and 14th opening event are of the "delamination" type. Figure 9 shows the surface of the contact after the 1st, 2nd and 4th cycles suggest the Au film is tearing and lifting from the substrate at AB and CD. It was found that while an MMB event was associated with a change in surface roughness of 1.06 nm, a delamination event had a much greater average change of 3.25 nm.

4. Discussion

4.1. Cold Switched Contact Sequence

The contact resistance, surface roughness (Figure 7), volume transfer (Figure 8) and surface imagery (Figure 6) all suggest that the contact pair experienced a delamination of the Au film from the upper hemispherical contact during the first switching cycle. Some of this material was then transferred back and forth between the contacts with the volume of transfer decreasing with continued cycles, shown in Figure 8. The initial phase of switching is well known to demonstrate a gradual decrease in contact resistance as the surfaces begin to conform to one another and 'bed in'. Laurvick et al also observe the initial phase of switching with Au-Au MEMS contacts coincides with the greatest variation in contact resistance during the switching lifetime; however they also noted that where the decrease in contact resistance was not smooth and gradual, it correlated with the premature failure of the device [4]. The observed delamination presents a significant defect in the contact surface that can reasonably be expected to lead to premature contact failure. The observation in this study of a delamination effect linked to unstable contact resistance suggests a mechanism for the premature failures observed in [4]. The trend observed between increasing roughness and contact resistance (Figure 7) supports this. As the surface volume change stabilizes the contact resistance is also stabilized, but at a higher level than the 0.45 Ω measured at the initial closure on the undamaged interface, suggestive the change in surface texture is at least partially responsible. As the material transfer is reduced, the contact interface will evidently be more stable, and therefore the contact resistance also stabilizes. This suggests the Au film is has at least partially re-adhered to the ball. Jensen et al observed the adhesive forces between Au-Au MEMS switches were dependent on both adhesive forces between surfaces in the apparent contact area but of also by the metal-metal adhesion

in the real contact area [30]. With the contact resistance primarily dependent on the real contact area any change in adhesion between contacts cannot be inferred from the contact resistance alone. It is noted that the observed detachment of the Au film from the substrate will allow significantly increased rates of strain in the film and thus an increased rate of strain-hardening. This may be a contributory factory to the increased contact resistance as a harder contact material evidently provides a smaller contact area for a given force.

Adhesion in Au contacts is a recognized problem and this presents a significant failure mechanism for the MEMS switch, particularly when the poor adhesion of Au to Si/SiO substrates is considered. In this study an adhesion promotor (Cr) was used, previously demonstrated by Lewis et al to enhance switching lifetimes in Au contacts [31]. However, while this study was carried out under controlled temperature and humidity, the test environment was not under hermetic seal or inert gas, and the presence of water vapor and hydrocarbon contamination is expected. These are both recognized as factors in influencing self-adhesion of Au, an effect would be reduced in a practical Au thin-film device by sealing under an inert atmosphere [30,32]. However, the intention of future work is investigating a novel contact material, capable of operating without hermetic encapsulation and offering the potential for reducing the potential for complications that arise from this process [33]. In this context this study provides a useful bench mark for Au film behavior in an ambient atmospheric environment for future investigation.

4.2. Hot Switched Contact Sequence 20mA

A wear scar appears after a single switching event that is described by a toroid where the thin-film surface shows partial tearing and wrinkling at opposing sides (Figure 9, cycles 1 and 2). The height of the features AB and CD shown in Figure 9 are ~500 nm. As this is the deposited Au film thickness it suggests that the film has torn, delaminated from the substrate and shifted laterally to expose the Si wafer. The toroidal wear shape is significant as it has been previously been shown analytically and empirically that the maximum current density occurs preferentially at the edges of the contact region [6,34]. The visual representation of the surface height in Figure 9 show the greatest change occurring at the 1st, 2nd and 4th cycles at the AB and CD features. The voltage waveform observed at these cycles was not representative of a molten metal bridge event and suggests the contact area has not decreased gradually, but suddenly. The change in surface roughness associated with this "delamination" type waveform is over three times higher than observed for the molten metal bridge type.

Cross sections comparing the AB and CD features in Figure 9 after the 1st and 20th cycle show they have reduced in scale after 20 cycles. The trend of decreasing surface roughness is also seen in Figure 10 from the 5rd to 20th switching cycle onwards. The 14th cycle shows a small increase in roughness and this is the final "delamination" type voltage waveform. It appears that the feature at CD is a tear in the Au film that is gradually closed as switching continues. During the initial phase of switching it is apparent that the local contact pressure in the real area of contact will be higher as the most prominent surface asperities in contact undergo plastic deformation and additional surrounding asperities begin to distribute the contact load more elastically as the contacts "bed in" [4,6]. It is during this initial phase where the higher local pressures and plastic deformation are most likely to result in cold welding. The observation of the delamination waveforms occurring in early switch operations (1st, 2nd and 4th) suggests a correlation with the period of highest plastic deformation. Recent study has shown that hot switched MEMS contact welding is observed regularly at conditions of 10 VDC and 80 mA, and sporadically at 10 VDC and 60mA; however the study did not specify the contact closure force, and the reported contact resistance suggests it was higher than this study [35].

As the switching sequence continues, it is apparent from Figure 9 that the tear in the thin-film Au observed at the CD feature of the contact region is visible reduced and appears to be smoothed out. The smoothing effect is confirmed by the progression of roughness from the 5th switching cycle (Figure 10). The surface roughness and contact resistance decrease, with all but one of the last 15 opening waveforms characterized by MMB type events. The observations of Laurvick et al, that over

long term switching the irregular progression of contact resistance corelated to premature device failure [4] is noted, as in this study the largest changes in contact resistance correlated with the largest changes in surface texture and the appearance of apparent tears in the Au film.

These observations suggest the delamination events are associated with a higher level of damage to the Au film, while the MMB type events correlate to decreased damage, film smoothing and perhaps even repair of the film.

5. Conclusions

The purpose of this investigation was to describe, outline and test the capabilities of a novel MEMS apparatus for the measurement of In-situ Contact Evolution. The ICE apparatus is demonstrated to resolve detail of microscopic wear occurring in-situ at the contact interface under low force conditions. The initial results show that the apparatus is capable of detection of wear in both cold (dry switching) and hot switching from the first cycling of the contacts.

During the first 20 cycles of a hot switched (20 mA, 4V) Au contact at MEMS scale closure force, it is shown that there are opening events with no apparent MMB. The opening event is characterized by a step change in the voltage across the device (sampled at 25 MHz) and linked to a quantifiably greater surface roughness change than the MMB event. This paper defines these as delamination events (DE). The ICE apparatus shows for the first time that these events result from the cold welding of the Au layers, and the subsequent tearing of the surface (delamination). It is interesting to note that the tearing of the surface film seems to prevent a MMB.

Acknowledgments: The authors would like to thank Dr. Kevin Cross from TaiCaan Technologies Ltd. for his assistance in the development of the apparatus control, and the EPSRC for their support in this work which is funded in part by grant EP/M508147/1.

Conflicts of Interest: The authors declare no conflict of interest

References

1. Rebeiz, G.M. *Rf mems: Theory, design, and technology*. John Wiley & Sons: 2004.
2. Iannacci, J. Rf-mems: An enabling technology for modern wireless systems bearing a market potential still not fully displayed. *Microsystem Technologies* **2015**, *21*, 2039-2052.
3. Toler, B.F.; Coutu, R.A.; McBride, J.W. A review of micro-contact physics for microelectromechanical systems (mems) metal contact switches. *J Micromech Microeng* **2013**, *23*.
4. Laurvick, T.V.; Coutu, R.A. Improving gold/gold microcontact performance and reliability under low-frequency ac through circuit loading. *IEEE Transactions on Components, Packaging and Manufacturing Technology* **2017**, *7*, 345-353.
5. Yunus, E.M.; McBride, J.W.; Spearing, S.M. The relationship between contact resistance and contact force on au-coated carbon nanotube surfaces under low force conditions. *Ieee T Compon Pack T* **2009**, *32*, 650-657.
6. Holm, R. *Electric contacts: Theory and application*. Springer Science & Business Media: 1958.
7. Hyman, D.; Mehregany, M. In *Contact physics of gold microcontacts for mems switches*, Proceedings of the Forty-Fourth IEEE Holm Conference on Electrical Contacts, 1998; IEEE: pp 133-140.
8. Gouldstone, A.; Koh, H.-J.; Zeng, K.-Y.; Giannakopoulos, A.; Suresh, S. Discrete and continuous deformation during nanoindentation of thin films. *Acta Mater* **2000**, *48*, 2277-2295.
9. Jensen, B.D.; Huang, K.; Chow, L.L.W.; Kurabayashi, K. Low-force contact heating and softening using micromechanical switches in diffusive-ballistic electron-transport transition. *Applied Physics Letters* **2005**, *86*.
10. Zhang, P.; Lau, Y.; Timsit, R.S. On the spreading resistance of thin-film contacts. *Ieee T Electron Dev* **2012**, *59*, 1936-1940.

11. Coutu, R.A.; McBride, J.W.; Starman, L.A. Improved micro-contact resistance model that considers material deformation, electron transport and thin film characteristics. In *Proceedings of the 55th IEEE Holm Conference on Electrical Contacts*, IEEE: Vancouver, Canada, 2009.
12. Toler, B.F.; Coutu Jr, R.A.; McBride, J.W. A review of micro-contact physics for microelectromechanical systems (mems) metal contact switches. *J Micromech Microeng* **2013**, *23*, 103001.
13. Malucci, R.D. In *The impact on current density and constriction resistance from bridge structures in real contacts*, Electrical Contacts, 2017 IEEE Holm Conference on, 2017; IEEE: pp 59-62.
14. Fukuyama, Y.; Sakamoto, N.; Kaneko, N.-H.; Kondo, T.; Toyoizumi, J.; Yudate, T. In *The effect of the distribution of α-spots in the peripheral part of an apparent contact point on constriction resistance*, Electrical Contacts, 2017 IEEE Holm Conference on, 2017; IEEE: pp 302-305.
15. Liu, H.; McBride, J.W. In *The influence of multiscale surface roughness on contact mechanics using finite element modeling: Applied to a au-coated cnt composite electrical contact surface*, Electrical Contacts, 2017 IEEE Holm Conference on, 2017; IEEE: pp 229-235.
16. Lewis, A.P.; McBride, J.W.; Jiang, L. Evolution of voltage transients during the switching of a mems relay with au/mwcnt contacts. *Components, Packaging and Manufacturing Technology, IEEE Transactions on* **2015**, *5*, 1747-1754.
17. Mcbride, J.; Yunas, E.; Spearing, S. Gold coated carbon nanotube surfaces as low force electrical contacts for mems devices: Part 1. In *The 59th IEEE Holm Conference on Electrical Contacts*, Newport, USA, 2009.
18. Ren, W. Unstable electrical contact behaviour at nanoscale for mems switch. In *28th International Conference on Electric Contacts*, Heriott Watt University: Edinburgh, UK, 2016; pp 213-218.
19. Stilson, C.; Coutu, R. In *Contact resistance evolution of highly cycled, lightly loaded micro-contacts*, SPIE MOEMS-MEMS 2014, San Francisco, USA, 2014; International Society for Optics and Photonics: San Francisco, USA.
20. Doduco. *Databook of electrical contacts*. Duduco GmbH: 2012.
21. Koren, P.; Nahemow, M.; Slade, P. The molten metal bridge stage of opening electrical contacts. *IEEE Transactions on Parts, Hybrids, and Packaging* **1975**, *11*, 4-10.
22. McBride, J. The wear processes of gold coated multi-walled carbon nanotube surfaces used as electrical contacts for micro-electro-mechanical switching. *Nanoscience and Nanotechnology Letters* **2010**, 2, 357-361.
23. Bull, T.; Mcbride, J. The influence of circuit parameters on molten metal bridge energy in a mems relay testing platform. *Proceedings of 2016 Twenty Eighth International Conference on Electrical Contacts* **2016**.
24. Leach, R.E. *Optical measurement of surface topography*. Springer: Berlin, 2011.
25. Nouira, H.; El-Hayek, N.; Yuan, X.; Anwer, N.; Salgado, J. In *Metrological characterization of optical confocal sensors measurements (20 and 350 travel ranges)*, Journal of Physics: Conference Series, 2014; IOP Publishing: p 012015.
26. Taicaan technologies xyris 4000. http://www.taicaan.com/xyris-4000/ (29th March 2018),
27. McBride, J.; Jiang, L.; Chianrabutra, C. In *Fine transfer in electrical switching contacts using gold coated carbon-nanotubes*, 26th International Conference on Electrical Contacts (ICEC 2012),, Beijing, China, 14-17 May 2012, 2012; IET: Beijing, China, pp 353-358.
28. Mcbride, J.W. A review of volumetric erosion studies in low voltage electrical contacts. *Ieice T Electron* **2003**, *86*, 908-914.
29. Slade, P.G. *Electrical contacts: Principles and applications, second edition*. CRC Press: 2014.
30. Jensen, B.D.; Huang, K.W.; Chow, L.L.W.; Kurabayashi, K. Adhesion effects on contact opening dynamics in micromachined switches. *J Appl Phys* **2005**, *97*.

472 31. Lewis, A.; Down, M.; Chianrabutra, C.; Jiang, L.; Spearing, S.; McBride, J. In *The effect on switching lifetime*
473 *of chromium adhesion layers in gold-coated electrical contacts under cold and hot switching conditions*, Holm
474 Conference on Electrical Contacts (HOLM), 2013 IEEE 59th, 2013; IEEE: pp 1-7.
475 32. Cognard, J. Adhesion to gold: A review. *Gold Bulletin* **1984**, *17*, 131-139.
476 33. Spearing, S.M. Materials issues in microelectromechanical systems (mems). *Acta Mater* **2000**, *48*, 179-
477 196.
478 34. Sawada, S.; Tsukiji, S.; Shimada, S.; Tamai, T.; Hattori, Y. In *Current density analysis of thin film effect in*
479 *contact area on led wafer*, 58th Holm Conference on Electrical Contacts, Portland, USA, 2012; IEEE:
480 Portland, USA, pp 1-6.
481 35. Lisec, T.; Stoppel, F.; Kaden, D.; Heinrich, F.; Neumann, A.; Wagner, B. In *Mems switch with prolonged*
482 *lifetime under hot switching conditions based on gold as contact material*, Solid-State Sensors, Actuators and
483 Microsystems (TRANSDUCERS), 2017 19th International Conference on, 2017; IEEE: pp 2043-2046.

MPDI Technologies 2019

technologies

MDPI

Article

Transients Contact Opening Forces in a MEMS switch using Au/MWCNT composite

Thomas G Bull* and John W McBride

Mechanical Engineering, University of Southampton, UK; tb10g11@soton.ac.uk
* Correspondence: tb10g11@soton.ac.uk; Tel.: +44-23-8059-5568

Received: date; Accepted: date; Published: date

Abstract: Most failures in micro electromechanical systems (MEMS) switches can be attributed to the degradation of contact surfaces and sticking contacts. A wear tolerant Au composite contact material, with conductive properties close to pure Au has been engineered to provide wear resistance and enhanced switching lifetime. Switching lifetimes of billions of cycles have been demonstrated, representing greatly increased performance over thin film Au. Below the arcing threshold (~12 V) the wear mechanism has been shown to be a combination of fine transfer of contact material by the molten metal bridge (MMB) phenomenon and a delamination of the Au. In this study the composite contact is hot switched at low current DC conditions (4 V DC and 20 mA) while the contact force is measured at the micro Newton scale in nanosecond resolution. The characteristic voltage waveform associated with the MMB is observed with forces detected as the contacts softens, melts, and separate. The presence of delamination events (DE) are also observed, where the contact opens abruptly with no MMB phenomenon apparent. The DE contact openings are associated with a transient peak force of 21.6 ± 2.3 μN while the MMB are linked to a lower peak force of 18.1 ± 2.5 μN.

Keywords: MEMS switching; molten metal bridge; surface wear; DC switching; hot switching; low current switching; contact sticking; contact forces

1. Introduction

The use of a metal-to-metal contact interface in a microelectromechanical system (MEMS) switch offers the advantages of a low contact resistance in the on-state while the air gap between contacts provides a high impedance in the off-state. These characteristics provide a low signal power loss with a RF supply (insertion loss) and a large ratio between the on and off state impedance (isolation). This presents improved performance over semiconductor alternatives such as field effect transistors (FET) and P-I-N diodes [1].

The MEMS switch contact is typically a thin film of metal on a silicon substrate, with the moving contact formed by etching away material to form a beam or cantilever. Precious metals such as gold or platinum are often used for their high conductivity and resistance to oxide formation [2]. While many strategies have been used to provide the actuation force for the switch by far the most common is electrostatic actuation. This uses a bias electrode to attract the cantilever to close contacts. Removing the bias voltage allows the residual spring force in the beam or cantilever to open the contacts. The mechanism is attractive as the bias electrode draws no current once charged. It is relatively fast acting and convenient to manufacture using micromachining techniques. The main disadvantages of the electrostatic actuation method are the large bias voltage required and low contact closure force. The cantilever design must be optimised for the opposing requirements of a high closure force to ensure a good contact interface and a large restorative spring force to reliably open the contact.

The main obstacle to a high reliability Ohmic MEMS switch is the switching surface, which has two common factors leading to device failure. The first is where the contacts become stuck together through processes such as cold welding, thermal welding or the accumulation of adhesive wear

polymers. The second is through damage and wear to the contact surface leading to an excessive increase in contact resistance [3,4]. Typically the metallic films are 10's or 100's of nm in thickness with very limited tolerance to wear. Mechanical effects of switching such as work hardening and cold-welding cause wear during switching with no electrical signal (cold switching). Operating the contacts while they carry an electrical signal (hot switching) of more than ~ 1 V and a several mA's causes an additional mechanism for wear driven by Joule heating and described by a process of fine transfer [5]. At contact opening as the contact force reduces the contact area shrinks and the current flow lines are constricted. The current constriction causes Joule heating with even a small potential drop across the contact sufficient to cause the softening, melting and boiling of the contact material at the final point of contact [6-9]. As the contacts separate a molten metal bridge (MMB) is formed between the contacts, that ruptures as it boils, interrupting the circuit. The softening, melting and boiling voltages for Au are respectively ~ 0.08, 0.43 and 0.88 V [7,10]. The MMB wear is described by a fine transfer process linked to the gradual and cumulative scattering of the melted contact material that wears away the contact over many millions of cycles [5]. If the contact area does not decrease smoothly and gradually there may be a step change in contact area where there is insufficient time for interface to reach thermal equilibrium. This represents a limiting case for the formation of a MMB [7,11]. Through in-situ surface measurement of a thin film Au contacts between hot switching cycles the contacts were observed to sometimes open without showing the characteristic MMB waveform. These events were linked to sections of the contact surface being torn away from the surface [12]. These events are therefore termed *Delamination Events* (DE) [13]. The DE can be characterized with an immediate transition from the closed contact potential to the open contact potential.

Figure 1 shows waveforms typical of the MMB (red graph) as the contact material melts, draws out a MMB that boils and ruptures before the contact opens, and the DE (black graph) as the contacts open instantaneously [9].

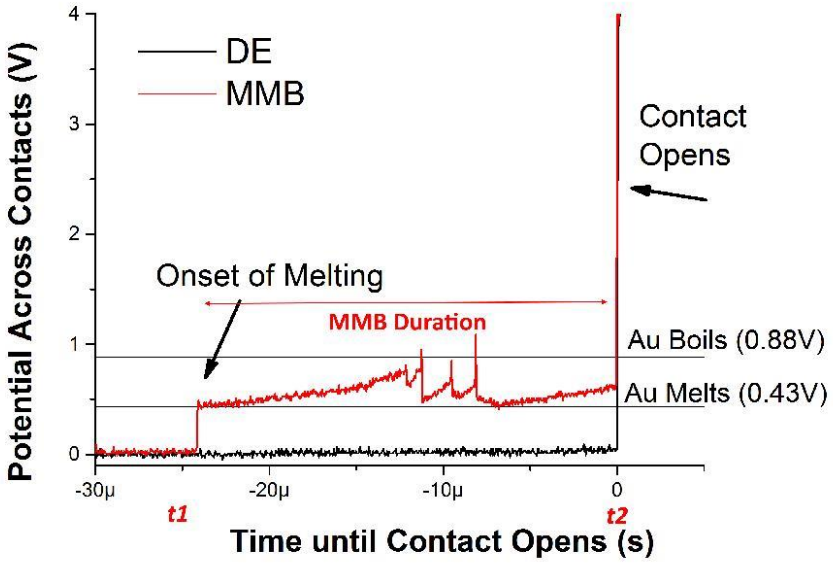

Figure 1. The contact potential during two hot switched opening events of a Au/MWCNT contact switched at 4 V and 20 mA. The red trace is characteristic of a molten metal bridge forming with steps

linked to the melting and boiling voltages for Au. The black trace is characteristic of a delamination event (DE) that shows no evidence of the contact material melting or boiling.

A proposed solution to the wear in thin Au films is a composite where the Au film is embedded in the upper surface of a forest of vertically-aligned multi-walled carbon nanotubes (MWCNT) [14,15]. The carbon nanotubes provide a mechanically compliant sublayer, allowing the conductive Au to conform to the incoming contact (Figure 2). This provides reduced contact pressure, increased contact area, and a mechanism to absorb the kinetic energy of contact closure [16], when compared to thin film Au-Au contacts. The vertical alignment of the nanotubes is crucial in achieving the extended lifetime as random or non-vertical alignments provide negligible benefit [17]. Au/MWCNT has been shown to increase contact lifetime [18]. Switching lifetimes of 4 x10^9 cycles at 4 μW DC power and 150 x10^6 cycles at 200 mW DC power have been demonstrated with the material [13,19].

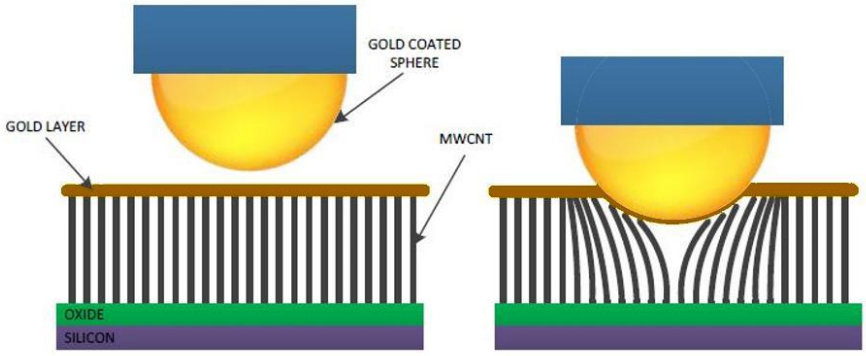

Figure 2. Illustration showing a composite contact formed by Au coating a field of vertically aligned multi-walled carbon nanotubes. The composite conforms to the incoming contact, enhancing the contact area and reducing the contact pressure.

In this study transient forces associated with the contact opening processes are investigated. The contacts are actuated by a piezoelectric cantilever to simulate MEMS scale closure force (150 μN) under low current hot switching conditions (4 V DC 20 mA). Contact force and potential are then monitored as the contact opens.

2. Materials and Methods

2.1. *Contact Manufacture*

The test contacts are: 1) an hemispherical upper contact, manufactured from a 2 mm diameter precision ground stainless-steel ball, coated with 20 nm Cr, then 500 nm Au and 2) a planar lower contact, of a SiO_2 on Si substrate (IDB Technologies, UK), with a 50 μm field of vertically-aligned multiwalled carbon nanotubes (MWCNT) grown by the thermal chemical vapour deposition (tCVD) of ethylene in a quartz reactor tube furnace. The MWCNT upper surface is coated with a 500 nm layer of Au by plasma enhanced chemical vapour deposition (peCVD) (Kurt J Lesker). Height and layer thickness are verified by exposing masked sections and measuring the step height with a laser surface profiler (TaiCaan Xyris 4000CL).

2.2. *Test Circuit*

The switching circuit is a simple series loop incorporating a 4 V lead acid battery with current controlled by a resistive load. The contact potential is measured by a high-speed oscilloscope (Tektronix MDO4054-3) with 1 GHz bandwidth and a sample rate of 2.5 GS/s (0.4 ns time resolution).

106 The circuit conditions are 4 V DC and 20 mA, chosen as they provide conditions where a mixture of
107 MMB and DE type contact openings are expected [13]. The circuit configuration for switching is
108 shown in Figure 3.

109 *2.3. Switching Arrangement and Force Measurement*

110 The test apparatus uses a frame, stage and focus controls of an optical microscope to position the two
111 contacts. The upper Au coated ball contact is fixed to the tip of a quartz force sensor (Kistler Model
112 9207 with 115 pC/N sensitivity) that is fixed to the head of the microscope frame. The lower contact
113 is fixed to a piezoelectric cantilever suspended from the stage of the microscope frame. The switch is
114 actuated by a square wave voltage provided by a signal generator. The system is housed inside a
115 chamber to stabilize temperature and damp air transmitted vibration. The apparatus is isolated from
116 floor transmitted vibrations by an optical grade damping table (Newport PG Series Breadboard with
117 ND30A isolators). The force transducer is linked to a charge amplifier (Kistler Type 5007 -3db
118 frequency response 2.3 GHz). The sensitivity for transient force is ~ 1 μN. The method is highly
119 sensitive to changes in dynamic forces but is described as a quasi-static force measurement because
120 the charge associated with a static force will decay over longer periods. The time constant for charge
121 decay is set to 0.01 s. The apparatus is housed in a metrology laboratory with temperature and
122 humidity controlled to better than 22.0 ± 0.2 °C and 40 ± 10 %RH.

123 *2.4. Experimental Procedure*

124 The contacts are positioned to achieve a static closed contact force of 150 μN. The static closed
125 force is determined using the same charge amplifier with a 20 s time constant. The contacts are
126 opened to a clearance of ~ 25 μm by applying a 20 V signal to the piezoelectric cantilever. The contact
127 closes when the signal to the piezoelectric cantilever is 0 V. The drive signal to the cantilever is an
128 offset 0 – 20 V square wave 0.5 Hz signal. The contacts are 'bedded in' for 1,000 cycles with no circuit
129 load to allow the contact interface to mechanically stabilize. After 1,000 cycles with no electrical signal
130 the load circuit is switched on. A further 100 cycles are carried out hot switching a 4 V DC, 20 mA
131 signal. The contact potential and transient forces associated with these 100 contact openings are
132 captured. The voltage and force signals are sampled at 0.4 ns over 80 μs (200,000 points).

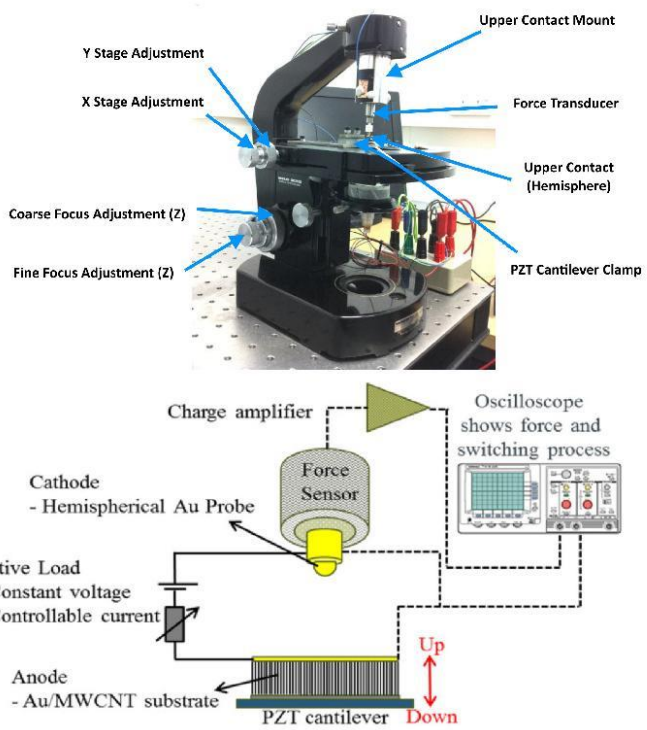

Figure 3. Switching circuit arrangement and experimental apparatus

2.5. Capture and Classification of Contact Opening Events

The point of contact opening is defined as occurring when the measured voltage exceeds 3 V. The opening event type is determined from the duration of the opening event.

Because the contact softening voltage (~0.08 V) is close to the noise floor of the oscilloscope (0.02 V resolution) the onset of contact melting is defined by applying a moving average filter. The filter removes the rapid fluctuations and allows the onset of contact softening to be distinguished from background noise. The contact opening waveform is resampled by the filter over a 2 µS window at 51-points. The starting point of the opening event, t_1 is defined as where the filtered waveform value rises to 0.08 V above closed contact potential for consecutive samples. The end point, t_2 of the opening event is defined as where the contact potential rises above 3 V. The opening event duration is the time elapsed between t_1 and t_2 as shown in Figure 1. This method gives a sensitivity to detect the opening event duration of ~ 2 µs.

The opening peak transient force is defined as the peak magnitude of force after the contact open. The arrangement of the contacts and a free body diagram showing the force sensor and the convention used for force direction is shown in Figure 4. Examples of Peak Transient Force are shown in Figure 5.

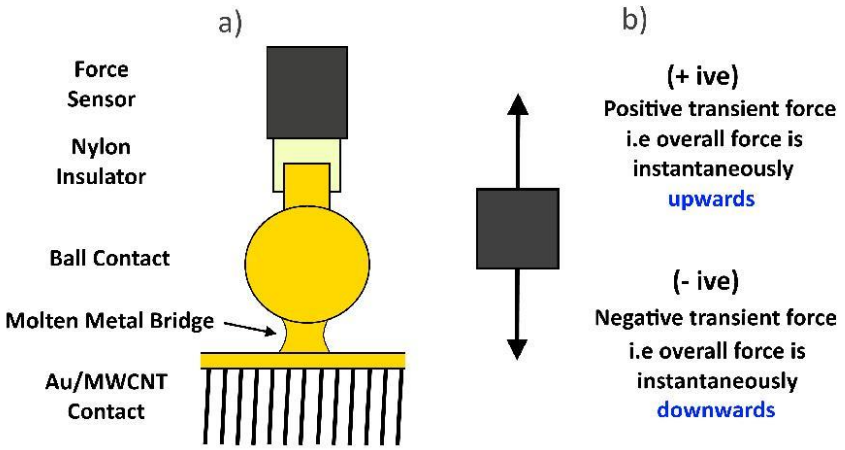

Figure 4. The contact force measurement arrangement a) and a free body diagram of the force sensor showing the convention used in graphs for positive and negative force (b)

3. Results

Figure 5 shows the voltage and force transients at opening. The Figure compares a DE (top) and MMB (bottom) from 500 ns before to 100 ns after the contact opens.

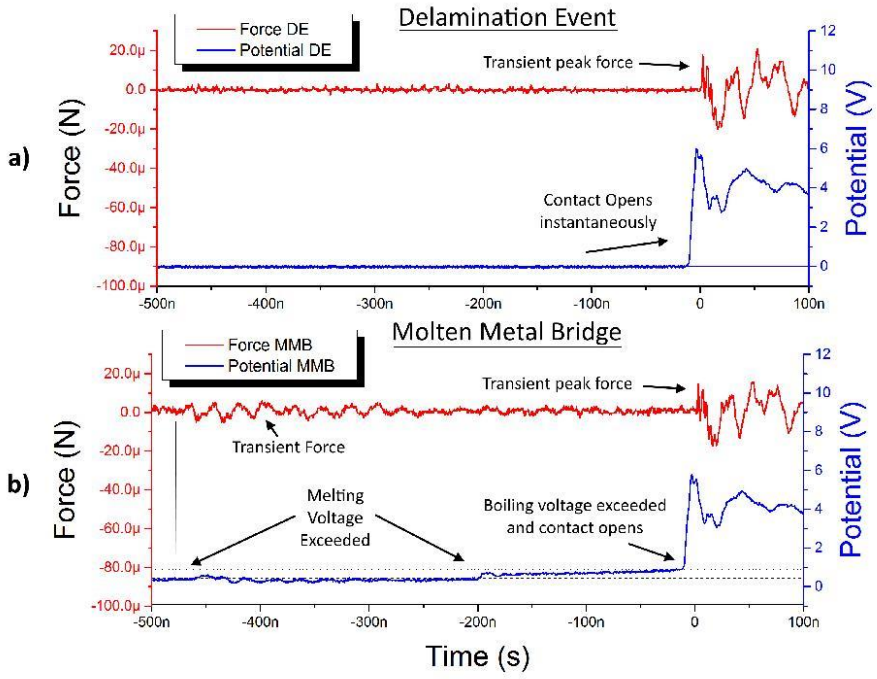

Figure 5. Examples of the force and contact voltage during a Delamination Event (top) and Molten Metal Bridge (bottom) from 500 ns before the contact opens with the transient peak force as the contact opens indicated.

The DE force graph Figure 5a (red trace) shows the force sensor at the noise floor (~ 1 μN) while the contact potential graph Figure 5 a) (blue trace) remains at the closed contact potential. At time = 0 the contact potential instantly rises above the open circuit voltage and a positive force event around 20 μN is detected. Both force and the voltage potential oscillate after this event.

The MMB force graph Figure 5b (red trace) shows force events above the noise floor of the force sensor. The contact potential varies above the normal closed contact potential, with steps shown to correspond with the melting voltage (horizontal dashed line) and boiling voltage (dotted black line) for Au. The contact potential rises to the boiling voltage for Au where it then rapidly rises above the open circuit voltage and a positive force event of ~ 20 μN is detected. The force and voltage oscillations observed are like the DE example.

3.1. The Molten Metal Bridge and the Transient Contact Force

While each MMB event is unique, a representative example is presented in Figure 6, over a longer time duration that Figure 5. Contact potential (blue) and the transient force experienced by the upper contact (red) are shown from 2 μS before to 1.5 μS after contact opening. The time scale shows t = 0 s as the contact opening. The event labelled as Transient Peak Force in both Figures 5 and 6 is a positive event showing the net force acting upwards on the upper contact has increased.

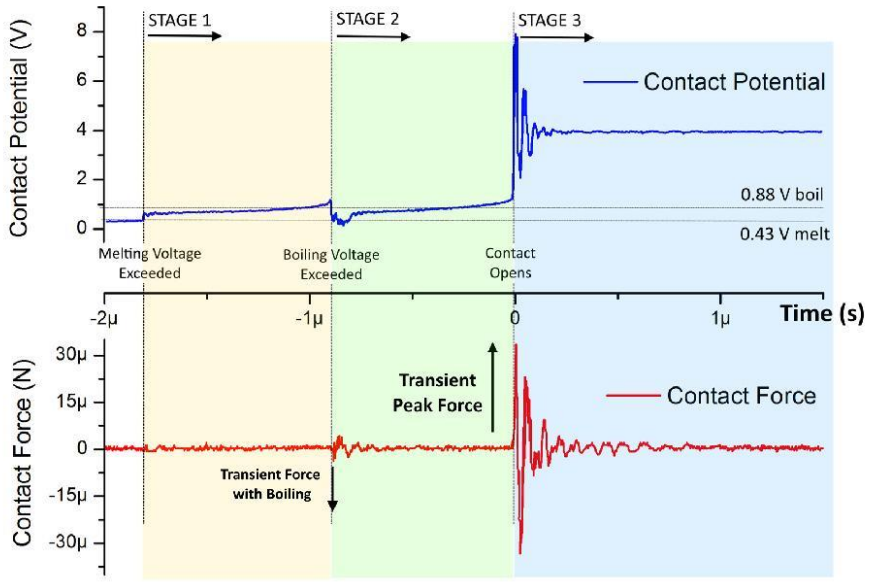

Figure 6. Molten metal bridge contact potential and the corresponding Transient Peak Force.

Stage 1 Melting Voltage Exceeded (from ~1.8 μs before contact opening)

As the contact potential steps from just below 0.4 V to above 0.6 V (this is above the melting voltage for Au), there is a very low-level force that is within the noise level of the sensor. At end of stage 1, the contact potential rises to 0.9 V before rapidly increasing to 1.1 V exceeding the boiling voltage for Au at time = -0.9 μS. The rapid increase from 0.9 V to 1.1 V occurs over 30 nS.

Stage 2 – Boiling Voltage Exceeded (from ~ 0.9 μs before contact opening)

At the start of stage 2, the contact potential drops sharply from 1.1 V to 0.2 V. After a further 150 ns the contact potential rises back to 0.6 V. When the contact potential drops from 1.1 V to 0.2 V a force transient is detected peaking at 5 μN and lasting 150 ns. The force is initially in the opposite direction to the opening force in Fig 6. is damped after 150 ns. From t = -0.75 μs the contact potential slowly rises from 0.6 V to 0.9 V and above the boiling voltage. The contact potential increases more rapidly from 0.9 to 1.1 V over 100 ns before a step change to nearly 7.8 V occurs.

Stage 3 – Contact Opens

This is the point at which the contacts are deemed to be open and the circuit has been interrupted. After the circuit is open the contact potential oscillates 5 times over 260 ns around the open circuit voltage of 4.1 V varying between a maximum of 7.8 V and a minimum of 2.2 V. The time period of each oscillation in contact potential is 52 ns. The force is initially positive and then oscillates 8 times over the next 700 ns with a time period of 87 ns. The peak force when the contact opens is defined as the *Transient Peak Force*.

3.2. The Classification of Delamination Events (DE) and Molten Metal Bridge (MMB) Events

The type of opening event is classified by the transient voltage waveform. DE show a single abrupt voltage step to the open circuit voltage while MMB show multiple stages of rising and falling contact potential as the bridge is formed. Figure 7 shows 100 consecutive hot opening events as both contact potential vs time (left) and the number of events of a given duration (right). The MMB events waveform are highly variable from one event to the next. It has previously been shown that groups of consecutive cycles at the same switching conditions are well described by a Gaussian distribution [9]. It is possible to distinguish a clear difference between the DE and MMB events in Fig 7 (left) as there are no MMB apparent with a duration of less than ~10 μs. However, it is difficult to see the number of DE as each trace is effectively overlaid. By evaluating the duration of each event and plotting the number of events at a given duration (Figure 7 right) it is very clear that there are two distinct type of event. Approximately half the events are classified with a duration under 7.5 μs while the remainder have a duration above 10 μs. Using this methodology, the short duration events are classified as DE and the longer duration events as MMB. No events are classified with a duration between 7.5 and 10 μs.

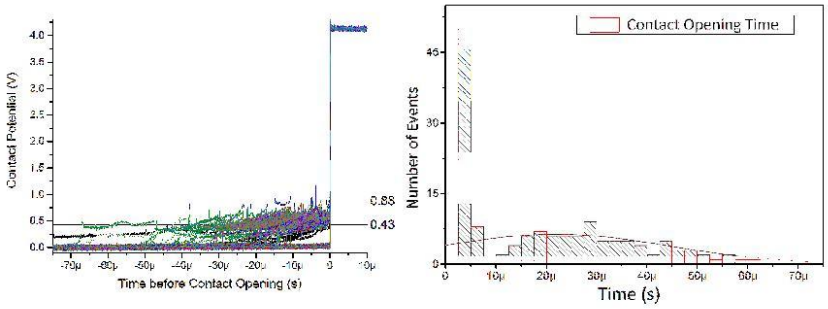

Figure 7. The transient voltage waveforms of 100 consecutive switching cycles (left) and a histogram showing the calculated duration of the opening event. The individual molten metal bridge (MMB) waveforms are highly variable but rise to 0.43 and 0.88 V prior to opening. The delamination events (DE) show no increase in the contact potential until the contact abruptly opens.

With the contact opening now classified as either MMB or DE events, the contact force can be evaluated and according to the type of opening event.

3.3. The Contact Opening Force for Delamination and Molten Metal Bridge Events

Figure 8 shows a histogram distribution of the Peak Transient Opening Force of the 100 hot switched (4 V DC, 20 mA) opening events. The colour scale shows the contact opening type by colour with MMB (blue) and DE (red) with a normal distribution curve fitted to each type. The figure demonstrates a nearly equal number of DE and MMB events.

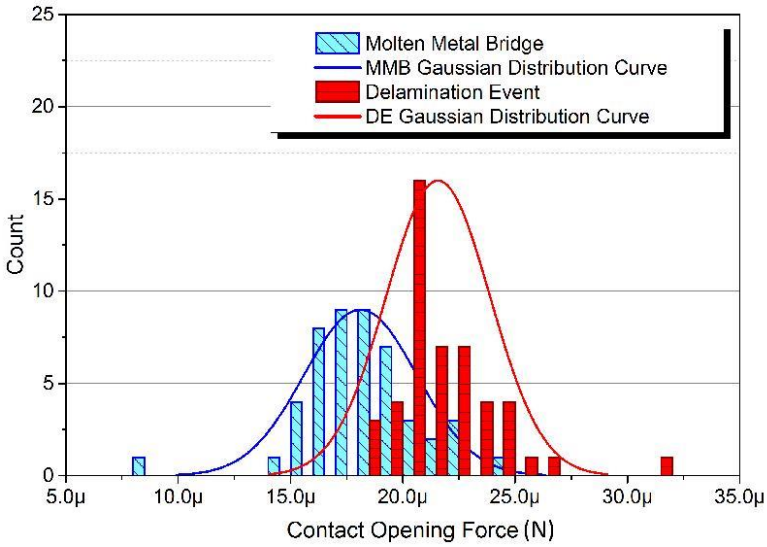

Figure 8 A histogram of the Transient Peak Force of 100 consecutive hot switched contact openings at 4V 20mA. Delamination events (DE) are shown in red while the molten metal bridge (MMB) events are shown in blue. The average Transient Peak Force is 18.1 µN for MMB and 21.6 µN for DE.

The distribution of Transient Peak Force for MMB is close to Gaussian distribution with a mean opening force and standard deviation of 18.1 ± 2.5 µN. The distribution of DE type demonstrates a slightly more leptokurtic (peakier) distribution with a higher mean opening force of 21.6 ± 2.3 µN. This represents the DE contact openings having a ~ 20% higher average Transient Peak Force than the MMB type.

4. Discussion

4.1. The Molten Metal Bridge and the Transient Contact Force

The results show that the MMB event can be detected by the force sensing method. The force events are synchronized with step changes in the contact potential linked to phase changes in the contact material predicted by the ϑ-ψ theorem [8].

Stage 1 – Melting Voltage

The first force event is a small shock or vibration caused by liquid surface tension as the MMB is formed. The observed force indicates that as the liquid bridge initially forms there is a small increase in adhesion force. Over the following 900 ns the contact potential rises smoothly as the constriction resistance increases, with no force transients detected at the contact. This indicates the contacts are separating while the molten bridge is elongating and reducing in cross section while its temperature rises.

Stage 2 – Boiling Voltage

As the contact potential reaches 0.9 V it begins to rise more quickly reaching 1.1 V before suddenly dropping to 0.2 V. The observed drop in potential across the contact shows the current path has rapidly decreased in resistance. This suggests that on this occasion the circuit path is not interrupted by the onset of boiling but rather it has been deformed or distorted to include a part of the contact that is much cooler and in still in solid phase. This event is not typical and attributed to the unique properties of the Au/MWCNT surface. The MWCNT under the Au coating is acting like a spring with the deformation of the surface returning its non-loaded condition. The introduction of cooler material to the MMB momentarily reduces the average temperature of the bridge to below the melting (freezing) point for around 80 ns before the potential again exceeds the melting voltage. This period is explained by the new solid material becoming heated to a molten state.

As the contacts are separating, the refreezing of MMB causes an instantaneous force. This is experienced as a force by the force transducer, followed by a mechanical ringing that is damped as the bridge re-liquifies. It is noted that this is in the opposite direction to the defined Transient Peak Force and indicates that the Au/MWCNT surface is applying a force to the upper contact, as would be expected with the spring like nature of the surface.

Stage 3 – Contact Opening

Prior to stage 3 in Figure 6. the potential rises steadily from 0.6 to 0.9 V, and before again increasing more rapidly after reaching 0.9 V; however, this time the contact potential rises instantaneously (in less than 4 ns) to over 3 V. Simultaneously a sudden increase in force of 32 μN is detected at the upper contact. This event describes the rupture of the molten bridge by boiling, and the contacts separating. For the contacts to separate they must be under enough opening force to overcome the adhesive forces between the contacts. As the MMB boils it is broken and the surface tension that was acting as an adhesive force between contacts is instantaneously removed. The measured Transient Peak Force is the upper contact experiencing a sudden decrease in adhesive force as the MMB is removed. The measured Transient Peak Force is therefore equal and opposite to the adhesive tension force in the MMB the instant before the bridge ruptures.

After the contacts have separated there is a transient ringing in both the electrical circuit and the response of the force transducer. The oscillation in force can be explained as mechanical vibration of the upper contact as MMB ruptures and its tension force is lost. The vibration characteristics are therefore related to the stiffness and the mass of the upper contact mount [20]. It is interesting to note that the time period of force and contact potential oscillations are of the same order at 52 and 87 ns respectively. Similar phenomenon were reported during opening of MEMS scale contacts, however the study used extremely low opening velocities that were unrepresentative of a practical device and subject to influence from environmental vibration [21].

Modelling Voltage Oscillation after Contact Separation

The observation of oscillation in contact potential following contact separation appears highly repeatable suggesting a ringing response in the electrical circuit. The response is modelled to check the empirically observed response matches the predicted response. The over voltage at the point of circuit rupture is critical to maintain below ~ 12 V as above this level micro arcing can be induced. The magnitude and time period consistent the circuit's inductance and capacitance are estimated from a series LCR model of the switching circuit behavior (Matlab Simulink 2015) according to the second order transient response (1).

$$V_s = LC\frac{d^2v_c(t)}{dt^2} + RC\frac{dv_c(t)}{dt} + v_c(t) \quad (1)$$

Capacitance is estimated using a parallel plate model, while inductance is estimated as the self-inductance of a single loop of wire. The modelled and empirically observed values for overvoltage, time period and damping time of the electrical ringing response are summarized in Table 1.

Table 1. Modelled vs Observed Electrical Ringing Characteristics at Contact Opening

	Peak Over Voltage (V)	Time Period (ns)	Damping Time /6dB (ns)
Experimental	3.7	52.5	260
Modelled	3.8	69.4	427

The modelled values for peak overvoltage and the frequency of the response closely correlate with the experimentally observed voltage transient at contact opening. The damping observed is higher than predicted by the model. This is expected as the model does not consider the influence of circuit capacitance changing (as would occur between real separating contacts), nor the dynamic impedance of the lead acid voltage source to a high frequency signal, both factors that would damp the response. The good agreement observed between the modelled and empirically observed values for overvoltage and frequency support the observation that the oscillation in the contact potential is the circuit electrically ringing after opening due to its micro-inductance and pico-capacitance. Both empirical and modelled responses indicate the MMB test circuit does not exceed the threshold voltage for arcing [10].

It is noted continuous increase in separation of contacts means the capacitance will change dynamically. Both more advanced modelling of capacitance and load circuit inductance are identified for future investigation.

4.2. Classification of MMB and DE

The classification of opening events by duration demonstrates a distribution with a clear region of separation. This shows the classification method is effective at separating the MMB and DE events. It is noted that the use of the moving average filter will result in overestimated DE duration, which are effectively instantaneous but, the primary purpose is to classify the opening event type and this method provides a clear distinction between MMB and DE. The switching conditions were chosen as they have previously been linked with a frequent occurrence of the DE. The occurrence of DE marks a limiting condition for the formation of the MMB. Increasing either the current of voltage from circuit conditions of 4V 20mA demonstrated the number of DE decreased, while as the number of switching cycles increased the frequency of the DE increased [13]. The limiting case to the formation for the MMB can be explained by step changes in the conduction area. A requirement for the Holm ϑ-ψ theorem is that Joule heating raises the conductor temperature nearly instantaneously to a point of thermal equilibrium [7]. This is reasonable assumption provided the contact area and therefore constriction resistance change gradually. If there is a step change in the contact area occurring (such as a delamination), this may occur too rapidly for thermal equilibrium so no MMB is formed. The time constant for thermal equilibrium is dependent only on the thermal conductivity and heat capacity per unit volume of the conducting material and proportional to the contact area. Illustratively, for a circular constriction of diameter 10 μm in a Au conductor the thermal equilibrium time constant is calculated as 0.198 μs. It is noted than the observed MMB duration and contact areas reported in low force studies of the Au/MWCNT material are of similar magnitude [9,12].

4.3. Distribution of Contact Opening Force

The distribution of Contact Opening Forces shows that DE are associated with a greater adhesion force between contacts than the MMB events. Figure 9. shows scanning electron micrographs of the Au/MWCNT contact surface before and after hot switching at 4 V DC and 20 mA. There is evidence of both softening and melting as well as mechanical flattened and cracking of the surface. It is proposed that because of the speed of the DE there is insufficient time for a MMB to form. The Contact Opening Forces observed are evidence the adhesive force released during a DE are ~ 20% greater than during the MMB formed at 4 V 20 mA circuit conditions.

In the MEMS switching regime contact opening force is limited. Small increases in adhesion are therefore linked to increase risk of the contacts failure by sticking [20]. It has previously been shown that varying the circuit conditions will influence the duration, thermal energy and size of the MMB [9].

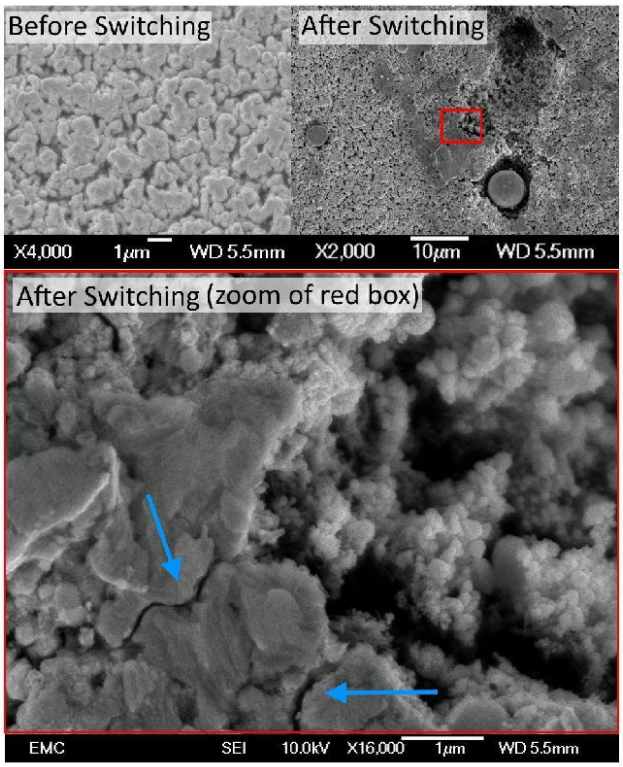

Figure 9. Electron micrographs of the Au/MWCNT surface before switching (top left) and after hot switching 1,000,000 cycles at 4 V 20 mA (top right). The main image (bottom) is magnified to show cracks in the surface (blue arrows) next to a region where Au is being worn away

5. Conclusion

The Contact Opening Forces in molten metal bridge (MMB) and delamination events (DE) have been investigated during hot switching of a Au/MWCNT composite contact at forces and switching conditions representative of the MEMS switch regime.

The magnitude and direction of micro force transients are observed under contact closure force and opening velocities realistic for a practical device. The force transients are linked to the melting and boiling processes that are also linked to a fine transfer wear process. A limiting case for the formation of the MMB is proposed where step changes in contact area occur too rapidly for thermal equilibrium.

Finally, the Transient Peak Force required is found to be ~ 20 % greater when DE are observed cf. MMB events.

Author Contributions: Conceptualization, J.M. and T.B.; methodology, T.B.; investigation, T.B.; resources, J.M.; writing—original draft preparation, T.B.; writing—review and editing, T.B. and J.M; supervision, J.M.; project administration, J.M.; funding acquisition, J.M.

Acknowledgments: The authors would like to thank the EPSRC for their support in this work which is funded in part by grant EP/M508147/1.

Conflicts of Interest: The authors declare no conflict of interest

References

1. Iannacci, J. RF-MEMS: an enabling technology for modern wireless systems bearing a market potential still not fully displayed. *Microsystem Technologies* **2015**, *21*, 2039-2052.
2. Coutu Jr, R.A.; Kladitis, P.E.; Leedy, K.D.; Crane, R.L. Selecting metal alloy electric contact materials for MEMS switches. *Journal of Micromechanics and Microengineering* **2004**, *14*, 1157.
3. Toler, B.F.; Coutu, R.A.; McBride, J.W. A review of micro-contact physics for microelectromechanical systems (MEMS) metal contact switches. *Journal of Micromechanics and Microengineering* **2013**, *23*, doi:Artn 103001
10.1088/0960-1317/23/10/103001.
4. Basu, A.; Adams, G.; McGruer, N. A review of micro-contact physics, materials, and failure mechanisms in direct-contact RF MEMS switches. *Journal of Micromechanics and Microengineering* **2016**, *26*, 104004.
5. McBride, J.W.; Liu, H.; Chianrabutra, C.; Lewis, A.P. The Wear of Hot Switching Au/Cr-Au/MWCNT Contact Pairs for MEMS Contacts. *Ieice Transactions on Electronics* **2015**, *E98c*, 912-918, doi:10.1587/transele.E98.C.912.
6. Price, M.; Jones, F.L. The electrical contact: the properties and rupture of the microscopic molten metal bridge. *Journal of Physics D: Applied Physics* **1969**, *2*, 589.
7. Slade, P.G. *Electrical Contacts: Principles and Applications, Second Edition*; CRC Press: 2014.
8. Holm, R. *Electric contacts: theory and application*; Springer Science & Business Media: 1958.
9. Bull, T.; Mcbride, J. The Influence of Circuit Parameters on Molten Metal Bridge Energy in a MEMS relay testing platform. *Proceedings of 2016 Twenty Eighth International Conference on Electrical Contacts* **2016**.
10. Doduco. *Databook of Electrical Contacts*; Duduco GmbH: 2012.
11. Timsit, R.S. Constriction resistance of thin film contacts. *IEEE Transactions on Components and Packaging Technologies* **2010**, *33*, 636-642.
12. Bull, T.G.; McBride, J.W. In-Situ Contact Surface Characterization in a MEMS Ohmic Switch under Low Current Switching. *MDPI Technologies* **2018**, *2*, 47.
13. Bull, T.G.; McBride, J.W.; Jiang, L. The influence of Circuit Parameters on Molten Bridge Surface Degradation in a Au/MWCNT MEMS Switch Contact. In Proceedings of 2018 IEEE Holm Conference on Electrical Contacts; pp. 359-365.
14. Mcbride, J.; Yunas, E.; Spearing, S. Gold coated Carbon Nanotube Surfaces as Low Force Electrical Contacts for MEMS devices: Part 1. In Proceedings of The 59th IEEE Holm Conference on Electrical Contacts, Newport, USA.
15. McBride, J.; Yunus, E.; Spearing, S. Improving the contact resistance at low force using gold coated carbon nanotube surfaces. *The European Physical Journal-Applied Physics* **2010**, *50*.
16. Down, M.; Lewis, A.P.; Jiang, L.; McBride, J.W. A nano-indentation study of the contact resistance and resistivity of a bi-layered Au/multi-walled carbon nanotube composite. *Applied Physics Letters* **2015**, *106*, 101911.
17. Kageyama, T.; Shinozaki, K.; Zhang, L.; Lu, J.; Takaki, H.; Lee, S.-S. Fabrication of an Au–Au/carbon nanotube-composite contacts RF-MEMS switch. *Micro and Nano Systems Letters* **2018**, *6*, 6.
18. Lewis, A.P.; McBride, J.W.; Jiang, L. Evolution of Voltage Transients During the Switching of a MEMS Relay With Au/MWCNT Contacts. *Components, Packaging and Manufacturing Technology, IEEE Transactions on* **2015**, *5*, 1747-1754.

404 19. McBride, J.W.; Bull, T.G. The in-situ wear of a hot and cold switched Au on Au coated MWCNT
405 electrical contact for a MEMS switch application. *IEEE Holm Conference on Electrical Contacts, Milwaukee,*
406 *WI* **2019**.
407 20. Jensen, B.D.; Huang, K.W.; Chow, L.L.W.; Kurabayashi, K. Adhesion effects on contact opening
408 dynamics in micromachined switches. *Journal of Applied Physics* **2005**, *97*, doi:Artn 103535
409 10.1063/1.1901837.
410 21. Ren, W.; Chang, C.; Chen, Y.; Xue, S.; Coutu, R.A. Investigation of the Surface Adhesion Phenomena
411 and Mechanism of Gold-Plated Contacts at Superlow Making/Breaking Speed. *IEEE Transactions on*
412 *Components, Packaging and Manufacturing Technology* **2015**, *5*, 771-778.

9.3 Conference Papers

ICEC Edinburgh 2016

The influence of circuit parameters on Molten Metal Bridge Energy in a MEMS relay testing platform

J.W.McBride[1,2], T.Bull
University of Southampton
Southampton, UK, SO17 1BJ
[2]University of Southampton Malaysia Campus
Nusajaya, 79200, Johor, Malaysia

Abstract— **A MEMs relay testing platform is described, consisting of an actuation cantilever and switching contacts, where the contact force is determined though the contact resistance measurement of Au coated Multi-walled Carbon Nano-tube (Au/MWCNT) sensor surface. The Au/MWCNT surface is further investigated under a range of DC switching condition to determine the limits of the non-arcing condition, or the minimum arcing voltage and current. The range of circuit conditions is also used to determine the degradation process of the surface in the non-arcing condition through the investigation of the molten metal bridge transient voltages, which have previously been linked to the failure of the surface as switching surface.**

Keywords-.

I. INTRODUCTION

Wear processes on the electrical contact surfaces, used in low voltage (2-12V) switching applications, exemplified by Micro-Electro-Mechanical (MEMS) switching devices or relays; can result in premature device failure, [1]. This becomes evident when the electrical contact surfaces are conventional metallic films. A proposed solution to minimize the electrical contact surface wear is to coat one or both surfaces with a sub-layer of carbon nano-tubes [2].

The process of switching an electrical load, even at the low voltage levels, is referred to as "hot switching" when related to MEMS relays; implying that the electrical load is outside the "dry circuit" condition; when the applied voltage and current have no physical influence on the surface [3]. A typical MEMS relay "hot switching" electrical load of, 1mA-10mA and 4V; although below the minimum arcing voltage associated with most commonly used metallic electrical contact surfaces (~12V); is above the softening and melting voltages for the metallic surfaces [4-6]. This leads to a transfer mechanism between the two surfaces known as "fine transfer", or molten metal bridge phenomena and this was first discussed in the context of the current study in [7]. The material transfer between electrical contacts in MEMS devices is similar to a problem encountered in switching devices used in telecommunication systems in the 1950's and 1960's. The research conducted during that period can be reviewed in [4-6]; however it is important to note that there is one important difference. Although the voltage levels used are comparable, the current levels are higher than those used in MEM relays, and typically of the order of 1A. It is apparent from the studies of "fine transfer" that a primary issue was the influence of the circuit inductance on the transient voltage during opening and closing. Although the steady-state circuit voltage (e.g. 4 V) is below the minimum arcing level (~12 V), the presence of circuit inductance can result in local micro-arcing phenomena, as transient voltages exceed the minimum arcing condition. The mechanism of "fine transfer", without the presence of micro-arcing was shown to be related to the physical properties of the metals used. This can best be described with reference to the ψ, θ theorem [4], where ψ is the electrical potential and θ the temperature in a metallic conductor.

The voltage required to result in the melting temperature and the boiling temperature of Au, commonly used as the metallic contact surface in MEMS; is for melting, 0.43V, and for boiling, 0.88V. Both voltage levels are below the steady state voltage used in MEMS relays. It therefore follows that during each opening and closing operation, the Au surface will result in the formation of a molten bridge, leading to the wear process. The direction of the wear or transfer process is far from trivial, and not fully described; an overview of the thermodynamic and other process is given in [5].

Metallic surfaces used in MEMS relays are often films on Si or other surfaces. If Au is used then the hard (Si) substrate limits the contact area, and even at low force (mN's), the resultant contact pressure can be sufficient to produce cold welding; thus resulting in delamination of the Au films during opening and closing. A proposed solution to both the "fine transfer" and the potential cold welding problems of Au surfaces has been to use a sub-layer of structured carbon nanotubes (CNT's). Recent studies have focused on the application of carbon nanotubes (CNT) as a potential solution to the MEMS electrical contact problem, where a "forest" of vertically aligned, multi-walled carbon nanotubes (MWCNT) sputter coated with a conductive gold layer. This is referred to

here as Au/MWCNT. This creates a CNT composite surface, with a high conductivity surface layer and a compliant under layer. In [8], a modified nano-indentation apparatus was used to determine the contact resistance as a function of contact force (1mN) and the data used to model the surfaces in [9]. In [10] the surfaces were tested under a range of current loading conditions and it was shown that the wear process although still dominated by the "fine transfer" process was further complicated at higher currents by apparent delamination of the surfaces, where the fine transfer process resulting from the molten metal bridge (MMB) thins the Au layer and then leads sticking and delamination. In [11] the MMB phenomena has been studied further on the Au/MWCNT surface and the MMB thermal energy used as an indicator of the failure phenomena. It was suggested in [11] that the roughness of the surface would affect the MMB duration. As shown in Fig.1. The idea proposed is that as the surface wears the initial roughness is smoothed by the MMB process from Fig 1a to Fig 1e; and that when the surface is smother i.e with lower roughness that the MMB bridge formation will cover a larger area. This idea has not been proven but it was observed in the same paper that as the contact surfaces wear with number of operations and close to the point of failure that the thermal energy of the MMB increases, suggesting a longer MMB period associated with a larger MMB area. The results are shown in Fig.2, for a Au/MWCNT surface mounted in a MEMS system with very low force (≈ 35μN), and with a 4 V and 50mA supply. The MMB energy is shown to increase from a stable 1.5 μJ to over 13 μJ at the failure point corresponding the increase in contact resistance also shown in Fig.2.

The objective of this paper is to investigate the same type of surface under a range of electrical loading conditions, to investigate the influence of the load on both the MMB transient at the opening phase and also to look for the onset of gap breakdown as voltage is increases. For the study we have selected two surfaces of differing surface roughness to investigate further the influence of the roughness on the MMB phenomena.

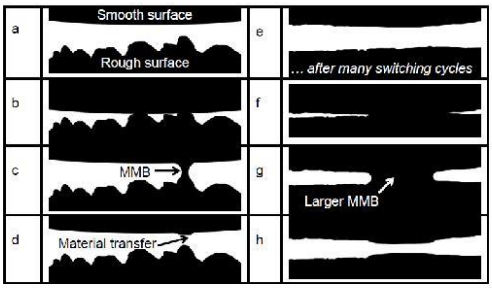

Fig.1 The evolution of MMB as a function of surface wear, [11]

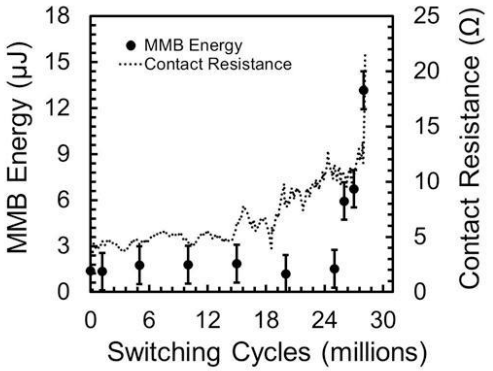

Fig.2 MMB energy and contact resistance versus number of switching cycles. Error bars calculated using standard error, for a Au/MWCNT surface in a MEMs system at 35μN and with a 4 V and 50mA load, [11].

II. Sample Fabrication

A. *Sample Fabrication*

The fabrication of the Au/MWCNT composite is reported in [10]. A 1.5 nm layer of Al_2O_3 and a catalyst layer of 10 nm Fe are initially sputtered on a silicon wafer. Vertical aligned MWCNTs are grown using thermal chemical vapor deposition (CVD), and ethylene is used as carbon source gas. The growth temperature is 875°C, and the growth time is used to control the height of MWCNT. The last step is sputtering a gold layer onto the nanotubes forest. In this paper, a composite with 500-nm Au sputtered on 50-μm CNT is investigated.

Fig. 3 shows a typical composite surface, with the nanotubes aligned. It is shown that the penetration depth varies from sample to sample; and is 6 μm for the samples presented.

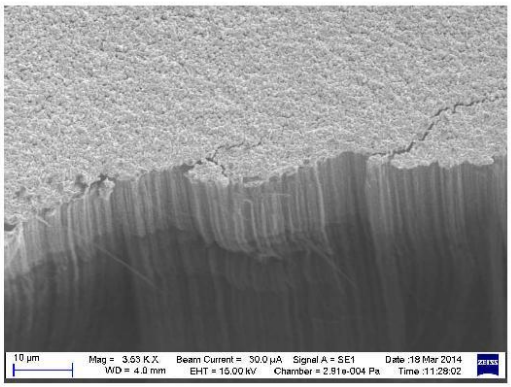

Fig. 3. SEM image of a nominal 500 nm gold coated on 50 μm CNT surface (angle of incidence of 55°), showing the penetration of gold into MWCNT. The surface is cut using a sharp slider to see the cross section of the surface.

B. Surface characterization

Two surfaces have been sued for the investigation, a rough surface and a relatively smooth surface. A TaiCaan XYRIS 4000WL 3D optical profiler was used to evaluate texture the composite surface. This measurement method is used as it offers the capability to evaluate the entire composite surface while retaining a high vertical measurement resolution (10nm). Fig. 4 shows the smooth surface over a 0.2mm x 0.2mm measurement region. The peak to valley measurement for the cross section highlighted is 1.651µm. Fig. 5 shows the rough surface over a measurement of the same area 0.2mm x 0.2mm, where the cross section shows a peak to valley of 31.425 µm.

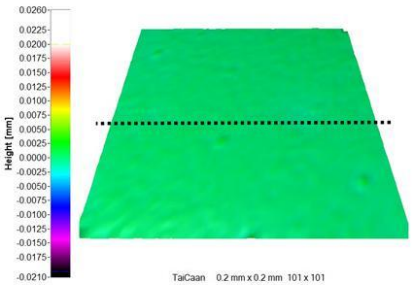

Fig. 4 Peak to Valley on 2D Cross Section (along dotted line) 1.651um

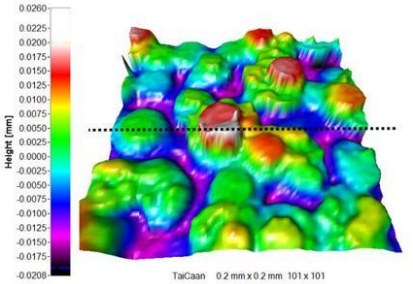

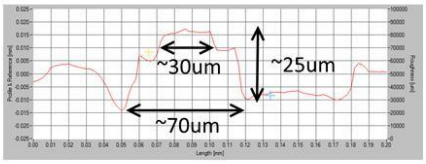

Fig. 5 Peak to Valley on 2D Cross Section (along dotted line) 31.425um

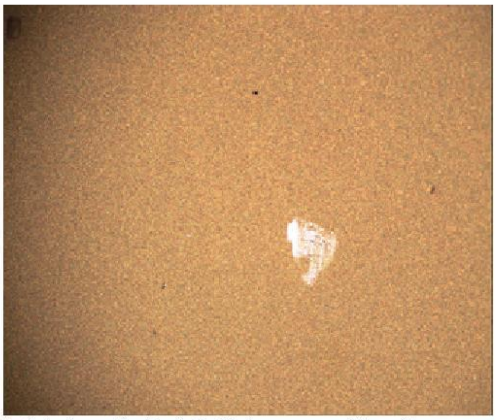

Fig 6. An image of surface in the Fig.4 over an area of 3mm x3mm

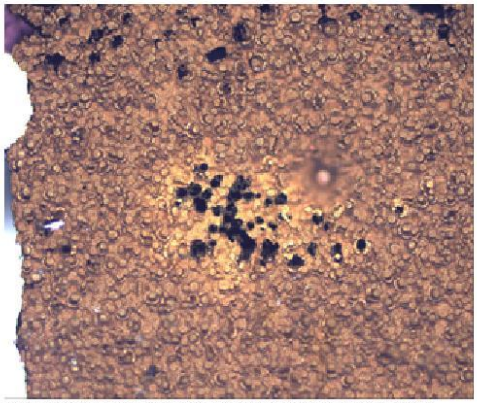

Fig.7 An image of surface in the Fig.5 over an area of 3mm x3mm

The rough surface shown in Fig's 5 and 7 consists of flattened peaks ~30um in diameter at the tip and ~30um in height. The composites were characterised for their variation in surface amplitude using a measured evaluation area of 1mm x 1mm and 201 x 201 data points (every 5um). The variation in amplitude was quantified statistically using the areal arithmetic mean absolute roughness parameter (Sa). A 0.25mm Gaussian filter was applied to the data to remove the influence of long wavelength surface features on the Sa parameter that do not influence the contact dynamics. The Areal surface roughness of the rough sample is Sa = 7.822um with a 0.25mm Gaussian filter, 1mm x 1mm, 201 x 201 measurements. The Area surface roughness of the smooth surface Sa = 0.231 with a 0.25mm Gaussian filter, 1mm x 1mm, 201 x 201 measurements.

C. *Experimenatl Method*

The experimental apparatus is the same as described in [10], and a schematic of the testing system is shown in Fig. 8. The setup is mounted on an anti-vibration workstation in an environmental controlled room with average humidity at 60.6% (variance of ±10%) and average temperature at 20 ºC (variance ±1 ºC). To simulate the repeated switching behaviour of MEMS switches, the Au/MWCNT composite was attached to a PZT cantilever which was actuated by a function generator. The contact force was 1 mN, and the load voltage was 4 V for all variation in current experiments presented. The experiments were performed with load current values of 10, 20, 50, 100 and 200 mA. To investigate the influence of the voltage on the MMB the current was held at 50 mA and the voltage varied from 4, 6, 8, 10, and 12 V. In all cases the surface is switched for 50 "Hot switching cycles", for a particular load condition. The point of contact is then moved and the test repeated at a new location on the surface for a new load condition. The voltage and current transients are stored and then evaluated for the thermal energy of the MMB for each switching operation, [11].

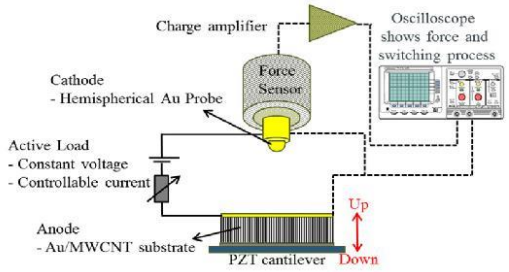

Fig 8. Schematic of the test apparatus used for the hot switching tests.

III. Results and Discussion

A. *Smooth Au/MWCNT surface.*

Fig's 9 and 10 shows the influence of the load current on the MMB energy over 50 switching cycles for the smooth surface described in Fig's 4 and 6, for the variation of the load current. Fig 9 is for all current values while Fig 10, focuses on the lower current values which are not clearly shown in Fig. 9. The first point to observe is that for 50 mA the MMB energies are lower here than in [11], with a typical average value of 100 nJ in Fig.10 compared to 1500 nJ as shown in Fig.2, [11]. The surface in [11] although not identical has a similar roughness value to the surface used here. The key difference between the two results is that a different test apparatus was used. In [11] the tests were performed on MEMS beam with a contact force of 35 µN compared to the PZT beam used here with a higher force of 1000 µN or 1 mN. It is conceivable that the lower contact force results in a lower opening velocity and thus extending the time period of the MMB, and increasing the MMB energy. This would need to be investigated further.

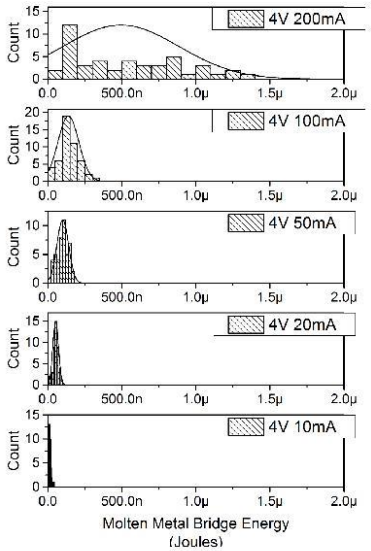

Fig.9 MMB Energy for smooth Au/MWCNT surface, for 4V, and varying load current

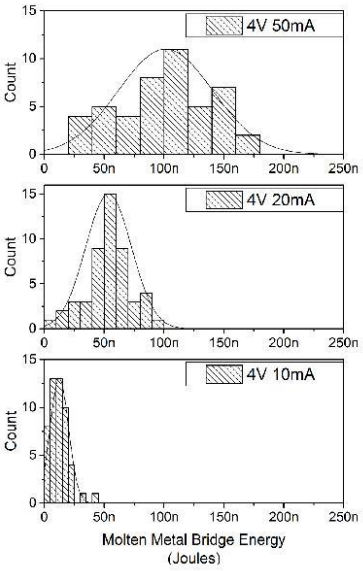

Fig.10 MMB Energy for the Rough Au/MWCNT surface, for 4V, and varying load current.

The MMB energy data in Fig. 9 shows the variability of the MMB process, with Gaussian curves modelling the variability. The higher the current the higher the energy as expected but also the higher the variability. Fig. 10 shows the same characteristics for the three lower load current values. The data in Fig.11 shows the influence of load voltage, and as expected there is no apparent tend with the supply voltage.

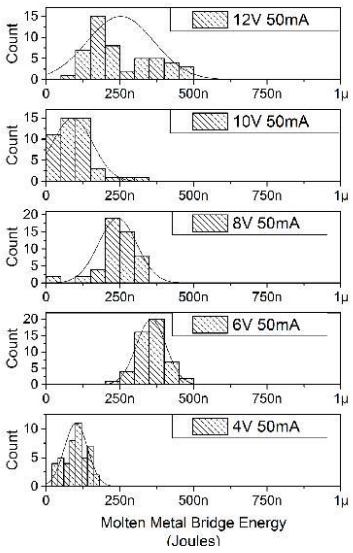

Fig.11 MMB Energy for Smooth Au/MWCNT surface, for 50 mA, and varying load voltage.

B. The Rougher Au/MWCNT surface.

Fig's 12 and 13 shows the influence of the load current on the MMB energy over 50 switching cycles for the rougher surface described in Fig's 5 and 7, for the variation of the load current. Fig 12 is for all current values while Fig 13, focuses on the lower current values which are not clearly shown in Fig. 12. Again the MMB energy for the 50 mA are lower here (280 nJ compared with 1500 nJ) than in [11], but actually higher than for the smother surface in Fig 10. This result contradicts the suggest process in Fig.1, as is the key observation in this work. According to Fig.1 the rougher surface would be expected to have a lower MMB. This result is important as it now suggests that the increase in MMB energy over the lifetime of the device is not linked to the surface roughness changes.

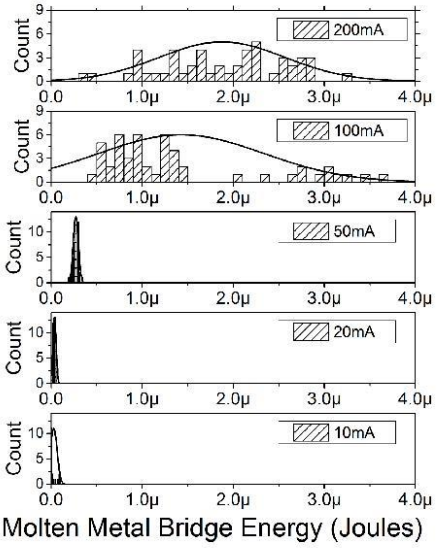

Fig.12 MMB Energy for Rough Au/MWCNT surface, for 4V, and varying load current.

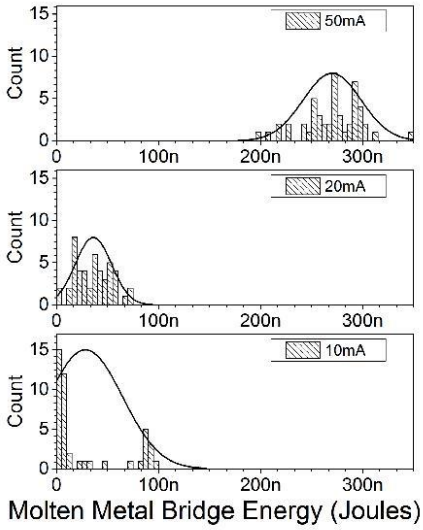

Fig.13 MMB Energy for the Rough Au/MWCNT surface, for 4V, and varying load current.

IV. Conclusions

The objective of the paper was to investigate the Au/MWNCT surface used for MEMS switching conditions, under a range of electrical loading conditions, to investigate the influence of the load on the MMB transient at the opening phase under "hot switching" conditions; and to test the hypothesis that the MMB energy was linked to the roughness of the surfaces. The results have shown that the MMB energy appears to be links to the surface roughness but in the opposite sense than expected. It is shown here that the MMB energy is linked closely to the load current and increases with the increase in surface roughness.

References

[1] B. F. Toler, R. A. Coutu, and J. W. McBride, "A review of micro-contact physics for microelectromechanical systems (MEMS) metal contact switches," J. Micromechanics Microengineering, vol. 23, no. 10, p. 103001, Oct. 2013

[2] E. M. Yunus, S. M. Spearing, and J. W. McBride, "The Relationship Between Contact Resistance and Contact Force on Au-Coated Carbon Nanotube Surfaces Under Low Force Conditions," IEEE Trans. Compon. Packag. Technol., vol. 32, no. 3, pp. 650–657, Sep. 2009.

[3] ASTM B539-02(2008). Standard Test Methods for Measuring Resistance of Electrical Connections (Static Contacts).

[4] Holm. R, Electrical Contacts: Theory and Application, 4th Edition, Springer, (1999)

[5] Llewellyn Jones F, The Physics of Electrical Contacts, Oxford Clarendon Press, (1957)

[6] Slade P, (Edit), Electrical Contacts, theory and applications, Marcel Dekker, (1999)

[7] JW McBride, "The wear processes of gold coated multi-walled carbon nanotube surfaces used as electrical contacts for micro-electro-mechanical switching", Nanoscience and Nanotechnology Letters 2 (4), 357-361.

[8] M. P. Down, A. P. Lewis, L. Jiang, and J. W. McBride, "A nano-indentation study of the contact resistance and resistivity of a bi-layered Au/multi-walled carbon nanotube composite," Appl. Phys. Lett., vol. 106, no. 10, p. 101911, Mar. 2015

[9] H. Liu, J. W. McBride, M. P. Down, and S. H. Pu, "Finite Element Model of a Bilayered Gold-Coated Carbon Nanotube Composite Surface," IEEE Trans. Compon. Packag. Manuf. Technol., vol. 5, no. 6, pp. 779–787, Jun. 2015.

[10] J. W. McBride, C. Chianrabutra, L. Jiang, and S. H. Pu, "The contact resistance performance of gold coated carbon-nanotube surfaces under low current switching," IEICE Trans. Electron., vol. E96–C, no. 9, pp. 1097–1103, Nov. 2012.

[11] A. P. Lewis, J. W. McBride, and L. Jiang, "Evolution of Voltage Transients During the Switching of a MEMS Relay With Au/MWCNT Contacts," IEEE Trans. Compon. Packag. Manuf. Technol., vol. 5, no. 12, pp. 1747–1754, Dec. 2015.

IEEE Holm Conference/ICEC 2018

The influence of Circuit Parameters on Molten Bridge Surface Degradation in a Au/MWCNT MEMS Switch Contact

Thomas. G. Bull, John W. McBride, and Liudi Jiang
Mechanical Engineering Dept, University of Southampton
tb10g11@soton.ac.uk

***Abstract*— The influence of circuit parameters on an Ohmic (metal-metal contact) MEMS (microelectromechanical system) switch contact pair are investigated under hot-switching (carrying current) circuit conditions below the arcing-threshold. A novel MEMS relay testing platform is used to investigate microscale contact surface change between individual switching events. The contact materials are a composite contact material of vertically-aligned carbon-nanotubes with a metallic (Au) layer, paired with an Au-coated ball contact. The evolution of the contact surface is evaluated along with the energy associated with the molten-metal bridge (MMB) phenomena. Circuit voltage is varied between 4 and 8 V DC and current between 20 and 50 mA to determine their influence on surface degradation. Two modes of voltage transient are observed. The first has been linked to the formation of a MMB and the second to a delamination event (DE) where the contacts separate with no MMB apparent. Results are presented on the relative likelihood of the DE or the MMB events occurring. After 100k cycles at switching conditions of 4V, 20 mA the contact surface demonstrates negligible wear. Increasing the current (4 V, 50 mA) or the voltage (8 V, 20 mA) both increase the average energy associated with opening and the contact wear. The increase in MMB energy and wear with supply voltage is unexpected and is discussed.**

***Index Terms*—MEMS switching, hot switching, low current switching, contact wear.**

I. Introduction

A microelectromechanical system (MEMS) switch or relay is a metal-metal contact switching device with at least one dimension at the micrometer (μm) scale. The metallic conductors typically consist of thin-films (<1 μm) formed by microfabrication techniques. The ohmic contact presents advantages over capacitive MEMS and solid state switching devices alternatives [1-3]. It can transmit signals ranging from DC to the radio frequency (RF) range. Power loss in the transmitted signal (insertion loss) is low due to the minimal on-state impedance of a metal-metal interface, while the mechanical opening mechanism provides an 'air gap' in the off-state, giving excellent signal attenuation and a large ratio in the off-to-on impedance (isolation) [1].

Contact failure can generally be classified as either contacts sticking together, or by excessive increase in contact resistance [4, 5]. Gold (Au) provides excellent conductive properties and protection against corrosion; however, these properties are offset by its relatively softness, vulnerability to wear, and self-adhesion [5, 6]. The use of harder metallics with higher melting points, such as Tungsten or Ruthenium can enhance contact wear resistance [4, 7]; but have lower conductivity and thus provide a higher contact resistance. A proposed solution is the use of a composite contact material, consisting of compliant sub-layer of multi-walled carbon nano-tubes (MWCNT) with a coating of Au (Au/MWCNT). This has been shown to provide both low contact resistance and enhanced tolerance for wear [8]. The composite is able to deform at low force, allowing the contacts to conform to each other, increasing the area available for conduction [9]. The Au/MWCNT composite has also been shown to provide extended contact lifetime when the switch is operated while carrying a load ("hot switching") [10, 11].

Below the arcing-threshold voltage (~12 V) [12] hot switching wear is linked to a process of softening, melting and boiling of the metallic contact surface as the contact opens. The wear mechanism is described with reference to the ψ-θ relationship where ψ is electric potential and θ the temperature in a conductor [13]. The ψ-θ relationship is valid provided no heat is lost from the conductor and the system reaches a steady state. As the contact opens the current constriction leads to Joule heating and, provided the contact voltage is sufficient, causes softening and melting at the tips of the contacting asperities. This creates a molten-metal bridge (MMB) between the opening contacts. If the bridge boils it must rupture. In the Au/MWCNT contact this process results in a 'fine transfer' of contact material [11]. The softening, melting and boiling voltages for Au are given as ~0.08, 0.43, and 0.88 V respectively [14]. While individual MMB events can be highly variable between consecutive events, a good correlation has been shown between average MMB energy and the circuit current according to an i^2 relationship [15].

The MMB energy has been shown to be linked to changes in the surface texture [15], and to improve the performance of the Au/MWCNT surface it is important to understand the nature of

"The authors would like to thank the EPSRC for their support in this work which is funded in part by grant EP/M508141/1

the contact wear. To study the evolution of the wear process a MEMS switch testing system has been developed [16], to investigate in-situ changes occurring in the contact surface. The system is novel and for the first time allows an accurate description of how surface wear evolves with the number of switching cycles. The system resolves sub-micron scale surface change between individual switching events.

A previous study investigated 'hot' (with current) and 'cold', or 'dry', switching (without current), of Au sputter films [16]. The study showed that, under contact forces of 100 µN, cold switching wear was detectable after a single switching event with the wear presented as a region of Au film delamination. Surface wear was also detected after a single switching event under hot switched conditions of 4 V and 20 mA and contact closure force of 500 µN. The wear pattern differed from the cold switched case and shows as a ring-shaped area surrounding the contact in which there was evidence of the film softening, tearing and delaminating. A voltage waveform across the contact was detected that showed no evidence of MMB formation. The event was associated with much greater increase in surface roughness than seen with a MMB event and was described as a delamination event (DE). The test system is termed the In-situ Contact Evolution (ICE) apparatus and is used here to investigate the surface evolution of a Au/MWCNT contact under hot switching conditions. The contact surface is investigated over 100,000 switching cycles at a contact closure force of 500 µN. The effects of changing the circuit current between 20 and 50 mA, and circuit voltage between 4 and 8 V DC are reported.

II. Materials

The configuration and design of the contact surfaces are detailed in [17]. In this paper the upper contact is a precision ground 2 mm diameter stainless steel ball. The ball is sputter coated with a 20 nm layer of Cr to enhance adhesion of the 500 nm Au layer. The lower (planar) contact surface is a Au/MWCNT composite. The contact is manufactured on a SiO_2 on Si substrate that is sputter coated with a layer of Al_2O_3 followed by an Fe catalyst layer. Carbon nanotubes are grown in a thermal reactor to 50 µm height and sputter coated with a 500 nm Au layer. The Au penetrates into the top of the nanotube forest resulting in a metal-matrix-composite (MMC) material [18]. The composite provides an upper layer with conductive properties and contact resistance properties close to that of an Au thin-film coating. The carbon nanotubes provide a compliant sublayer allowing the composite to conform, increasing contact area and tolerance to mechanical damage.

III. Experimental Apparatus

The In-situ Contact Evolution (ICE) apparatus, has been developed from a commercial surface profiler [19] to allow the investigation of the contact surface and high frequency contact cycling for accelerated lifetime testing (up to 3 kHz). Contact cycling can be interrupted at any time to measure the contact surface profile, before the contacts are realigned to their original positions. A piezoelectric actuator provides the force to operate the switching mechanism. The mechanism has been designed so that the actuator can operate a MEMS scale cantilever for indirect contact operation; however, in this investigation the Au coated ball contact is mounted directly on the tip of the actuator for direct actuation of the switching mechanism.

The apparatus specifications are provided in Table 1. A schematic of the system operation is presented in Fig. 1.

TABLE I
In-situ Contact Evolution (ICE) Apparatus Specification

Measurement Principle	Vertical (Z) Resolution	XY Range	XY On-axis Accuracy	Sensor Spatial (XY) Resolution
Point Autofocus	10 nm	25 mm x 25 mm	±50 nm	<1 µm

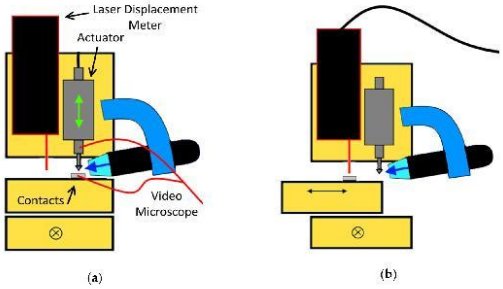

Fig. 1. A schematic of the In-situ Contact Evolution (ICE) Apparatus during a) switch cycling and b) measurement of the contact surface.

The actuator position is controlled by a square wave signal. A switching frequency of 0.5 Hz is used when capturing the contact opening voltage waveforms, 10 Hz when hot switching upto 10,000 cycles, and 200 Hz to 100,000 switching cycles and beyond. The square wave signal maximizes the velocity of the contact closure so providing the most mechanically demanding contact closure condition.

Static contact closure force is determined by calibrating the contact force to contact resistance for the contact pair. Contact force is measured by piezo quartz force transducer (Model 9207, Kistler AG, Switzerland) integrated to a separate apparatus previously described in [20]. In the ICE apparatus the initial contact position is adjusted until the contact resistance is achieved that corresponds to the calibrated contact force. The contact position is stabilized by an isolation system that damps vibration and stabilizes temperature to a variation of no more than ±0.2 ℃ in 24 hours. Contact resistance is measured using the 4-wire method. The voltage waveform at contact opening is captured using a high-speed oscilloscope. A detailed description of the ICE apparatus, its associated instrumentation, isolation systems and specification is given in [16]. In this experiment the force is set to 0.5 mN. The Au coated ball and Au/MWCNT contact pair are investigated under three different

TABLE II
Test Conditions

Test Name	Voltage and Current	Contact Force	Surface Measured at Cycles
4-20	4 V, 20 mA	500 µN	1-10, 100, 1k, 10k, 100k, 1M
4-50	4 V, 50 mA	500 µN	1-10, 100, 1k, 10k, 100k
8-20	8 V, 20 mA	500 µN	1-10, 100, 1k, 10k, 100k

hot switched conditions summarized in Table II. The switching process is interrupted to measure the contact surface and contact resistance. The first 10 cycles are measured. Measurements are then repeated at 100, 1k, 10k and 100k cycles. For convenience the test conditions are referred to by the voltage and current as the 4-20, 4-50 and 8-20 cases.

The MMB energy, and the contact opening waveform are captured for 150 consecutive events immediately after surface measurement. The contact waveform is classified as a MMB if the contact potential rises to the melting and boiling voltages associated with Au. Where the potential across the contacts rises from the voltage drop associated with the closed contact resistance, to above 3 V without apparent transition to the levels for melting or boiling the opening is termed a delamination event (DE) [16]. The time resolution of the waveform is 200 ns. Fig. 2 shows a waveform characteristic of the MMB and the DE. The energy associated with the MMB waveform is calculated by integration of the area under the waveform.

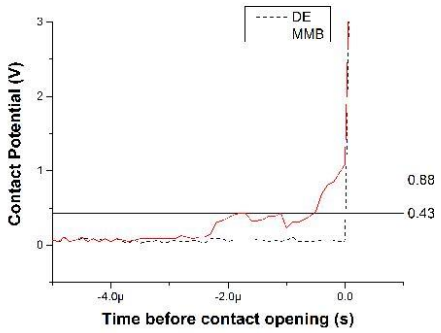

Fig. 2. Voltage waveforms across the contacts immediately before contact opening. The solid red line is characteristic of a MMB event, the dashed black line is termed a DE event. The DE has previously been associated with a greater level of surface damage than the MMB type in Au/Si contacts [16].

IV. Results

The change in contact resistance over the testing period is presented for each case in Fig. 3. All three switching conditions show a decrease in contact resistance after a single hot switching cycle. Over the first 10 cycles the contact resistance shows a degree of variability, as expected as the two surfaces start to conform. After the first 10 cycles the contact resistance is sampled at logarithmic decades of switching cycles and shows a stable contact resistance between 0.34 and 0.39 Ω, at 100k cycles.

Fig. 4 shows the number of molten metal bridge (MMB) and delamination events (DE) recorded over consecutive cycles at each decade of contact cycling expressed as the percentage of MMB events observed. A decreasing percentage of MMB therefore indicates increasing numbers of DE. It is important to note that the resolution of the waveform capture is 200 ns and any MMB events of shorter duration are classified as a DE. At each sample interval 150 consecutive opening events are sampled, except at 10 cycles, where only the first 10 cycles are evaluated. Both the 4-20 and 4-50 cases show a decrease in the percentage of MMB events at 10k cycles before increasing at 100k cycles. It is interesting to note that for the 4-20 case, at 10k cycles there are only 10% of events that are MMB, implying that 90% of the opening event occur without the representative waveform shown in Fig. 2. For the other examples although the MMB event waveform is the most common there are high percentages of events with the DE type waveform.

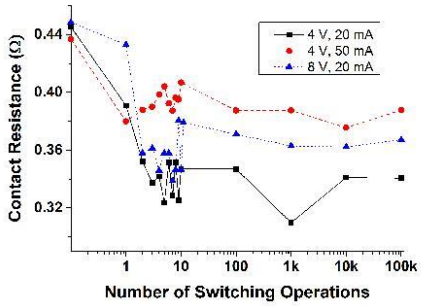

Fig. 3. The evolution of contact resistance with number of switching cycles for circuit conditions of 4V 20mA, 4V 50mA and 8V 20mA.

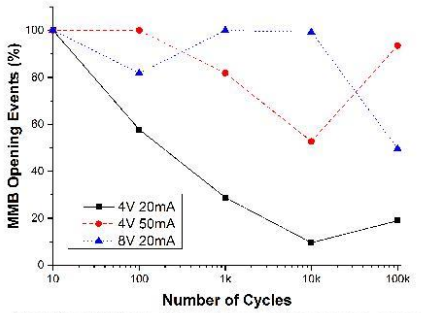

Fig. 4. The ratio of MMB to DE events over 150 consecutive cycles at 4V 20mA, 4V 50mA and 8V 20mA.

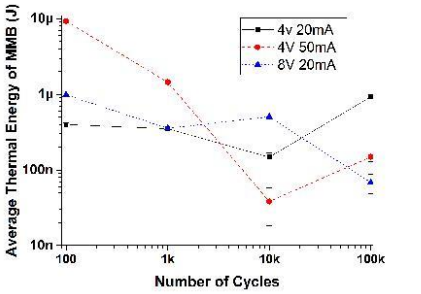

Fig. 5. The average thermal energy associated with a MMB opening event for circuit conditions of 4V 20mA, 4V 50mA and 8V 20mA.

The average MMB energy associated with the contact opening event is presented in Fig. 5, only for the waveforms where the MMB is present. The associated thermal energy is calculated by integration of the area under the transient voltage waveform illustrated in Fig. 2 and the average value is presented. The error bars represent the maximum-minimum energy of an MMB within the sampled data.

The 4-20 case shows relatively stable energy with increasing switching cycles to 100k cycles. This is as expected, as the Au/MWCNT contact has demonstrated lifetimes in excess of 70M cycles at these circuit conditions [20]. In both the 4-50 and 8-20 cases there are general trends for the average energy to decrease with increasing contact cycles. The overall average thermal energy (from evaluations at 100, 1k, 10k and 100k switching cycles) for the 4-20, 4-50 and 820 cases are 0.13, 2.65 and 1.69 µJ respectively. The average energy value 2.65 µJ for the 4-50 case is in keeping with the values presented by Lewis *et al.* under the same circuit conditions of 1.54 µJ during the stable lifetime [10]. The primary differences for this investigation are the use of a greater contact force here (500 vs 35 µN) and a ball contact instead rather than a cantilever beam contact. A significant observation is that increased circuit voltage results in increased MMB energy over the first 10k switching cycles (4-20 cf. 8-20). This is interesting as the circuit voltage has not previously been linked to the MMB energy. The 4-50 case shows the highest overall average energy as expected. When compared to the 4-20 case the increase in MMB energy is proportional to an i^2 relationship. It is also noted that the trend of the energy in the 4-20 and 4-50 cases follows a similar pattern to the percentage of MMB openings in Fig. 3.

The areal (3-D) surface roughness, S_a of the contact surface is presented in Fig. 6, as a function of the number of cycles. The surface S_a parameter is the 3-d (areal) surface roughness. S_a is the absolute arithmetic absolute average of surface heights in the evaluation area, defined in (2). The S_a parameter is used as the mean average provides a highly stable parameter to quantify surface texture; however, S_a only evaluates amplitude changes of the surface (height) and does not evaluate the scale (spatial frequency) of the texture

$$S_a = \frac{1}{A}\iint_A |z(x,y)|\ dxdy \qquad (2)$$

The evaluation area, A of 150 µm (x) by 150 µm (y) is measured for height (z) at equally spaced 250 nm intervals (361,201 data points). The surface is levelled according to a linear least squares plane-of-best-fit to the surface data. The zero datum in Fig. 6 for surface roughness is defined as the S_a value for the new un-switched surface. All switching conditions demonstrate an increase in surface roughness from the very first hot switched cycle. Over the first 10 cycles the trend is for surface roughness to vary slightly and stabilize. This shows a similar, but inverted, trend to the evolution of the contact resistance in Fig. 3. The largest overall increase in roughness in the first 10 cycles is 27 nm. The average roughness change is an increase of 12 nm. The 4-20 case demonstrates stable surface roughness to 100k switching cycles, with a small overall increase of 9 nm. Both the 8-20 and 4-50 cases show progressive increase in surface roughness with switching cycles. The 4-50 case increases in roughness more rapidly (by 185 nm after 100k cycles). The 8-20 case follows the same trend but shows a lower increase in surface roughness (116 nm after 100k cycles).

The evolution of the contact surface height distribution is presented in Fig. 6. Each image represents a plan view of the Au/MWCNT surface over a 150 µm by 150 µm region. To clearly indicate the location of the highest surface peaks (contact asperities) and deepest troughs (locations of wear), the height scale is restricted to three colors – points higher than 5 µm (peaks) are white, with points lower than -5 µm (troughs) black. All other heights are shown as grey. Each column represents a switching condition and each row compares the same number of switching cycles.

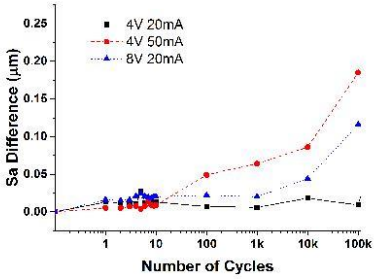

Fig. 6. The change in S_a surface roughness with number of switching cycles for circuit conditions of 4V 20mA, 4V 50mA and 8V 20mA. Zero roughness is defined at the surface roughness before any switching has occurred.

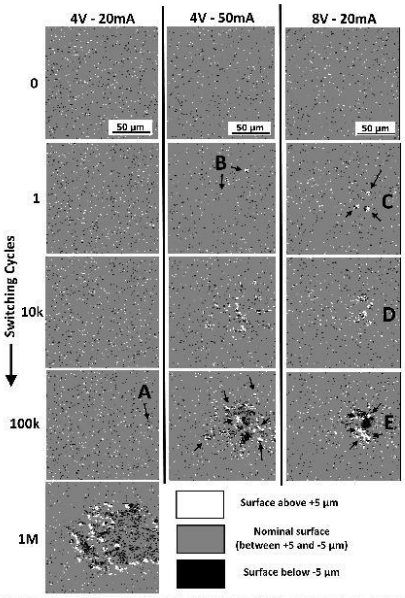

Fig. 7. Surface height maps of the 0.15 mm by 0.15 mm contact region of the Au/MWCNT contact surface switched at (left) 4V 20mA, (middle) 4V 50mA and (right) 8V 20mA. The surface height map is shown after 0 (before switching), 1, 10k and 100k hot switched cycles. The location of peaks (above + 5 µm) are shown in white, with troughs (below -5 µm) shown in black. The remaining surface is shown as grey.

Both the 4-50 and 8-20 cases show measurable features after only a single switching operation, labelled B and C respectively. Features B and C shows circular regions 3-6 µm in diameter. The edges are raised ~5 µm above the nominal surface on one side and depressed ~ 5 µm below the surface on the opposite side.

In the 4-50 case there are two raised features separated by ~ 60 µm (feature B), while the 8-20 case shows three features separated by approximately 30 µm (feature C). After 10k cycles features are apparent at the same locations; however, the features show greater evidence of wear. In the 4-50 case the wear is described by features that are around 5 µm in height spread over a region approximately 100 µm in diameter. After 100k cycles a similar wear region and distribution of high points is seen to 10k cycles; however, there are significant areas where the surface has been penetrated by 5 to 6 µm. The wear region is irregular, made up of 4 or 5 sub-regions.

The 8-20 case shows a smaller region of wear when compared to the 4-50 case after 10k cycles. The features of 8-20 are however broadly similar with a single significant difference, labelled feature D (Fig. 7). Feature D presents as a donut shaped region ~ 10 µm in diameter but the edges show a significant increase in height. After 100k cycles the 8-20 case shows multiple areas raised ~20 µm above the nominal surface, labelled feature E with arrows. A donut feature is still apparent at the previous location of feature D. In the 8-20 case the most apparent change after 100k cycles is a region of continuous wear of 5 to 6 µm in depth. The 4-20 case demonstrates negligible wear to 100k cycles.

Fig. 8 shows the volume of the asperities tips with switching cycles. The calculation is performed using commercial surface analysis software (Boddies 2.18, TaiCaan Technologies, UK). The volume is defined by a plane 5 µm above the nominal surface and any surface above this height. It therefore describes the total volume of the features shown in Fig. 7 as white. The unswitched surface (i.e. 0 cycles) is plotted as 0.1 cycles on the logarithmic axis for convenience.

After a single switching cycle all three cases show a measurable increase in the asperity volume, before a small decrease after 100 cycles. From 100 to 100k cycles the 4-20 case shows a consistent volume but the 4-50 and 8-20 cases show an increase in volume, with the 8-20 case showing the greatest increase.

Fig. 9 shows the surface height map of the Au/MWCNT contact after 100k cycles. In each image a 150 µm x 150 µm area of the contact surface is shown. The surface height in each image is linked to the same ± 6 µm colour scale and relates to the 100k cycles 'row' in the Fig. 7. The dotted line indicates the location of the inset 2-D cross section. The scale of the cross section a 150 µm length and 40 µm in height in each image.

After 100k cycles the 4-20 case shows minimal surface change while both the 4-50 and 8-20 case show significant evidence of wear. The 8-20 case shows the surface wear is confined to a smaller area than the 4-50 case, with the 2-D cross section showing the peaks higher (~20 µm v. 10 µm) and less numerous. In the 8-20 case the highest peaks are located immediately at the perimeter of the material loss region, while in the 4-50 case they are spread out and occur mostly in regions with no obvious material loss.

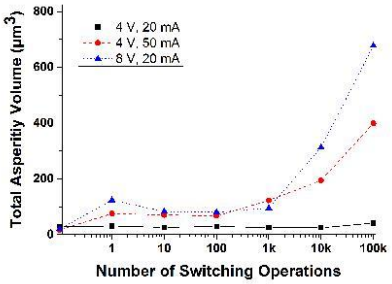

Fig. 8. The total asperity tip volume above a 5 µm datum plane for conditions of 4V 20mA, 4V 50mA and 8V 20mA.

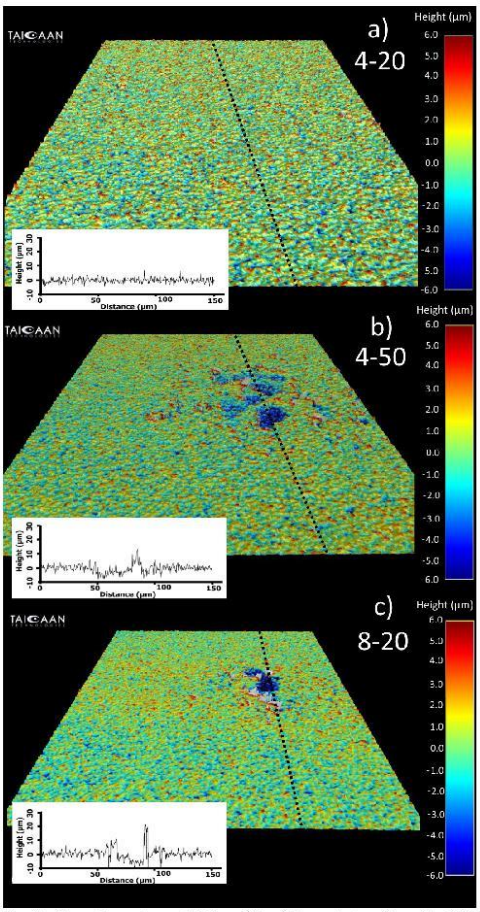

Fig. 9. The colour enhanced 3-D profile of the contact surface after 100,000 hot switched cycles for the (a) 4-20, (b) 4-50 and (c) 8-20 cases. The contact region is 150 µm by 150 µm. The colour scale represents regions of height difference. A 2-D cross section along the black dotted line is inset to each image at the same scale.

V. Discussion

Both MMB and DE type openings are observed under all three circuit conditions. The frequency of the MMB and DE events show variability, but as previously noted the 4-20 case shows the highest occurrence of the DE events (Fig. 4), the least variability and lowest overall average MMB energy (Fig 5.). The frequent occurrence of the DE waveform is unexpected, as in a previous study of Au/Si contacts it was associated with the delamination and tearing of the conductive film and greater increase in surface roughness, when compared with MMB events [8, 16]. In the case of Au/MWCNT contact materials it was previously observed that delamination occurred after the contact surface was worn to a thinner Au layer by the MMB process [8]. The increased current (4-50) and voltage (8-20) cases both show much greater evidence of surface change, and an increased number of MMB events with a higher average opening energy than the 4-20 case. In the 4-50 case this is the anticipated result, with the MMB energy linked to Joule heating and therefore an i^2 relationship. The 2.5-fold increase in circuit current between the 4-20 and 4-50 cases is expected to result in a 6.25-fold increase in the thermal energy. This trend is broadly observed as the ratio of the MMB energy between the 4-20 and 4-50 cases (Fig. 5). The increased voltage case (8-20 cf. 4-20 case) was not expected to show an increase in the opening energy or surface wear. It was previously shown during investigation of a rough and smooth Au/MWCNT surface that for the same circuit conditions the rougher surface demonstrated a higher energy associated with the MMB [15]; however, there is no clear explanation for the increase in surface wear with an increase in circuit voltage below the arcing threshold. The previous investigation showed no consistent correlation between the circuit voltage and the energy associated with the MMB over a range of 4 to 12 V; however, a much lower number of switching cycles were evaluated and a slight increase in the MMB energy was observed between conditions of 4V, 50 mA and 8V, 50 mA [15]. This is a subject for future investigation.

Surface changes are detected in each case with new surface features detectable after only a single switching cycle in both the 4-50 and 8-20 cases. The 8-20 case demonstrates a more concentrated region of wear to the 4-50 case, with the surface material depleted and drawn into peaks (Fig. 9) that are observed after a single switching operation (Fig 7). The surface roughness alone does not clearly describe the differences in the surfaces; however, it is quantified by surface asperity volume. Previous investigation has shown the transfer of Au contact material is always observed from the Au/MWCNT to the Au contact, and independent of polarity or gravity [10]. The mechanism proposed is differential cooling in the MMB caused by the material properties of the contacts resulting in asymmetrical MMB rupture. The wear observed in this study suggests that the rupture occurs towards the Au contact. The dimensions of the peak features shown (Figs. 7 and 9) are suggestive of the dimensions of the MMB formed. These are in agreement with previous observation, with the significant difference that a much lower current has been used in this investigation (20 to 50 mA vs 10 to 100 A) [21].

VI. Conclusion

The paper demonstrates the ability of a novel MEMS contact testing system to determine small scale wear features associated with molten metal bridge phenomena (MMB) between the opening contacts. The system shows a high sensitivity such that wear from a single hot switching cycle (4V- 20 mA) can be measured.

The result of testing three switching conditions over a number of cycles (up to 1 Million), has shown, as follows;

1. A stable contact resistance between 0.34 and 0.39 Ω
2. The percentage of events where there is no apparent MMB. This observation is important and was previously also observed on Au/Si contacts [13]. For the 4 V, 20 mA condition only 30% of the opening events experience a MMB, after the initial switching period.
3. In a further new observation, the supply voltage, increasing from 4 V to 8 V, with 20 mA has been shown to have an influence on the surface wear. The MMB phenomena is not normally linked to the supply voltage. This unexpected result is shown in an analysis of the wear regions, by evaluating the asperity tip volume 5 µm above a datum plane fitted to the unworn surface. There is no clear explanation for this result, which will be explored in further investigations.

Acknowledgment

The authors wish to express thanks to Kevin J. Cross for pre-release access a beta version of Boddies Extreme software paper (BEX 1.0.14, TaiCaan Technologies, UK) used for surface analysis and image rendering.

References

[1] G. M. Rebeiz, *RF MEMS: theory, design, and technology*: John Wiley & Sons, 2004.

[2] G. M. Rebeiz, and J. B. Muldavin, "RF MEMS switches and switch circuits," *IEEE Microwave magazine,* vol. 2, no. 4, pp. 59-71, 2001.

[3] H. Shen, S. B. Gong, and N. S. Barker, "DC-Contact RF MEMS Switches using Thin-Film Cantilevers," *2008 European Microwave Integrated Circuits Conference (Eumic)*, pp. 382-385, 2008.

[4] B. F. Toler, R. A. Coutu, and J. W. McBride, "A review of micro-contact physics for microelectromechanical systems (MEMS) metal contact switches," *Journal of Micromechanics and Microengineering,* vol. 23, no. 10, Oct, 2013.

[5] T. V. Laurvick, and R. A. Coutu, "Improving Gold/Gold Microcontact Performance and Reliability Under Low-Frequency AC Through Circuit Loading," *IEEE Transactions on Components, Packaging and Manufacturing Technology,* vol. 7, no. 3, pp. 345-353, 2017.

[6] M. Libansky, J. Zima, J. Barek, A. Reznickova, V. Svorcik, and H. Dejmkova, "Basic electrochemical properties of sputtered gold film electrodes," *Electrochimica Acta,* vol. 251, pp. 452-460, 2017.

[7] A. Basu, G. Adams, and N. McGruer, "A review of micro-contact physics, materials, and failure mechanisms in direct-contact RF MEMS switches," *Journal of Micromechanics and Microengineering,* vol. 26, no. 10, pp. 104004, 2016.

[8] J. W. McBride, H. Liu, C. Chianrabutra, and A. P. Lewis, "The Wear of Hot Switching Au/Cr-Au/MWCNT Contact Pairs for MEMS Contacts," *Ieice Transactions on Electronics,* vol. E98c, no. 9, pp. 912-918, Sep, 2015.

[9] M. P. Down, L. Jiang, and J. W. McBride, "Investigating the benefits of a compliant gold coated multi-walled carbon nanotube

contact surface in micro-electro mechanical systems switching," *Applied Physics Letters,* vol. 107, no. 7, Aug 17, 2015.

[10] A. P. Lewis, J. W. McBride, and L. Jiang, "Evolution of Voltage Transients During the Switching of a MEMS Relay With Au/MWCNT Contacts," *Components, Packaging and Manufacturing Technology, IEEE Transactions on,* vol. 5, no. 12, pp. 1747-1754, 2015.

[11] J. McBride, "The wear processes of gold coated multi-walled carbon nanotube surfaces used as electrical contacts for micro-electro-mechanical switching," *Nanoscience and Nanotechnology Letters,* vol. 2, no. 4, pp. 357-361, 2010.

[12] K. L. Kaiser, *Electromagnetic compatibility handbook*: CRC press, 2004.

[13] R. Holm, *Electric contacts: theory and application*: Springer Science & Business Media, 1958.

[14] P. G. Slade, *Electrical Contacts: Principles and Applications, Second Edition*, p.^pp. 1311: CRC Press, 2014.

[15] T. Bull, and J. Mcbride, "The Influence of Circuit Parameters on Molten Metal Bridge Energy in a MEMS relay testing platform," *Proceedings of 2016 Twenty Eighth International Conference on Electrical Contacts*, 2016.

[16] T. G. Bull, and J. W. McBride, "In-Situ Contact Surface Characterization in a MEMS Ohmic Switch under Low Current Switching," *MDPI Technologies,* vol. 2, no. 6, pp. 47, 2018.

[17] J. McBride, E. Yunus, and S. Spearing, "Improving the contact resistance at low force using gold coated carbon nanotube surfaces," *The European Physical Journal Applied Physics,* vol. 50, no. 1, pp. 12904, 2010.

[18] H. Liu, J. W. McBride, and M. Z. M. Yusop, "Surface characterization of a Au/CNT composite for a MEMS switching application." pp. 751-754.

[19] "Taicaan Technologies Xyris 4000," 29th March 2018; http://www.taicaan.com/xyris-4000/.

[20] J. W. McBRIDE, C. Chianrabutra, L. Jiang, and S.-H. Pu, "The contact resistance performance of gold coated carbon-nanotube surfaces under low current switching," 2012.

[21] M. Price, and F. L. Jones, "The electrical contact: the properties and rupture of the microscopic molten metal bridge," *Journal of Physics D: Applied Physics,* vol. 2, no. 4, pp. 589, 1969.

IEEE Holm Conference 2019

The in-situ wear of a hot and cold switched Au on Au coated MWCNT electrical contact for a MEMS switch application

J.W.McBride
Dept of Mechanical Engineering
University of Southampton Southampton, UK
jwm@soton.ac.uk

T. G. Bull
Dept of Mechanical Engineering
University of Southampton Southampton, UK
tb10g11@soton.ac.uk

***Abstract*— The electrical contacts in metal-metal MEMS switches are normally made from thin (< 1 µm) metallic film, e.g. (Au). The low contact force in a MEMS device results in a small area for conduction; to increase the area, a composite contact material has been developed. Sputter coated Au, applied to vertically-aligned multi-walled carbon nanotubes, (Au-MWCNT composite), has been shown to increase contact area and extend switching lifetime by orders of magnitude. In this study the Au-MWCNT composite contact is paired with a Au coated hemisphere contact under a contact force of 150 µN, in an In-situ Contact Evolution (ICE) apparatus, to evaluate the durability of the contacts for two DC switching conditions; cold switching, at 4 V, 4 µA, (16 µW) and hot switching at 4 V, 50 mA (200mW). Under cold switching the contacts are shown to maintain a low stable resistance for 4 Billion cycles. The result leads to a re-evaluation of an established fine transfer model, used to predict switching life times.**

Keywords—MEMS switching, cold switching cycles, fine transfer model.

I. INTRODUCTION

A micro-electro-mechanical system (MEMS) switch or relay normally uses metallic thin film conductors formed by microfabrication techniques. These devices are partially limited by the durability of the electrical contacts. They are expected to be used to transmit signals ranging from DC to the radio frequency (RF) range. In the RF application, power loss in the transmitted signal (insertion loss) is low due to the minimal on-state impedance of a metal-metal interface, while the mechanical opening mechanism provides an 'air gap' in the off-state, giving excellent signal attenuation and a large ratio in the off-to-on impedance (isolation) [1,2].

Whilst MEMS relays boast a number of advantages over PIN and FET devices, notably the high isolation, low on-resistance and excellent frequency performance, one of the major disadvantages of MEMS relays is that the electric contacts are prone to failure [3,4]. With no or low (< 0.5 mA, < 0.2 V) electrical load conditions referred to as "cold switching" the lifetime may reach billions of cycles; however failure occurs sooner with the application of higher electrical loads (> 0.5 mA, > 1 V), referred to as "hot switching" [5]. A recent investigation using a full MEMS device, with RF hot switching a Au-CNT composite contact registered limited life-time of 1,000's of cycles, [6], as an improvement over the metal-to-metal interface. There are limited studies comparing the DC and RF performance of MEMS devices; but in a micro relay study, a good performance with RF loads up to 37 W at frequencies up to 3 GHz, was noted, [7].

Contact failure mechanisms at these low voltage (<12 V) and low current (<1 A) conditions, be can be classified as either; adhesion, where the contacts stick; or by an excessive increase in contact resistance, [5,8]. Gold (Au) provides excellent conductive properties and protection against corrosion; however, these properties are offset by the relatively softness, vulnerability to wear, and self-adhesion [9,10]. The use of harder metallic surfaces with higher melting points, such as Tungsten or Ruthenium can enhance contact wear resistance [3,4]; but have lower conductivity and thus a higher contact resistance.

A possible solution to the durability issue has been developed using a composite contact material, consisting of compliant sub-layer of vertically aligned multi-walled carbon nano-tubes (MWCNT) with a coating of Au, generally referred to as Au/MWCNT or simply Au/CNT (in this paper), shown in Fig.1. This has been shown to provide both low contact resistance and enhanced tolerance for wear, [5,11-14]. Under "hot switching" with a DC power supply of 4 V and 10 mA, a MEMS test device was tested to 0.5 Billion operations without failure in [13]. The material is yet to be tested in a full MEMS device but a similar composite material using non-aligned nano-tubes has been investigated in a real device in [6], where the benefits to the durability were not significant. This suggests that the alignment of the carbon nano-tubes is very important for the improved performance. Using the vertically aligned CNT structure the composite deforms, allowing the contacts to conform to each other, increasing the area available for conduction [12].

A. The Fine Transfer Mechanism under DC conditons

Below the arcing-threshold voltage (~12 V) surface wear, defined in [14] as "fine transfer", is linked to a process of softening, melting and boiling of the metallic contact surface as the contact opens, referred to as molten metal bridge (MMB) phenomena, shown schematically in Fig.2. The wear mechanism is described with reference to the ψ-θ relationship where ψ is electric potential and θ the temperature in a conductor, [14]. The softening, melting and boiling voltages for Au are given as ~0.08, 0.43, and 0.88 V respectively. The wear process results in a preferential transfer between the opening contacts, when the molten bridge breaks. For the composite surface studied here the direction of fine transfer has been shown to be from the Au/CNT surface to the Au ball surface, irrespective of the circuit polarity. In addition to the fine transfer mechanism a delamination process has also been described, where small elements of the surface are torn from the coating, by an adhesion process, [15]. This was explored

in [11], where it was shown that the addition of a Cr adhesive layer on the metallic ball contact had a significant influence in reducing the delamination of the ball. It was observed in [15] that some opening transient voltages did not show the characteristic softening and melting voltages. These instant openings have been attributed to the delamination phenomena, where an asperity scale element of the surface film is removed and transferred to the ball contact. The delamination phenomena has been linked to a process where the MMB phenomena first thins the Au upper coating before the delamination occurs, and thus would be related to the current level. Higher currents would thin the upper surface more quickly, leading to a more rapid breakdown once the delamination starts, [14].

B. *Fine Transfer Model*

An increase in contact resistance, leading to a failure condition, during the fine transfer process [14], was shown to occur when the Au upper surface of the Au/CNT composite had depleted to such an extent that the conduction path was no longer through the Au but through the CNT surface. The surface area of the depleted region was measured and from this, for a known value of the thickness of the Au layer, a maximum volume of material transferred was determined (V_{max}). A model for the fine transfer process was then proposed, where for a given current loading (I) and for a known number of cycles to failure, (N_f);

$$N_f = \frac{V_{max}}{k\, I^2} \qquad (1)$$

where k, is determined experimentally for one condition and then applied for all other conditions. In [14] the conditions used for the definition of k, were, 4 V, 20 mA with a contact force of 1 mN. The contact material used was similar to that used in this work, (50 µm high CNT sputter coated with a 500 nm Au). In Eq. (1) it is assumed that the transfer of material is only driven by the DC power and therefore proportional to I^2.

In this paper the durability of the Au/CNT surface is explored further. To enable this and to provide a detailed study of the wear processes in MEMS contacts an In-situ Contact Evolution (ICE) apparatus is used, [15]. The system was used in [16] to conduct a preliminary study of the influence of the DC power on the wear of the Au/CNT surface. It was shown that an increase in the supply voltage used (from 4 to 8 V) increased the fine transfer process. This unexpected result suggests a further layer of complexity in the fine transfer mechanism described in Eq. (1).

There are two studies undertaken here, all under DC conditions with a fixed contact force of 150 µN. The first is a bench-mark test under "near" cold switching conditions, 4 V and 4 µA (16 µW) and the second a hot switching test, at 4 V and 50 mA (200 mW).

II. Methodology

A. *In-situ Contact Evolution (ICE) apparatus*

The ICE testing platform, [15,16], utilises a commercial metrology frame [17] for stability, integrating a 3D laser profiling system into the testing platform such that after a set number of cycles the contact surfaces can be separated and measured before returning the surfaces to the same switching position to allow the switching tests to continue. The positioning system provides on-axis repeatability of better than ± 50 nm in each axis. The system has been demonstrated on a flat Au coated Si substrate mated with a Au coated ball, (1mm radius), and shows the ability to measure wear after a single switching cycle under "cold switching" conditions, [16].

To undertake this study in reasonable time limits, the samples need to be cycled at a high frequency. In [13] testing was conducted with a self actuated cantilever, cycling at 100 Hz; at this frequency the 0.5 Billion cycles were completed in 58 days. In this study switching is conducted at 1.1 kHz. Arriving at 0.5 Billion DC switching cycles in <5 days

A piezoelectric actuator provides the force to operate the switching mechanism, and has been designed so that the actuator can operate a MEMS scale cantilever for indirect contact operation. In this investigation because of the high frequency testing (1.1 kHz) the ball contact is mounted directly on the tip of the actuator, therefore reducing the dependency on the dynamic response of a cantilever. A schematic of the system operation is shown in Fig. 3, where the actuator switching is shown in (a), and in (b) the two lower X,Y stages, allow for the surface to be moved under the laser for the measurement of the contact surface (CS).

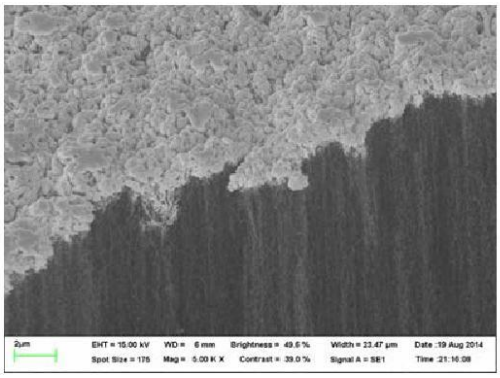

Fig. 1. Au/CNT surface showing the Au coating at the dge of the sample, with Au penatrtion into the CNT surface.

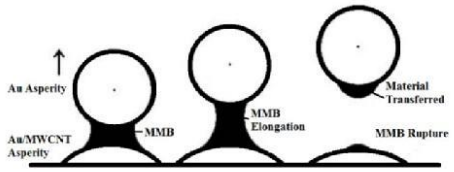

Fig. 2. The fine transfer model showing the molten metal bridge as the contacts open.

B. *Contact Materials*

The upper contact is a 2 mm diameter stainless steel ball, sputter coated with a 20 nm layer of Cr to enhance adhesion of the 500 nm Au layer, [11]. The lower (planar) contact surface is a Au/CNT composite, shown in Fig.1. The contact is manufactured on a SiO_2 on Si substrate that is sputter coated with a layer of Al_2O_3 followed by an Fe catalyst layer. Carbon nanotubes are grown in a thermal reactor to 50 µm height and sputter coated with a 500 nm Au layer, referred to as a 505

surface, [18]. The Au penetrates into the top of the nanotube forest resulting in a metal-matrix-composite material. The composite provides an upper layer with conductive properties and contact resistance properties close to that of an Au thin-film coating. Carbon nanotubes provide a compliant sublayer allowing the composite to conform, increasing contact area, [19]. A (505) Au/CNT sample is used for both experimental conditions, with the point of contact moved and the upper ball contact changed between experiments.

C. *Contact Force and Resistance*

Contact force measurement is not included in the ICE apparatus. The force is determined from a calibrated force, contact resistance relationship for the 505 material shown in Fig. 4; where the force is measured by a transducer (Model 9207, Kistler AG, Switzerland) integrated to a second apparatus previously described in [15].

The ICE apparatus is mounted on anti-vibration table in a temperature controlled environment 22 ± 0.2 °C. The contact resistance (CR) is measured using the 4-wire method, allowing the contacts to settle over a 30 second period. The initial contact resistance is below 1 Ω and the failure condition defined as occurring when the resistance increases significantly higher than 3 Ω. Previous studies have shown that at failure the CR increases to a high value (10's Ω) over a short duration of cycling, [13,15].

D. *Experimental Conditions*

Experiment 1). DC, Cold switching test.

To determine the cold switching performance of the 505 surface, the sample is tested at 1.1kHz, with a DC resistive load, 4 V, 4 µA. At this level the MMB bridge phenomena will be minimal and the sample expected to maintain a low resistance (CR) for Billions of switch cycles. The sample surface (CS) was measured at 0, cycles, and then every Billion cycles. With resistance (CR) measured at 100 Million cycles intervals. The contact force was maintained using a fixed displacement of the ball contact.

Experiment 2). DC, Hot switching test.

A new contact ball is used at a new Au/CNT surface location, on the same 505 sample. As the MMB transient voltage will be present in the test the switching frequency is dropped to 300Hz, so that the MMB process has time to complete. The load is DC resistive 4V, 50 mA, for bench marking with previous experiments under similar conditions, [13].

In [13], using a low force 30 µN MEMS actuated cantilever, the contacts failed under the same DC conditions at 28 Million cycles. In this experiment the initial force was set at 150 µN and adjusted after each CS measurement, such that the initial CR was maintained. This implies that the ball contact displacement increased and the force will correspondingly increase slightly with the number of cycles.

E. *Measurement of Volumetric Wear*

The measurement of the contact surface (CS) using the ICE apparatus is undertaken with 0.5 µm spatial and 10 nm height resolution, in the same metrology fame. This allows the subtraction of the CS surface before the test from the measured surface without the need to align data. The subtraction of the surface allows the form of the surface to be removed and the resulting surface is the difference and therefore the material removed. The data is processed using BEX, commercial software [17], allowing the evaluation of the volume of material below a datum surface to be measured directly. This is an improvement over the methodology used in [14], where only the area was measured, and the thickness of the film assumed.

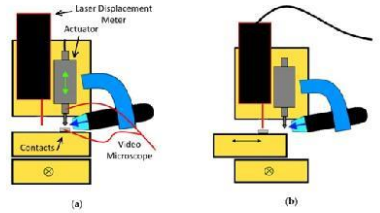

Fig. 3. In-situ Contact Evolution (ICE) Apparatus during, a) switch cycling and b) measurement of the Au/CNT contact surface (CS).

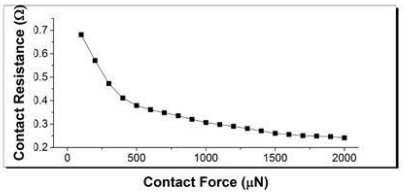

Fig. 4. The relationship between CR and contact force for the 50 µm high CNT, sputter coated with a 500 nm Au, or (505) surface

III. Results

A. *Experiment 1, 4 Billion cylces, DC cold switching, 1.1 kHz, at DC 4 V, 4 µA.*

There are no MMB events measured in the transient voltage, sampled at 10 MHz. The full period of 1 cycle is 900 µsec. Fig 5, shows the CR result for the surface. The initial resistance is 0.4 Ω and this is shown to gradually increase with the number of cycles. The test programme was halted at 4 Billion switching cycles after 40 days without surface failure, as defined by an increase in CR above 3Ω.

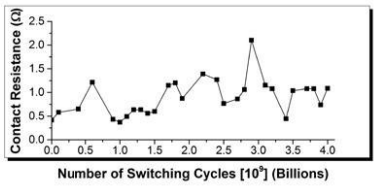

Fig. 5. Contact Resistance (CR) with cold switching cycles. DC Cold switching, at 1.1 kHz, 4 V, 4 µA.

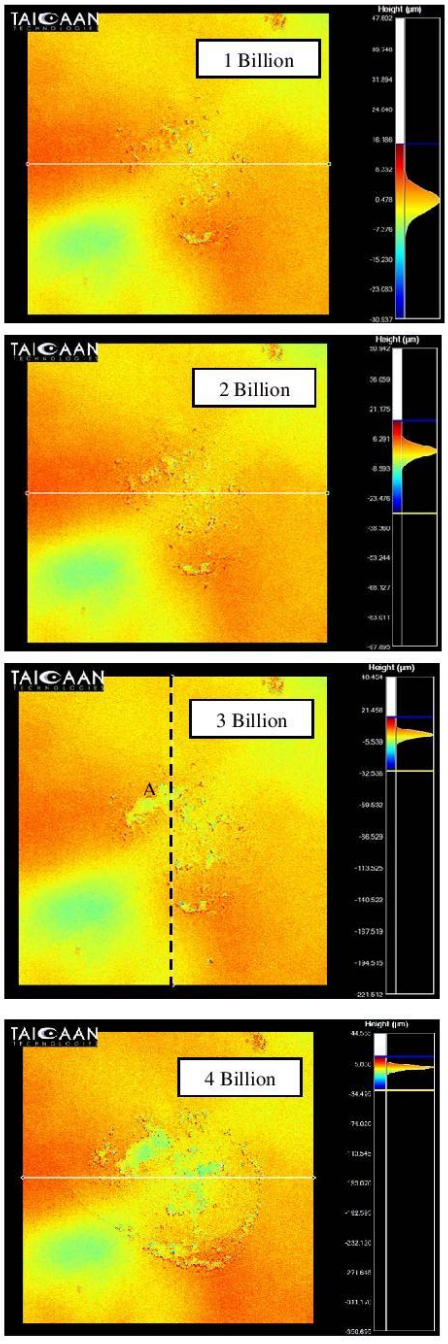

Fig. 6. The evolution of the Au/CNT surface measured in the ICE in a sequence of 1-4 Billion switching cycles, switching at DC 4V and 4 µA, (Cold switching). Each data set, is 1001x1001 data over 0.5mm x 0.5mm, leveled and the colour scale set, +15 to -30 µm.

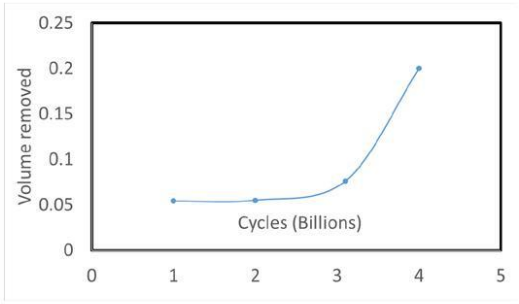

Fig. 7. Experiment 1; Cold switching 4 V, 4 µA volume of surface removed from Au/CNT (x10^{-3} mm^3) with switching cycles (Billion).

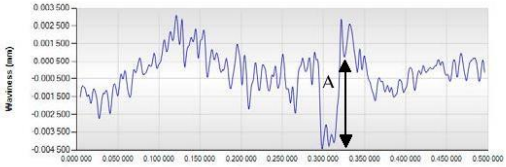

Fig. 8. Cross section of Fig 6, (at 3 Billion cycles) using the vertical central line shown, with a 8 µm Gauss (waviness) filter to smooth the surface.

Fig. 6, shows the evolution of the contact surface (CS), where there is a gradual increase in the wear with switching cycles. The wear is apparent within the central region for all images, with an approximate 150 µm radius. At 4 Billion cycles the outer ring of the contact region is apparent.

Fig. 7, is the removal of volume from the surface with the number of cycles. As the Au layer depletes the CR increases as more of the current flow occurs through the CNT surface.

Fig. 8 is a cross section of the data for 3 Billion cycles fitted with a 8 µm gaussian filter to remove the high spatial frequency surface components associated with the tops of the CNT, shows that the surface is degraded by a 5 µm removal of the upper surface at A, and this is consistence for the other areas of wear on the surface, as with previous observations of the Au/CNT surface, [7].

B. Experiment 2. DC hot switching, 300 Hz, 4 V, 50 mA

In this study the power switched is increased to 0.2 W, DC hot switching (4 V and 50 mA), compared to 16 µW, cold switching in Experiment 1. The surface evolution is shown in Fig 9 and the CR in Fig. 10. The MMB events associated with hot switching lead to a more rapid degradation of the Au/CNT surface, when compared with experiment 1, Fig 6. The 140 Million cycles reached in this test exceeds previous testing at this current level (50mA), [13], where an actuated MEMS cantilever was tested to failure at 28 million cycles.

In this comparative test, the key difference with the data in [13] is the contact force; 150 µN used here, compared to 35 µN in [13]. It is also noted that in [13] the contact surface was nominally a flat on flat, although due to alignment issues this was realised as a line contact. In this experiment we are using the more common ball on flat arrangement.

The volume change of the surface has been evaluated after fitting a 1mm radius reference surface to the deformed surface

in Fig. 9 at the end of the test, the volume removed is 0.154 ($x10^{-3}$) mm^3. The deformation of the surface is evidenced in cross section after 10 Million cycles, where the central region is deformed by 8 µm, as shown for the CS after 10 Million cycles. This deformation of the surface was not apparent in the cold switching test (Fig. 6) in experiment 1, because the actuator displacement was fixed in the former and increased slightly in experiment 2.

Fig 10 shows the onset of failure as the CR reached exceeds 2 Ω, an increase of more than x3 from the nominal 0.4 Ω at the start of the test. The contact resistance remains between 0.4 and 0.5 Ω for the duration of the test until the onset of failure at 140 Million cycles.

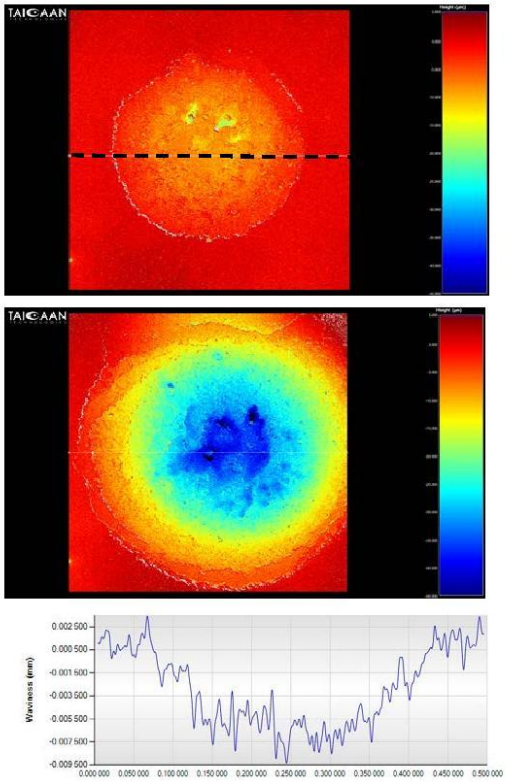

Fig. 9. Evolution of the Au/CNT surface in Experiment 2, with 10 and 140 Million Switching cycles, 4V 50 mA, with cross section profile from 10 Million cyles, smoothed with 8 µm Gauss filter. Data format 1001x1001 over 0.5mm x 0.5mm, leveled and the colour scale set, +5 to -45 µm.

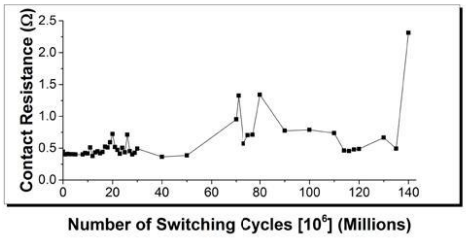

Fig. 10. Contact Resistance (CR) with hot switching cycles. DC hot switching, at 0.3 kHz, 4 V, 50 mA.

C. *Results summary*

Table 1 shows an overview of the experiment results and includes data from previous work, [13,14]. There are 4 notes (a-d), as follows:

a) The contacts did not fail at 4 Billion cycles, the experiment was halted. The volume measured does not correspond to the fail condition.
b) The contact force started at 150 µN, but increased slightly with the number of cycles.
c) With the low force cantilever test the location of the contact spot on the Au/CNT surface could not be located. Data was presented in [13] for the cantilever surface only.
d) The cycles to failure was published as 70 Million [14], but this was extended in [11], because there was significant contact bonce in the system, here averaged at 13 bounces per switching cycle. Each bounce corresponds to a new opening event.

TABLE 1. SUMMARY OF RESULTS

Exp.	Summary Data for 505 surface		
	Contact Force, and DC current	*Cycles to failure*	*Wear Volume (10-3) mm(3)*
1	150 µN, 4 µA	4 Billion [a]	0.2
2	150 µN [b], 50 mA	140 Million	0.154
[13]	35 µN, 50 mA	28 Million	Not measured [c]
[14]	1000 µN, 20 mA	910 Million [d]	0.444

IV. DISCUSSION

The results in experiment 1, show a contact surface exceeding 4 Billion switching cycles under a nominal cold switching condition. It is important to note that at the conclusion of the test the CR had not exceeded the 3Ω, the failure condition limit.

A. *The influence of the DC current*

The strict definition of cold switching requires zero voltage and current, but in experiment 1, a DC load of 4 V and 4 µA was used. Using these values, with the same V_{max} value used to determine k in Eq (1), (note the surface used to define k was a 505 surface as used here), although the contact force used was 1 mN compared to the 150 µN, used here; as follows; k = 1.22 $x10^{-9}$, and V_{max} = 4.44 $x10^{-4}$ mm^3, (see Table 1).

A key issue with the existing theory for the fine transfer mechanism is that when the current level is 4 µA as used in experiment 1, the failure point is predicted to be at 22.8 x 10^6 Billion cycles. This massive increase in predicted lifetime is not apparent in the surfaces shown in Fig. 6, where there is clear and measured evidence of wear processes. For the current range below 1 mA it is apparent that the fine transfer process described in Eq.1 should be re-evaluated.

The data shown in Fig. 5&6, indicated that the surface has not failed at 4 Billion cycles, it is therefore necessary to estimate the failure point. For this discussion we shall assume failure, at 6.92 Billion cycles. This value is determined from the average transfer rate in Fig. 7, for a reduced, V_{max} = 0.27 x10^{-3} (mm^3) based on a reduced area for the lower contact force used in experiment 1.

Firstly, Eq.1 is based on an assumed I^2 relationship, linked to the thermal behaviour of the MMB. This was assumed to be the driving factor in [14], but the evidence here suggests this is not the case. Fig 11, from [13], shows that for a similar surface over a range of higher current levels, the MMB duration is linear with the current (10-200 mA). If we now assume that during the MMB process the voltage (u) remains constant to a first approximation (the molten metal voltage). Then the energy (E) associated with the MMB is a linear function of I, as shown in Eq.(2);

$$E = \int_{t_1}^{t_2} u \times I \, dt \qquad (2)$$

where t_1 and t_2 are the start on end of the MMB period.

If we assume the rate of transfer of material in the MMB process is linked to the MMB energy in Eq.2, then it will be proportional to the I and not the I^2. This observation changes the value of k determined in Eq.(1), to k = 2.43 x 10^{-11}. This change in Eq.1 results in a predicted 4550 Billion cycles to failure at 4 µA. This number of cycles remains much higher than the estimated 6.92 Billion. A further adjustment is required for low currents.

B. *The influence of contact force*

The existing model (Eq.1) does not account for contact force on the assumption that the process was driven by the MMB, however it is apparent from the data shown in Fig.6 that in the cold switching condition, even with no apparent MMB, there is wear. It is proposed that the wear observed in Fig.6 is linked to asperity level adhesion linked linearly to the applied force; then to a first approximation, the existing model can be developed as the sum of the current relationship and the new force relationship, as;

$$N_f = \frac{V_{max}}{k_1 I + k_2 F} \qquad (3)$$

where V_{max} is also a function of F, since the maximum area of Au removed from the Au/CNT surface is expected to reduce with the contact force. In this new relationship,

k_1 = is the newly defined value of 2.43 x 10^{-11} and not linked to force.

k_2 = function of contact area and therefore force.

The model based on Eq. 3 is shown in Fig. 12. In this model the maximum cycles to failure at a current below 500 µA is limited by the adhesion process to between 1 and 15 Billion cycles, linked to contact force; while above 500 µA, is linked primarily to the current level (I).

C. *Predicting cycles to failure.*

The model is consistent with a previous study [13], where with a MEMS cantilever with 30 µN force, a 50 mA experiment resulted in 28 Million cycles to failure; Eq (3) predicts 28.5 Million, on the assumption that the V_{max} is much reduced for the line contact in [13]. As noted in Table 1, it was not possible to detect the wear on the Au/CNT surface after an detailed SEM study.

For experiment 2 presented in this study, the new fine transfer model predicts 214 Million cycles to failure, compared to the 140 Million cycles observed. The error could be accommodated by the increasing contact force after each CS measurement, noted in experiment 2.

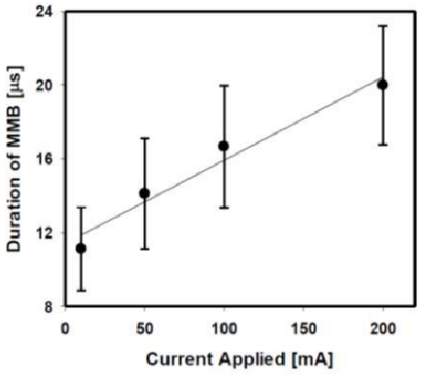

Fig. 11. The MMB duration with applied current, [13].

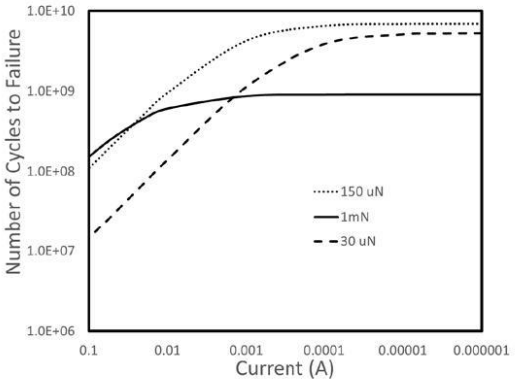

Fig. 12. The new model of the fine transfer process linked to failure for the 505 Au/CNT surface, based on Eq.3.

D. *Limitations of the new fine transfer model.*

It is noted that the new fine transfer model Eq.(3) does not account for;

- the wear condition associated with delamination, evidenced at higher contact forces and current levels above 50 mA.
- variation in the opening velocity of the contacts. It is however considered that the later will only be a secondary influence, as all system will open with an acceleration profile from rest.
- variation in the properties of the surface. A key factor will be the thickness of the Au layer used, and the penetration in to the CNT surface.
- variation in the applied voltage, there is evidence in [15], that increasing the voltage increased the fine transfer associated with the MMB. It has been noted that this result is unexpected and requires further investigation.

V. CONCLUSIONS

The Au/CNT surface investigated shows a stable contact resistance under near cold switching conditions for 4 Billion switching cycles.

The surface has been measured in-situ, over the test and shows evidence of wear. This observation has resulted in a re-evaluation of a fine transfer model used to predict contact failure in MEMS switching contacts. The new fine transfer model is linked to the DC current level and the contact force. The new fine transfer model has been tested against known results from other test conditions and shows a good correlation.

VI. ACKNOWLEDGMENT

The authors would like to acknowledge the software developed by Dr K. Cross at TaiCaan Technologies Ltd, for the integration of surface scanning into ICE apparatus.

REFERENCES

[1] G. M. Rebeiz, RF MEMS: theory, design, and technology: John Wiley & Sons, 2004.

[2] Jacapo Iannacci, RF-MEMS Technology for High performance passice, IOP Books, 2017.

[3] B. F. Toler, R. A. Coutu, and J. W. McBride, "A review of micro-contact physics for microelectromechanical systems (MEMS) metal contact switches," Journal of Micromechanics and Microengineering, vol. 23, no. 10, Oct, 2013.

[4] A. Basu, G. Adams, and N. McGruer, "A review of micro-contact physics, materials, and failure mechanisms in direct-contact RF MEMS switches," Journal of Micromechanics and Microengineering, 2016, vol. 26, no. 10, pp. 104004.

[5] C. Chianrabutra, L. Jiang, A. P. Lewis, and J. W. McBride, "Evaluating the influence of current on the wear processes of Au/Cr-Au/MWCNT switching surfaces," in 59th IEEE Holm Conference on Electrical Contacts, Newport, RI, 2013, pp. 344-349.

[6] T. Kageyama1, K. Shinozaki, L. Zhang, J. Lu, H. Takaki, S. Lee, " Fabrication of an Au–Au/carbon nanotube-composite contacts RF-MEMS switch", Micro and Nano Sytem Letters, 2018, 6:6.

[7] W. Johler, "Basic Investigations for Switching of RF Signals", IEEE Holm conference on Electrical Contacts, 2017, 10.1, pp 229-238.

[8] K. W. Gilbert, S. Mall, and K. D. Leedy, "Characterization of Gold–Gold Microcontact Behavior Using a Nanoindenter Based Setup," Journal of Adhesion Science and Technology, 2010, vol. 24, pp. 2597-2615.

[9] T. V. Laurvick, and R. A. Coutu, "Improving Gold/Gold Microcontact Performance and Reliability Under Low-Frequency AC Through Circuit Loading," IEEE Transactions on Components, Packaging and Manufacturing Technology, 2017, vol. 7, no. 3, pp. 345-353.

[10] M. Libansky, J. Zima, J. Barek, A. Reznickova, V. Svorcik, and H. Dejmkova, "Basic electrochemical properties of sputtered gold film electrodes," Electrochimica Acta, 2017, vol. 251, pp. 452-460.

[11] J. W. McBride, H. Liu, C. Chianrabutra, and A. P. Lewis, "The Wear of Hot Switching Au/Cr-Au/MWCNT Contact Pairs for MEMS Contacts," Ieice Transactions on Electronics, 2015, vol. E98c, no. 9, pp. 912-918.

[12] M. P. Down, L. Jiang, and J. W. McBride, "Investigating the benefits of a compliant gold coated multi-walled carbon nanotube contact surface in micro-electro mechanical systems switching," Applied Physics Letters, 2015, vol. 107 (7), 071901.

[13] A. P. Lewis, J. W. McBride, and L. Jiang, "Evolution of Voltage Transients During the Switching of a MEMS Relay With Au/MWCNT Contacts," IEEE Transactions on Components, Packaging and Manufacturing Technology, 2015, vol. 5, no. 12, pp. 1747-1754.

[14] J. McBride, "The wear processes of gold coated multi-walled carbon nanotube surfaces used as electrical contacts for micro-electro-mechanical switching," Nanoscience and Nanotechnology Letters, 2010, vol. 2, no. 4, pp. 357-361.

[15] T.G. Bull, J. W. McBride, and L. Jiang. "The influence of Circuit Parameters on Molten Bridge Surface Degradation in a Au/MWCNT MEMS Switch Contact", IEEE Holm Conference on Electrical Contacts, Albuqurque NM, 2018, pp 356-361pp.

[16] T. G. Bull, and J. W. McBride, "In-Situ Contact Surface Characterization in a MEMS Ohmic Switch under Low Current Switching," MDPI Technologies, 2018, vol. 2, no. 6, pp. 47.

[17] Taicaan Technologies XYRIS 4000CL, non contact confocal laser metrology system, http://www.taicaan.com

[18] J. McBride, E. Yunus, and S. Spearing, "Improving the contact resistance at low force using gold coated carbon nanotube surfaces," The European Physical Journal Applied Physics, 2010, vol. 50, no. 1, pp. 12904.

[19] H. Liu, J.W. McBride, "A Finite Element Based Contact Resistance Model for Rough Surfaces: Applied to a Bi-layered Au/MWCNT Composite", IEEE Transactions on Components, Packaging and Manufacturing Technology, 2018, Vol: 8, (6), pp 919 – 926.

BSSM 2018

Investigating Micro-scale Surface Change of an Ohmic MEMS Switch Contact between Switching Cycles

T.G. Bull[1a], L. Jiang[2] and J.W. McBride[1]

[1]Mechatronics Engineering Group, University of Southampton, Highfield Campus, UK

[2]Engineering Materials Group, University of Southampton, Highfield Campus, UK

[a] tb10g11@soton.ac.uk

Abstract. The leading cause of failure of the Ohmic (metal-metal contact) MEMS switch is through micro-scale wear of the contact surface. The wear is caused by both dynamic mechanical forces and the electrical signal. Characterisation of these contact surfaces has importance in understanding how the surfaces change as a result of wear, as well as the dominant mechanisms of wear for given switching conditions. Measurement of these surfaces has previously limited to measurement at the conclusion of switching. The following describes a novel apparatus for the investigation of the Ohmic MEMS switch contact surface inbetween individual switching cycles, and its use in investigating the early stages of micro-wear during low force (<1 mN) switching of a thin-film Au contact.

Introduction

Ohmic MEMS switches are micrometre-scale electrical components designed to complete, or interrupt, an electrical signal path through making or breaking a conductive pathway. They offer potential for low cost, low insertion-loss and high-isolation switching, of particular value for high frequency signals where the performance of solid-state alternatives falls off. The devices are manufactured using microfabrication techniques, with the conductive contact surfaces formed of metallic thin-films. Practical surface roughness ensures the true contact area is much smaller than the apparent contact area, and limited to locations where surface asperities on opposing contacts touch, or 'a'-spots. A circuit may only be completed where there is a metallic pathway between contacts at an 'a'-spot, thus they cause a constriction of current flow lines and the surface texture gives rise to a constriction resistance. As a consequence, micro-scale wear can have a profound influence on device performance, with the majority of Ohmic MEMS switch failures attributed to the contact surface interface itself **[1,2].**

Several difficulties exist in analytically predicting switching performance. Simplifications that allow macro switch behaviour to be accurately predicted, such as diffusive conduction dominating, materials behaving according to their bulk properties and well distributed 'a'-spots do not hold for the MEMS contact. Several improvements to micro-contact theory have been made; however the distribution and size of the 'a'-spots remain a parameter that can usually only be determined by empirical measurement of the surface **[3,4].** As well as the mechanical effects, the influence of carrying power when operated (hot switching) must also be evaluated on the surface wear process. When hot switching below the arcing threshold this is best described with reference to the Voltage-Temperature relationship that predicts the formation of a molten-metal bridge as contacting asperities undergo separation that driving a fine transfer wear process **[5]**.

The contact wear process is exceptionally complex and not fully described by current literature. Investigating the contact surface in-situ requires the resolution of a-spot features at the micro-scale. The following describes an apparatus to measure the contact surface at the micro-scale, between individual switching cycles and its use to investigate the dry switched wear of a thin film Au contact surface undergoing switching at low force conditions.

Ohmic MEMS Switch Contact Testing Apparatus

An overview of the apparatus is presented in Figure 1. The system allows the precision control of

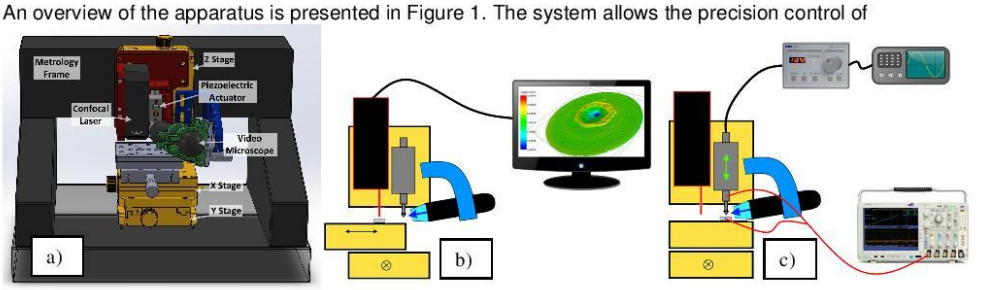

Figure 1. a) the apparatus design and major components, b) schematic of apparatus measuring contact surface with displacement laser and c) schematic of apparatus switching contact

a stationary contact relative to a mobile contact. Separation and reposition of contacts is achieved in an X,Y & Z coordinate reference frame using three motorised linear translation stages (Figure 1a, b & c – shown in yellow). A piezoelectric nano actuator provides fine Z control (10 nm) of the mobile contact and high speed cycling (> 1.25 kHz) for enhanced-rate contact lifetime-testing.

The lower, planar contact is held on the XY stages such that it can be located in the XY reference coordinates. A granite structure supports the Z translation stage above the XY stages. The Z stage also carries, a video microscope, for visually showing the contact positions) and a laser displacement meter. The fixed contact surface is mapped by translating the XY reference frame below the laser displacement meter (shown in Figure 1b) such that a raster scanning displacement mapping of the contact surface is recorded.

The electrical characterisation of the contact resistance at closure is recorded using a 4-wire Kelvin probe method and micro Ohmmeter (Keithley, USA). While the voltage transient at opening, corresponding to the molten-metal bridge rupture is recording using a high speed digital storage oscilloscope (Tektronix, USA). Visualisation of the contact approaching the surface is achieved using a 400x video microscope integrated to the system.

Evolution of the Surface of a Dry Switched Au Thin Film Contact

The evolution of a thin film Au contact is presented in colour maps of the measured surface height (Figure 2.a,b &c). The transfer of contact material back and forth between contacts as a result of individual switching cycles is demonstrated. The transfer pattern is validated by examination of the surface after switching using conventional microscopy (Figure 2d).

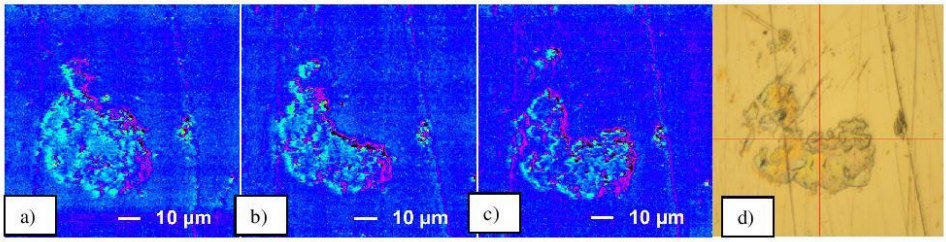

Figure 2. Contact surface mapping showing film delamination and transfer between contacts after a) 3 switching cycles, b) 4 switching cycles, c) 10 switching cycles and d) same region under 500x conventional microscopy after switching

Conclusion

A novel apparatus for investigating the contact evolution of an Ohmic MEMS switch contact is described and demonstrated detecting wear on a thin film Au contact at MEMS scale forces. The apparatus is capable of resolving the microscopic change in contact morphology as the result of individual switching operations. The wear process of a simple Au film contact is then investigated between individual switching events during initial contact "bedding in". The surface damage process is revealed to be a complex wear arising from plastic contact separation linked to film delamination wear, as well as molten metal bridge events, responsible for more subtle surface wear. The wear process is shown not to be a simple cumulative process; rather the process is highly complex with seemingly catastrophic damage arising very early from a low number of switching cycles. This damage is shown to be partially or fully repaired by subsequent switching events and provides insight to the unpredictable and catastrophic failure mode previous observed in Au films where they are employed as MEMS contacts.

References

[1] Toler, B.F., Coutu Jr, R.A. and McBride, J.W., 2013. A review of micro-contact physics for microelectromechanical systems (MEMS) metal contact switches. *Journal of Micromechanics and Microengineering*, *23*(10), p.103001.
[2] Rebeiz, G.M., 2004. *RF MEMS: theory, design, and technology*. John Wiley & Sons. P
[3] Holm, R, Electric Contacts, Theory and Applications
[4] Coutu Jr, R.A., McBride, J.W. and Starman, L.A., 2009, September. Improved micro-contact resistance model that considers material deformation, electron transport and thin film characteristics. In *Electrical Contacts, 2009 Proceedings of the 55th IEEE Holm Conference on* (pp. 298-302). IEEE.
[5] Lewis, A.P., McBride, J.W. and Jiang, L., 2015. Evolution of voltage transients during the switching of a MEMS relay with Au/MWCNT contacts. *IEEE Transactions on Components, Packaging and Manufacturing Technology*, *5*(12), pp.1747-1754.

Postgrad Conference 2017

AN INVESTIGATION OF THE APPICLATION OF GOLD COATED MULTI-WALLED-CARBON-NANOTUBE SURFACES FOR USE IN LOW CURRENT SWITCHING

T. Bull[1], L. Jiang[2], J. McBride[1 3]

[1]Mechatronics, Faculty of Engineering and the Environment, University of Southampton, UK
[2]Engineering Materials, Faculty of Engineering and the Environment, University of Southampton, UK
[3] University of Southampton, Malaysia Campus

INTRODUCTION

Micro-Electro-Mechanical-System (MEMS) switches are sub-millimetre scale devices that integrate a mechanical mechanism to control the switching of an electrical signal. Mechanical switches offer superlative performance over semiconductor alternatives in terms of their isolation (the ratio of the on-off state impedance) and insertion loss (the ratio of the on-off power dissipation of the switch).
Wear processes on the electrical contact surfaces, used in low voltage (2-12V) switching applications, exemplified by MEMS switching devices or relays, can result in premature device failure [1]. This becomes evident when the electrical contact surfaces are conventional metallic films. A proposed solution to minimize the electrical contact surface wear is to apply a sub-layer of carbon nano-tubes [2] to one or both surfaces – creating a gold/multi-walled-carbon-nanotube (Au/MWCNT) composite material. The carbon-nanotube layer serves to provide some compliance thus reducing local contact pressure and increasing the area available for contact material transfer. This provides a contact with a greatly increased lifespan over conventional metallic films where cold welding and film delamination are notable failure mechanisms. The predominant wear mechanism in the Au/MWCNT composite under low voltage, hot switching operation is a fine transfer of contact material. This is related to the circuit conditions and the properties of the contact material. During contact opening the circuit conditions give rise to a molten metal bridge (MMB) phenomena between the contacts. This process is investigated using a MEMS relay testing platform.

METHODOLOGY

The MEMS relay testing platform consists of an Au-Au/MWCNT contact pair (Figure 1) switched by a piezoelectric actuator. Contact pressure is monitored and controlled using a force transducer and Vernier adjustment of the switch actuator position. A DC circuit current is applied and the opening contact voltage transient measured using a high speed digital oscilloscope. The measured voltage transient is related to the thermal energy involved in the MMB and volume of material transfer. Circuit conditions are investigated over a range of circuit parameters below the arcing threshold and for different Au/MWCNT surface roughness [3].

RESULTS AND DISCUSSION

The results show that while the individual energy of an MMB events varies significantly between consecutive events for the same circuit parameters they show a normal distribution when evaluated over multiple consecutive events. Peak and average thermal energy show a clear rise as circuit current is increased. No clear trend is observed with circuit voltage. Increase in surface roughness of the composite correlates to an increase in the MMB energy which is contrary to the expected trend. This suggests that surface roughness – a parameter that only considers the amplitude variation of the surface – is insufficient to characterise the surface texture meaningfully as it relates to the MMB energy.

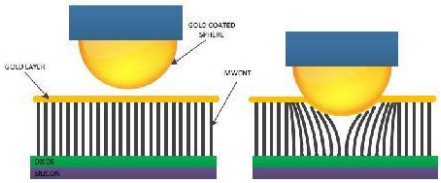

Figure 1: A Gold coated multi-walled-carbon nanotube (Au/MWCNT) and Gold coated hemisphere contact pair.

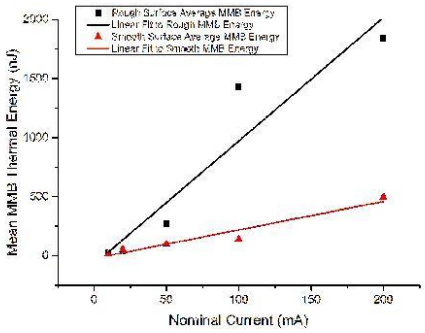

Figure 2: The average thermal energy of 100 repeat MMB events for a smooth (red) and a rough (black) Au/MWCNT surface.

CONCLUSIONS AND FUTURE WORK

The results have shown that the MMB energy appears to be linked to the surface roughness but in the opposite sense than expected. It is shown here that the MMB energy is linked closely to the load current and increases with the increase in surface roughness.
Future work will focus on developing a testing rig to operate at a higher cyclic rate with reduced contact force typical of a commercial MEMS switch mechanism. This will allow accelerated lifetime testing of the order of 10^9 cycles < 1 week. This will require the miniaturisation and micromanipulation of the apparatus along with the design, manufacture and investigation of a scaled down MEMS switch device utilising the novel Au/MWCNT composite.

REFERENCES

[1] B. F. Toler, R. A. Coutu, and J. W. McBride, *"A review of micro-contact physics for microelectromechanical systems (MEMS) metal contact switches,"* J. Micromechanics Microengineering, vol. 23, no. 10, p. 103001, Oct. 2013

[2] E. M. Yunus, S. M. Spearing, and J. W. McBride, *"The Relationship Between Contact Resistance and Contact Force on Au-Coated Carbon Nanotube Surfaces Under Low Force Conditions,"* IEEE Trans. Compon. Packag. Technol., vol. 32, no. 3, pp. 650–657, Sep. 2009.

[3] Bull T, McBride J, *The Influence of Circuit Parameters on Molten Metal Bridge Energy in a MEMS relay testing platform.* Proceedings of 2016 Twenty Eight International Conference on Electrical Contacts, 2016.

References

1. Brown, E.R., *RF-MEMS switches for reconfigurable integrated circuits.* Ieee Transactions on Microwave Theory and Techniques, 1998. **46**(11): p. 1868-1880.

2. Petersen, K., *Micromechanical membrane switches on silicon.* IBM Journal of Research and Development, 1979. **23**(4): p. 376-385.

3. Bouchard, J., *IHS iSuppli Teardown Analysis Service Identifies First Use of RF MEMS Part, Set to be Next Big Thing in Cellphone Radios*. 2012: https://technology.ihs.com/389456/ihs-isuppli-teardown-analysis-service-identifies-first-use-of-rf-mems-part-set-to-be-next-big-thing-in-cellphone-radios.

4. Rebeiz, G.M., *RF MEMS: theory, design, and technology*. 2004: John Wiley & Sons.

5. Iannacci, J., *RF-MEMS: an enabling technology for modern wireless systems bearing a market potential still not fully displayed.* Microsystem Technologies, 2015. **21**(10): p. 2039-2052.

6. Muldavin, J.B. and G.M. Rebeiz, *All-metal high-isolation series and series/shunt MEMS switches.* IEEE Microwave and wireless components letters, 2001. **11**(9): p. 373-375.

7. Toler, B., et al., *Unique Fabrication Method for Novel MEMS Micro-contact Structure*, in *MEMS and Nanotechnology, Volume 5*. 2014, Springer. p. 49-55.

8. Maciel, J. *RF MEMS switches are reliable: a comprehensive technology overview*. 27/7/2016].

9. Spearing, S.M., *Materials issues in microelectromechanical systems (MEMS).* Acta Materialia, 2000. **48**(1): p. 179-196.

10. Basha, S.J., et al., *Microcantilever Based RF MEMS Switch for Wireless Communication.* Microelectronics and Solid State Electronics, 2016. **5**(1): p. 1-6.

11. Czaplewski, D.A., et al., *Lifetime limitations of ohmic, contacting RF MEMS switches with Au, Pt and Ir contact materials due to accumulation of 'friction polymer'on the contacts.* Journal of Micromechanics and Microengineering, 2012. **22**(10): p. 105005.

12. Coutu, R.A., et al., *Microswitches with sputtered Au, AuPd, Au-on-AuPt, and AuPtCu alloy electric contacts.* IEEE transactions on Components and Packaging Technologies, 2006. **29**(2): p. 341-349.

13. Coutu, R.A., J.W. McBride, and L.A. Starman, *Improved micro-contact resistance model that considers material deformation, electron transport and thin film characteristics*, in *Proceedings of the 55th IEEE Holm Conference on Electrical Contacts*. 2009, IEEE: Vancouver, Canada.

14. Yunus, E., J. McBride, and S. Spearing, *Low force electrical switching using gold coated vertically aligned multi-walled carbon nanotubes surfaces.* IEICE Technical Report, 2008. **108**(296): p. 61-64.

15. McBride, J., et al. *Gold coated carbon-nanotube surfaces as low force electrical contacts for MEMS devices: Part II, fine transfer mechanisms*. in *2011 IEEE 57th Holm Conference on Electrical Contacts (Holm)*. 2011. IEEE.

16. Down, M., et al., *A nano-indentation study of the contact resistance and resistivity of a bi-layered Au/multi-walled carbon nanotube composite.* Applied Physics Letters, 2015. **106**(10): p. 101911.

17. Down, M., L. Jiang, and J. McBride, *Investigating the benefits of a compliant gold coated multi-walled carbon nanotube contact surface in micro-electro mechanical systems switching.* Applied Physics Letters, 2015. **107**(7): p. 071901.

18. Lewis, A.P., et al., *Electromechanical Investigation into the Influence of MWCNT Height on the Performance of Au/MWCNT Composites for Electrical Contacts.* Proceedings of the 2015 Sixty-First Ieee Holm Conference on Electrical Contacts (Holm), 2015: p. 376-380.

19. Lewis, A.P., J.W. McBride, and L. Jiang, *Evolution of Voltage Transients During the Switching of a MEMS Relay With Au/MWCNT Contacts.* Components, Packaging and Manufacturing Technology, IEEE Transactions on, 2015. **5**(12): p. 1747-1754.

20. van Spengen, W.M., *Capacitive RF MEMS switch dielectric charging and reliability: a critical review with recommendations.* Journal of Micromechanics and Microengineering, 2012. **22**(7).

21. Bordas, C., et al. *Carbon nanotube based dielectric for enhanced RF MEMS reliability*. in *2007 IEEE/MTT-S International Microwave Symposium*. 2007. IEEE.

22. Tavassolian, N., *DIELECTRIC CHARGING IN CAPACITIVE RF MEMS SWITCHES WITH SILICON NITRIDE AND SILICON DIOXIDE* May 2011, Georgia Institute of Technology.

23. Goldsmith, C., et al. *Understanding and improving longevity in RF MEMS capacitive switches*. in *MOEMS-MEMS 2008 Micro and Nanofabrication*. 2008. International Society for Optics and Photonics.

24. Chang, J.-S., et al. *Wafer level glass frit bonding for MEMS hermetic packaging*. in *Microsystems Packaging Assembly and Circuits Technology Conference (IMPACT), 2010 5th International*. 2010. IEEE.

25. Mahajan, A., et al., *Studies on the thermal decomposition of multiwall carbon nanotubes under different atmospheres.* Materials Letters, 2013. **90**: p. 165-168.

26. Goggin, R., et al. *Commercialization of a reliable RF MEMS switch with integrated driver circuitry in a miniature QFN package for RF instrumentation applications*. in *2015 IEEE MTT-S International Microwave Symposium*. 2015. IEEE.

27. Omron, *RF MEMS Switch: What you need to know*. 2013. p. 13.

28. Wong, O.-Y., et al. *An overview of charge pumping circuits for flash memory applications*. in *ASIC (ASICON), 2011 IEEE 9th International Conference on*. 2011. IEEE.

29. Feng, Y. and N.S. Barker, *Electrostatic RF MEMS Switch Working on 500~750 GHz.* 2016.

30. Mcbride, J., E. Yunas, and S. Spearing, *Gold coated Carbon Nanotube Surfaces as Low Force Electrical Contacts for MEMS devices: Part 1*, in *The 59th IEEE Holm Conference on Electrical Contacts*. 2009: Newport, RI, USA.

31. Grimwade, M., *The metallurgy of gold.* Interdisciplinary Science Reviews, 1992. **17**(4): p. 371-381.

32. Nutting, J. and J. Nuttall, *The malleability of gold.* Gold Bulletin, 1977. **10**(1): p. 2-8.

33. Aguilar, M., A. Oliva, and P. Quintana, *The effect of electrical current (DC) on gold thin films.* Surface science, 1998. **409**(3): p. 501-511.

34. Hyman, D. and M. Mehregany. *Contact physics of gold microcontacts for MEMS switches*. in *Electrical Contacts-1998. Proceedings of the Forty-Fourth IEEE Holm Conference on Electrical Contacts (Cat. No. 98CB36238)*. 1998. IEEE.

35. Jensen, B.D., et al., *Low-force contact heating and softening using micromechanical switches in diffusive-ballistic electron-transport transition.* Applied Physics Letters, 2005. **86**(2).

36. Antler, M., *Tribological properties of gold for electric contacts.* IEEE Transactions on parts, hybrids, and packaging, 1973. **9**(1): p. 4-14.

37. Tringe, J., et al., *A single asperity study of Au/Au electrical contacts.* Journal of Applied Physics, 2003. **93**(8): p. 4661-4669.

38. Dickrell, D.J. and M.T. Dugger. *The effects of surface contamination on resistance degradation of hot-switched low-force MEMS electrical contacts*. in *Proceedings of the Fifty-First IEEE Holm Conference on Electrical Contacts, 2005.* 2005. IEEE.

39. Jensen, B.D., et al., *Adhesion effects on contact opening dynamics in micromachined switches.* Journal of Applied Physics, 2005. **97**(10): p. 103535.

40. McMurry, J., *Fundamentals of Organic Chemistry, ; Brooks.* Cole, California, 1994.

41. Tsoukleri, G., et al., *Subjecting a graphene monolayer to tension and compression.* small, 2009. **5**(21): p. 2397-2402.

42. Nessim, G.D., *Properties, synthesis, and growth mechanisms of carbon nanotubes with special focus on thermal chemical vapor deposition.* Nanoscale, 2010. **2**(8): p. 1306-1323.

43. Kroto, H.W., et al., *C60: Buckminsterfullerene.* Nature, 1985. **318**(6042): p. 162-163.

44. Iijima, S., *Helical microtubules of graphitic carbon.* nature, 1991. **354**(6348): p. 56.

45. Popov, V.N., *Carbon nanotubes: properties and application.* Materials Science and Engineering: R: Reports, 2004. **43**(3): p. 61-102.

46. José-Yacamán, M., et al., *Catalytic growth of carbon microtubules with fullerene structure.* Applied physics letters, 1993. **62**(6): p. 657-659.

47. Kumar, M. and Y. Ando, *Chemical vapor deposition of carbon nanotubes: a review on growth mechanism and mass production.* Journal of nanoscience and nanotechnology, 2010. **10**(6): p. 3739-3758.

48. Bhaviripudi, S., et al., *CVD synthesis of single-walled carbon nanotubes from gold nanoparticle catalysts.* Journal of the American Chemical Society, 2007. **129**(6): p. 1516-1517.

49. Baker, R., P. Harris, and S. Terry, *Unique form of filamentous carbon.* Nature, 1975. **253**(5486): p. 37-39.

50. Hofmann, S., et al., *Surface diffusion: the low activation energy path for nanotube growth.* Physical review letters, 2005. **95**(3): p. 036101.

51. Falvo, M.R., et al., *Bending and buckling of carbon nanotubes under large strain.* Nature, 1997. **389**(6651): p. 582-584.

52. Kayastha, V.K., et al., *High-density vertically aligned multiwalled carbon nanotubes with tubular structures.* Applied Physics Letters, 2005. **86**(25): p. 253105.

53. Bradford, P.D., et al., *Tuning the compressive mechanical properties of carbon nanotube foam.* Carbon, 2011. **49**(8): p. 2834-2841.

54. Zhang, R., et al., *Growth of half-meter long carbon nanotubes based on Schulz–Flory distribution.* Acs Nano, 2013. **7**(7): p. 6156-6161.

55. Yunus, E.M., J.W. McBride, and S.M. Spearing, *The Relationship Between Contact Resistance and Contact Force on Au-Coated Carbon Nanotube Surfaces Under Low Force Conditions.* Ieee Transactions on Components and Packaging Technologies, 2009. **32**(3): p. 650-657.

56. McBride, J., E. Yunus, and S. Spearing, *Improving the contact resistance at low force using gold coated carbon nanotube surfaces.* The European Physical Journal Applied Physics, 2010. **50**(1): p. 12904.

57. McBride, J., L. Jiang, and C. Chianrabutra. *Fine transfer in electrical switching contacts using gold coated carbon-nanotubes*. in *26th International Conference on Electrical Contacts (ICEC 2012),*. 2012. Beijing, China: IET.

58. Chianrabutra, C., et al., *Evaluating the influence of current on the wear processes of Au/Cr-Au/MWCNT switching surfaces.* Proceedings of 2013 Ieee 59th Holm Conference on Electrical Contacts (Holm), 2013.

59. Down, M.P., L. Jiang, and J.W. McBride, *Investigating the benefits of a compliant gold coated multi-walled carbon nanotube contact surface in micro-electro mechanical systems switching.* Applied Physics Letters, 2015. **107**(7).

60. Down, M., *Mechanical and Electrical Characerisation of Carbon Nanotube Composite Surfaces for MEMS Switching Applications*, in *Faculty of Engineering and the Environment*. 2015, University of Southampton.

61. Agarwal, A., S.R. Bakshi, and D. Lahiri, *Carbon nanotubes: reinforced metal matrix composites*. 2016: CRC press.

62. YUKIYOSHI, Y., et al., *Electrical contact resistance performance of precious-metal-electroplated carbon nanotube films under micro loads.* Mechanical Engineering Journal, 2016. **3**(5): p. 15-00346-15-00346.

63. Izuo, S.-I., et al., *RF-MEMS switch using carbon nanotube composite gold electroplating.* IEEJ Transactions on Sensors and Micromachines, 2010. **130**: p. 165-169.

64. Kageyama, T., et al., *Fabrication of an Au–Au/carbon nanotube-composite contacts RF-MEMS switch.* Micro and Nano Systems Letters, 2018. **6**(1): p. 6.

65. McBride, J., A. Lewis, and M. Down. *Evaluating contact force based on displacement measurement of cantilever beams for MEMS switches and sensor applications*. in *IEEE Sensors 2015*. 2015. Busan, South Korea: IEEE.

66. Slade, P.G., *Electrical Contacts: Principles and Applications, Second Edition*. 2014, Boca Raton, FL, USA: CRC Press.

67. Maxwell, J.C., *A treatise on electricity and magnetism*. 1873, Oxford,: Clarendon press.

68. Thomas, T. and S. Probert, *Establishment of contact parameters from surface profiles.* Journal of Physics D: Applied Physics, 1970. **3**(3): p. 277.

69. Greenwood, J., *Constriction resistance and the real area of contact.* British Journal of Applied Physics, 1966. **17**(12): p. 1621.

70. Holm, R., *Electric contacts: theory and application*. 1958, Berlin, Germany: Springer Science & Business Media.

71. Greenwood, J. *50 Years Since GW66*. in *28th International Conference on Electric Contacts*. 2016. Edinburgh.

72. Myers, M., M. Leidner, and H. Schmidt. *Effect of contact parameters on current density distribution in a contact interface*. in *Electrical Contacts (Holm), 2011 IEEE 57th Holm Conference on*. 2011. IEEE.

73. Malucci, R.D. *The impact of spot size and location on current density*. in *Electrical Contacts, 2009 Proceedings of the 55th IEEE Holm Conference on*. 2009. IEEE.

74. Greenwood, J. and J. Tripp, *The contact of two nominally flat rough surfaces.* Proceedings of the institution of mechanical engineers, 1970. **185**(1): p. 625-633.

75. Abbott, E. and F. Firestone, *Specifying surface quality: a method based on accurate measurement and comparison.* SPIE MILESTONE SERIES MS, 1995. **107**: p. 63-63.

76. Bowden, F.P. and D. Tabor, *The area of contact between stationary and moving surfaces.* Proc. R. Soc. Lond. A, 1939. **169**(938): p. 391-413.

77. Bowden, F.P. and D. Tabor, *The friction and lubrication of solids*. Vol. 1. 2001: Oxford university press.

78. Yamada, K., et al., *Mechanisms of elastic contact and friction between rough surfaces.* Wear, 1978. **48**(1): p. 15-34.

79. Chang, W., I. Etsion, and D.B. Bogy, *An elastic-plastic model for the contact of rough surfaces.* Journal of tribology, 1987. **109**(2): p. 257-263.

80. Zhang, P., Y. Lau, and R.S. Timsit, *On the spreading resistance of thin-film contacts.* IEEE Transactions on Electron Devices, 2012. **59**(7): p. 1936-1940.

81. Timsit, R.S., *Constriction resistance of thin film contacts.* IEEE Transactions on Components and Packaging Technologies, 2010. **33**(3): p. 636-642.

82. Malucci, R.D. *Single and multi-spot current density distribution*. in *Electrical Contacts (Holm), 2016 IEEE 62nd Holm Conference on*. 2016. IEEE.

83. Mikrajuddin, A., et al., *Size-dependent electrical constriction resistance for contacts of arbitrary size: from Sharvin to Holm limits.* Materials Science in Semiconductor Processing, 1999. **2**(4): p. 321-327.

84. Pennec, F., et al., *Impact of the surface roughness description on the electrical contact resistance of ohmic switches under low actuation forces.* IEEE Transactions on Components, Packaging and Manufacturing Technology, 2012. **2**(1): p. 85-94.

85. Doduco, *Databook of Electrical Contacts*, ed. H. Vinaricky, Behrens. 2012, Pforzheim, Germany: Duduco GmbH.

86. Kumar, G., G. Prasad, and R. Pohl, *Experimental determinations of the Lorenz number.* Journal of materials science, 1993. **28**(16): p. 4261-4272.

87. Kittel, C., *Introduction to solid state physics*. 7th ed. 1995.

88. Koren, P., M. Nahemow, and P. Slade, *The molten metal bridge stage of opening electrical contacts.* IEEE Transactions on Parts, Hybrids, and Packaging, 1975. **11**(1): p. 4-10.

89. Price, M. and F.L. Jones, *The electrical contact: the properties and rupture of the microscopic molten metal bridge.* Journal of Physics D: Applied Physics, 1969. **2**(4): p. 589.

90. Slade, P. and M. Nahemow, *Initial separation of electrical contacts carrying high currents.* Journal of Applied Physics, 1971. **42**(9): p. 3290-3297.

91. Wakatsuki, N. and T. Watanabe, *Electric Characteristics and Contact Area Features of Melting when Making and Breaking Contacts.* Proceedings of the 2015 Sixty-First Ieee Holm Conference on Electrical Contacts (Holm), 2015: p. 76-81.

92. Malucci, R.D. *The impact on current density and constriction resistance from bridge structures in real contacts*. in *Electrical Contacts, 2017 IEEE Holm Conference on*. 2017. IEEE.

93. Warham, J., *The effect of inductance on fine transfer between platinum contacts.* Proceedings of the IEE-Part I: General, 1953. **100**(124): p. 163-168.

94. Stilson, C. and R. Coutu. *Micro-contact Resistance of Au-Au on Engineered Contact Surfaces using Gray-scale Lithography*. in *ICEC 2014; The 27th International Conference on Electrical Contacts; Proceedings of*. 2014. VDE.

95. Bull, T. and J. Mcbride, *The Influence of Circuit Parameters on Molten Metal Bridge Energy in a MEMS relay testing platform*, in *Proceedings of 2016 Twenty Eighth International Conference on Electrical Contacts*. 2016: Edinburgh, UK.

96. The Instruments, S.a.A.S., *Recommended Environments for Standards Laboratories*, I. 1-55617-977-4, Editor. 2006, ISA: NC, USA.

97. Bouchaud, J. and H. Wicht, *RF MEMS: status of the industry and application roadmap.* Frequenz, 2005. **59**(1-2): p. 24-26.

98. Ya, M.L., A.N. Nordin, and N. Soin, *Design and Analysis of a Low-Voltage Electrostatic Actuated RF CMOS-MEMS Switch.* 2013 Ieee Regional Symposium on Micro and Nanoelectronics (Rsm 2013), 2013: p. 41-44.

99. Maciel, J., et al. *Lifetime characteristics of ohmic MEMS switches*. in *Proc. SPIE*. 2004.

100. Muskett, C. and R. Hood, *Vibration Damage to Occupied Buildings*. 1990.

101. Standard, B., *BS 7385-2: 1993-Evaluation and measurement for vibration in buildings: Guide to damage levels from groundbourne vibration*. 1993, British Standards Institution, London, United Kingdom.

102. McBRIDE, J.W., et al., *The contact resistance performance of gold coated carbon-nanotube surfaces under low current switching.* 2012.

103. Lewis, A.P., J.W. McBride, and L.D. Jiang, *Evolution of Voltage Transients During the Switching of a MEMS Relay With Au/MWCNT Contacts.* IEEE Transactions on Components Packaging and Manufacturing Technology, 2015. **5**(12): p. 1747-1754.

104. Ren, W., et al., *Experimental Investigation and Understanding of the Intermittent Molten Bridge Phenomena and Mechanism of Contacts With Superlow Opening Speed.* IEEE Transactions on Components, Packaging and Manufacturing Technology, 2016. **6**(3): p. 418-423.

105. Ren, W., et al., *Investigation of the Surface Adhesion Phenomena and Mechanism of Gold-Plated Contacts at Superlow Making/Breaking Speed.* IEEE Transactions on Components, Packaging and Manufacturing Technology, 2015. **5**(6): p. 771-778.

106. Ren, W., *Unstable electrical contact behaviour at nanoscale for MEMS switch*, in *28th International Conference on Electric Contacts*. 2016, Heriott Watt University: Edinburgh, UK. p. 213-218.

107. Toler, B., C. Stilson, and R. Coutu. *Contact resistance evolution of au-au micro-contacts with encapsulated ag colloids*. in *2013 IEEE 59th Holm Conference on Electrical Contacts (Holm 2013)*. 2013. IEEE.

108. !!! INVALID CITATION !!! {}.

109. Kondo, D., S. Sato, and Y. Awano, *Low-temperature synthesis of single-walled carbon nanotubes with a narrow diameter distribution using size-classified catalyst nanoparticles.* Chemical physics letters, 2006. **422**(4): p. 481-487.

110. Futaba, D.N., et al., *84% catalyst activity of water-assisted growth of single walled carbon nanotube forest characterization by a statistical and macroscopic approach.* The Journal of Physical Chemistry B, 2006. **110**(15): p. 8035-8038.

111. Zhu, L., et al., *Growth and electrical characterization of high-aspect-ratio carbon nanotube arrays.* Carbon, 2006. **44**(2): p. 253-258.

112. Zhang, G., et al., *Ultra-high-yield growth of vertical single-walled carbon nanotubes: Hidden roles of hydrogen and oxygen.* Proceedings of the National Academy of Sciences of the United States of America, 2005. **102**(45): p. 16141-16145.

113. Xu, Y.-Q., et al., *Vertical array growth of small diameter single-walled carbon nanotubes.* Journal of the American Chemical Society, 2006. **128**(20): p. 6560-6561.

114. Watanabe, M., M. Hamano, and M. Harazono, *The role of atmospheric oxygen and water in the generation of water marks on the silicon surface in cleaning processes.* Materials Science and Engineering: B, 1989. **4**(1-4): p. 401-405.

115. Libansky, M., et al., *Basic electrochemical properties of sputtered gold film electrodes.* Electrochimica Acta, 2017. **251**: p. 452-460.

116. Begtrup, G., et al., *Extreme thermal stability of carbon nanotubes.* physica status solidi (b), 2007. **244**(11): p. 3960-3963.

117. Yeh, P., *Introduction to photorefractive nonlinear optics*. Vol. 14. 1993: Wiley-Interscience.

118. GmbH, A.I. *Alicona infiniteFocus Technical Specifications*. 23/7/16]; Available from: http://www.alicona.com/products/infinitefocus/.

119. Chianrabutra, C., *Switching Characteristics of Gold Coated Carbon Nanotubes under MEMS Conditions*, in *Electromechanical Engineering*. 2014, University of Southampton.

120. McBride, J.W., et al., *The Wear of Hot Switching Au/Cr-Au/MWCNT Contact Pairs for MEMS Contacts.* Ieice Transactions on Electronics, 2015. **E98c**(9): p. 912-918.

121. Bull, T.G. and J.W. McBride, *In-Situ Contact Surface Characterization in a MEMS Ohmic Switch under Low Current Switching.* MDPI Technologies, 2018. **2**(6): p. 47.

122. Lewis, A.P., et al. *Development of a MEMS test platform for investigating the use of multi-walled CNT composites electric contacts*. in *Electronics Packaging Technology Conference (EPTC 2013), 2013 IEEE 15th*. 2013. IEEE.

123. Calvert, J.R. and R.A. Farrar, *An engineering data book*. 2008: Palgrave Macmillan.

124. Shelby, J., *Viscosity and thermal expansion of lithium aluminosilicate glasses.* Journal of Applied Physics, 1978. **49**(12): p. 5885-5891.

125. Laurvick, T.V. and R.A. Coutu, *Improving Gold/Gold Microcontact Performance and Reliability Under Low-Frequency AC Through Circuit Loading.* IEEE Transactions on Components, Packaging and Manufacturing Technology, 2017. **7**(3): p. 345-353.

126. Lewis, A., et al. *The effect on switching lifetime of chromium adhesion layers in gold-coated electrical contacts under cold and hot switching conditions*. in *2013 IEEE 59th Holm Conference on Electrical Contacts (Holm 2013)*. 2013. IEEE.

127. Cognard, J., *Adhesion to gold: A review.* Gold Bulletin, 1984. **17**(4): p. 131-139.

128. Lisec, T., et al. *MEMS switch with prolonged lifetime under hot switching conditions based on gold as contact material*. in *2017 19th International Conference on Solid-State Sensors, Actuators and Microsystems (TRANSDUCERS)*. 2017. IEEE.

129. Collins, P.G., et al., *Current saturation and electrical breakdown in multiwalled carbon nanotubes.* Physical review letters, 2001. **86**(14): p. 3128.

130. Zhang, K., G.M. Stocks, and J. Zhong, *Melting and premelting of carbon nanotubes.* Nanotechnology, 2007. **18**(28): p. 285703.

131. Masahito, S., et al., *Measuring the electrical resistivity and contact resistance of vertical carbon nanotube bundles for application as interconnects.* Nanotechnology, 2011. **22**(8): p. 085302.

132. Wang, P., R. Xiang, and S. Maruyama, *Thermal Conductivity of Carbon Nanotubes and Assemblies.* 2018.

133. McBride, J., *The wear processes of gold coated multi-walled carbon nanotube surfaces used as electrical contacts for micro-electro-mechanical switching.* Nanoscience and Nanotechnology Letters, 2010. **2**(4): p. 357-361.

134. Carslaw, H.S. and J.C. Jaeger, *Conduction of heat in solids.* Oxford: Clarendon Press, 1959, 2nd ed., 1959.

135. Bull, T.G., J.W. McBride, and L. Jiang. *The influence of Circuit Parameters on Molten Bridge Surface Degradation in a Au/MWCNT MEMS Switch Contact*. in *2018 IEEE Holm Conference on Electrical Contacts*. 2018. Albuquerque, NM, USA: IEEE.

136. Micro, M. *MM3100 - 6 Channel SPST RF-Micro-Switch*. 2018; Available from: https://www.menlomicro.com/uploads/7/8/8/9/78891034/menlo_mm3100_datasheet.pdf.

137. Johler, W. *Basic investigations for switching of RF signals*. in *Electrical contacts-2007, the 53rd ieee holm conference on*. 2007. IEEE.

138. Devices, A. *0Hz/DC to 14GHz, Single-Pole, Four-Throw MEMS Switch with Integrated Driver*. 2018; Available from: https://www.analog.com/en/products/adgm1304.html.

139. Rebeiz, G.M., L.P.B. Katehi, and N.S. Barker, *Special issue on MEMS devices for RF systems - Guest editorial.* Ieee Transactions on Microwave Theory and Techniques, 2003. **51**(1): p. 257-258.

140. Manz, B. *The High-Performance RF MEMS Switch Has Arrived*. 2018; Available from: https://www.electronicdesign.com/analog/high-performance-rf-mems-switch-has-arrived-pdf-download.

141. Van Caekenberghe, K., *RF MEMS on the radar.* IEEE Microwave magazine, 2009. **10**(6).

142. MenloMicro. *Application Notes for the MM3100 Switch*. Available from: https://www.menlomicro.com/uploads/7/8/8/9/78891034/menlo_mm3100_application_note.pdf.

143. Pheasant, S. and C.M. Haslegrave, *Bodyspace: Anthropometry, ergonomics and the design of work*. 2016: CRC Press.

144. Liu, H., J.W. McBride, and M.Z.M. Yusop. *Surface characterization of a Au/CNT composite for a MEMS switching application*. in *Nanotechnology (IEEE-NANO), 2016 IEEE 16th International Conference on*. 2016. Sendai, Japan: IEEE.